Forensic Study of Early Failures with Unbonded Concrete Overlays


Prepared by:
Shad Sargand, Roger Green, Junqing Zhu, and Issam Khoury

Prepared for:
The Ohio Department of Transportation,
Office of Statewide Planning & Research

State Job Number 134996

November 2017
Final Report

Ohio Research Institute for Transportation and the Environment

U.S. Department of Transportation
Federal Highway Administration

Technical Report Documentation Page

1. Report No.	2. Government Accession No.	3. Recipient's Catalog No.
FHWA/OH-2017-38		

4. Title and Subtitle	5. Report Date
Forensic Study of Early Failures with Unbonded Concrete Overlays	**November 2017**
	6. Performing Organization Code

7. Author(s) (include ORCID ID)	8. Performing Organization Report No.
Shad Sargand (ORCID 0000-0002-1633-1045), Roger Green (ORCID 0000-0003-2497-825X), Junqing Zhu (ORCID 0000-0003-4134-4064), and Issam Khoury (ORCID 0000-0003-4856-7535)	

9. Performing Organization Name and Address	10. Work Unit No. (TRAIS)
Ohio Research Institute for Transportation and the Environment (ORITE) **233 Stocker Center** **Ohio University** **Athens, OH 45701-2979**	
	11. Contract or Grant No.
	SJN 134996

12. Sponsoring Agency Name and Address	13. Type of Report and Period Covered
Ohio Department of Transportation **Office of Statewide Planning and Research** **1980 West Broad St., MS 3280** **Columbus, OH 43223**	**Final Report, August 2014 – September 2017**
	14. Sponsoring Agency Code

15. Supplementary Notes

16. Abstract

A forensic investigation was conducted to identify failure mechanisms responsible for early failures of unbonded concrete overlays on selected projects in Ohio, including I-70 in Madison County, I-77 in Washington and Noble Counties, and I-90 in Lake County, plus a project in US Route 30 in Ashland County that was one of the better performing jointed plain concrete (JPC) overlays in Ohio. Standard NCHRP procedures (Report 747) were generally followed. Field inspections included visual assessment; distress survey; falling weight deflectometer; MITScan; and collection of core specimens. Laboratory testing included core dimensions, material mechanical properties, and petrographic analysis. HIPERPAV analysis was conducted to evaluate the concrete strength development in early stage. A finite element analysis was conducted to evaluate structural failure mechanisms. Recommendations were made for ODOT to improve performance and prevent similar failures in the future.

17. Keywords	18. Distribution Statement
Forensic investigation, unbonded concrete overlay, rigid pavement, finite element method, falling weight deflectometer, MITScan, HIPERPAV, petrographic	**No restrictions. This document is available to the public through the National Technical Information Service, Springfield, Virginia 22161**

19. Security Classification (of this report)	20. Security Classification (of this page)	21. No. of Pages	22. Price
Unclassified	**Unclassified**	**248**	

Form DOT F 1700.7 (8-72) **Reproduction of completed pages authorized**

SI* (MODERN METRIC) CONVERSION FACTORS

APPROXIMATE CONVERSIONS TO SI UNITS

Symbol	When You Know	Multiply By	To Find	Symbol
LENGTH				
in	inches	25.4	millimeters	mm
ft	feet	0.305	meters	m
yd	yards	0.914	meters	m
mi	miles	1.61	kilometers	km
AREA				
in^2	square inches	645.2	square millimeters	mm^2
ft^2	square feet	0.093	square meters	m^2
yd^2	square yards	0.836	square meters	m^2
ac	acres	0.405	hectares	ha
mi^2	square miles	2.59	square kilometers	km^2
VOLUME				
fl oz	fluid ounces	29.57	milliliters	mL
gal	gallons	3.785	liters	L
ft^3	cubic feet	0.028	cubic meters	m^3
yd^3	cubic yards	0.765	cubic meters	m^3
NOTE: Volumes greater than 1000 L shall be shown in m^3.				
MASS				
oz	ounces	28.35	grams	g
lb	pounds	0.454	kilograms	kg
T	short tons (2000 lb)	0.907	megagrams (or "metric ton")	Mg (or "t")
TEMPERATURE (exact)				
°F	Fahrenheit temperature	5(°F-32)/9 or (°F-32)/1.8	Celsius temperature	°C
ILLUMINATION				
fc	foot-candles	10.76	lux	lx
fl	foot-Lamberts	3.426	candela/m^2	cd/m^2
FORCE and PRESSURE or STRESS				
lbf	poundforce	4.45	newtons	N
lbf/in^2 or psi	poundforce per square inch	6.89	kilopascals	kPa

APPROXIMATE CONVERSIONS FROM SI UNITS

Symbol	When You Know	Multiply By	To Find	Symbol
LENGTH				
mm	millimeters	0.039	inches	in
m	meters	3.28	feet	ft
m	meters	1.09	yards	yd
km	kilometers	0.621	miles	mi
AREA				
mm^2	square millimeters	0.0016	square inches	in^2
m^2	square meters	10.764	square feet	ft^2
m^2	square meters	1.195	square yards	yd^2
ha	hectares	2.47	acres	ac
km^2	square kilometers	0.386	square miles	mi^2
VOLUME				
mL	milliliters	0.034	fluid ounces	fl oz
L	liters	0.264	gallons	gal
m^3	cubic meters	35.71	cubic feet	ft^3
m^3	cubic meters	1.307	cubic yards	yd^3
MASS				
g	grams	0.035	ounces	oz
kg	kilograms	2.202	pounds	lb
Mg (or "t")	megagrams (or "metric ton")	1.103	short tons (2000 lb)	T
TEMPERATURE (exact)				
°C	Celsius temperature	1.8°C + 32	Fahrenheit temperature	°F
ILLUMINATION				
lx	lux	0.0929	foot-candles	fc
cd/m^2	candela/m^2	0.2919	foot-Lamberts	fl
FORCE and PRESSURE or STRESS				
N	newtons	0.225	poundforce	lbf
kPa	kilopascals	0.145	poundforce per square inch	lbf/in^2 or psi

* SI is the symbol for the International Symbol of Units. Appropriate rounding should be made to comply with Section 4 of ASTM E380.

(Revised September 1993)

Forensic Study of Early Failures with Unbonded Concrete Overlays

Prepared by:
Shad Sargand, Roger Green, Junqing Zhu, and Issam Khoury

Ohio Research Institute for Transportation and the Environment
Russ College of Engineering and Technology
Ohio University
Athens, Ohio 45701-2979

Prepared in cooperation with the Ohio Department of Transportation
and the U.S. Department of Transportation, Federal Highway Administration

November 2017

Acknowledgments

The authors would like to thank the ODOT Technical Liaisons and other key personnel providing assistance during this project:

- Mr. Adam Au (Office of Pavement Engineering)
- Mr. Aric Morse (Office of Pavement Engineering)
- Mr. Dwayne McKinney (Office of Pavement Engineering)
- Mr. Robert Loughry (Office of Pavement Engineering)
- Mr. Andrew Clouse (Office of Pavement Engineering)
- Mr. Patrick W. Bierl (Office of Pavement Engineering)
- Mr. David Miller (Office of Pavement Engineering)

The authors also thank ODOT's Office of Statewide Planning & Research for their time and assistance. The authors would like to thank graduate students Anwer Al-Jhayyish and Abdul Qaium Fekrat at Ohio University, who also contributed significantly to the completion of this project. The authors also thank the subcontractors, Dr. Jan Olek and his collaborators at Purdue, who contributed the petrographic analysis of core samples, including scanning electron microscope and entrapped air voids analysis, and Stantec at Tonawanda NY, who conducted the international roughness index and image scans on MAD-70 and WAS/NOB-77.

Table of Contents

Appendices

List of Figures

List of Tables

1 Introduction

1.1 Problem Statement

The installation of an unbonded concrete overlay (UBCO) is one of the techniques employed by the Ohio Department of Transportation (ODOT) to rehabilitate deteriorated concrete pavements. Most of the unbonded concrete overlays constructed in Ohio have significantly extended pavement life [Williams and Chou, 1994], such as Project 1998-0119 in Ashland County. Others have failed prematurely, including the projects evaluated in this report: ODOT Project 1999-0295 in Madison County, Project 2005-3000 in Washington and Noble Counties, and Project 2005-0518 in Lake County. The performance of the above projects, in terms of pavement condition rating (PCR), as well as the average performance of all jointed plain concrete overlays on the Ohio highway system, and the ODOT PMS prediction model for unbonded concrete overlays, developed in 2012, are shown in Figure 1.

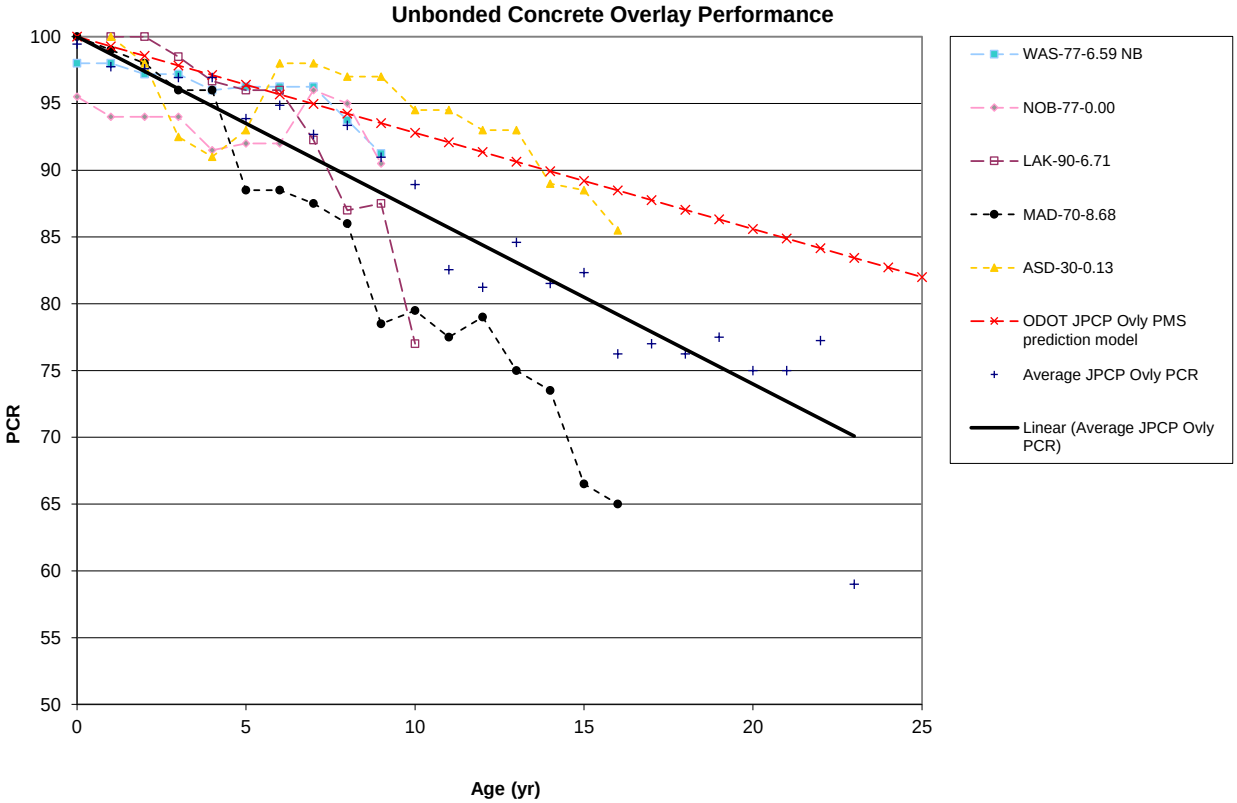

Figure 1 ODOT pavement condition rating versus age for unbonded overlay projects studied in this project.

Project 1999-0295 overlaid an existing 9 in (230 mm) jointed, reinforced, dowelled concrete pavement on I-70 in Madison County (MAD-70) with a 9 in (230 mm) jointed, plain, dowelled concrete (Item 452) pavement on a 1 in (25 mm) asphalt (Item 448) bondbreaker, constructed during 1999 and 2000. By 2008, significant transverse cracking, corner breaks, and slab settlement had appeared. In 2009, ODOT conducted an initial forensic investigation which included a distress survey, pavement coring, FWD deflection measurements, and observations of the removed pavement during repair. Data from the ODOT Office of Pavement Engineering showed 15% of all slabs in the eastbound direction and 5% of all slabs in the westbound direction

had cracks (the orientation of cracks was not identified). Results of the initial forensic study were inconclusive. The pavement continues to deteriorate and additional repairs have been made since 2009. Figure 2a) shows transverse cracking found on MAD-70.

Project 2005-3000 overlaid an existing 9 in (230 mm) jointed, reinforced, dowelled concrete pavement on I-77 in Washington and Noble Counties (WAS/NOB-77) with an 8 in (200 mm) jointed, plain, dowelled concrete (Item 452) pavement on a 1 in (25 mm) asphalt (Item 448) bondbreaker in 2006. The ODOT PCR data indicates transverse cracks appear immediately in the southbound lanes. Longitudinal cracking appeared in the northbound lanes in 2008 and the southbound lanes in 2010. Spalling of the joints appeared in the southbound direction in 2010 and the northbound lane in 2015. In 2014, corner breaks appeared in the southbound direction and pressure damage appeared in the northbound lanes. In 2015, pumping was rated in both directions. Figure 2b) shows longitudinal cracking found on WAS/NOB-77.

Both overlays were constructed using 15 ft (4.6 m) joint spacing. Cracking in slabs of this length was not expected this early. When a pavement experiences premature distress, it may be a result of poor design, poor construction technique, substandard construction material, higher than anticipated truck volumes, heavier than anticipated traffic loads, environmental factors such as the climate during pavement placing or curing, warping and curling stresses, or a combination of these. A forensic investigation is needed to consider all these cases and identify the factors that did contribute to the distresses. Once these factors are identified, steps can be taken to eliminate or reduce the occurrence of distress on future projects thus reducing the economic impact to ODOT and the exposure of the travelling public to unsafe conditions, such as differential settlement and potholes.

Two projects were added to this study. The first was added because it appeared to possibly have a different failure mechanism. Project 2005-0518 overlaid an existing 10 in (254 mm) jointed, reinforced, dowelled concrete pavement on I-90 in Lake County (LAK-90) east of Cleveland with a 9.5 in (241 mm) jointed, plain, dowelled concrete (Item 452) on a 1 in (25 mm) asphalt bondbreaker (Item 442) in 2005. Longitudinal joint spalling was observed in the westbound direction in 2008 and the eastbound direction in 2013. Transverse joint spalling was observed in the westbound direction in 2010 and the eastbound direction in 2012. Longitudinal cracking was observed in the eastbound direction in 2012. In 2013, corner breaks and transverse cracking was observed in the eastbound direction and in the westbound direction in 2014 and 2015, respectively. Faulting in the westbound direction was observed in 2014. Both directions were patched with full depth rigid repairs in 2015. The longitudinal cracking predominant on LAK-90 was a different type of distress than seen on the other project sites. Longitudinal cracking on LAK-90 was multiple hairline cracks present in nearly every slab whereas cracking on WAS/NOB-77 were typically a single low severity crack of occasional or frequent occurrence. Therefore, the data collected from a forensic study on LAK-90 was expected to complement that collected on MAD-70 and WAS/NOB-77, and would provide a more complete picture of the causes of early failures of unbonded overlays on rigid pavements. The climate in northern Ohio is different, and the soil is a different type than at the other two project sites.

The other project added to this study was one of the better performing jointed plain unbonded concrete overlays in Ohio and was included to verify the findings of this research. Project 1998-0119 overlaid an existing 9 in (229 mm) jointed, reinforced, dowelled concrete pavement on US-30 in Ashland County (ASD-30) with a 9 in (229 mm) jointed, plain, dowelled concrete on a 1 in (25 mm) asphalt bondbreaker (Item 403).

a)  b) 

Figure 2 a) Transverse cracking on MAD-70; b) Longitudinal cracking on WAS/NOB-77

1.2 Objectives

This project includes forensic evaluations of MAD-70-8.68 (project 1999-0295) and WAS/NOB-77-6.63/0.00 (Project 2005-3000) to identify mechanisms responsible for premature distresses. LAK-90 and ASD-30 were added later. The evaluations generally followed NCHRP procedures, based on the research team's two decades of experience conducting similar studies of Ohio's road system and climate conditions, and included nondestructive and destructive testing methods.

The pavements were modeled during construction using HIPERPAV. A finite element model of load response of unbonded overlays was generated using ABAQUS and a sensitivity analysis performed. The results of the modeling and the forensic evaluations were analyzed to identify mechanisms responsible for the premature distresses at each site.

The research team recommended changes to design procedures, plan details, construction inspection procedures and/or materials and construction specifications to eliminate or delay the formation of these distresses in future projects of this type.

In addition, the research team reviewed the NCHRP procedure by noting any differences in results that would have come from a strict adherence to NCHRP procedure versus results using the team's best engineering judgment. These differences were noted as possible indications where the NCHRP method could use some improvement for implementation in future forensic studies.

2 Literature Review

Liao [2011], in his University of Minnesota dissertation, proposed a design method for unbonded concrete overlays (UBCOs) based on fracture mechanics. The ultimate load capacity of the unbonded concrete overlay structure was related to the fundamental material properties and geometric dimensions using a two-dimensional cohesive zone model to predict reflective cracking. The concept of this method is similar to the stress equivalency concept in the Portland Cement Association (PCA) method. The structural equivalency determined not by stress values, but by the maximum load achieved during the simulated failure in an UBCO system compared to an equivalent single layer PCC pavement. The three-layer UBCO system was modeled with an existing crack in the existing Portland cement concrete (PCC) pavement, as shown in the right portion of Figure 3, to account for PCC overlay failure from reflective cracking. The maximum load before failure is determined from the cohesive zone model using the finite element analysis program ABAQUS. The UBCO should be designed to have load-carrying capacity equal to that of a new single-layer PCC pavement, as shown in the left side of Figure 3. A set of equations and design procedures were presented using on the results of a series of the finite element simulations.

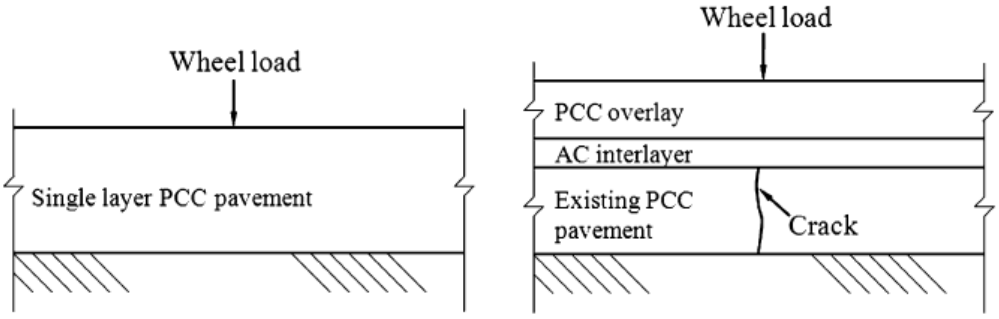

Figure 3 Structural equivalency proposed by Liao [2011].

In 2006, Ohio University conducted an experiment at the request of the New York State Department of Transportation (NYSDOT) to evaluate performance of unbonded concrete overlays placed over three sections of I-86 in Cattaraugus County, New York, each subjected to a different treatment [Sargand, Khoury, & Padilla-Llano, 2012]. The existing pavement on the first section was left untreated; the second section was broken and seated; and the third section was rubblized. Each section was overlaid with a 3 in (76 mm) porous asphalt bondbreaker, and then overlaid with 8.86 in (225 mm) PCC. Each section was instrumented with LVDTs, strain gages, and thermocouples, and the performance was monitored. Falling Weight Deflectometer (FWD) testing was also conducted on these sections to determine response to dynamic loads. By November, 2009, mid-panel top-down cracks were observed in 90% of the pavement slabs in the untreated section compared to about 5% of the sections in the rubblized and broken and seated sections. The researchers concluded that the environmental effects were more critical on concrete pavements than dynamic loads based on the strain measurements. The researchers also suggested NYSDOT should break and seat the existing pavement before placing an unbonded concrete overlay.

In 2002, Illinois Department of Transportation reported a study of unbonded concrete overlay on I-74 in Knox County, IL [Heckel, 2002]. The overlay was constructed in 1995. A continuously reinforced concrete overlay of 9.25 in (235 mm) was placed on an asphalt bondbreaker 3 in (76 mm) to 4.5 in (114 mm) thick. The existing concrete pavement was a 7 in

(178 mm) continuously reinforced PCC with a 4 in (102 mm) bituminous aggregate mix base. The concrete had severe D-cracking and many punch-outs before the overlay was applied. An earlier asphalt concrete overlay exhibited transverse, longitudinal, and reflective cracks. Performance was monitored since construction of the PCC overlay through traffic count, Condition Rating Survey (CRS) values, visual distress surveys, International Roughness Index (IRI), Load Transfer Efficiency (LTE), and Falling Weight Deflectometer (FWD). As of December 31, 2001, 31.6 percent of the design traffic had passed, which means the design traffic will be reached over approximately 18 years of service, assuming a growth rate of 3% per year. The CRS and IRI showed little deterioration during six years of service. Table 1 presents the FWD results over the same time frame, which also showed minimal deterioration. Overall, the unbonded concrete overlay performance until 2001 was excellent and no maintenance or patching had been necessary.

Table 1 FWD results collected over the first six years of service on I-74 in Knox County IL [Heckel, 2002]

	Temperature		Normalized deflection		Area		LTE
Date	(°F)	(°C)	(mil/kip)	(mm/MN)	(in)	(mm)	(%)
Jul-95	90	32	2	11.4	31	787.4	NC
Aug-96	77	25	2.2	12.6	31.6	802.64	NC
Jul-97	85	29	2.4	13.7	31.4	797.56	92.6
Apr-99	56	13	2.1	12.0	31	787.4	92.6
Jul-01	94	34	2.3	13.1	30.8	782.32	91.6

Researchers from the University of Waterloo monitored and reported on the ten-year performance of an UBCO constructed and instrumented during the rehabilitation of Bloor Street in Toronto during 2003. The street was subjected to high volumes of heavy transit traffic, which had led to heavy damage to on the old pavement. 150 mm (5.9 in) PCC and a 25 mm (1 in) HMA "bondbreaker" were overlaid on an existing PCC pavement of thickness 200 mm (7.9 in). Strain gages were placed at various locations in the pavement layers. The strain measured in the overlay section remained fairly low. A general trend of increasing compressive strains was observed throughout the first ten years of service at the top and bottom of the pavement. The author suggested that compressive strain at the bottom may be the result of a bond between the two concrete layers, which is to say that the bondbreaker layer did not function as intended. As shown in the right portion of Figure 4, both slabs are behaving monolithically with the neutral axis located in the old slab. This bonding may add additional structural capacity, but is undesirable because reflective cracking is likely [Kivi et al., 2013].

Figure 4 Comparison of overlay strain profiles: a) unbonded; b) bonded [Kivi et al., 2013].

Visual condition surveys showed the overlay section remained in very good condition after ten years of service. Overall, the overlay section has shown excellent performance in its first ten years of service, with no major functional or structural issues. The author concluded that concrete overlays are excellent rehabilitation options for urban pavements subjected to high traffic volumes.

Hansen and Liu [2013] from the University of Michigan investigated unbonded concrete overlays that were experiencing premature distresses in Michigan. The distresses included corner breaks and longitudinal cracking originating at the joints. The evaluation consisted of nondestructive testing at the site and laboratory testing of core samples. The researchers confirmed the major cause of distress was pumping, which was a direct result of poor drainage. The poor drainage was either because of construction related factors that blocked water from reaching the drainage trench or because no drainage system was built. The researchers also found the rate of IRI increase was related to the quality of pavement drainage. A finite element analysis using EverFE predicted concrete overlays are more sensitive than regular JPCP to slab cracking from loss of joint support.

In 2004, Sargand [2005] from Ohio University conducted a forensic investigation on I-75 in Hancock County. The road was constructed in 1990 with 6 in (152 mm) recycled concrete aggregate (RCA) as base and 11 in (280 mm) reinforced concrete at top. The joint spacing was 27 ft (8.2 m). Various distresses were observed approximately 10 years later, including spalling, transverse cracking, punch outs, and shoulder deterioration. Dynamic Cone Penetrometer (DCP) tests were conducted by the research team to determine the resilient modulus of the base at selected locations. ODOT provided FWD test data, cracking records, core samples and pictures. The resilient modulus of the base was found to be high in some locations, indicating the presence of moisture-induced hardening. The researchers concluded there was an excess amount of fine materials in the RCA, which was hardened when water seeped into base and caused a variability of stiffness. The stiffness of the base resulted in a loss of support under the concrete pavement, and thus led to various types of cracking.

3 Methods

3.1 Visual Assessment

The study of an unbonded concrete overlay (UBCO) project began with a site visit where a visual assessment of the general condition of the pavement was made. Typically the most distressed segment was identified for more detailed study and a corresponding "control section" of similar length with minor distress designated for comparison. Photographs were taken of some distressed spots, such as those in Figure 2.

3.2 Distress Survey

A detailed visual distress survey was conducted on the designated distressed section and the corresponding control section. Distress survey sheets were used to record locations and types of distresses (e.g. cracking, spalling, pothole, and patching), mark locations where cores were collected (possibly at a later date), and add other notes pertaining to the project, such as joints selected for MIT Scanning.

Archived distress surveys conducted by ODOT in prior years were consulted as well. The distress surveys of I-90 and US-30 were conducted by reviewing PathWeb images provided by ODOT from their most recent surveys in 2014. PathWeb is a web-based viewing software allowing users to see right-of-way and distress imagery on the roadway on which data were collected. Figure 5 is a sample road surface image from I-90. The number of cracks per every 0.1 mile (0.16 km) was counted by reviewing the images and the numbers plotted with respect to mile marker. If video scans were available, these were accessed and the cracks per station counted from the images for the overlay project. These data were plotted along with the temperature at the time of construction for each station. For US-30, some of the images were blurred and Google Street View images were used to for assistance in counting cracks.

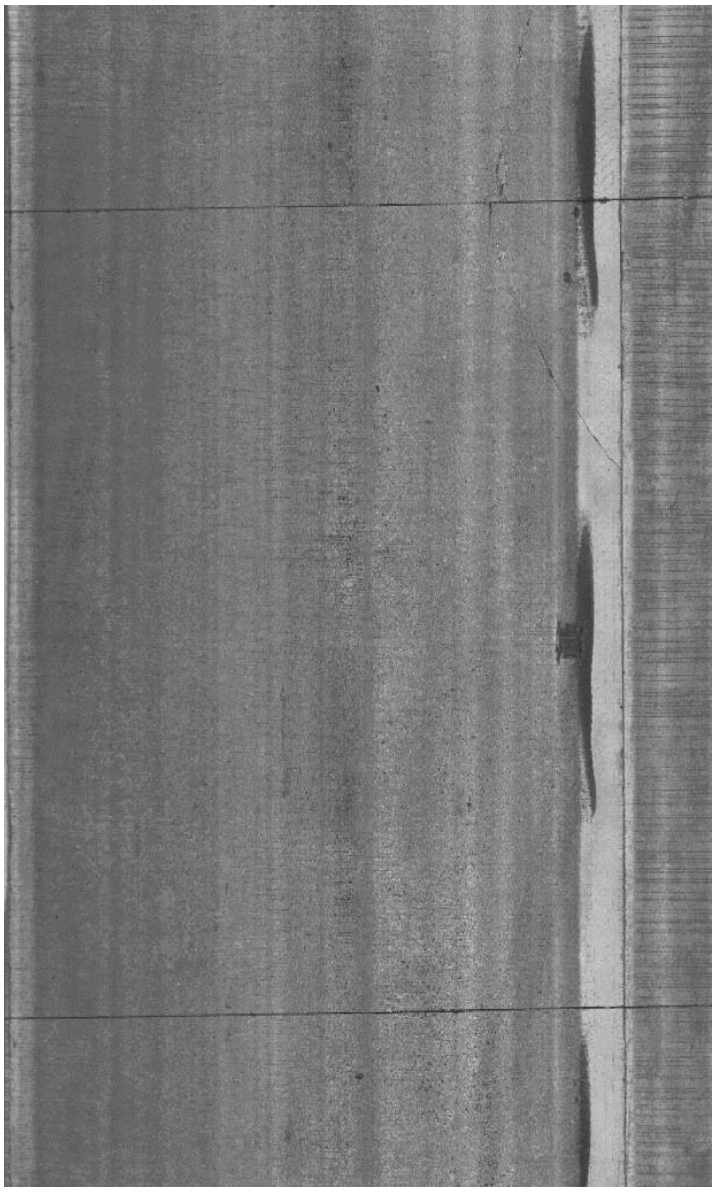

Figure 5 PathWeb Road Surface Image for LAK-90

Subcontractor Stantec Consulting Services made video distress surveys of I70- and I-77 using their Road Tester 3000 (RT3000) vehicle. The RT3000 unit simultaneously collects pavement condition, GPS, and digital image data streams and can, therefore, collect all surface condition data, ride quality, rutting, and imagery components. The data collection vehicle used for this assignment uses sub-systems for the collection of ride quality data, right-of-way imagery, GPS, as well as the INO Laser Road Imaging System.

The Stantec system could also compute the International Roughness Index (IRI), which could be compared to earlier ODOT IRI measurements where applicable. It should be noted that Stantec adopted a lane numbering convention where Lane 1 was the inside (passing) lane and the highest number was the outside (driving lane) with EB designating eastbound lanes and WB designating westbound lanes (and NB for northbound and SB for southbound). Correlating to the ODOT lane convention defined by facing up station (EB or NB) and numbering left to right, for a

6-lane east-west highway, the corresponding lanes are ODOT Lane 1 = Stantec WB3, ODOT Lane 2 = Stantec WB2, ODOT Lane 3 = Stantec WB1, ODOT Lane 4 = Stantec EB1, ODOT Lane 5 = Stantec EB2, and ODOT Lane 6 = Stantec EB3.

The Stantec data were averaged for each lane and plotted on a bar chart that marked criteria for "Good", "Acceptable", and "Not Acceptable" performance. The criterion for each level is given in Table 2.

Table 2 Correlation of IRI to pavement condition levels

Condition Level	IRI (in/mile)	IRI (m/m)
Good	IRI < 95	IRI < 1.5×10^{-3}
Acceptable	95 ≤ IRI ≤170	1.50×10^{-3} ≤ IRI ≤ 2.68×10^{-3}
Not Acceptable	170 < IRI	2.68×10^{-3} < IRI

Images were used to identify the extent of spalling, corner breaks, and transverse cracking, and longitudinal cracking. This information, as well as the IRI data, was used to identify the worst and best performing sections, in terms of severity of individual distress and ride quality, for the forensic investigation.

3.3 Falling Weight Deflectometer (FWD)

The Falling Weight Deflectometer (FWD) drops a known weight from a known adjustable height, creating an impulse load designed to simulate a single heavy wheel passing over the pavement structure [Alavi, LeCates, and Tavares, 2008]. The model of FWD used in this project is Dynatest 8002, shown in Figure 6. The FWD load creates deflections in the pavement surface which are measured by geophones located at selected distances from load application point, as diagrammed in Figure 7; one geophone is located at the center of the load plate, on which the impact load is dropped, labelled Df_1. FWD results were used to estimate the load transfer efficiency (LTE), joint support ratio (JSR), mid-slab spreadability (SPR), and normalized deflection at the load plate location (NDf_1) along the sections. Averages of these parameters were calculated for each section.

Figure 6 FWD used by ODOT

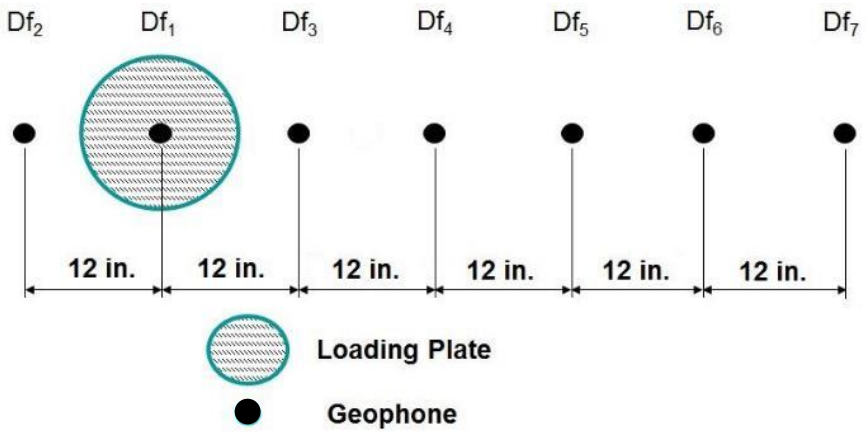

Figure 7 FWD geophone arrangement used in the test (12 in =0.305 m)

When FWD testing is performed at a joint, the LTE of the joint can be calculated using the following equations:

$$LTE_a = 100(\frac{Df_3}{Df_1})$$

$$LTE_l = 100(\frac{Df_2}{Df_1})$$

where Df_1, Df_2, and Df_3 are the measured deflections of Sensor 1, Sensor 2, and Sensor 3, respectively; and the sub-indexes a and l refer to the approach (a) or leave (l) position of the load plate (i.e. whether the drop represents a tire just before or just after it crosses the joint), as shown in Figure 8; note in the photos ODOT's FWD has an empty geophone cradle between the load plate and the 12 in (0.305 m) cradle (Df_3). LTE indicates the pavement's ability to transfer loads across the joints. The LTE varies depending on the support material, pavement temperature, aggregate interlock at the joints, and whether the joints have dowel bars [Sargand, Edwards, and Kim, 2002].

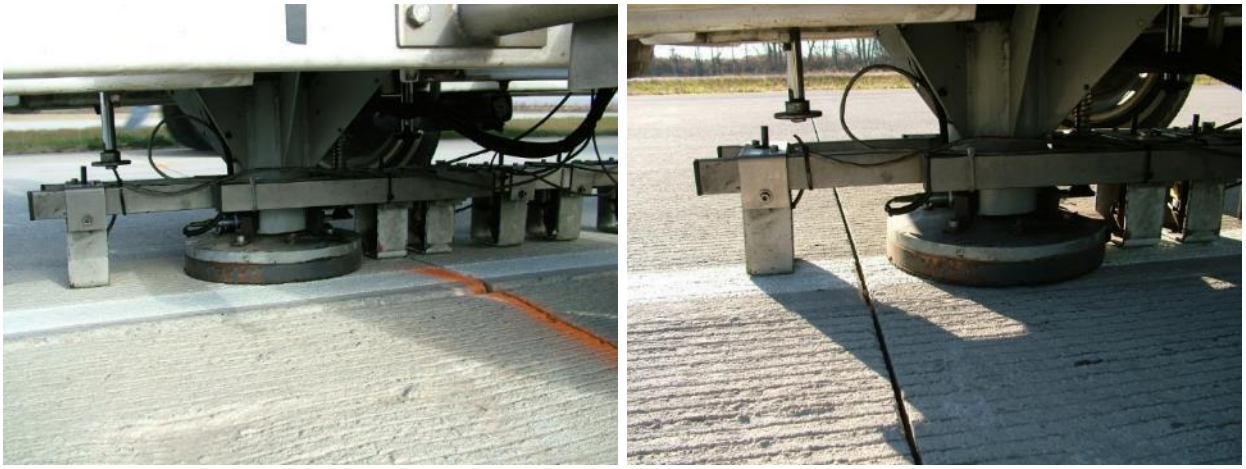

Figure 8 a) Joint approach position; b) Joint leave position. Note that sensor cradle immediately to right of the load plate is empty.

The joint support ratio (JSR) is the ratio between the deflection Df_1 in the leave position and in the approach position. It depends on the support condition at each side of the joint and can be used to identify the presence of voids under the slabs. JSR = 1.0 indicates equal support conditions at both sides of the joint (Sargand Edwards, and Kim, 2002). The JSR is calculated using this equation:

$$JSR = \frac{Df_{1l}}{Df_{1a}}$$

where the sub-indexes *a* and *l* refer to approach and leave, as before.

Mid-slab spreadability (SPR) is the average of the deflections measured by all the geophones normalized to that at the load plate, Df_1. SPR depends on the elastic modulus of the different layers in the pavement structure, the geometry of the load area, and the arrangement and number of seismometers [Sargand Edwards, and Kim, 2002]. SPR values are indicators of the geometry of the deflection basin and the bending stiffness of the pavement structure. For an FWD equipped with seven geophones, SPR is calculated as follows,

$$SPR = \frac{\sum_{i=1}^{7} Df_i}{7Df_1}$$

The deflections measured at each geophone during an FWD drop depend on the magnitude of the applied load, the geometry of the slab, its flexural stiffness, the support conditions, and other properties of the pavement [Sargand Edwards, and Kim, 2002]. In order to remove the effect of the applied load, the deflections are normalized by dividing by the load. If the deflection measured at the load plate is Df_1, the normalized deflection NDf_1 is given by

$$NDf_1 = \frac{Df_1}{P}$$

where *P* is the applied load. Notice that equations for LTE and SPR produce identical results regardless whether or not deflections are normalized.

The research team analyzed previously obtained FWD measurements made by ODOT on the UBCO project. For example, on the MAD-70 project, the FWD loads were applied every 200 ft (61 m) to 500 ft (152 m) at these locations on the slab: joint approach, joint leave, and mid-slab. This way, a representative sample of pavement response along the whole section was recorded. The results provided a general idea of the response of the tested section and were used to identify areas with the worst performance for detailed investigation, in conjunction with the visual assessment and IRI results.

Based on the results of pre-existing FWD tests, IRI, and distress survey, the worst performing section was selected for more detailed FWD testing, which was performed specifically for this project. FWD measurements were made at each joint and slab of the selected distressed segment and the corresponding control segment. The deflection data were normalized to load weight and then used to compute load transfer efficiency (LTE), Joint Support Ratio (JSR), and spreadability (SPR).

3.4 MITScan

The widely adopted Federal Highway Administration (FHWA) recommended limits for horizontal and vertical alignment (rotation) are ¼ in (6.4 mm) over 12 in (305 mm) or 2% [FHWA 1990]. The American Concrete Pavement Association (ACPA) follows guidance in National Cooperative Highway Research Program (NCHRP) Synthesis 56 [Copas and Pennock, 1979] and

an FHWA memo from 1989 and recommends limits of $^{3}/_{8}$ in (9.5 mm) over 12 in (305 mm) or 3%. ODOT adopted limits on misalignment with the 2013 Construction and Materials Specifications Manual. The required dowel bar tolerances are given in Table 3. Figure 9 illustrates various types of dowel misalignment. The potential impacts of various types of dowel misalignment on pavement performance, as identified by Tayabji [1986], are summarized in Table 4. Baskets were used to hold the dowel bars during placing of the pavement. ODOT has MITScan equipment and made the readings for each project except LAK 90 which was experiencing materials related distress and did not exhibit signs of dowel bar alignment related stress. The data were analyzed by the Ohio University team.

Table 3 Dowel bar tolerances from ODOT 2013 Construction and Material Specifications

	Acceptance Tolerance		Rejection Criterion	
Alignment Parameter	(in)	(mm)	(in)	(mm)
Horizontal Translation	0.50	13	2.00	51
Longitudinal Translation	2.00	51	2.30	58
Depth Translation	0.50	13	0.66	17
Horizontal Rotation	0.50	13	0.70	18
Vertical Rotation	0.50	13	0.70	18

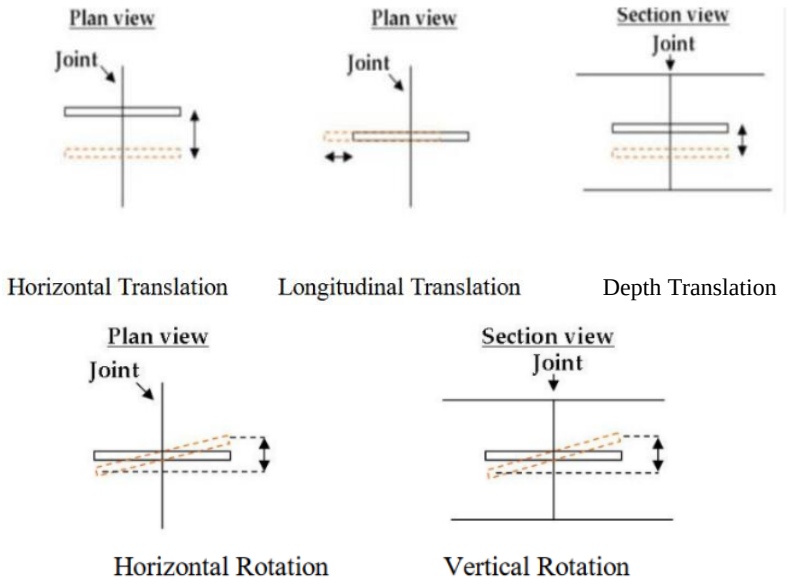

Figure 9 Types of dowel misalignment [ODOT, 2013, p. 261].

Table 4 Impacts of dowel misalignment [Taybji, 1986].

Type of Misalignment	Effect on Spalling	Cracking	Load Transfer
Horizontal Translation	No	No	Yes
Longitudinal Translation	No	No	Yes
Depth Translation	Yes	No	Yes
Horizontal Rotation	Yes	Yes	Yes
Vertical Rotation	Yes	Yes	Yes

Figure 10 shows a sample MITScan reading from a joint on I-70 EB. The bar locations are noted by dark red spots at the left, and these are resolved into the positions marked to their right, which graphically indicates the orientation of each bar and deviation from design placement. Note in the figure one red spot is at the bottom, below where x=0, indicating a bar outside the scan zone, probably due to not being able to operate the apparatus along the inside edge of the lane due to the presence of traffic control and moving traffic in the adjoining lane. The detected bars are numbered 1 through 11, though there should be 12. Furthermore, Bar 2 appears to be located at a midpoint between two dark spots, and may be a spurious reading. The section of the figure to the left of the raw scan represents the resolving of the magnetic readings into dowel bar locations, including indications of various types of misalignment. For example Bar 1 and Bar 11 are clearly rotated. Bars 1, 3, 4, and 5 have longitudinal translation, as indicated by the green outlines. Vertical displacements are noted on the z-x graph that is the third section of the figure, with the plus signs (circles) indicating the vertical (z) position of the left (right) end of each bar.

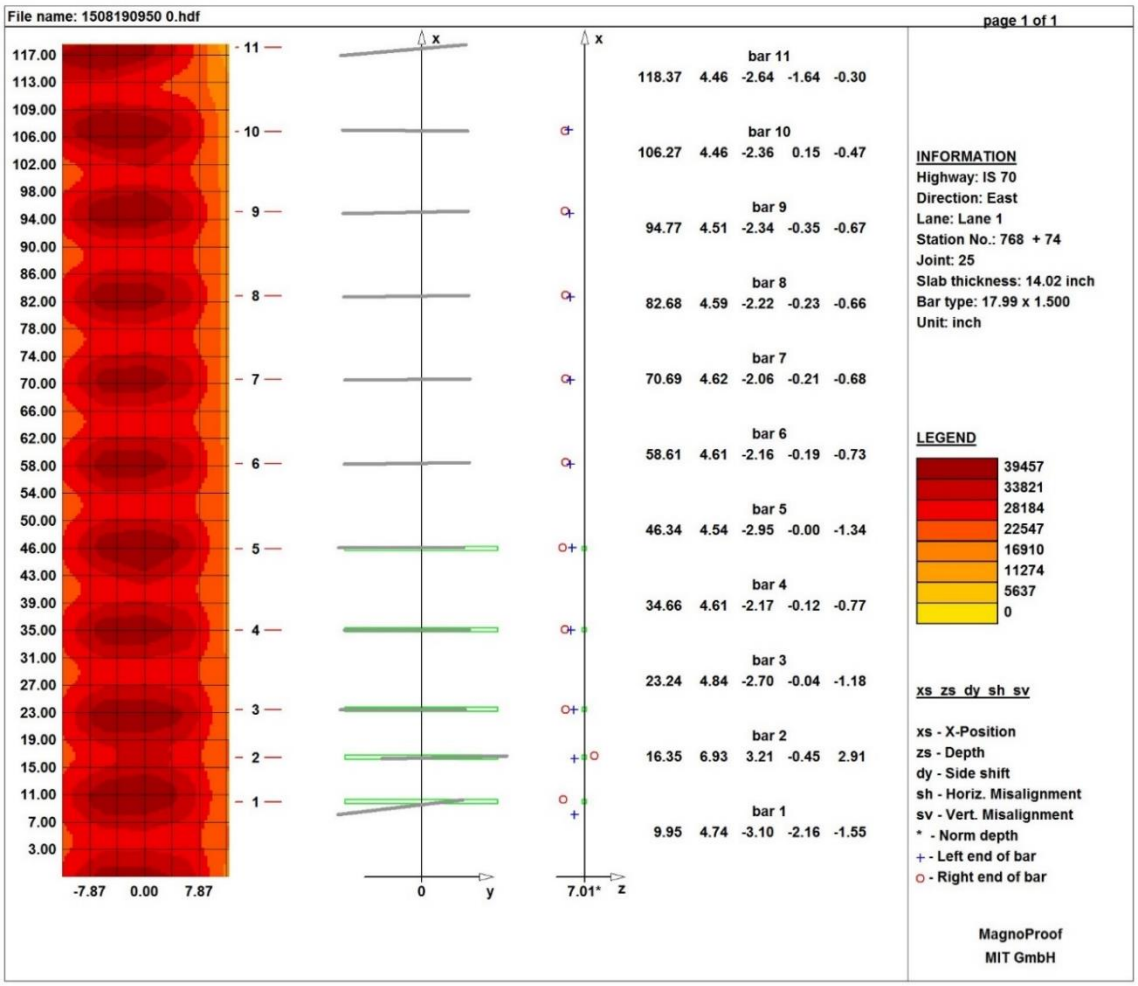

Figure 10 Sample MITScan reading from Joint 25 on I70 EB. Bar locations are denoted by dark red spots in at the left, and these are recsolved into the positions marked to their right, which graphically indicates the oreintation of each bar and deviation from design placement.

3.5 Slab Removal

On MAD-70, selected slabs of the overlay were cut and removed so the research team could examine the condition of the bottom of the slab and bondbreaker layer, particularly at joints. This work was conducted where possible during contract repair operations.

3.6 PCC Coring

Several 4 in (100 mm) cores were collected at each site. Physical dimensions of the cores were measured – width and depth of the overlay and bondbreaker. Only intact samples were measured for the purpose of thickness determination. Some cores were set aside for shipment to Dr. Jan Olek at Purdue University for petrographic analysis and Energy Dispersive X-ray spectroscopy (EDX) analysis to verify the mix design and to determine if material-related distress was present. The other cores were used for materials testing at Ohio University. Cores were generally collected near cracks or corner breaks as well as mid-slab with no distress on bad sections. On good sections, cores were generally taken from mid-slab or near joints. In each direction, on each test section, an intact control slab was identified and 5 cores collected across mid-slab. Core locations were typically marked on distress survey sheets. After a core was removed, the condition of the bondbreaker underneath was examined visually.

3.7 Laboratory testing

3.7.1 PCC Core Sample Preparation

The cores reserved for laboratory analysis were prepared to meet the requirements of AASHTO T22 and AASHTO T24. Cores for compressive strength test and splitting tensile test were cut to the length of 8 in (200 mm), to obtain a length to diameter ratio between 1.9 and 2.1. Cores for coefficient of thermal expansion test were cut to the length of 7 in (180 mm) in accordance with AASHTO T 336. The ends of all specimen were sawed flat and perpendicular to the longitudinal axis of the core. Uneven specimens were capped according to AASHTO T231. After cutting all the specimens, length and diameter were re-measured to verify dimensions. The specimens were then sealed in freezer storage bags for moisture conditioning. Figure 11 shows the saw used for cutting the cores and a specimen in a sealed bag for moisture conditioning.

a)  b) 

Figure 11 a) Saw used in core preparation; b) Core specimen in a sealed bag for moisture conditioning.

3.7.2 Compressive Strength Test

The compressive strength tests were conducted in accordance with ASTM Standard C39 "Standard Test Method for Compressive Strength of Cylindrical Concrete Specimens". Prior to the test, the width of each specimen was measured along the diameter twice (D_1 and D_2) at right angles at approximately midheight and averaged. This average diameter D was rounded to the nearest 0.01 in (0.25 mm) and was used to calculate the cross-sectional area A of the specimen. During the test, the load rate was maintained within 35±7 psi/s (240±48 kPa/s). The test machine automatically recorded the maximum load P, once the load has decreased to less than 95% of the peak value, where the decrease indicates fracture of the specimen. Figure 12a) shows the test machine and Figure 12b) shows an example of the fractured specimen after testing.

The results were averaged for each direction and were rounded to the nearest 10 psi (69 kPa). Some cores were used for the Elastic Modulus and Poisson's ratio test before being used for compressive strength test. The compressive strength of the specimen was calculated by using

$$f'_c = \frac{P}{A}$$

where:
$f'c$ is the compressive strength, psi.
P is the maximum load applied during the test, lb.
A is the specimen's average cross-sectional area.

The fracture pattern was recorded after each test. The compressive strength measurements were compared to ODOT's design strength of 4000 psi (28 MPa).

a)  b) 

Figure 12 Compressive Strength Test Setup a) compression tester; b) fractured core in device.

3.7.3 Splitting Tensile Strength Test

The splitting tensile strength test was conducted in accordance with AASHTO Standard T 198 "Standard Method of Test for Splitting Tensile Strength of Cylindrical Concrete Specimens" (ASTM C496). For each core, the diameter was measured to the nearest 0.01 in (0.25 mm) and length was measured to the nearest 0.1 in (2.5 mm) before testing. Diametric lines were drawn on each end of the specimen to aid positioning. Plywood strips were placed between the specimen

and the upper and lower bearing blocks in the test device, with the specimen positioned so that the lines marked on the ends are vertical and centered over the plywood strip, as shown in the test setup depicted in Figure 13. The loading stress rate was maintained within the range 100 psi/min (0.69 MPa) to 200 psi/min (1.38 MPa)), which corresponds to 5024 lb/min (22 kN) to 10048 lb/min (45 kN) force for a 4 in (102 mm) × 8 in (203 mm) specimen. The maximum applied load *P* was recorded automatically at failure. Tensile strength was averaged for each route and rounded to the nearest 5 psi (0.034 MPa). The equation used for calculating the tensile strength is

$$T = \frac{2P}{\pi LD}$$

where:
T is splitting tensile strength, psi.
P is maximum applied load recorded by the test machine, lb.
L is the specimen length, in.
D is the specimen diameter, in.

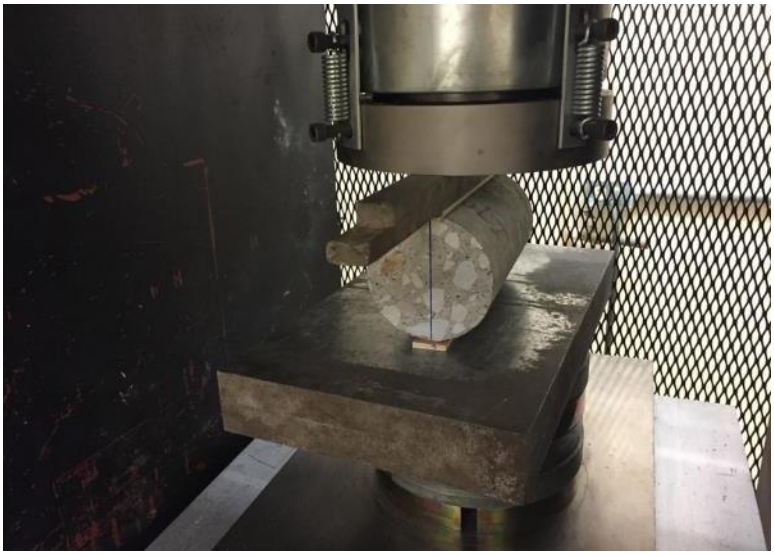

Figure 13 Splitting Tensile Test Setup

ODOT designs for a Modulus of Rupture of 700 psi (4.83 MPa). The splitting tensile strength of concrete is usually 60% to 80% of the modulus of rupture, and this was compared to the measured results.

3.7.4 Coefficient of Thermal Expansion

The Coefficient of Thermal Expansion (CTE) test was conducted in accordance with AASHTO Standard Method T 336 "Standard Method of Test for Coefficient of Thermal Expansion of Hydraulic Cement Concrete", using the apparatus shown in Figure 14. The test result is the average of the two CTE values obtained from two test segments. The CTE was calculated using equation:

$$CTE = \frac{\Delta L_a}{L_0\, \Delta T}$$

where:

L_0 is measured length of specimen at room temperature, mm
ΔT is measured temperature change, °C
ΔL_a is actual length change of specimen during temperature change, mm, determined by:

$$\Delta L_a = \Delta L_m + \Delta L_f$$

where:
ΔL_m is measured change in length of the specimen during temperature change, mm
ΔL_f is change in length of the measuring apparatus during temperature change, mm, determined by:

$$\Delta L_f = C_f \times L_0 \times \Delta T$$

Where C_f is a correction factor accounting for the change in length of the measurement apparatus with temperature. Results were compared to typical values recorded by FHWA for the given type of aggregate [FHWA, 2011].

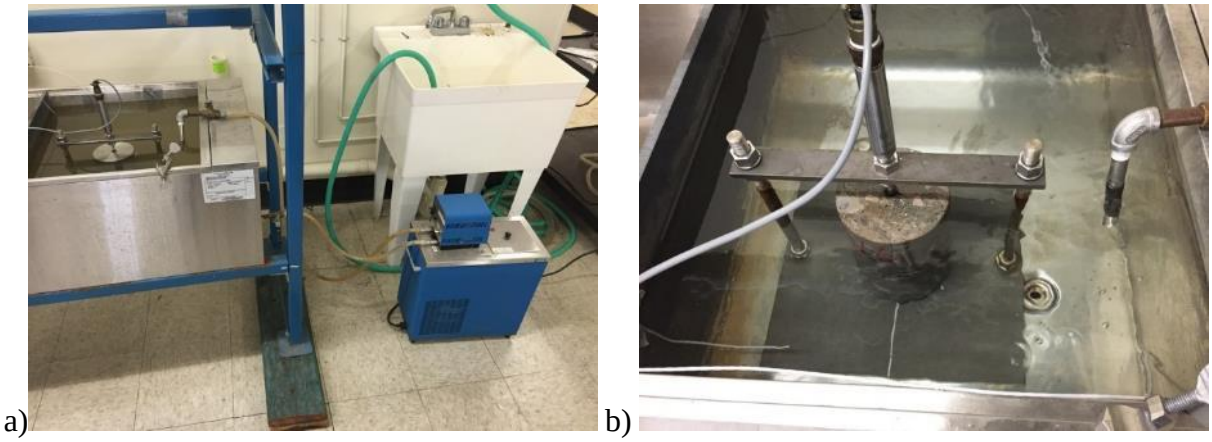

a) b)

Figure 14 Coefficient of Thermal Expansion (CTE) test setup.

3.7.5 Elastic Modulus and Poisson's Ratio

The test was conducted in accordance with ASTM Standard Test Method C 469 "Standard Test Method for Static Modulus of Elasticity and Poisson's Ratio of Concrete in Compression". Two strain gauges were installed on the surface of the core specimen, one corresponding to longitudinal strain and the other one corresponding to horizontal strain. The strain gauge used was the model PL-60-11-3LT from Tokyo Sokki Kenkyujo Company, which was specifically designed for use on concrete or rock materials. A MEGADAC data acquisition system was used to record strain and load data. The load was applied at a rate of 35±7 psi/s (241±48 kPa/s), which is the same rate as in the compression test. Figure 15 shows the setup for the test. According to the standard, the specimen was loaded to up to 40% of its compressive strength. The specimens were loaded twice, first to seat the gauges, then to apply the test load. Readings from the second load were recorded 200 times per second. For elastic modulus, applied load and longitudinal strain were recorded as P_1 at the point when the longitudinal strain ε_1=50 με and as P_2, ε_2 when the applied load is equal to 40% of the ultimate load. For Poisson's ratio, transverse strains were recorded at same points as ε_{t1} and ε_{t2}. The specimens used for this test were reused for compressive strength test after this test was finished.

The modulus of elasticity was calculated using equation:

$$E = \frac{S_2 - S_1}{\varepsilon_2 - 0.000050}$$

where:
E is modulus of elasticity, psi,
S_2 is stress corresponding to P_2, 40% of ultimate load,
S_1 is stress in psi from load P_1 corresponding to a longitudinal strain, ε_1, of 50 με,
ε_2 is longitudinal strain produced by stress S_2.

Poisson's ratio was calculated by using equation:

$$\nu = \frac{\varepsilon_{t2} - \varepsilon_{t1}}{\varepsilon_2 - 0.000050}$$

where:
ν is Poisson's ratio,
ε_{t2} is transverse strain at mid-height of the specimen produced by stress S_2 from load P_2,
ε_{t1} is transverse strain at mid-height of the specimen produced by stress S_1 from load P_1.

The modulus of elasticity results were compared to ODOT's design value of 5 million psi (35 GPa). The Posson's ratio values were compared to the normal values in the literature.

a)  b) 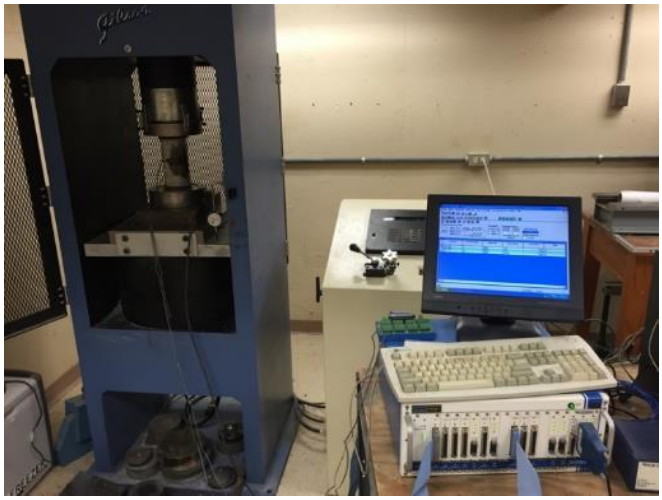

Figure 15 Elastic Modulus and Poisson's Ratio Test Setup

3.8 Petrographic analysis

The petrographic analysis was performed by Professor Jan Olek and his team at Purdue University. Purdue also studied some cores with a Scanning Electron Microscope (SEM) and/or performed air voids analysis. The Purdue team also noted the presence of deicing chemical residue in the form of Friedel's salt and chlorides. The petrographic analysis also included examining for the presence of ettringite and slag aggregate.

3.9 HIPERPAV simulation

The early age performance of each overlay project, except ASD-30, was simulated using HIPERPAV software (http://www.hiperpav.com/) with mix data from the project and environmental data from the project site on the dates of construction; ASD-30 was not simulated because construction data were not available,. HIPERPAV is a simulation tool for determining the early age (first 3 days after construction) behavior of Portland cement concrete pavement. It was first developed by the Federal Highway Administration in 1996. The latest version is HIPERPAV III (Version 3.20.006) and it was used in this project to study the effect of climate on early age performance of the Portland cement concrete pavement in UBCO projects.

4 I-70 in Madison County

4.1 Project Information

Project 1999-0295 overlaid a 9 in (229 mm) jointed, reinforced, dowelled concrete pavement on I-70 in Madison County (MAD-70) with a 9 in (229 mm) jointed, plain, dowelled concrete (ODOT Item 452) pavement on a 1 in (25 mm) asphalt (ODOT Item 448) bondbreaker and was constructed during 1999 and 2000. By 2008, significant transverse cracking, corner breaks, and slab settlement were present, especially in the eastbound direction. As a result, in 2009, the Department conducted an initial forensic investigation that included a distress survey, pavement coring, FWD deflection measurements, and observations of the removed pavement during repair. The 2009 distress survey disclosed 15% of all slabs in the eastbound direction and 5% of all slabs in the westbound direction had transverse cracks. Results of the initial forensic study were inconclusive. The pavement continues to deteriorate and additional repairs have been made since 2009. As of 2014, ADT = 56200 and ADTT = 15070. Figure 16 shows the location map of the MAD-70 project and identifies the forensic investigation locations within the project. Figure 17 shows the pavement structure of MAD-70 UBCO section.

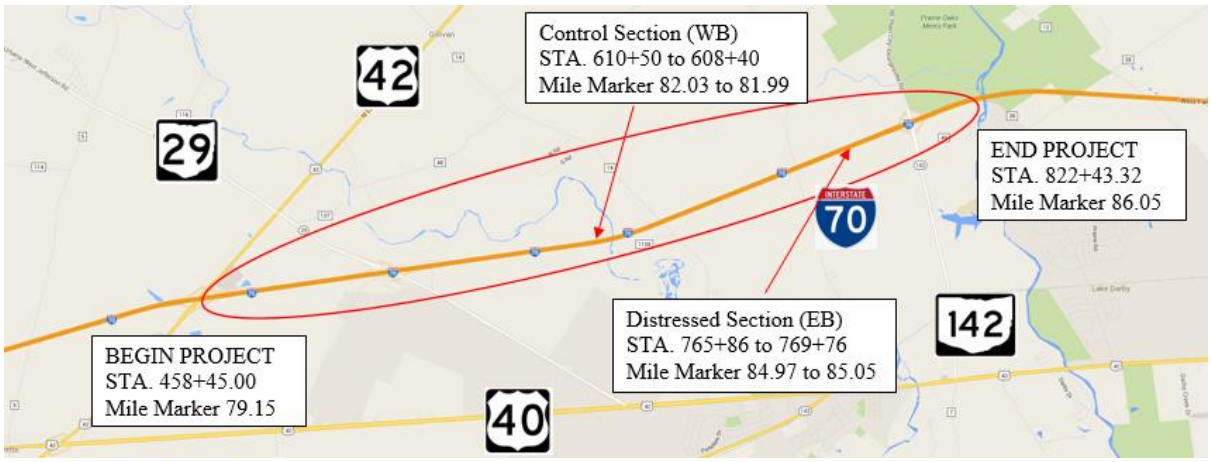

Figure 16 Location Map of MAD-70

4.2 Visual Assessment

A visual inspection was conducted along the unbonded concrete overlay sections in March 2015 before tests started. A few observations were made and summarized below.

In the eastbound direction, various distresses were found including patching, faulting, transverse cracking, corner breaks and joint spalling. Figure 18 shows pictures of faulting and a transverse crack on I-70 eastbound. An eastbound segment consisting of 26 slabs was selected for more thorough inspection; 20 of the 26 slabs exhibited distress. Three had been replaced recently with concrete repairs. Only three were still in good condition. The westbound direction appeared to suffer relatively less damage, and less distress was observed. Figure 19a) shows a corner break and Figure 19b) shows joint spalling found on westbound direction. In the selected westbound section, only two joints out of 15 showed signs of distress. The distress map in Figure 20 illustrates the locations and types of distresses found in the selected distressed section and in the other direction.

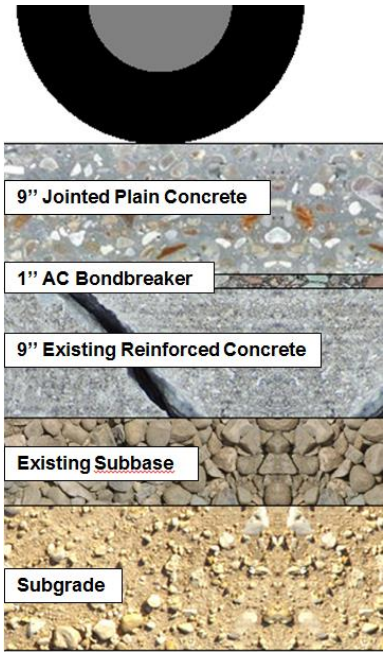

Figure 17 Pavement Structure of MAD-70 UBCO section (1 in = 25.4 mm)

a)  b) 

Figure 18 a) MAD-70 EB faulting (ODOT photo June 25, 2008); b) MAD-70 EB transverse cracking (April 22, 2015)

a)  b) 

Figure 19 a) MAD-70 WB corner breaks (March 30, 2015); b) MAD-70 WB joint spalling at bottom of picture, filled with water (August 19, 2015)

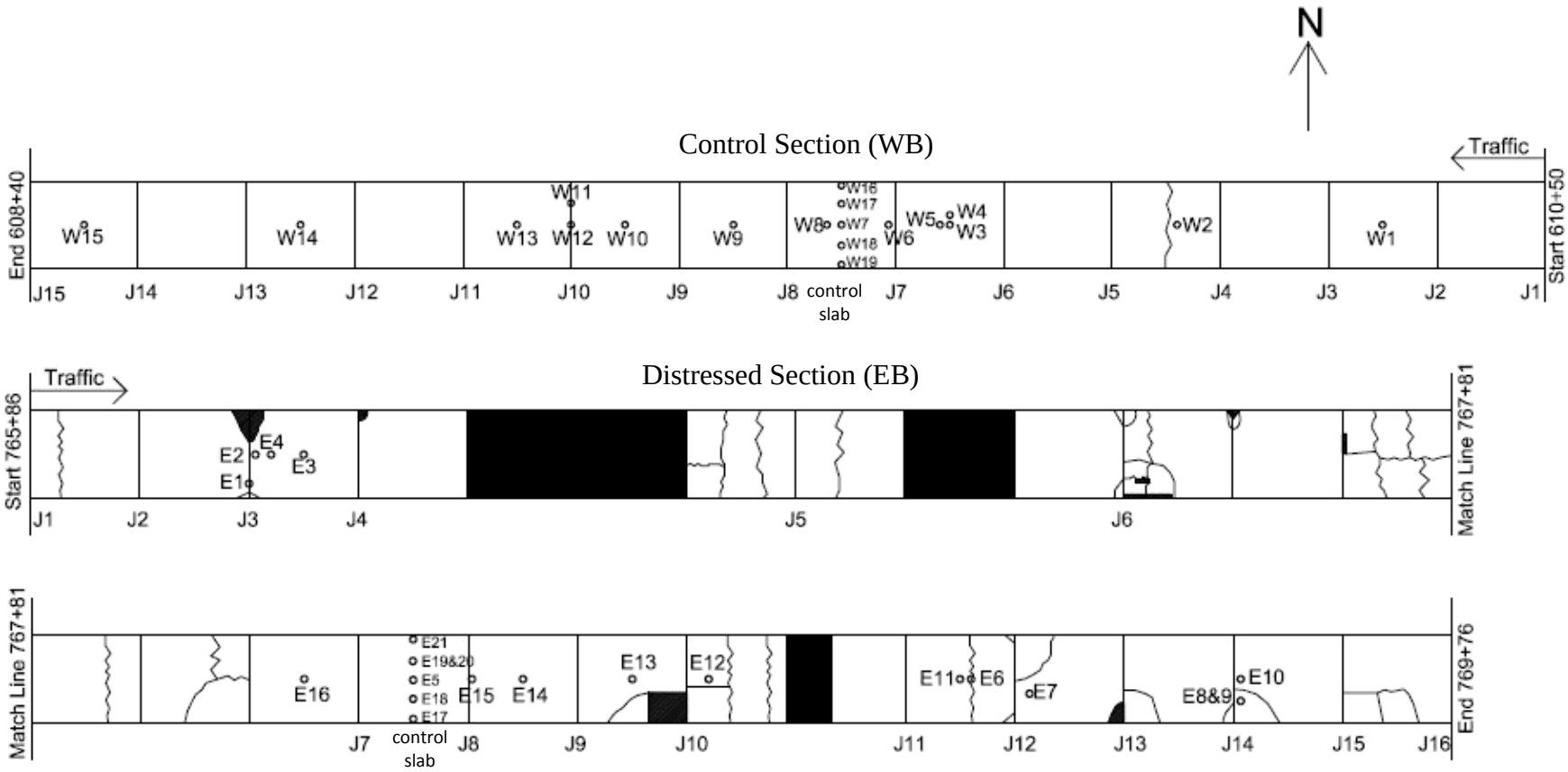

Figure 20 Distress Map and Coring plan on MAD-70. Numbered joints were scanned by the MITScanner.

4.3 Distress Survey

Distress surveys were conducted by ODOT in 2008 and 2009 along the whole length of MAD-70 UBCO sections. Cracks per station were calculated and plotted over the length of the project in Figure 21 and Figure 22. Replacement of cracked slabs between 2009 and 2015 was responsible for the decreased amount of cracking shown in the figures. High and low temperatures during construction were added to the graphs to determine if temperature or temperature differential had an effect on cracking. Temperature and temperature differential have effects on early age (first 3 days) cracking, and the extent of the cracking be predicted using HIPERPAV. However, as seen in Figure 21 and Figure 22, a direct relationship is not apparent between long term cracking and temperature at time of construction. Shaded areas are full-depth concrete pavement segments. From the graph, it can be seen the number of cracks per station increased from 2008 to 2009. This suggests the pavement was still deteriorating. As seen in Figure 20, there is no direct relationship between placement minimum/maximum temperature and cracking. However, other factors, in combination with temperature, such as wetting the bond breaker surface prior to overlay placement, affect the stress development and strength gain, and are included in the discussion of the HIPERPAV analysis. Comparing eastbound with westbound direction, it can be seen the eastbound direction experienced much more cracking than the westbound direction. Comparing the UBCO section with the full-depth reconstruction section, it can be seen that the UBCO section had more cracks.

A video distress survey was conducted on MAD-70 by Stantec Consulting Services Ltd. using their Road Tester 3000 (RT3000) vehicle on May 22, 2015. The average IRI is illustrated below in Figure 23 through Figure 25. As mentioned earlier, Stantec adopted a lane numbering convention where Lane 1 was the inside (passing) lane and the highest number was the outside (driving lane) with EB designating eastbound lanes and WB designating westbound lanes. Correlating to the ODOT lane convention defined by facing up station (EB in this case) and numbering left to right, the corresponding lanes are ODOT Lane 1 = Stantec WB3, ODOT Lane 2 = Stantec WB2, ODOT Lane 3 = Stantec WB1, ODOT Lane 4 = Stantec EB1, ODOT Lane 5 = Stantec EB2, and ODOT Lane 6 = Stantec EB3. As can be seen from the graphs, the overall ride quality for most of the tested lanes was "Good" (IRI <95 in/mi = 1.5×10^{-3} m/m), where "Good" meets the IRI criterion in Table 2. The only exception was the outside tested lane (EB3 = ODOT Lane 6) for MAD-70 which showed "Acceptable" condition (1.50×10^{-3} m/m = 95 in/mi ≤ IRI ≤ 170 in/mi = 2.68×10^{-3} m/m). A significant amount of roughness was observed during testing at the bridge approach slabs, bridge joints and bridge decks and these were was removed from the analysis as anomalies. The westbound lanes of MAD-70 are smoother than the eastbound lanes. For MAD-70 EB3 (ODOT Lane 6), Mileage Point (MP) 82 and MP 85 are in worse condition compared to other segments of the highway. For MAD-70 WB1 (ODOT Lane 3), MP 82 and MP 85 are in worse condition compared to other segments of the highway. Plots of the 50 ft (15 m) IRI moving average are provided in Appendix A. The 2015 results are also incorporated in Figure 21 and Figure 22. The slight decrease in cracking at some places may be due to repairs made in 2009.

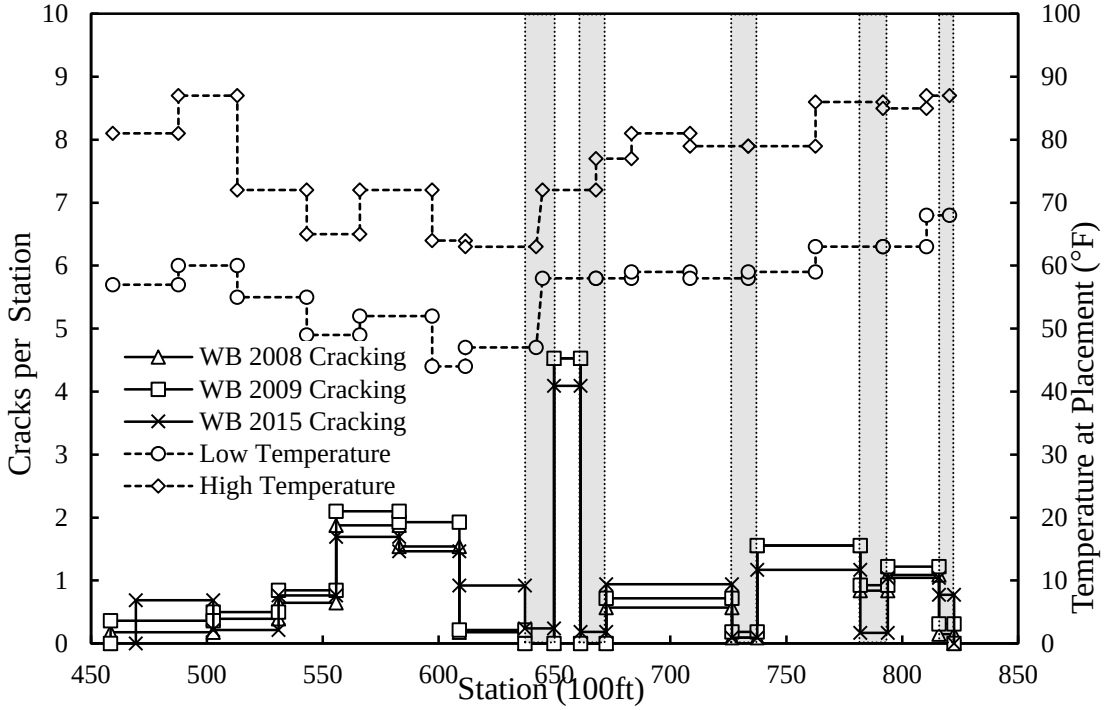

Figure 21 MAD-70 Westbound cracking plot (100 ft = 30.5 m).

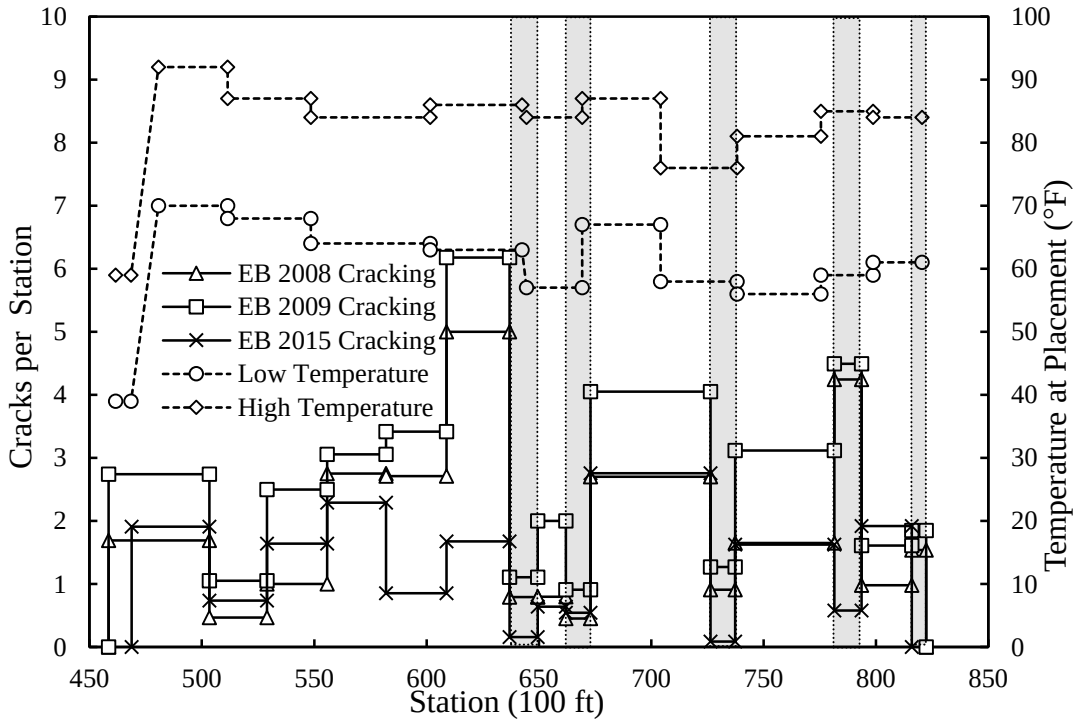

Figure 22 MAD-70 Eastbound cracking plot (100 ft = 30.5 m).

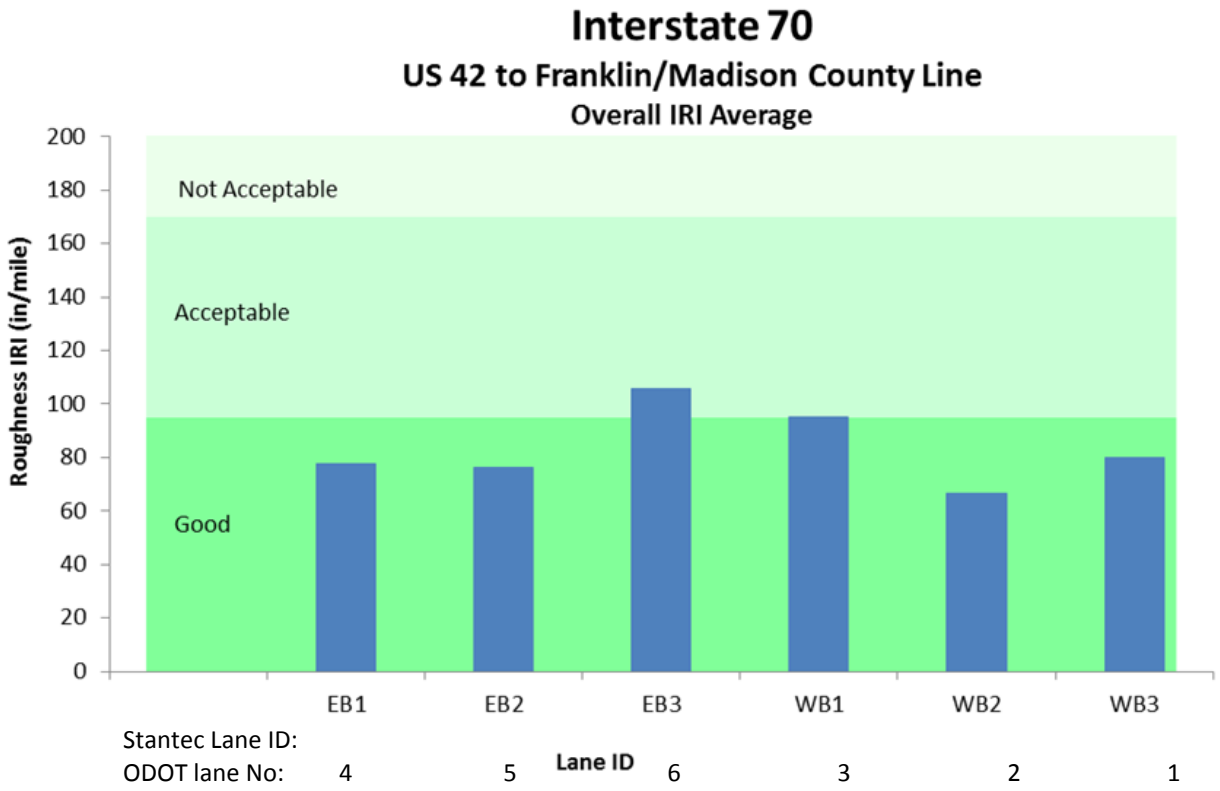

Figure 23 Average IRI on MAD-70, all lanes, measured May 22, 2015. Graph by Stantec. (1 in/mi = 1.58×10^{-5} m/m).

Table 5 Correlation of IRI to pavement condition levels

Condition Level	IRI (in/mile)	IRI (m/m)
Good	IRI < 95	IRI < 1.5×10^{-3}
Acceptable	95 ≤ IRI ≤170	1.50×10^{-3} ≤ IRI ≤ 2.68×10^{-3}
Not Acceptable	170 < IRI	2.68×10^{-3} < IRI

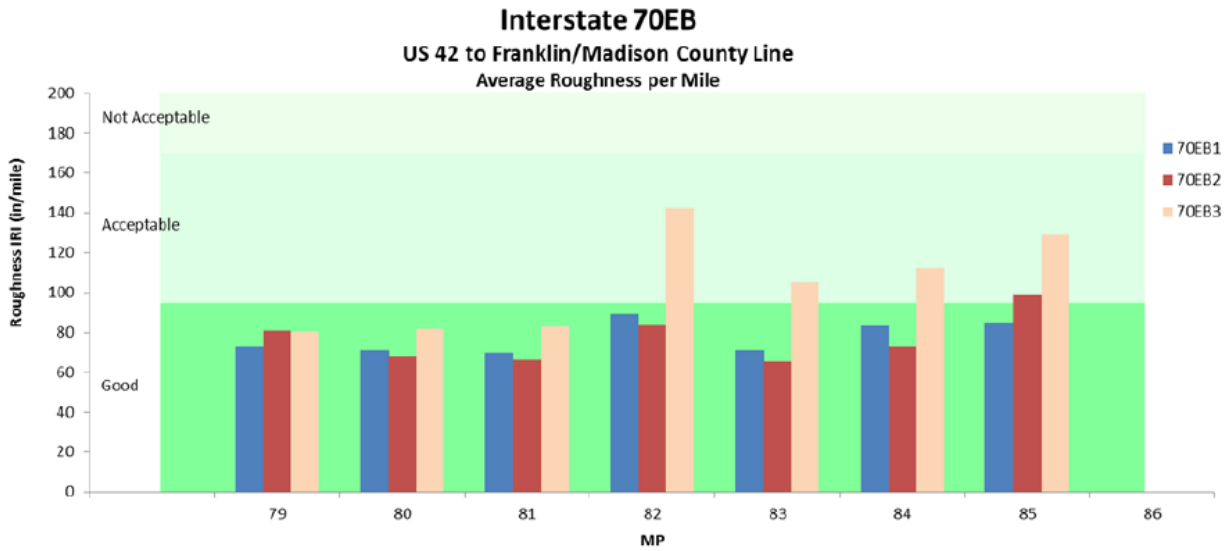

Figure 24 Average IRI of MAD-70, May 22, 2015, EB lanes. Graph by Stantec. (1 in/mi = 1.58×10^{-5} m/m) (Lanes: 70EB1 = ODOT Lane 4, 70EB2 = ODOT Lane 5, 70EB3 = ODOT Lane 6).

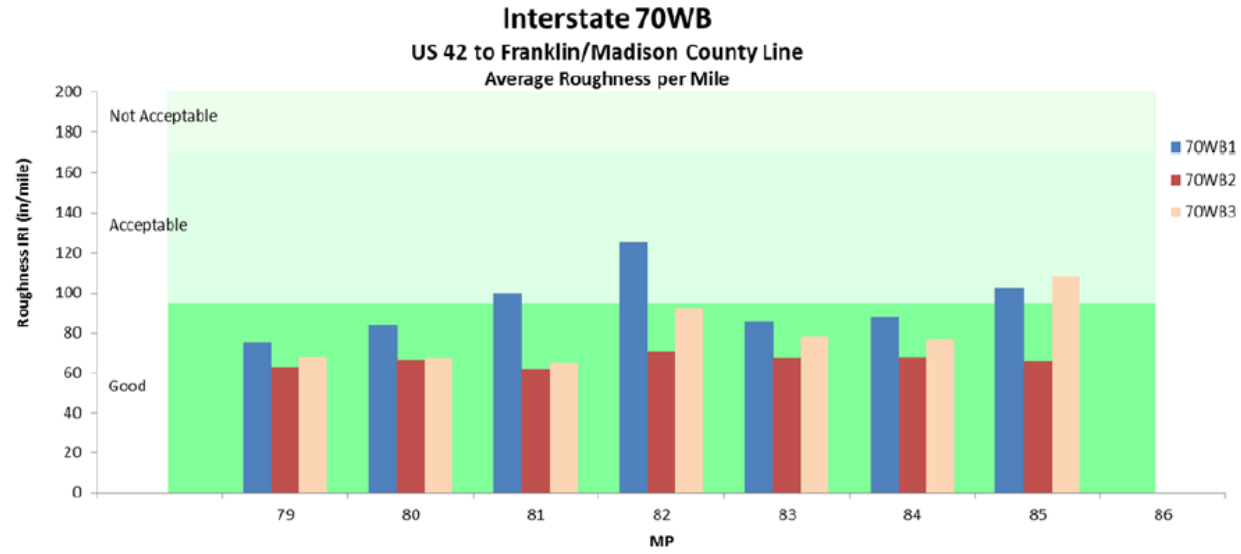

Figure 25 Average IRI of MAD-70, May 22, 2015, WB Lanes. Graph by Stantec. (1 in/mi = 1.58×10^{-5} m/m) (Lanes: 70WB1 = ODOT Lane 3, 70WB2 = ODOT Lane 2, 70WB3 = ODOT Lane 1).

Table 6 presents major distresses identified on MAD-70 based on the distress survey and visual assessment. The PCR history table provided by ODOT was used to confirm the distresses. Primary and contributing factors were listed below as provided on the NCHRP PCC distress types and causes table (Table 35 and Table 36). Possible causes were listed based on NCHRP tables as well as research team's judgement.

Table 6 Major distresses identified on MAD-70 and possible causes

Project	Major Distress	Primary Factors	Contributing Factors	Possible Causes
MAD-70	transverse cracking	Design features; Load; Construction	Temperature; Materials	loss of support; fatigue; curling and warping; dowel misalignment; poor construction practices; freeze-thaw and moisture-related settlement; materials related problem; high volumes of heavy traffic.
	corner break	Load	Design features; Water; Temperature	
	slab settlement	N/A	Design features; Load; Water; Construction	
	faulting	Design; Load; Water	Temperature; Materials	

4.4 Falling Weight Deflectometer (FWD) Test

4.4.1 Pre-investigation FWD results

The FWD measurements were conducted by ODOT along the entire length of the MAD-70 project. The FWD loads were applied every 200 ft (61 m) to 500 ft (152 m) at these locations on the slab: joint approach, joint leave, and mid-slab. This way, a representative sample of pavement response along the whole section was recorded. The results gave a general idea of the response of the tested section and were used to identify areas with the worst performance for further investigation. Figure 26 and Figure 27 present normalized joint deflections of the I-70 UBCO sections, while Figure 28 and Figure 29 show the LTEs. Shaded areas are full-depth concrete pavement sections. Data in the graph were compiled from FWD testing conducted in 2009 and 2014. Findings from these graphs are summarized below:

- Full-depth sections have higher joint deflections than UBCO sections. This can be explained by the fact that UBCO has old concrete pavement acting as a base, which is much stiffer than 304 aggregate base in the full-depth section.
- Comparing eastbound direction with westbound direction, eastbound direction has higher and more variable joint deflections. LTE of eastbound direction is lower and more variable than westbound direction.
- Comparing data of 2014 with those of 2009, joint deflections increased by a small percentage while LTE dropped significantly from 2009. Note that the joints tested in 2014 were not necessarily the same ones tested in 2009.

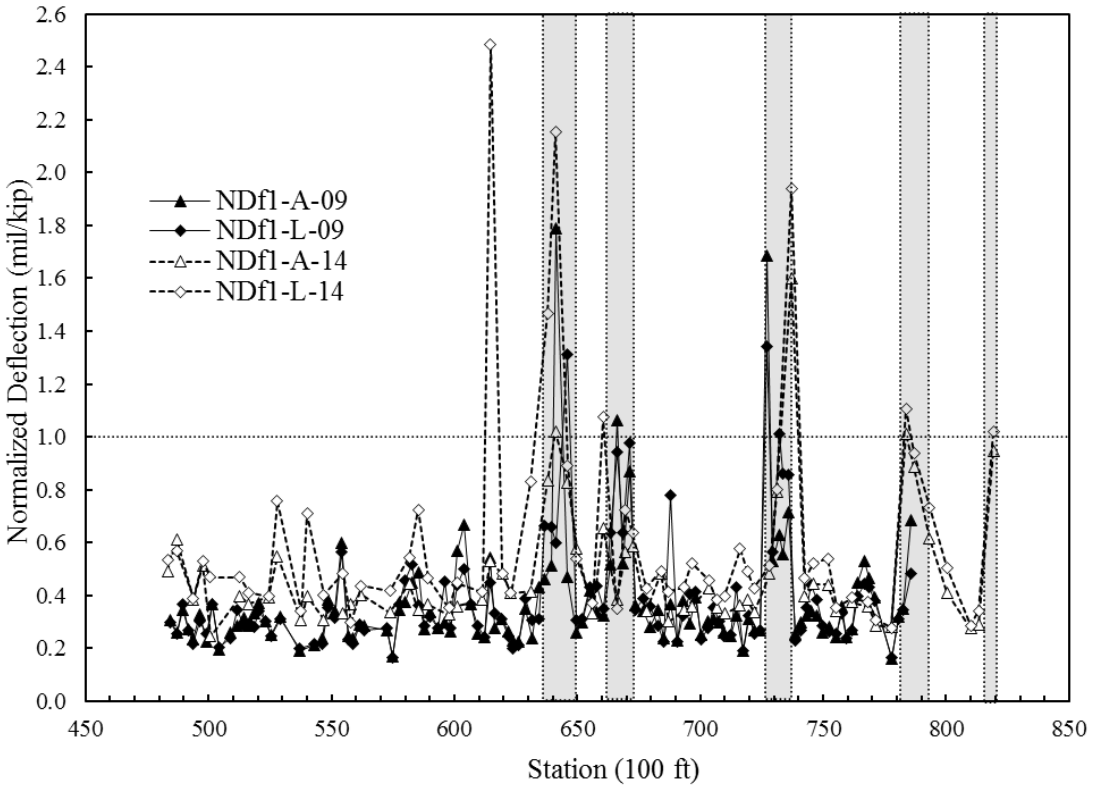

Figure 26 I-70 eastbound normalized joint deflections measured in 2009 and 2014 (1 mil/kip = 5.71 mm/MN, 100 ft = 30.5 m).

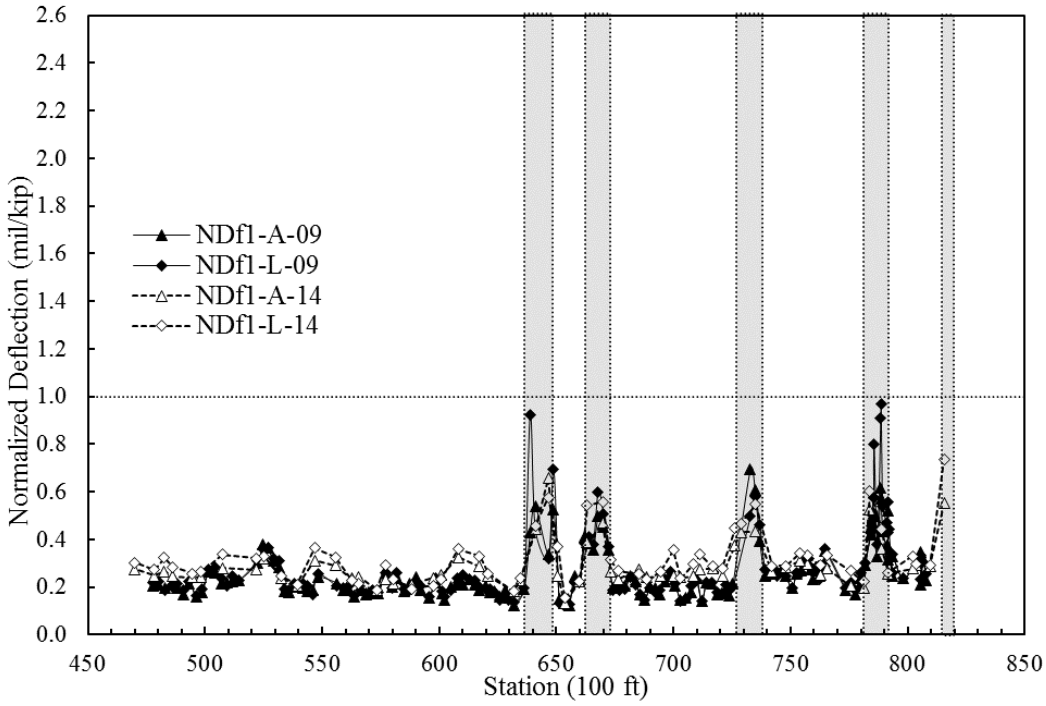

Figure 27 I-70 westbound normalized joint deflections measured in 2009 and 2014 (1 mil/kip = 5.71 mm/MN, 100 ft = 30.5 m).

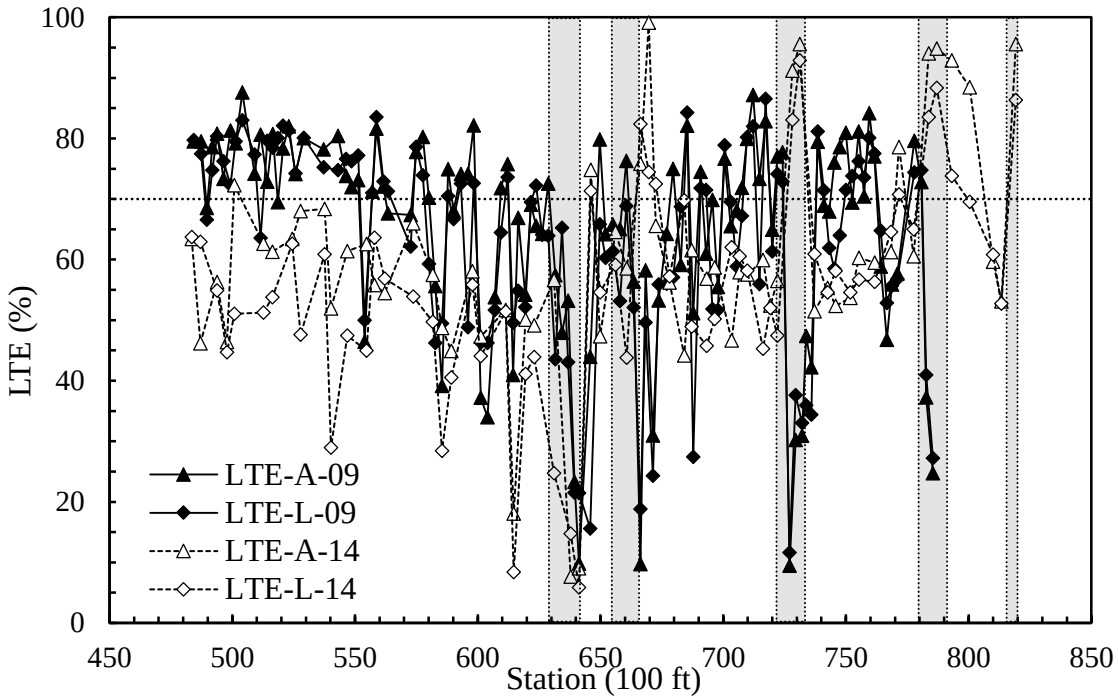

Figure 28 I-70 eastbound load transfer efficiency measured in 2009 and 2014 (100 ft = 30.5 m).

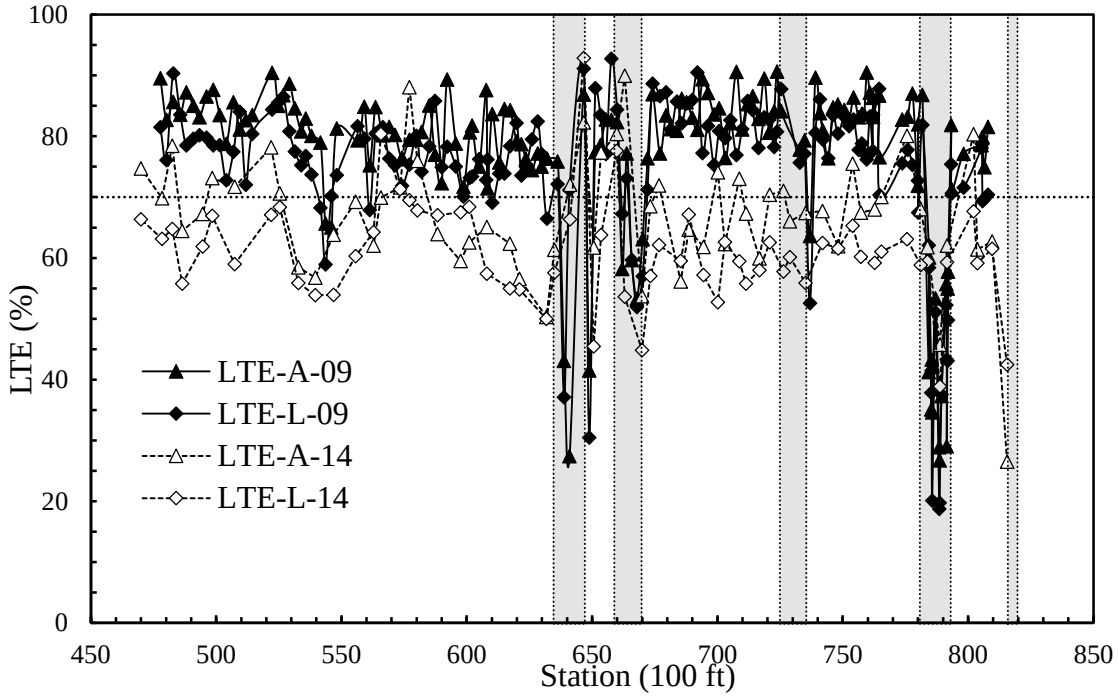

Figure 29 I-70 westbound load transfer efficiency measured in 2009 and 2014 (100 ft = 30.5 m).

4.4.2 Results of FWD testing on selected sections

Based on the results of FWD tests, IRI, and distress survey, the worst performing section was selected for more testing, which was performed on August 19, 2015. A control section, the best performing in terms of deflection, IRI, and distress, was selected to be compared with the worst performing section. The selected eastbound distressed section consisted of 26 slabs of total length 390 ft (119 m) ranging from eastbound Station 765+86 to Station 769+76, or interstate mile markers 84.97 to 85.05. This section included various distress types representative of the deteriorated eastbound direction. The selected westbound control section included 14 slabs of total length 210 ft (64 m) from Station 610+50 to Station 608+40, or interstate mile markers 82.03 to 81.99. The locations of both selected sections are shown in Figure 16 above.

4.4.2.1 Load Transfer Efficiency (LTE)

Figure 30 shows the load transfer efficiency (LTE) results of selected test sections. LTE is generally poor on the eastbound distressed section of MAD-70. Most distressed section joints have LTE less than 70% and the variation is large from joint to joint; in some joints the LTE is less than 20%. This indicates the dowels are ineffective. The westbound control section joints showed satisfactory LTE; only one joint had LTE at 70% or less. The temperature during testing in both directions was high and slab expansion would have tended to lead to joint interlock, which would improve LTE, thus the joints with low LTE would be expected to perform even worse at lower temperatures.

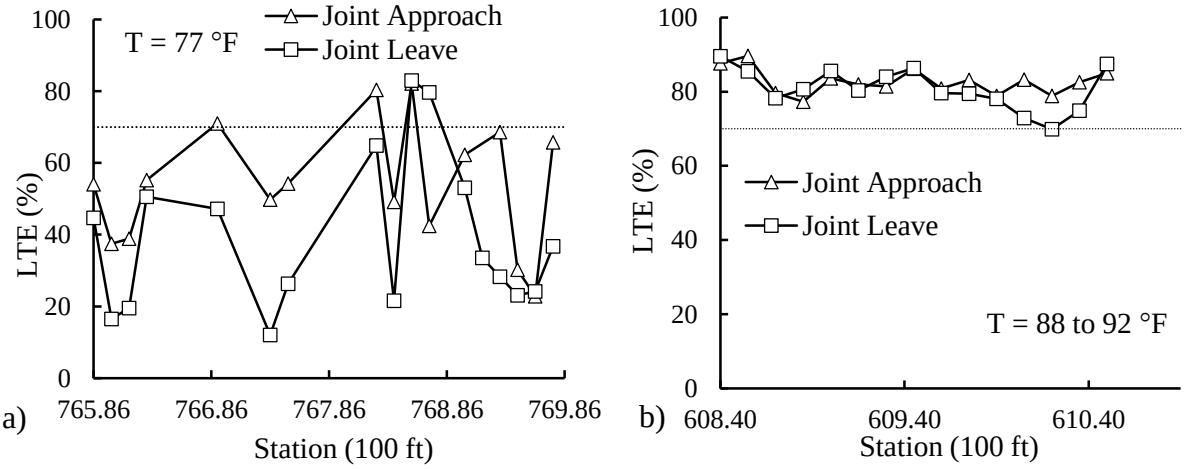

Figure 30 a) MAD-70 EB distressed section Load Transfer Efficiency; b) MAD-70 WB control section Load Transfer Efficiency (100 ft = 30.5 m). (T = pavement surface temperature)

4.4.2.2 Normalized Deflections

Figure 31 shows the normalized deflection results of the selected sections. Eastbound MAD-70 distressed section showed high normalized joint deflections, as great as 3.7 mil/kip (21 mm/MN), with a lot of variation from joint to joint. Deflections on the joint leave position are relatively

higher than that on the joint approach position. The MAD-70 westbound control section showed small and uniform joint deflections, most below 0.25 mil/kip (1.43 mm/MN).

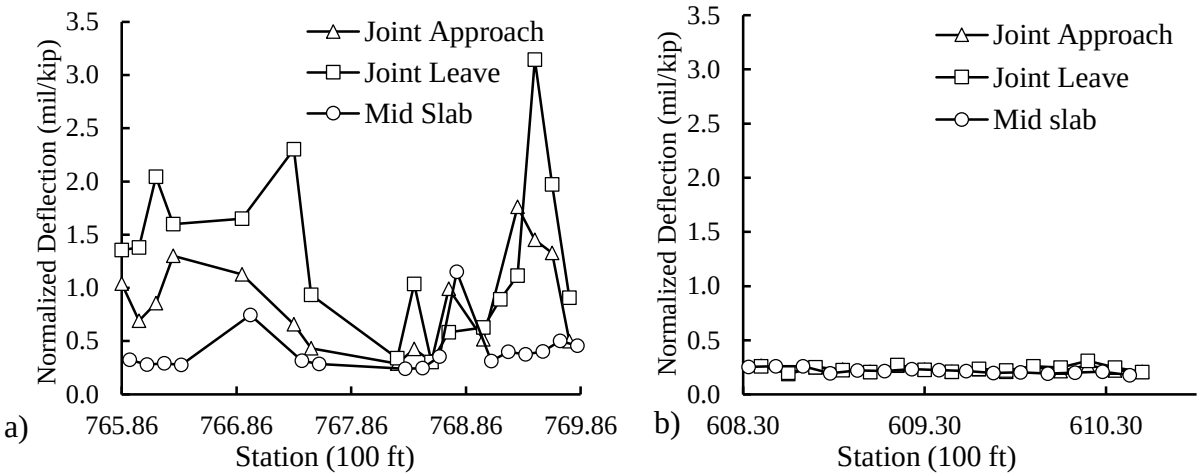

Figure 31 a) MAD-70 EB distressed section Normalized Deflections; b) MAD-70 WB control section Normalized Deflections (1 mil/kip = 5.71 mm/MN, 100 ft = 30.5 m).

4.4.2.3 JSR and SPR

Figure 32 presents the Joint Support Ratio (JSR) results and Figure 33 presents mid-slab spreadability (SPR) results. For MAD-70 EB distressed section direction, JSR values are significantly greater than 1, which indicates joint support condition is unbalanced; the joint leave side has much greater deflection than the joint approach side. This indicates voids under joint leave side. This is consistent with distresses found on the leave side, as shown in Figure 18. Joint 6, 14, and 15 with high JSR values all had large corner break slab on the leave side. All JSR values on westbound control section of MAD-70 are close to 1, which means equal joint support condition on both sides of joints. Mid-slab SPR values are variable in the eastbound direction distressed section, while SPR values on westbound direction control section are uniform and close to 0.75. This indicates a lower level of deterioration than on the distressed section, consistent with observations of pavement condition.

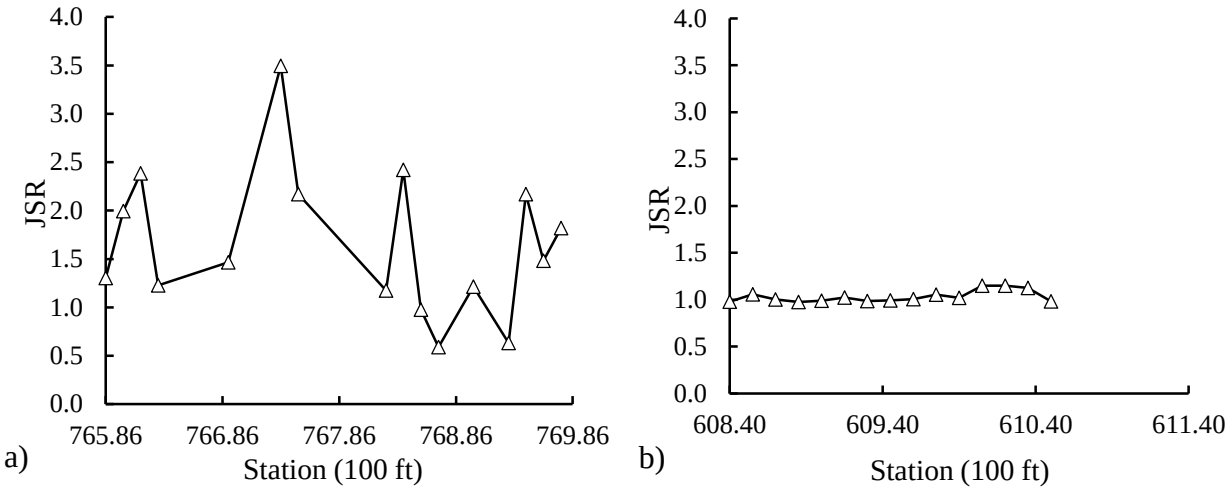

Figure 32 a) MAD-70 EB distressed section Joint Support Ratio; b) MAD-70 WB control section Joint Support Ratio (100 ft = 30.5 m).

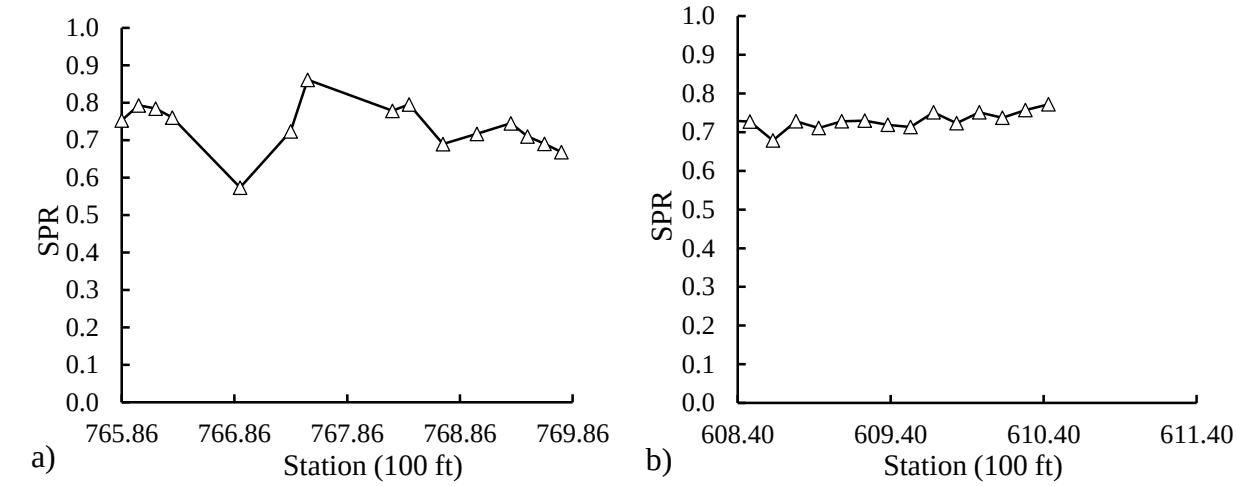

Figure 33 a) MAD-70 EB distressed section Mid-slab Spreadability; b) MAD-70 WB control section Mid-slab Spreadability (100 ft = 30.5 m).

4.5 MITScan and slab removal

Baskets were used to hold the dowel bars during placing of the pavement. Following the standard arrangement of dowel bars in 12 ft (3.66 m) wide lanes, there were 12 bars per joint, distributed with the first bar 6 in (152 mm) from the lane edge, then one bar every 12 in (305 mm) with the last bar placed 6 in (152 mm) from the other edge of the lane. The MITScan was performed by ODOT on August 19, 2015. Figure 20 above shows the locations of scanned joints (labelled e.g. "J1", "J2", etc.). In total, 16 joints were scanned in the eastbound direction of MAD-70; 15 joints in the westbound direction. The distribution of dowel misalignment is presented in Table 7. It can be seen from the table that alignment in the westbound control section is generally better than in the eastbound distressed section. For example dowel bar misalignment by vertical rotation was 29.2% over 0.7 in (18 mm) compared to 4.1% for the control section. However, misalignment in Depth Translation and in Horizontal Translation were both highly prevalent. For Horizontal

Translation, only 10.8% of dowels met the acceptance criterion in the control section, while in the distressed section the acceptance rate was a mere 1.9%, and 85.7% met or exceeded the rejection criterion. When the offset is removed by computing the dowel bar spacing, the acceptance rate is 86.2% in the distressed section, and 99.2% on the control section. The respective rejection rates are 6.9% and 0.0%. Detailed tables of the MITScan data are in Appendix B. It should be noted that a few scanned joints in I-70 EB (Joint 55, Joint 25, Joint 19, and possibly Joint 13, as indicated in Appendix B1) had several anomalously high or low spacings between some dowel bars, possibly due to repairs on the distressed pavement, though an effort was made to avoid reconstructed joints with the MITScanner.

Table 7 Distribution of dowel misalignment in selected MAD-70 sections. Acceptance and rejection criteria are from Table 3.

Section	Type of Misalignment	accept		reject	No. Bars
		$\lvert d \rvert \leq 0.5$	$0.5 < \lvert d \rvert \leq 0.7$	$\lvert d \rvert > 0.7$	
EB (distressed)	Horizontal Rotation	91.3%	1.9%	6.8%	161
	Vertical Rotation	57.1%	13.7%	29.2%	161
		$\lvert d \rvert \leq 0.5$	$0.5 < \lvert d \rvert \leq 0.66$	$\lvert d \rvert > 0.66$	
	Depth Translation	57.1%	8.7%	34.2%	161
		$\lvert d \rvert \leq 2$	$2 < \lvert d \rvert \leq 2.3$	$\lvert d \rvert > 2.3$	
	Longitudinal Translation	89.4%	3.7%	6.8%	161
		$\lvert d \rvert \leq 0.5$	$0.5 < \lvert d \rvert \leq 2$	$\lvert d \rvert > 2$	
	Horizontal Translation	1.9%	12.4%	85.7%	161
	Dowel Bar Spacing	86.2%	6.9%	6.9%	145
Section	Type of Misalignment	$\lvert d \rvert \leq 0.5$	$0.5 < \lvert d \rvert \leq 0.7$	$\lvert d \rvert > 0.7$	# Bars
WB (control)	Horizontal Rotation	98.6%	1.4%	0.0%	148
	Vertical Rotation	89.2%	6.8%	4.1%	148
		$\lvert d \rvert \leq 0.5$	$0.5 < \lvert d \rvert \leq 0.66$	$\lvert d \rvert > 0.66$	
	Depth Translation	60.1%	23.0%	16.9%	148
		$\lvert d \rvert \leq 2$	$2 < \lvert d \rvert \leq 2.3$	$\lvert d \rvert > 2.3$	
	Longitudinal Translation	93.2%	6.1%	0.7%	148
		$\lvert d \rvert \leq 0.5$	$0.5 < \lvert d \rvert \leq 2$	$\lvert d \rvert > 2$	
	Horizontal Translation	10.8%	36.5%	52.7%	148
	Dowel Bar Spacing	99.2%	0.8%	0.0%	133

Some deteriorated joints and slabs on MAD-70 were repaired on April and September 2015. During the repair work on the eastbound forensic section, on September 15, 2015, the Ohio University research team was in the field to document the condition underneath the overlay slabs. A joint repair slab with 3 ft (0.92m) on either side of a transverse joint was lifted out as shown in Figure 34. Distress in the segment included joint spalling and corner breakage with settlement. In Figure 34b), it can be seen clearly in the circled area that the bottom half of concrete near the joint remained in the hole. Figure 35 shows the state of the bondbreaker layer beneath the segment. In Figure 35a), a ridge of concrete chunks was left on the bondbreaker after the segment had been removed. This confirms the tenting distress found during coring. On near right side of Figure 35b), the bondbreaker was in poor condition, which was due to water retained from lack of drainage as evidenced by the presence of saw slurry. Other observations made during slab removal include:

- Excessive water was found trapped in the asphalt bondbreaker layer at multiple locations, for example as shown in Figure 36a).
- Some bondbreaker material was soft and deteriorated as seen in Figure 36b).
- "Tenting" distress was found at some joints.
- There was no evidence the joints or cracks in the underlying concrete pavement were reflecting into the unbonded overlay. The underlying concrete pavement base appeared to be complete and smooth.

a) 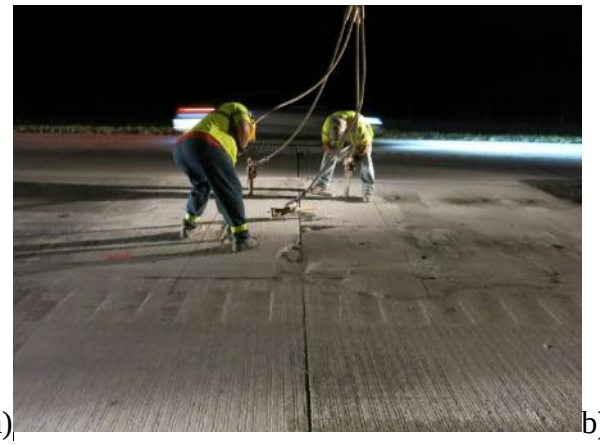 b) 

Figure 34 a) Segment being prepared for removal, September 15, 2015; b) Segment being lifted. Circled area shows gap where missing concrete remained in hole.

a)  b) 

Figure 35 a) Area under segment after removal showing tenting distress (circled); b) Same area under different lighting showing saw slurry from trapped water at lower right.

a)  b) 

Figure 36 a) Water trapped in the bondbreaker layer; b) Deteriorated bondbreaker

4.6 PCC Coring

In total 36 cores were collected from MAD-70 selected sections on August 19, 2015 from the locations indicated in Figure 20; 22 cores were sent to Purdue University for petrographic and Energy Dispersive X-ray spectroscopy (EDX) analysis to verify the mix design and to determine if material-related distress is an issue. The rest of the cores were tested in Ohio University laboratories to determine mechanical properties. Cores were generally collected near cracks or corner breaks on the distressed forensic section. On the "control" forensic section, cores were generally taken from mid-slab or near joints. In each direction, on each test section, an intact control slab was identified and 5 cores collected across mid-slab. Figure 37 and Figure 38 present pictures taken during coring on the distressed section (EB).

Figure 39 is a photograph taken during construction of the MAD-70 overlay in 1999 showing the bondbreaker surface was dry when concrete was placed, contrary to specification, which requires wetting measures. The dry surface can produce stress due to differential moisture levels in the slab [National Concrete Pavement Technology Center, 2006]

a)  b) 

Figure 37 a) Tenting in a failed joint; b) Deteriorated AC bondbreaker. Photos taken August 19, 2015.

a)  b) 

Figure 38 Core holes retaining water.

Figure 39 Concrete overlay being placed on a dry bondbreaker surface on MAD-70 in 1999.

Water drained very slowly from the core holes on both sections, as seen in Figure 38, indicating a lack of drainage for water entering the pavement through the joints. It is likely this water saturated the asphalt bondbreaker near joints and cracks. The cores sent to Purdue were taken from a failed joint with tenting distress, a good joint, at mid-slab from a segment of three slabs with no cracks, and from a slab with a mid-slab crack.

In the distressed section (EB):

- Core E2, E7, E8, E15, E19 and E21 have no bondbreaker material; Core E10 had only deteriorated pieces. 5 of these core holes are located next to or near the joints. Figure 37b) shows deteriorated AC bondbreaker in core hole next to the joint.
- Tenting was found in a failed joint and was beginning in a joint that looked good from the surface (Figure 37a).
- Bondbreaker in core hole adjacent to a corner break had a small gap between bondbreaker and the overlay slab.

In the control section (WB):

- Bondbreaker was found in all core holes, including those at joints, and at an average thickness of 1.9 in (48 mm) they were 46% thicker than in the eastbound direction, which averaged 1.3 in (33 mm). Table 7 in next section presents the thickness results. Only one joint had bondbreaker that was damaged but in the hole the bondbreaker felt solid.
- Only two joints out of 15 showed any signs of distress. The worst one was cored. The core collected in the wheel path had deteriorated to aggregate and concrete fragments typical of tenting. A core on the transverse joint broke and also showed signs of tenting (Figure 19b).
- A core was collected at a small crack which verified the presence of top down cracking, shown in Figure 40.

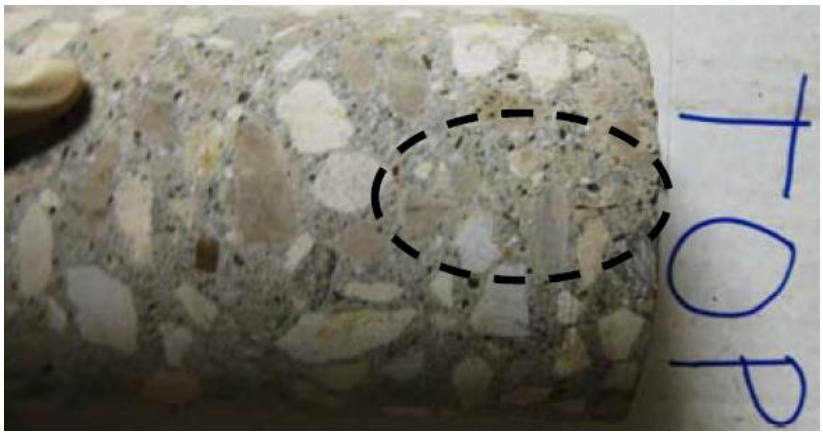

Figure 40 Top-down hairline crack on core W4 from MAD-70 westbound. Photo from report by Dr. Jan Olek of Purdue University.

4.7 Laboratory testing results

Diameter and length (thickness) were measured in the lab after collection. Only intact samples were measured and recorded. Damaged samples were excluded from thickness measuring. The thickness of the PCC pavement and AC bondbreaker in each direction was determined by averaging their thicknesses from core samples. Table 8 summarizes the measured thickness of all

cores taken from each section; 14 cores were tested at Ohio University for mechanical properties, and the remaining cores were sent to Purdue University for petrographic examination. Table 9 and Table 10 present the summary of laboratory testing results for the eastbound and westbound directions, respectively. Detailed test data can be found in Appendix C.

Cores E1 and W14 were used for the Elastic Modulus and Poisson's ratio test before being used for compressive strength test. Most cores displayed a Type 3 fracture pattern, which is columnar vertical cracking through both ends with no well-formed cones. Specimens S2 and S4 showed a Type 2 pattern, which has a well-formed cone on one end, vertical cracks running through caps, and no well-defined cone on other end. ODOT's current design strength is 4000 psi (28 MPa), which was exceeded by the measured values.

ODOT presently designs for a Modulus of Rupture of 700 psi (4.83 MPa). The splitting tensile strength of concrete is usually 60% to 80% of the modulus of rupture. Considering this conversion factor, the obtained splitting tensile strength of I-70 indicates the modulus of rupture is at least 819 psi (5.65 MPa) for EB or 900 psi (6.21 MPa) for WB, which exceeds the designed modulus of rupture value.

The CTE value is 7.41×10^{-6}/°C (4.12×10^{-6}/°F) for EB direction and 7.76×10^{-6}/°C (4.31×10^{-6}/°F) for WB direction. These values are a little low (17% and 13% respectively) for Portland cement concrete with dolomite aggregate, they are near enough to be regarded as typical. The FHWA average value for the CTE of dolomite concrete is $8.92\pm0.73\times10^{-6}$/°C ($4.95\pm0.40\times10^{-6}$/°F) [FHWA, 2011]. The petrography report cited the main coarse aggregate minerals as calcite, dolomite, and dolomitic calcite.

ODOT currently designs for a modulus of elasticity of 5 million psi (35 GPa). The I-70 EB concrete is about 56% of this design value and the I-70 WB is 88% of the design value. The Posson's ratio value is close to the normal range of 0.1 to 0.2.

Table 8 Thickness of PCC and AC bondbreaker of MAD-70

Direction	units	PCC overlay thickness			C_V (%)	No. Cores	Bondbreaker thickness			C_V (%)	No. Cores
		Max.	Min.	Avg.			Max.	Min.	Avg.		
EB (distressed)	(in)	10.1	8.7	9.3	5.8	19	2	0.8	1.3	23.7	14
	(mm)	257	221	236			51	20	33		
WB (control)	(in)	9.2	8.8	9	1.3	17	2.2	1.5	1.9	10.0	18
	(mm)	234	224	229			56	38	48		

Table 9 Lab Testing Summary of EB distressed section of MAD-70

EB Core	Compressive strength ($f'c$)		Tensile strength		Elastic modulus (E)		Poisson's ratio (υ)	CTE (α)	
	(psi)	(MPa)	(psi)	(MPa)	(10^6psi)	(GPa)		(10^{-6}/°F)	(10^{-6}/°C)
E7	8710	60.05							
E8	8950	61.71							
E12	7360	50.75			2.8	19.31	0.22		
E10			701	4.83					
E13			635	4.38					
E14			625	4.31					
E16								4.11	7.40
Average	8340	57.50	655	4.52	2.8	19.31	0.22	4.11	7.40

Table 10 Lab Testing Summary of WB control section of MAD-70

WB Core	Compressive strength ($f'c$)		Tensile strength		Elastic modulus (E)		Poisson's ratio (υ)	CTE (α)	
	(psi)	(MPa)	(psi)	(MPa)	(10^6psi)	(GPa)		(10^{-6}/°F)	(10^{-6}/°C)
W1	10920	75.29							
W2	10580	72.95							
W14	9450	65.16			4.41	30.41	0.15		
W5			565	3.90					
W9			745	5.14					
W13			845	5.83					
W15								4.31	7.76
Average	10310	71.08	720	4.96	4.41	30.41	0.15	4.31	7.76

Findings from the laboratory tests included the following:

1. The bondbreaker thickness of I-70 eastbound is thinner than I-70 westbound. This reduced thickness potentially made the EB bondbreaker more susceptible to pumping damage, which led to decreased structural support to the slabs and created transverse cracking, faulting, and corner breaks.
2. Cores obtained from I-70 eastbound and westbound met ODOT specifications for tensile strength.
3. A core from I-70 WB had an elastic modulus about 12% below design value, while a core from I-70 EB had a modulus 44% below design value.
4. By examining core photos and coring locations, it was found that for I-70 eastbound, no bondbreaker was found in any cores from holes adjacent to joints or cracks, while cores from mid-slab locations had bondbreaker attached. For I-70 westbound, bondbreaker was found in almost every core.

4.8 Petrographic analysis

The petrographic analysis was performed by Purdue University. Figure 42 and Figure 43 show the list of tested specimens from MAD-70 as well as their locations in the test section. Core E1, E2, E3 and E6 from the eastbound lanes and Cores W4, W7 and W11 from the westbound lanes were also studied with a Scanning Electron Microscope (SEM). Core E3, E15, E18 from eastbound lanes and Cores W6, W7 from westbound lanes were subjected to air voids analysis. Findings from SEM analysis of the cores are presented below from the subcontractor report.

Core E2:

- Slag cement was present.
- Air Void system was severely compromised.
- Calcium carbonate was frequently encountered in the top sample whereas calcium hydroxide was frequently encountered in the bottom sample.
- Figure 41 shows ettringite infilling of air voids found on bottom sample from Core E2.

Core E3:

- Slag cement was present.

- Ettringite deposits were rarely encountered in the top sample but more frequently encountered in the bottom sample.
- No Chlorides were detected in the bottom sample but the top sample had high frequency of occurrence of Friedel's salt. Friedel's salt is a consequence of the reaction of chlorides applied in anticing chemicals with constituents of the concrete; it tends to fill air voids.

Core E6:

- Calcium carbonate was found in the vicinity of cracks.
- Deposits of Friedel's salt found.

Cores E1, W4, W7 and W11:

- The matrix of all the cores seemed to have a good and uniform air void system except Core W11 which had a very poor pore system.
- Although cracks were observed in the matrix of all cores, the most extensive cracking was observed in Core W11. The matrix of this core contained mainly horizontal cracks (most likely due to the lack of sufficient quality air voids system which resulted in freeze/thaw damage). Some of the cracks were filled with ettringite and carbonated calcium hydroxide ($Ca(OH)_2$).
- The matrix of all the cores seemed to be carbonated to the depth of at least 1 in (25 mm).
- All of the analyzed cores contained essentially the same type of coarse aggregate: calcite, dolomite, dolomitic calcite. As for the fine aggregate, it contained mainly feldspar, quartz, dolomite, calcite and mudstone minerals. The sizes of fine dolomite and calcite particles were close to those of cement grains. In few cases, fine siliceous particles contained inclusions of iron oxide.
- Slag grains, which have a composition similar to akermanite (calcium-magnesium-alumina silicate), were present in the matrix. Some of the finer slag particles showed signs of reaction (hydration).
- Deposits of Friedel's salt were found in all the cores tested.
- Evidence of gypsum and thaumasite-like phase formation was observed in Cores E1 and W4.
- The matrix from all cores contained deposits of ettringite/monosulfate crystals in air voids (as large deposits) and in the paste (as small crystals). In some cases, deposits were found in the cracks within the matrix and at the interface. Some of these deposits may be due to the sulfate ions being liberated from internal sulfate source as a pyrite in a mudstone particle. In several cases, the deposits of ettringite were observed near or in the mudstone particles.

Table 11 summarizes the air void analysis results of MAD-70 cores. ODOT designs concrete with 6±2% air void content. All the tested specimens had air void content within this range. The maximum value of the spacing factor for moderately exposed concrete is usually assumed to be 0.008 in (0.20 mm), though somewhat larger values may be adequate for mild exposure, while lesser values may be required for severe exposure, especially if deicing chemicals are in contact with the concrete. All tested specimens were within the maximum allowed spacing factor.

Table 11 Summary of the air void analysis of cores from MAD-70

		Eastbound			Westbound	
Core ID		E3	E15	E18	W6	W7
Air void content		4.32%	6.64%	4.6%	7.97%	6.98%
Paste content		22.96%	28%	21.6%	31.94%	28.97 %
Spacing factor	(in)	0.003	0.003	0.008	0.0019	0.0017
	(mm)	0.088	0.077	0.20	0.049	0.042

Summary of findings from petrographic analysis as well as remarks:

- Concrete from both directions were found to be well cured. Air void content and spacing factor were generally acceptable.
- Infilling of the air voids with Ettringite leads to a durability problem in the PCC, such as the tenting/joint deterioration found in both the eastbound and westbound direction.
- Friedel's salt deposits were frequently found in almost all tested cores. Friedel's salt comes from chlorides in dissolved road salt that fills voids. This potentially lowers the freezing temperature and leads to more freeze-thaw cycles.
- Slag cement is beneficial because it typically reduces the permeability of the concrete, eliminating or at least delaying the infilling of air voids.

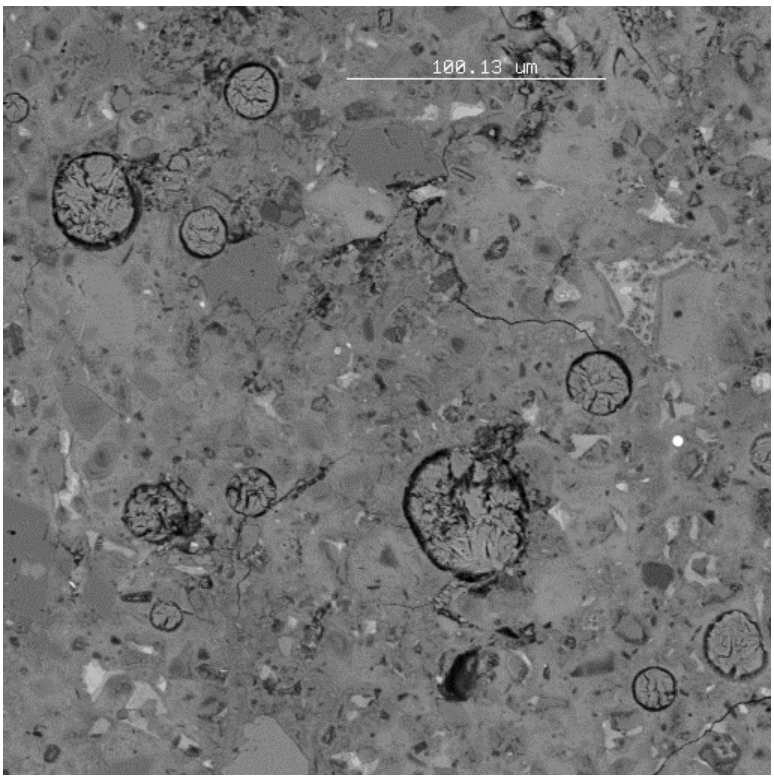

Figure 41 Ettringite infilling of air voids on Core E2 bottom sample (100.13 µm = 3.94 mil). From report by Dr. Jan Olek of Purdue University.

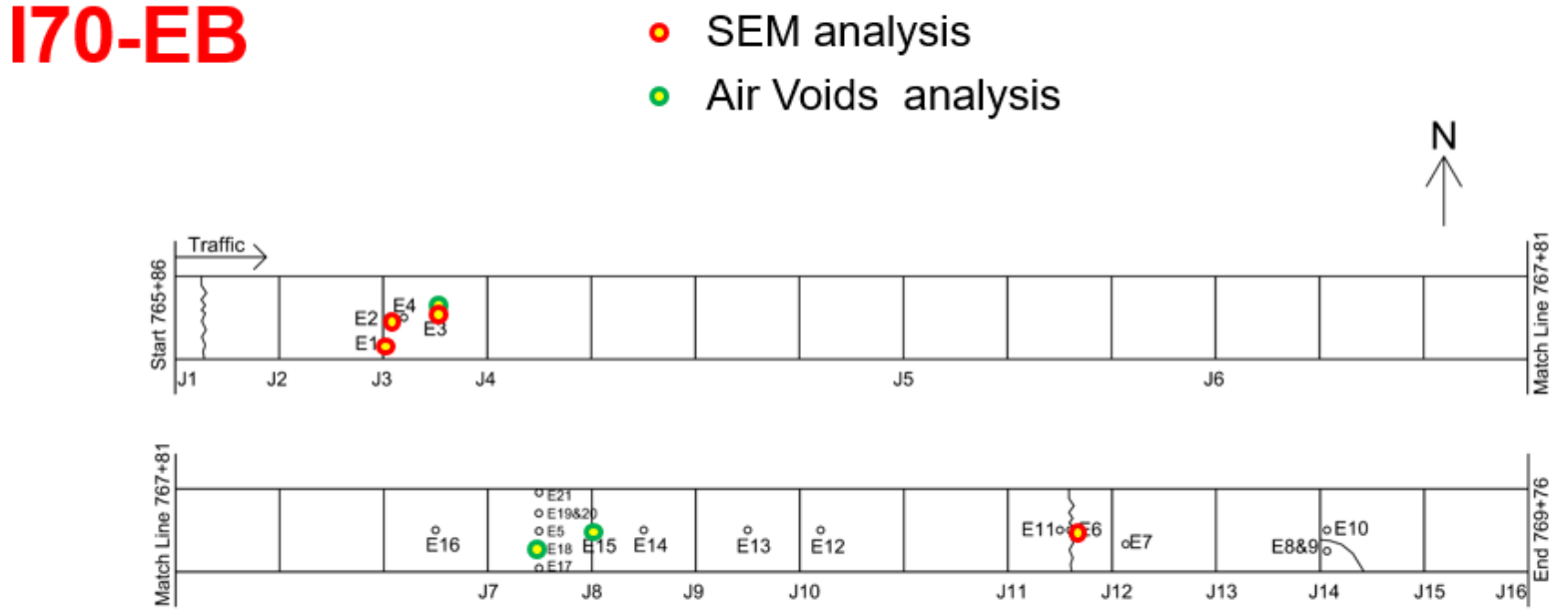

I70 Eastbound Core Sample Profile

#	Station	Destination	Notes	#	Station	Destination	Notes
E1	766+17	Purdue	wheelpath, spalled joint; shattered	E12	768+72	OU	
E2	766+17	Purdue	center of lane, spalled joint; horizontally cracked	E13	768+64	OU	
E3	766+24	Purdue	center of slab, core for additional testing	E14	768+49	OU	
E4	766+20	Purdue	center of lane, 3' from joint, cotrol of E1&E2	E15	768+42	Purdue	center of lane, joint of no distress; horizontally cracked
E5	768+35	Purdue	center of slab; control for E15	E16	768+20	OU	
E6	769+12	Purdue	midslab crack; vertically cracked	E17	768+35	Purdue	
E7	769+19	OU		E18	768+35	Purdue	
E8-top	769+48	OU	overlay core	E19-top	768+35	Purdue	overlay core
E9-bottom	769+48	OU	old concrete core	E20-bottom	768+35	Purdue	old concrete core
E10	769+48	OU		E21	768+35	Purdue	
E11	769+11	Purdue	control for E6				

Figure 42 Location map and list of petrographic cores collected on MAD-70 eastbound. From report by Dr. Jan Olek of Purdue University.

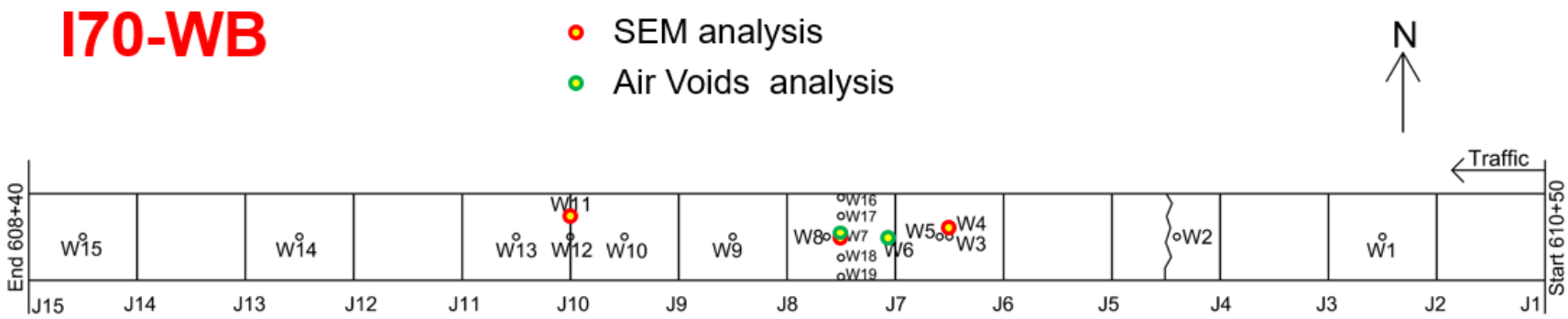

I70 Westbound Core Sample Profile							
#	Station	Destination	Notes	#	Station	Destination	Notes
W1	610+27	OU		W11	609+15	Purdue	wheelpath, spalled joint; shattered
W2	609+99	OU	next to a crack	W12	609+15	Purdue	center of lane, spalled joint; broken
W3	609+69	Purdue	center of slab, control for W4, W6&W7	W13	609+7	OU	
W4	609+69	Purdue	wheelpath, hairline crack	W14	608+75	OU	next to a core taken at construction
W5	609+68	OU	center of lane, joint of no distress	W15	608+48	OU	
W6	609+61	Purdue		W16	609+54	Purdue	
W7	609+54	Purdue	centerof lane, midslab crack; vertically cracked	W17	609+54	Purdue	
W8	609+52	Purdue	center of lane, control for W7 or additional testing	W18	609+54	Purdue	
W9	609+40	OU		W19	609+54	Purdue	
W10	609+25	Purdue	center of lane, control for W11&W12				

Figure 43 Location map and list of petrographic cores collected on MAD-70 westbound. From report by Dr. Jan Olek of Purdue University.

4.9 HIPERPAV Results

Table 12 presents the PCC mix used on the MAD-70 overlay evaluated with HIPERPAV. Class C Option 3 concrete from ODOT specifications was used with limestone aggregate. The water to cementitious material ratio was 0.5. Type D admixture was used. Single coat curing method was applied. Defaults were used for initial PCC mix temperature and initial support layer temperature. Weather data were estimated from three nearby weather stations in Columbus, Dayton, and Mansfield. High and low temperatures on dates of construction were extracted from the construction diary and were used in the analysis. The dates the mainline UBCO was constructed and corresponding temperatures are presented in Table 15, along with the analysis results for two cases, dry base and moist base, where in the latter the asphalt bondbreaker was wetted before placing the concrete overlay. All the analysis passed for moist base case, but when constructed with dry base, the concrete failed prematurely 6 out of 17 days (35%). Appendix D shows the analysis results for each day.

Table 12 MAD-70 PCC Mix Design.

Density unit	Coarse Aggregate	Fine Aggregate	Cement (Type I)	Water	GGBF Slag	Total
(lb/yd^3)	1670	1310	385	275	165	3805
(kg/m^3)	991	777	228	163	98	2257

Table 13 HIPERPAV Analysis Results for all construction days on MAD-70.

Direction	Day number	Date	Air temperature (°F)		Air temperature (°C)		Analysis result (pass/fail)	
			low	high	low	high	moist base	dry base
Eastbound	1	8/17/1999	70	92	21.1	33.3	pass	pass
	2	8/18/1999	68	87	20.0	30.6	pass	pass
	3	8/20/1999	64	84	17.8	28.9	pass	pass
	4	8/23/1999	63	86	17.2	30.0	pass	pass
	5	8/27/1999	67	87	19.4	30.6	pass	pass
	6	8/30/1999	58	76	14.4	24.4	pass	pass
	7	8/31/1999	56	81	13.3	27.2	pass	fail
	8	9/2/1999	61	84	16.1	28.9	pass	pass
Westbound	9	5/12/2000	60	87	15.6	30.6	pass	fail
	10	5/15/2000	55	72	12.8	22.2	pass	pass
	11	5/16/2000	49	65	9.4	18.3	pass	fail
	12	5/17/2000	52	72	11.1	22.2	pass	fail
	13	5/18/2000	44	64	6.7	17.8	pass	fail
	14	5/19/2000	47	63	8.3	17.2	pass	fail
	15	5/24/2000	58	72	14.4	22.2	pass	pass
	16	5/30/2000	59	79	15.0	26.1	pass	pass
	17	6/1/2000	63	85	17.2	29.4	pass	pass
	Fail (count)						0	6
	Fail (%)						0%	35%

A comparison was made between moist and dry base to see the effect of wetting the base before placing concrete. Figure 44 shows comparison of concrete strength development placed on August 31, 1999. The simulation indicated the concrete on moist base cured much faster than concrete on dry base. The tensile strength at 72 hours is 263.4 psi (1.816 MPa) for concrete on moist base and 209.4 psi (1.444 MPa) for concrete on dry base. Figure 49 shows the crack risk plot. In the dry case, the stress to strength ratio exceeds 100% at about 16 hours, indicating crack formation. The stress-strength ratio of the concrete on moist base stays below 75%. Figure 46 and Figure 47 show the concrete strength and crack risk, respectively, computed for concrete placed on May 12, 2000, during the next construction season. There is a similar discrepancy in tensile strength at 72 hours with 230.0 psi (1.586 MPa) for concrete on moist base and 182.3 psi (1.257 MPa) for concrete on a dry base. In Figure 47, the dry base stress to strength ratio breaks 100% at about 15 hours, while the moist base case tops out at about 85%.

Figure 39, a photograph taken during construction, shows that no wetting measure taken on that particular day of construction. It is not known on how many days the wetting measure was skipped. Based on the HIPERPAV analysis, it is obvious concrete placed on a moist base cures much faster and is stronger in the first 72 hours, and is less likely to crack, than concrete placed on a dry base.

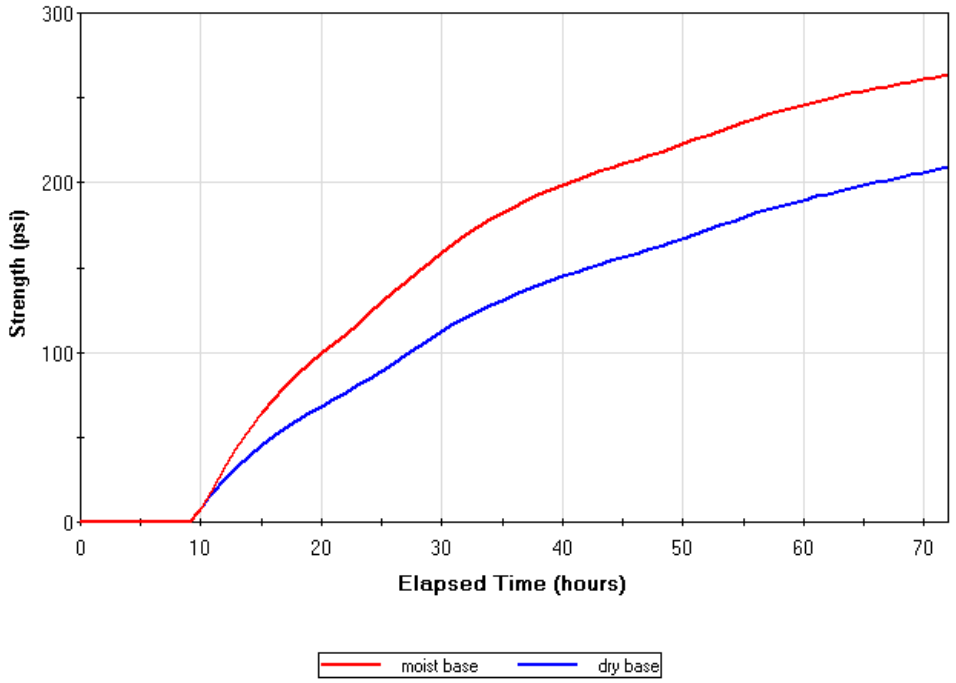

Figure 44 Strength versus elapsed time in HIPERPAV, MAD-70 overlay August 31, 1999.

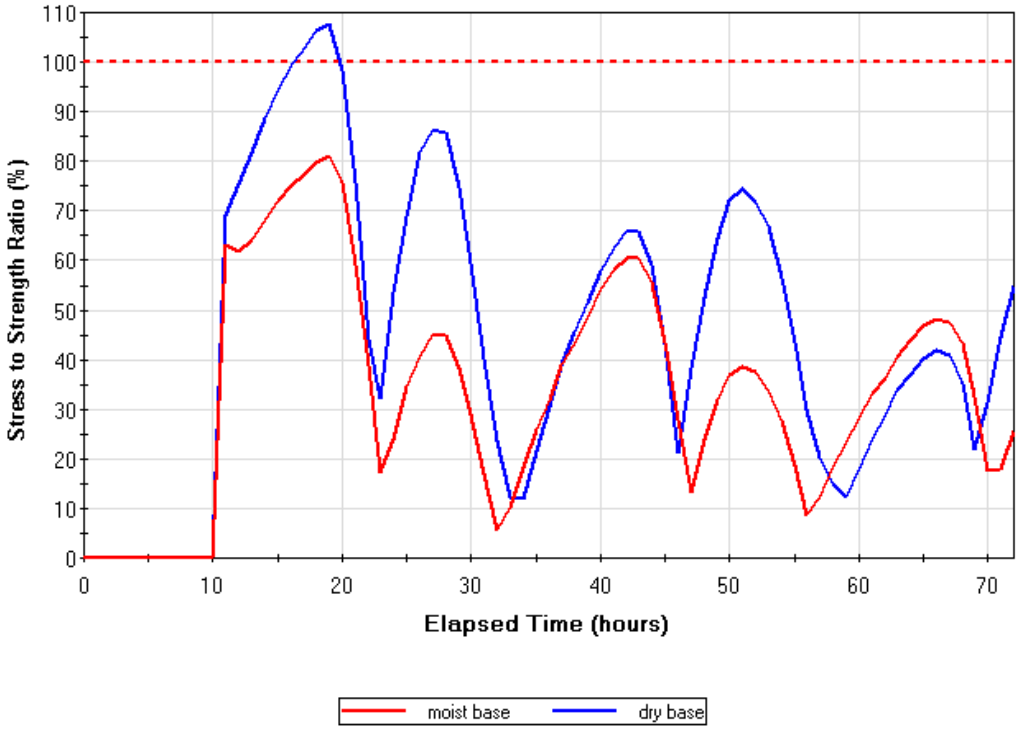

Figure 45 Stress to strength ratio versus elapsed time in HIPERPAV, MAD-70 overlay August 31, 1999.

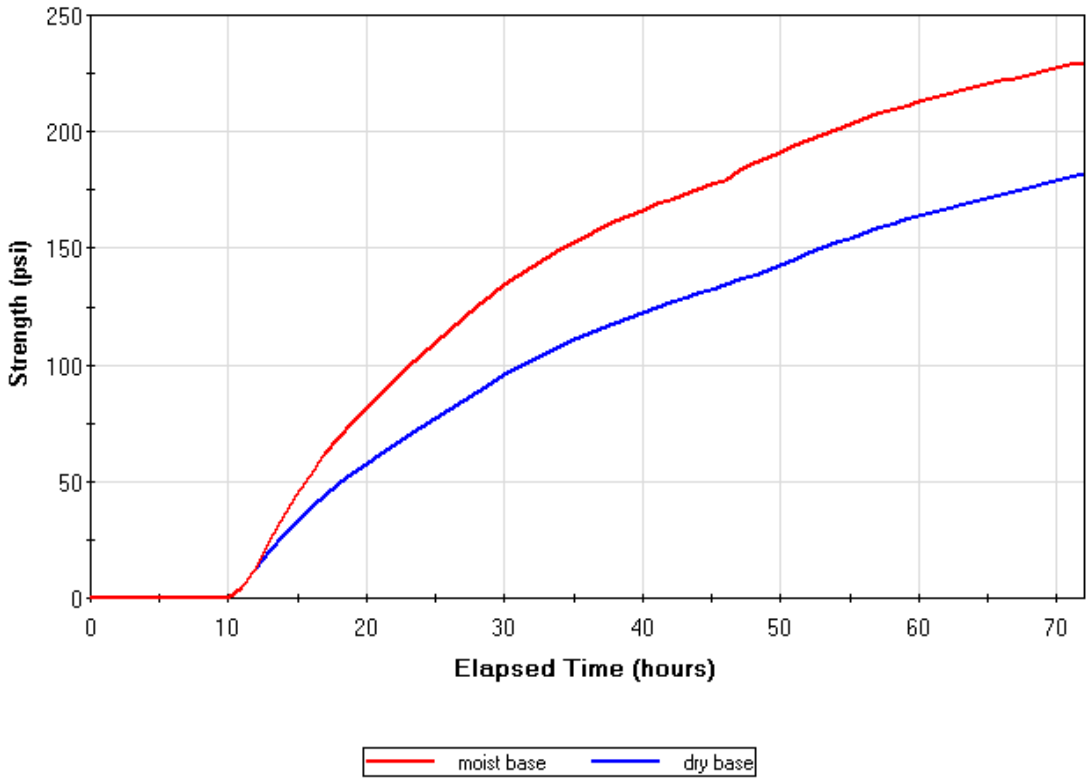

Figure 46 Strength versus elapsed time in HIPERPAV, MAD-70 overlay, May 12, 2000.

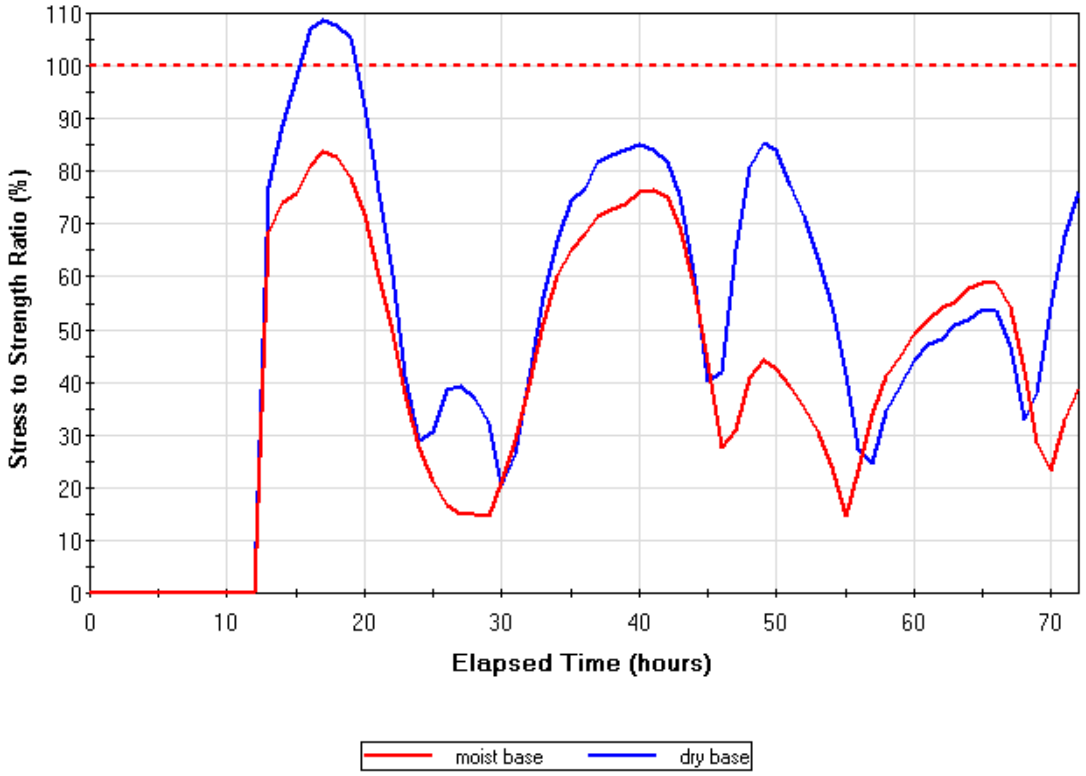

Figure 47 Stress to strength ratio versus elapsed time in HIPERPAV, MAD-70 overlay, May 12, 2000.

4.10 Findings

Key findings from the forensic investigation of the overlay on MAD-70 are summarized below:

- Water drained slowly from the core holes, indicating a lack of drainage. It is possible this water saturated the asphalt bondbreaker near joints and cracks.
- A thin bondbreaker is more susceptible to water damage when subjected to heavy truck traffic. The thicker bondbreaker layer on the relatively undamaged westbound side of the pavement provided two advantages: it reduced the stress transmitted below more than a thin layer, and the thicker layer was able to absorb more water and provide volume for water to migrate into when pressure was applied by a load, reducing the potential for early deterioration. However, the thicker bondbreaker is not a solution to the presence of moisture, as the deterioration is merely delayed if the moisture problem is not addressed.
- The tenting observed was a result of the formation of ettringite that moved into and filled the air voids. The reduced air voids in the concrete resulted in cracking and shortened durability.
- In addition, water would dissolve salt applied to the road surface for deicing and then accumulate because of the poor drainage. The dissolved salt penetrated into the concrete, further reducing air voids and causing concrete deterioration.
- The westbound direction also showed more consistency in measured properties, thickness, and dowel bar alignment, indicating better construction and material quality control.
- Based on review of a photograph taken during construction, the asphalt bondbreaker was dry before the concrete overlay was placed.

- During slab removal, there was no indication the underlying cracks and joints in the original pavement had an effect on the location of cracking or deterioration in the UBCO.
- Petrographic analysis findings summary.
    - Concrete from both sections were found to be well cured.
    - Slag cement is good practice.
    - Freeze-thaw is potentially a cause of damage indicated by the low air voids due to infilling.
    - Top-down cracking was observed.

5 I-77 in Washington and Noble County

5.1 Project Information

Project 2005-3000 overlaid a 9 in (229 mm) jointed, reinforced, dowelled concrete pavement on I-77 in Washington and Noble Counties (WAS/NOB-77) with an 8 in (203 mm) jointed, plain, dowelled concrete (ODOT Item 452) pavement on a 1 in (25 mm) plan thickness asphalt (ODOT Item 448) bondbreaker in 2006. Approximately 4 years after opening to traffic, transverse and longitudinal cracking began to appear. As of 2014, ADT = 16,530 and ADTT = 1,250. Figure 48a) shows the location of the project on a map, and Figure 48b) shows the build-up of the project section.

a)

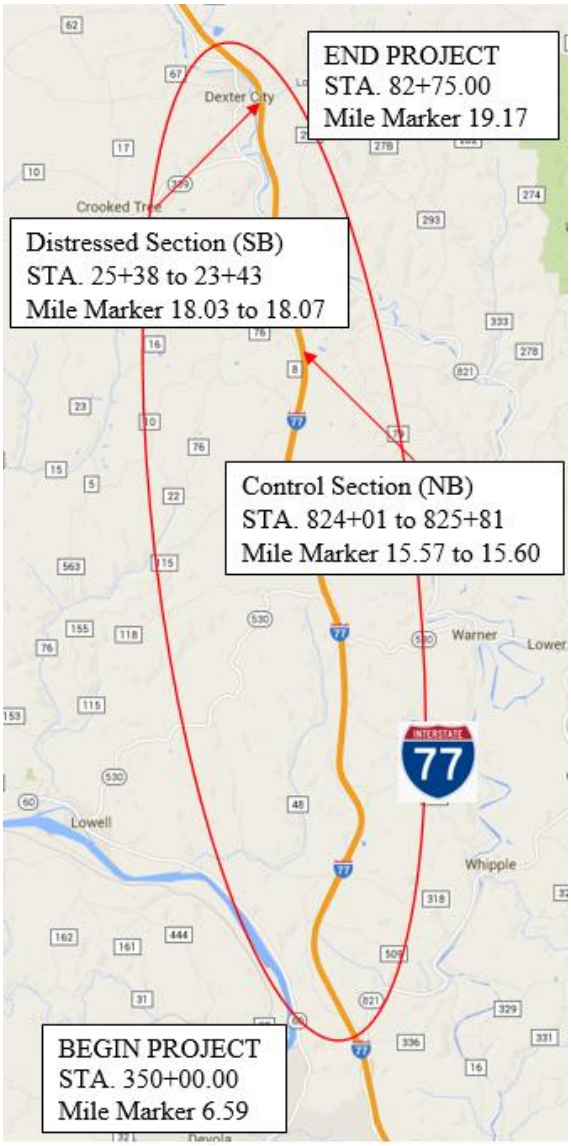

b)

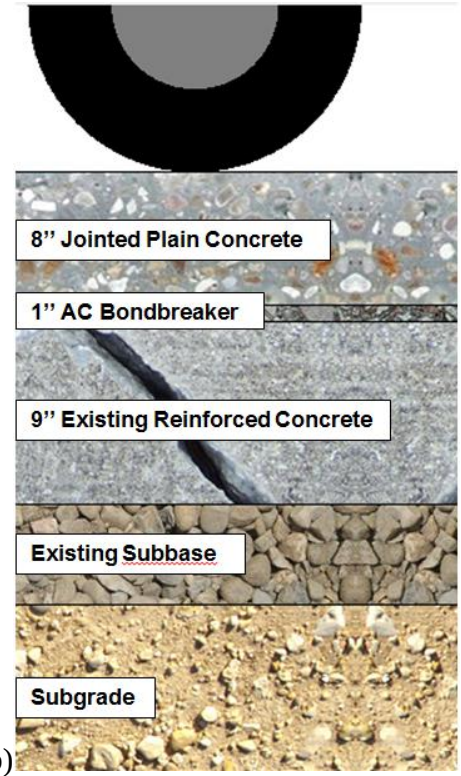

Figure 48 a) Location map; b) Pavement structure of WAS/NOB-77 UBCO section

5.2 Visual Assessment

A visual assessment of the condition of WAS/NOB-77 was conducted on December 8, 2014. The dominant distress found in the UBCO was longitudinal cracking, such as the example in Figure 49a). Other distresses such as transverse crack, patching, and joint spalling, seen on Figure 49b), were also found on I-77. Figure 50 shows the bondbreaker being wetted before placing the concrete overlay, in accordance with specifications.

a)  b) 

Figure 49 a) longitudinal cracking and joint spalling found on WAS/NOB-77 SB; b) joint spalling found on WAS/NOB-77 NB. Photos taken December 8, 2014.

a)  b) 

Figure 50 Wetting the bondbreaker before placing concrete. Photos dated Oct. 10, 2006.

5.3 Distress Survey

A video distress survey was conducted May 23, 2015 on the whole project by Stantec Consulting Services Ltd. (Stantec) using Stantec's Road Tester 3000 (RT3000) vehicle. As can be seen from the graphs in Figure 51 through Figure 53, the International Roughness Index (IRI) of I-77 is generally good (< 95 in/mi or 1.50×10^{-3} m/m). There is no significant difference between two directions. MP16 and MP19 on I-77 northbound direction are in relatively worse condition compared to other segments of the project. The outside lane (NB2, ODOT Lane 4) is performing better than the inside lane (NB1, ODOT Lane 3), with the exception of segments at MP6, MP7,

and MP12. MP19 on southbound direction showed worse performance compared to other segments of the project. Plots of the 50 ft (15 m) IRI moving average are provided in Appendix A.

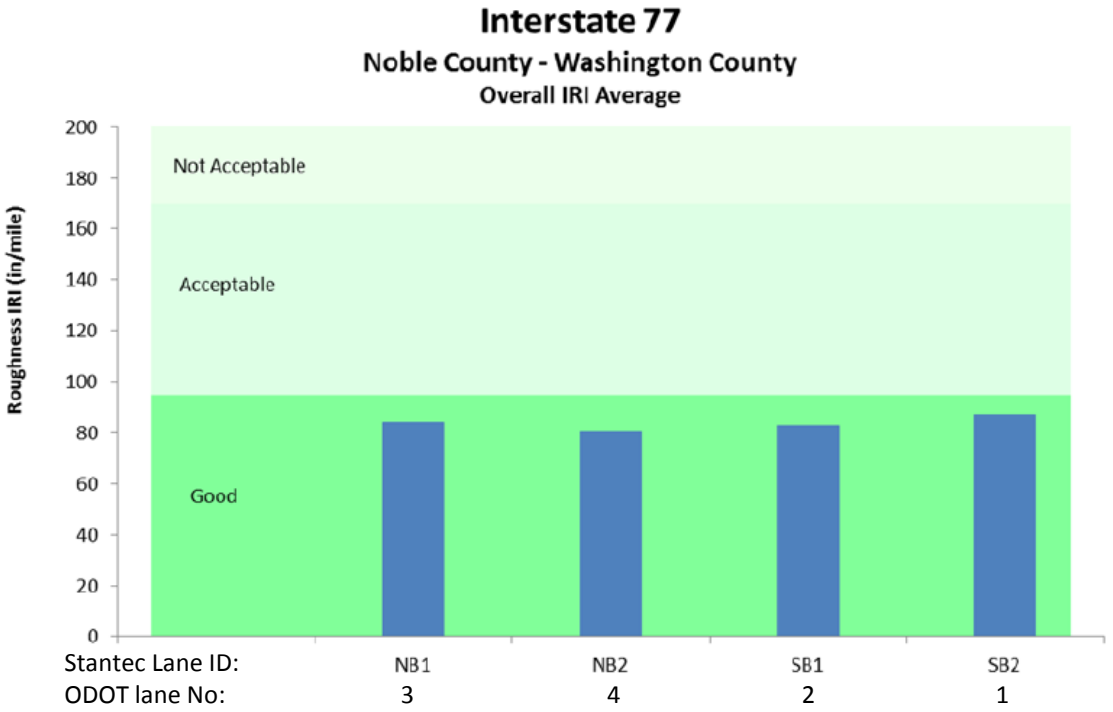

Figure 51 Average Measured IRI of WAS/NOB-77, all lanes, May 23, 2015. Graph by Stantec. (1 in/mi = 1.58×10^{-5} m/m).

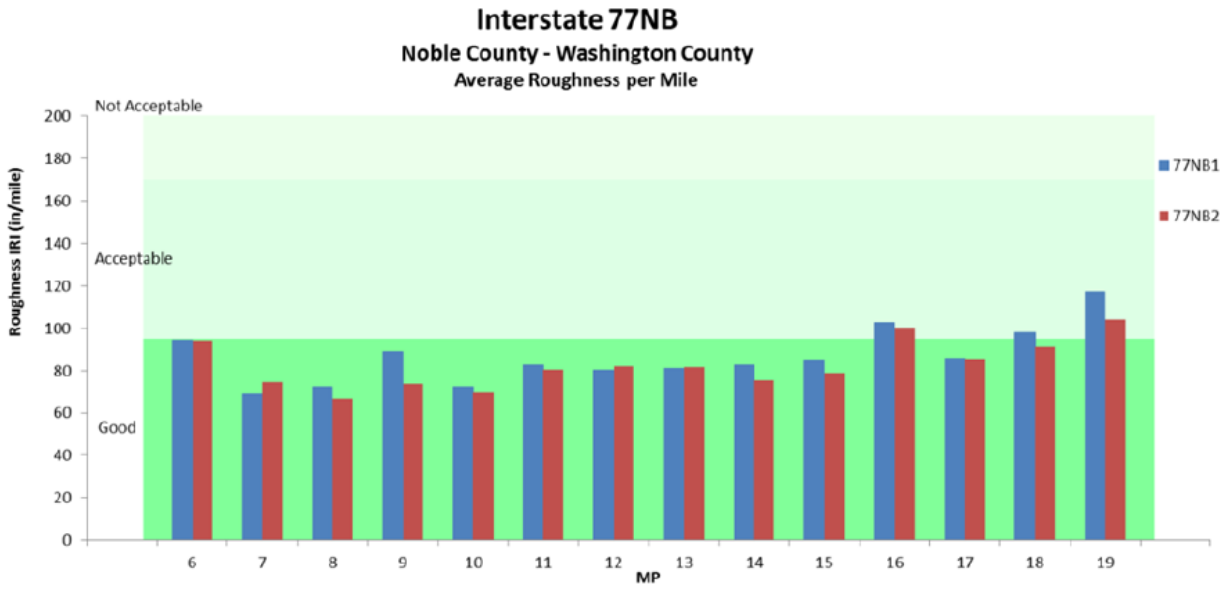

Figure 52 Average IRI of WAS/NOB-77, northbound lanes May 23, 2015. Graph by Stantec. (1 in/mi = 1.58×10^{-5} m/m) (Lanes: 77NB1 = ODOT Lane 3, 77NB2 = ODOT Lane 4).

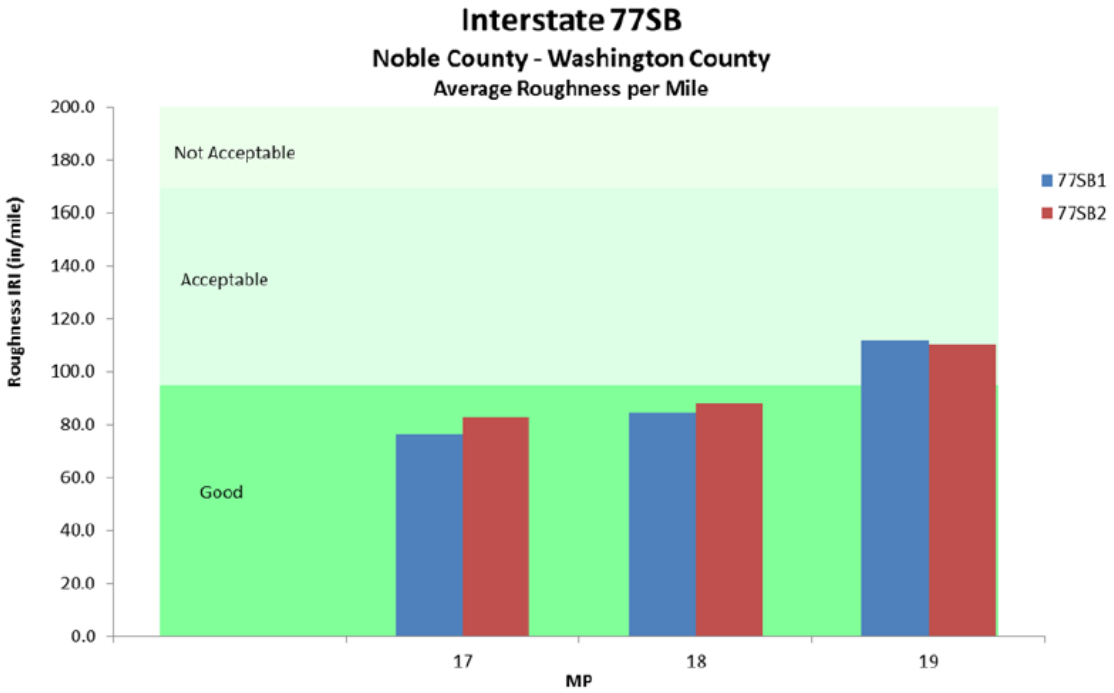

Figure 53 Average IRI of WAS/NOB-77, southbound lanes May 23, 2015. Graph by Stantec. (1 in/mi = 1.58×10^{-5} m/m) (Lanes: 77SB1 = ODOT Lane 2, 77SB2 = ODOT Lane 1).

Table 14 presents major distresses identified on WAS/NOB-77 based on the distress survey and visual assessment. The PCR history table provided by ODOT was used to confirm the distresses. Primary and contributing factors were listed below as provided on the NCHRP PCC distress types and causes table (Table 35 and Table 36). Possible causes were listed based on NCHRP tables as well as research team's judgement.

Table 14 Major distresses identified on WAS/NOB-77 and possible causes

Project	Major Distress	Primary Factors	Contributing Factors	Possible Causes
WAS/NOB-77	Longitudinal Cracking	Design features; Load; Construction	Temperature; Materials	Dowel bar related problem; poor construction practices; material related problem.
	Joint Spalling	Materials	Design features; Temperature; Load; Construction	

5.4 FWD

5.4.1 Pre-investigation FWD results

Figure 54 through Figure 57 present the initial FWD results along the entire length of the I-77 UBCO project, collected December 8-9, 2014. Shaded areas are full-depth sections. For I-77 northbound, the readings began at station 350+00 in Washington County and ended at station 82+51 in Noble County. In the plots, stations in Noble County were added to the end station 930+65 in Washington County for convenience and consistency (e.g. Station 950+65 in the plots is actually Station 20+00 in Noble County). It can be seen from the plots that normalized

deflections are mostly less than 0.4 mil/kip (2.3 mm/MN), and the variation is very small along the whole length. A majority of the LTE values for the unbonded overlay were less than 70%.

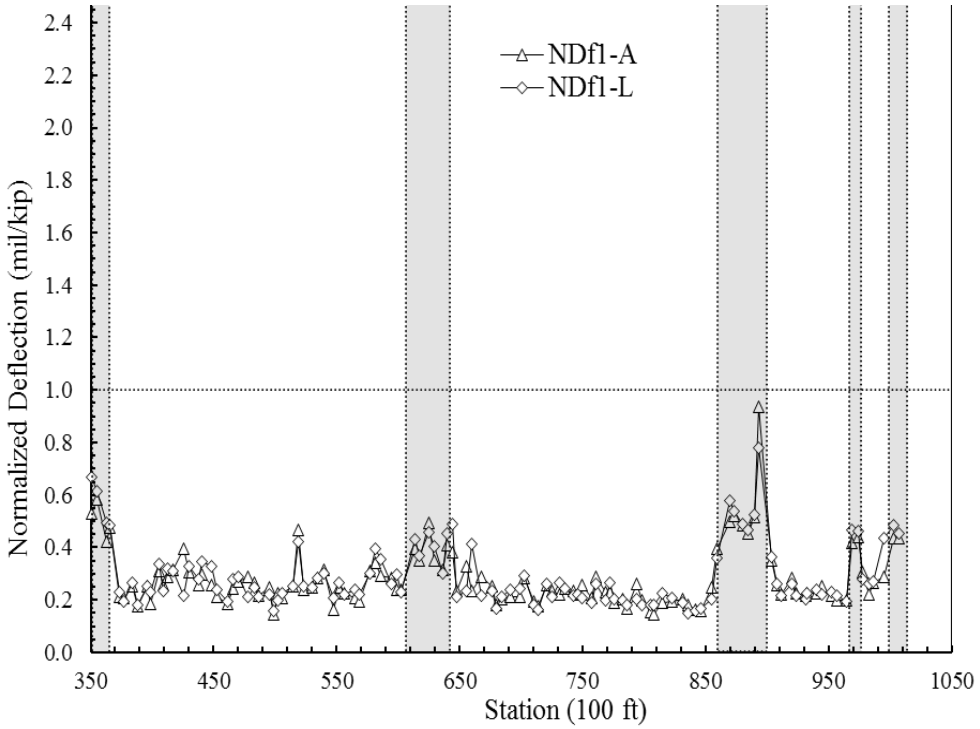

Figure 54 I-77 northbound normalized joint deflections (1 mil/kip = 5.71 mm/MN, 100 ft = 30.5 m)

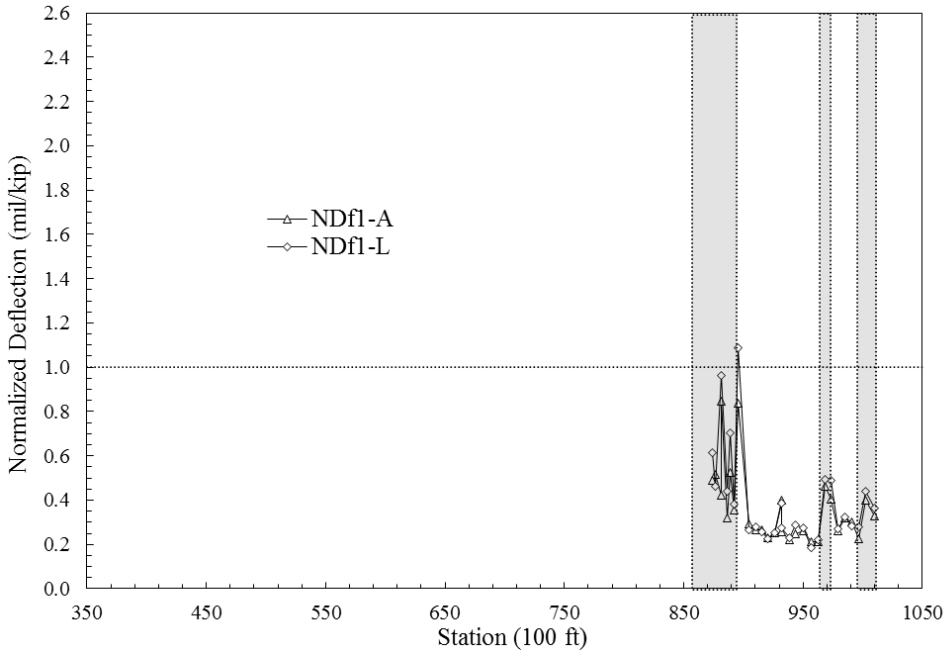

Figure 55 I-77 southbound normalized joint deflections (1 mil/kip = 5.71 mm/MN, 100 ft = 30.5 m)

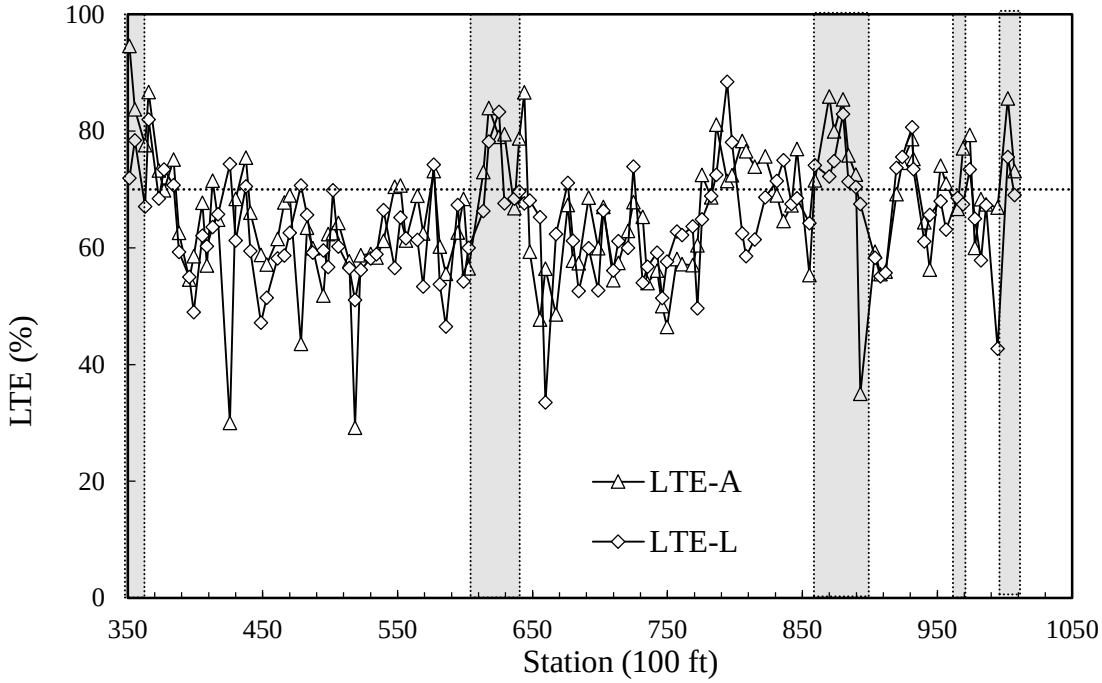

Figure 56 I-77 northbound load transfer efficiency (LTE) (100 ft = 30.5 m)

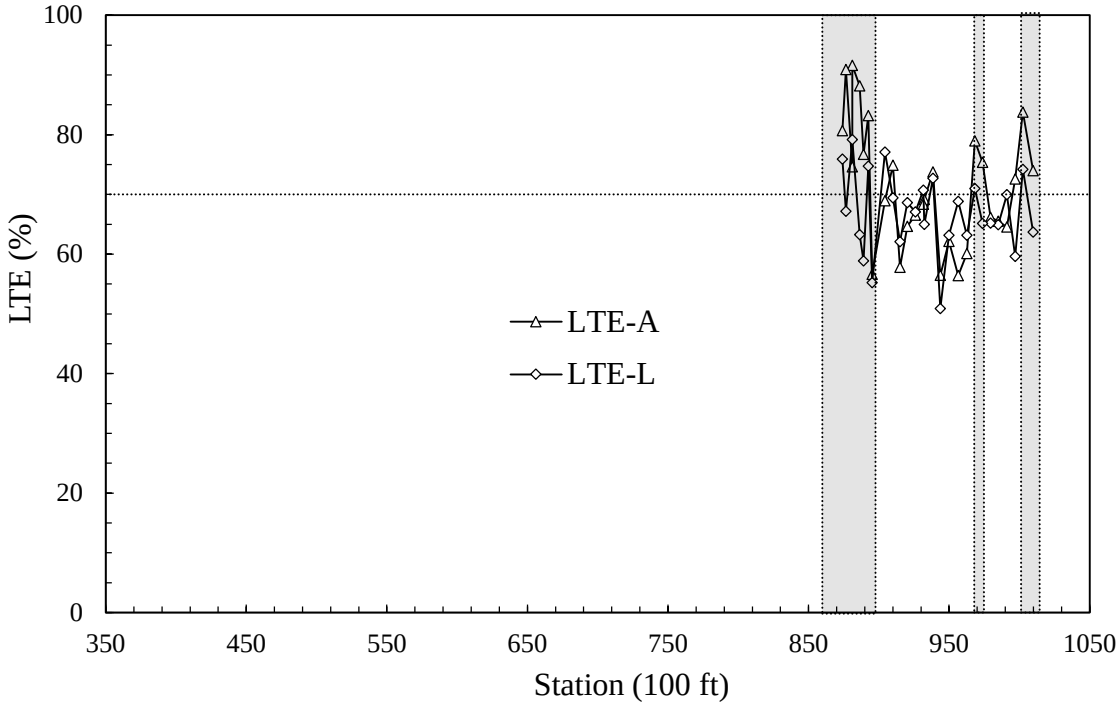

Figure 57 I-77 southbound load transfer efficiency (LTE) (100 ft = 30.5 m)

5.4.2 FWD test results on selected section

For WAS/NOB-77, the selected northbound control section extended from Station 824+01 to Station 825+81, running from state mile marker 15.57 to 15.60. The control section length is

180 ft (55 m), consisting of 12 slabs. This section was selected to represent an undamaged or control section that had endured normal wear. The selected damaged segment extended from southbound Station 25+38 to Station 3+43, running from state mile marker 18.03 to 18.07. The length is 195 ft (59 m), consisting of 13 slabs. This distressed section was selected to represent deteriorated pavement. The locations of the selected sections are shown in Figure 48. The distresses of the selected sections were mapped as shown in Figure 58. Detailed FWD measurements were made on October 8, 2015.

Figure 59 shows the LTE results of the selected damaged and control sections. The LTE results are generally good on both sections, above 70% with one exception on the control side. Figure 60 shows the normalized deflections of the selected sections. I-77 control and distressed sections showed small and uniform joint deflections, most of which are below 0.25 mil/kip. Figure 61 and Figure 62 respectively present the JSR and SPR results of selected control and distressed sections.

High LTE of joints in the distressed section in the southbound direction may include contributions from temperature-induced horizontal compressive stress in the concrete pavement pushing slabs together and creating aggregate interlock or increased friction. Coring verified the previous evaluation of joint condition. For example, the last joint in the control section in the northbound direction was cored and found to have a horizontal crack at the dowel bar level.

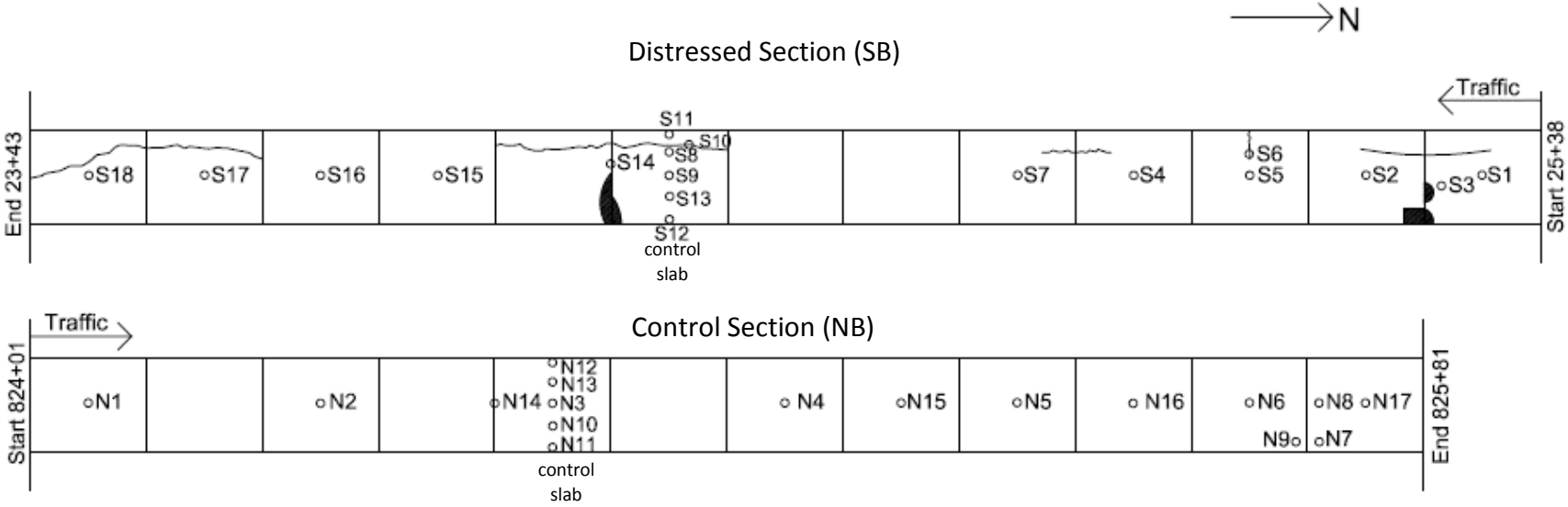

Figure 58 Distress map and coring plan for WAS/NOB-77

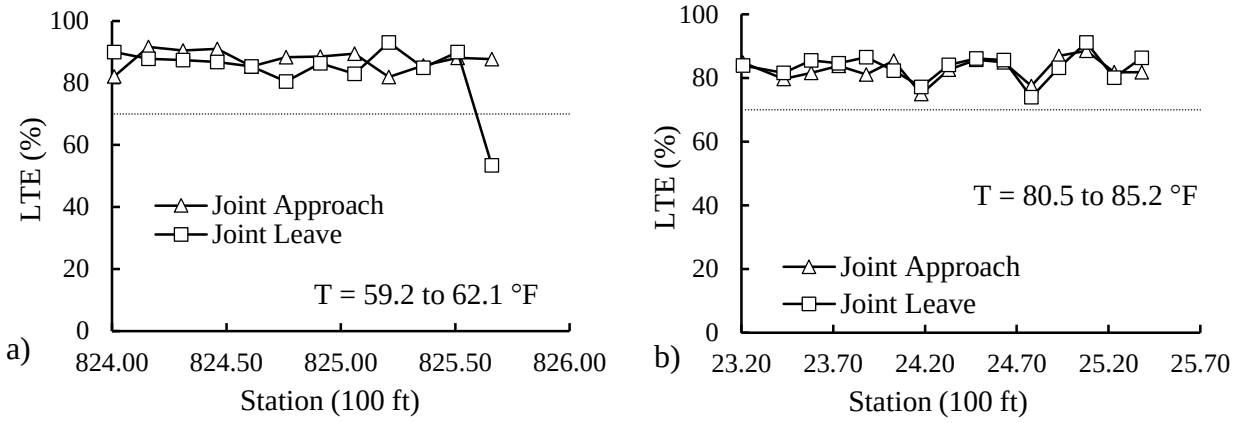

Figure 59 a) I-77 NB control section Load Transfer Efficiency; b) I-77 SB distressed section Load Transfer Efficiency (100 ft = 30.5 m). (T = pavement surface temperature)

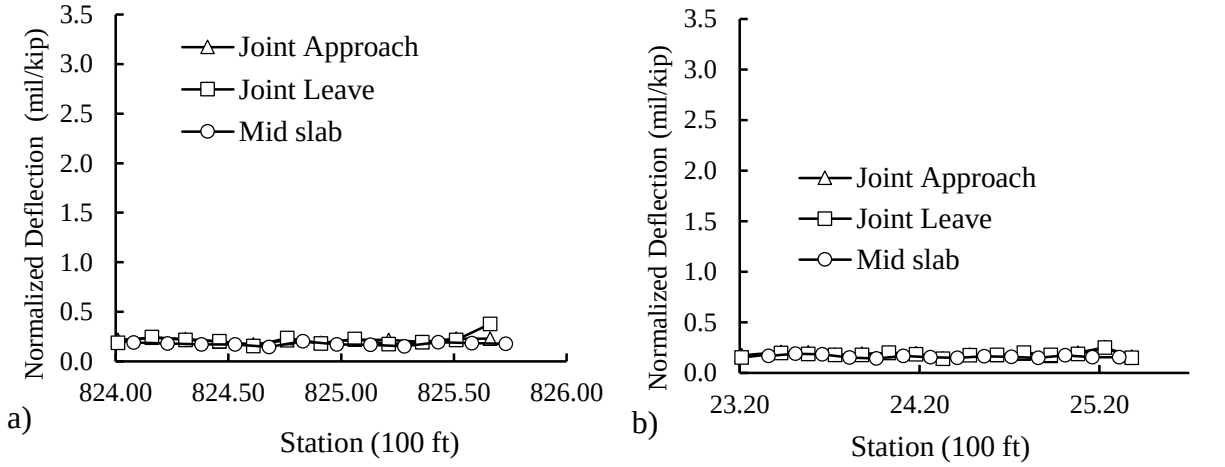

Figure 60 a) WAS/NOB-77 NB control section Normalized Deflections; b) WAS/NOB-77 SB distressed section Normalized Deflections (1 mil/kip = 5.71 mm/MN, 100 ft = 30.5 m).

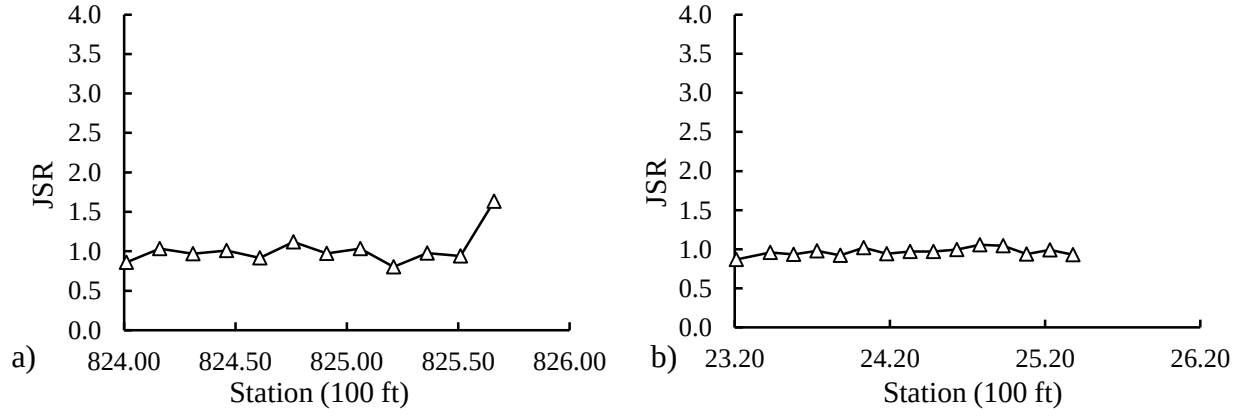

Figure 61 a) WAS/NOB-77 NB control section JSR; b) WAS/NOB-77 SB distressed section JSR (100 ft = 30.5 m).

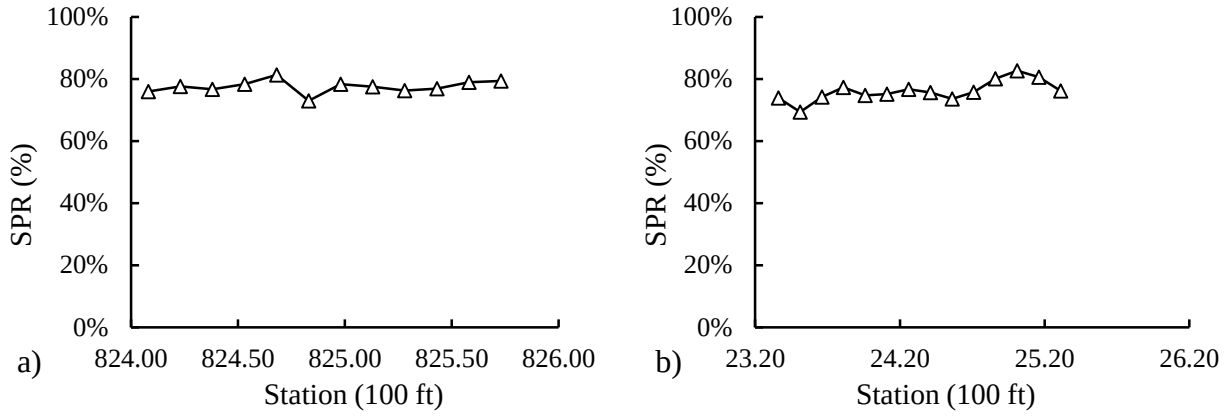

Figure 62 a) WAS/NOB-77 NB control section SPR; b) WAS/NOB-77 SB distressed section SPR (100 ft = 30.5 m).

5.5 MITScan and dowel bar misalignment

MITScan readings were made on I-77 by ODOT on November 10, 2015. Joints were scanned in each direction, 13 northbound and 13 southbound, with 12 dowel bars per joint. Both directions showed poor dowel bar alignment, as shown in Table 15. The biggest contrast was in the Horizontal Translation category, where 76.4% of bars were acceptable, though the rejection rate was 0.0%; however, the control section had an acceptance rate of only 2.0%, and a rejection rate of 75.0%. However, the two directions are much more comparable when the dowel bar spacing is considered instead of the horizontal translation. The acceptance rate for the distressed (control) section is 94.7% (91.4%), and the rejection rate is 0.0% for both. Detailed tables of the MITScan data are in Appendix B.

Table 15 Distribution of dowel misalignment in selected WAS/NOB-77 sections, as of November 10, 2015. Acceptance and rejection criteria are from Table 3.

Section	Type of Misalignment	accept		reject	No. Bars
		$\|d\| \leq 0.5$	$0.5 < \|d\| \leq 0.7$	$\|d\| > 0.7$	
SB (distressed)	Horizontal Rotation	89.6%	7.6%	2.8%	144
	Vertical Rotation	63.9%	16.7%	19.4%	144
		$\|d\| \leq 0.5$	$0.5 < \|d\| \leq 0.66$	$\|d\| > 0.66$	
	Depth Translation	98.6%	1.4%	0.0%	144
		$\|d\| \leq 2$	$2 < \|d\| \leq 2.3$	$\|d\| > 2.3$	
	Longitudinal Translation	79.9%	9.7%	10.4%	144
		$\|d\| \leq 0.5$	$0.5 < \|d\| \leq 2$	$\|d\| > 2$	
	Horizontal Translation	76.4%	23.6%	0.0%	144
	Dowel Bar Spacing	94.7%	5.3%	0.0%	131
Section	Type of Misalignment	$\|d\| \leq 0.5$	$0.5 < \|d\| \leq 0.7$	$\|d\| > 0.7$	# Bars
NB (control)	Horizontal Rotation	69.7%	20.4%	9.9%	152
	Vertical Rotation	83.6%	11.8%	4.6%	152
		$\|d\| \leq 0.5$	$0.5 < \|d\| \leq 0.66$	$\|d\| > 0.66$	
	Depth Translation	84.9%	9.2%	5.9%	152
		$\|d\| \leq 2$	$2 < \|d\| \leq 2.3$	$\|d\| > 2.3$	
	Longitudinal Translation	90.1%	6.6%	3.3%	152
		$\|d\| \leq 0.5$	$0.5 < \|d\| \leq 2$	$\|d\| > 2$	
	Horizontal Translation	2.0%	23.0%	75.0%	152
	Dowel Bar Spacing	91.4%	8.6%	0.0%	139

5.5.1 Dowel Bar Inserter

Figure 63 has photos taken during the construction of WAS/NOB-77. As shown in the photos, a dowel bar inserter (DBI) was used; dowel bar baskets were used in the construction of MAD-70. The use of dowel bar inserter may have contributed to the misalignment of dowel bars in WAS/NOB-77 sections. The other concern associated with the inserter is the adequacy of consolidation of concrete over the inserted bars, resulting in segregation of aggregate. This is a result of the insertion process, which involves the inserter vibrating the bar while pushing it into the concrete. The vibrations have the effect of pushing larger pieces of aggregate down or to the

side of the bar, so that the concrete that fills the hole over the bar tends to have smaller aggregate and a greater probability of entrapped air voids forming within the concrete or as a gap between the top of the dowel bar and the concrete. As a result, the material properties of the concrete above the dowel bar may differ from that below the bar, for example the strength and modulus, as reported by Larson, Vanikar, and Forster [1993]. Over the long term, the concrete near the dowel bars can then be subject to vertical longitudinal cracking, horizontal cracking, and defects associated with the air voids in the concrete and/or directly above the dowel bar.

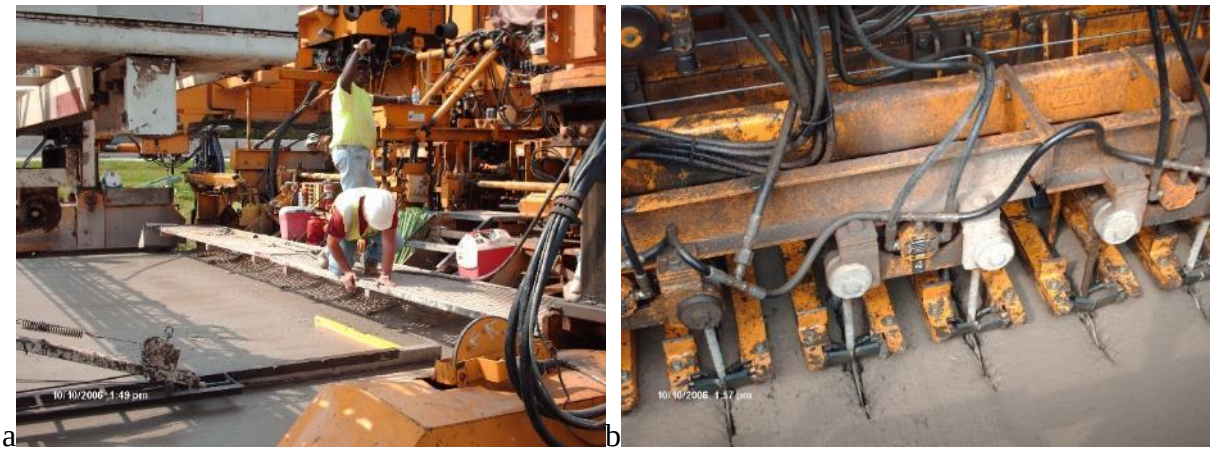

Figure 63 Pictures of DBI used in construction of WAS/NOB-77. Photos dated October 10, 2006.

Issues with dowel bar inserters affecting the integrity of the concrete above the dowel were previously identified on the WAY-30 test road, though after publication of the technical reports [Sargand, Figueroa, and Romanello, 2008; Sargand and Figueroa, 2010]. The problem was investigated by collecting several cores at the joints, through the dowel bars. These cores included tangential cores, where the coring device was placed tangent to the joint so that the core was collected from one slab, and on-joint cores, where the coring device was centered over the joint directly over a dowel bar, collecting equally from both slabs. The tangential cores were then sawn in vertically with the cut line parallel to the dowel bar, with cuts extending from either end of the core to the dowel bar. Some of these cores were further rotated perpendicularly and sliced into thirds. The on-joint cores were too damaged for this slicing treatment.

Figure 64 shows a tangential core collected at a location on WAY-30 with longitudinal cracking. The crack runs between pieces of aggregate above the dowel bar, while it runs through the aggregate below it, which is an indication that the cement was stronger below. The core is opened at the crack to show one half in Figure 65, where some entrapped air voids are visible, along with a gap above the dowel bar and some corrosion of the steel. Figure 66 shows a tangential core before cutting; note the gap visible above the dowel bar. Figure 67 shows two sliced cores with the dowel bars exposed; the bar in the half-core on the right is held in place with adhesive tape, which can also be seen in Figure 68, along with the space above the bar. Figure 69 shows the other half-core, which also has some space above the bar, but also some large entrapped air voids showing some moisture intrusion. Figure 70 shows the middle slices from two WAY-30 tangential cores, showing more evidence of entrapped air voids and smaller aggregate above the dowel bars.

Figure 64 Tangential core collected over a dowel bar from WAY-30 at a location with a longitudinal crack. Note crack runs between aggregate above dowel bar, then runs through the aggregate underneath, indicating the concrete is stronger underneath.

Figure 65 Tangential core with longitudinal crack, opened to show deterioration of concrete, gap above dowel bar, and corrosion of bar.

Figure 66 Uncut tangential core form WAY-30 showing gap above dowel bar.

Figure 67 Two tangential cores collected at a joint on WAY-30, after sawing in half.

Figure 68 Close-up of tangential core from WAY-30 showing space above dowel bar and some entrapped air voids. Note that the dowel bar is held in place with clear adhesive tape.

Figure 69 Close-up of tangential core from WAY-30 showing entrapped air voids and moisture penetration above dowel bar.

Figure 70 Slices from WAY-30 tangential cores showing more detail of entrapped air voids in area above dowel bars.

5.6 PCC Coring

The procedures used to collect cores described in Section 3.6 were followed to obtain cores from I-77 on October 8, 2015. The coring plan is presented in Figure 58 above. Bondbreaker was found in almost all core holes, except S4 and S7. The thickness of the bondbreaker was significantly greater than the design thickness of 1 in (25 mm). Figure 71 shows a core (N14) collected from WAS/NOB-77 northbound at a joint away from a dowel bar. Figure 72 shows a core (N7) drilled near a joint on the northbound side showing a horizontal crack at dowel bar level, while Figure 73 shows a more severe horizontal crack in a core (S14) near a joint in the southbound direction. Even though longitudinal cracking was not widespread, there were differences in the concrete above and below the dowel bar due to the DBI vibrations.

Figure 71 Core collected at a joint on WAS-NOB-77 northbound.

Figure 72 Horizontal crack at dowel level near joint from northbound side of WAS/NOB-77.

Figure 73 Core with horizontal crack at dowel level from southbound side of WAS/NOB-77.

5.7 Laboratory testing results

In total 35 cores were collected from WAS/NOB-77, following the coring plan in Figure 58; 20 cores were sent to Dr. Jan Olek of Purdue University for petrographic analysis, and the remaining 15 were used in laboratory tests at Ohio University, following the same methods used for MAD-70. The thicknesses of the PCC overlay and AC bondbreaker in each direction are presented in Table 16. The average thickness of the PCC overlay is 8.2 in (208 mm) for NB control section and 8.4 in (213 mm) for SB distressed section. The average thickness of AC bondbreaker is 2.9 in (74 mm) for NB control section and 2.2 in (56 mm) for SB distressed section. The bondbreaker thickness is significantly greater than the design thickness of 1 in (25 mm). ODOT District 10 personnel confirmed a second lift of asphalt was placed to achieve a smooth surface on which to place concrete. The rest of the thicknesses are within range compared to typical values. A summary of testing results are presented in Table 17 for the northbound direction and in Table 18 for the southbound direction; detailed test data can be found in Appendix C. The obtained splitting tensile strength is 880 psi from NB and 895 psi from SB, which are relatively high; other properties were comparable to standard values.

Table 16 Thickness of PCC and AC bondbreaker layers of WAS/NOB-77

Direction		PCC Thickness					Bondbreaker Thickness				
		Max.	Min.	Avg.	C_V (%)	#Cores	Max.	Min.	Avg.	C_V (%)	#Cores
NB (control)	(in)	8.5	7.8	8.2	1.9	17	3.2	2.7	2.9	7.1	17
	(mm)	216	198	208			81	69	74		
SB (distressed)	(in)	8.9	8.1	8.4	2.4	18	2.8	1.1	2.2	24.7	15
	(mm)	226	206	213			71	28	56		

Table 17 I-77 NB control section cores laboratory testing summary

Core	Compressive strength ($f'c$)		Tensile strength		Elastic modulus (E)		Poisson's ratio (υ)	CTE (α)	
	(psi)	(MPa)	(psi)	(MPa)	(10^6psi)	(GPa)		(10^{-6}/°F)	(10^{-6}/°C)
N2	8760	60.40							
N4	9030	62.26							
N15	8960	61.78			4.02	27.72	0.17		
N5			870	6.00					
N9			915	6.31					
N16			850	5.86					
N17								5.09	9.16
NB Avg	8920	61.50	880	6.07	4.02	27.72	0.17	5.09	9.16

Table 18 I-77 SB distressed section cores laboratory testing summary

Core	Compressive strength ($f'c$)		Tensile strength		Elastic modulus (E)		Poisson's ratio (υ)	CTE (α)	
	(psi)	(MPa)	(psi)	(MPa)	(10^6psi)	(GPa)		(10^{-6}/°F)	(10^{-6}/°C)
S2	9570	65.98							
S4	8320	57.36							
S7	8260	56.95			5.01	34.54	0.16		
S5			970	6.69					
S6			895	6.17					
S18			760	5.24					
S16								4.87	8.77
SB Avg	8720	60.12	875	6.03	5.01	34.54	0.16	4.87	8.77

5.8 Petrographic analysis

Figure 74 and Figure 75 show the list of tested specimens and their locations on WAS/NOB-77. Cores N8 and N14 from northbound lanes and Cores S3, S10, and S14 from southbound lanes were used for SEM analysis. Cores N3 and N12 from northbound lanes and Cores S3 and S9 from southbound lanes were used for air voids analysis. Findings from SEM analysis of the cores are presented below from the subcontractor report by Dr. Jan Olek of Purdue University:

S3:

- Most air voids were filled with ettringite.
- Few chloride deposits were found in calcium silicate hydrate gel.
- Cracks were found around air voids filled with ettringite.

S10:

- Most air voids were filled with ettringite.
- Deposits of Friedel's salt were found.
- A carbonated layer was found on the top surface.
- Few cracks were filled with ettringite.

S14:

- Extensive deposits of ettringite were located in the in air voids, cracks and in the interfacial transition zone.
- The highest volume of ettringite was found among all the samples, concentrated in the big (170-200 μm (6.7-7.9 mil)) air voids.
- Microcracking was observed in association with the ettringite deposits.

N8:

- Ettringite deposits compromised the air void system.
- No chloride was detected in the bottom sample.

N14:

- The top portion of the sample extracted from the top of the core had high content of unhydrated cement particles.
- The sample extracted from the top of the core showed higher chlorides in CSH and as Friedel's salt whereas no chloride was detected in the sample extracted from the bottom of the core.

- Higher infilling of air voids with ettringite was observed in the sample extracted from the bottom of the core compared to the sample extracted from the top of the core.

Table 19 presents the air void analysis results. Air voids of all tested specimens were acceptable. The spacing factor of Cores N3 and N12 exceeded the maximum value of 0.008 in (0.20 mm), which means potentially reduced freeze-thaw durability.

Table 19 Summary of the air void analysis of cores from WAS/NOB-77

		Northbound (control)		Southbound (distressed)	
Core ID		N3	N12	S3	S9
Air void content		3.85%	4.87%	8.00%	7.07%
Paste content		21.7%	22.3%	22.6%	21.6%
Spacing factor	(in)	0.014	0.013	0.0067	0.005
	(mm)	0.35	0.33	0.169	0.132

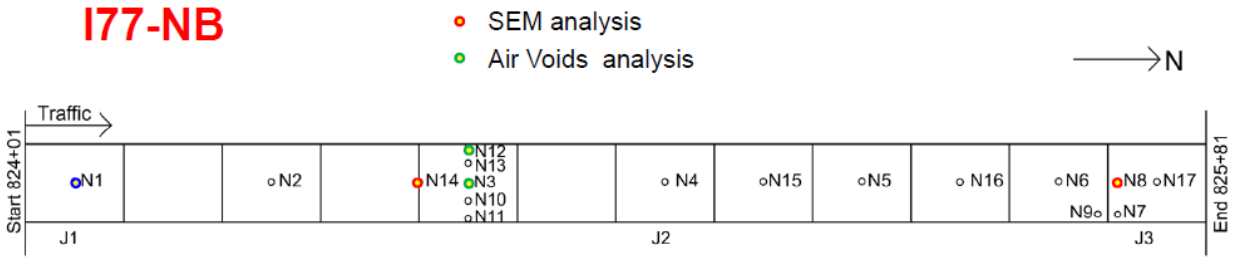

I77 Northbound Core Sample Profile

#	Station	Destination	Notes	#	Station	Destination	Notes
N1	824+9	Purdue		N10	824+69	Purdue	
N2	824+39	OU		N11	824+69	Purdue	
N3	824+69	Purdue		N12	824+69	Purdue	
N4	824+99	OU		N13	824+69	Purdue	
N5	825+29	OU		N14	824+61	Purdue	
N6	825+59	Purdue		N15	825+14	OU	
N7	825+67	OU	horizontal crack	N16	825+34	OU	
N8	825+67	Purdue		N17	825+64	OU	
N9	825+65	OU					

Figure 74 Location map and list of petrographic cores collected on WAS/NOB-77 northbound. From report by Dr. Jan Olek of Purdue University.

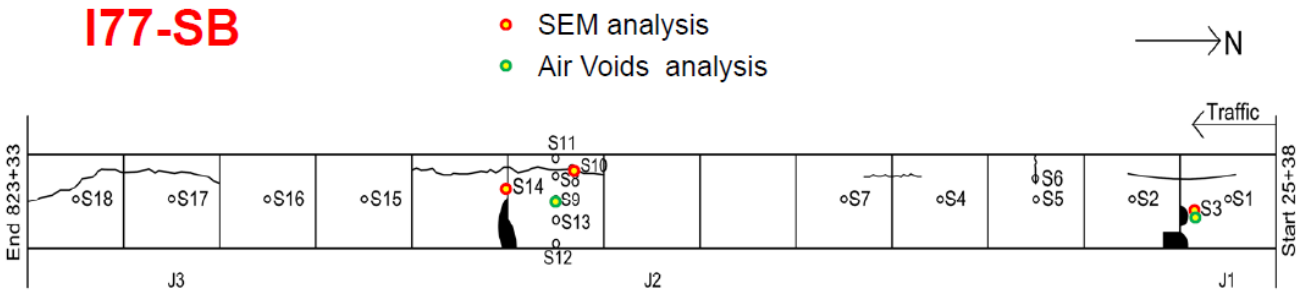

I77 Southbound Core Sample Profile							
#	Station	Destination	Notes	#	Station	Destination	Notes
S1	25+30	Purdue		S10	24+26	Purdue	
S2	25+15	OU		S11	24+25	Purdue	
S3	25+19	Purdue		S12	24+25	Purdue	
S4	24+85	OU		S13	24+25	Purdue	
S5	25+00	OU		S14	24+17	Purdue	horizontal crack in approach slab
S6	25+00	OU		S15	23+94	OU	
S7	24+70	OU		S16	23+79	OU	
S8	24+25	Purdue		S17	23+64	Purdue	
S9	24+25	Purdue		S18	23+49	OU	

Figure 75 Location map and list of petrographic cores collected on WAS/NOB-77 southbound. From report by Dr. Jan Olek of Purdue University.

5.9 HIPERPAV Results

Original HIPERPAV runs were obtained from ODOT. The inputs were examined and re-run. In total 13 construction days were examined. Class C Option 3 concrete from ODOT specifications was used with the mix design given in Table 20. The water to cementitious material ratio was 0.42, and the aggregate type was siliceous gravel. Type D admixture was used. A single coat curing method was applied. Other inputs including weather data were kept the same as the original runs. Table 21 shows selected construction dates and temperatures, which were extracted from original files. The selected dates were actual dates that mainline UBCOs were constructed. All of the construction days passed the HIPERPAV analysis. Appendix D shows the analysis results for each construction day.

Table 20 WAS/NOB-77 PCC mix design.

Density unit	Coarse Aggregate	Fine Aggregate	Cement (Type I)	Water	GGBF Slag	Total
(lb/yd^3)	1667	1167	385	229	165	3613
(kg/m^3)	989	692	228	136	98	2143

Table 21 HIPERPAV analysis results for all construction days on WAS/NOB-77.

Direction	Day number	Date	Air temperature (°F)		Air temperature (°C)		Analysis result (pass/fail)
			low	high	low	high	
NB	1	5/24/2006	58	74	14.4	23.3	pass
	2	5/30/2006	67	91	19.4	32.8	pass
	3	6/7/2006	57	76	13.9	24.4	pass
	4	6/8/2006	56	77	13.3	25.0	pass
	5	6/9/2006	49	75	9.4	23.9	pass
SB	6	7/6/2006	51	75	10.6	23.9	pass
	7	7/7/2006	55	79	12.8	26.1	pass
	8	7/14/2006	68	83	20.0	28.3	pass
NB	9	9/7/2006	54	77	12.2	25.0	pass
	10	9/8/2006	55	80	12.8	26.7	pass
	11	9/11/2006	60	77	15.6	25.0	pass
	12	9/14/2006	55	2	12.8	-16.7	pass
	13	9/15/2006	54	73	12.2	22.8	pass

5.10 Findings

Key findings from the forensic investigation of the overlay on WAS/NOB-77 are summarized below:

- Longitudinal cracking is the predominant type of distress observed.
- There were differences in the concrete above and below the dowel bar due to the DBI vibrations.
- The asphalt bondbreaker thickness is significantly thicker than the plan thickness of 1 in (25 mm), averaging 2.9 in (74 mm) on NB and 2.2 in (56 mm) on SB. Two lifts of asphalt were placed during construction to make the surface level before placing the concrete.
- Laboratory testing shows good material strength and properties for the concrete.
- Poor dowel bar alignment was found on the selected sections. For example, 19.4% of scanned dowel bars exceeded ODOT dowel bar vertical rotation alignment rejection criteria on SB section (distressed section). The dowel bar inserter may have contributed to the dowel misalignment.
- A horizontal crack was found on a core at dowel bar level near the joint. It was likely caused by dowel bar misalignment.

6 I-90 in Lake County

6.1 Project Information

Project 2005-0518 overlaid the existing 10 in (254 mm) jointed, reinforced, dowelled concrete pavement on I-90 in Lake County (LAK-90) with a 9.5 in (241 mm) jointed, plain, dowelled concrete (ODOT Item 452) on a 1 in (25 mm) asphalt bondbreaker (Item 442) in 2006 and 2007. As of 2014 on the 6-lane portion, ADT = 58,900 and ADTT = 6,690; on the 4-lane portion ADT = 47,120 and ADTT = 6,650. Figure 76 shows the location map of this project. Selected sections are also shown on the map. Longitudinal cracking was observed in the eastbound direction as early as 2012. In 2013, corner breaks and transverse cracking were observed in the eastbound direction; in the westbound direction corner breaks were seen in 2014 and transverse cracking in 2015. Faulting in the westbound direction was observed in 2014. Both directions were patched with full-depth concrete repairs in 2015. The longitudinal cracking included multiple hairline cracks present in nearly every slab.

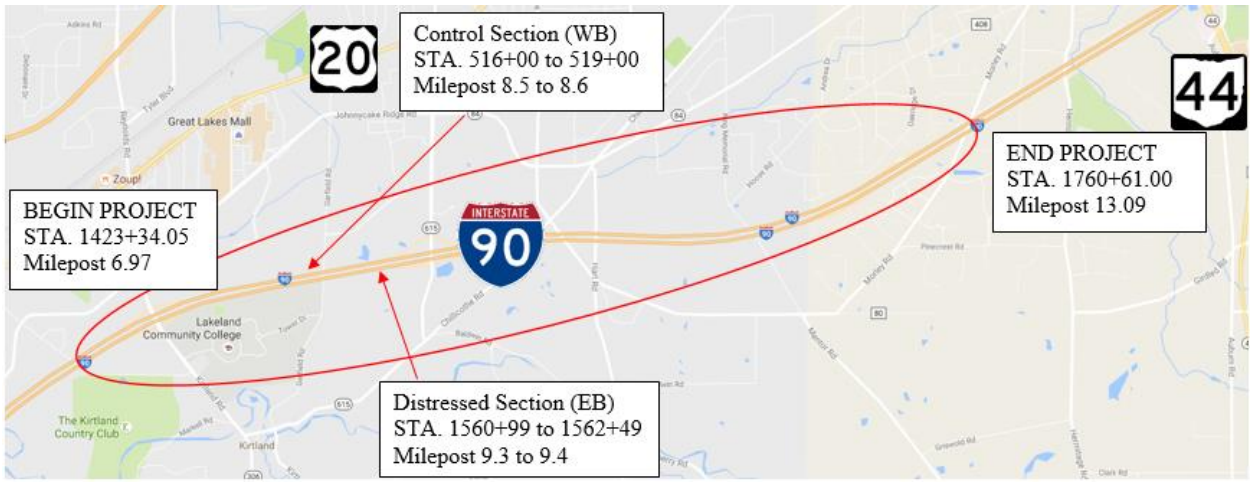

Figure 76 Location map of LAK-90.

6.2 Visual Assessment

Figure 77 below shows longitudinal cracking found on both directions of LAK-90 during a visual assessment on August 5, 2016.

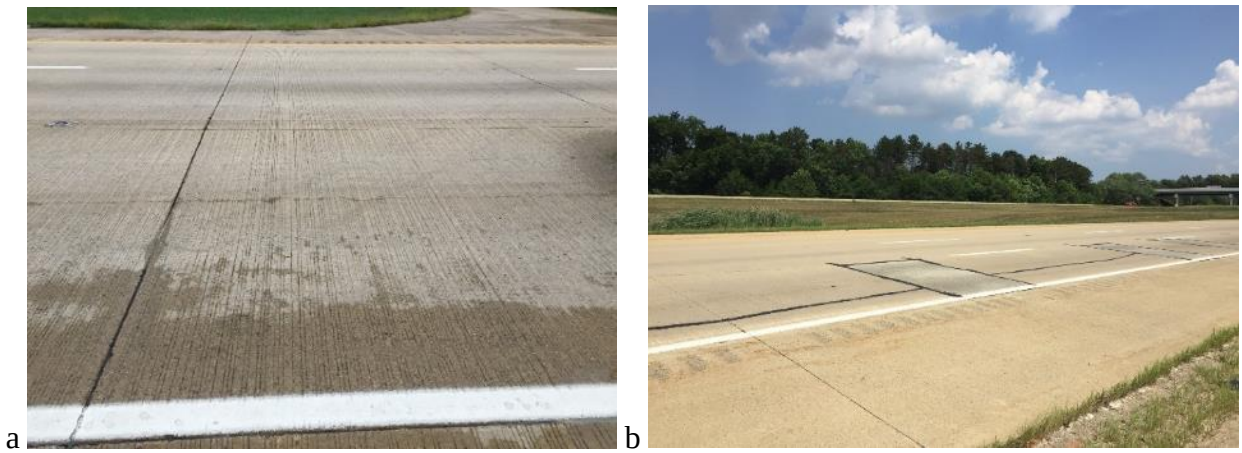

Figure 77 a) longitudinal cracking on WB I-90; b) repaired longitudinal cracking on EB I-90. Photos taken August 5, 2016.

6.3 Distress Survey

The distress survey of I-90 was conducted by reviewing PathWeb images provided by ODOT from their most recent survey on July 28, 2014. The number of cracks per every 0.1 mile (0.16 km) was counted by reviewing the images, such as Figure 5 and the numbers were plotted with respect to mile marker; the results are shown in Figure 78 and Figure 79 for eastbound and westbound directions, respectively. Shaded areas indicate full-depth concrete pavement sections (PCC thickness=13 in (330 mm)). As can be seen from the plot, on the eastbound direction, the maximum amount of cracks occurred between Mile Marker 10.3 and 10.4 with the value of 10 cracks per 0.1 mi (0.16 km). On the westbound direction, the maximum amount of cracks occurred between Mile Marker 12.3 and 12.4 with the value of 14 cracks per 0.1 mi (0.16 km).

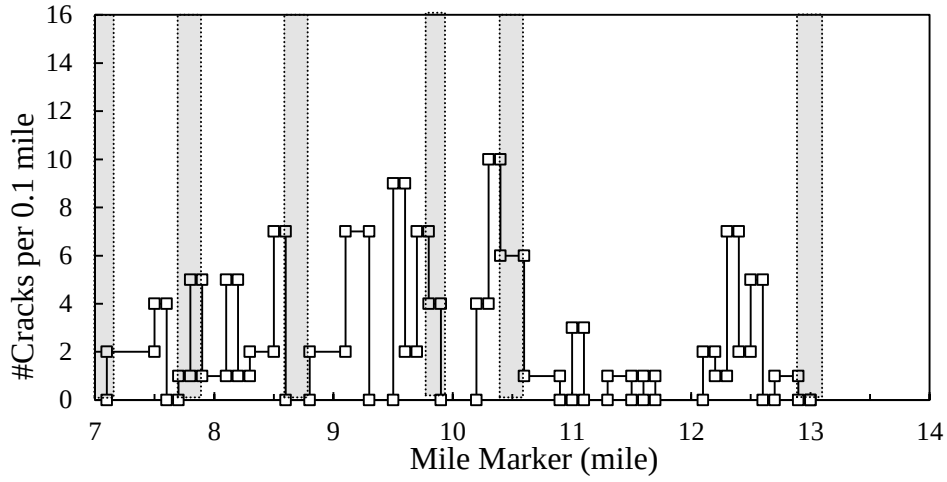

Figure 78 LAK-90 EB cracking plot (1 mi = 1.61 km)

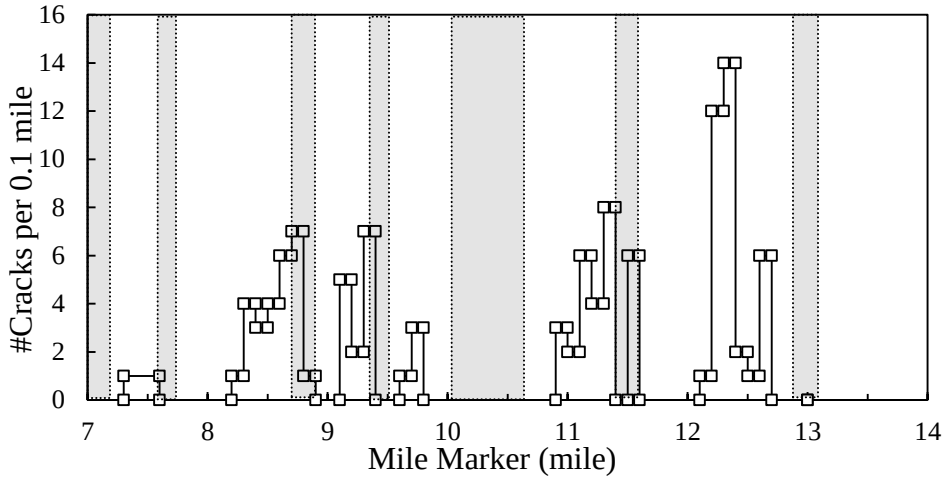

Figure 79 LAK-90 WB cracking plot (1 mi = 1.61 km)

Table 22 below presents major distress identified on LAK-90 based on distress survey and visual assessment. PCR history table provided by ODOT was also used to confirm the distresses. Primary and contributing factors were listed below as provided on the NCHRP PCC distress types and causes table (Table 35 and Table 36). Possible causes were listed based on NCHRP tables as well as researcher's judgement.

Table 22 Major distresses identified on LAK-90 and possible causes

Project	Major Distress	Primary Factors	Contributing Factors	Possible Causes
LAK-90	Transverse Cracking	Design features; Load; Construction	Temperature; Materials	Poor construction practices; materials related problem;
	Longitudinal Cracking	Design features; Load; Construction	Temperature; Materials	

6.4 FWD

6.4.1 Pre-investigation FWD results

Initial FWD measurements were made on LAK-90 on June 15, 2016. Figure 80 and Figure 81 present the normalized joint deflections (NDf_1) of the LAK-90 UBCO sections. LTE results are shown in Figure 82 and Figure 83. The shaded areas indicate full-depth concrete pavement sections. Overall, the normalized joint deflections are below 1 mil/kip, except for joint-leave deflection at mile marker 10.602 and joint-leave defection at 12.998 on the westbound direction, which are 1.578 mils/kip and 1.164 mils/kip. These two locations are full-depth concrete. In the LTE plots, these two joints had very low LTE values of 9.5% and 20.9% on joint leave position. The rest joints of westbound direction had LTE values above 80% with a few exceptions which are between 80% and 60%. On the eastbound direction, LTE values were above 80% mostly also with a few exceptions as low as 31.9% at mile marker 10.552.

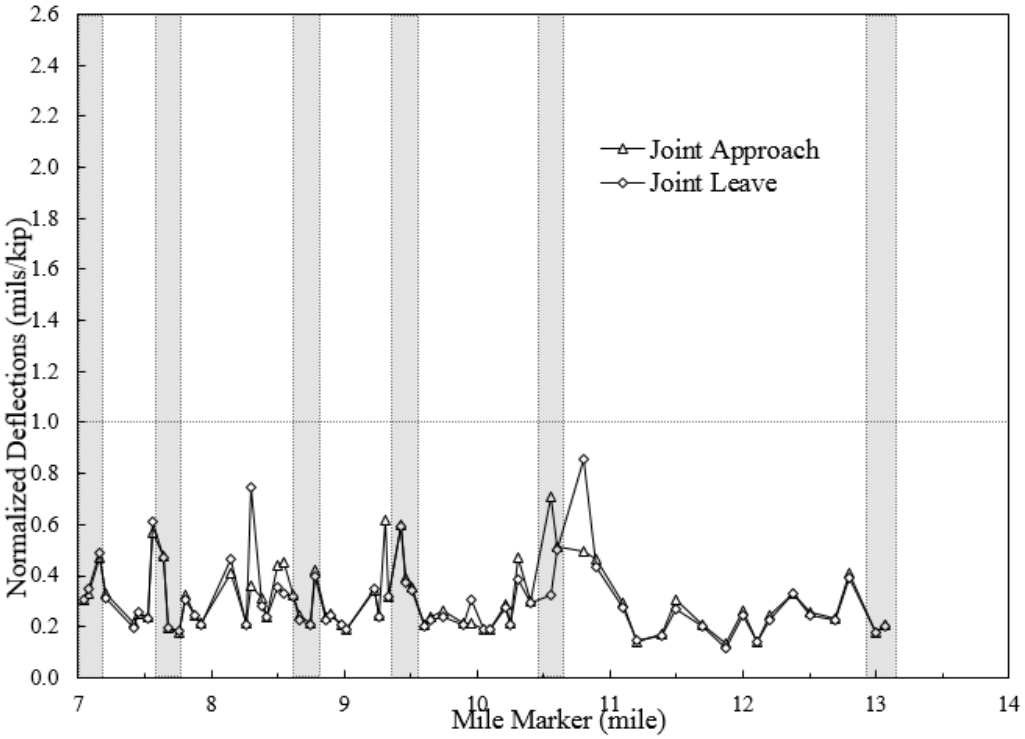

Figure 80 LAK-90 Eastbound Normalized Joint Deflection (1 mil/kip = 5.71 mm/MN; 1 mi = 1.61 km)

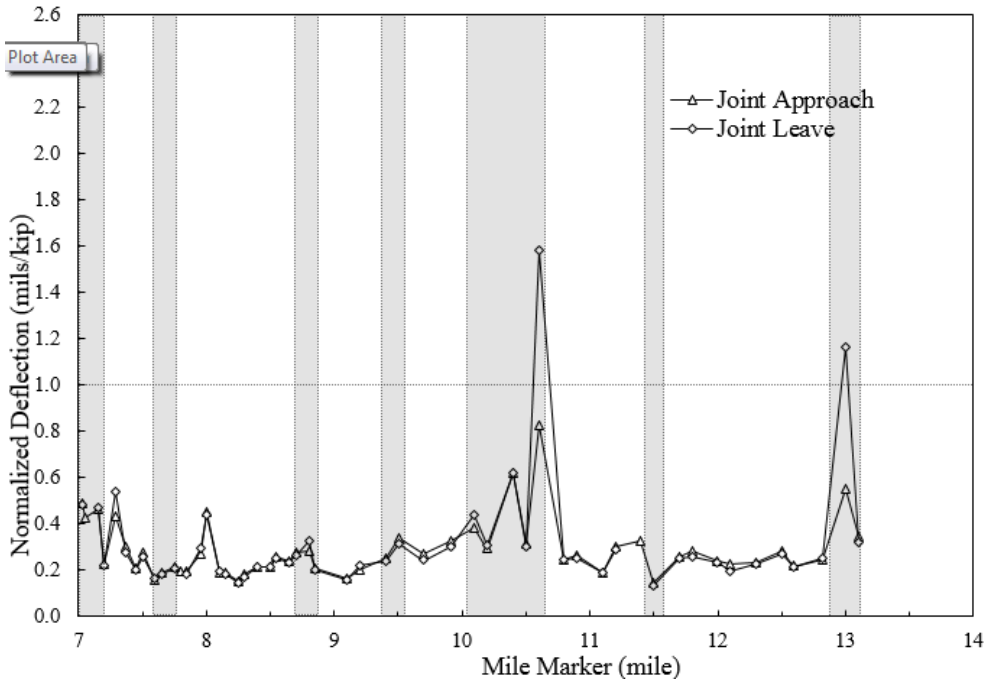

Figure 81 LAK-90 Westbound Normalized Joint Deflection (1 mil/kip = 5.71 mm/MN; 1 mi = 1.61 km).

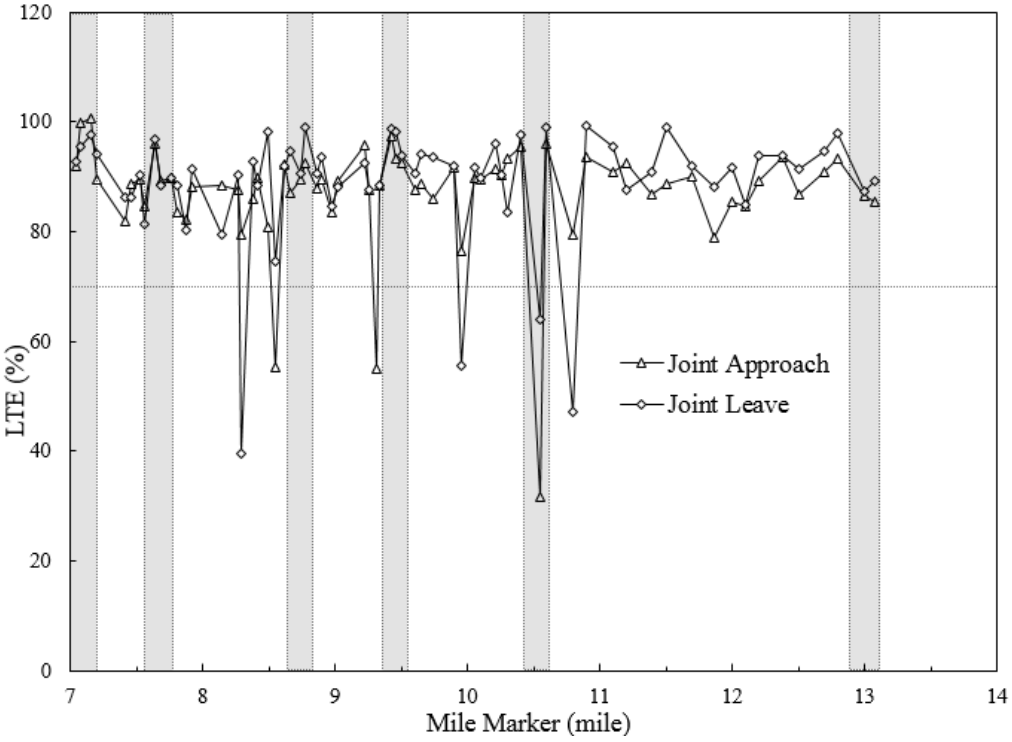

Figure 82 LAK-90 Eastbound Load Transfer Efficiency (1 mi = 1.61 km)

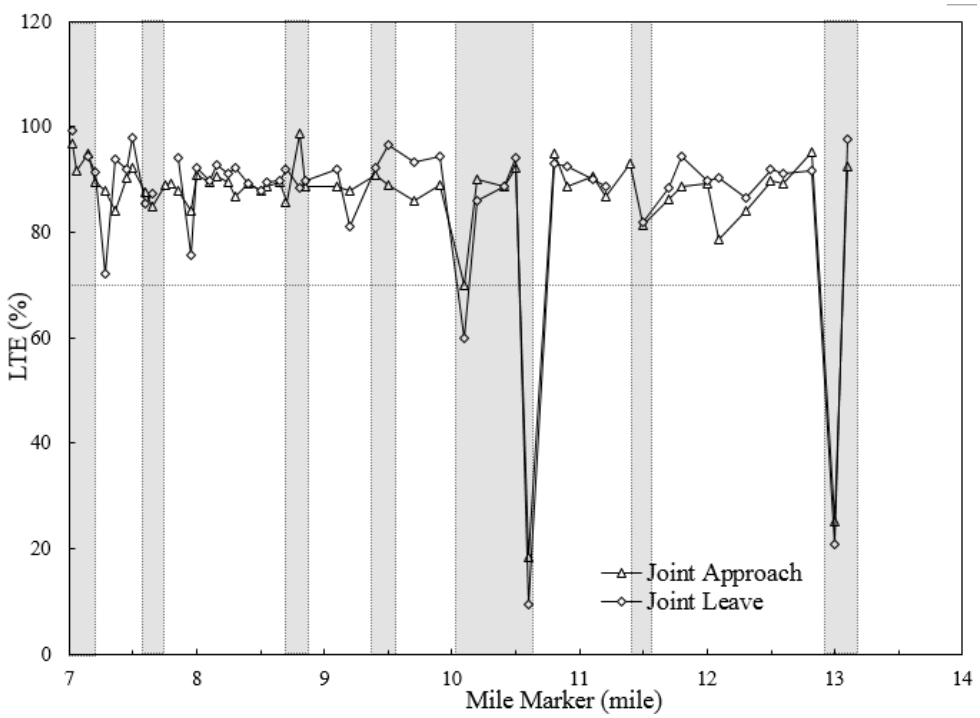

Figure 83 LAK-90 Westbound Load Transfer Efficiency (1 mi = 1.61 km)

6.4.2 FWD results on selected sections

Based on the distress survey and pre-investigation FWD results, a distressed section and a control section were selected for more detailed study. The selected distressed section was from station 1560+99 to 1562+49 in the eastbound direction, milepost 9.3 to 9.4. The selected control section was from station 516+00 to 519+00 in the westbound direction, milepost 8.5 to 8.6. The location of the selected sections are shown in Figure 76. Figure 84 through Figure 87 present FWD results of selected section in each direction, from data collected August 31, 2016. Section from station 1564+00 to 1565+90 in the eastbound direction is full-depth concrete pavement.

Figure 84 presents the LTE results on the selected sections. In the distressed section, LTE values are mostly above 80% with a few exceptions that were below 80%. These points are consistent with joint distress/repair shown on Figure 89. The segment from station 1564+00 to 1565+90 in the distressed section is full-depth concrete pavement. This section had LTE values over 100%. In the control section, all LTE values are near 90%, which indicates good load transfer.

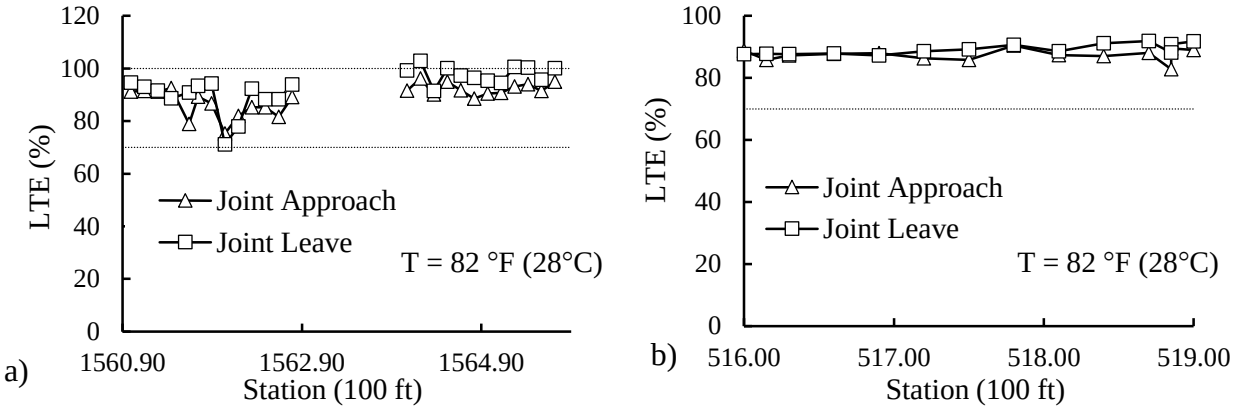

Figure 84 a) LAK-90 EB distressed section Load Transfer Efficiency; b) LAK-90 WB control section Load Transfer Efficiency (100 ft = 30.5 m) (T = pavement surface temperature).

Figure 85 presents the normalized deflections on selected sections. In the distressed section, deflections are generally between 0.2 mil/kip (1.14 mm/MN) and 0.4 mil/kip (2.28 mm/MN) with variations from joint to joint. The full-depth section in the distressed section have higher deflections. In the control section, all deflections are near 0.2 mil/kip (1.14 mm/MN) with much lower variation. Figure 86 presents the Joint Support Ratio (JSR) results, which are close to 1 for both distressed and control sections. Figure 87 presents the spreadability (SPR) results. SPR values are all close to 80%, which indicates good spreadability overall. In summary, based on deflection data, pavement structure was not the cause of the distresses.

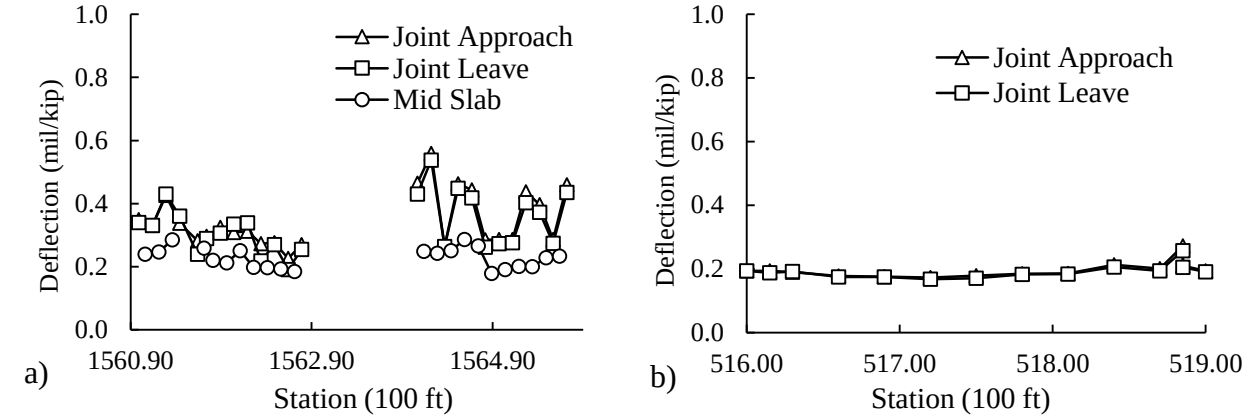

Figure 85 a) LAK-90 EB distressed section Normalized Deflection; b) LAK-90 WB control section Normalized Deflection (1 mil/kip = 5.71 mm/MN, 100 ft = 30.5 m).

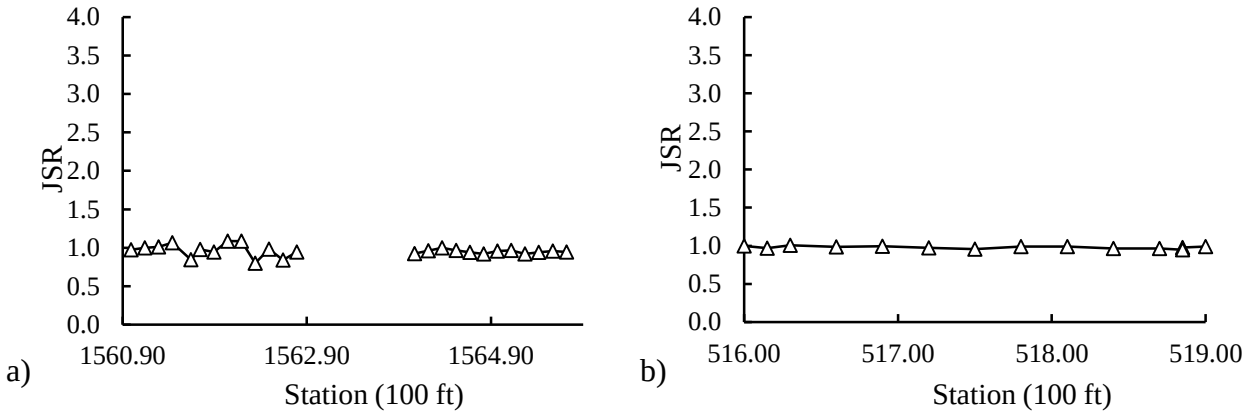

Figure 86 a) LAK-90 EB distressed section Joint Support Ratio; b) LAK-90 WB control section Joint Support Ratio (100 ft = 30.5 m).

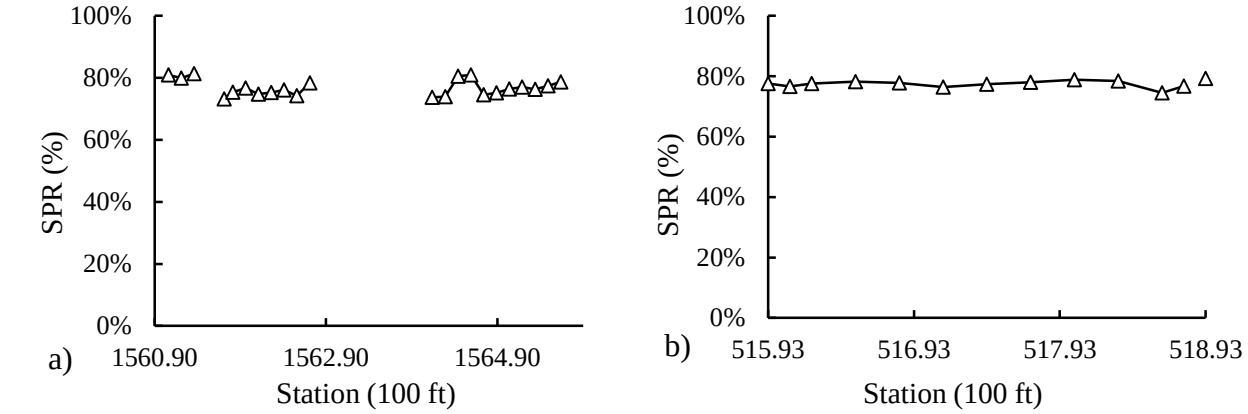

Figure 87 a) LAK-90 EB distressed section Mid-slab Spreadability; b) LAK-90 WB control section Mid-slab Spreadability (100 ft = 30.5 m).

6.5 PCC Coring

Figure 88 shows the drilling process used to collect cores from LAK-90 on August 31, 2016. Figure 89 shows the coring plans on LAK-90. Intact bondbreaker was found in all 18 cores collected.

a)  b) 

Figure 88 a) Core drilling on LAK-90, August 31, 2016; b) Concrete core samples.

6.6 Lab testing results

Table 23 presents the measured thickness of LAK-90 cores. The average thickness of the PCC overlay is 9.6 in (244 mm) on both directions, only slightly greater than the design thickness of 9.5 in (241 mm). The average thickness of AC bondbreaker is 1.1 in (28 mm) on EB and 1.3 in (33 mm) on WB, 10% and 30% greater respectively than the design thickness of 1 in (25 mm). Table 24 presents the lab testing results. The average splitting tensile strength is 635 psi (4.38 MPa). All material strength properties met or exceeded ODOT specifications or design values, except the elastic modulus, which at 3.94 million psi (27.17 GPa) was 21% less than the 5 million psi (34 GPa)

Table 23 Measured Thickness of LAK-90 Cores

Direction	units	PCC overlay thickness			C_V	No.	Bondbreaker thickness			C_V	No.
		Max.	Min.	Avg.	(%)	Cores	Max.	Min.	Avg.	(%)	Cores
EB (distressed)	(in)	9.9	8.9	9.6	3.3	7	1.4	0.9	1.1	13.0	7
	(mm)	251	226	244			36	23	28		
WB (control)	(in)	9.7	9.2	9.6	1.7	11	1.6	1	1.3	13.0	11
	(mm)	246	234	244			41	25	33		

Table 24 LAK-90 Cores Lab Testing Summary (EB = distressed, WB = control section)

Core	Compressive strength ($f'c$)		Tensile strength		Elastic modulus (E)		Poisson's ratio (υ)	Density		CTE (α)	
	(psi)	(MPa)	(psi)	(MPa)	(10^6psi)	(GPa)		(lb/ft^3)	(kg/m^3)	(10^{-6}/°F)	(10^{-6}/°C)
L2 (EB)	6750	46.54			3.94	27.17	0.19	134.8	2159		
L6 (EB)	6990	48.19						135.8	2175		
L17 (WB)	7810	53.85						137.0	2195		
L7 (EB)			595	4.10				134.8	2159		
L8 (WB)			645	4.45				135.4	2169		
L12 (WB)			660	4.55				135.3	2167		
L13 (WB)										5.85	10.53
Average	7180	49.50	635	4.38	3.94	27.17	0.19	135.5	2171	5.85	10.53

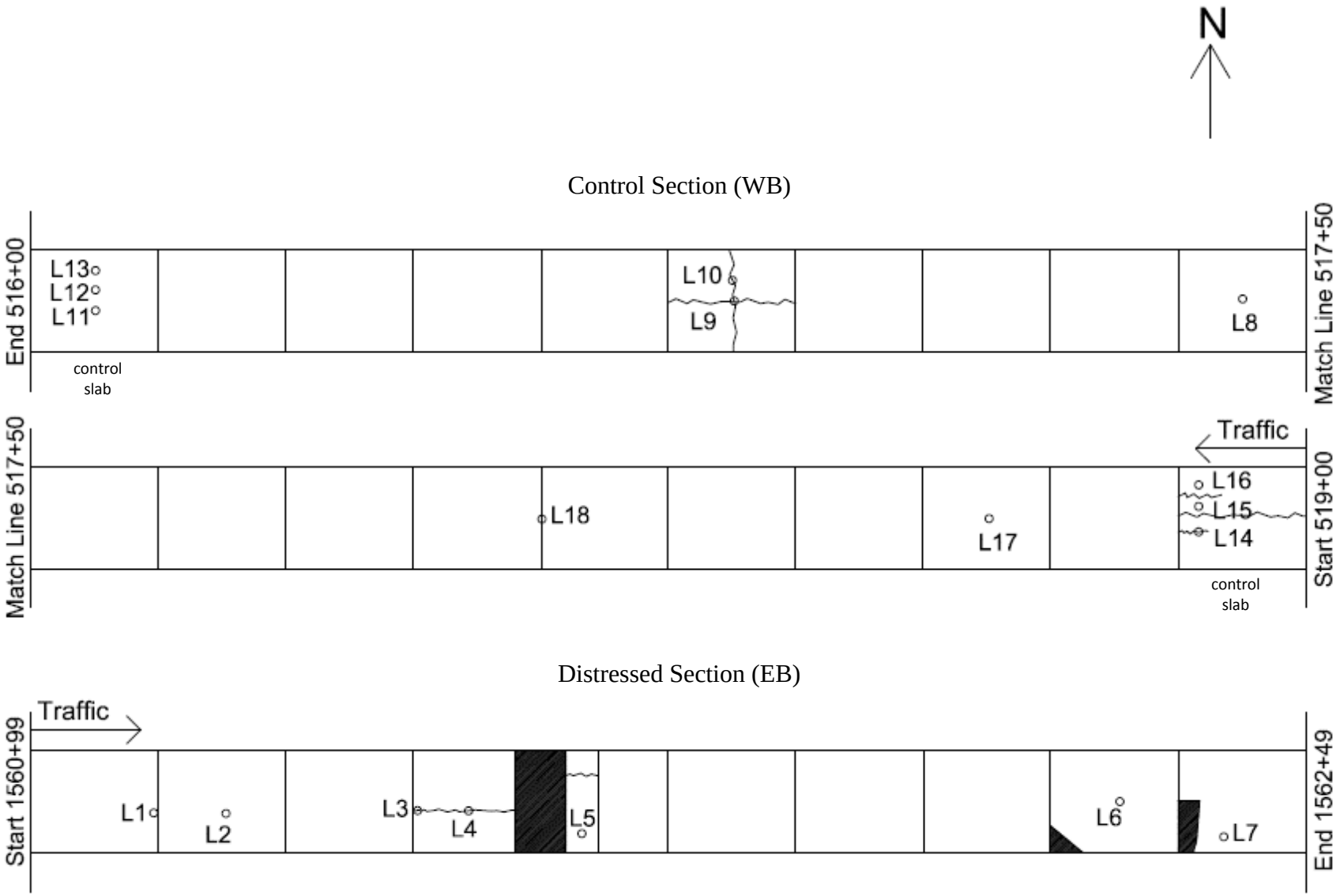

Figure 89 Distress Map and Coring plan on LAK-90.

6.7 Petrographic analysis

Cores L1 and L4 from the distressed eastbound lane and Cores L9 and L18 from the control westbound lane were used for petrographic analysis. Location of the cores can be determined by looking at Figure 89 above. Core L1 was used for specific gravity and coarse slag aggregate analyses, the latter also including Core L18. Results are summarized in Table 25. Findings from the SEM analysis of the cores are presented below from the subcontractor report by Dr. Jan Olek of Purdue University:

L1 (EB) Top:
- Mostly empty air voids of varying sizes.
- Microcracks in the paste.

L1 (EB) Bottom:
- Paste essentially crack free.
- Empty air void system.

L4 (EB) Top:
- Presence of numerous cracks in the paste.
- Cracks are narrow empty and appear to be originating form larger air voids.
- Air voids were empty.
- Numerous deposits of ettringite and Friedel's salt found in the paste matrix.
- Evidence of the slag cement in the matrix.

L4 (EB) Bottom:
- Crack intensity appeared to be higher in L4 bottom compared to that of the L4 top.
- Cracks are narrow empty and appear to be originating form larger air voids.
- Air voids were empty.
- Numerous deposits of ettringite and Friedel's salt were found in the paste matrix.
- Slag cements were found.

L9 (WB) Top:
- Extensive deposition of ettringite and Friedel's salt within the paste matrix.
- Evidence of the slag cement in the matrix.

L9 (WB) Bottom:
- Sample contains slag aggregate.
- Paste showing signs of extensive microcracking that appears to be originating from the numerous (mostly empty) air voids.
- Some of the smaller air voids filled with ettringite.
- Evidence of chlorides within the calcium silicate hydrate gel and monosulfate within the matrix.

L18 (WB) Top:
- Numerous (mostly large (~100μm or 3.9 mil) and empty) air voids.
- Microcracks developing in the matrix between the air voids and (in some cases) along the periphery of the aggregates.
- Smaller air voids filled with ettringite.
- Occasional Friedel's salt deposits within the matrix.

Table 25 Specific gravity and coarse slag aggregate analysis results on LAK-90.

			Specific Gravity		Coarse slag aggregate	
Direction	Core ID	Sample	Bulk	Bulk SSD	Distribution	Proportion
EB (distressed)	L1	top	2.098	2.199	36.7%	36.0%
		bottom	2.104	2.212	34.5%	34.2%
WB (control)	L18	top				37.3%

6.8 HIPERPAV Results

Table 26 presents the PCC mix evaluated with HIPERPAV. Class C Option 3 concrete from ODOT specifications was used. The water to cement ratio is 0.5. Type D admixture was used. Weather data were estimated from three nearby weather stations in Cleveland, Youngstown, and Akron. Actual daily temperature during construction from 2006 to 2007 were collected from National Centers for Environmental Information using their Climate Data Online tool, which reported data from the Kirtland weather station, which is near LAK-90. Figure 90 shows the daily temperatures during the time of construction together with PCC mix temperatures. The daily temperatures were inputted in the HIPERPAV for analysis.

Table 27 shows selected construction dates and temperatures, which were extracted from original files. The selected dates were actual dates that mainline UBCOs were constructed. In total 16 days were analyzed with actual daily temperatures starting from 10/10/2006 to 10/25/2006; 8 days (50%) showed early failure, 7 (44%) where top surface stress exceeded strength, and 2 (12%) where bottom surface stress exceeded strength – October 15, 2006 failed both at the top and the bottom. When the analysis was rerun using without the slag (Type I) cement in the mix, only two days (13%) failed. This suggests that the slag cement slows the curing and strength development in the PCC during the first 72 hours. Temperature, PCC stress, and strength plots of each construction day are attached in Appendix D.

Table 26 LAK-90 PCC Mix Design

Density unit	Coarse Aggregate	Fine Aggregate	Cement (Type I)	Water	GGBF Slag	Total
(lb/yd^3)	1385	1385	385	275	165	3595
(kg/m^3)	822	822	228	163	98	2133

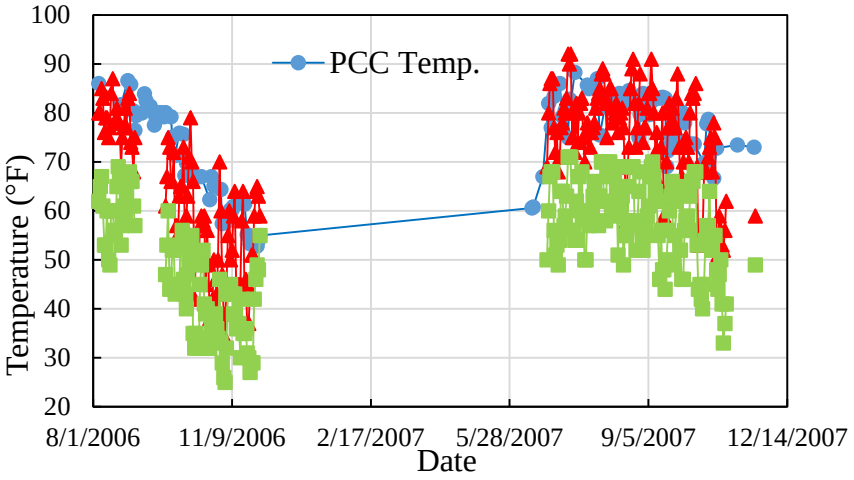

Figure 90 Daily temperature and PCC mix temperature during construction of LAK-90

Table 27 HIPERPAV analysis results for all construction days on LAK-90.

Direction	Day number	Date	Air temperature (°F)		Air temperature (°C)		Analysis result (pass/fail)	
			low	high	low	high	w/slag	no slag
EB	1	10/10/2006	52	79	11.1	26.1	fail	pass
	2	10/11/2006	55	70	12.8	21.1	fail	pass
	3	10/12/2006	35	66	1.7	18.9	pass	fail
	4	10/13/2006	32	42	0.0	5.6	pass	pass
	5	10/14/2006	35	52	1.7	11.1	fail	pass
	6	10/15/2006	34	50	1.1	10.0	fail	fail
	7	10/16/2006	32	50	0.0	10.0	pass	pass
	8	10/17/2006	45	57	7.2	13.9	pass	pass
	9	10/18/2006	49	59	9.4	15.0	pass	pass
	10	10/19/2006	52	58	11.1	14.4	fail	pass
	11	10/20/2006	41	59	5.0	15.0	pass	pass
	12	10/21/2006	39	45	3.9	7.2	fail	pass
	13	10/22/2006	40	56	4.4	13.3	fail	pass
	14	10/23/2006	32	49	0.0	9.4	pass	pass
	15	10/24/2006	32	38	0.0	3.3	pass	pass
	16	10/25/2006	36	40	2.2	4.4	fail	pass
Fail (count)							8	2
Fail (%)							50%	13%

As an example, Figure 91 presents the temperature as a function of time for three days starting on construction day October 10, 2006. Figure 92 shows the development of PCC tensile strength and stress after construction. The blue line is the tensile strength line and yellow region

shows high stress on the top surface of concrete and green region shows high stress on the bottom surface. It can be seen that stress on the top surface begins to exceed strength at 5 am. Figure 93 directly compares tensile strength development with and without slag cement in the mix for cement placed on Oct. 10, 2006. At 72 hours, the PCC tensile strength is 217.3 psi (1.50 MPa) without slag cement, and 160.3 psi (1.11 MPa) with the slag cement. Figure 94 shows the stress to strength ratio for the same date; the slag cement crosses the 100% line, indicating failure, about 16 hours after placement.

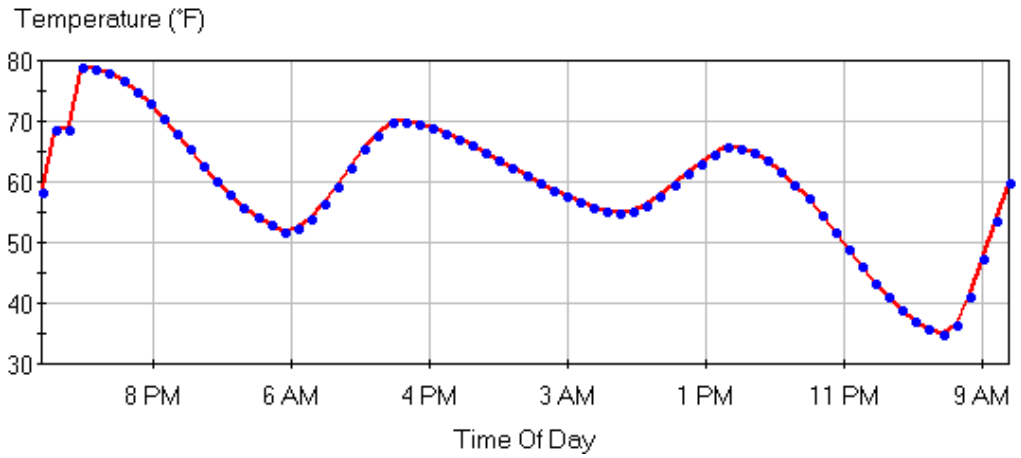

Figure 91 Temperatures at LAK-90 for three days after construction on October 10, 2006

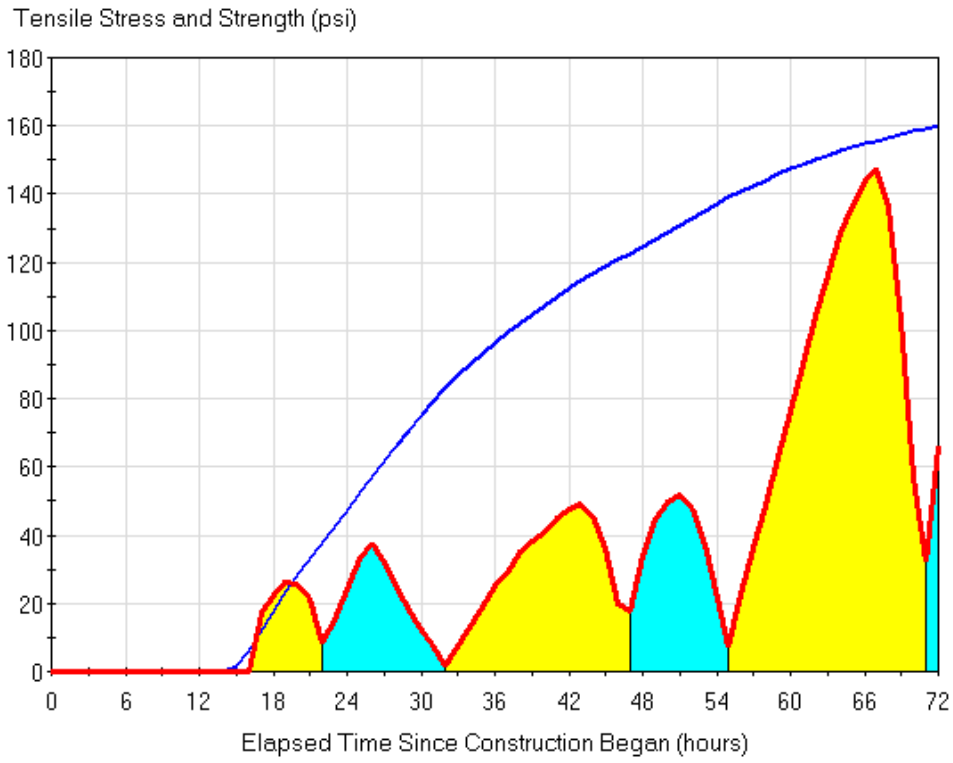

Figure 92 PCC Tensile strength and stress development after construction on LAK-90, October 10, 2006 (1 psi = 6.89 kPa).

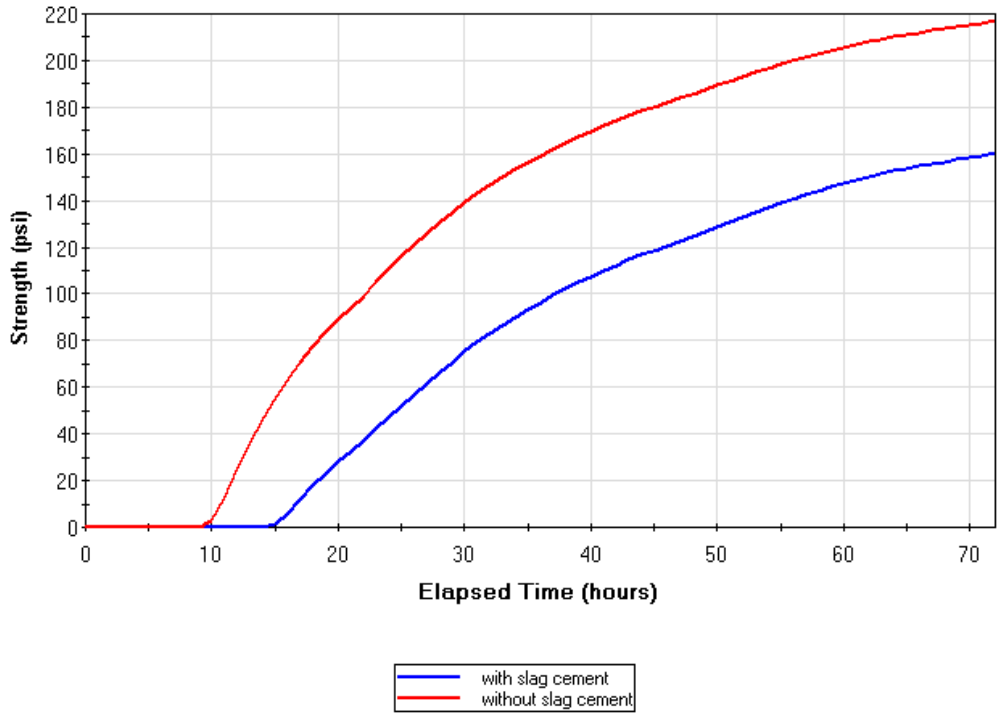

Figure 93 Early stage PCC tensile strength development comparison from HIPERPAV, LAK-70 overlay with and without slag cement, October 10, 2006 (1 psi = 6.89 kPa).

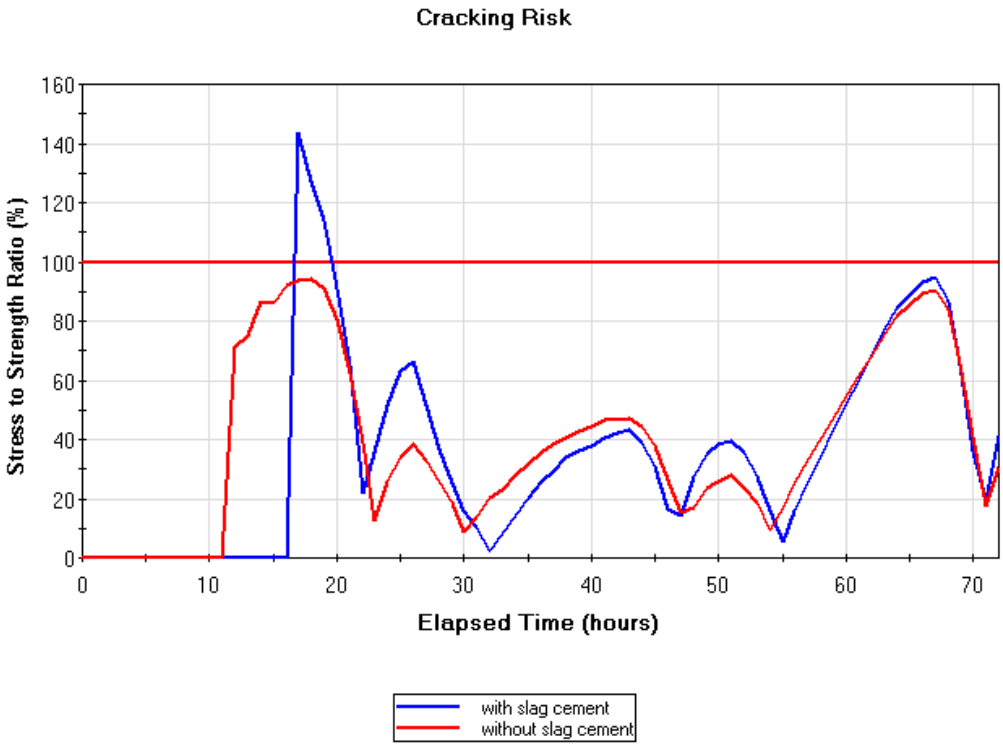

Figure 94 Stress to strength ratio versus elapsed time in HIPERPAV, LAK-70 overlay with and without slag cement, October 10, 2006.

6.9 Findings

Key findings from the forensic investigation of the overlay on LAK-90 were summarized below:

- The coring found the bondbreaker layer intact. Insufficient time has passed to determine if the moisture and loading will damage the bondbreaker.
- Laboratory testing shows good material strength and other mechanical properties for the concrete.
- Cracking was found on the surface of the concrete. The HIPERPAV results showed for 7 out of 15 days, early cracking at the surface would be expected when actual temperatures from October 10, 2006 through October 25, 2006 are used. This was a result of placing concrete containing slag cement during low temperature days which was not in accordance with ODOT specifications.

7 US-30 in Ashland County

7.1 Project Information

ODOT pavement condition rating (PCR) collected on jointed plain unbonded concrete overlays (UBCO) was plotted versus age in Figure 95. These data were used to select an excellent performing UBCO, ASD-30-0.13, to validate conclusions from the forensic investigations conducted for this study at other locations. Figure 1 above shows the PCR histories for ASD-30-0.13 along with the other projects in this study.

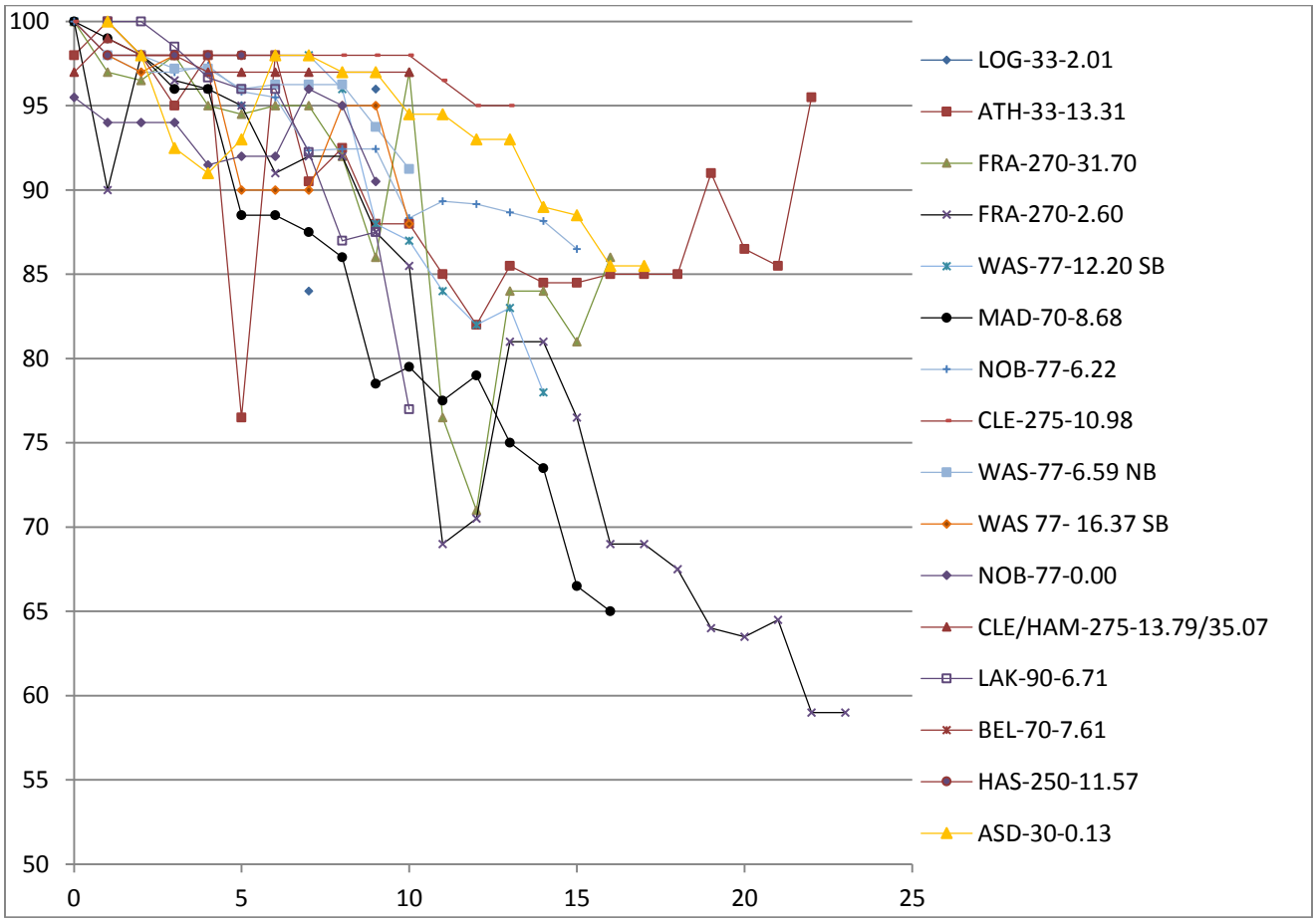

Figure 95 ODOT pavement condition rating versus age for jointed plain concrete unbonded overlay projects.

Project 1998-0119 overlaid an existing 9 in (23 cm) jointed, reinforced, dowelled concrete pavement on US-30 in Ashland County with a 9 in (23 cm) jointed, plain, dowelled concrete (ODOT Item 451) on a 1 in (2.5 cm) asphalt bondbreaker (ODOT Item 403). Average daily traffic (ADT) and average daily truck traffic (ADTT) was 12500 and 3480, respectively, in 2012. Figure 96 shows the location map of ASD-30. The selected sections are also presented in the map. The Station numbers were in meters, and the slab length (joint spacing) is 5 m (16.4 ft).

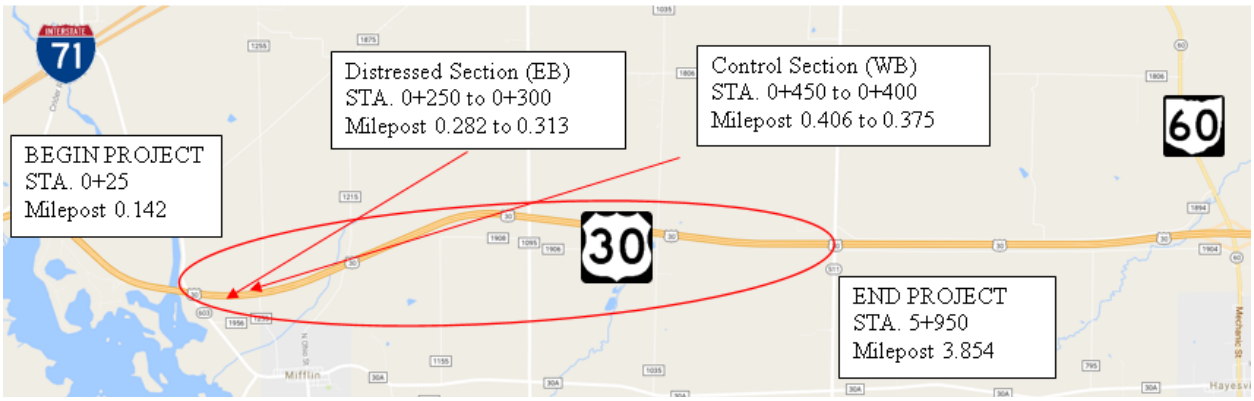

Figure 96 Location map of ASD-30.

7.2 Visual Assessment

The ASD-30 site was visited on July 8, 2016, and some photographs showing the state of the pavement were taken, such as the minor joint spalling and longitudinal cracking shown in Figure 97.

a)  b) 

Figure 97 Pavement distress observed on ASD-30, July 8, 2016: a) Joint spalling; b) Longitudinal cracking

7.3 Distress Survey

A distress survey using PathWeb images was conducted. The latest data available on PathWeb for ASD-30 are from August 2014. Some of the images were blurred and Google Street View was used to for assistance in counting cracks. The images of ASD-30 on Google Street View were collected from August 2013. Based on the survey, the eastbound passing lane experienced more distresses, including longitudinal cracking and joint failure. Westbound appeared to be in good condition overall. Figure 98 presents the cracking statistics of eastbound passing lane. Cracks per 0.1 mile (0.16 km) were counted and plotted with respect to milepost.

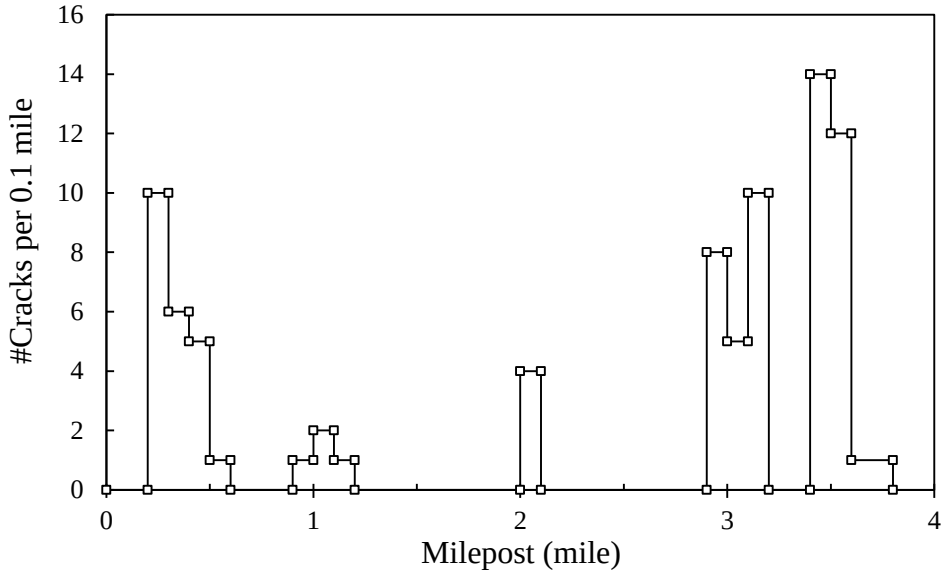

Figure 98 ASD-30 Eastbound Passing Lane Cracking Plot (1 mile = 1.6 km)

Table 28 below presents major distresses identified on ASD-30 based on the distress survey and visual assessment. The PCR history table provided by ODOT was used to confirm the distresses. Primary and contributing factors were listed below as provided on the NCHRP PCC distress types and causes table (Table 35 and Table 36). Possible causes were listed based on NCHRP tables as well as research team's judgement.

Table 28 Major distresses identified on ASD-30 and possible causes

Project	Major Distress	Primary Factors	Contributing Factors	Possible Causes
ASD-30	Longitudinal Cracking	Design features; Load; Construction	Temperature; Materials	Dowel bar related problem.
	Joint Spalling	Materials	Design features; Temperature; Load; Construction	

7.4 FWD results on selected sections

Based on the distress survey and field inspection, a distressed section and a control section were selected. The selected distressed section was from station 0+250 to +300 in the eastbound direction, covering mileposts 0.282 to 0.313. The selected control section was from station 0+450 to 0+400 in the westbound direction, mileposts 0.406 to 0.375. The location of the selected sections are shown in Figure 96. Figure 99 through Figure 102 present FWD results of the selected sections on both directions of ASD-30, from data collected September 20, 2016.

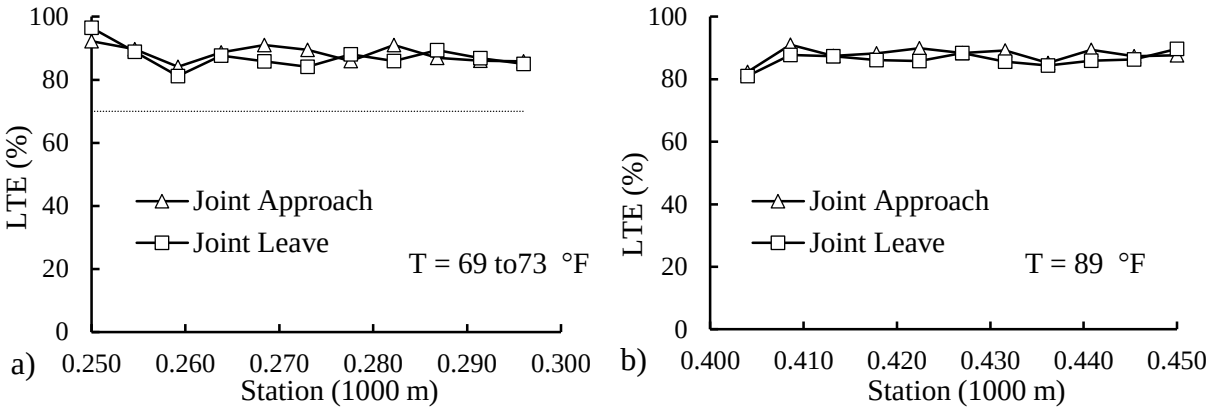

Figure 99 ASD-30 Load Transfer Efficiency a) Eastbound; b) ASD-30 Westbound (1000 m = 3281 ft). (T = pavement surface temperature)

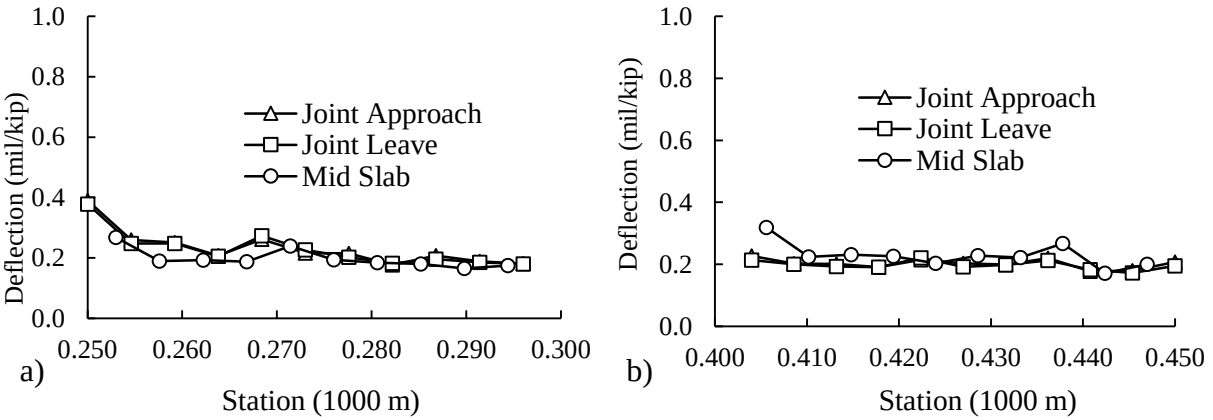

Figure 100 ASD-30 Normalized Deflections a) Eastbound; b) Westbound (1 mil/kip = 5.71 mm/MN, 1000 m = 3281 ft).

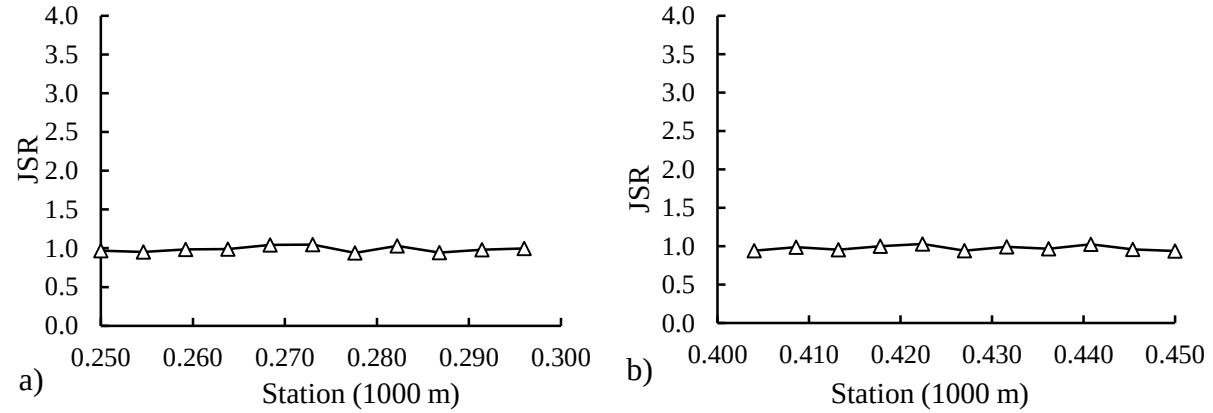

Figure 101 ASD-30 Joint Support Ratio a) Eastbound; b) Westbound (1000 m = 3281 ft).

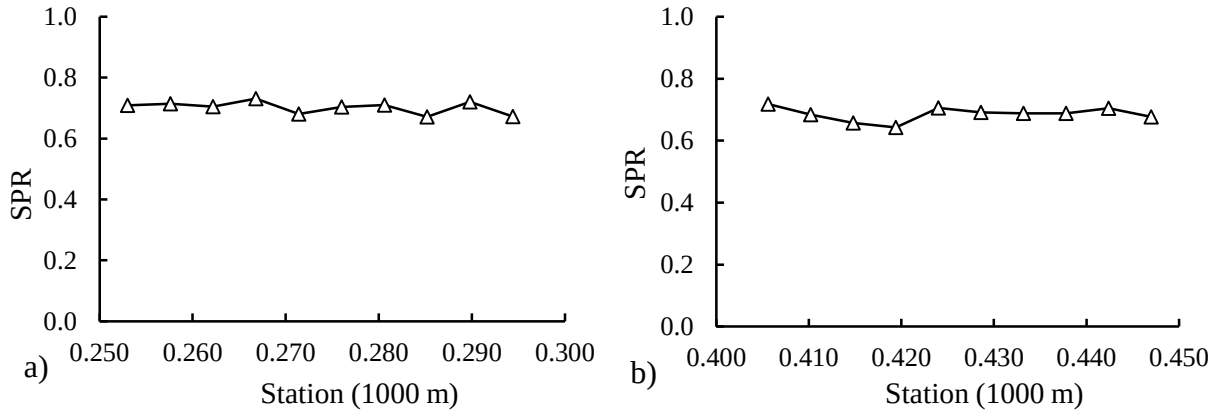

Figure 102 ASD-30 Mid-slab Spreadability a) Eastbound; b) Westbound (1000 m = 3281 ft).

7.5 MITScan and dowel bar misalignment

MITScan readings were made on US-30 by ODOT on May 11, 2017. Joints were scanned in each direction, 11 eastbound and 11 westbound, with 12 dowel bars per joint. Results for various types of misalignments of scanned dowel bars are presented in Table X below. Overall, horizontal rotation alignment appears to be acceptable on each direction. However, vertical rotation alignment is relatively bad with 22.7% of bars over the rejection limit on eastbound, and 14.4% of bars over the rejection limit on westbound. Horizontal translation misalignment is severe on both directions, with 54.6% over the rejection limit on eastbound direction and 66.7% on westbound direction. However, when dowel bar spacing is considered and the initial offset subtracted out, the acceptance rate is 93.2% on the control section and 98.2% on the distressed section, and the rejection rate 0.0% in both directions.

Table 29 Distribution of dowel misalignment in selected ASD-30 sections, as of May 11, 2017. Acceptance and rejection criteria are from Table 3.

Section	Type of Misalignment	Accept		Reject	No. Bars
		|d|≤0.5	0.5<|d|≤0.7	|d|>0.7	
EB (distressed)	Horizontal Rotation	95.8%	1.7%	2.5%	119
	Vertical Rotation	35.3%	42.0%	22.7%	119
		|d|≤0.5	0.5<|d|≤0.66	|d|>0.66	
	Depth Translation	72.3%	16.0%	11.8%	119
		|d|≤2	2<|d|≤2.3	|d|>2.3	
	Longitudinal Translation	70.6%	20.2%	9.2%	119
		|d|≤0.5	0.5<|d|≤2	|d|>2	
	Horizontal Translation	9.2%	36.1%	54.6%	119
	Dowel Bar Spacing	98.2%	0.8%	0.0%	108
Section	Type of Misalignment	|d|≤0.5	0.5<|d|≤0.7	|d|>0.7	# Bars
WB (control)	Horizontal Rotation	88.3%	2.7%	9.0%	111
	Vertical Rotation	47.7%	37.8%	14.4%	111
		|d|≤0.5	0.5<|d|≤0.66	|d|>0.66	
	Depth Translation	60.5%	33.3%	6.1%	114
		|d|≤2	2<|d|≤2.3	|d|>2.3	
	Longitudinal Translation	78.4%	11.7%	9.9%	111
		|d|≤0.5	0.5<|d|≤2	|d|>2	
	Horizontal Translation	0.9%	32.5%	66.7%	114
	Dowel Bar Spacing	93.2%	6.8%	0.0%	103

7.6 PCC Coring

Figure 103 presents the distress survey and coring plan on ASD-30 in both directions. Coring occurred on September 20, 2016. A horizontal crack at dowel level was found in one of the core holes, shown in Figure 104.

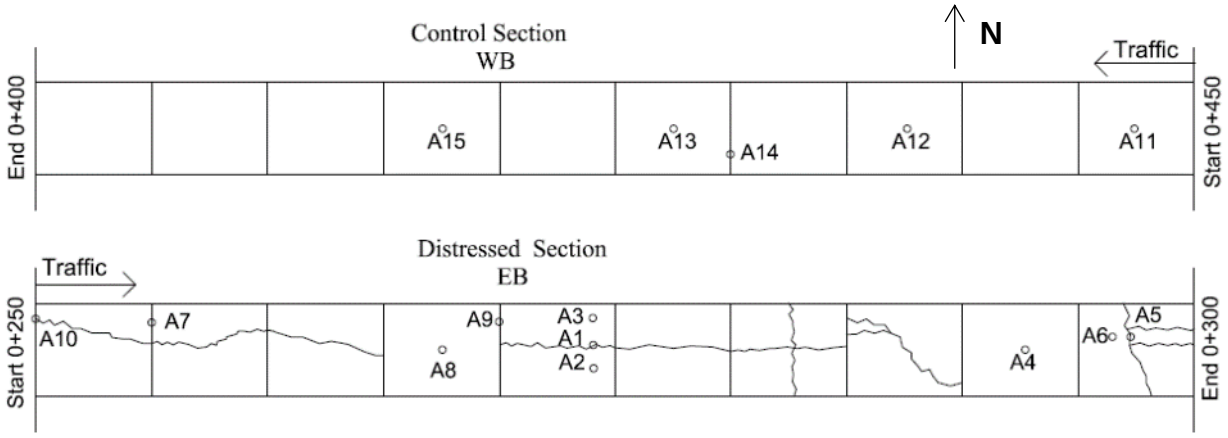

Figure 103 Distress map and coring plan on ASD-30. Note section numbers are in meters (1 m = 1.094 yd = 3.28 ft)

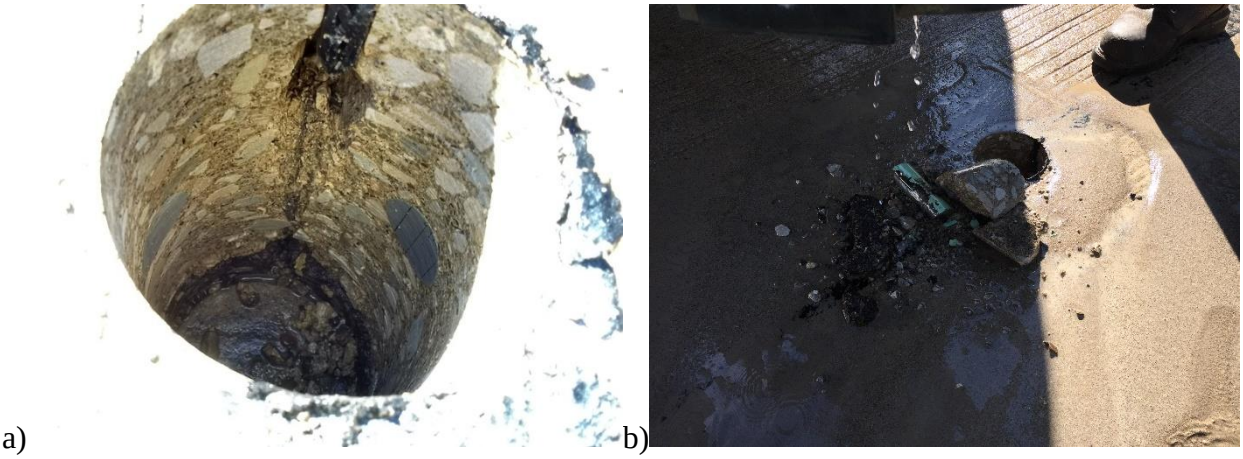

Figure 104 Horizontal crack at the dowel level

7.7 Lab testing results

Table 30 shows the measured layer thicknesses as found in the laboratory using the collected cores. The average thickness of PCC overlay is 9.2 in (23.4 cm) on both directions. The average thickness of AC bondbreaker is 1.1 in (2.8 cm) on EB and 0.8 in (2.1 cm) on WB.

Table 30 Measured Layer Thicknesses of ASD-30 cores

Direction	units	PCC overlay thickness			C_V (%)	No. Cores	Bondbreaker thickness			C_V (%)	No. Cores
		Max.	Min.	Avg.			Max.	Min.	Avg.		
EB (distressed)	(in)	9.3	9.1	9.2	0.8	7	1.4	1	1.1	12.2	7
	(cm)	23.6	23.1	23.4			3.6	2.5	2.8		
WB (control)	(in)	9.7	8.9	9.2	3.4	5	0.9	0.8	0.8	4.8	5
	(cm)	24.6	22.6	23.4			2.3	2.0	2.0		

When compared to the other projects investigated for this study, ASD-30 had the lowest coefficient of variation for both the concrete overlay thickness and bondbreaker thickness, as shown in Table

31, with the exception of the control direction (WB) overlay. The higher coefficient of variation for ASD was approximately equal to average coefficient of variation for the other three projects, indicating better control of thickness on ASD-30.

Table 31 Coefficient of Variation of overlay and bondbreaker layer thicknesses for all pavements in this study.

	Coefficient of Variation (%)							
	PCC overlay thickness				Bondbreaker thickness			
Direction	MAD-70	WAS/NOB-77	LAK-90	ASD-30	MAD-70	WAS/NOB-77	LAK-90	ASD-30
Distressed: EB or SB	5.8%	2.4%	3.3%	0.8%	23.7%	24.7%	13%	12.2%
Control: WB or NB	1.3%	1.9%	1.7%	3.4%	10%	7.1%	13%	4.8%

Table 32 presents the lab testing results. The average splitting tensile strength is 630 psi (4.34 MPa).

Table 32 ASD-30 Lab Testing Summary (EB = distressed section, WB = control section)

Core	Compressive strength ($f'c$)		Tensile strength		Elastic modulus (E)		Poisson's ratio (υ)	CTE (α)	
	(psi)	(MPa)	(psi)	(MPa)	(10^6psi)	(GPa)		(10^{-6}/°F)	(10^{-6}/°C)
A3	9130	62.95							
A4	8880	61.23							
A6	8130	56.05							
A8			580	4.00					
A11			555	3.83					
A12			745	5.14					
A13								5.17	9.31
A15					4.45	30.68	0.22		
Average	8710	60.05	630	4.34	4.45	30.68	0.22	5.17	9.31

7.8 Petrographic analysis

Core A2 from the distressed eastbound lane and Core A14 from the control westbound lane were used for petrographic SEM analysis. The location of each core can be determined by looking at Figure 103 above. Findings from the SEM analysis of the cores are presented below from the subcontractor report by Dr. Jan Olek of Purdue University:

A2 (EB) Top:

- Matrix (paste) mostly crack-free (only occasional isolated cracks).
- Deposits of ettringite, Friedel's salt, and brucite (magnesium hydroxide) found within the matrix.
- Empty air voids of non-uniform size.

A2 (EB) Bottom:

- Matrix (paste) mostly crack-free (only occasional isolated cracks).
- Deposits of ettringite, Friedel's salt, and brucite within the paste.
- Empty air voids.

A14 (WB) Top:

- Most of the air-voids filled with ettringite.
- Many microcracks within the matrix.
- Numerous deposits of monosulfate within the matrix.
- Ettringite deposits within the air-voids.

A14 (WB) Bottom):

- Generally low frequency of the air voids.
- Many smaller air voids filled with ettringite.
- Relatively high level of microcracks within the matrix.
- Paste carbonated in places with occasional deposits of brucite.

7.9 Findings

The following observations were drawn from the examination of ASD-30:

- Control of concrete overlay and bondbreaker thickness during construction was very good.
- Observed distress was primarily longitudinal cracking
- Material related distress was observed in cracks and joints.
- A thin bondbreaker performed well on ASD-30
- Truck traffic on ASD-30 is significantly lower than that on MAD-70, which may explain the performance given the thin bondbreaker layer.

8 Finite Element Analysis

8.1 ABAQUS Model Characterization

The general purpose three-dimensional finite element program ABAQUS was used for finite element analysis. Figure 105 and Figure 106 show side view and plan view respectively of the model used in the analysis.

The model consists of a pavement shoulder, driving lane, and passing lane across with 3 slabs along each lane. Dowel bar and tie bars were provided at all transverse joints and longitudinal joints respectively. The normal slab dimensions in the traffic lanes are 15 ft (4.57 m) by 12 ft (3.66 m) and the shoulder slab dimension is 15 ft (4.57 m) by 10 ft (3.05 m). The build-up of the model is the same as I-70: 9 in (229 mm) concrete overlay placed over 1 in (2.5 cm) asphalt bondbreaker on 9 in (229 mm) original PCC atop 6 in (152 mm) aggregate base over a subgrade thickness of 60 in (1.52 m). Based on the study of damage analysis of JPCP by Purdue University [Sotelino, Asgari, Saksa, & Cedeno, 2005], a subgrade depth of 1.5 m (59.1 in.) is sufficient for analysis purpose. The dowel bar is 18 in (457 mm) long and 1.25 in (32 mm) in diameter. The tie bar dimension is 30 in (762 mm) long and 5/8 in (15.9 mm) in diameter.

The coordinate system was oriented with the positive X axis in the direction of traffic and the negative Z axis down from pavement surface into the subgrade. Thus the positive Y axis is transverse to traffic in the plane of the pavement, pointing across the pavement shoulder and the traffic lanes. The origin was at the pavement surface, at the outside edge of the shoulder slab at the point first crossed by the traffic.

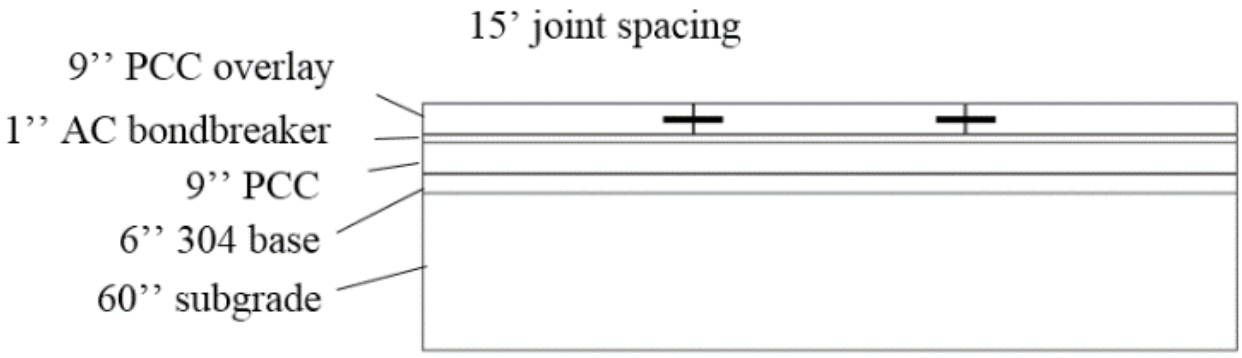

Figure 105 Side view of FE model (1” = 25.4 mm, 1’ = 0.305 m)

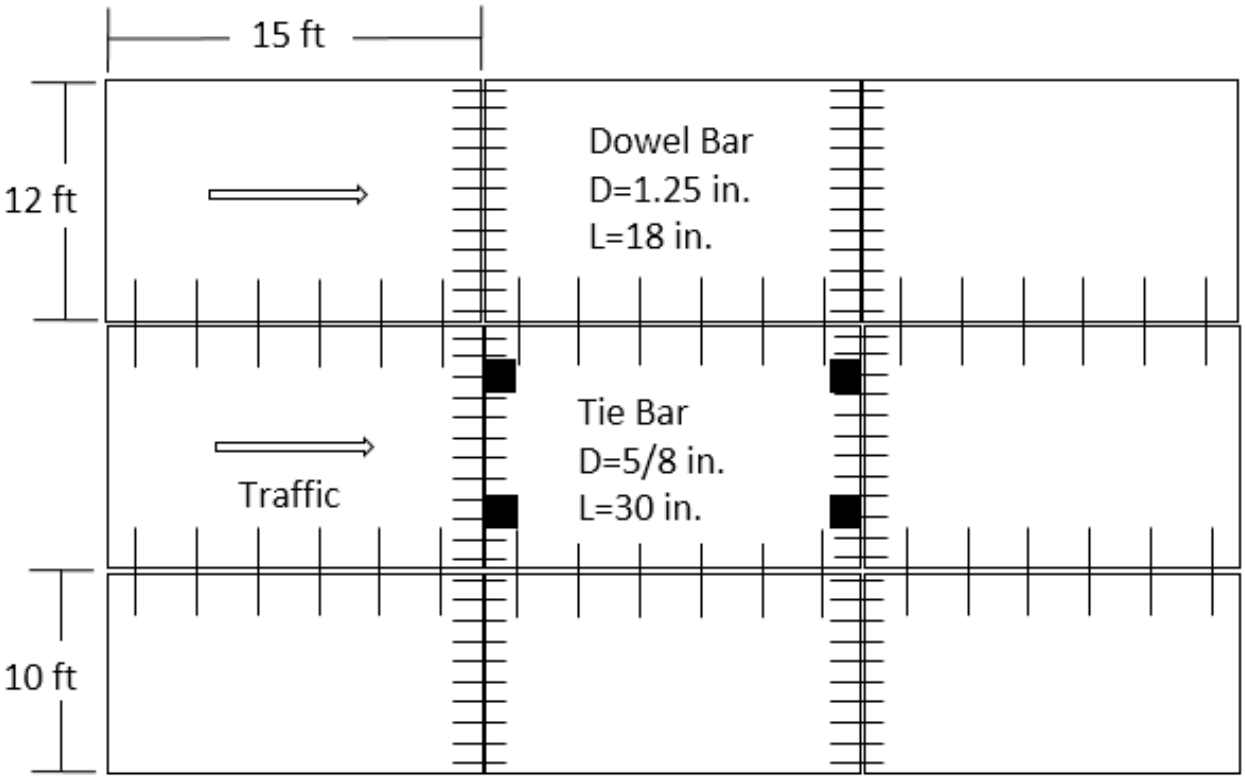

Figure 106 Plan view of FE model (1 in = 25.4 mm, 1 ft = 0.305 m)

8.1.1 Mesh

Both coarse and fine mesh were used in the FEA model. The fine mesh was used on the center slab, with element size 3 in×1.5 in×1.125 in (76.2 mm×38.1 mm×28.6 mm). This was done to accurately apply the nonlinear temperature gradient through the depth of the slab. The other reason is to achieve better dowel bar section stress development. The stress in the rest of the slabs are not the main concern, it was deemed unnecessary to use a detailed model for all other slabs. Coarse mesh was used for all other slabs to reduce computation time. The size is 9 in×3 in×2.25 in (229 mm×76.2 mm×54.0 mm). Figure 107 shows the mesh of the FE model. The dowel bar and tie bar meshes are shown in Figure 108.

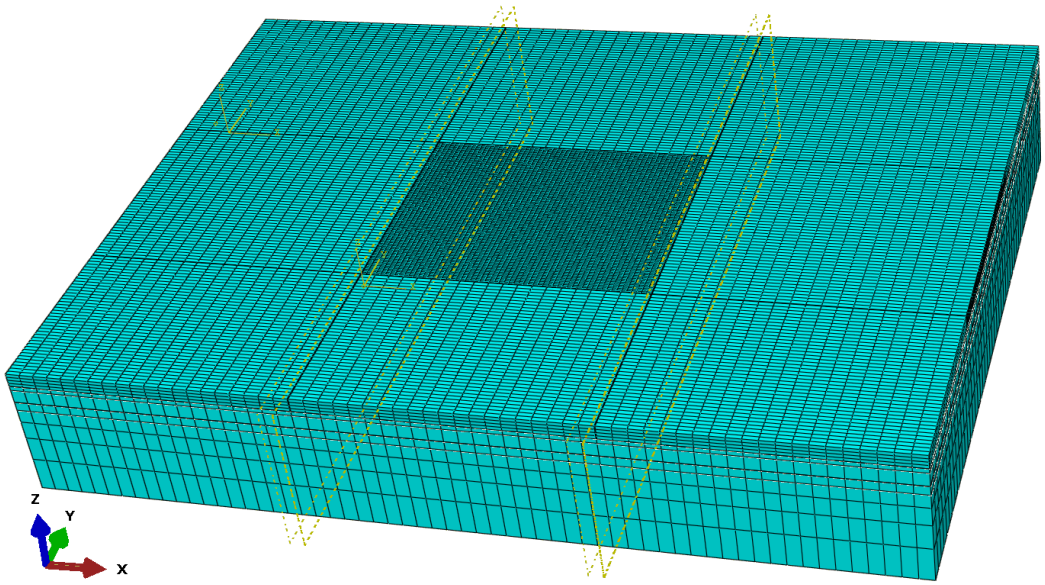

Figure 107 Mesh of the PCC Overlay FE model

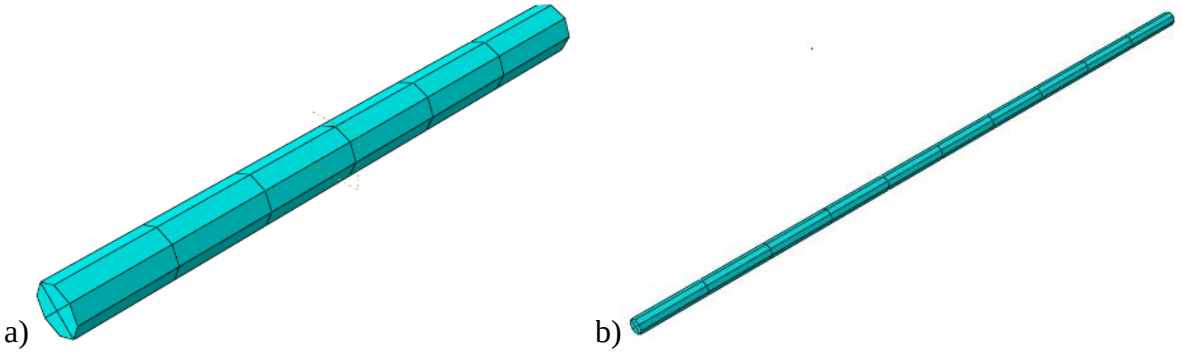

Figure 108 a) Dowel bar mesh; b) Tie bar mesh

8.1.2 Boundary conditions

Boundary conditions were set up so that the bottom of the pavement model was fully constrained in all directions. All sides of the model were restrained in their normal direction, but no constraints were applied at the concrete slab boundaries.

8.1.3 Material properties

Materials used in this analysis were assumed to have linear elastic behavior that could be modeled using only the elastic modulus and Poisson's ratio. Density (unit weight) was also inputted, but self-weight was considered only for overlay slabs. Table 33 presents the material properties used in this model.

Table 33 Material Properties (English units were used in the FEA)

Part	Material	E		ν	γ		α	
		(psi)	(MPa)		(lb/in^3)	(kg/m^3)	(1/°F)	(1/°C)
Slab	Concrete	4,000,000	27,579	0.15	0.087	2408	5.50E-06	9.90E-06
Bondbreaker	Asphalt	400,000	2,758	0.3	0.085	2353	—	—
Base	Crushed Stone	35,000	241	0.35	0.081	2242	—	—
Subgrade	Medium Clay	5,000	34	0.45	0.06	1661	—	—
Dowel & tie bars	Steel	29,000,000	199,948	0.3	—	—	—	—

8.1.4 Interactions

ABAQUS allows two methods of modeling the mechanical interaction between elements at interfaces. The first method uses zero-thickness interface elements which are formulated to calculate the contact direction, contact area, and the normal and shear stresses transmitted at the surface of contact. The second method uses the contact interaction option, where the interaction is selected from several friction models. Based on the study of Hammons [1998], it is recommended to use the contact interaction method for its simplicity and slightly higher accuracy. In this study, contact interaction method was used for all surface interactions.

Surface-to-surface contact was defined between layers in terms of normal and tangential behaviors. For normal behaviors between surfaces, hard contact was assumed, meaning minimum penetration was allowed between surfaces. For tangential behavior between surfaces, different methods were used depending on the materials involved.

For the overlay-asphalt interface, a basic Coulomb friction model was used to define horizontal behavior. The concept of the basic Coulomb friction model, according to the ABAQUS User's Manual [2011], is that the two contact surfaces will "stick", that is they can carry shear stresses up to a certain magnitude across their interface before they start sliding relative to one another. Figure 109 illustrates the Coulomb friction model. The critical shear stress is defined as a fraction of the contact pressure, given by a friction coefficient. The friction coefficient is usually obtained from tangent of internal friction angle of base material. Based on literature, a friction coefficient of 0.9 was used in this analysis. Separation was allowed between overlay and bondbreaker. For other layer interfaces, rough tangential behavior was defined, which means no slip occurred between surfaces; and no separation was allowed.

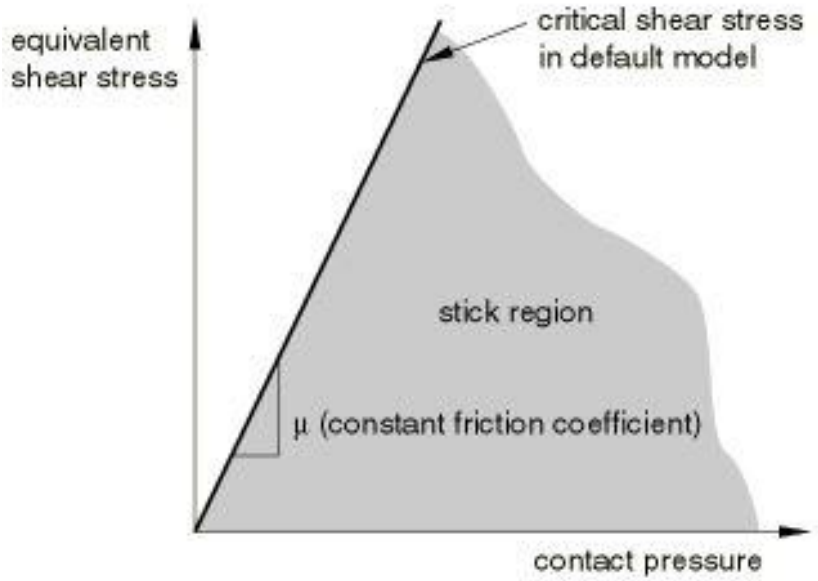

Figure 109 Slip regions for the basic Coulomb friction model [ABAQUS Standard User's Manual, Version 6.11, 2011]

Dowel bars are embedded (bonded) to slab on one side, and are allowed to slide in slab on the other side. For the part that is allowed to slide, hard contact was defined for normal behavior and penalty with friction coefficient of 0.01 was defined for tangential behavior. This way dowel bars can move horizontally along the longitudinal direction and only vertical stress can be carried. Tie bars are bonded to slabs on both sides, and thus can carry horizontal forces between slabs.

8.1.5 Environmental loading from temperature gradient

Temperature gradients through the depth of concrete pavement cause curling which diminishes support from the underlying layers and can magnify load-related stresses. Changes in ambient temperature also cause slab expansion and contraction which affect transverse cracking and joint performance.

When a negative gradient exists (i.e. the top is cooler than the bottom), the corners of the slab will tend to curl upward, as seen in Figure 110a). This causes gaps to form underneath the slab corners while the center of the slab remains in contact with the subgrade. When a positive temperature gradient exists (i.e. the top is warmer than the bottom), the corners of the slab will tend to curl downward and push into the subgrade, and a gap will form underneath the center of the slab, as seen in Figure 110b).

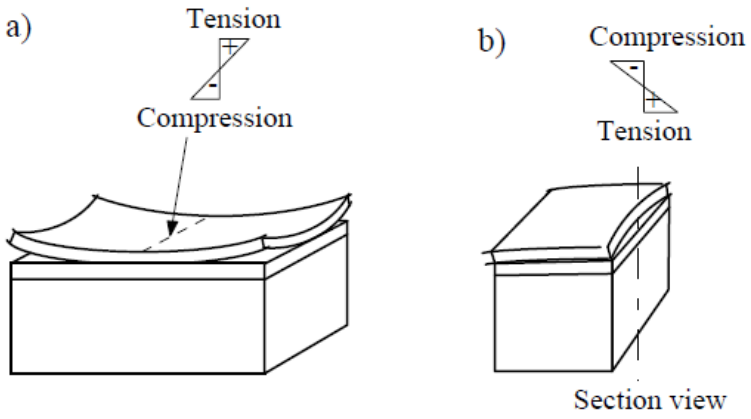

Figure 110 a) Upward curling due to negative temperature gradient; b) Downward curling due to positive temperature gradient

In this study a nonlinear negative temperature gradient was applied through the depth of overlay slab. The temperature gradient was calculated from the Integrated Climatic Model (ICM) program developed by Dempsey, Herlache, and Patel [1986]. The ICM program uses input pavement properties and appropriate climatic data to calculate temperature gradients through the depth of pavement. In this study, climatic data from OSU airport weather station in Columbus, Ohio was used and pavement properties from I-70 UBCO sections were used to calculate temperature gradient through concrete overlay depth. Table 34 and Figure 111 show the resulting negative temperature gradient used in the analysis. Previous research by Thompson, Dempsey, and Hill [1987] showed the temperature change in the supporting layers of a concrete pavement is very small. Thus, in this work, the temperature differential is applied solely to the concrete overlay slab.

Table 34 Negative temperature gradient used in the FEA

Depth	(in)	0	-1	-2	-3	-4	-5	-6	-7	-8	-9
	(mm)	0	-25	-51	-76	-102	-127	-152	-178	-203	-229
Temperature	(°F)	-16.88	-14.07	-11.5	-9.16	-7.05	-5.17	-3.53	-2.12	-0.94	0
	(°C)	-27.16	-25.59	-24.17	-22.87	-21.69	-20.65	-19.74	-18.96	-18.30	-17.78

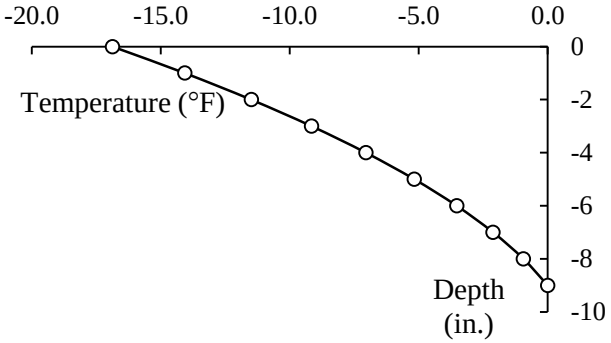

Figure 111 Nonlinear negative temperature gradient (1 in = 25.4 mm)

8.1.6 Applied load from trucks

A wheel load for a standard AASHTO HS-20 truck, shown in Figure 112, was used as the applied load, for which 32,000 lb (142 kN) load is carried by the four tires in a single axle. The tire pressure was assumed to be 111 psi (765 kPa) and the contact area of one tire was taken as 72 in^2 (46500 mm^2). Figure 113a) shows the footprint of a dual tire, computed to be 12 in×12 in (93000 mm^2). The load was positioned just inside of two transverse joints on one slab to maximize the effect. Figure 113b) shows the load position.

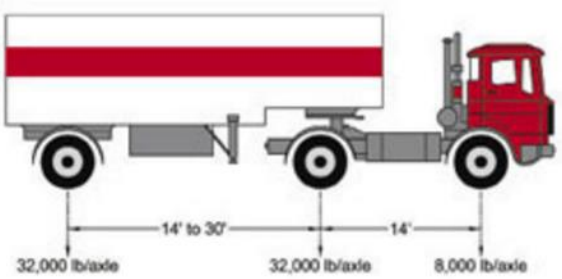

Figure 112 AASHTO HS-20 truck (1 ft = 0.305 m, 8000 lb = 36 kN).

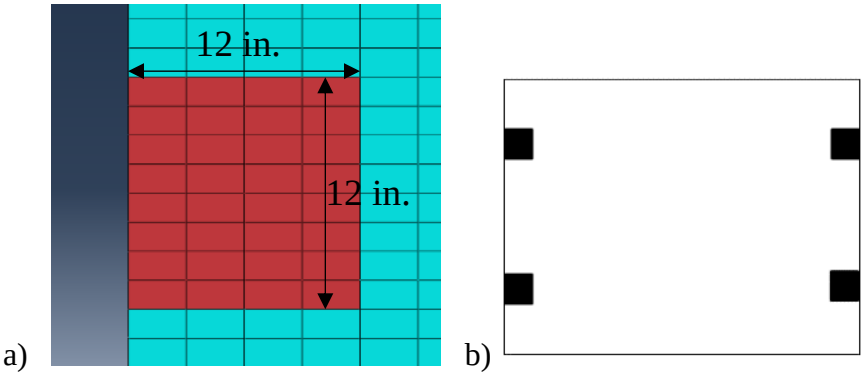

Figure 113 a) Footprint of a dual tire of AASHTO HS-20 truck (1 in = 25.4 mm); b) tire load positions marked in black on the outline of a slab.

8.2 Parametric Study of FE Model

To gain deeper insights into the structural performance of UBCO pavements, a parametric study was conducted using the developed FE model. Factors considered in the analysis include the effects of loss of support, AC bondbreaker thickness, and joint spacing (slab size). The stresses developed in the center slab were recorded and plotted along Line 1 and Line 2 on the top surface of slab as shown in Figure 114. Vertical deflections along Line 1 and Line 2 was also recorded and plotted.

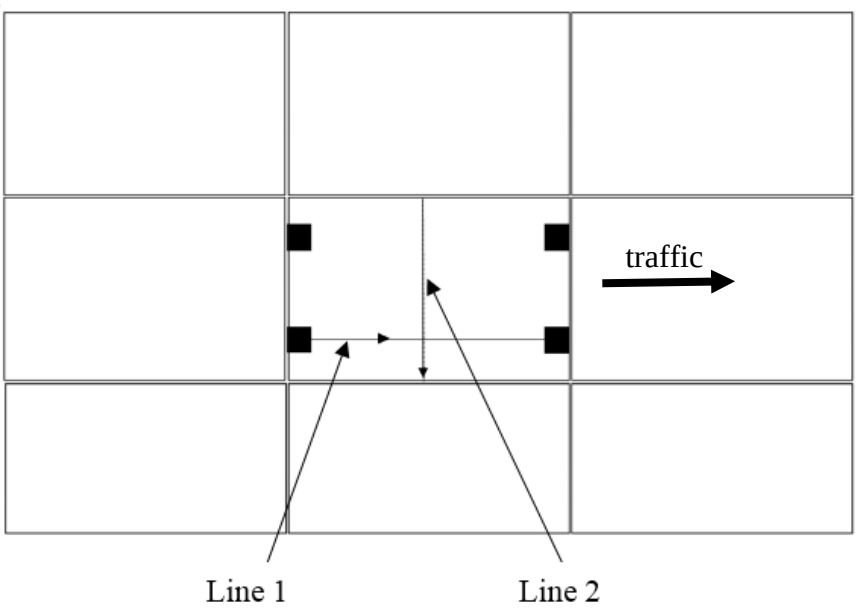

Figure 114 Definition of Line 1 and Line 2. Traffic direction is to the right.

8.2.1 Case 1: Effect of loss of material under transverse joints

To study the effect of loss of material under the joints, four different models were developed, based on the length of the loss of support zone under the slab ends. Each end of the slab was assumed to have a rectangular area of loss of support that extended the full transverse width of the slab (12 ft = 3.66 m) and a longitudinal length of 0 in (0 m) (i.e. no loss of support), 12 in (0.305 m), 24 in (0.610 m), and 36 in (0.910 m) loss of support. The loss of support was modeled by removing the AC material under the joints with a rectangular shape. An illustration of 24 in (0.610 m) loss of support is shown in Figure 115.

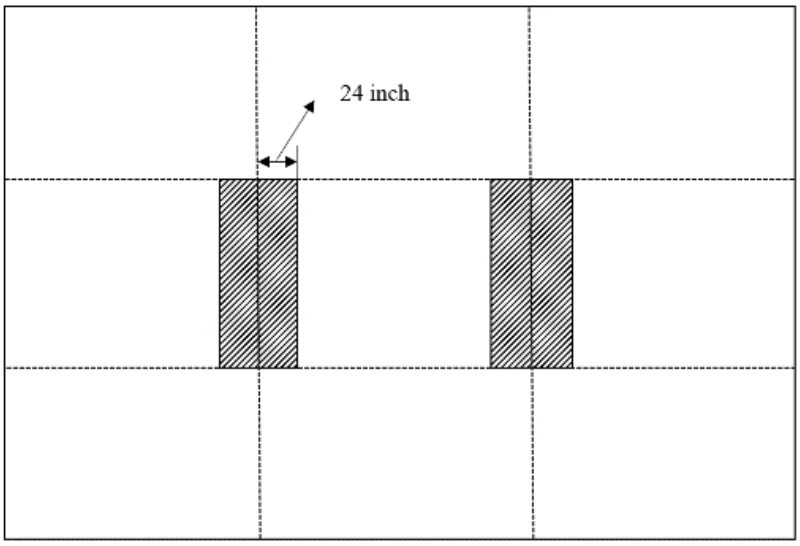

Figure 115 Illustration of 24 in (0.610 m) loss of support under transverse joints, indicated by shading.

8.2.1.1 Wheel load with no negative temperature (W)

Figure 116 and Figure 117 present the maximum principal stress distribution and vertical deflection along Line 1 and Line 2 with only wheel loads. Stress along Line 1 and Line 2 increased with more loss of support. Maximum stress reaches 210 psi (1447 kPa) with 36-in (0.91 m) loss of support compared with 69 psi (475 kPa) with no loss of support. Deflections along Line 1 increased at the edges with more loss of support and remained nearly unchanged in the middle. The difference of deflections along Line 2 is relatively small. The slab is moving upwards near the longitudinal edge and is moving downwards near the center.

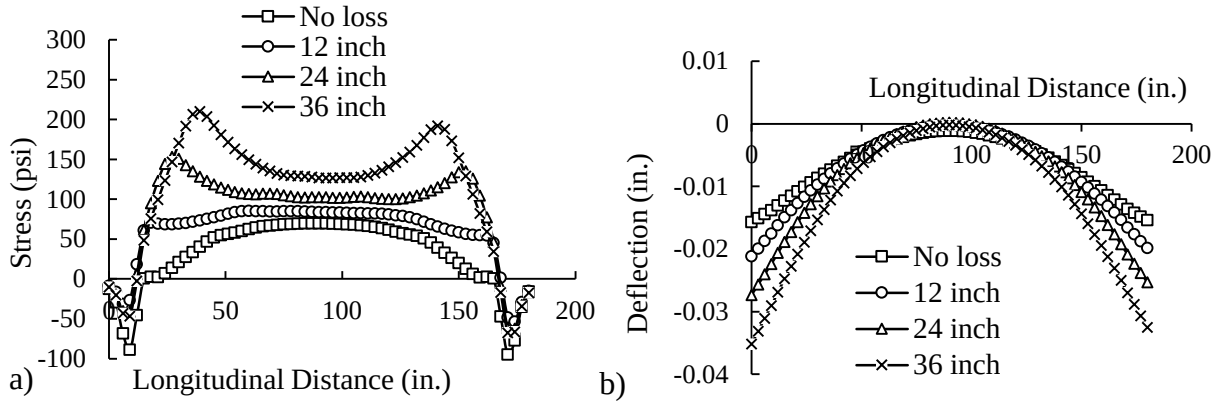

Figure 116 Case 1 (W) a) Maximum principal stress along Line 1; b) Deflection along Line 1. Line 1 is parallel to traffic. (1 in = 25.4 mm; 1 psi = 6.9 kPa)

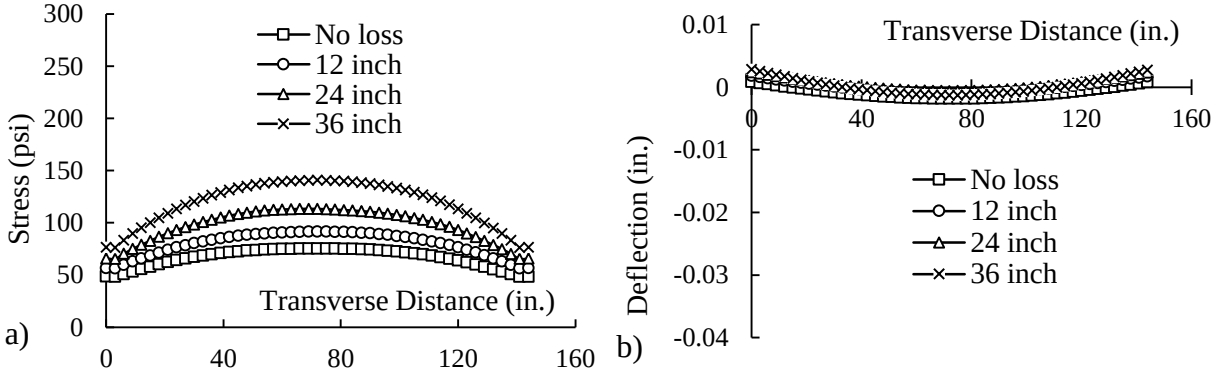

Figure 117 Case 1 (W) a) Maximum principal stress along Line 2; b) Deflection along Line 2. Line 2 is transverse to traffic. (1 in = 25.4 mm; 1 psi = 6.9 kPa)

8.2.1.2 Negative temperature gradient with no wheel loading (T)

Figure 118 and Figure 119 present the maximum principal stress distribution and vertical deflection along Line 1 and Line 2 with only negative temperature gradient. Generally, the loss of materials under the joints had no or very little effect in this case. Stresses and deflections remained unchanged along both Line 1 and Line 2 with or without loss of support. This can be explained by

the fact that with negative temperature gradient, the slab curls up on the corners and edges to create loss of support.

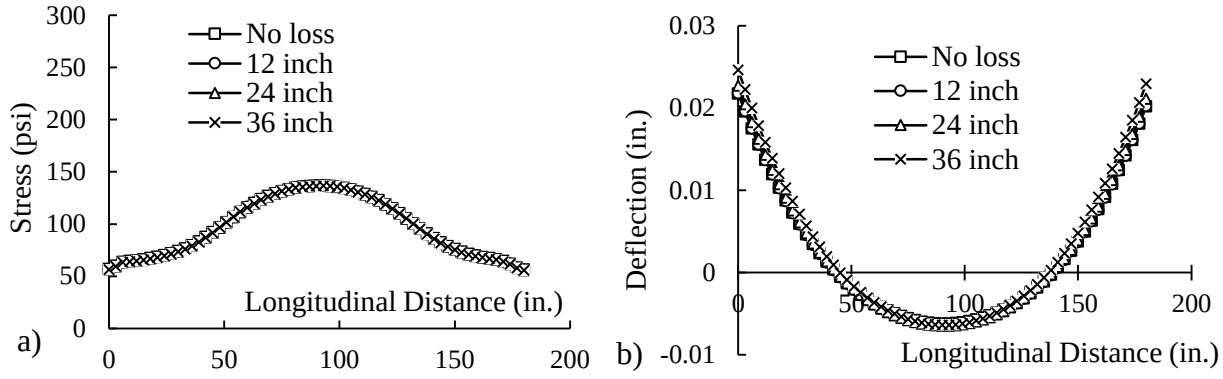

Figure 118 Case 1 (T) a) Maximum principal stress along Line 1; b) Deflection along Line 1. Line 1 is parallel to traffic. (1 in = 25.4 mm; 1 psi = 6.9 kPa)

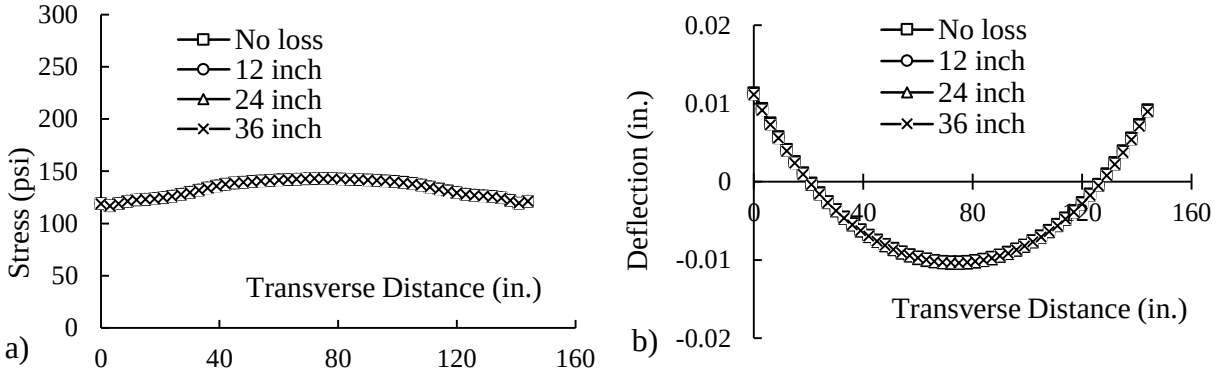

Figure 119 Case 1 (T) a) Maximum principal stress along Line 2; b) Deflection along Line 2. Line 2 is transverse to traffic. (1 in = 25.4 mm; 1 psi = 6.9 kPa)

8.2.1.3 Negative temperature gradient with wheel loading (T+W)

Figure 120 and Figure 121 present the maximum principal stress distribution and vertical deflections along Line 1 and Line 2. From Figure 120a), it can be seen that stress in the middle of the slab increased with more loss of support. The stress increased rapidly near the 36 in (0.91 m) position of Line 1 to 276.3 psi (1905 kPa). The surface of the slab between 36 in (0.91 m) to 144 in (3.66 m) position along Line 1 is under great tension due to loss of support. The stress distribution of 12 in (0.305 m) and 24 in (0.61 m) loss of support is analogous but less obvious. Deflections along Line 1 also increased with more loss of support. The maximum deflection increased from 0.0057 in (0.145 mm) to 0.0158 in (0.401 mm). Stress along Line 2 increased with more loss of support. The stress in the middle of the slab increased from 261.1 psi (1800 kPa) with no loss of support to 294.2 psi (2028 kPa) with 36 in (0.91 m) loss of support. Deflection along Line 2 generally remained unchanged with or without loss of support.

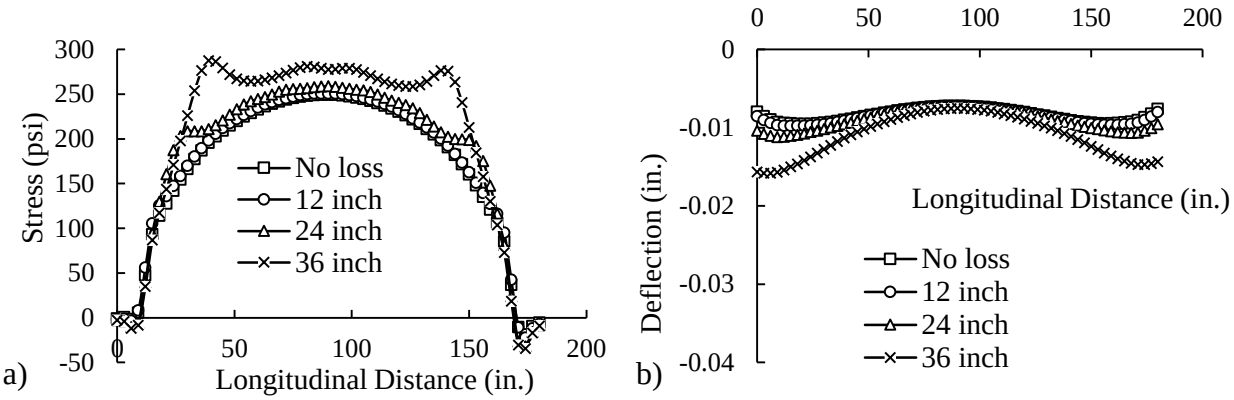

Figure 120 Case 1 (T+W) a) Maximum principal stress along Line 1; b) Deflection along Line 1. Line 1 is parallel to traffic. (1 in = 25.4 mm; 1 psi = 6.9 kPa)

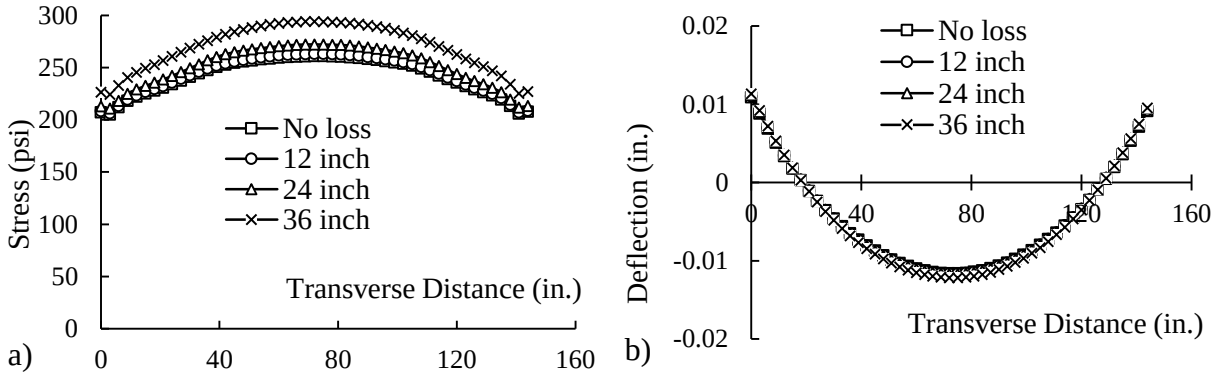

Figure 121 Case 1 (T+W) a) Maximum principal stress along Line 2; b) Deflection along Line 2. Line 2 is transverse to traffic. (1 in = 25.4 mm; 1 psi = 6.9 kPa)

8.2.2 Case 2: Effect of AC Bondbreaker Thickness

To study the effect of the thickness of asphalt bondbreaker, three models with different thickness of asphalt bondbreaker was used: 1 in (25 mm), 3 in (76 mm) and 5 in (127 mm). Other conditions remain unchanged. Loading composition includes wheel loading only (W); negative temperature only (T); negative temperature with wheel loading (T+W).

8.2.2.1 Wheel loading with no negative temperature (W)

Figure 122 presents the maximum principal stress distribution and deflection along Line 1 due to wheel loading only. Figure 123 presents the stress and deflection along Line 2. As can be seen, stresses along Line 1 and Line 2 decrease with thicker AC bondbreaker. The vertical deflections along Line 1 are negative, indicating the slab is pressed into the bondbreaker. The slab on the 1 in (25 mm) thick bondbreaker shows the most deflection at the ends and the least negative deflection in the center, indicating the most bending of the slab, while the 5 in (127 mm) bondbreaker yields the least bending distortion of the slab.

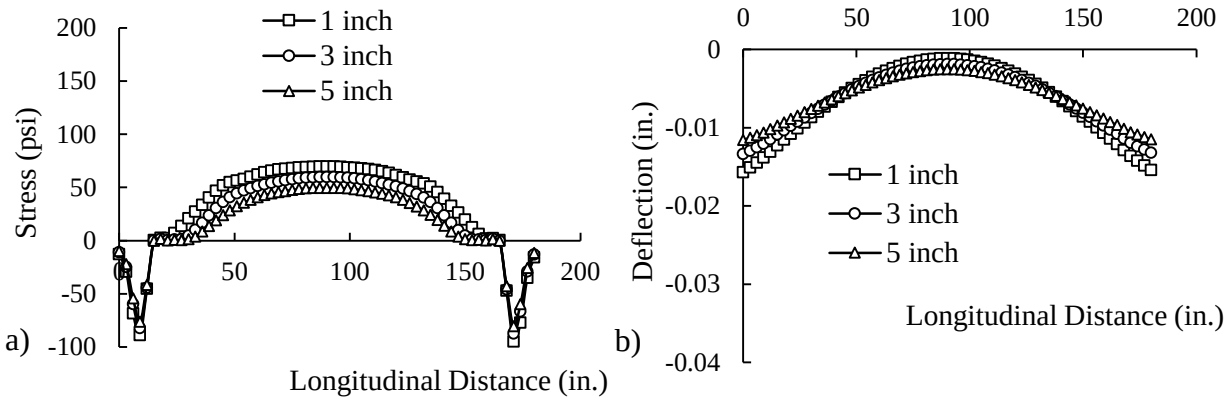

Figure 122 Case 2 (W) a) Maximum principal stress along Line 1; b) Deflection along Line 1. Line 1 is parallel to traffic. (1 in = 25.4 mm; 1 psi = 6.9 kPa)

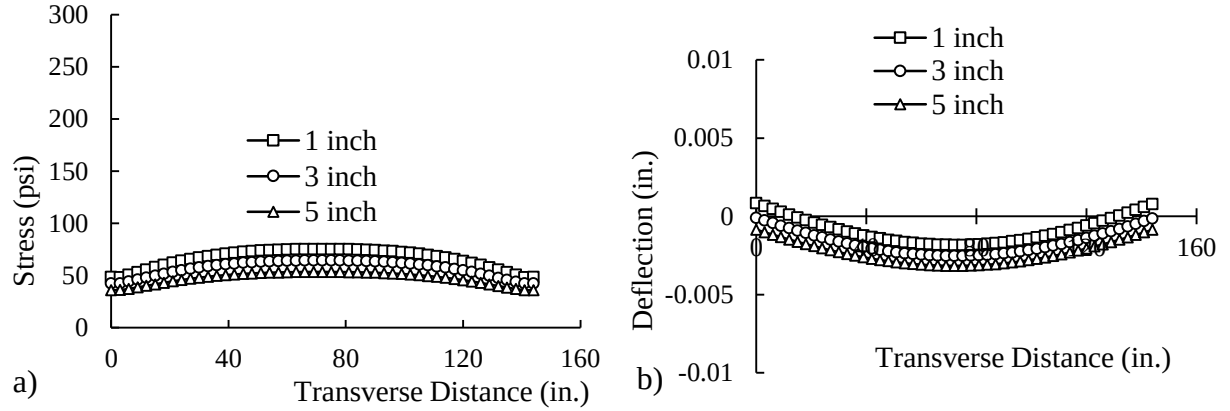

Figure 123 Case 2 (W) a) Maximum principal stress along Line 2; b) Deflection along Line 2. Line 2 is transverse to traffic. (1 in = 25.4 mm; 1 psi = 6.9 kPa)

8.2.2.2 Negative temperature gradient with no wheel loading (T)

Figure 124 and Figure 125 present the maximum principal stress distribution and deflections along Line 1 and Line 2. As can be seen, the negative temperature gradient causes the slab to curl upwards. The edges and corners of the slab lost contact with the bondbreaker. The maximum stress along Line 1 and Line 2 increases with thicker bondbreaker. This difference is greater in the middle of the slab, while in the edges the difference is less. The deflections, however, decrease with thicker bondbreaker. Similarly, the difference is greater in the middle of the slab.

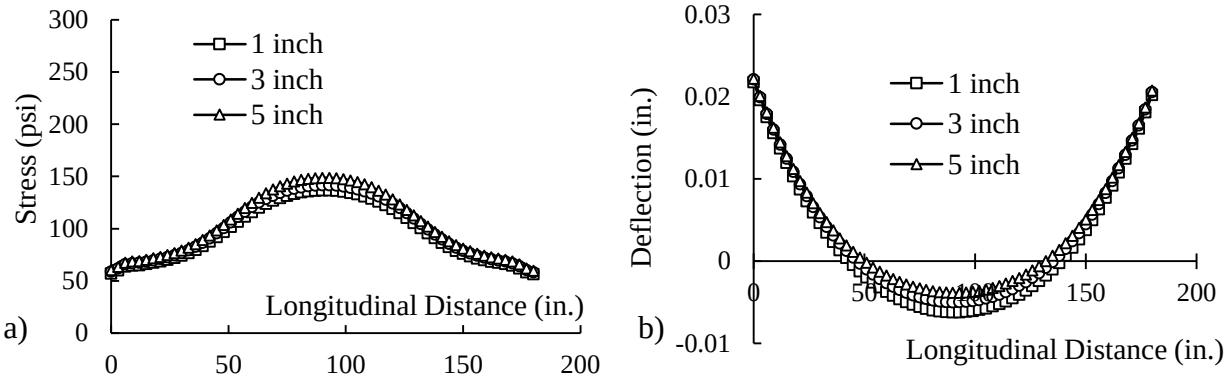

Figure 124 Case 2 (T) a) Maximum principal stress along Line 1; b) Deflection along Line 1. Line 1 is parallel to traffic. (1 in = 25.4 mm; 1 psi = 6.9 kPa)

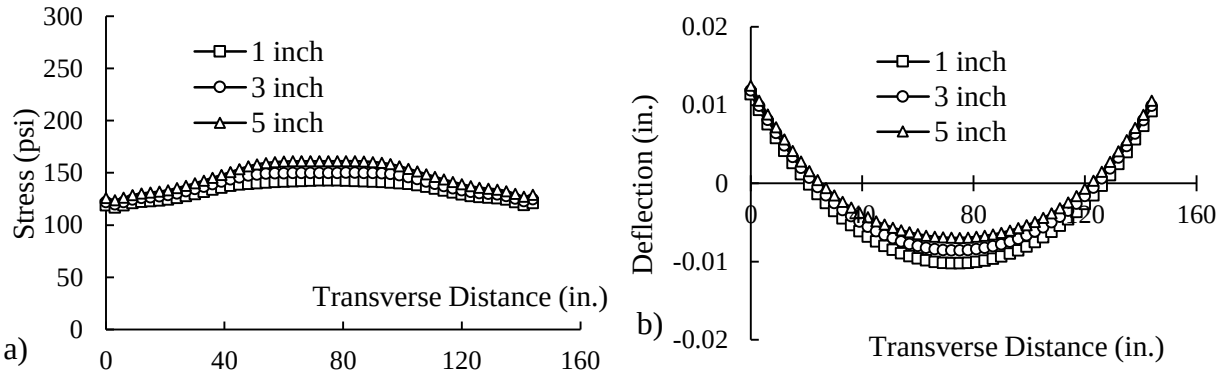

Figure 125 Case 2 (T) a) Maximum principal stress along Line 2; b) Deflection along Line 2. Line 2 is transverse to traffic. (1 in = 25.4 mm; 1 psi = 6.9 kPa)

8.2.2.3 Negative temperature gradient with wheel loading (T+W)

Figure 126 presents the maximum principal stress distribution and deflections along Line 1 due to negative temperature and wheel loading. Figure 127 presents the stress and deflections along Line 2. The difference of stress along Line 1 is very small. The model with thicker bondbreaker has slightly lower stress in the middle of the slab. Stress along Line 2 decreases with thicker bondbreaker. Deflections along Line 1 and Line 2 decrease with thicker bondbreaker thickness.

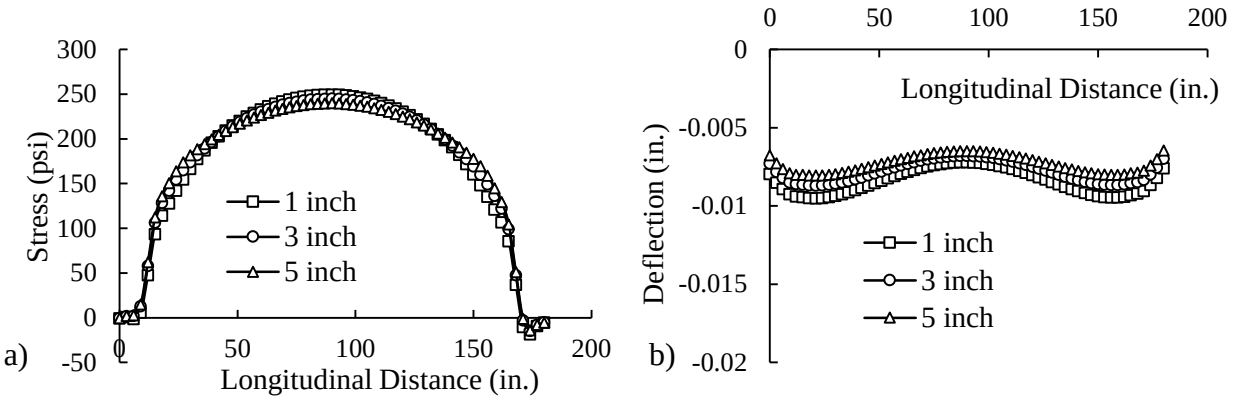

Figure 126 Case 2 (T+W) a) Maximum principal stress along Line 1; b) Deflection along Line 1. Line 1 is parallel to traffic. (1 in = 25.4 mm; 1 psi = 6.9 kPa)

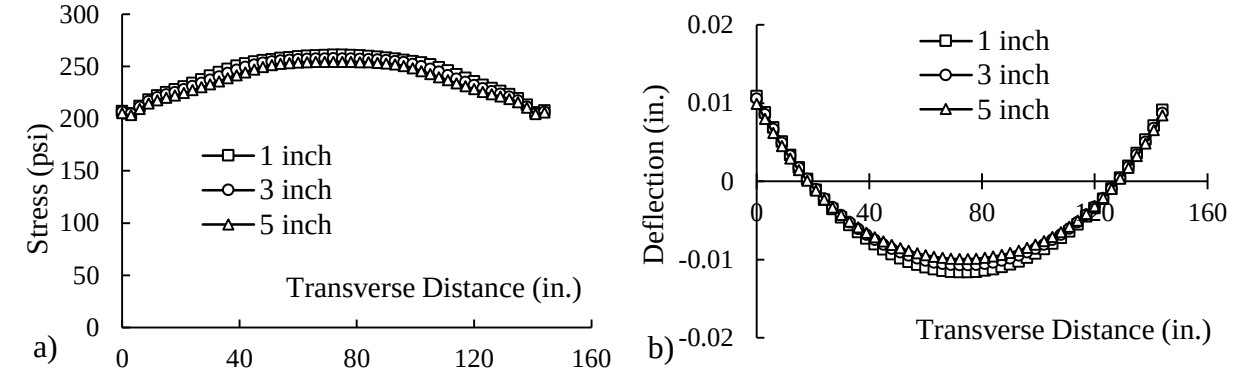

Figure 127 Case 2 (T+W) a) Maximum principal stress along Line 2; b) Deflection along Line 2. Line 2 is transverse to traffic. (1 in = 25.4 mm; 1 psi = 6.9 kPa)

8.2.3 Case 3: Effect of Joint Spacing

To study the effect of joint spacing, two models were developed with 13 ft (4.0 m) and 15 ft (4.6 m) joint spacing or slab length. When the rear wheel load is applied at the left edge of the 13 ft (4.0 m) slab, as shown in Figure 128, the same as for the 15 ft (4.6 m) slab, the front axle lies on the adjacent 13 ft (4.0 m) slab rather than at the other end of the same 15 ft (4.6 m) slab, as in Figure 113b).

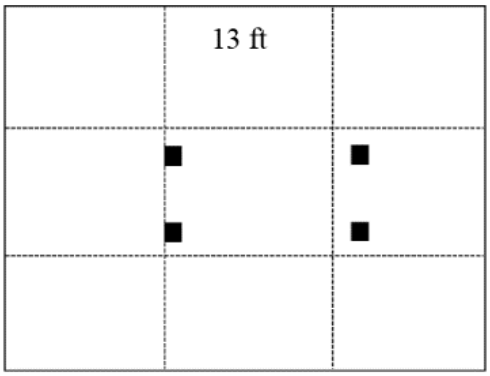

Figure 128 Wheel loading on 13 ft (4.0 m) joint spacing model. Compare to Figure 113b).

8.2.3.1 Wheel loading with no negative temperature gradient (W)

Figure 129 and Figure 130 present the maximum principal stress distribution and deflections along Line 1 and Line 2 due to wheel loading only. It can be seen from the plots that stress didn't change much along Line 1 and Line 2. Deflections along Line 1 remained unchanged from 15 ft (4.6 m) to 13 ft (4.0 m) joint spacing. Deflections along Line 2 decreased from 15 ft (4.6 m) to 13 ft (4.0 m) joint spacing, but the difference is very small.

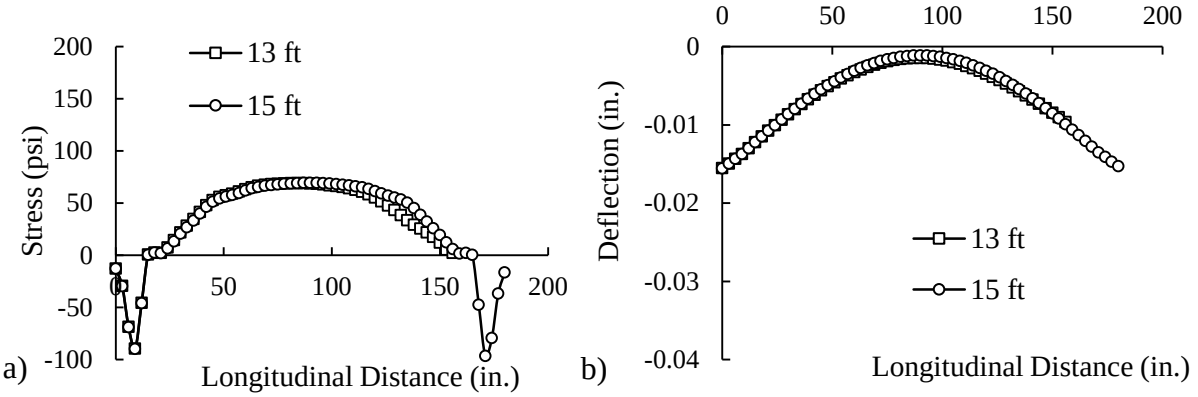

Figure 129 Case 3 (W) a) Maximum principal stress along Line 1; b) Deflection along Line 1. Line 1 is parallel to traffic. (1 in = 25.4 mm; 1 psi = 6.9 kPa)

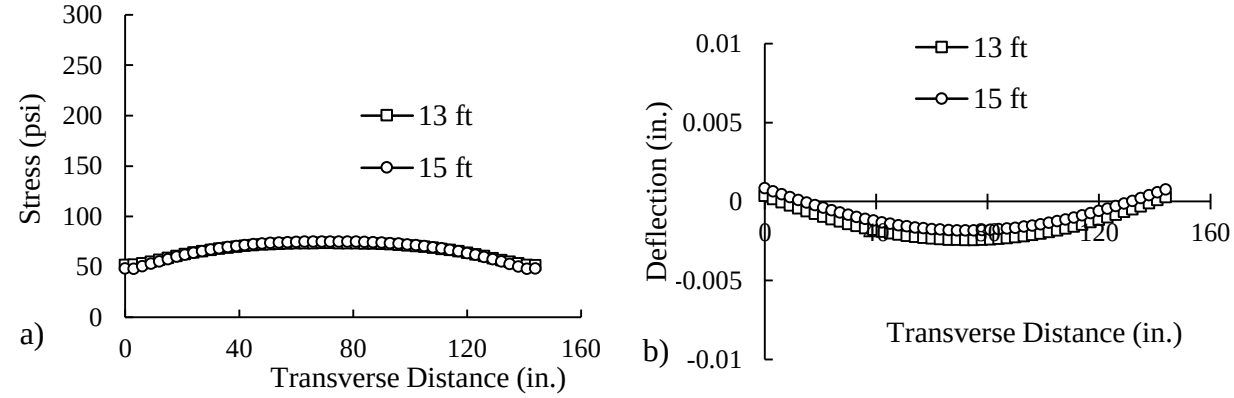

Figure 130 Case 3 (W) a) Maximum principal stress along Line 2; b) Deflection along Line 2. Line 2 is transverse to traffic. (1 in = 25.4 mm; 1 psi = 6.9 kPa)

8.2.3.2 Negative temperature gradient with no wheel loading (T)

Figure 131 and Figure 132 present the maximum principal stress distribution and deflections along Line 1 and Line 2 due to negative temperature only. It can be seen from the plots that the deflections didn't change much due to different joint spacing. Stress along Line 2 and middle of Line 1 decreased with smaller joint spacing.

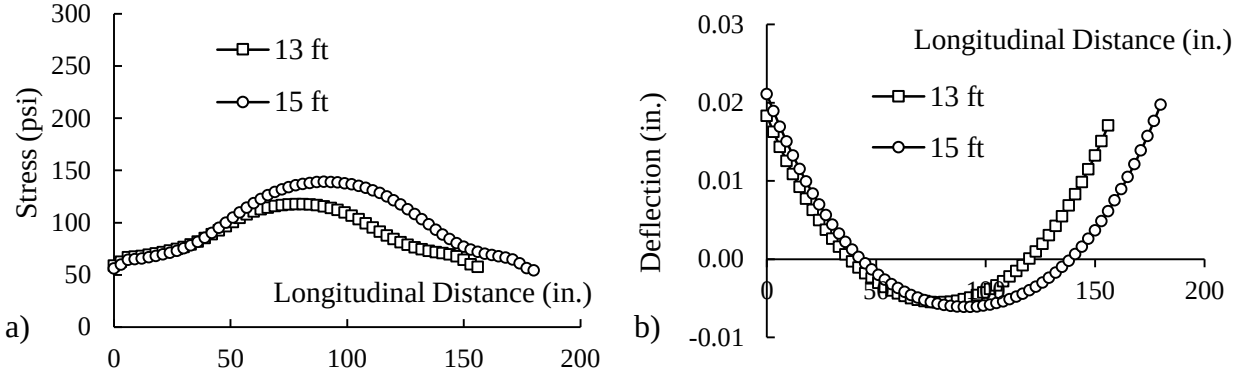

Figure 131 Case 3 (T) a) Maximum principal stress along Line 1; b) Deflection along Line 1. Line 1 is parallel to traffic. (1 in = 25.4 mm; 1 psi = 6.9 kPa)

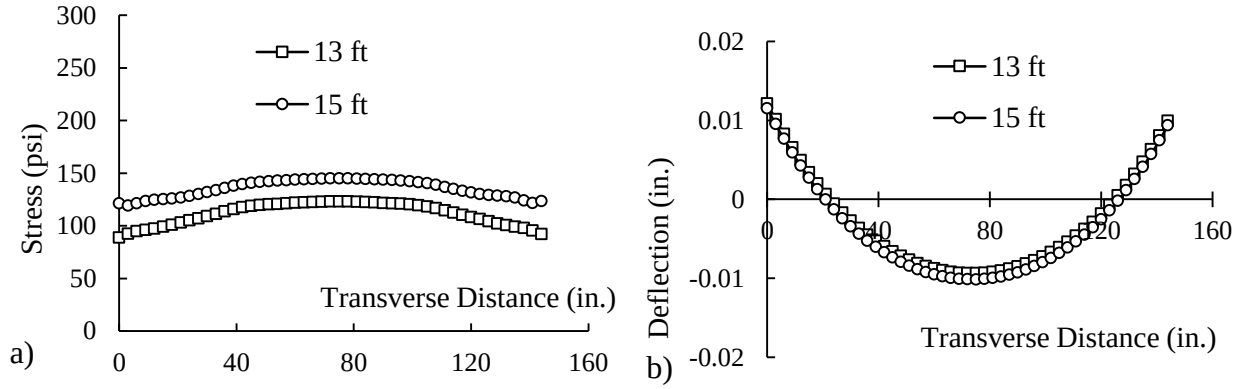

Figure 132 Case 3 (T) a) Maximum principal stress along Line 2; b) Deflection along Line 2. Line 2 is transverse to traffic. (1 in = 25.4 mm; 1 psi = 6.9 kPa)

8.2.3.3 Negative temperature gradient with wheel loading (T+W)

Figure 133 and Figure 134 present the maximum principal stress distribution and deflections along Line 1 and Line 2 due to negative temperature with wheel loading. The stress decreased with shorter joint spacing. Deflection along line 1 increased with shorter joint spacing on the loaded side of the slab. On the other side of the slab, however, deflection dropped significantly with 13 ft (4.0 m) joint spacing.

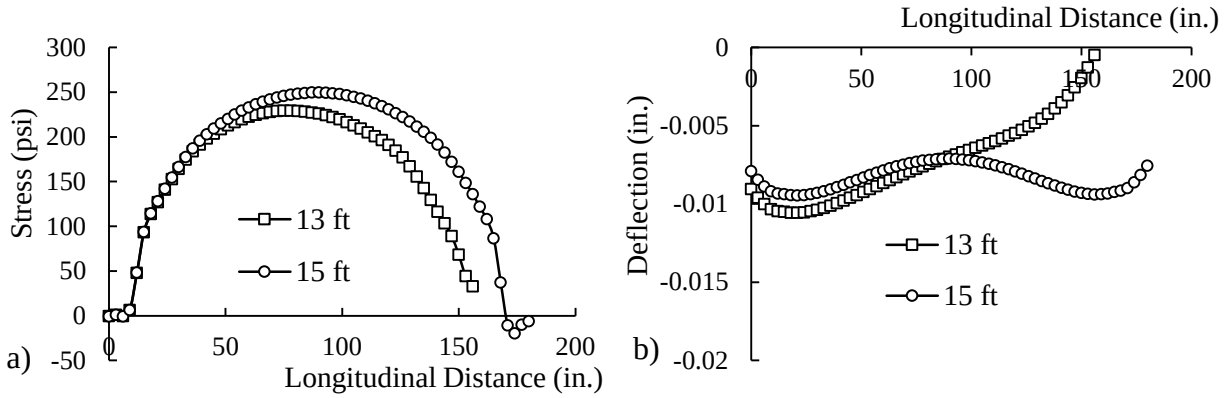

Figure 133 Case 3 (T+W) a) Maximum principal stress along Line 1; b) Deflection along Line 1. Line 1 is parallel to traffic. (1 in = 25.4 mm; 1 psi = 6.9 kPa)

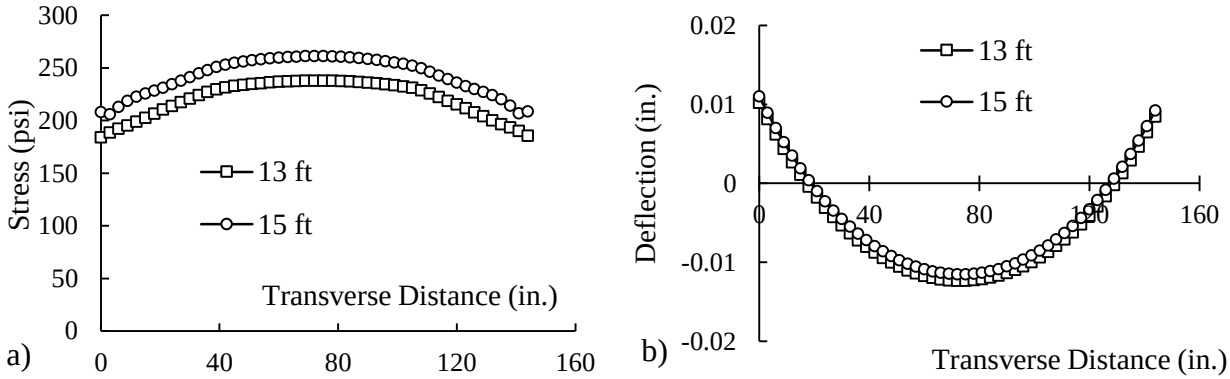

Figure 134 Case 3 (T+W) a) Maximum principal stress along Line 2; b) Deflection along Line 2. Line 2 is transverse to traffic. (1 in = 25.4 mm; 1 psi = 6.9 kPa)

8.3 Finite Element Modeling Summary

Based on the finite element modeling of UBCO pavement using ABAQUS, some observations are provided below.

- When there is material loss under the joints, stress on the surface of the slab increases when wheel loads are applied. The maximum stress occurred on the wheel path near the loss of support area. When the length of the loss of support area is 36 in (0.91 m), the maximum stress reaches 204 psi (1406 kPa) on the wheel path, but if there is no loss of support, the maximum stress is 69 psi (475 kPa) at the same location.
- Deflection increases at the edges of the slab when there is material loss under the joints.
- Loss of material under the joints has no effect on the case when the only load is a negative temperature gradient.
- When wheel and negative temperature gradient loads are combined, the stress increased up to 293.3 psi (2021 kPa) at mid-slab with 36-inch loss of support. The middle of the slab is under greater tension compared with no loss of support.
- Stress under wheel loading decreases with thicker AC bondbreaker. The maximum stress due to wheel loading decreased from 69 psi (0.48 MPa) to 59 psi (0.41 MPa) when

bondbreaker thickness increased from 1 in (25 mm) to 3 in (76 mm) and to 49 psi (0.34 MPa) when bondbreaker thickness increased to 5 in (127 mm).

- Stress under negative temperature gradient increases with thicker AC bondbreaker. The trends indicate maximum stress due to negative temperature gradient increased from 145 psi (1.00 MPa) to 152 psi (1.05 MPa) when the bondbreaker thickness increased from 1 in (25 mm) to 3 in (76 mm) and to 162 psi (112 MPa) when the bondbreaker thickness increased to 5 in (127 mm).
- When both wheel and negative temperature gradient loadings are combined, stress decreases in the middle of the slab with thicker AC bondbreaker, while stress at the edges increases with thicker AC bondbreaker.
- Deflection under wheel loading increases with thicker AC bondbreaker, while deflection under temperature gradient decreases with thicker AC bondbreaker. When both loadings combined, deflection decreases with thicker AC bondbreaker.
- Joint spacing has no or little effect on stress under wheel loading case only. Stress under negative temperature gradient decreases with shorter joint spacing. When both loadings are combined, stress in the middle of the slab decreased from 261 psi (1801 kPa) with 15 ft (4.6 m) joint spacing to 239 psi (1654 kPa) with 13 ft (4.0 m) joint spacing.
- Aggregate interlock between slabs was not considered. Aggregate interlock would increase LTE between slabs, which would give more conservative results.
- More accurate results can be obtained using 20-node elements. However, it takes significantly longer computation time with 20-node elements. Therefore the 8-node element was used in this study.
- A positive temperature gradient was not considered in this study, since it results in compression on the top surface of slab, while in this analysis top-down cracking is expected.

From the finite element analysis, it was found that:

- The design thickness of the concrete overlay was adequate and thickness design of the concrete was not a cause of premature failure.
- When a loss of bondbreaker occurs under the joints, the slab is under great tension when truck load and negative temperature gradient were applied together.
- A thicker bondbreaker layer reduces stresses in the overlay slab under truck load.
- A shorter joint spacing reduces stresses under a negative temperature gradient.
- The FEM considered joint spacings of 13 ft (4.0 m) and 15 ft (4.6 m), both of which performed about equally well when modeled under conditions of roughly 90% LTE. As the pavement ages and the LTE declines, it is expected that the shorter joint spacing will perform better.

9 Review of NCHRP Procedures

9.1 Introduction to NCHRP Procedures

Hundreds of forensic investigations have been performed on pavements in the United States in recent decades, mostly to investigate the underlying causes of premature failure. NCHRP Report 747, entitled *Guide for conducting forensic investigation on highway pavements* [Rada, et al., 2013], provides a systematic, practical, and logical procedure for conducting forensic investigations of pavements and collecting data for use in performance-prediction models. NCHRP Report 747 also provides guidance for using the data to determine the reasons behind premature failures or exceptionally good performance. Figure 135 shows the flowchart mapping the investigation approach suggested by NCHRP Report 747. Reasons for conducting forensic investigations include one or a combination of the following, quoted from the report [Rada, et al., 2013]:

- *Determining reasons for poor pavement performance/premature failures.*
- *Understanding exceptional pavement performance and/or longevity.*
- *Validating pavement performance prediction (actual versus predicted).*
- *Closing-out/conducting final investigations of experimental test sections.*
- *Collecting project specific data for:*
  - *Rehabilitation design;*
  - *Litigation purposes (e.g., settling disputes or defending/supporting claims and lawsuits).*
- *Collecting general data to:*
  - *Support development and/or calibration of pavement performance prediction models,*
  - *Understand/quantify long-term effects of traffic and environment on material properties.*
  - *Evaluate specific design and/or construction practices.*
- *Certifying pavement-related warranties.*
- *Evaluating new pavement-related products or techniques.*

Types and causes of PCC distress are listed in Table 35, and a summary of materials related distresses, symptoms, and causes is given in Table 36.

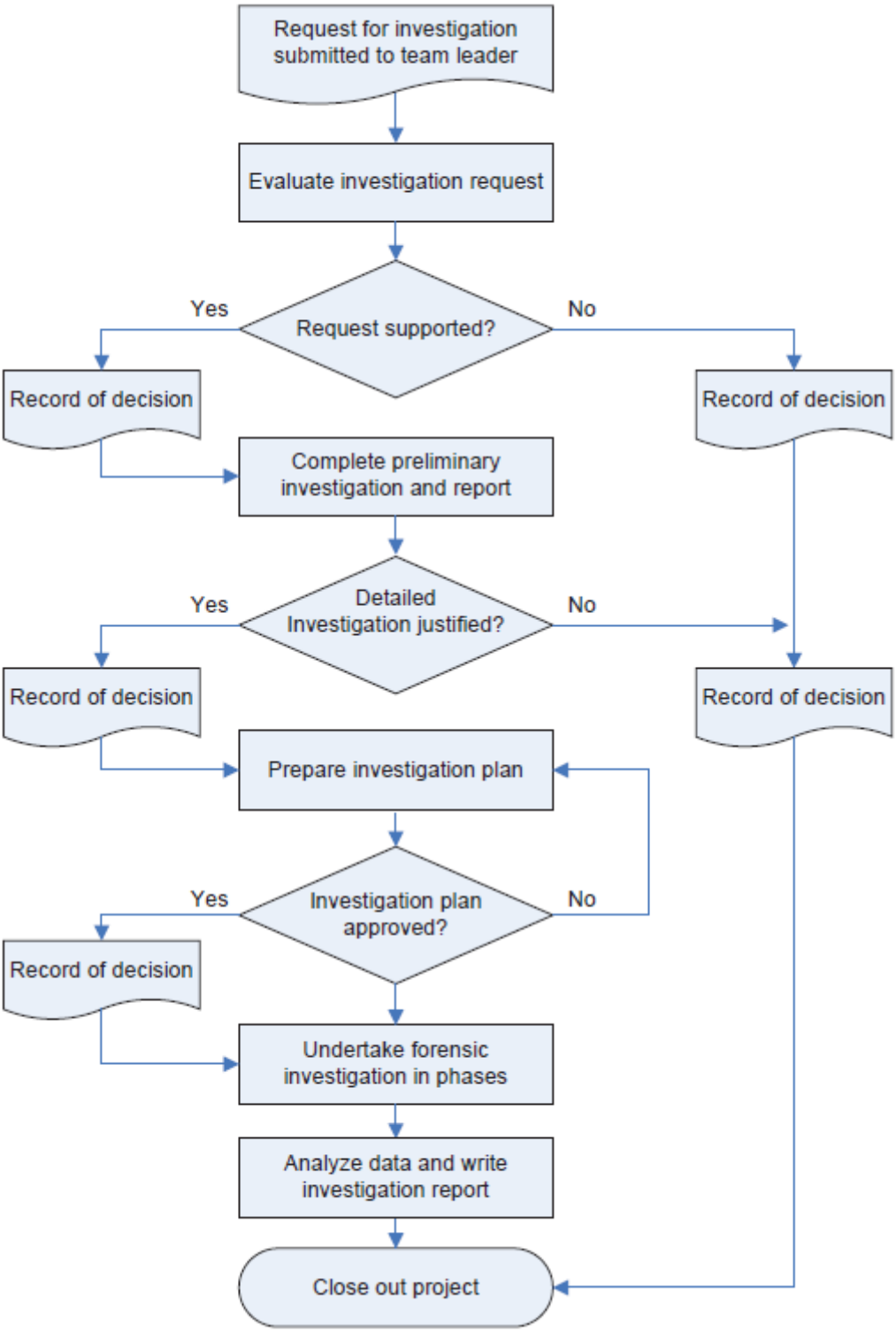

Figure 135 Recommended general approach to forensic investigations [Rada, et al., 2013].

Table 35 Example PCC distress types and possible causes [Rada, et al., 2013].

Structural Distress	Contributing Factors[1]					
	Pavement Design	Load	Water	Temp.	Pavement Materials	Construct.
Structural Distress						
Cracking[2]						
Transverse	P	P	N	C	C	P
Longitudinal	P	P	N	C	C	P
Corner	C	P	C	C	N	N
Intersecting	C	P	C	N	C	N
Possible causes of cracking: Fatigue, joint spacing too long, shallow or late joint sawing, base or edge restraint, loss of support, freeze-thaw and moisture-related settlement/heave, dowel bar lock-up, curling, and warping.						
Joint/Crack Deterioration						
Spalling	C	C	N	C	P	C
Pumping[2]	C	P	P	N	C	N
Blowups	C	N	N	P	C	N
Joint Seal Damage[2]	C	C	C	C	P	C
Possible causes of joint/crack deterioration: Incompressibles in joint/crack, material durability problems, subbase pumping, dowel socketing or corrosion, keyway failure, metal or plastic inserts, rupture and corrosion of steel in JRCP, high reinforcing steel.						
Punchouts[2]	P	P	C	N	C	N
Possible causes of punchouts: Loss of support, low steel content, inadequate concrete slab thickness, poor construction procedures.						
Durability						
D-cracking	N	N	P	C	P	N
Alkali-Silica Reactivity (ASR)	N	N	P	C	P	N
Freeze-thaw damage	N	N	P	P	P	C
Possible causes of durability distresses: Poor aggregate quality, poor concentrate mixture quality, water in the pavement structure.						
Functional Distress						
Roughness						
Faulting[2]	P	P	P	C	C	N
Heave/swell[2]	C	N	P	P	C	N
Settlement[2]	C	C	C	N	N	C
Patch deterioration	C	C	C	C	C	C
Possible causes of roughness: Poor load transfer, loss of support, subbase pumping, backfill settlement, freeze-thaw, and moisture-related settlement/heave, curling and warping, and poor construction practices.						
Surface Polishing	N	C	N	N	P	N
Possible causes of surface polishing: High volumes of traffic, poor surface texture, wide uniform tine spacing, wide joint reservoirs, and wheel path abrasion because of studded tires or chains.						
Noise	P	C	N	N	C	P
Possible causes of noise: High volumes of traffic, poor surface texture, wide uniform tine spacing, wide joint reservoirs, and wheel path abrasion because of studded tires or chains.						
Surface Defects						
Scaling	N	N	C	C	P	P
Popouts	N	N	C	C	P	C
Crazing	N	N	N	C	C	P
Plastic shrinkage cracks	N	N	N	C	C	P
Possible causes of surface defects: Over-finishing the surface, poor concrete mixture, reactive aggregates, and poor curing practices.						

[1] P= Primary Factor C= Contributing Factor N= Negligible Factor

[2] Loss of support is an intermediary phase between the contributing factors and these distresses. Loss of support is affected by load, water, and design factors.

Table 36 Summary of key Materials Related Distresses (MRD) in PCC pavements [Rada, et al., 2013]

Type of MRD	Surface Distress Manifestations and Locations	Causes/ Mechanisms
Materials Related Distress Due to Physical Mechanisms		
Freeze-Thaw Deterioration of Hardened Cement Paste	Scaling, spalling, or map cracking, generally initiating near joints or cracks; possible internal disruption of concrete matrix.	Deterioration of saturated cement paste due to repeated freeze-thaw cycles.
Deicer Scaling/ Deterioration	Scaling or crazing of the slab surface with possible alteration of the concrete pore system and/or the hydrated cement paste leading to staining at joints/cracks.	Deicing chemicals can amplify freeze-thaw deterioration and may interact chemically with cement hydration products.
Freeze-Thaw Deterioration of Aggregate	Cracking parallel to joints and cracks and later spalling; may be accompanied by surface staining.	Freezing and thawing of susceptible coarse aggregates results in fracturing and/or excessive dilation of aggregate.
Materials Related Distress Due to Chemical Mechanisms		
Alkali-Silica Reactivity (ASR)	Map cracking over entire slab area and accompanying expansion-related distresses (joint closure, spalling, and blowups).	Reactions involving hydroxyl and alkali ions in pore solution and reactive silica in aggregate resulting in the build-up of expansive pressures within aggregate, until tensile strength of surrounding paste matrix is exceeded, resulting in cracks.
Alkali-Carbonate Reactivity (ACR)	Map cracking over entire slab area and accompanying pressure-related distresses (spalling, blowups).	Expansive reaction involving hydroxyl and alkali ions in pore solution and certain dolomitic aggregates resulting in dedolomitization and brucite formation.
External Sulfate Attack	Fine cracking near joints and slab edges or map cracking over entire slab area, ultimately resulting in joint or surface deterioration.	Expansive formation of ettringite that occurs when external sources of sulfate (e.g., groundwater, deicing chemicals) react with the calcium sulfoaluminates.
Internal Sulfate Attack	Fine cracking near joints and slab edges or map cracking over entire slab area.	Formation of ettringite from internal sources of sulfate that results in expansive disruption in the paste phase or fills available air voids, reducing freeze-thaw resistance.
Corrosion of Embedded Steel	Spalling, cracking, and deterioration at areas above or surrounding embedded steel.	Chloride ions penetrate concrete, resulting in corrosion of embedded steel, and formation of high-volume oxidation products and resultant expansion.

9.2 Investigation Plan

Based on the NCRHP Report 747 [Rada et al., 2013] procedures and the Ohio University research team's extensive experience conducting forensic investigations, an investigation plan was proposed and executed in this project. The investigation included preliminary investigation stage and forensic investigation stage following the NCHRP procedures. The preliminary investigation work included:

- Collect and review relevant project information (i.e. structural design, material design), existing NDT and Destructive Testing results, and construction diaries.
- Conduct literature review.

The forensic investigation stage work included:

- Initial visual assessment.
- Distress survey/profile
- FWD testing on the project.
- Identify a precise locations for forensic investigation. The first location should include the problems under investigation to the fullest extent possible. The second section, on a different portion of the same project, has little or no distress and serves as a control.
- Additional visual assessment in selected distressed and control sections.
- Additional non-destructive testing on selected distressed and control sections.
- Destructive testing and sampling on distressed and control sections.
- Laboratory testing and petrographic analysis of specimens collected.
- Finite element analysis and HIPERPAV analysis as needed.

Field work includes falling weight deflectometer test; video distress survey; core extraction, and slab removal. Lab work includes petrographic analysis and mechanical properties testing of PCC core samples. Common types of non-destructive testing equipment include FWD, profilometers, and MITScan. Section 3.3 gives a brief introduction of non-destructive testing equipment used for this study. The analysis of FWD data is presented in Section 3.4. Section 3.5 presents the MITScan and destructive field testing. Coring is discussed in Section 3.6 and laboratory testing conducted on the cores is discussed in Section 3.7.

9.3 Recommendations regarding NCHRP procedures

NCHRP Report 747 provides 24 forms that may be used to document the forensic investigation. The forms used and the degree of detail captured will depend on the specific nature of the investigation, the level of specificity required, and the amount of information required to implement any findings [Rada et al., 2013]. Table 37 provides the complete list of 24 forms, with those applicable to this study marked. In this project, only core log forms were used for convenience. The rest of the applicable forms were not used because they are either for solely administrative purposes or the content of the form has been covered in the report. Future forensic investigations on UBCO pavements may refer to this table and utilize selected forms.

Table 37 List of forensic investigation forms from NCHRP Report 747 [Rada et al., 2013].

#	Form Name	Applicable
Form #1	Forensic Investigation Request	**Y**
Form #2	Preliminary Investigation	**Y**
Form #3	Decision to Proceed	**Y**
Form #4	Preliminary Investigation Report	
Form #5	Forensic Investigation Team	**Y**
Form #6	Pre-Investigation Site Visit	**Y**
Form #7	Photograph Record	**Y**
Form #8	Visual Assessment Form (Asphalt/Surface Treatment)	
Form #9	Visual Assessment Form (Portland Cement Concrete)	**Y**
Form #10	Initial Non-Destructive Testing Plan	**Y**
Form #11	Initial Forensic Investigation Plan	**Y**
Form #12	Interim Report Cover Sheet	**Y**
Form #13	Final Non-Destructive Testing Plan	**Y**
Form #14	Destructive Testing Plan	**Y**
Form #15	Final Forensic Investigation Plan	**Y**
Form #16	Forensic Investigation Site Report	**Y**
Form #17a	Core Log (Single Core)	
Form #17b	Core Log (Multi Core)	**Y**
Form #18	Test Pit Profile	
Form #19a	Asphalt Concrete/Asphalt Surface Treatment Layer Log	
Form #19b	Portland Cement Concrete Layer Log	**Y**
Form #20	Gravel and Stabilized Layer Log	
Form #21	Sample Log	
Form #22	Density and Moisture Content	
Form #23	Dynamic Cone Penetrometer	
Form #24	Final Report Cover Sheet	**Y**

10 Summary, Conclusions, and Recommendations

10.1 Summary

The thicknesses of the PCC overlays for each project, based on statistics compiled from the measurements of all cores, are plotted in Figure 136, along with design thicknesses. The measured thicknesses are each close to the design value, though MAD-70 distressed section shows a greater variability in the measurements than the other sections, particularly the MAD-70 control section. The thickness design was not found to be an issue for any of the overlay projects.

The thicknesses of the AC bondbreaker layers are given in Figure 137. The design thickness was 1 in (25 mm) for each project, but the MAD-70 Westbound and WAS/NOB-77 bondbreaker thicknesses are far greater than the design values, with the control sections being thicker than the distressed sections.

The compressive and tensile strength of the PCC layer in each section is given in Figure 138 and Figure 139, respectively. In all cases, these strengths exceed the ODOT design criteria indicated by the red line. The elastic modulus (*E*) values are plotted in Figure 140; only WAS/NOB-77 meets the current ODOT criterion of 5 million psi (34.5 GPa), while the others fall short by up to about 20%, except MAD-70 distressed, which at 2.8 million psi (19.3 GPa) is 44% below the ODOT criterion. Note that only one specimen was measured from each section on MAD-70 and WAS/NOB-77, and only one specimen for the sites LAK-90 and ASD-30, with LAK-90 control and ASD-30 distressed sections not included. The coefficient of thermal expansion values for each site are plotted in Figure 141, representing three values for each section except LAK-90 distressed and ASD-30 distressed, which were not measured.

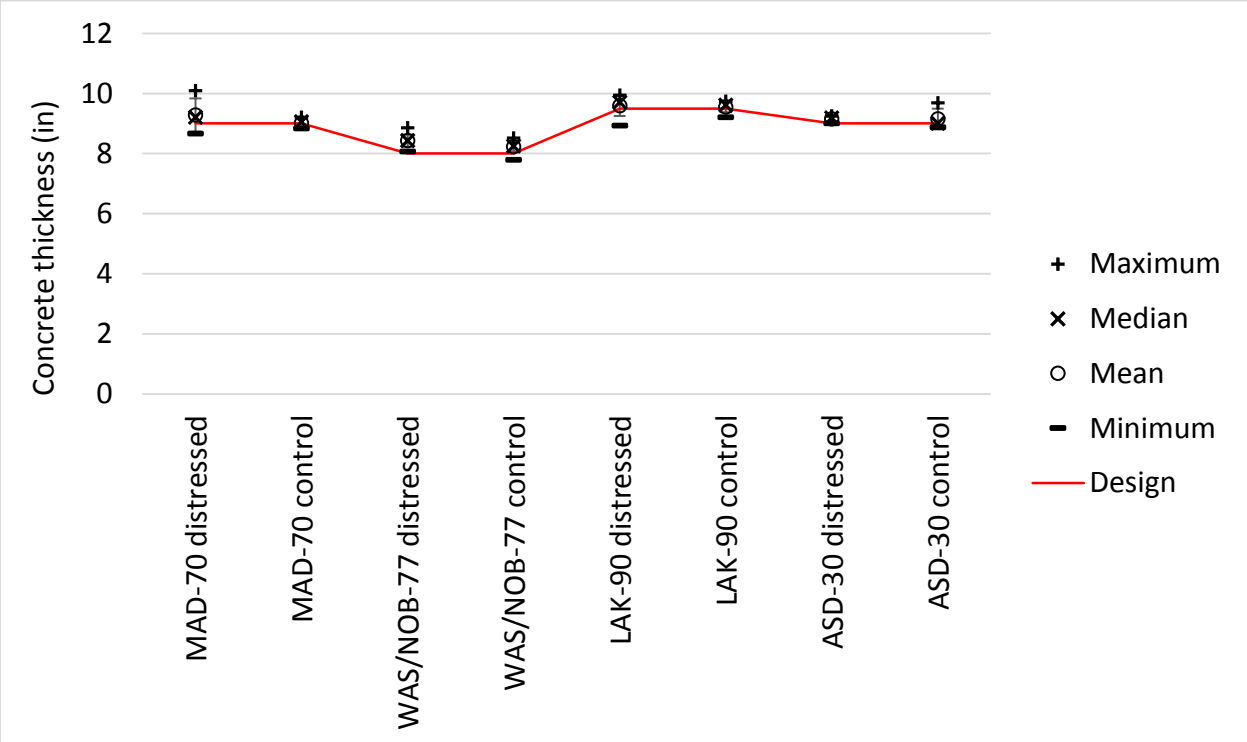

Figure 136 PCC Overlay thicknesses of each project compared to design values (1 in =25.4 mm).

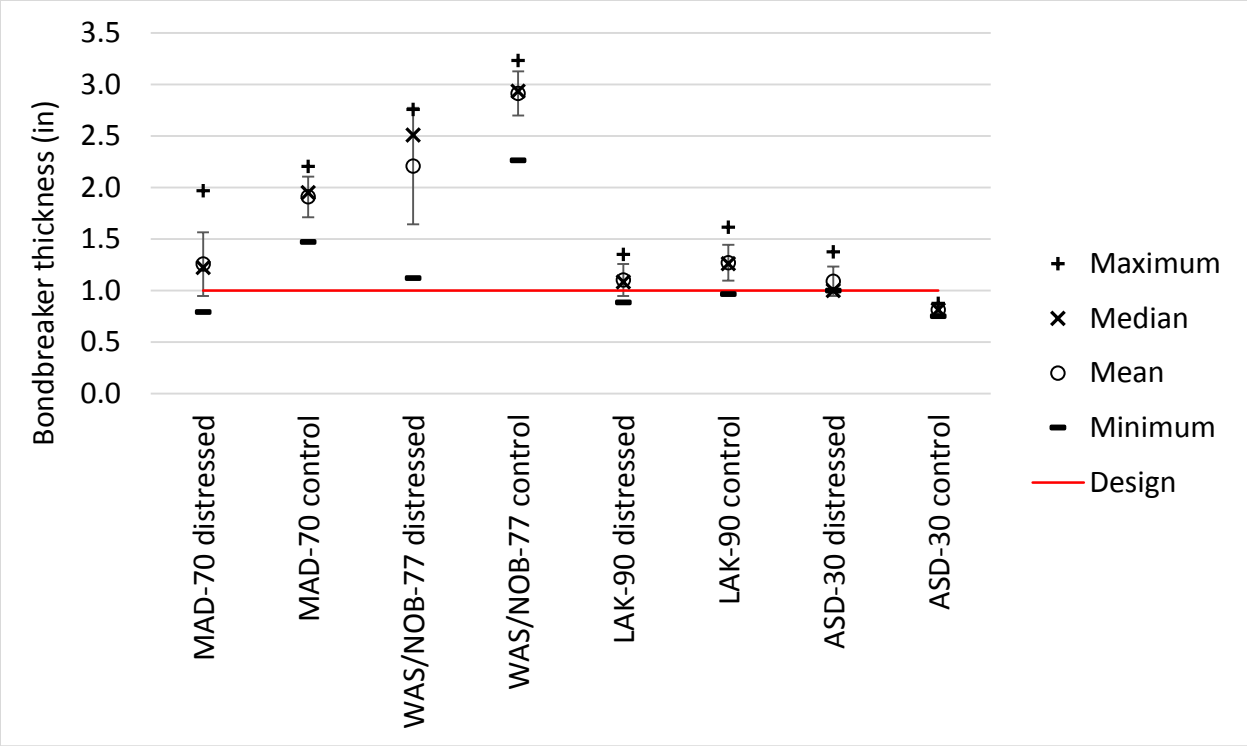

Figure 137 Bondbreaker thicknesses of each project compared to design values (1 in =25.4 mm).

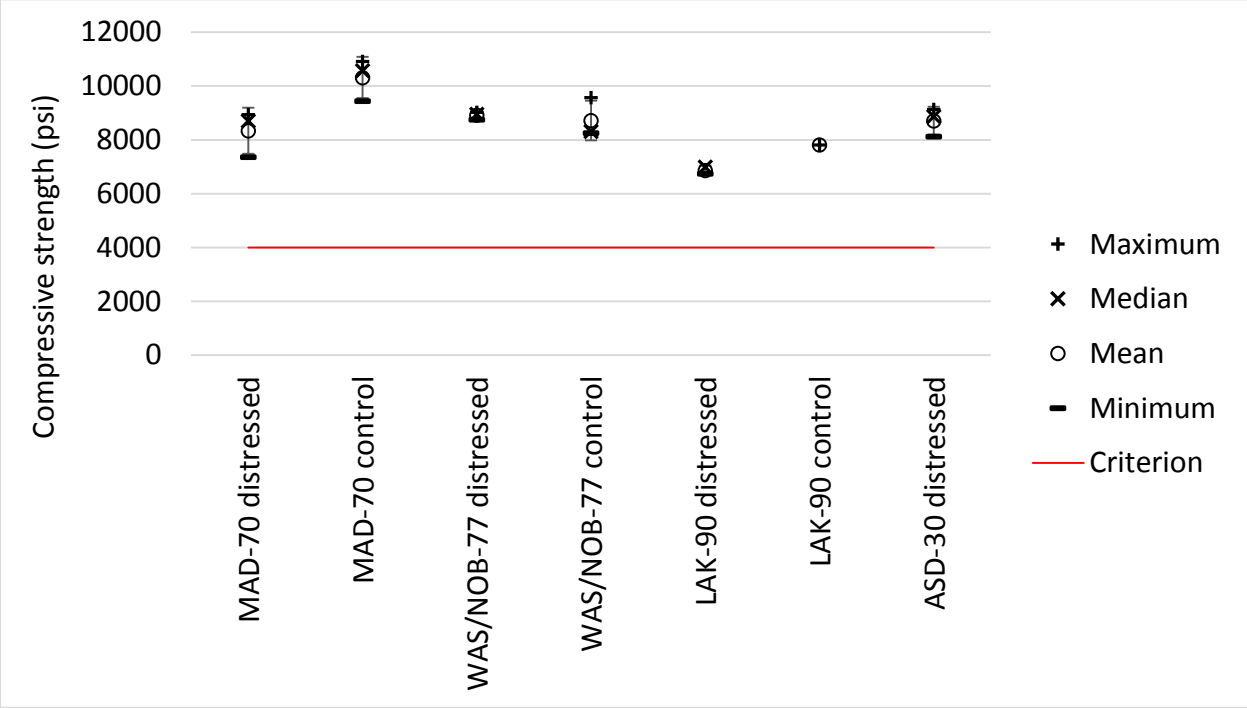

Figure 138 Compressive strength of PCC overlay for each project (1000 psi = 6.89 MPa).

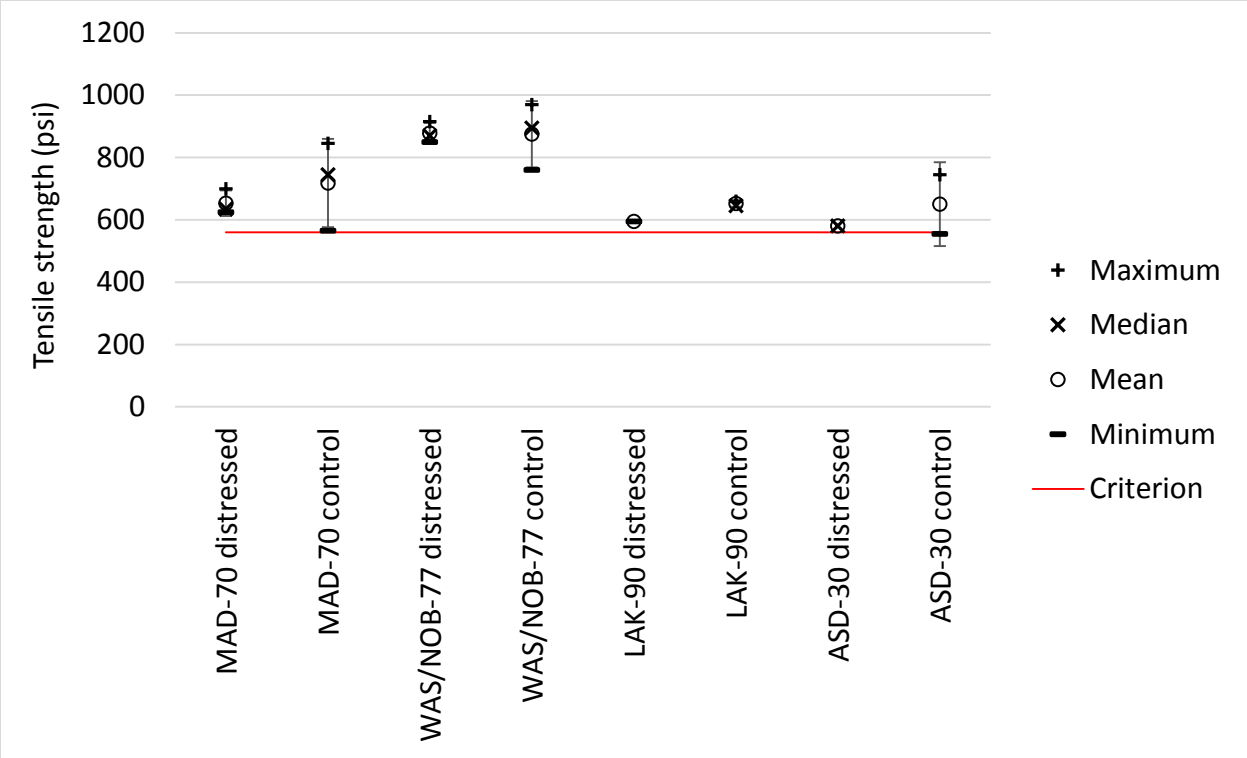

Figure 139 Tensile strength of PCC overlay for each project (1000 psi = 6.89 MPa).

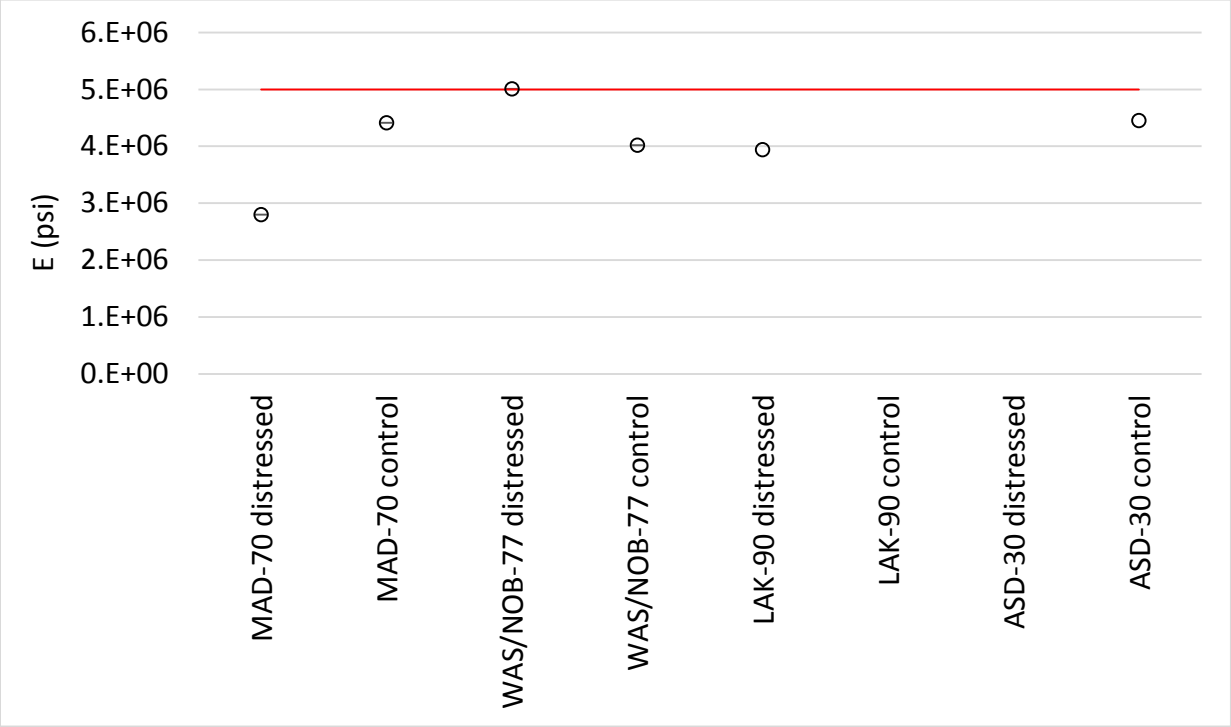

Figure 140 Elastic modulus (*E*) of PCC overlay for each project (1E+06 psi = 6.89 GPa). Note this parameter was not measured for LAK-90 control or ASD-30 distressed sections.

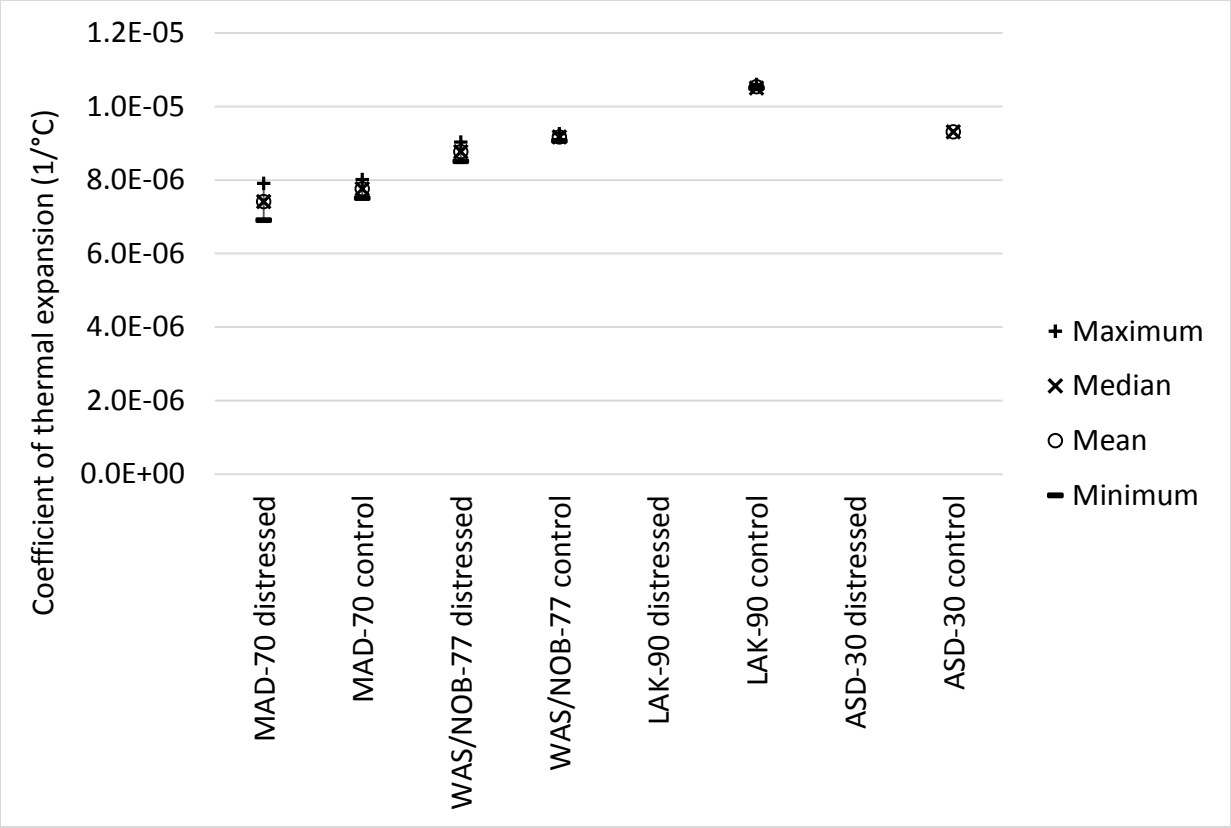

Figure 141 Coefficient of thermal expansion for each project (1/°C = 1.8/°F). Note this parameter was not measured for LAK-90 distressed or ASD-30 distressed sections.

Table 38 presents the MITScan results of all scanned sections (MAD-70, WAS/NOB-77, and ASD-30). In terms of horizontal rotation, I-77 NB has the most misalignment of this type, with 9.9% over the rejection limit and 69.7% under the acceptance limit. The acceptance rates of other sections are at least 88.3%. US-30 WB has 9.0% over the rejection limit and I-70 EB has 6.8% over the rejection limit. Other rejection rates were 2.8% or less.

In terms of vertical rotation, I-70 EB has the highest rejection rate of 29.2%, followed by US-30 EB at 22.7% and I-77 SB at 19.4%. The lowest acceptance, however, is on US-30 EB, which is only 35.3%. US-30 WB also has a low acceptance rate of 47.7%.

In terms of depth translation, I-70 EB has the highest rejection rate of 34.2%, and an acceptance rate of 57.1%. I-70 WB, US-30 WB, and US-30 EB also have relatively low acceptance rates (60.1%, 60.5%, and 72.3%, respectively).

In terms of longitudinal translation, I-77 SB has the highest rejection rate of 10.4%. US-30 WB and US-30 EB have respective rejection rates of 9.2% and 9.9%. The acceptance rate was lowest on US-30 EB at 70.6%, followed by US-30 WB and I-77 SB at 78.4% and 79.9%, respectively

In terms of horizontal translation, all sections have high rejection rates except for I-77 SB, which is believed to be a result of a test error. When scanning the transverse joints on most test sections, the crew couldn't run the MIT Scan-2 from the very edge of the joint because of the traffic on the adjacent lane. This resulted in the first bar missing from most of the scans and the x-position measurements were recorded with an offset that threw the measured x positions off from

expected values. Therefore, the x-position of scanned bars deviates significantly from the designed x-position and resulted in high horizontal translation misalignment. If the anomalous I-77 SB results are disregarded, the acceptance rate is 10.8% (I-70 WB) or 9.2% (US-30 EB) or well below that. Rejection rates range from 85.7% (I-70 WB) to 52.7% (I-70 EB).

If the first bar in each joint is used as a reference point, and the distance between each bar and its preceding neighbor is measured and compared to the design value of 12 in (305 mm), with the same acceptance and rejection criteria as before, the alignment appears to be much better. For the distressed section on I-70 EB, the acceptance rate is 86.21% and the rejection rate is 6.90%, most likely due to a number of bars positioned at anomalous spacings possibly during repairs, though an effort was made to avoid scanning obviously repaired joints. For all the other sections, the acceptance rates are above 90%, and the rejection rate is 0.00%. While the horizontal translation readings produced very low acceptance rates, those are clearly the effect of the positioning of the origin of the x axis origin, which was difficult given the limited lane width the vehicle was operated in due to traffic control. The dowel bar spacings are much closer to the design value of 12 in (305 mm) in each case, but other than the low rating on the damaged section of MAD-70, there is no clear relationship between dowel bar spacing or horizontal position and the performance of the observed overlay.

Although the MITScan was performed on over 100 bars and 11 joints in each test section, only four locations and eight test sections were evaluated, which statistically are too few locations to draw recommendations with confidence. However, some trends were observed when comparing dowel bar alignment values with visible distress, which should be investigated further by ODOT. Sections with high vertical rotation, at least 19% of the bars exceeding rejection criteria, had longitudinal cracking while the sections with less than 7% of the bars exceeding criteria had no longitudinal cracking. A trend was also observed when comparing depth translation, the distressed section on MAD-70 with 29.2% of the bars exceeding the rejection criteria had a much lower load transfer efficiency, 54.0% on average on the approach side and 39.1% on the leave side, and below 20% for some joints, while the control sections with less than 15% of the bars exceeding the rejection criteria had LTE everywhere greater than 70%. No observed correlation was noted between MITScan results and spalling or transverse cracking.

Table 38 Summary of MITScan results. In the third column, D indicates the designated distressed section and C the corresponding control section.

Misalignment Type	Section		accept		reject	
			|d| ≤0.5	0.5< |d| ≤0.7	|d| >0.7	No. Bars
Horizontal Rotation	I-70 EB	D	91.30%	1.90%	6.80%	161
	I-70 WB	C	98.60%	1.40%	0.00%	148
	I-77 SB	D	89.60%	7.60%	2.80%	144
	I-77 NB	C	69.70%	20.40%	9.90%	152
	US-30 EB	D	95.80%	1.70%	2.50%	119
	US-30 WB	C	88.30%	2.70%	9.00%	111
Vertical Rotation	I-70 EB	D	57.10%	13.70%	29.20%	161
	I-70 WB	C	89.20%	6.80%	4.10%	148
	I-77 SB	D	63.90%	16.70%	19.40%	144
	I-77 NB	C	83.60%	11.80%	4.60%	152
	US-30 EB	D	35.30%	42.00%	22.70%	119
	US-30 WB	C	47.70%	37.80%	14.40%	111
	Section		|d| ≤0.5	0.5< |d| ≤0.66	|d| >0.66	No. Bars
Depth Translation	I-70 EB	D	57.10%	8.70%	34.20%	161
	I-70 WB	C	60.10%	23.00%	16.90%	148
	I-77 SB	D	98.60%	1.40%	0.00%	144
	I-77 NB	C	84.90%	9.20%	5.90%	152
	US-30 EB	D	72.30%	16.00%	11.80%	119
	US-30 WB	C	60.50%	33.30%	6.10%	114
	Section		|d| ≤2	2< |d| ≤2.3	|d| >2.3	No. Bars
Longitudinal Translation	I-70 EB	D	89.40%	3.70%	6.80%	161
	I-70 WB	C	93.20%	6.10%	0.70%	148
	I-77 SB	D	79.90%	9.70%	10.40%	144
	I-77 NB	C	90.10%	6.60%	3.30%	152
	US-30 EB	D	70.60%	20.20%	9.20%	119
	US-30 WB	C	78.40%	11.70%	9.90%	111
	Section		|d| ≤0.5	0.5< |d| ≤2	|d| >2	No. Bars
Horizontal Translation	I-70 EB	D	1.90%	12.40%	85.70%	161
	I-70 WB	C	10.80%	36.50%	52.70%	148
	I-77 SB	D	76.40%	23.60%	0.00%	144
	I-77 NB	C	2.00%	23.00%	75.00%	152
	US-30 EB	D	9.20%	36.10%	54.60%	119
	US-30 WB	C	0.90%	32.50%	66.70%	114
Dowel Bar Spacing	I-70 EB	D	86.21%	6.90%	6.90%	145
	I-70 WB	C	99.25%	0.75%	0.00%	133
	I-77 SB	D	94.66%	5.34%	0.00%	131
	I-77 NB	C	91.37%	8.63%	0.00%	139
	US-30 EB	D	98.15%	1.85%	0.00%	108
	US-30 WB	C	93.20%	6.80%	0.00%	103

10.2 Conclusions and Recommendations

The conclusions for the investigation of premature distresses at each unbonded overlay project selected for this study are given below. The primary causes of premature distress were impacted by different factors at each site. There was some commonality between the sites, however. The main causes of the distresses appear to be the presence of water and poor construction quality control.

Regarding water issues:

- Since water is damaging both the AC bondbreaker and PCC overlay, and even though a thicker bondbreaker with increased binder will help protect the pavement, as long as water is present, the PCC will still be prematurely damaged.
- The best solution is to get rid of the water, and the recommended overlay construction techniques are the use of fabric, permeable bondbreaker, fracturing the existing slabs prior to placing the unbonded overlay, or a combination of these.

Regarding poor construction quality control, specific examples were identified by the forensic investigation:

- Not wetting bondbreaker before placing concrete.
- Misalignment of dowel bars.
- Vibration of concrete by dowel bar insert, leading to segregation, entrapped air voids, and different material properties in the PCC above and below the dowel bars.
- Placing concrete when the air temperature and temperature variation over the three days after placing the concrete create stresses in the pavement which exceed the strength of the concrete.

Regarding microcracking observed on petrographic examination of cores from WAS/NOB-77, LAK-90, and ASD-30:

- The petrographer believes these microcracks are likely shrinkage related. Many parameters contribute to shrinkage. The detailed records (i.e. mixture composition, batching tickets, temperature and the wind conditions at the time of concrete placement, evidence of curing (or lack thereof)) required to confirm the causes on these projects were not readily available.

Specific conclusions regarding individual projects appear below.

10.2.1 MAD-70 (1999)

- The major contributions to distress came from the presence of water in the joints. This excess water was not able to drain, leading to negative impacts on both asphalt and concrete at the joints.
- On the concrete, it appears there were some mineral constituents in the concrete that migrated into the air voids. In the majority of petrographic specimens, the air voids are filled. There are two consequences: chemical deterioration that weakens the concrete, and the filled air voids will permit freeze-thaw processes to break the concrete. Tenting was observed at the joints as a consequence.
- Also road salt applied during winter dissolved and moved into the joints. Because the lack of drainage, the salt is retained in the water and migrates into the concrete.
- The excess water was also trapped in the thin layer of the bondbreaker. Traffic loads caused high pore water pressure, damaging the asphalt and causing loss of support under

the overlay slab. This led to corner breaks, faulting, and in some places to mid-panel breaks, both of which were observed in the field visit.

- Since there is no drainage, the trapped water created optimal conditions for premature distresses. This could be solved by draining the water, which can be done using fabrics or permeable asphalt of sufficient thickness – 2.5 in (64 mm) or greater for permeable asphalt constructed using AASHTO #67 or #57 aggregate.
- The bondbreaker was thicker in the westbound direction, which performed better than the eastbound direction. The westbound direction also showed more consistency in measured properties, thickness, and dowel bar alignment, indicating better construction and material quality control.
- Based on review of photographs taken during construction, the asphalt bondbreaker was dry before the concrete overlay was placed.
- During slab removal, there was no indication the underlying cracks and joints in the original pavement had an effect on the location of cracking or the deterioration in the overlay.
- The petrographic analysis, besides finding the filled air voids, did verify that the concrete was well cured and that the slag cement content was not an issue.
- Top-down cracking was observed in both of the two cores collected at mid-slab, one in each direction.
- The concrete was placed on dry bondbreaker, absorbing moisture from the concrete, reducing the water available for hydration, which could have had an impact on the strength of the concrete. However the PCC still had good strength in laboratory tests.
- Ohio is using slag cement and not sealing joints. These practices may continue, as both improve the performance [Olek, 2016].

10.2.2 WAS/NOB-77 (2005)

- The overall performance was good. Distress was limited in both directions.
- Longitudinal cracking was the predominant type of distress observed.
- The asphalt bondbreaker thickness was significantly thicker than the plan thickness of 1 in (25 mm), averaging 2.9 in (74 mm) on NB and 2.2 in (56 mm) on SB. Two lifts of asphalt were placed during construction.
- Laboratory testing showed good material strength and properties for the concrete.
- Poor dowel alignment was found on the selected sections. 19.4% of scanned dowel bars exceeded ODOT dowel bar vertical alignment rejection criteria on the more distressed SB section. The dowel bar inserter may have contributed to the dowel misalignment. While no direct correlation between dowel bar alignment and distress was noted, the misalignment is presented as an indication of poor construction quality control.
- A horizontal crack was found at dowel bar level on a core taken near the joint. The crack was likely caused by dowel bar misalignment.
- ODOT should further investigate whether the dowel inserter is properly positioning dowel bars into the pavement and/or creating entrapped air voids above the dowel bars. Also, it appears the vibrations from the inserter created segregation that likely weakened the concrete above the dowel bars.

10.2.3 LAK-90 (2005)

- The PCC mix contained slag aggregate and slag cement. In a very short period of time after construction in 2005 a significant amount of cracking was observed on the surface in both longitudinal and transverse directions, because the slower curing of the slag cement made it vulnerable to low temperatures.
- In this project since the pavement expressed distress in so short a time, there is not much impact from the bondbreaker. The failure is clearly in the concrete.
- HIPERPAV simulation of early age indicates some sections had cracked because the concrete was placed at a lower temperature than recommended. In particular, at about 18 hours after placement, the tensile stress at the top surface of the concrete exceeded the strength.

10.2.4 ASD-30 (1998)

- This project had generally performed well. The variability of the mechanical properties of the materials was low. Distress was limited to longitudinal cracking and minor distress at joints.

10.2.5 Finite Element Model

- The 3-D FEM was used to simulate the stresses due to temperature and cyclic loads, and the level of stress was significantly higher in zones where cracks were observed, particularly when the environmental and traffic loads occurred in concert.
- The 3-D FEM indicated the design thickness of the concrete overlay was adequate and thickness design of the concrete was not a cause of premature failure.
- The 3-D FEM demonstrated the improved performance of 13 ft (4.0 m) joint spacing due to decreased stress under negative temperature gradient.
- The 3-D FEM also verified a thicker bondbreaker layer reduces stresses in the overlay slab under truck load and a shorter joint spacing reduces stresses under a negative temperature gradient.

10.3 Implementation

To implement the recommendations of this research, ODOT should focus on the following items concerning design, water drainage, and construction QC/QA.

With regards to design:

- Consider a lower elastic modulus value for design of concrete pavement.
- Use a 13 ft (4.0 m) joint spacing as recommended in Sargand and Abdalla [2006].

Concerning construction, several QC/QA procedures in the specifications are critical to the long term performance of the unbonded overlay and need to be strictly monitored and enforced, specifically:

- Dowel bar alignment, especially the rotational criteria
- Wetting of the bondbreaker prior to placing concrete
- Proper usage of HIPERPAV prior to placing concrete
- Contractor procedures for controlling thickness of bondbreaker and concrete pavement.

Water in the pavement system damages the pavement due to transport of chemicals which infill voids in the concrete and weaken the bond between asphalt and aggregate in the bondbreaker. Techniques which may improve drainage of unbonded overlays include:

- Use performance engineered mixtures (PEM) which include supplementary cementitious material to reduce permeability in concrete
- Insure underdrains are functioning
- Provide a permeable bondbreaker and/or base by taking measures such as
    - Fracturing existing slabs before placing bondbreaker and overlay
    - Installing a fabric bondbreaker or permeable asphalt bondbreaker.

10.3.1 Fabric bondbreaker

Nonwoven geotextiles have been used in Germany since the 1980s as a bondbreaker for concrete overlays, where they have also been used to separate PCC pavements from cement-treated bases in new pavements [CP Road Map, 2009]. The geotextile layer must be thick enough to allow water to flow laterally through the fabric and drain at the pavement edge. The geotextile interlayer was tested in Missouri and Oklahoma in 2008 [CP Road Map, 2009]. Information about geotextile interlayers has been synthesized and included in the National Concrete Pavement Technology Center publications *Guide to Concrete Overlays* [Harrington and Fick, 2014] and *Guide Specifications for Concrete Overlays* [NCPTC, 2016]. The latter publication focuses more on provisions which should be included in contract specifications. For example, the quality control plan should include tests measuring mass per unit area, thickness under load, and tensile strength [NCPTC, 2016]. Material requirements and test procedures are given in a table which appears in both documents and is reproduced in Table 39 [Harrington and Fick, 2014, p. 79; NCPTC, 2016, p. 10]. Drainage of the fabric interlayer is accomplished by terminating the aggregate into an aggregate base under the shoulder, which is connected to an underdrain and/or daylighted. Drainage plans are depicted in the *Guide to Concrete Overlays* [Harrington and Fick, 2014, p. 73-74].

10.3.2 Permeable asphalt bondbreaker

The now inactive ODOT CMS Item 308, Asphalt Treated Free Draining Base (ATFDB) is similar to the permeable base used on the NYSDOT I-86 project discussed in Chapter 2 of this report. Figure 142 shows a comparison of the aggregate gradations permitted for Item 308, which can be either AASHTO #57 or AASHTO #67 at the discretion of the contractor, and the gradation used on I-86, NYSDOT Type 1. The ODOT mix could be a finer gradation with a smaller top size. The ODOT specification requires an asphalt content between 1.5% and 3.5% whereas the NYSDOT requires an asphalt content between 2.0% and 4.0%. Should ODOT chose to use a permeable asphalt bondbreaker, it is recommended the Department evaluate their Item 308 specification, make revisions as needed, and reactivate.

Table 39 Geotextile Separation Layer Material Requirements [Harrington and Fick, 2014, p. 79; NCPTC, 2016, p. 10].

Property	Requirements	Test Procedure
Geotextile Type	Nonwoven, needle-punched, no thermal treatment to include calendaring†	EN 13249, Annex F (Certification)
Color	Uniform/nominally same color fibers	(Visual Inspection)
Weight (mass per unit area) [13]	≥ 450 g/m^2 (13.3 oz/yd^2) ≥ 500 g/m^2 (14.7 oz/yd^2) ≤ 550 g/m^2 (16.2 oz/yd^2)	ISO 9864 (ASTM D 5261)
Thickness under load (pressure)	[a] At 2 kPa (0.29 psi): ≥ 3.0 mm (0.12 in.) [b] At 20 kPa (2.9 psi): ≥ 2.5 mm (0.10 in.) [c] At 200 kPa (29 psi): ≥ 0.10 mm (0.04 in.)	ISO 9863-1 (ASTM D 5199)
Wide-width tensile strength	≥ 10 kN/m (685 lb/ft)	ISO 10319 (ASTM D 4595)
Wide-width maximum elongation	≤ 130 percent	ISO 10319 (ASTM D 4595)
Water permeability in normal direction under load (pressure)	≥ 1 x 10^{-4} m/s (3.3 x 10^{-4} ft/s) at 20 kPa (2.9 psi)	DIN 60500-4 (modified ASTM D 5493)
In-plane water permeability (transmissivity) under load (pressure)	[a] ≥ 5 x 10^{-4} m/s (1.6 x 10^{-3} ft/s) at 20 kPa (2.9 psi) [b] ≥ 2 x 10^{-4} m/s (6.6 x 10^{-4} ft/s) at 200 kPa (2.9 psi)	ISO 12958 (ASTM D 6574) or ISO 12958 (modified ASTM D 4716)
Weather resistance	Retained strength ≥ 60 percent (70% average)	EN 12224 (ASTM D 4355 @ 500 hr exposure for grey, white, or black material only)
Alkali resistance	≥ 96 percent polyproplene/polyethylene	EN 13249, Annex B (Certification)

† Calendering is a process that passes the geotextile through one or more heated rollers during manufacturing, modifying the surface of the geotextile. Calendering may reduce the absorption properties of the geotextile on the calendered side

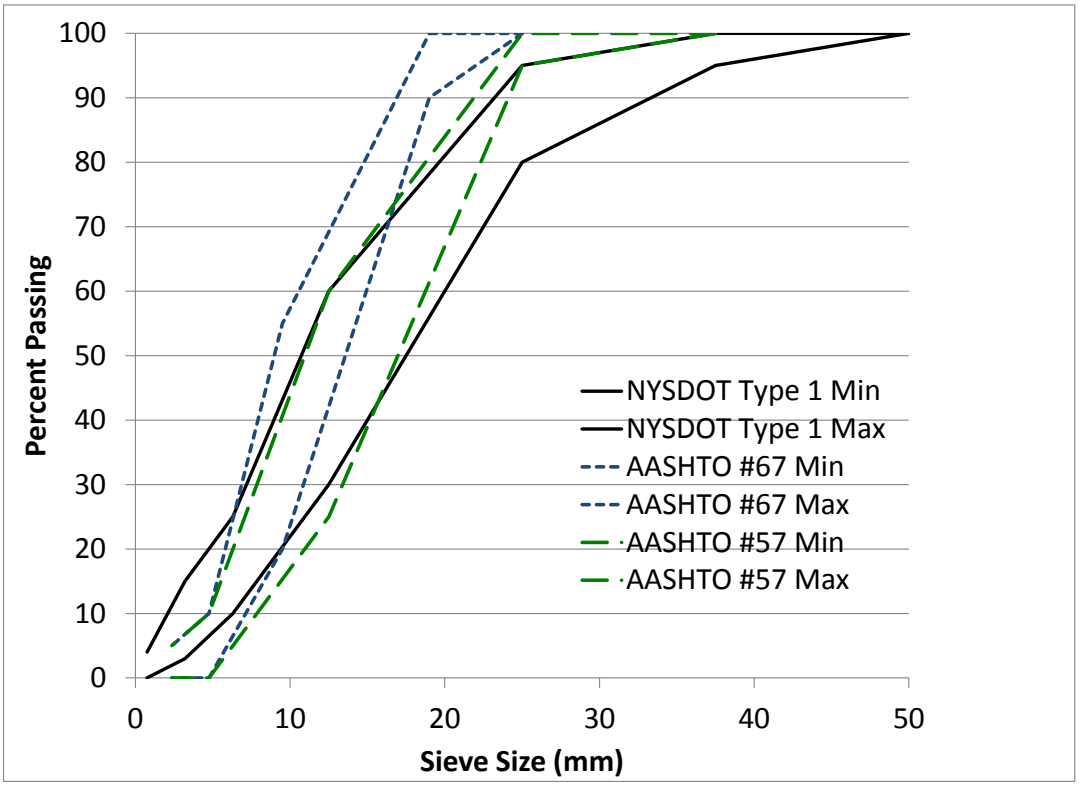

Figure 142. Comparison of aggregate gradations for former ODOT CMS Item 308, which can be either AASHTO #67 or AASHTO #57, and NYSDOT Type 1 aggregate used on I-86 in New York. (25.4 mm = 1 in).

11 References

AASHTO. (1993). *Guide for Design of Pavement Structures*. Washington, DC: American Association of State Highway and Transportation Officials.

AASHTO. (2008). *Mechanistic-Empirical Pavement Design Guide - A Manual of Practice*. Washington, DC: American Association of State Highway and Transportation Officials.

Abaqus/Standard User's Manual, Version 6.11. (2011). Providence, RI: Dassault Systèmes Simulia Corp.

ACI Committee 325. (2006). *Concrete Overlays for Pavement Rehabilitation*. Farmington Hills: American Concrete Institute Publication ACI 325.13R-06.

Alavi, S., LeCates, J.F., and Tavares, M.P. (2008). *Falling Weight Deflectometer Usage: A Synthesis of Highway Practice*, NCHRP Synthesis 381, Washington DC, Transportation Research Board.

Copas, Thomas L., and Pennock, Herbert A. (1979). *Joint-Related Distress In PCC Pavement: Cause, Prevention And Rehabilitation*, NCHRP Synthesis 56, Washington DC, Transportation Research Board. Alden 7th floor TE278.2 .N37 1979

CP Road Map, 2009, "Use of Nonwoven Geotextiles as Interlayers in Concrete Pavement Systems, MAP Brief 7-1, Federal Highway Administration, Washington, DC, May 2009.

Dale Harrington and Gary Fick, 2014, *Guide to Concrete Overlays*, third edition, National Concrete Pavement Technology Center (NCPTC), Institute for Transportation, Iowa State University, Ames IA, May 2014. Available at http://www.cptechcenter.org/technical-library/documents/Overlays_3rd_edition.pdf, accessed May 8, 2017.

Dempsey, B. J., Herlache, W. A., and Patel, A. J. (1986). "The Climatic-Materials-Structural Pavement Analysis Program". *Transportation Research Record*, No. 1095, pp. 111-123.

Federal Highway Administration (FHWA), (1990). *Concrete Pavement Joints*. Washington DC, Federal Highway Administration, United States Department of Transportation.

Federal Highway Administration (FHWA), (2011). "Coefficient of Thermal Expansion in Concrete Pavement Design". Advanced Concrete Pavement Technology TechBrief FHWA-HIF-09-15, Washington DC, Federal Highway Administration, United States Department of Transportation, October 2011.

Hammons, M. I. (1998). *Advanced Pavement Design: Finite Element Modeling for Rigid Pavement Joints, Report II: Model Development*. Washington, DC: U.S. Department of Transportation Federal Aviation Administration.

Hansen, W., and Liu, Z. (2013). *Improved Performance of JPCP Overlays*. Lansing, Michigan: Michigan Department of Transportation Report No. RC-1574.

Heckel, L.B., (2002). Performance of an Unbonded Concrete Overlay on I-74. Springfield, IL: Illinois Department of Transportation Bureau of Materials and Physical Research.

Huang, Y. H. (2004). *Pavement Analysis and Design*. Upper Saddle River, New Jersy: Pearson Prentice Hall.

Kivi, A., Tighe, S. L., Fung, R., & Grajek, J. (2013). "Ten Year Performance Evaluation of Unbonded Concrete Overlay and Jointed Plain Concrete Pavement: A Toronto Case Study". *Conference of the Transportation Association of Canada.* Winniepeg, Manitoba.

Larson, R.M., Vanikar, S., and Forster, S., (1993). *U.S. Tour of European Concrete Highways (US Tech) Follow-up Tour of Germany and Austria*, Washington DC, Federal Highway Administration.

Liao, M. (2011). *Towards Fracture Mechanics-Based Design of Unbonded Concrete Overlay Pavements* (Doctoral Dissertation). Minneapolis, MN: University of Minnesota.

National Concrete Pavement Technology Center (2006). "Concrete Pavement Construction Basics: Tech Note". Ames, Iowa. National Concrete Pavement Technology Center. August, 2006.

National Concrete Pavement Technology Center (NCPTC), 2016, *Guide Specifications for Concrete Overlays*, Institute for Transportation, Iowa State University, Ames IA, September 2015/revised February 2016. Available at http://www.cptechcenter.org/technical-library/documents/overlay_guide_specifications.pdf, accessed May 8, 2017.

Ohio Department of Transportation (ODOT). (2013). *Construction and Material Specifications*. Columbus, OH. Ohio Department of Transportation.

Ohio Department of Transportation (ODOT). (2014). *Pavement Design Manual*. Columbus, OH. Ohio Department of Transportation.

Olek, Jan (2016), Purdue University, test results presentation, December 19, 2016.

Rada, G. R., Jones, D. J., Harvey, J. T., Senn, K. A., & Thomas, M. (2013). *Guide for Conducting Forensic Investigations of Highway Pavements*. NCHRP Report 747. Washington D.C.: Transportation Research Board.

Sargand. (2000). *Effectiveness of Base Type on The Performance of PCC Pavement on ERI/LOR 2*, Interim Report for Project Entitled: "Continued Monitoring of Instrumented Pavement in Ohio". Athens, Ohio: Department of Civil Engineering, Ohio University.

Shad M. Sargand, William Edwards, and Huntae Kim, (2002), *Determination of Pavement Layer Stiffness On The Ohio SHRP Test Road Using Backcalculation Technique*, Final Report, ODOT/FHWA (July 2002).

Sargand, S. (2005). *Forensic Study of Cracking of Concrete on I75 Southbound near Finlay*. Athens, Ohio: Ohio Research Institute for Transportation and the Environment.

Shad Sargand and Basel Abdalla, (2006), *Truck/Pavement/Economic Modeling and In-Situ Field Test Data Analysis Applications – Volume 2: Verificiation and Validation of Finite Element Models for Rigid Pavement Using In-Situ Data – Selection of Joint Spacing*, Report No. FHWA/OH-2006/3B for Ohio Department of Transportation, State Job No. 147700, Pooled Fund Study SPR2(203), June 2006.

Shad Sargand, J. Ludwig Figueroa, and Michael Romanello, (2008), *Instrumentation of the Way-30 Test Pavements*, Technical Report No. FHWA/OH-2008/7 for the Ohio Department of Transportation, State Job No. 14815, June 2008.

Shad Sargand and J. Ludwig Figueroa, (2010), *Monitoring and Modeling of Pavement Response and Performance Task A: Ohio*, Technical Report No. FHWA/OH-2010/03A for the Ohio Department of Transportation, Pooled Fund Project TPF-5(121), State Job No. 134287, June 2010.

Sargand, S., Khoury, I., and Padilla-Llano, D. (2012). *Monitoring and Modeling of Pavement Response and Performance Task B: New York Vol 2: I86 PCC*. Athens, Ohio: Department of Civil Engineering, Ohio University.

Smith, K. E. (2002). *Portland Cement Concrete Overlays: State of the Technology Synthesis*. Washington, DC: Federal Highway Administration.

Sotelino, E. D., Asgari, A., Saksa, A., & Cedeno, G. (2005). *Damage Analysis of Jointed Palin Concrete Pavements in Indiana Part I: Finite Element Modeling and Damage Analysis*. Purdue University, School of Civil Engineering. West Lafayette: Indiana Department of Transportation Report No. FHWA/IN/JTRP-2004/30.

Tayabji, S., and Okamoto, P. (1985). "Thickness Design of Concrete Resurfacing". *Third International Conference on Concrete Pavement Design and Rehabilitation*, West Lafayette, IN: Purdue University, pp. 367-379.

Tayabji, S. D. (1986). "Dowel Placement Tolerances for Concrete Pavement". *Transportation Research Record* No. 1062. Washington D.C.: Transportation Research Board

Thompson, M.R., Dempsey, B.J., and Hill, H., (1987). "Characterizing Temperature Effects for Pavement Analysis and Design". *Transportation Research Record* No. 1121, pp. 14-22.

Torres, H. N., Roesler, J., Rasmussen, R. O., & Harrington, D. (2012). *Guide to The Design of Concrete Overlays Using Existing Methodologies*. National Concrete Pavement Technology Center.

Williams, G. J., and Chou, E. Y. (1994). *Performance Evaluation of Rigid Pavement Rehabilitation Techniques*. ODOT Report No. ST/SS/94-002. University of Toledo, Department of Civil Engineering. Toledo, Ohio.

Appendix A: IRI data

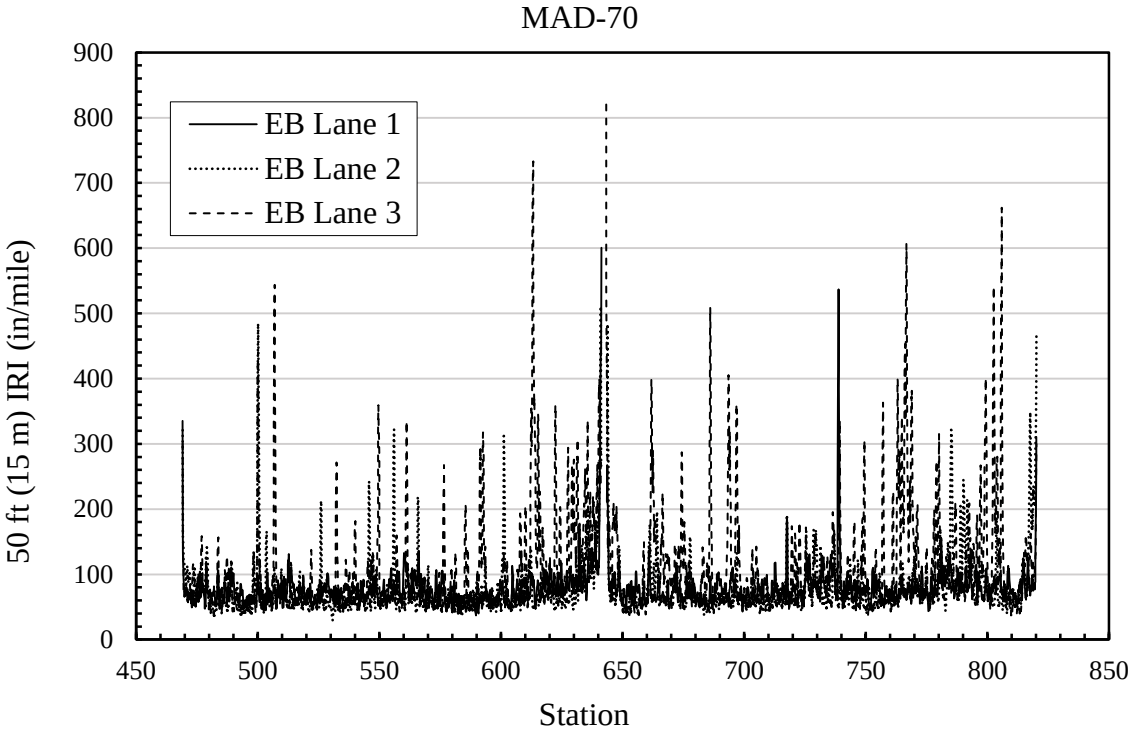

MAD-70 EB 50 ft (15 m) IRI Moving Average (100 ft = 30.5 m; 1 in/mi = 1.58×10^{-5})

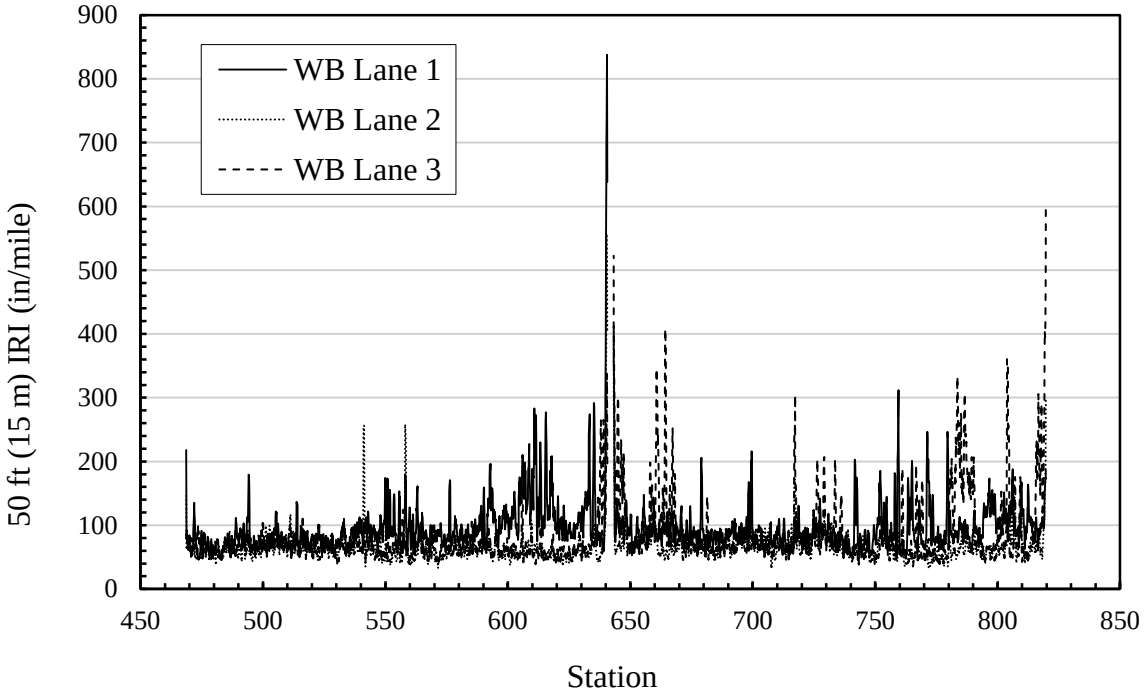

MAD-70 WB 50 ft (15 m) IRI Moving Average (100 ft = 30.5 m; 1 in/mi = 1.58×10^{-5})

WAS/NOB-77

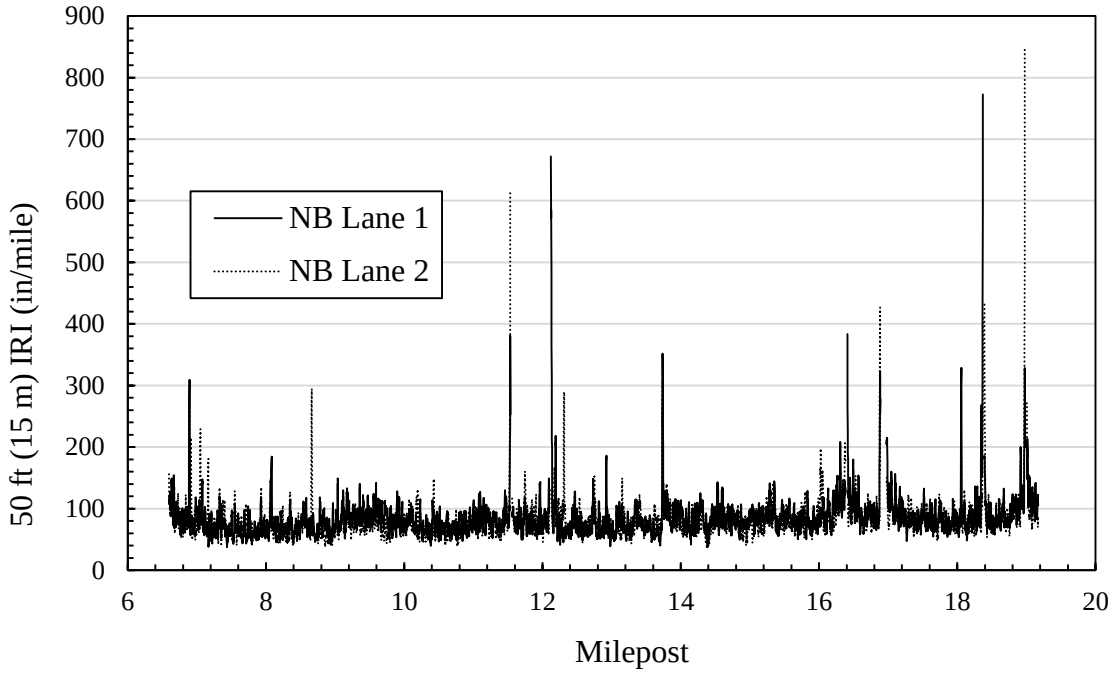

WAS/NOB-77 NB 50 ft (15 m) IRI Moving Average (1 mi = 1.6 km; 1 in/mi = 1.58×10^{-5})

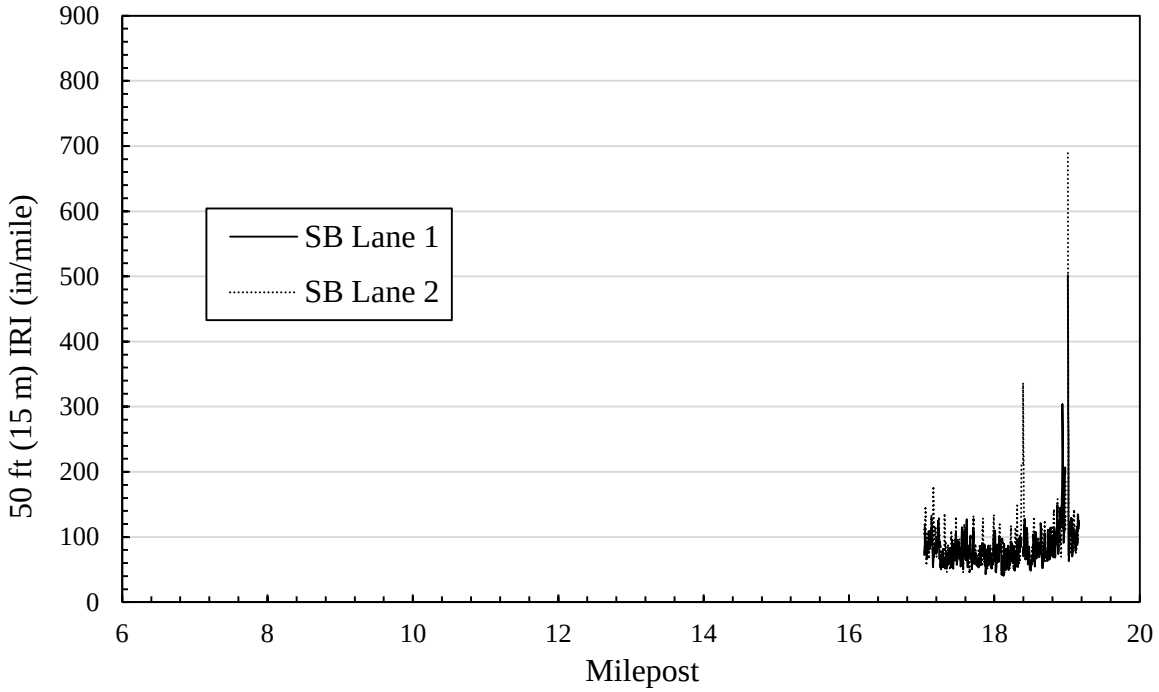

WAS/NOB-77 SB 50 ft (15 m) IRI Moving Average (1 mi = 1.6 km; 1 in/mi = 1.58×10^{-5})

Appendix B: MITScan data

B1: MAD-70 EB distressed section MITScan data collected by ODOT August 19, 2015

Highway	Direction	Station Number	Joint	Lane	Bar Number	X-Position		Depth		Depth Deviation		Side Shift		Misalignment		Horizontal Misalignment		Vertical Misalignment		Minimal Cover	
HW	Dir	SNo	Jo	La	BNo	xs		zs		dz		dy		s		sh		sv		c	
-	-	-	-	-	-	(in)	(mm)	(in)	(mm)	(in)	(mm)	(in)	(mm)	(in)	(mm)	(in)	(mm)	(in)	(mm)	(in)	(mm)
IS 70	East	775-22	79	La. 1	1	0.17	4.3	3.8	97	-3.2	-81	0.1	3	0.4	10	-0.4	-10	0.1	3	3	76
IS 70	East	775-22	79	La. 1	2	12.56	319.0	3.8	97	-3.2	-81	1.3	33	0.8	20	-0.4	-10	0.7	18	2.7	69
IS 70	East	775-22	79	La. 1	3	24.6	624.8	3.8	97	-3.2	-81	0.9	23	0.7	18	-0.5	-13	0.6	15	2.7	69
IS 70	East	775-22	79	La. 1	4	36.61	929.9	3.7	94	-3.3	-84	0.6	15	0.6	15	-0.5	-13	0.3	8	2.8	71
IS 70	East	775-22	79	La. 1	5	48.64	1235.5	3.7	94	-3.3	-84	0	0	0.5	13	-0.5	-13	0.1	3	2.9	74
IS 70	East	775-22	79	La. 1	6	60.63	1540.0	3.7	94	-3.3	-84	-0.2	-5	0.4	10	-0.4	-10	0	0	3	76
IS 70	East	775-22	79	La. 1	7	72.69	1846.3	3.8	97	-3.2	-81	-0.5	-13	0.5	13	-0.4	-10	-0.1	-3	3	76
IS 70	East	775-22	79	La. 1	8	84.71	2151.6	3.8	97	-3.2	-81	-0.2	-5	0.4	10	-0.4	-10	0.1	3	3	76
IS 70	East	775-22	79	La. 1	9	96.65	2454.9	3.7	94	-3.3	-84	-0.6	-15	0.3	8	-0.3	-8	0	0	3	76
IS 70	East	775-22	79	La. 1	10	108.89	2765.8	3.8	97	-3.2	-81	-0.1	-3	0.5	13	-0.5	-13	0.2	5	3	76
IS 70	East	774-50	73	La. 1	1	9.24	234.7	4.3	109	-2.7	-69	1.2	30	0.4	10	0.1	3	0.3	8	3.4	86
IS 70	East	774-50	73	La. 1	2	21.6	548.6	4.4	112	-2.6	-66	1.2	30	0.4	10	-0.1	-3	0.4	10	3.4	86
IS 70	East	774-50	73	La. 1	3	33.59	853.2	4.2	107	-2.8	-71	1.1	28	0.3	8	-0.2	-5	0.3	8	3.4	86
IS 70	East	774-50	73	La. 1	4	45.58	1157.7	4.2	107	-2.8	-71	1.2	30	0.4	10	-0.2	-5	0.3	8	3.3	84
IS 70	East	774-50	73	La. 1	5	57.61	1463.3	4.2	107	-2.8	-71	1.2	30	0.4	10	-0.3	-8	0.3	8	3.3	84
IS 70	East	774-50	73	La. 1	6	69.58	1767.3	4.2	107	-2.9	-74	1	25	0.2	5	-0.1	-3	-0.1	-3	3.3	84
IS 70	East	774-50	73	La. 1	7	81.69	2074.9	4.4	112	-2.6	-66	0.9	23	0.3	8	-0.1	-3	-0.2	-5	3.6	91
IS 70	East	774-50	73	La. 1	8	93.65	2378.7	4.2	107	-2.8	-71	0.8	20	0.4	10	-0.3	-8	-0.2	-5	3.3	84
IS 70	East	774-50	73	La. 1	9	105.69	2684.5	4.4	112	-2.6	-66	1	25	0.6	15	-0.5	-13	-0.2	-5	3.6	91
IS 70	East	774-50	73	La. 1	10	117.55	2985.8	4.5	114	-2.5	-64	0.4	10	0.6	15	0.2	5	-0.5	-13	3.5	89
IS 70	East	773-78	67	La. 1	1	9.89	251.2	3.7	94	-3.3	-84	-1.7	-43	0.7	18	-0.3	-8	-0.7	-18	2.6	66
IS 70	East	773-78	67	La. 1	2	22.25	565.2	3.7	94	-3.3	-84	-1.2	-30	0.5	13	0.1	3	-0.5	-13	2.7	69
IS 70	East	773-78	67	La. 1	3	34.22	869.2	3.8	97	-3.2	-81	1.5	38	1.1	28	0.1	3	1.1	28	2.5	64
IS 70	East	773-78	67	La. 1	4	46.29	1175.8	3.7	94	-3.3	-84	1.1	28	1	25	-0.2	-5	0.9	23	2.5	64
IS 70	East	773-78	67	La. 1	5	58.13	1476.5	3.7	94	-3.3	-84	-2	-51	0.6	15	-0.2	-5	-0.6	-15	2.7	69
IS 70	East	773-78	67	La. 1	6	70.25	1784.4	3.9	99	-3.2	-81	-1.6	-41	0.5	13	-0.1	-3	-0.5	-13	2.9	74
IS 70	East	773-78	67	La. 1	7	82.34	2091.4	3.9	99	-3.1	-79	-1.5	-38	0.5	13	0	0	-0.5	-13	2.9	74
IS 70	East	773-78	67	La. 1	8	94.32	2395.7	4	102	-3	-76	-1	-25	0.3	8	0	0	-0.3	-8	3.1	79
IS 70	East	773-78	67	La. 1	9	106.18	2697.0	4.1	104	-2.9	-74	-0.6	-15	0.1	3	0	0	-0.1	-3	3.3	84
IS 70	East	773-78	67	La. 1	10	118.11	3000.0	4.6	117	-2.4	-61	1.4	36	0.8	20	-0.3	-8	0.8	20	3.5	89
IS 70	East	773-6	61	La. 1	1	6.48	164.6	3.8	97	-3.3	-84	0.5	13	0.3	8	-0.2	-5	0.3	8	2.9	74
IS 70	East	773-6	61	La. 1	2	18.83	478.3	3.8	97	-3.2	-81	0.8	20	0.4	10	-0.1	-3	0.4	10	2.8	71
IS 70	East	773-6	61	La. 1	3	30.86	783.8	3.7	94	-3.3	-84	0.9	23	0.6	15	0	0	0.6	15	2.7	69
IS 70	East	773-6	61	La. 1	4	42.89	1089.4	3.7	94	-3.3	-84	1	25	0.6	15	-0.1	-3	0.6	15	2.7	69
IS 70	East	773-6	61	La. 1	5	54.86	1393.4	3.8	97	-3.2	-81	0.4	10	0.4	10	-0.2	-5	0.3	8	2.9	74
IS 70	East	773-6	61	La. 1	6	66.87	1698.5	3.8	97	-3.3	-84	0.4	10	0.3	8	0	0	0.3	8	2.8	71
IS 70	East	773-6	61	La. 1	7	79	2006.6	4	102	-3	-76	1.1	28	0.7	18	-0.2	-5	0.7	18	3	76
IS 70	East	773-6	61	La. 1	8	90.98	2310.9	4	102	-3.1	-79	0.8	20	0.5	13	-0.2	-5	0.4	10	3	76
IS 70	East	773-6	61	La. 1	9	102.89	2613.4	4	102	-3	-76	-0.5	-13	0.2	5	0.1	3	-0.2	-5	3.2	81

IS 70	East	773-6	61	La. 1	10	114.28	2902.7	4.2	107	-2.8	-71	-0.6	-15	0.1	3	-0.1	-3	0	0	3.5	89
IS 70	East	772-34	55	La. 1	1	10.6	269.2	4.7	119	-2.3	-58	-1.6	-41	2.1	53	-1.2	-30	-1.7	-43	3.1	79
IS 70	East	772-34	55	La. 1	2	17.51	444.8	4.2	107	-2.8	-71	-0.9	-23	1.4	36	-1.4	-36	-0.1	-3	3.4	86
IS 70	East	772-34	55	La. 1	3	24.8	629.9	4.1	104	-2.9	-74	1.2	30	1	25	-0.6	-15	0.7	18	3	76
IS 70	East	772-34	55	La. 1	4	32.02	813.3	3.9	99	-3.1	-79	0.9	23	1.2	30	-1.2	-30	0.4	10	3	76
IS 70	East	772-34	55	La. 1	5	39.28	997.7	3.8	97	-3.2	-81	0.5	13	0.6	15	-0.5	-13	0.2	5	3	76
IS 70	East	772-34	55	La. 1	6	46.21	1173.7	4	102	-3	-76	1.2	30	0.8	20	-0.3	-8	0.7	18	2.9	74
IS 70	East	772-34	55	La. 1	7	53.15	1350.0	5.4	137	-1.6	-41	0.9	23	0.6	15	-0.5	-13	0.4	10	4.5	114
IS 70	East	772-34	55	La. 1	8	60.34	1532.6	3.9	99	-3.1	-79	0.6	15	0.2	5	0.2	5	0.1	3	3.1	79
IS 70	East	772-34	55	La. 1	9	71.91	1826.5	3.9	99	-3.1	-79	0.5	13	0.3	8	0.2	5	0.1	3	3.1	79
IS 70	East	772-34	55	La. 1	10	83.84	2129.5	3.8	97	-3.2	-81	0.7	18	0.2	5	0.2	5	0	0	3	76
IS 70	East	772-34	55	La. 1	11	95.77	2432.6	3.9	99	-3.1	-79	0.8	20	0.4	10	0.3	8	0.2	5	3	76
IS 70	East	772-34	55	La. 1	12	108	2743.2	3.9	99	-3.1	-79	0.6	15	0.3	8	0.2	5	0.2	5	3	76
IS 70	East	771-62	49	La. 1	1	2.49	63.2	4.2	107	-2.8	-71	0.5	13	0.9	23	0.9	23	-0.2	-5	3.3	84
IS 70	East	771-62	49	La. 1	2	14.41	366.0	4.1	104	-2.9	-74	0.7	18	0.3	8	0.3	8	0	0	3.3	84
IS 70	East	771-62	49	La. 1	3	26.53	673.9	4	102	-3	-76	1.1	28	0.3	8	0.2	5	0.2	5	3.2	81
IS 70	East	771-62	49	La. 1	4	38.58	979.9	4.1	104	-2.9	-74	0.7	18	0.1	3	0.1	3	0.1	3	3.3	84
IS 70	East	771-62	49	La. 1	5	50.63	1286.0	4.1	104	-2.9	-74	0.7	18	0.1	3	0	0	0.1	3	3.3	84
IS 70	East	771-62	49	La. 1	6	62.59	1589.8	4	102	-3	-76	0.8	20	0.1	3	0	0	0.1	3	3.2	81
IS 70	East	771-62	49	La. 1	7	74.61	1895.1	4	102	-3	-76	0.9	23	0.1	3	0.1	3	0	0	3.3	84
IS 70	East	771-62	49	La. 1	8	86.61	2199.9	4	102	-3	-76	0.9	23	0.3	8	0.1	3	-0.3	-8	3.1	79
IS 70	East	771-62	49	La. 1	9	98.57	2503.7	4.1	104	-2.9	-74	0.8	20	0.1	3	0.1	3	-0.1	-3	3.3	84
IS 70	East	771-62	49	La. 1	10	110.77	2813.6	4	102	-3	-76	1	25	0.4	10	-0.3	-8	-0.2	-5	3.1	79
IS 70	East	770-18	37	La. 1	1	2.9	73.7	4.4	112	-2.6	-66	-1.8	-46	0.5	13	-0.1	-3	-0.4	-10	3.5	89
IS 70	East	770-18	37	La. 1	2	15.12	384.0	4.4	112	-2.6	-66	-1.8	-46	0.3	8	-0.2	-5	-0.3	-8	3.5	89
IS 70	East	770-18	37	La. 1	3	27.11	688.6	4.4	112	-2.6	-66	-1.4	-36	0.3	8	-0.2	-5	-0.2	-5	3.5	89
IS 70	East	770-18	37	La. 1	4	39.12	993.6	4.3	109	-2.7	-69	-1.3	-33	0.4	10	-0.2	-5	-0.3	-8	3.4	86
IS 70	East	770-18	37	La. 1	5	51.12	1298.4	4.3	109	-2.7	-69	-1.2	-30	0.4	10	-0.2	-5	-0.3	-8	3.4	86
IS 70	East	770-18	37	La. 1	6	63.14	1603.8	4.3	109	-2.7	-69	-1.2	-30	0.3	8	-0.2	-5	-0.3	-8	3.4	86
IS 70	East	770-18	37	La. 1	7	75.13	1908.3	4.3	109	-2.7	-69	-1.4	-36	0.3	8	0.1	3	-0.3	-8	3.4	86
IS 70	East	770-18	37	La. 1	8	85.97	2183.6	4.2	107	-2.8	-71	-4.3	-109	3.4	86	1.7	43	-3	-76	2	51
IS 70	East	770-18	37	La. 1	9	99.11	2517.4	4.2	107	-2.8	-71	-1.5	-38	0.2	5	0.1	3	-0.2	-5	3.4	86
IS 70	East	770-18	37	La. 1	10	111.37	2828.8	4.2	107	-2.9	-74	-2	-51	0.6	15	0.5	13	-0.3	-8	3.3	84
IS 70	East	770-90	43	La. 1	1	2.75	69.9	4.6	117	-2.5	-64	-1.4	-36	0.4	10	-0.2	-5	-0.4	-10	3.6	91
IS 70	East	770-90	43	La. 1	2	14.78	375.4	4.6	117	-2.4	-61	-1.7	-43	0.7	18	-0.4	-10	-0.6	-15	3.5	89
IS 70	East	770-90	43	La. 1	3	27.3	693.4	4.6	117	-2.4	-61	-0.2	-5	0.7	18	0.6	15	0.5	13	3.6	91
IS 70	East	770-90	43	La. 1	4	38.95	989.3	4.4	112	-2.6	-66	0.9	23	0.2	5	-0.2	-5	0.1	3	3.6	91
IS 70	East	770-90	43	La. 1	5	50.96	1294.4	4.4	112	-2.7	-69	1.1	28	0.3	8	-0.3	-8	0.2	5	3.5	89
IS 70	East	770-90	43	La. 1	6	63.26	1606.8	4.2	107	-2.8	-71	1.4	36	0.4	10	0	0	0.3	8	3.3	84
IS 70	East	770-90	43	La. 1	7	74.98	1904.5	4.1	104	-2.9	-74	1.6	41	0.4	10	0.2	5	0.4	10	3.2	81
IS 70	East	770-90	43	La. 1	8	86.83	2205.5	4.8	122	-2.2	-56	2.7	69	1.9	48	0.4	10	1.9	48	3.1	79
IS 70	East	770-90	43	La. 1	9	99.08	2516.6	4.9	124	-2.1	-53	2.7	69	2.1	53	-0.3	-8	2	51	3.2	81
IS 70	East	770-90	43	La. 1	10	111.74	2838.2	4.8	122	-2.2	-56	2.6	66	2	51	-0.8	-20	1.8	46	3.1	79
IS 70	East	769-46	31	La. 1	1	3.46	87.9	4.6	117	-2.4	-61	1.6	41	0.9	23	0.3	8	0.8	20	3.4	86
IS 70	East	769-46	31	La. 1	2	15.73	399.5	4.7	119	-2.4	-61	1.9	48	1	25	0.1	3	1	25	3.4	86
IS 70	East	769-46	31	La. 1	3	27.77	705.4	4.6	117	-2.4	-61	1.8	46	0.9	23	0.1	3	0.9	23	3.4	86
IS 70	East	769-46	31	La. 1	4	39.84	1011.9	4.6	117	-2.4	-61	1.8	46	0.9	23	0.1	3	0.9	23	3.4	86
IS 70	East	769-46	31	La. 1	5	51.85	1317.0	4.6	117	-2.4	-61	1.8	46	0.9	23	0	0	0.9	23	3.4	86
IS 70	East	769-46	31	La. 1	6	63.85	1621.8	4.5	114	-2.5	-64	1.5	38	0.4	10	0.1	3	0.4	10	3.5	89

IS 70	East	769-46	31	La. 1	7	75.92	1928.4	4.5	114	-2.5	-64	1.4	36	0.5	13	0.2	5	0.4	10	3.6	91
IS 70	East	769-46	31	La. 1	8	87.86	2231.6	4.6	117	-2.4	-61	1.8	46	1	25	0.3	8	1	25	3.4	86
IS 70	East	769-46	31	La. 1	9	99.85	2536.2	4.6	117	-2.4	-61	1.8	46	1.1	28	0.3	8	1.1	28	3.3	84
IS 70	East	769-46	31	La. 1	10	112.26	2851.4	4.6	117	-2.4	-61	1.9	48	1.3	33	-0.2	-5	1.3	33	3.2	81
IS 70	East	768-74	25	La. 1	1	9.58	243.3	4.7	119	-2.3	-58	-3.1	-79	2.7	69	-2.2	-56	-1.6	-41	3.2	81
IS 70	East	768-74	25	La. 1	2	16.34	415.0	6.9	175	-0.1	-3	3.2	81	2.9	74	-0.4	-10	2.9	74	4.7	119
IS 70	East	768-74	25	La. 1	3	23.25	590.6	4.8	122	-2.2	-56	-2.7	-69	1.2	30	0	0	-1.2	-30	3.5	89
IS 70	East	768-74	25	La. 1	4	34.72	881.9	4.6	117	-2.4	-61	-2.2	-56	0.8	20	-0.1	-3	-0.8	-20	3.5	89
IS 70	East	768-74	25	La. 1	5	46.51	1181.4	4.5	114	-2.5	-64	-3	-76	1.3	33	0	0	-1.3	-33	3.1	79
IS 70	East	768-74	25	La. 1	6	58.65	1489.7	4.6	117	-2.4	-61	-2.2	-56	0.8	20	-0.2	-5	-0.7	-18	3.5	89
IS 70	East	768-74	25	La. 1	7	70.69	1795.5	4.6	117	-2.4	-61	-2.1	-53	0.7	18	-0.2	-5	-0.7	-18	3.5	89
IS 70	East	768-74	25	La. 1	8	82.7	2100.6	4.6	117	-2.4	-61	-2.2	-56	0.7	18	-0.2	-5	-0.7	-18	3.5	89
IS 70	East	768-74	25	La. 1	9	94.74	2406.4	4.5	114	-2.5	-64	-2.3	-58	0.8	20	-0.3	-8	-0.7	-18	3.4	86
IS 70	East	768-74	25	La. 1	10	106.42	2703.1	4.5	114	-2.5	-64	-2.4	-61	0.5	13	0.2	5	-0.5	-13	3.5	89
IS 70	East	768-74	25	La. 1	11	118.25	3003.6	4.5	114	-2.5	-64	-2.6	-66	1.7	43	-1.6	-41	-0.3	-8	3.6	91
IS 70	East	768-2	19	La. 1	1	7.1	180.3	3.8	97	-3.2	-81	2.6	66	1.6	41	0.9	23	1.4	36	2.3	58
IS 70	East	768-2	19	La. 1	2	23.33	592.6	4	102	-3	-76	1	25	0.8	20	-0.4	-10	0.7	18	2.9	74
IS 70	East	768-2	19	La. 1	3	35.57	903.5	4	102	-3	-76	1.2	30	0.8	20	-0.3	-8	0.7	18	2.9	74
IS 70	East	768-2	19	La. 1	4	47.6	1209.0	3.9	99	-3.1	-79	0.9	23	0.6	15	-0.2	-5	0.6	15	2.9	74
IS 70	East	768-2	19	La. 1	5	59.56	1512.8	3.9	99	-3.1	-79	0.8	20	0.5	13	-0.2	-5	0.5	13	2.9	74
IS 70	East	768-2	19	La. 1	6	71.6	1818.6	4	102	-3	-76	1.6	41	1.1	28	-0.2	-5	1	25	2.7	69
IS 70	East	768-2	19	La. 1	7	83.56	2122.4	4	102	-3	-76	1.5	38	1	25	-0.1	-3	1	25	2.8	71
IS 70	East	768-2	19	La. 1	8	95.48	2425.2	4	102	-3	-76	1.5	38	1	25	0	0	1	25	2.7	69
IS 70	East	768-2	19	La. 1	9	107.77	2737.4	4	102	-3	-76	1.6	41	1.1	28	0.3	8	1.1	28	2.7	69
IS 70	East	767-30	13	La. 1	1	2.54	64.5	4	102	-3	-76	1.3	33	0.9	23	0.2	5	0.8	20	2.9	74
IS 70	East	767-30	13	La. 1	2	14.61	371.1	4	102	-3	-76	1.5	38	0.8	20	0.1	3	0.8	20	2.8	71
IS 70	East	767-30	13	La. 1	3	28.48	723.4	3.7	94	-3.3	-84	1.6	41	0.5	13	0.3	8	0.4	10	2.7	69
IS 70	East	767-30	13	La. 1	4	39.12	993.6	3.7	94	-3.3	-84	0.9	23	0.3	8	0	0	0.3	8	2.8	71
IS 70	East	767-30	13	La. 1	5	50.7	1287.8	3.6	91	-3.4	-86	1.2	30	0.4	10	-0.1	-3	0.4	10	2.7	69
IS 70	East	767-30	13	La. 1	6	62.22	1580.4	3.7	94	-3.3	-84	1.3	33	0.5	13	0	0	0.5	13	2.7	69
IS 70	East	767-30	13	La. 1	7	72.66	1845.6	3.5	89	-3.5	-89	1.7	43	0.6	15	0.3	8	0.5	13	2.6	66
IS 70	East	767-30	13	La. 1	8	86.43	2195.3	3.8	97	-3.2	-81	1.8	46	0.6	15	0	0	0.6	15	2.7	69
IS 70	East	767-30	13	La. 1	9	98.6	2504.4	3.8	97	-3.2	-81	1.6	41	0.3	8	0	0	0.3	8	2.9	74
IS 70	East	767-30	13	La. 1	10	110.84	2815.3	3.9	99	-3.1	-79	2.2	56	1.1	28	-0.5	-13	1	25	2.7	69
IS 70	East	766-58	7	La. 1	1	0.96	24.4	3.8	97	-3.2	-81	-0.3	-8	0.5	13	-0.4	-10	0.3	8	2.9	74
IS 70	East	766-58	7	La. 1	2	13.29	337.6	3.8	97	-3.3	-84	0.8	20	0.7	18	-0.2	-5	0.7	18	2.7	69
IS 70	East	766-58	7	La. 1	3	25.3	642.6	3.8	97	-3.2	-81	1.3	33	1	25	-0.2	-5	1	25	2.6	66
IS 70	East	766-58	7	La. 1	4	37.31	947.7	3.8	97	-3.2	-81	1.2	30	0.9	23	-0.2	-5	0.9	23	2.6	66
IS 70	East	766-58	7	La. 1	5	49.31	1252.5	3.8	97	-3.2	-81	1.3	33	0.9	23	-0.1	-3	0.9	23	2.6	66
IS 70	East	766-58	7	La. 1	6	61.3	1557.0	3.8	97	-3.2	-81	1.5	38	1.1	28	-0.2	-5	1	25	2.5	64
IS 70	East	766-58	7	La. 1	7	73.32	1862.3	3.8	97	-3.2	-81	1.4	36	1.1	28	-0.3	-8	1	25	2.6	66
IS 70	East	766-58	7	La. 1	8	85.28	2166.1	3.8	97	-3.2	-81	1.5	38	1	25	-0.2	-5	1	25	2.5	64
IS 70	East	766-58	7	La. 1	9	97.22	2469.4	3.9	99	-3.2	-81	1.4	36	1.1	28	-0.2	-5	1.1	28	2.6	66
IS 70	East	766-58	7	La. 1	10	109.5	2781.3	3.9	99	-3.1	-79	0.3	8	0.6	15	0	0	0.6	15	2.8	71
IS 70	East	765-86	1	La. 1	1	1.75	44.5	4	102	-3	-76	-0.8	-20	1.3	33	-1.3	-33	0.2	5	3.1	79
IS 70	East	765-86	1	La. 1	2	13.94	354.1	4	102	-3	-76	-0.6	-15	0.6	15	-0.5	-13	0.3	8	3.1	79
IS 70	East	765-86	1	La. 1	3	25.91	658.1	4	102	-3	-76	-0.6	-15	0.3	8	-0.3	-8	0.1	3	3.1	79
IS 70	East	765-86	1	La. 1	4	37.99	964.9	3.9	99	-3.1	-79	-1	-25	0.4	10	0	0	-0.4	-10	3	76
IS 70	East	765-86	1	La. 1	5	50	1270.0	4	102	-3.1	-79	-0.3	-8	0.3	8	0	0	0.3	8	3.1	79

IS 70	East	765-86	1	La. 1	6	62.03	1575.6	4	102	-3	-76	-0.6	-15	0.3	8	-0.2	-5	0.2	5	3.1	79
IS 70	East	765-86	1	La. 1	7	74.04	1880.6	4	102	-3	-76	-0.5	-13	0.1	3	-0.1	-3	-0.1	-3	3.2	81
IS 70	East	765-86	1	La. 1	8	85.97	2183.6	4	102	-3	-76	-1.3	-33	0.5	13	0	0	-0.5	-13	3	76
IS 70	East	765-86	1	La. 1	9	97.92	2487.2	4	102	-3	-76	-0.3	-8	0.2	5	0.2	5	0.2	5	3.2	81
IS 70	East	765-86	1	La. 1	10	109.49	2781.0	4.2	107	-2.8	-71	-0.7	-18	0.4	10	-0.1	-3	0.4	10	3.2	81
IS 70	East	766-58	7	La. 1	1	9.21	233.9	3.8	97	-3.2	-81	1.5	38	0.9	23	0	0	0.9	23	2.6	66
IS 70	East	766-58	7	La. 1	2	21.59	548.4	3.8	97	-3.2	-81	1.5	38	1	25	-0.2	-5	1	25	2.6	66
IS 70	East	766-58	7	La. 1	3	33.58	852.9	3.7	94	-3.3	-84	1.6	41	1	25	-0.3	-8	1	25	2.5	64
IS 70	East	766-58	7	La. 1	4	45.65	1159.5	3.8	97	-3.3	-84	0.5	13	0.3	8	-0.2	-5	0.2	5	2.9	74
IS 70	East	766-58	7	La. 1	5	57.54	1461.5	3.8	97	-3.2	-81	1.5	38	1	25	-0.2	-5	1	25	2.5	64
IS 70	East	766-58	7	La. 1	6	69.5	1765.3	3.8	97	-3.2	-81	1.4	36	1	25	-0.1	-3	1	25	2.6	66
IS 70	East	766-58	7	La. 1	7	81.91	2080.5	4.7	119	-2.3	-58	-0.2	-5	1.6	41	-0.9	-23	1.3	33	3.3	84
IS 70	East	766-58	7	La. 1	8	93.67	2379.2	3.9	99	-3.1	-79	1.4	36	1.3	33	-0.6	-15	1.1	28	2.6	66
IS 70	East	766-58	7	La. 1	9	105.43	2677.9	3.9	99	-3.1	-79	1.3	33	1.2	30	0	0	1.2	30	2.5	64
IS 70	East	766-58	7	La. 1	10	117.29	2979.2	4.1	104	-3	-76	-0.8	-20	0.9	23	-0.2	-5	0.8	20	2.9	74
IS 70	East	766-58	7	La. 1	1	3.71	94.2	3.7	94	-3.3	-84	0.6	15	0.8	20	-0.1	-3	0.7	18	2.6	66
IS 70	East	766-58	7	La. 1	2	16.13	409.7	3.7	94	-3.3	-84	0.6	15	0.7	18	-0.3	-8	0.7	18	2.6	66
IS 70	East	766-58	7	La. 1	3	28.19	716.0	3.7	94	-3.4	-86	-0.5	-13	0.2	5	-0.1	-3	0.2	5	2.8	71
IS 70	East	766-58	7	La. 1	4	40.2	1021.1	3.7	94	-3.3	-84	-0.7	-18	0.4	10	-0.2	-5	0.3	8	2.8	71
IS 70	East	766-58	7	La. 1	5	52.28	1327.9	3.7	94	-3.3	-84	1.4	36	1.2	30	-0.3	-8	1.1	28	2.4	61
IS 70	East	766-58	7	La. 1	6	64.27	1632.5	3.7	94	-3.3	-84	-0.8	-20	0.2	5	-0.2	-5	0.1	3	2.9	74
IS 70	East	766-58	7	La. 1	7	76.19	1935.2	3.8	97	-3.2	-81	1	25	1.1	28	-0.2	-5	1.1	28	2.5	64
IS 70	East	766-58	7	La. 1	8	88.12	2238.2	3.7	94	-3.3	-84	-1.4	-36	0.2	5	0	0	0.1	3	2.8	71
IS 70	East	766-58	7	La. 1	9	99.72	2532.9	4	102	-3	-76	-2	-51	0.1	3	0	0	-0.1	-3	3.2	81

B2: MAD-70 WB control section MITScan data collected by ODOT August 19, 2015

Highway	Direction	Station Number	Joint	Lane	Bar Number	X-Position		Depth		Depth Deviation		Side Shift		Misalignment		Horizontal Misalignment		Vertical Misalignment		Minimal Cover	
HW	Dir	SNo	Jo	La	BNo	xs		zs		dz		dy		s		sh		sv		c	
-	-	-	-	-	-	(in)	(mm)	(in)	(mm)	(in)	(mm)	(in)	(mm)	(in)	(mm)	(in)	(mm)	(in)	(mm)	(in)	(mm)
IS 70	West	784-58	157	La. 1	1	6.29	159.8	4.4	112	-2.6	-66	1.2	30	0.3	8	0.3	8	0.1	3	3.6	91
IS 70	West	784-58	157	La. 1	2	18.6	472.4	4.5	114	-2.5	-64	1.2	30	0.1	3	-0.1	-3	0	0	3.7	94
IS 70	West	784-58	157	La. 1	3	30.6	777.2	4.5	114	-2.5	-64	1.1	28	0.1	3	-0.1	-3	0.1	3	3.7	94
IS 70	West	784-58	157	La. 1	4	42.62	1082.5	4.5	114	-2.5	-64	1	25	0.2	5	-0.1	-3	0.1	3	3.7	94
IS 70	West	784-58	157	La. 1	5	54.48	1383.8	4.5	114	-2.5	-64	0.8	20	0.1	3	0	0	0.1	3	3.7	94
IS 70	West	784-58	157	La. 1	6	66.61	1691.9	4.6	117	-2.4	-61	0.2	5	0.1	3	-0.1	-3	0	0	3.8	97
IS 70	West	784-58	157	La. 1	7	78.77	2000.8	4.4	112	-2.6	-66	-0.2	-5	0.3	8	0.2	5	0.2	5	3.5	89
IS 70	West	784-58	157	La. 1	8	90.48	2298.2	4.5	114	-2.5	-64	0	0	0.2	5	-0.1	-3	0.1	3	3.6	91
IS 70	West	784-58	157	La. 1	9	102.67	2607.8	4.6	117	-2.4	-61	-0.2	-5	0.2	5	0.2	5	0.1	3	3.8	97
IS 70	West	784-58	157	La. 1	10	114.62	2911.3	4.5	114	-2.5	-64	-0.9	-23	0.5	13	0.5	13	-0.1	-3	3.7	94
IS 70	West	784-58	157	La. 1	1	6.43	163.3	3.9	99	-3.1	-79	1.6	41	0.6	15	-0.2	-5	0.6	15	2.8	71
IS 70	West	784-58	157	La. 1	2	18.78	477.0	4	102	-3	-76	1.6	41	0.5	13	-0.2	-5	0.5	13	3	76
IS 70	West	784-58	157	La. 1	3	30.79	782.1	4.1	104	-2.9	-74	1.8	46	0.8	20	-0.2	-5	0.8	20	2.9	74
IS 70	West	784-58	157	La. 1	4	42.8	1087.1	4	102	-3	-76	1.6	41	0.6	15	-0.2	-5	0.5	13	3	76
IS 70	West	784-58	157	La. 1	5	54.81	1392.2	4.2	107	-2.8	-71	1.7	43	1	25	-0.2	-5	1	25	3	76
IS 70	West	784-58	157	La. 1	6	66.85	1698.0	4.2	107	-2.8	-71	1.7	43	1	25	-0.2	-5	1	25	2.9	74

IS 70	West	784-58	157	La. 1	7	78.89	2003.8	4.2	107	-2.8	-71	2.1	53	1	25	0	0	1	25	3	76
IS 70	West	784-58	157	La. 1	8	90.86	2307.8	4.2	107	-2.8	-71	1.8	46	1	25	-0.1	-3	1	25	2.9	74
IS 70	West	784-58	157	La. 1	9	102.72	2609.1	4.1	104	-2.9	-74	1.3	33	0.8	20	0	0	0.8	20	2.9	74
IS 70	West	784-58	157	La. 1	10	114.55	2909.6	4.1	104	-2.9	-74	0.4	10	0.5	13	0.4	10	0.3	8	3.2	81
IS 70	West	783-86	151	La. 1	1	5	127.0	3.9	99	-3.1	-79	1.5	38	0.6	15	-0.1	-3	0.6	15	2.9	74
IS 70	West	783-86	151	La. 1	2	17.39	441.7	4	102	-3	-76	1.4	36	0.5	13	-0.1	-3	0.5	13	3	76
IS 70	West	783-86	151	La. 1	3	29.37	746.0	4	102	-3	-76	1.4	36	0.6	15	-0.2	-5	0.5	13	3	76
IS 70	West	783-86	151	La. 1	4	41.37	1050.8	4	102	-3	-76	1.5	38	0.5	13	-0.1	-3	0.5	13	3	76
IS 70	West	783-86	151	La. 1	5	53.45	1357.6	4	102	-3	-76	1.3	33	0.5	13	-0.1	-3	0.4	10	3	76
IS 70	West	783-86	151	La. 1	6	65.53	1664.5	4	102	-3	-76	1.6	41	0.6	15	-0.1	-3	0.6	15	2.9	74
IS 70	West	783-86	151	La. 1	7	77.55	1969.8	4	102	-3.1	-79	1.4	36	0.7	18	-0.1	-3	0.7	18	2.8	71
IS 70	West	783-86	151	La. 1	8	89.46	2272.3	4	102	-3	-76	1.3	33	0.5	13	-0.1	-3	0.5	13	3	76
IS 70	West	783-86	151	La. 1	9	101.32	2573.5	4	102	-3	-76	0.9	23	0.4	10	0	0	0.4	10	3.1	79
IS 70	West	783-86	151	La. 1	10	113.09	2872.5	4.2	107	-2.8	-71	-0.9	-23	0.3	8	-0.1	-3	-0.3	-8	3.3	84
IS 70	West	783-14	145	La. 1	1	10.46	265.7	3.9	99	-3.1	-79	1.7	43	0.8	20	0.5	13	0.6	15	2.9	74
IS 70	West	783-14	145	La. 1	2	22.86	580.6	4	102	-3	-76	1.6	41	0.5	13	0.1	3	0.5	13	3	76
IS 70	West	783-14	145	La. 1	3	34.92	887.0	4	102	-3	-76	1.6	41	0.5	13	-0.2	-5	0.5	13	3	76
IS 70	West	783-14	145	La. 1	4	46.95	1192.5	4	102	-3	-76	1.5	38	0.5	13	-0.3	-8	0.5	13	3	76
IS 70	West	783-14	145	La. 1	5	59.02	1499.1	4.1	104	-3	-76	1.4	36	0.5	13	-0.3	-8	0.4	10	3.1	79
IS 70	West	783-14	145	La. 1	6	71.06	1804.9	4	102	-3	-76	1.3	33	0.5	13	-0.2	-5	0.4	10	3.1	79
IS 70	West	783-14	145	La. 1	7	83.07	2110.0	4	102	-3	-76	1.1	28	0.5	13	-0.2	-5	0.4	10	3	76
IS 70	West	783-14	145	La. 1	8	94.95	2411.7	4	102	-3	-76	0.9	23	0.4	10	-0.1	-3	0.3	8	3.1	79
IS 70	West	783-14	145	La. 1	9	106.88	2714.8	4.1	104	-2.9	-74	-0.2	-5	0.1	3	0.1	3	0	0	3.3	84
IS 70	West	783-14	145	La. 1	10	119.52	3035.8	4.3	109	-2.8	-71	-1.2	-30	0.7	18	-0.6	-15	-0.4	-10	3.3	84
IS 70	West	782-42	139	La. 1	1	5.51	140.0	3.9	99	-3.2	-81	1	25	0.5	13	0.1	3	0.5	13	2.9	74
IS 70	West	782-42	139	La. 1	2	17.83	452.9	3.9	99	-3.1	-79	0.9	23	0.3	8	0	0	0.3	8	3	76
IS 70	West	782-42	139	La. 1	3	29.87	758.7	3.9	99	-3.1	-79	0.8	20	0.3	8	0	0	0.3	8	3	76
IS 70	West	782-42	139	La. 1	4	41.92	1064.8	3.9	99	-3.1	-79	0.9	23	0.3	8	0	0	0.3	8	3	76
IS 70	West	782-42	139	La. 1	5	53.93	1369.8	3.9	99	-3.1	-79	0.8	20	0.3	8	-0.1	-3	0.3	8	3	76
IS 70	West	782-42	139	La. 1	6	65.96	1675.4	3.9	99	-3.2	-81	0.8	20	0.3	8	-0.1	-3	0.3	8	3	76
IS 70	West	782-42	139	La. 1	7	77.98	1980.7	3.8	97	-3.2	-81	0.9	23	0.4	10	-0.1	-3	0.4	10	2.9	74
IS 70	West	782-42	139	La. 1	8	89.97	2285.2	3.8	97	-3.2	-81	0.8	20	0.3	8	0	0	0.3	8	2.9	74
IS 70	West	782-42	139	La. 1	9	101.85	2587.0	3.9	99	-3.1	-79	0.9	23	0.4	10	0	0	0.4	10	2.9	74
IS 70	West	782-42	139	La. 1	10	113.62	2885.9	4.1	104	-2.9	-74	0.5	13	0.2	5	0.1	3	0.2	5	3.2	81
IS 70	West	781-70	133	La. 1	1	4.94	125.5	3.9	99	-3.1	-79	1.5	38	0.2	5	-0.1	-3	0.2	5	3.1	79
IS 70	West	781-70	133	La. 1	2	17.12	434.8	4	102	-3	-76	1.5	38	0.3	8	-0.3	-8	0	0	3.2	81
IS 70	West	781-70	133	La. 1	3	29.17	740.9	4	102	-3	-76	1.4	36	0.4	10	-0.4	-10	0.1	3	3.2	81
IS 70	West	781-70	133	La. 1	4	41.2	1046.5	4	102	-3	-76	1.4	36	0.4	10	-0.4	-10	0.1	3	3.2	81
IS 70	West	781-70	133	La. 1	5	53.21	1351.5	4	102	-3	-76	1.2	30	0.3	8	-0.3	-8	0.1	3	3.2	81
IS 70	West	781-70	133	La. 1	6	65.25	1657.4	4	102	-3	-76	1.2	30	0.2	5	-0.2	-5	0.1	3	3.2	81
IS 70	West	781-70	133	La. 1	7	77.3	1963.4	4	102	-3	-76	1.1	28	0.3	8	-0.2	-5	0.2	5	3.1	79
IS 70	West	781-70	133	La. 1	8	89.25	2267.0	4	102	-3	-76	0.8	20	0	0	0	0	0	0	3.2	81
IS 70	West	781-70	133	La. 1	9	101.21	2570.7	4	102	-3	-76	0.6	15	0.2	5	0.1	3	0.1	3	3.2	81
IS 70	West	781-70	133	La. 1	10	113.08	2872.2	4	102	-3	-76	-0.2	-5	0.4	10	0.4	10	0	0	3.2	81
IS 70	West	780-98	127	La. 1	1	4.54	115.3	3.8	97	-3.2	-81	0.4	10	0.2	5	-0.1	-3	0.1	3	3	76
IS 70	West	780-98	127	La. 1	2	16.74	425.2	3.9	99	-3.1	-79	0.3	8	0.2	5	-0.1	-3	0.1	3	3.1	79
IS 70	West	780-98	127	La. 1	3	28.67	728.2	3.9	99	-3.1	-79	0.1	3	0	0	0	0	0	0	3.2	81
IS 70	West	780-98	127	La. 1	4	40.85	1037.6	3.9	99	-3.1	-79	0.4	10	0.2	5	-0.2	-5	0.1	3	3.1	79
IS 70	West	780-98	127	La. 1	5	52.83	1341.9	3.9	99	-3.1	-79	1.2	30	0.4	10	-0.1	-3	0.4	10	3	76

IS 70	West	780-98	127	La. 1	6	64.82	1646.4	3.9	99	-3.1	-79	1.2	30	0.3	8	-0.1	-3	0.3	8	3	76
IS 70	West	780-98	127	La. 1	7	76.87	1952.5	3.8	97	-3.2	-81	1.2	30	0.3	8	0	0	0.3	8	3	76
IS 70	West	780-98	127	La. 1	8	88.83	2256.3	3.8	97	-3.2	-81	1.2	30	0.4	10	-0.1	-3	0.4	10	2.9	74
IS 70	West	780-98	127	La. 1	9	100.8	2560.3	3.8	97	-3.2	-81	1.2	30	0.3	8	0	0	0.3	8	2.9	74
IS 70	West	780-98	127	La. 1	10	112.93	2868.4	3.8	97	-3.2	-81	1.2	30	0.3	8	0.1	3	0.3	8	2.9	74
IS 70	West	780-26	121	La. 1	1	0.82	20.8	3.9	99	-3.1	-79	1.8	46	0.5	13	-0.4	-10	0.4	10	3	76
IS 70	West	780-26	121	La. 1	2	12.96	329.2	3.8	97	-3.2	-81	2.2	56	0.6	15	-0.3	-8	0.6	15	2.8	71
IS 70	West	780-26	121	La. 1	3	24.92	633.0	3.9	99	-3.2	-81	2	51	0.6	15	-0.2	-5	0.6	15	2.8	71
IS 70	West	780-26	121	La. 1	4	36.98	939.3	3.9	99	-3.1	-79	2.1	53	0.7	18	-0.1	-3	0.7	18	2.8	71
IS 70	West	780-26	121	La. 1	5	49.07	1246.4	3.9	99	-3.1	-79	1.9	48	0.6	15	-0.2	-5	0.6	15	2.8	71
IS 70	West	780-26	121	La. 1	6	61.09	1551.7	3.9	99	-3.1	-79	1.8	46	0.5	13	-0.2	-5	0.5	13	2.9	74
IS 70	West	780-26	121	La. 1	7	72.99	1853.9	3.8	97	-3.2	-81	1.6	41	0.4	10	-0.2	-5	0.4	10	2.9	74
IS 70	West	780-26	121	La. 1	8	84.99	2158.7	3.8	97	-3.2	-81	1.6	41	0.4	10	-0.2	-5	0.3	8	2.9	74
IS 70	West	780-26	121	La. 1	9	96.93	2462.0	3.9	99	-3.1	-79	1.5	38	0.4	10	-0.2	-5	0.4	10	2.9	74
IS 70	West	780-26	121	La. 1	10	109.27	2775.5	3.8	97	-3.2	-81	1.6	41	0.5	13	-0.4	-10	0.4	10	2.9	74
IS 70	West	780-26	121	La. 1	1	3.09	78.5	4	102	-3	-76	0.4	10	0.4	10	-0.2	-5	0.4	10	3.1	79
IS 70	West	780-26	121	La. 1	2	15.26	387.6	4	102	-3.1	-79	0.3	8	0.4	10	-0.2	-5	0.4	10	3	76
IS 70	West	780-26	121	La. 1	3	27.21	691.1	4	102	-3	-76	0.4	10	0.4	10	-0.1	-3	0.4	10	3.1	79
IS 70	West	780-26	121	La. 1	4	39.28	997.7	4	102	-3	-76	-0.3	-8	0.3	8	-0.2	-5	0.2	5	3.2	81
IS 70	West	780-26	121	La. 1	5	51.29	1302.8	4.1	104	-2.9	-74	-0.8	-20	0.2	5	-0.2	-5	-0.1	-3	3.3	84
IS 70	West	780-26	121	La. 1	6	63.25	1606.6	4.1	104	-2.9	-74	-1.3	-33	0.3	8	-0.1	-3	-0.3	-8	3.2	81
IS 70	West	780-26	121	La. 1	7	75.34	1913.6	4.2	107	-2.8	-71	-1.4	-36	0.4	10	-0.2	-5	-0.4	-10	3.2	81
IS 70	West	780-26	121	La. 1	8	87.33	2218.2	4.2	107	-2.8	-71	-1.4	-36	0.4	10	-0.2	-5	-0.4	-10	3.2	81
IS 70	West	780-26	121	La. 1	9	99.26	2521.2	4.1	104	-2.9	-74	-1.4	-36	0.4	10	-0.1	-3	-0.4	-10	3.2	81
IS 70	West	780-26	121	La. 1	10	111.5	2832.1	4.1	104	-2.9	-74	-1.6	-41	0.5	13	0.2	5	-0.5	-13	3.1	79
IS 70	West	779-54	115	La. 1	1	11.43	290.3	4.2	107	-2.8	-71	0.4	10	0.2	5	-0.1	-3	-0.2	-5	3.4	86
IS 70	West	779-54	115	La. 1	2	23.65	600.7	4.3	109	-2.7	-69	0.4	10	0.2	5	-0.2	-5	-0.1	-3	3.5	89
IS 70	West	779-54	115	La. 1	3	35.85	910.6	4.3	109	-2.7	-69	0.7	18	0.3	8	-0.3	-8	0.1	3	3.4	86
IS 70	West	779-54	115	La. 1	4	47.81	1214.4	4.1	104	-2.9	-74	1	25	0.4	10	-0.3	-8	0.3	8	3.2	81
IS 70	West	779-54	115	La. 1	5	59.75	1517.7	4.1	104	-2.9	-74	1.1	28	0.4	10	-0.2	-5	0.4	10	3.2	81
IS 70	West	779-54	115	La. 1	6	71.8	1823.7	4.2	107	-2.8	-71	1.1	28	0.4	10	-0.2	-5	0.3	8	3.2	81
IS 70	West	779-54	115	La. 1	7	83.79	2128.3	4.2	107	-2.8	-71	1.1	28	0.3	8	-0.1	-3	0.3	8	3.3	84
IS 70	West	779-54	115	La. 1	8	95.69	2430.5	4.1	104	-2.9	-74	1.1	28	0.3	8	-0.1	-3	0.3	8	3.2	81
IS 70	West	779-54	115	La. 1	9	107.93	2741.4	4.1	104	-2.9	-74	0.9	23	0.7	18	-0.6	-15	0.1	3	3.3	84
IS 70	West	778-82	109	La. 1	1	11.41	289.8	3.9	99	-3.2	-81	-1.4	-36	0.3	8	-0.2	-5	-0.3	-8	3	76
IS 70	West	778-82	109	La. 1	2	23.66	601.0	3.9	99	-3.1	-79	-1.7	-43	0.2	5	-0.1	-3	-0.2	-5	3.1	79
IS 70	West	778-82	109	La. 1	3	35.73	907.5	4	102	-3.1	-79	-1.7	-43	0.3	8	-0.1	-3	-0.2	-5	3.1	79
IS 70	West	778-82	109	La. 1	4	47.77	1213.4	4	102	-3	-76	-1.8	-46	0.3	8	-0.1	-3	-0.2	-5	3.1	79
IS 70	West	778-82	109	La. 1	5	59.72	1516.9	4.1	104	-2.9	-74	-1.8	-46	0.3	8	-0.1	-3	-0.3	-8	3.2	81
IS 70	West	778-82	109	La. 1	6	71.77	1823.0	4.1	104	-2.9	-74	-1.9	-48	0.4	10	0	0	-0.4	-10	3.2	81
IS 70	West	778-82	109	La. 1	7	83.92	2131.6	4.1	104	-2.9	-74	-1.7	-43	0.3	8	-0.2	-5	-0.2	-5	3.2	81
IS 70	West	778-82	109	La. 1	8	95.7	2430.8	4	102	-3	-76	-1.4	-36	0.4	10	-0.3	-8	-0.2	-5	3.2	81
IS 70	West	778-82	109	La. 1	9	107.41	2728.2	4.2	107	-2.8	-71	0.5	13	0.3	8	0.2	5	0.3	8	3.3	84
IS 70	West	778-10	103	La. 1	1	7.56	192.0	3.7	94	-3.3	-84	1.3	33	0.2	5	0.1	3	0.2	5	2.9	74
IS 70	West	778-10	103	La. 1	2	19.82	503.4	3.8	97	-3.3	-84	1.5	38	0.3	8	0.1	3	0.3	8	2.9	74
IS 70	West	778-10	103	La. 1	3	31.83	808.5	3.9	99	-3.1	-79	1.4	36	0.4	10	0	0	0.3	8	2.9	74
IS 70	West	778-10	103	La. 1	4	43.92	1115.6	3.9	99	-3.1	-79	1.5	38	0.3	8	0	0	0.3	8	3	76
IS 70	West	778-10	103	La. 1	5	55.89	1419.6	4	102	-3.1	-79	1.4	36	0.3	8	0	0	0.3	8	3	76
IS 70	West	778-10	103	La. 1	6	67.93	1725.4	4	102	-3	-76	1.5	38	0.3	8	0	0	0.3	8	3.1	79

IS 70	West	778-10	103	La. 1	7	79.96	2031.0	4	102	-3	-76	1.6	41	0.3	8	0	0	0.3	8	3.1	79
IS 70	West	778-10	103	La. 1	8	91.93	2335.0	4	102	-3	-76	1.6	41	0.3	8	0.1	3	0.3	8	3.1	79
IS 70	West	778-10	103	La. 1	9	103.75	2635.3	4.1	104	-2.9	-74	1.6	41	0.3	8	0.1	3	0.3	8	3.2	81
IS 70	West	778-10	103	La. 1	10	115.58	2935.7	4.3	109	-2.7	-69	1.4	36	0.2	5	0.2	5	0.1	3	3.5	89
IS 70	West	777-38	97	La. 1	1	8.59	218.2	3.8	97	-3.2	-81	1.3	33	0.5	13	0	0	0.5	13	2.8	71
IS 70	West	777-38	97	La. 1	2	20.85	529.6	3.9	99	-3.1	-79	1.5	38	0.5	13	0.1	3	0.5	13	2.9	74
IS 70	West	777-38	97	La. 1	3	32.86	834.6	4	102	-3	-76	1.2	30	0.5	13	0	0	0.5	13	3	76
IS 70	West	777-38	97	La. 1	4	44.88	1140.0	4	102	-3	-76	1.4	36	0.4	10	0	0	0.4	10	3	76
IS 70	West	777-38	97	La. 1	5	56.84	1443.7	4	102	-3	-76	1.1	28	0.5	13	0	0	0.5	13	3.1	79
IS 70	West	777-38	97	La. 1	6	68.9	1750.1	4.1	104	-3	-76	1.3	33	0.4	10	0	0	0.4	10	3.1	79
IS 70	West	777-38	97	La. 1	7	80.85	2053.6	4	102	-3	-76	1.3	33	0.4	10	0	0	0.4	10	3.1	79
IS 70	West	777-38	97	La. 1	8	92.83	2357.9	4	102	-3	-76	1.4	36	0.3	8	0	0	0.3	8	3.1	79
IS 70	West	777-38	97	La. 1	9	104.7	2659.4	4	102	-3	-76	1.3	33	0.4	10	0	0	0.4	10	3.1	79
IS 70	West	777-38	97	La. 1	10	116.63	2962.4	4.1	104	-2.9	-74	1.6	41	0.3	8	-0.1	-3	0.3	8	3.3	84
IS 70	West	776-66	91	La. 1	1	3.05	77.5	3.7	94	-3.3	-84	1	25	0.4	10	-0.2	-5	0.4	10	2.8	71
IS 70	West	776-66	91	La. 1	2	15.08	383.0	3.8	97	-3.2	-81	1.2	30	0.4	10	-0.1	-3	0.3	8	2.8	71
IS 70	West	776-66	91	La. 1	3	27.11	688.6	3.8	97	-3.2	-81	0.9	23	0.4	10	-0.2	-5	0.3	8	2.9	74
IS 70	West	776-66	91	La. 1	4	39.14	994.2	3.9	99	-3.1	-79	0.9	23	0.3	8	-0.2	-5	0.3	8	3	76
IS 70	West	776-66	91	La. 1	5	51.16	1299.5	3.9	99	-3.1	-79	0.7	18	0.3	8	-0.1	-3	0.3	8	3	76
IS 70	West	776-66	91	La. 1	6	63.2	1605.3	3.9	99	-3.1	-79	0.8	20	0.3	8	-0.2	-5	0.3	8	3	76
IS 70	West	776-66	91	La. 1	7	75.2	1910.1	4	102	-3.1	-79	0.7	18	0.3	8	-0.1	-3	0.2	5	3.1	79
IS 70	West	776-66	91	La. 1	8	87.16	2213.9	3.9	99	-3.1	-79	0.7	18	0.3	8	-0.2	-5	0.2	5	3	76
IS 70	West	776-66	91	La. 1	9	99.04	2515.6	3.9	99	-3.1	-79	0.8	20	0.3	8	-0.2	-5	0.2	5	3	76
IS 70	West	776-66	91	La. 1	10	110.78	2813.8	4.1	104	-2.9	-74	0.5	13	0.1	3	-0.1	-3	0	0	3.3	84
IS 70	West	775-94	85	La. 1	1	8.3	210.8	3.3	84	-3.7	-94	-2.1	-53	0.3	8	0	0	-0.3	-8	2.5	64
IS 70	West	775-94	85	La. 1	2	20.65	524.5	3.4	86	-3.6	-91	-1.5	-38	0.1	3	0	0	-0.1	-3	2.7	69
IS 70	West	775-94	85	La. 1	3	32.69	830.3	3.5	89	-3.6	-91	-1.9	-48	0.2	5	-0.1	-3	-0.1	-3	2.8	71
IS 70	West	775-94	85	La. 1	4	44.73	1136.1	3.5	89	-3.5	-89	-1.9	-48	0.3	8	-0.1	-3	-0.3	-8	2.7	69
IS 70	West	775-94	85	La. 1	5	56.73	1440.9	3.6	91	-3.5	-89	-2.2	-56	0.4	10	-0.1	-3	-0.4	-10	2.7	69
IS 70	West	775-94	85	La. 1	6	68.77	1746.8	3.6	91	-3.4	-86	-2.1	-53	0.5	13	-0.1	-3	-0.5	-13	2.7	69
IS 70	West	775-94	85	La. 1	7	80.73	2050.5	3.6	91	-3.4	-86	-2.1	-53	0.5	13	-0.1	-3	-0.5	-13	2.7	69
IS 70	West	775-94	85	La. 1	8	92.69	2354.3	3.5	89	-3.5	-89	-2.1	-53	0.5	13	-0.1	-3	-0.4	-10	2.7	69
IS 70	West	775-94	85	La. 1	9	104.48	2653.8	3.6	91	-3.4	-86	-2.2	-56	0.5	13	0.2	5	-0.5	-13	2.7	69
IS 70	West	775-94	85	La. 1	10	116.31	2954.3	3.9	99	-3.1	-79	-2.5	-64	0.7	18	0.2	5	-0.6	-15	2.9	74

B3: WAS/NOB-77 SB distressed section MITScan data collected by ODOT November 10, 2015

Highway	Direction	Station Number	Joint	Lane	Bar Number	X-Position		Depth		Depth Deviation		Side Shift		Misalignment		Horizontal Misalignment		Vertical Misalignment		Minimal Cover	
HW	Dir	SNo	Jo	La	BNo	xs		zs		dz		dy		s		sh		sv		c	
-	-	-	-	-	-	(in)	(mm)	(in)	(mm)	(in)	(mm)	(in)	(mm)	(in)	(mm)	(in)	(mm)	(in)	(mm)	(in)	(mm)
IS 77	South	23-45	14	La. 1	1	5.51	140.0	4.1	104	0	0	-1.7	-43	0.2	5	0	0	-0.2	-5	3.3	84
IS 77	South	23-45	14	La. 1	2	17.93	455.4	3.6	91	-0.5	-13	-0.8	-20	0.4	10	-0.4	-10	-0.1	-3	2.9	74
IS 77	South	23-45	14	La. 1	3	30.21	767.3	3.9	99	-0.2	-5	1.8	46	1	25	0	0	1	25	2.7	69
IS 77	South	23-45	14	La. 1	4	42.19	1071.6	3.8	97	-0.3	-8	1.5	38	0.8	20	0.2	5	0.7	18	2.8	71
IS 77	South	23-45	14	La. 1	5	54.4	1381.8	3.9	99	-0.1	-3	1.9	48	1.3	33	0.7	18	1.1	28	2.8	71

IS 77	South	23-45	14	La. 1	6	66.35	1685.3	3.8	97	-0.3	-8	1.9	48	1.2	30	0.8	20	0.8	20	2.7	69
IS 77	South	23-45	14	La. 1	7	78.34	1989.8	3.8	97	-0.2	-5	1.8	46	1.3	33	0.9	23	1	25	2.7	69
IS 77	South	23-45	14	La. 1	8	90.61	2301.5	3.9	99	-0.2	-5	1.9	48	0.7	18	0.4	10	0.5	13	3	76
IS 77	South	23-45	14	La. 1	9	102.48	2603.0	3.9	99	-0.1	-3	2	51	0.5	13	0	0	0.5	13	3.1	79
IS 77	South	23-45	14	La. 1	10	114.37	2905.0	4	102	-0.1	-3	1.9	48	1.1	28	0.4	10	1	25	2.8	71
IS 77	South	23-45	14	La. 1	11	126.69	3217.9	4	102	0	0	1.7	43	0.7	18	0.1	3	0.7	18	3.1	79
IS 77	South	23-60	13	La. 1	1	5.46	138.7	4.1	104	0.1	3	1	25	0.5	13	-0.1	-3	0.5	13	3.2	81
IS 77	South	23-60	13	La. 1	2	17.85	453.4	3.9	99	-0.1	-3	0.8	20	0.3	8	-0.2	-5	0.3	8	3.2	81
IS 77	South	23-60	13	La. 1	3	30.2	767.1	4.2	107	0.2	5	0.9	23	0.4	10	0.3	8	0.2	5	3.5	89
IS 77	South	23-60	13	La. 1	4	41.95	1065.5	4.1	104	0.1	3	1.2	30	0.2	5	0.1	3	0.2	5	3.4	86
IS 77	South	23-60	13	La. 1	5	54.26	1378.2	4.3	109	0.3	8	1.4	36	0.7	18	0.4	10	0.6	15	3.4	86
IS 77	South	23-60	13	La. 1	6	66.27	1683.3	4.1	104	0.1	3	1.5	38	0.3	8	0.2	5	0.3	8	3.3	84
IS 77	South	23-60	13	La. 1	7	78.37	1990.6	4.2	107	0.2	5	1.6	41	0.6	15	-0.1	-3	0.6	15	3.3	84
IS 77	South	23-60	13	La. 1	8	90.6	2301.2	4.2	107	0.2	5	2	51	0.2	5	-0.2	-5	0	0	3.6	91
IS 77	South	23-60	13	La. 1	9	102.45	2602.2	4.3	109	0.3	8	2.2	56	0.5	13	-0.5	-13	-0.1	-3	3.6	91
IS 77	South	23-60	13	La. 1	10	114.41	2906.0	4.3	109	0.2	5	1.7	43	0.3	8	0.2	5	0.2	5	3.5	89
IS 77	South	23-60	13	La. 1	11	126.66	3217.2	4.5	114	0.4	10	1.8	46	0.1	3	-0.1	-3	-0.1	-3	3.8	97
IS 77	South	23-75	12	La. 1	1	5.35	135.9	4.2	107	0.2	5	1.1	28	0.7	18	0	0	0.7	18	3.2	81
IS 77	South	23-75	12	La. 1	2	17.74	450.6	3.8	97	-0.2	-5	0.6	15	0.4	10	-0.1	-3	0.3	8	3	76
IS 77	South	23-75	12	La. 1	3	29.95	760.7	3.8	97	-0.2	-5	-0.2	-5	0.3	8	0.2	5	-0.1	-3	3.2	81
IS 77	South	23-75	12	La. 1	4	41.9	1064.3	3.8	97	-0.2	-5	1.4	36	0.5	13	0.2	5	0.5	13	3	76
IS 77	South	23-75	12	La. 1	5	54.15	1375.4	4	102	0	0	1.7	43	1	25	0.3	8	0.9	23	2.9	74
IS 77	South	23-75	12	La. 1	6	66.14	1680.0	3.8	97	-0.2	-5	1.8	46	0.9	23	0.4	10	0.7	18	2.8	71
IS 77	South	23-75	12	La. 1	7	78.17	1985.5	3.8	97	-0.2	-5	1.8	46	0.8	20	0.5	13	0.7	18	2.8	71
IS 77	South	23-75	12	La. 1	8	90.33	2294.4	3.9	99	-0.2	-5	2.3	58	0.6	15	0.2	5	0.6	15	2.9	74
IS 77	South	23-75	12	La. 1	9	102.41	2601.2	4	102	0	0	2.4	61	0.5	13	-0.1	-3	0.5	13	3.1	79
IS 77	South	23-75	12	La. 1	10	114.24	2901.7	3.8	97	-0.2	-5	1.9	48	0.8	20	0.5	13	0.6	15	2.9	74
IS 77	South	23-75	12	La. 1	11	126.46	3212.1	3.9	99	-0.1	-3	1.8	46	0.5	13	0.2	5	0.5	13	3.1	79
IS 77	South	23-90	11	La. 1	1	5.46	138.7	4.4	112	0.4	10	2.5	64	2	51	0	0	2	51	2.8	71
IS 77	South	23-90	11	La. 1	2	17.69	449.3	3.8	97	-0.2	-5	-1.1	-28	0.2	5	-0.2	-5	0.1	3	3.1	79
IS 77	South	23-90	11	La. 1	3	29.97	761.2	4.1	104	0.1	3	1.6	41	1.2	30	0	0	1.2	30	2.8	71
IS 77	South	23-90	11	La. 1	4	41.92	1064.8	3.9	99	-0.1	-3	1.4	36	0.8	20	0.1	3	0.8	20	2.9	74
IS 77	South	23-90	11	La. 1	5	54.1	1374.1	4.2	107	0.2	5	2.1	53	1.5	38	0.5	13	1.5	38	2.9	74
IS 77	South	23-90	11	La. 1	6	66.07	1678.2	4.1	104	0.1	3	2	51	1.2	30	0.4	10	1.1	28	2.9	74
IS 77	South	23-90	11	La. 1	7	78.07	1983.0	4.1	104	0.1	3	1.9	48	1.1	28	0.5	13	1	25	3	76
IS 77	South	23-90	11	La. 1	8	90.4	2296.2	4.1	104	0.1	3	2.4	61	0.6	15	-0.2	-5	0.6	15	3.2	81
IS 77	South	23-90	11	La. 1	9	102.19	2595.6	4.2	107	0.2	5	2.6	66	1	25	-0.7	-18	0.8	20	3.2	81
IS 77	South	23-90	11	La. 1	10	114.08	2897.6	4.1	104	0.1	3	1.7	43	0.6	15	0.1	3	0.5	13	3.2	81
IS 77	South	23-90	11	La. 1	11	126.48	3212.6	4.1	104	0.1	3	1.6	41	0.5	13	0.3	8	0.4	10	3.3	84
IS 77	South	24-5	10	La. 1	1	5.51	140.0	4.5	114	0.4	10	1	25	0.8	20	0.1	3	0.8	20	3.4	86
IS 77	South	24-5	10	La. 1	2	17.71	449.8	4	102	0	0	2.1	53	1.4	36	0.1	3	1.4	36	2.7	69
IS 77	South	24-5	10	La. 1	3	29.73	755.1	4.1	104	0	0	2	51	1.3	33	0.5	13	1.2	30	2.9	74
IS 77	South	24-5	10	La. 1	4	41.57	1055.9	4.1	104	0.1	3	2.3	58	1.5	38	0.4	10	1.5	38	2.7	69
IS 77	South	24-5	10	La. 1	5	53.9	1369.1	4.3	109	0.3	8	2.5	64	1.9	48	0.4	10	1.8	46	2.8	71
IS 77	South	24-5	10	La. 1	6	65.87	1673.1	4.1	104	0.1	3	2.2	56	1.4	36	0.4	10	1.4	36	2.8	71
IS 77	South	24-5	10	La. 1	7	77.93	1979.4	4.2	107	0.2	5	2.4	61	1.7	43	0.5	13	1.7	43	2.8	71
IS 77	South	24-5	10	La. 1	8	90.25	2292.4	4.1	104	0.1	3	2.2	56	0.9	23	-0.2	-5	0.9	23	3	76
IS 77	South	24-5	10	La. 1	9	102.3	2598.4	4.1	104	0.1	3	2.2	56	0.7	18	-0.1	-3	0.7	18	3.2	81
IS 77	South	24-5	10	La. 1	10	114.06	2897.1	4.1	104	0.1	3	2	51	0.9	23	0.3	8	0.8	20	3	76

IS 77	South	24-5	10	La. 1	11	126.42	3211.1	4.2	107	0.2	5	2	51	0.7	18	0.3	8	0.7	18	3.3	84
IS 77	South	24-20	9	La. 1	1	5.36	136.1	4.3	109	0.2	5	-1.1	-28	0.3	8	0	0	-0.3	-8	3.5	89
IS 77	South	24-20	9	La. 1	2	17.99	456.9	4.2	107	0.2	5	0.8	20	0.5	13	-0.3	-8	0.5	13	3.3	84
IS 77	South	24-20	9	La. 1	3	30.35	770.9	4.3	109	0.3	8	0.9	23	0.5	13	0.4	10	0.2	5	3.6	91
IS 77	South	24-20	9	La. 1	4	42.29	1074.2	4.3	109	0.3	8	1.4	36	0.3	8	-0.1	-3	0.2	5	3.5	89
IS 77	South	24-20	9	La. 1	5	54.53	1385.1	4.4	112	0.4	10	1.5	38	0.5	13	0.2	5	0.4	10	3.6	91
IS 77	South	24-20	9	La. 1	6	66.45	1687.8	4.3	109	0.3	8	1.7	43	0.5	13	0.4	10	0.3	8	3.5	89
IS 77	South	24-20	9	La. 1	7	78.48	1993.4	4.4	112	0.4	10	1.6	41	0.6	15	0.3	8	0.6	15	3.5	89
IS 77	South	24-20	9	La. 1	8	91.02	2311.9	4.6	117	0.6	15	3.3	84	0.1	3	-0.1	-3	0	0	3.9	99
IS 77	South	24-20	9	La. 1	9	102.8	2611.1	4.7	119	0.6	15	4.2	107	0.3	8	0	0	-0.3	-8	3.9	99
IS 77	South	24-20	9	La. 1	10	114.54	2909.3	4.4	112	0.4	10	2.6	66	0.4	10	0.3	8	-0.1	-3	3.7	94
IS 77	South	24-20	9	La. 1	11	127.04	3226.8	4.5	114	0.5	13	1.9	48	0.7	18	0.5	13	-0.4	-10	3.6	91
IS 77	South	24-35	8	La. 1	1	5.31	134.9	4.2	107	0.2	5	0.7	18	0.2	5	-0.1	-3	-0.2	-5	3.5	89
IS 77	South	24-35	8	La. 1	2	17.99	456.9	4	102	0	0	0.6	15	0.3	8	-0.3	-8	0.2	5	3.3	84
IS 77	South	24-35	8	La. 1	3	30.15	765.8	4.1	104	0.1	3	1	25	0.5	13	0	0	0.5	13	3.3	84
IS 77	South	24-35	8	La. 1	4	41.81	1062.0	4.1	104	0.1	3	1.1	28	0.3	8	0	0	0.3	8	3.3	84
IS 77	South	24-35	8	La. 1	5	54.06	1373.1	4.4	112	0.3	8	1.3	33	1	25	0.4	10	0.9	23	3.3	84
IS 77	South	24-35	8	La. 1	6	66.06	1677.9	4.2	107	0.2	5	1.5	38	0.8	20	0.3	8	0.7	18	3.2	81
IS 77	South	24-35	8	La. 1	7	78.06	1982.7	4.3	109	0.3	8	1.2	30	0.7	18	0.2	5	0.7	18	3.3	84
IS 77	South	24-35	8	La. 1	8	90.26	2292.6	4.2	107	0.1	3	1.7	43	0.7	18	0.6	15	0.3	8	3.4	86
IS 77	South	24-35	8	La. 1	9	102.25	2597.2	4.2	107	0.1	3	2.1	53	0.1	3	0.1	3	-0.1	-3	3.5	89
IS 77	South	24-35	8	La. 1	10	114.24	2901.7	4.1	104	0.1	3	2.1	53	0.3	8	0.3	8	0	0	3.4	86
IS 77	South	24-35	8	La. 1	11	126.77	3220.0	4.2	107	0.2	5	2.2	56	0.4	10	0.4	10	0	0	3.6	91
IS 77	South	24-50	7	La. 1	1	5.38	136.7	4.1	104	0.1	3	-0.9	-23	0.2	5	-0.1	-3	-0.2	-5	3.4	86
IS 77	South	24-50	7	La. 1	2	17.68	449.1	3.7	94	-0.3	-8	0.2	5	0.6	15	-0.5	-13	0.4	10	2.9	74
IS 77	South	24-50	7	La. 1	3	29.72	754.9	3.9	99	-0.1	-3	-0.3	-8	0.3	8	0.1	3	0.2	5	3.2	81
IS 77	South	24-50	7	La. 1	4	41.56	1055.6	3.9	99	-0.1	-3	1.1	28	0.7	18	0.1	3	0.7	18	2.9	74
IS 77	South	24-50	7	La. 1	5	53.88	1368.6	4.1	104	0	0	1.8	46	1.4	36	0.5	13	1.3	33	2.8	71
IS 77	South	24-50	7	La. 1	6	65.92	1674.4	3.9	99	-0.1	-3	1.9	48	1.2	30	0.7	18	1	25	2.8	71
IS 77	South	24-50	7	La. 1	7	77.97	1980.4	3.9	99	-0.1	-3	1.4	36	1.2	30	1	25	0.8	20	2.9	74
IS 77	South	24-50	7	La. 1	8	90.14	2289.6	3.9	99	-0.2	-5	1.7	43	0.7	18	0.1	3	0.7	18	2.9	74
IS 77	South	24-50	7	La. 1	9	102.22	2596.4	4	102	0	0	1.4	36	0.3	8	0.2	5	0.3	8	3.2	81
IS 77	South	24-50	7	La. 1	10	113.9	2893.1	3.9	99	-0.1	-3	1.7	43	0.9	23	0.6	15	0.6	15	3	76
IS 77	South	24-50	7	La. 1	11	126.21	3205.7	4.1	104	0.1	3	1.5	38	1.1	28	1.1	28	0.4	10	3.3	84
IS 77	South	24-65	6	La. 1	1	4.67	118.6	4.1	104	0.1	3	1.6	41	0.3	8	-0.3	-8	-0.1	-3	3.4	86
IS 77	South	24-65	6	La. 1	2	16.95	430.5	3.9	99	-0.2	-5	1.7	43	0.6	15	-0.3	-8	0.5	13	3	76
IS 77	South	24-65	6	La. 1	3	29.2	741.7	3.9	99	-0.1	-3	1.7	43	0.7	18	-0.1	-3	0.7	18	3	76
IS 77	South	24-65	6	La. 1	4	41.26	1048.0	3.8	97	-0.2	-5	1.6	41	0.3	8	-0.1	-3	0.3	8	3.1	79
IS 77	South	24-65	6	La. 1	5	53.68	1363.5	4	102	0	0	1.9	48	0.7	18	0	0	0.7	18	3.1	79
IS 77	South	24-65	6	La. 1	6	65.6	1666.2	3.9	99	-0.2	-5	2.5	64	0.3	8	0	0	0.3	8	3.1	79
IS 77	South	24-65	6	La. 1	7	77.41	1966.2	4	102	0	0	1.9	48	0.6	15	0.2	5	0.6	15	3.1	79
IS 77	South	24-65	6	La. 1	8	89.58	2275.3	4	102	0	0	2.1	53	0.4	10	-0.1	-3	0.3	8	3.2	81
IS 77	South	24-65	6	La. 1	9	101.4	2575.6	4.1	104	0.1	3	2.2	56	0.4	10	0	0	0.4	10	3.3	84
IS 77	South	24-65	6	La. 1	10	113.02	2870.7	3.9	99	-0.1	-3	1.9	48	0.6	15	0.4	10	0.5	13	3.1	79
IS 77	South	24-65	6	La. 1	11	125.07	3176.8	4.1	104	0.1	3	1.9	48	0.3	8	0.1	3	0.3	8	3.3	84
IS 77	South	24-80	5	La. 1	1	5.85	148.6	4	102	0	0	0.8	20	0.3	8	-0.2	-5	0.2	5	3.3	84
IS 77	South	24-80	5	La. 1	2	18.49	469.6	4	102	0	0	0.2	5	0.5	13	-0.5	-13	0	0	3.4	86
IS 77	South	24-80	5	La. 1	3	30.84	783.3	4.1	104	0.1	3	-0.3	-8	0.2	5	-0.1	-3	-0.2	-5	3.4	86
IS 77	South	24-80	5	La. 1	4	42.66	1083.6	4	102	0	0	0.8	20	0.2	5	0.1	3	0.1	3	3.3	84

IS 77	South	24-80	5	La. 1	5	55.1	1399.5	4.2	107	0.2	5	1.1	28	0.8	20	0.6	15	0.6	15	3.3	84
IS 77	South	24-80	5	La. 1	6	67.04	1702.8	4	102	0	0	1.8	46	0.7	18	0.6	15	0.3	8	3.2	81
IS 77	South	24-80	5	La. 1	7	79.01	2006.9	4.2	107	0.2	5	1.6	41	0.7	18	0.6	15	0.3	8	3.5	89
IS 77	South	24-80	5	La. 1	8	91.06	2312.9	4.3	109	0.2	5	2.8	71	0.1	3	0.1	3	0.1	3	3.6	91
IS 77	South	24-80	5	La. 1	9	102.73	2609.3	4.3	109	0.3	8	2.6	66	0.1	3	0	0	0	0	3.7	94
IS 77	South	24-80	5	La. 1	10	114.36	2904.7	4.2	107	0.2	5	1.9	48	0.6	15	0.5	13	0.3	8	3.4	86
IS 77	South	24-80	5	La. 1	11	126.54	3214.1	4.4	112	0.4	10	1.8	46	0.4	10	0.3	8	0.3	8	3.7	94
IS 77	South	24-95	4	La. 1	1	5.55	141.0	4.2	107	0.2	5	-0.8	-20	0.1	3	0.1	3	0	0	3.6	91
IS 77	South	24-95	4	La. 1	2	17.69	449.3	4.1	104	0.1	3	-0.9	-23	0.2	5	-0.2	-5	-0.1	-3	3.5	89
IS 77	South	24-95	4	La. 1	3	29.87	758.7	4.2	107	0.2	5	-2	-51	0.7	18	0.5	13	-0.5	-13	3.3	84
IS 77	South	24-95	4	La. 1	4	41.68	1058.7	4.2	107	0.2	5	-1.4	-36	0.4	10	0.4	10	-0.2	-5	3.5	89
IS 77	South	24-95	4	La. 1	5	54.23	1377.4	4.4	112	0.3	8	-1.2	-30	0.4	10	0.4	10	0.1	3	3.7	94
IS 77	South	24-95	4	La. 1	6	66.13	1679.7	4.2	107	0.2	5	1	25	1	25	0.3	8	0.9	23	3.1	79
IS 77	South	24-95	4	La. 1	7	78.09	1983.5	4.3	109	0.3	8	1	25	1	25	0.2	5	1	25	3.2	81
IS 77	South	24-95	4	La. 1	8	90.19	2290.8	4.2	107	0.2	5	0.5	13	0.5	13	0.3	8	0.5	13	3.4	86
IS 77	South	24-95	4	La. 1	9	102.31	2598.7	4.3	109	0.3	8	-1.2	-30	0.6	15	0	0	-0.6	-15	3.4	86
IS 77	South	24-95	4	La. 1	10	114.07	2897.4	4.2	107	0.2	5	-1.2	-30	0.5	13	0.4	10	-0.4	-10	3.4	86
IS 77	South	24-95	4	La. 1	11	126.46	3212.1	4.4	112	0.4	10	-1	-25	0.3	8	0.1	3	-0.2	-5	3.7	94
IS 77	South	25-25	2	La. 1	1	5.51	140.0	3.9	99	-0.1	-3	1.1	28	0.3	8	-0.1	-3	0.3	8	3.1	79
IS 77	South	25-25	2	La. 1	2	17.69	449.3	3.5	89	-0.5	-13	1.7	43	0.7	18	-0.6	-15	0.3	8	2.8	71
IS 77	South	25-25	2	La. 1	3	29.84	757.9	3.7	94	-0.3	-8	1.5	38	0.3	8	0	0	0.3	8	3	76
IS 77	South	25-25	2	La. 1	4	41.68	1058.7	3.7	94	-0.3	-8	1.8	46	0.3	8	0	0	0.3	8	3	76
IS 77	South	25-25	2	La. 1	5	53.67	1363.2	4.1	104	0.1	3	0.7	18	0.5	13	0.3	8	0.4	10	3.3	84
IS 77	South	25-25	2	La. 1	6	66.15	1680.2	4.2	107	0.2	5	1.7	43	0.1	3	0.1	3	0.1	3	3.5	89
IS 77	South	25-25	2	La. 1	7	78.47	1993.1	4	102	0	0	1.9	48	0.7	18	0.6	15	0.4	10	3.1	79
IS 77	South	25-25	2	La. 1	8	90.19	2290.8	3.8	97	-0.2	-5	2.5	64	0.6	15	0.2	5	0.5	13	2.9	74
IS 77	South	25-25	2	La. 1	9	102.22	2596.4	3.9	99	-0.1	-3	2.4	61	0.4	10	-0.2	-5	0.4	10	3.1	79
IS 77	South	25-25	2	La. 1	10	114.04	2896.6	3.8	97	-0.2	-5	2.1	53	0.4	10	0.4	10	0.1	3	3.1	79
IS 77	South	25-25	2	La. 1	11	125.45	3186.4	4.3	109	0.2	5	2.4	61	0.6	15	-0.3	-8	0.5	13	3.4	86
IS 77	South	25-40	1	La. 1	1	5.45	138.4	4	102	0	0	0.7	18	0.2	5	-0.2	-5	0	0	3.3	84
IS 77	South	25-40	1	La. 1	2	17.91	454.9	3.6	91	-0.4	-10	1.4	36	0.6	15	-0.6	-15	0.1	3	2.9	74
IS 77	South	25-40	1	La. 1	3	30.3	769.6	4	102	0	0	1.7	43	0.1	3	0.1	3	0.1	3	3.3	84
IS 77	South	25-40	1	La. 1	4	42.1	1069.3	3.9	99	-0.1	-3	1.8	46	0.2	5	-0.1	-3	0.2	5	3.2	81
IS 77	South	25-40	1	La. 1	5	54.5	1384.3	4.1	104	0.1	3	2	51	0.8	20	0.1	3	0.7	18	3.1	79
IS 77	South	25-40	1	La. 1	6	66.34	1685.0	3.9	99	-0.1	-3	2	51	0.4	10	0.2	5	0.4	10	3.1	79
IS 77	South	25-40	1	La. 1	7	78.33	1989.6	4	102	0	0	2	51	0.3	8	0.1	3	0.3	8	3.2	81
IS 77	South	25-40	1	La. 1	8	90.4	2296.2	3.9	99	-0.1	-3	2	51	0.4	10	0.4	10	0.2	5	3.2	81
IS 77	South	25-40	1	La. 1	9	102.4	2601.0	4.1	104	0.1	3	2	51	0.1	3	-0.1	-3	0	0	3.4	86
IS 77	South	25-40	1	La. 1	10	114.33	2904.0	4	102	0	0	1.9	48	0.5	13	0.5	13	0.1	3	3.4	86
IS 77	South	25-40	1	La. 1	11	126.25	3206.8	4.2	107	0.2	5	2	51	0.4	10	0.4	10	0	0	3.6	91
IS 77	South	25-40	1	La. 1	12	138.28	3512.3	4.1	104	0	0	1.3	33	0.4	10	0.3	8	-0.3	-8	3.3	84

B4: WAS/NOB-77 NB control section MITScan data collected by ODOT November 10, 2015

Highway	Direction	Station Number	Joint	Lane	Bar Number	X-Position		Depth		Depth Deviation		Side Shift		Misalignment		Horizontal Misalignment		Vertical Misalignment		Minimal Cover	
HW	Dir	SNo	Jo	La	BNo	xs		zs		dz		dy		s		sh		sv		c	
-	-	-	-	-	-	(in)	(mm)	(in)	(mm)	(in)	(mm)	(in)	(mm)	(in)	(mm)	(in)	(mm)	(in)	(mm)	(in)	(mm)
IS 77	North	824-0	1	La. 1	1	7.32	185.9	4.3	109	0.3	8	1.2	30	0.8	20	-0.2	-5	0.7	18	3.3	84
IS 77	North	824-0	1	La. 1	2	19.38	492.3	4.1	104	0.1	3	1.4	36	0.5	13	0.4	10	0.3	8	3.3	84
IS 77	North	824-0	1	La. 1	3	31.24	793.5	4.3	109	0.3	8	1.6	41	0.6	15	0.5	13	0.4	10	3.5	89
IS 77	North	824-0	1	La. 1	4	43.28	1099.3	4.3	109	0.3	8	1.6	41	0.9	23	0.8	20	0.2	5	3.6	91
IS 77	North	824-0	1	La. 1	5	55.21	1402.3	4.3	109	0.3	8	1.6	41	0.6	15	0.6	15	0.2	5	3.6	91
IS 77	North	824-0	1	La. 1	6	67.21	1707.1	4.3	109	0.2	5	1.8	46	0.2	5	0.1	3	0.2	5	3.6	91
IS 77	North	824-0	1	La. 1	7	79.46	2018.3	4.4	112	0.4	10	1.9	48	0.5	13	0.4	10	0.4	10	3.6	91
IS 77	North	824-0	1	La. 1	8	91.54	2325.1	4.2	107	0.2	5	2	51	0.7	18	0.7	18	0.1	3	3.5	89
IS 77	North	824-0	1	La. 1	9	103.58	2630.9	4.2	107	0.2	5	2.2	56	0.5	13	0.4	10	0.3	8	3.4	86
IS 77	North	824-0	1	La. 1	10	115.26	2927.6	4.2	107	0.1	3	2.2	56	0.8	20	0.7	18	0.3	8	3.4	86
IS 77	North	824-0	1	La. 1	11	127.21	3231.1	4.3	109	0.3	8	1.9	48	0.7	18	0.7	18	0	0	3.7	94
IS 77	North	824-0	1	La. 1	12	139.52	3543.8	4.6	117	0.6	15	1.3	33	0.6	15	0.5	13	-0.1	-3	3.9	99
IS 77	North	824-15	2	La. 1	1	8.52	216.4	4.1	104	0.1	3	-0.5	-13	0.2	5	-0.2	-5	0	0	3.5	89
IS 77	North	824-15	2	La. 1	2	20.99	533.1	4.1	104	0.1	3	-1.4	-36	0.6	15	0	0	-0.6	-15	3.2	81
IS 77	North	824-15	2	La. 1	3	32.64	829.1	4.1	104	0.1	3	-1.6	-41	0.6	15	0	0	-0.6	-15	3.1	79
IS 77	North	824-15	2	La. 1	4	44.75	1136.7	4.1	104	0.1	3	-1.6	-41	1	25	0.7	18	-0.7	-18	3.2	81
IS 77	North	824-15	2	La. 1	5	56.76	1441.7	4.2	107	0.2	5	-1.7	-43	1.2	30	0.6	15	-1	-25	3.1	79
IS 77	North	824-15	2	La. 1	6	68.67	1744.2	4.2	107	0.1	3	-1.6	-41	0.8	20	0.2	5	-0.8	-20	3.1	79
IS 77	North	824-15	2	La. 1	7	80.83	2053.1	4.2	107	0.2	5	-1.7	-43	0.8	20	0.6	15	-0.5	-13	3.3	84
IS 77	North	824-15	2	La. 1	8	92.85	2358.4	4.1	104	0.1	3	-1.8	-46	1.2	30	0.7	18	-0.9	-23	3.1	79
IS 77	North	824-15	2	La. 1	9	104.83	2662.7	4.1	104	0.1	3	-1.6	-41	0.7	18	0	0	-0.7	-18	3.1	79
IS 77	North	824-15	2	La. 1	10	116.62	2962.1	4.1	104	0.1	3	-1.4	-36	0.8	20	0.3	8	-0.7	-18	3.1	79
IS 77	North	824-15	2	La. 1	11	128.53	3264.7	4.2	107	0.2	5	-0.8	-20	0.6	15	0	0	-0.5	-13	3.3	84
IS 77	North	824-15	2	La. 1	12	141.01	3581.7	4.3	109	0.3	8	0.6	15	0.3	8	0.2	5	-0.2	-5	3.6	91
IS 77	North	824-30	3	La. 1	1	3.57	90.7	4	102	0	0	0.5	13	0.1	3	-0.1	-3	0	0	3.4	86
IS 77	North	824-30	3	La. 1	2	15.42	391.7	4	102	0	0	1.5	38	0.5	13	0.5	13	0.1	3	3.3	84
IS 77	North	824-30	3	La. 1	3	27.41	696.2	4.2	107	0.2	5	1.6	41	0.3	8	0.2	5	0.1	3	3.5	89
IS 77	North	824-30	3	La. 1	4	39.55	1004.6	4.2	107	0.2	5	1.7	43	0.6	15	0.6	15	0.2	5	3.5	89
IS 77	North	824-30	3	La. 1	5	51.42	1306.1	4.2	107	0.1	3	1.4	36	0.6	15	0.4	10	-0.5	-13	3.3	84
IS 77	North	824-30	3	La. 1	6	63.22	1605.8	4.2	107	0.2	5	1.7	43	0.3	8	0.3	8	-0.1	-3	3.5	89
IS 77	North	824-30	3	La. 1	7	75.73	1923.5	4.5	114	0.5	13	1.5	38	0.4	10	0.4	10	0.1	3	3.8	97
IS 77	North	824-30	3	La. 1	8	87.84	2231.1	4.3	109	0.2	5	2	51	0.7	18	0.6	15	-0.3	-8	3.5	89
IS 77	North	824-30	3	La. 1	9	99.7	2532.4	4.3	109	0.3	8	2.1	53	0.1	3	0	0	-0.1	-3	3.7	94
IS 77	North	824-30	3	La. 1	10	111.45	2830.8	4.4	112	0.3	8	1.8	46	0.9	23	0.9	23	-0.2	-5	3.7	94
IS 77	North	824-30	3	La. 1	11	124.11	3152.4	4.3	109	0.2	5	2.2	56	0.1	3	0.1	3	0	0	3.6	91
IS 77	North	824-30	3	La. 1	12	136.06	3455.9	4.2	107	0.2	5	2.4	61	0.1	3	0	0	-0.1	-3	3.5	89
IS 77	North	824-45	4	La. 1	1	2.31	58.7	4.2	107	0.2	5	2.8	71	2.1	53	0.3	8	2.1	53	2.5	64
IS 77	North	824-45	4	La. 1	3	14.31	363.5	3.9	99	-0.1	-3	-2	-51	0.7	18	0.2	5	-0.7	-18	2.9	74
IS 77	North	824-45	4	La. 1	4	26.13	663.7	4	102	0	0	-1.5	-38	0.4	10	0.3	8	-0.2	-5	3.2	81
IS 77	North	824-45	4	La. 1	5	38.13	968.5	4	102	0	0	-1.4	-36	0.8	20	0.8	20	-0.3	-8	3.2	81

IS 77	North	824-45	4	La. 1	6	50.04	1271.0	4	102	0	0	-1.7	-43	1.1	28	0.7	18	-0.8	-20	3	76
IS 77	North	824-45	4	La. 1	7	61.95	1573.5	4	102	0	0	-0.8	-20	0.3	8	0.2	5	-0.2	-5	3.3	84
IS 77	North	824-45	4	La. 1	8	74.1	1882.1	4.1	104	0.1	3	-1.1	-28	0.5	13	-0.1	-3	-0.5	-13	3.3	84
IS 77	North	824-45	4	La. 1	9	86.15	2188.2	4	102	0	0	0.8	20	1.1	28	1.1	28	-0.1	-3	3.4	86
IS 77	North	824-45	4	La. 1	10	98.13	2492.5	4.2	107	0.2	5	1.7	43	0.3	8	0.3	8	0.2	5	3.4	86
IS 77	North	824-45	4	La. 1	11	110.02	2794.5	4.4	112	0.3	8	1.7	43	0.9	23	0.9	23	-0.2	-5	3.6	91
IS 77	North	824-45	4	La. 1	12	122.9	3121.7	4.3	109	0.3	8	1.4	36	1	25	1	25	0	0	3.6	91
IS 77	North	824-45	4	La. 1	13	134.46	3415.3	4.4	112	0.4	10	1.6	41	0.5	13	0.5	13	0	0	3.8	97
IS 77	North	824-60	5	La. 1	1	10.19	258.8	4	102	0	0	0.3	8	0.6	15	0.6	15	-0.1	-3	3.3	84
IS 77	North	824-60	5	La. 1	2	22.64	575.1	4.2	107	0.1	3	-0.1	-3	0.5	13	0.5	13	-0.2	-5	3.4	86
IS 77	North	824-60	5	La. 1	3	34.73	882.1	4.2	107	0.1	3	0.9	23	1	25	1	25	0.3	8	3.4	86
IS 77	North	824-60	5	La. 1	4	46.49	1180.8	4.2	107	0.2	5	0.5	13	0.6	15	0.6	15	-0.1	-3	3.5	89
IS 77	North	824-60	5	La. 1	5	58.39	1483.1	4.5	114	0.5	13	0.1	3	0.3	8	-0.2	-5	-0.2	-5	3.7	94
IS 77	North	824-60	5	La. 1	6	71.2	1808.5	4.4	112	0.4	10	0.9	23	0.5	13	0.5	13	0.1	3	3.8	97
IS 77	North	824-60	5	La. 1	7	82.92	2106.2	4.1	104	0.1	3	1.7	43	0.9	23	0.8	20	0.2	5	3.3	84
IS 77	North	824-60	5	La. 1	8	94.8	2407.9	4.1	104	0.1	3	2	51	0.5	13	0.3	8	0.4	10	3.3	84
IS 77	North	824-60	5	La. 1	9	106.58	2707.1	4	102	0	0	2.2	56	0.8	20	0.7	18	0.4	10	3.2	81
IS 77	North	824-60	5	La. 1	10	118.34	3005.8	4.2	107	0.2	5	2.1	53	0.9	23	0.9	23	0.1	3	3.6	91
IS 77	North	824-60	5	La. 1	11	131.01	3327.7	4.4	112	0.4	10	0.8	20	1	25	0.8	20	-0.5	-13	3.6	91
IS 77	North	824-75	6	La. 1	1	9.59	243.6	4.3	109	0.3	8	0.1	3	0.5	13	-0.2	-5	-0.4	-10	3.4	86
IS 77	North	824-75	6	La. 1	2	21.94	557.3	4.5	114	0.5	13	0	0	0.4	10	0.2	5	-0.3	-8	3.8	97
IS 77	North	824-75	6	La. 1	3	33.91	861.3	4.7	119	0.6	15	-0.1	-3	0.8	20	0.7	18	-0.3	-8	3.8	97
IS 77	North	824-75	6	La. 1	4	45.8	1163.3	4.7	119	0.7	18	-0.2	-5	1	25	0.5	13	-0.9	-23	3.6	91
IS 77	North	824-75	6	La. 1	5	57.83	1468.9	4.7	119	0.7	18	-0.2	-5	0.6	15	0	0	-0.6	-15	3.8	97
IS 77	North	824-75	6	La. 1	6	70.04	1779.0	4.8	122	0.8	20	-0.1	-3	0.5	13	0.5	13	-0.2	-5	4.1	104
IS 77	North	824-75	6	La. 1	7	82.05	2084.1	4.8	122	0.7	18	-0.1	-3	1	25	0.7	18	-0.7	-18	3.8	97
IS 77	North	824-75	6	La. 1	8	94.05	2388.9	4.8	122	0.8	20	0.3	8	0.6	15	-0.2	-5	-0.6	-15	3.9	99
IS 77	North	824-75	6	La. 1	9	105.87	2689.1	4.7	119	0.6	15	0.5	13	0.9	23	0.8	20	-0.4	-10	3.8	97
IS 77	North	824-75	6	La. 1	10	118.13	3000.5	4.8	122	0.8	20	0.4	10	0.8	20	0.5	13	-0.6	-15	3.9	99
IS 77	North	824-75	6	La. 1	11	130.4	3312.2	4.8	122	0.8	20	0.8	20	0.7	18	0.6	15	-0.4	-10	4	102
IS 77	North	824-90	7	La. 1	1	1.1	27.9	3.9	99	-0.1	-3	0.6	15	0.4	10	0.1	3	0.4	10	3.1	79
IS 77	North	824-90	7	La. 1	3	13.38	339.9	3.7	94	-0.3	-8	1.3	33	0.1	3	0.1	3	0.1	3	3	76
IS 77	North	824-90	7	La. 1	4	25.37	644.4	3.9	99	-0.2	-5	1.1	28	0.3	8	0.2	5	0.2	5	3.1	79
IS 77	North	824-90	7	La. 1	5	37.51	952.8	4	102	0	0	1.5	38	0.8	20	0.7	18	0.5	13	3.1	79
IS 77	North	824-90	7	La. 1	6	49.41	1255.0	4	102	0	0	0.6	15	0.4	10	0.4	10	-0.2	-5	3.3	84
IS 77	North	824-90	7	La. 1	7	61.3	1557.0	4	102	0	0	0.9	23	0.2	5	0.1	3	0.2	5	3.3	84
IS 77	North	824-90	7	La. 1	8	73.35	1863.1	4.1	104	0.1	3	1.4	36	0.6	15	0.3	8	0.5	13	3.3	84
IS 77	North	824-90	7	La. 1	9	85.41	2169.4	4.1	104	0	0	0.9	23	0.6	15	0.6	15	0	0	3.4	86
IS 77	North	824-90	7	La. 1	10	97.4	2474.0	4.1	104	0.1	3	1.7	43	0.4	10	0	0	0.4	10	3.3	84
IS 77	North	824-90	7	La. 1	11	108.96	2767.6	4	102	0	0	1.8	46	0.4	10	0.3	8	0.2	5	3.3	84
IS 77	North	824-90	7	La. 1	12	121.06	3074.9	4.5	114	0.5	13	1.4	36	0.6	15	0.6	15	-0.1	-3	3.8	97
IS 77	North	824-90	7	La. 1	13	133.82	3399.0	4.5	114	0.5	13	0.7	18	0.5	13	0.4	10	-0.2	-5	3.8	97
IS 77	North	825-5	8	La. 1	1	8.45	214.6	4.2	107	0.2	5	-1.9	-48	0.7	18	-0.3	-8	-0.6	-15	3.3	84
IS 77	North	825-5	8	La. 1	2	20.48	520.2	4.1	104	0.1	3	0.7	18	0.3	8	0.3	8	-0.1	-3	3.4	86
IS 77	North	825-5	8	La. 1	3	32.3	820.4	4.4	112	0.3	8	0.8	20	0.3	8	0.3	8	0.1	3	3.7	94
IS 77	North	825-5	8	La. 1	4	44.31	1125.5	4.4	112	0.4	10	0.8	20	0.8	20	0.8	20	0.1	3	3.7	94
IS 77	North	825-5	8	La. 1	5	56.35	1431.3	4.5	114	0.4	10	0.4	10	0.5	13	0.5	13	-0.1	-3	3.8	97
IS 77	North	825-5	8	La. 1	6	68.46	1738.9	4.5	114	0.4	10	0.4	10	0.1	3	0	0	0	0	3.8	97
IS 77	North	825-5	8	La. 1	7	80.65	2048.5	4.6	117	0.6	15	0.1	3	0.2	5	0.2	5	-0.2	-5	3.9	99

IS 77	North	825-5	8	La. 1	8	92.68	2354.1	4.5	114	0.5	13	0.7	18	0.5	13	0.5	13	-0.2	-5	3.8	97
IS 77	North	825-5	8	La. 1	9	104.71	2659.6	4.4	112	0.4	10	0.9	23	0.3	8	-0.2	-5	-0.3	-8	3.7	94
IS 77	North	825-5	8	La. 1	10	116.42	2957.1	4.5	114	0.5	13	1.1	28	0.6	15	0.6	15	-0.1	-3	3.8	97
IS 77	North	825-5	8	La. 1	11	129.01	3276.9	4.6	117	0.6	15	0.9	23	0.5	13	0.5	13	-0.2	-5	3.9	99
IS 77	North	825-20	9	La. 1	1	6.5	165.1	4	102	0	0	-1.8	-46	0.7	18	0.2	5	-0.6	-15	3	76
IS 77	North	825-20	9	La. 1	2	18.61	472.7	3.8	97	-0.2	-5	1.7	43	0.4	10	0.4	10	0.2	5	3.1	79
IS 77	North	825-20	9	La. 1	3	30.46	773.7	3.9	99	-0.1	-3	2	51	0.6	15	0.4	10	0.4	10	3.1	79
IS 77	North	825-20	9	La. 1	4	42.65	1083.3	4	102	-0.1	-3	2.1	53	1	25	0.9	23	0.3	8	3.2	81
IS 77	North	825-20	9	La. 1	5	54.67	1388.6	3.9	99	-0.1	-3	1.9	48	0.5	13	0.4	10	0.1	3	3.2	81
IS 77	North	825-20	9	La. 1	6	66.51	1689.4	3.9	99	-0.1	-3	2	51	0.3	8	0.2	5	0.3	8	3.2	81
IS 77	North	825-20	9	La. 1	7	78.65	1997.7	4.1	104	0.1	3	2.2	56	0.5	13	0.3	8	0.4	10	3.2	81
IS 77	North	825-20	9	La. 1	8	90.8	2306.3	4	102	0	0	2.2	56	0.6	15	0.6	15	0.3	8	3.3	84
IS 77	North	825-20	9	La. 1	9	102.77	2610.4	4	102	0	0	2.3	58	0.4	10	0.1	3	0.3	8	3.2	81
IS 77	North	825-20	9	La. 1	10	114.58	2910.3	4	102	0	0	2.6	66	0.7	18	0.6	15	0.4	10	3.2	81
IS 77	North	825-20	9	La. 1	11	126.42	3211.1	4.3	109	0.3	8	2.6	66	0.6	15	0.5	13	0.2	5	3.5	89
IS 77	North	825-20	9	La. 1	12	139.17	3534.9	4.6	117	0.6	15	2.8	71	0.8	20	0.7	18	0.1	3	3.9	99
IS 77	North	825-35	10	La. 1	1	4.78	121.4	3.9	99	-0.1	-3	-1	-25	0.5	13	0.2	5	-0.5	-13	3	76
IS 77	North	825-35	10	La. 1	2	16.57	420.9	3.7	94	-0.4	-10	1.9	48	0.5	13	0.1	3	0.5	13	2.8	71
IS 77	North	825-35	10	La. 1	3	28.4	721.4	3.8	97	-0.2	-5	1.9	48	0.7	18	0.3	8	0.7	18	2.9	74
IS 77	North	825-35	10	La. 1	4	40.42	1026.7	3.9	99	-0.1	-3	2	51	0.8	20	0.7	18	0.5	13	3	76
IS 77	North	825-35	10	La. 1	5	52.41	1331.2	3.9	99	-0.1	-3	1.8	46	0.5	13	0.5	13	0.2	5	3.2	81
IS 77	North	825-35	10	La. 1	6	64.38	1635.3	3.9	99	-0.1	-3	1.7	43	0.4	10	0.2	5	0.3	8	3.1	79
IS 77	North	825-35	10	La. 1	7	76.53	1943.9	4.1	104	0.1	3	1.8	46	0.6	15	0.2	5	0.6	15	3.2	81
IS 77	North	825-35	10	La. 1	8	88.46	2246.9	4	102	0	0	1.5	38	0.4	10	0.3	8	0.3	8	3.2	81
IS 77	North	825-35	10	La. 1	9	100.16	2544.1	4.2	107	0.2	5	1	25	0.1	3	0	0	0.1	3	3.6	91
IS 77	North	825-35	10	La. 1	10	112.11	2847.6	4.5	114	0.4	10	1	25	0.2	5	0.2	5	0	0	3.8	97
IS 77	North	825-35	10	La. 1	11	125.48	3187.2	4.2	107	0.2	5	1.6	41	0.9	23	0.8	20	0.3	8	3.5	89
IS 77	North	825-35	10	La. 1	12	136.94	3478.3	3.8	97	-0.2	-5	1.8	46	0.6	15	0.5	13	0.4	10	3	76
IS 77	North	825-50	11	La. 1	1	0.68	17.3	3.8	97	-0.2	-5	1.2	30	0.5	13	-0.1	-3	0.5	13	3	76
IS 77	North	825-50	11	La. 1	3	12.89	327.4	3.8	97	-0.2	-5	1.6	41	0.3	8	0.3	8	0	0	3.1	79
IS 77	North	825-50	11	La. 1	4	24.83	630.7	4.1	104	0	0	1.5	38	0.3	8	0.1	3	0.3	8	3.3	84
IS 77	North	825-50	11	La. 1	5	36.89	937.0	4	102	0	0	1.4	36	0.7	18	0.6	15	0	0	3.4	86
IS 77	North	825-50	11	La. 1	6	48.98	1244.1	4.1	104	0.1	3	1.4	36	0.4	10	0.3	8	-0.2	-5	3.4	86
IS 77	North	825-50	11	La. 1	7	61	1549.4	4.1	104	0.1	3	1.4	36	0	0	0	0	0	0	3.5	89
IS 77	North	825-50	11	La. 1	8	73.1	1856.7	4.2	107	0.2	5	1.6	41	0.2	5	0.2	5	0	0	3.6	91
IS 77	North	825-50	11	La. 1	9	85.14	2162.6	4.1	104	0.1	3	1.5	38	1.1	28	1	25	-0.4	-10	3.3	84
IS 77	North	825-50	11	La. 1	10	97.21	2469.1	4.2	107	0.2	5	1.7	43	0.1	3	0.1	3	-0.1	-3	3.5	89
IS 77	North	825-50	11	La. 1	11	108.77	2762.8	4.3	109	0.2	5	1.1	28	0.8	20	0.7	18	-0.3	-8	3.5	89
IS 77	North	825-50	11	La. 1	12	121.42	3084.1	4.3	109	0.3	8	1.4	36	0.3	8	0.3	8	-0.1	-3	3.6	91
IS 77	North	825-50	11	La. 1	13	133.37	3387.6	4.3	109	0.3	8	1.5	38	0.4	10	0.4	10	-0.1	-3	3.6	91
IS 77	North	825-65	12	La. 1	1	11.41	289.8	4.2	107	0.2	5	0	0	0.3	8	-0.1	-3	-0.3	-8	3.5	89
IS 77	North	825-65	12	La. 1	2	23.47	596.1	4.5	114	0.4	10	0	0	0	0	0	0	0	0	3.8	97
IS 77	North	825-65	12	La. 1	3	35.52	902.2	4.5	114	0.5	13	0.2	5	0.5	13	0.5	13	0	0	3.9	99
IS 77	North	825-65	12	La. 1	4	47.49	1206.2	4.5	114	0.5	13	0	0	0.5	13	0.2	5	-0.4	-10	3.7	94
IS 77	North	825-65	12	La. 1	5	59.47	1510.5	4.6	117	0.5	13	0	0	0.3	8	-0.2	-5	-0.2	-5	3.8	97
IS 77	North	825-65	12	La. 1	6	71.65	1819.9	4.7	119	0.6	15	-0.1	-3	0.3	8	0.3	8	-0.2	-5	3.9	99
IS 77	North	825-65	12	La. 1	7	83.66	2125.0	4.6	117	0.6	15	0	0	0.8	20	0.6	15	-0.5	-13	3.7	94
IS 77	North	825-65	12	La. 1	8	95.69	2430.5	4.6	117	0.6	15	0.1	3	0.4	10	0	0	-0.4	-10	3.8	97
IS 77	North	825-65	12	La. 1	9	107.48	2730.0	4.5	114	0.5	13	0.1	3	0.6	15	0.5	13	-0.3	-8	3.7	94

IS 77	North	825-65	12	La. 1	10	119.83	3043.7	4.6	117	0.6	15	0	0	0.7	18	0.6	15	-0.3	-8	3.8	97
IS 77	North	825-65	12	La. 1	12	132.52	3366.0	4.6	117	0.5	13	0.2	5	0.5	13	0.4	10	-0.3	-8	3.8	97
IS 77	North	825-80	13	La. 1	1	3.02	76.7	4.2	107	0.2	5	-2	-51	0.8	20	-0.3	-8	-0.8	-20	3.2	81
IS 77	North	825-80	13	La. 1	2	15.01	381.3	4.3	109	0.2	5	-0.5	-13	0.7	18	-0.1	-3	-0.7	-18	3.3	84
IS 77	North	825-80	13	La. 1	3	27.08	687.8	4.4	112	0.4	10	0.1	3	0.3	8	-0.1	-3	-0.3	-8	3.6	91
IS 77	North	825-80	13	La. 1	4	39.29	998.0	4.4	112	0.4	10	-0.2	-5	0.7	18	0.6	15	-0.4	-10	3.6	91
IS 77	North	825-80	13	La. 1	5	51.32	1303.5	4.5	114	0.5	13	0	0	0.6	15	0.3	8	-0.4	-10	3.7	94
IS 77	North	825-80	13	La. 1	6	63.32	1608.3	4.6	117	0.6	15	-0.2	-5	0.6	15	-0.1	-3	-0.6	-15	3.6	91
IS 77	North	825-80	13	La. 1	7	75.44	1916.2	4.7	119	0.7	18	-0.2	-5	0.5	13	0.2	5	-0.5	-13	3.9	99
IS 77	North	825-80	13	La. 1	8	87.45	2221.2	4.6	117	0.6	15	-0.2	-5	0.7	18	0.4	10	-0.6	-15	3.6	91
IS 77	North	825-80	13	La. 1	9	99.46	2526.3	4.7	119	0.7	18	0.2	5	0.5	13	-0.1	-3	-0.5	-13	3.8	97
IS 77	North	825-80	13	La. 1	10	111.18	2824.0	4.6	117	0.6	15	0.4	10	0.7	18	0.5	13	-0.5	-13	3.7	94
IS 77	North	825-80	13	La. 1	11	123.52	3137.4	4.7	119	0.6	15	0.2	5	0.7	18	0.6	15	-0.3	-8	3.9	99
IS 77	North	825-80	13	La. 1	12	135.74	3447.8	4.4	112	0.4	10	0.7	18	0.5	13	0.3	8	-0.4	-10	3.6	91

B5: ASD-30 EB distressed section MITScan data collected by ODOT May 11, 2017

Highway	Direction	Station Number	Joint	Lane	Bar Number	X-Position		Depth		Depth Deviation		Side Shift		Misalignment		Horizontal Misalignment		Vertical Misalignment		Minimal Cover	
HW	Dir	SNo	Jo	La	BNo	xs		zs		dz		dy		s		sh		sv		c	
-	-	-	-	-	-	(in)	(mm)	(in)	(mm)	(in)	(mm)	(in)	(mm)	(in)	(mm)	(in)	(mm)	(in)	(mm)	(in)	(mm)
US 30	East	0-250	1	La. 2	01	7.50	190.5	4.0	102	-0.5	-12	-1.1	-29	0.4	10	0.2	5	-0.3	-8	3.1	79
US 30	East	0-250	1	La. 2	02	19.91	505.7	4.1	103	-0.4	-11	-1.5	-39	0.6	14	0.3	6	-0.5	-13	3.1	78
US 30	East	0-250	1	La. 2	03	31.94	811.2	4.1	103	-0.4	-11	-1.3	-32	0.5	12	0.3	8	-0.4	-9	3.1	80
US 30	East	0-250	1	La. 2	04	43.93	1115.7	4.0	103	-0.5	-12	-1.2	-30	0.5	12	0.2	5	-0.4	-11	3.1	78
US 30	East	0-250	1	La. 2	05	55.86	1418.9	4.0	101	-0.5	-13	-0.6	-16	0.3	7	0.2	4	-0.2	-6	3.1	79
US 30	East	0-250	1	La. 2	06	67.87	1723.9	3.9	99	-0.6	-15	-0.6	-15	0.3	9	0.2	4	-0.3	-8	3.0	77
US 30	East	0-250	1	La. 2	07	79.86	2028.4	3.9	98	-0.6	-16	0.1	4	0.2	4	0.2	4	0.0	0	3.1	79
US 30	East	0-250	1	La. 2	08	91.85	2333.1	3.9	99	-0.6	-16	-0.1	-2	0.2	5	0.1	2	-0.2	-4	3.1	78
US 30	East	0-250	1	La. 2	09	103.94	2640.2	4.4	112	-0.1	-3	2.3	59	1.4	36	0.2	5	1.4	36	2.9	75
US 30	East	0-250	1	La. 2	10	115.89	2943.6	3.7	93	-0.8	-21	0.5	12	0.1	4	0.0	-1	0.1	4	2.9	72
US 30	East	0-250	1	La. 2	11	128.50	3263.8	4.1	105	-0.4	-10	-0.3	-7	1.4	34	1.2	31	-0.6	-14	3.1	79
US 30	East	0-255	2	La. 2	01	9.97	253.3	3.9	98	-0.7	-17	1.3	34	0.5	13	0.0	0	0.5	13	2.9	72
US 30	East	0-255	2	La. 2	02	22.43	569.7	3.9	100	-0.6	-15	1.4	35	0.5	13	0.1	1	0.5	13	2.9	74
US 30	East	0-255	2	La. 2	03	34.39	873.5	3.9	99	-0.6	-15	1.2	31	0.4	9	0.0	1	0.4	9	3.0	76
US 30	East	0-255	2	La. 2	04	46.38	1178.1	3.9	100	-0.6	-14	1.3	33	0.5	12	0.1	2	0.5	11	3.0	75
US 30	East	0-255	2	La. 2	05	58.44	1484.4	3.9	99	-0.6	-16	1.2	30	0.4	10	0.0	1	0.4	10	2.9	75
US 30	East	0-255	2	La. 2	06	70.41	1788.3	3.8	97	-0.7	-17	1.2	31	0.5	13	0.1	4	0.5	13	2.8	72
US 30	East	0-255	2	La. 2	07	82.36	2091.9	3.8	97	-0.7	-18	1.0	24	0.3	9	0.1	2	0.3	9	2.9	73
US 30	East	0-255	2	La. 2	08	94.35	2396.6	4.0	102	-0.5	-13	0.4	10	0.2	6	0.1	3	0.2	5	3.2	81

US 30	East	0-255	2	La. 2	09	106.43	2703.2	3.8	96	-0.7	-18	0.7	17	0.2	4	0.0	0	0.2	4	2.9	75
US 30	East	0-255	2	La. 2	10	118.09	2999.6	3.8	97	-0.7	-17	0.2	5	0.1	2	0.1	2	0.0	0	3.1	78
US 30	East	0-260	3	La. 2	01	4.49	114.0	4.0	102	-0.5	-13	1.7	43	0.7	19	0.2	4	0.7	18	2.9	74
US 30	East	0-260	3	La. 2	02	16.76	425.6	4.1	103	-0.5	-11	1.7	42	0.6	16	0.1	3	0.6	16	3.0	76
US 30	East	0-260	3	La. 2	03	28.75	730.2	4.1	104	-0.4	-10	1.8	46	0.7	18	0.3	7	0.7	17	3.0	77
US 30	East	0-260	3	La. 2	04	40.77	1035.6	4.1	105	-0.4	-10	1.6	42	0.6	15	0.1	4	0.6	15	3.1	78
US 30	East	0-260	3	La. 2	05	52.79	1340.9	4.1	104	-0.4	-11	1.8	46	0.7	18	0.1	4	0.7	17	3.0	76
US 30	East	0-260	3	La. 2	06	64.85	1647.2	4.0	102	-0.5	-13	1.7	42	0.6	15	0.1	3	0.6	14	3.0	75
US 30	East	0-260	3	La. 2	07	76.81	1951.0	3.9	100	-0.6	-14	1.8	45	0.7	19	0.2	5	0.7	18	2.8	72
US 30	East	0-260	3	La. 2	08	88.79	2255.3	3.9	100	-0.6	-15	1.5	39	0.6	15	0.1	2	0.6	14	2.9	74
US 30	East	0-260	3	La. 2	09	100.82	2560.8	3.9	98	-0.6	-16	1.5	39	0.5	14	0.1	3	0.5	13	2.9	73
US 30	East	0-260	3	La. 2	10	112.76	2864.2	3.9	100	-0.6	-15	1.3	33	0.4	11	0.0	1	0.4	11	3.0	75
US 30	East	0-260	3	La. 2	11	124.54	3163.2	4.1	104	-0.4	-11	1.5	38	0.5	13	0.1	2	0.5	13	3.1	78
US 30	East	0-265	4	La. 2	01	5.83	148.2	4.2	106	-0.3	-8	2.2	55	0.8	20	0.2	6	0.7	19	3.1	78
US 30	East	0-265	4	La. 2	02	18.23	463.1	4.2	107	-0.3	-8	2.0	51	0.8	19	0.3	7	0.7	18	3.1	79
US 30	East	0-265	4	La. 2	03	30.33	770.3	4.2	107	-0.3	-8	2.1	53	0.7	18	0.0	1	0.7	18	3.1	78
US 30	East	0-265	4	La. 2	04	42.31	1074.7	4.2	107	-0.3	-7	2.0	51	0.7	17	-0.1	-3	0.7	17	3.1	80
US 30	East	0-265	4	La. 2	05	54.34	1380.3	4.2	106	-0.3	-8	2.1	54	0.7	19	-0.2	-4	0.7	18	3.1	78
US 30	East	0-265	4	La. 2	06	66.37	1685.7	4.1	104	-0.4	-10	1.9	49	0.6	16	-0.2	-5	0.6	15	3.1	78
US 30	East	0-265	4	La. 2	07	78.41	1991.5	4.1	103	-0.5	-11	2.0	52	0.7	17	-0.1	-2	0.7	17	3.0	76
US 30	East	0-265	4	La. 2	08	90.40	2296.3	4.0	103	-0.5	-12	1.8	45	0.6	14	-0.1	-3	0.5	14	3.0	77
US 30	East	0-265	4	La. 2	09	102.47	2602.7	4.0	102	-0.5	-13	1.8	46	0.6	14	-0.1	-3	0.5	14	3.0	76
US 30	East	0-265	4	La. 2	10	114.45	2906.9	4.0	101	-0.5	-13	1.5	39	0.5	12	-0.1	-2	0.5	12	3.0	76
US 30	East	0-265	4	La. 2	11	126.32	3208.6	4.1	103	-0.4	-11	1.4	36	0.5	13	0.0	-1	0.5	13	3.1	78
US 30	East	1-270	5	La. 2	01	4.54	115.2	4.6	117	0.1	2	2.4	60	0.5	13	-0.2	-6	0.4	11	3.6	92
US 30	East	1-270	5	La. 2	02	16.63	422.4	4.5	114	0.0	0	2.5	63	0.7	17	-0.5	-12	0.4	11	3.5	89
US 30	East	1-270	5	La. 2	03	28.49	723.8	4.5	114	0.0	-1	2.5	65	0.6	15	-0.3	-9	0.5	12	3.5	88
US 30	East	1-270	5	La. 2	04	40.55	1029.9	4.6	116	0.1	2	2.4	60	0.5	14	-0.4	-9	0.4	11	3.6	92
US 30	East	1-270	5	La. 2	05	52.67	1337.7	4.5	115	0.0	1	2.4	60	0.6	16	-0.5	-11	0.4	11	3.6	91
US 30	East	1-270	5	La. 2	06	64.69	1643.2	4.5	114	0.0	-1	2.2	55	0.5	14	-0.4	-11	0.3	8	3.6	91
US 30	East	1-270	5	La. 2	07	76.73	1948.9	4.4	112	-0.1	-2	2.1	54	0.6	15	-0.5	-12	0.4	10	3.5	88
US 30	East	1-270	5	La. 2	08	88.69	2252.8	4.4	112	-0.1	-2	1.8	45	0.6	16	-0.5	-14	0.3	8	3.5	89
US 30	East	1-270	5	La. 2	09	100.80	2560.4	4.9	125	0.4	11	-0.8	-21	1.0	26	-0.5	-12	-0.9	-23	3.7	95
US 30	East	1-270	5	La. 2	10	112.78	2864.6	4.3	110	-0.2	-4	1.4	34	0.4	11	-0.4	-10	0.2	5	3.5	89
US 30	East	1-270	5	La. 2	11	124.51	3162.7	4.5	114	0.0	-1	1.1	29	0.4	10	0.2	5	0.3	9	3.6	90
US 30	East	1-275	6	La. 2	01	2.97	75.4	4.1	105	-0.4	-10	2.3	58	0.7	18	-0.2	-4	0.7	18	3.0	77
US 30	East	1-275	6	La. 2	03	15.09	383.2	4.1	105	-0.4	-10	2.2	56	0.6	16	-0.2	-5	0.6	15	3.1	78
US 30	East	1-275	6	La. 2	04	27.19	690.6	4.1	105	-0.4	-9	2.3	58	0.7	18	-0.2	-4	0.7	18	3.0	77

US 30	East	1-275	6	La. 2	05	39.14	994.2	4.2	106	-0.3	-8	2.2	56	0.7	18	-0.2	-6	0.6	17	3.1	79
US 30	East	1-275	6	La. 2	06	51.23	1301.2	4.2	106	-0.3	-8	2.2	56	0.7	18	-0.2	-4	0.7	18	3.1	79
US 30	East	1-275	6	La. 2	07	63.24	1606.4	4.2	106	-0.3	-8	2.0	52	0.7	17	-0.2	-5	0.6	16	3.1	79
US 30	East	1-275	6	La. 2	08	75.26	1911.5	4.2	106	-0.3	-8	2.0	51	0.7	17	-0.1	-3	0.7	17	3.1	79
US 30	East	1-275	6	La. 2	09	87.24	2215.8	4.2	107	-0.3	-8	1.8	47	0.6	16	-0.2	-6	0.6	15	3.1	80
US 30	East	1-275	6	La. 2	10	99.35	2523.6	4.1	105	-0.4	-9	1.9	47	0.6	14	-0.1	-2	0.6	14	3.1	79
US 30	East	1-275	6	La. 2	11	111.29	2826.8	4.1	104	-0.4	-11	1.6	40	0.4	9	0.0	-1	0.4	9	3.2	80
US 30	East	1-275	6	La. 2	12	122.89	3121.4	4.2	108	-0.3	-7	1.4	35	0.2	6	0.0	-1	0.2	6	3.4	86
US 30	East	1-280	7	La. 2	01	2.90	73.5	4.1	105	-0.4	-9	2.0	50	0.7	17	0.2	5	0.6	16	3.1	78
US 30	East	1-280	7	La. 2	03	15.12	384.1	4.2	107	-0.3	-8	1.9	49	0.7	17	0.2	5	0.6	16	3.1	80
US 30	East	1-280	7	La. 2	04	27.19	690.5	4.3	109	-0.2	-5	2.0	50	0.7	18	0.0	0	0.7	18	3.2	81
US 30	East	1-280	7	La. 2	05	39.13	993.9	4.3	110	-0.2	-4	1.9	47	0.6	15	0.0	-1	0.6	15	3.3	83
US 30	East	1-280	7	La. 2	06	51.18	1300.0	4.3	110	-0.2	-4	1.9	47	0.7	17	0.0	0	0.7	17	3.3	83
US 30	East	1-280	7	La. 2	07	63.26	1606.7	4.3	109	-0.2	-5	1.7	43	0.6	15	-0.1	-2	0.6	15	3.3	83
US 30	East	1-280	7	La. 2	08	75.27	1911.8	4.3	109	-0.2	-6	1.7	44	0.7	17	0.0	0	0.7	17	3.2	81
US 30	East	1-280	7	La. 2	09	87.30	2217.5	4.3	108	-0.3	-6	1.5	38	0.6	15	-0.1	-2	0.6	15	3.2	82
US 30	East	1-280	7	La. 2	10	99.31	2522.6	4.1	104	-0.4	-10	1.3	33	0.3	7	0.0	0	0.3	7	3.2	81
US 30	East	1-280	7	La. 2	11	111.24	2825.5	4.0	103	-0.5	-12	1.1	28	0.3	7	0.1	2	0.3	7	3.2	80
US 30	East	1-280	7	La. 2	12	122.85	3120.3	4.1	104	-0.4	-11	1.1	28	0.2	5	0.2	5	0.1	3	3.3	84
US 30	East	1-285	8	La. 2	01	11.58	294.0	4.3	110	-0.2	-5	2.3	58	1.1	27	0.8	19	0.8	19	3.2	81
US 30	East	1-285	8	La. 2	03	24.37	618.9	4.4	113	-0.1	-2	2.4	61	0.9	24	0.4	11	0.8	21	3.3	83
US 30	East	1-285	8	La. 2	04	36.43	925.4	4.4	113	-0.1	-2	2.3	58	0.8	20	0.1	1	0.8	20	3.3	84
US 30	East	1-285	8	La. 2	05	48.47	1231.2	4.5	113	-0.1	-1	2.3	59	0.9	22	-0.1	-1	0.9	22	3.3	83
US 30	East	1-285	8	La. 2	06	60.51	1537.0	4.4	113	-0.1	-2	2.1	54	0.8	21	-0.1	-3	0.8	21	3.3	83
US 30	East	1-285	8	La. 2	07	72.52	1842.1	4.4	112	-0.1	-2	2.1	54	0.8	21	-0.1	-2	0.8	21	3.2	82
US 30	East	1-285	8	La. 2	08	84.68	2151.0	4.4	113	-0.1	-2	1.9	49	0.7	18	-0.1	-2	0.7	18	3.3	84
US 30	East	1-285	8	La. 2	09	96.58	2453.2	4.2	107	-0.3	-8	2.0	51	0.7	17	-0.1	-2	0.7	17	3.1	79
US 30	East	1-285	8	La. 2	10	108.26	2749.7	4.3	110	-0.2	-5	1.8	45	0.5	13	-0.1	-3	0.5	12	3.3	85
US 30	East	1-285	8	La. 2	11	120.10	3050.5	4.5	114	0.0	0	1.9	48	0.5	14	0.0	1	0.5	14	3.5	88
US 30	East	1-290	9	La. 2	01	1.52	38.6	4.4	112	-0.1	-2	2.0	50	0.9	22	-0.3	-6	0.8	21	3.3	83
US 30	East	1-290	9	La. 2	03	13.94	354.1	4.3	110	-0.2	-4	2.0	51	0.8	20	0.0	1	0.8	20	3.2	81
US 30	East	1-290	9	La. 2	04	26.04	661.5	4.4	111	-0.2	-4	2.0	52	0.9	22	0.1	3	0.9	22	3.2	81
US 30	East	1-290	9	La. 2	05	37.99	965.0	4.4	111	-0.2	-4	2.0	51	0.7	19	0.0	0	0.7	19	3.2	82
US 30	East	1-290	9	La. 2	06	49.99	1269.7	4.4	111	-0.1	-4	2.1	53	0.8	21	0.0	0	0.8	21	3.2	81
US 30	East	1-290	9	La. 2	07	62.00	1574.8	4.3	110	-0.2	-5	2.0	51	0.7	18	-0.1	-3	0.7	17	3.2	82
US 30	East	1-290	9	La. 2	08	74.02	1880.2	4.3	110	-0.2	-5	2.0	52	0.8	20	0.0	1	0.8	20	3.2	81
US 30	East	1-290	9	La. 2	09	86.06	2185.9	4.4	111	-0.2	-4	1.9	47	0.7	18	0.0	-1	0.7	18	3.3	83
US 30	East	1-290	9	La. 2	10	98.15	2492.9	4.3	110	-0.2	-5	1.8	46	0.7	17	0.0	0	0.7	17	3.2	82

US 30	East	1-290	9	La. 2	11	110.23	2799.8	4.3	109	-0.2	-6	1.7	43	0.6	16	0.0	0	0.6	16	3.2	81
US 30	East	1-290	9	La. 2	12	121.84	3094.8	4.3	110	-0.2	-5	1.7	44	0.7	17	0.0	1	0.7	17	3.2	82
US 30	East	1-295	10	La. 2	01	4.13	104.9	4.1	105	-2.9	-73	-2.0	-52	2.1	54	1.6	42	-1.3	-34	2.7	69
US 30	East	1-295	10	La. 2	02	16.22	411.9	4.1	105	-2.9	-73	-2.5	-63	1.3	32	0.7	17	-1.1	-27	2.9	73
US 30	East	1-295	10	La. 2	03	28.67	728.3	4.2	108	-2.8	-70	-1.0	-25	0.2	5	0.0	0	-0.2	-5	3.4	86
US 30	East	1-295	10	La. 2	04	40.73	1034.5	4.2	108	-2.8	-70	-1.4	-36	0.5	12	-0.1	-3	-0.5	-12	3.3	83
US 30	East	1-295	10	La. 2	05	52.68	1338.2	4.2	108	-2.8	-70	-1.2	-31	0.3	8	-0.1	-2	-0.3	-8	3.3	85
US 30	East	1-295	10	La. 2	06	64.70	1643.3	4.3	109	-2.7	-69	-1.4	-37	0.5	12	-0.1	-3	-0.5	-12	3.3	84
US 30	East	1-295	10	La. 2	07	76.69	1947.9	4.3	109	-2.7	-69	-1.5	-37	0.4	9	0.0	-1	-0.4	-9	3.3	85
US 30	East	1-295	10	La. 2	08	88.76	2254.5	4.2	108	-2.8	-70	-1.8	-45	0.5	13	-0.1	-3	-0.5	-13	3.2	82
US 30	East	1-295	10	La. 2	09	100.84	2561.4	4.2	107	-2.8	-71	-1.5	-39	0.5	11	-0.1	-2	-0.4	-11	3.2	82
US 30	East	1-295	10	La. 2	10	112.91	2867.8	4.2	108	-2.8	-70	-1.7	-43	0.6	16	-0.2	-6	-0.6	-15	3.2	81
US 30	East	1-295	10	La. 2	11	124.59	3164.6	4.3	110	-2.7	-68	-1.5	-38	0.6	16	0.0	-1	-0.6	-16	3.2	82
US 30	East	2-300	11	La. 2	01	1.87	47.5	4.0	100	-0.6	-14	3.1	79	1.3	34	0.1	3	1.3	34	2.5	64
US 30	East	2-300	11	La. 2	03	14.01	355.8	4.3	108	-0.3	-7	1.7	44	0.6	15	0.1	3	0.6	15	3.2	82
US 30	East	2-300	11	La. 2	04	26.30	668.0	4.3	109	-0.2	-6	1.7	44	0.6	15	0.1	3	0.6	15	3.2	82
US 30	East	2-300	11	La. 2	05	38.32	973.3	4.3	109	-0.2	-5	1.7	42	0.5	13	0.1	1	0.5	13	3.3	84
US 30	East	2-300	11	La. 2	06	50.37	1279.4	4.3	109	-0.2	-5	1.7	44	0.6	15	0.1	2	0.6	15	3.3	83
US 30	East	2-300	11	La. 2	07	62.43	1585.6	4.3	109	-0.2	-6	1.6	41	0.5	12	0.1	1	0.5	12	3.3	83
US 30	East	2-300	11	La. 2	08	74.41	1889.9	4.3	109	-0.2	-6	1.7	43	0.6	16	0.1	3	0.6	16	3.2	82
US 30	East	2-300	11	La. 2	09	86.46	2196.0	4.3	110	-0.2	-4	1.6	41	0.6	15	0.1	2	0.6	15	3.3	84
US 30	East	2-300	11	La. 2	10	98.57	2503.8	4.3	109	-0.2	-5	1.6	41	0.7	18	0.2	5	0.7	18	3.2	81
US 30	East	2-300	11	La. 2	11	110.60	2809.4	4.2	108	-0.3	-7	1.5	39	0.5	14	0.1	2	0.5	14	3.2	82
US 30	East	2-300	11	La. 2	12	122.26	3105.4	4.3	109	-0.2	-5	1.8	45	0.6	16	0.2	5	0.6	16	3.3	83

B6: ASD-30 WB control section MITScan data collected by ODOT May 11, 2017

Highway	Direction	Station Number	Joint	Lane	Bar Number	X-Position		Depth		Depth Deviation		Side Shift		Misalignment		Horizontal Misalignment		Vertical Misalignment		Minimal Cover	
HW	Dir	SNo	Jo	La	BNo	xs		zs		dz		dy		s		sh		sv		c	
-	-	-	-	-	-	(in)	(mm)	(in)	(mm)	(in)	(mm)	(in)	(mm)	(in)	(mm)	(in)	(mm)	(in)	(mm)	(in)	(mm)
US 30	West	0-450	1	La. 2	01	9.25	235.1	4.1	103	-0.5	-12	1.5	38	0.5	14	-0.3	-7	0.5	12	3.1	78
US 30	West	0-450	1	La. 2	02	21.82	554.2	4.1	105	-0.4	-9	1.6	40	0.6	16	-0.1	-4	0.6	16	3.1	78
US 30	West	0-450	1	La. 2	03	33.81	858.7	4.2	106	-0.3	-8	1.5	39	0.5	14	-0.2	-5	0.5	13	3.2	81
US 30	West	0-450	1	La. 2	04	45.85	1164.6	4.3	109	-0.2	-6	1.6	41	0.6	16	-0.1	-3	0.6	15	3.2	82
US 30	West	0-450	1	La. 2	05	57.85	1469.3	4.3	110	-0.2	-4	1.6	40	0.5	14	-0.1	-3	0.5	14	3.3	84
US 30	West	0-450	1	La. 2	06	69.71	1770.7	4.4	112	-0.1	-3	1.6	40	0.6	16	0.0	0	0.6	16	3.3	84
US 30	West	0-450	1	La. 2	07	81.79	2077.5	4.3	110	-0.2	-4	1.4	35	0.6	15	0.0	-1	0.6	15	3.3	84

US 30	West	0-450	1	La. 2	08	93.74	2381.1	4.3	110	-0.2	-5	1.3	33	0.6	16	0.0	-1	0.6	16	3.3	83
US 30	West	0-450	1	La. 2	09	105.65	2683.4	4.2	108	-0.3	-7	0.8	20	0.3	7	0.0	-1	0.3	7	3.3	85
US 30	West	0-450	1	La. 2	10	117.28	2978.9	4.3	110	-0.2	-4	0.1	2	0.1	2	0.0	1	0.1	2	3.5	90
US 30	West	0-445	2	La. 2	01	9.69	246.0	4.5	114	0.0	-1	2.2	55	0.7	18	0.0	0	0.7	18	3.4	86
US 30	West	0-445	2	La. 2	02	22.29	566.2	4.5	115	0.0	0	1.9	49	0.6	15	-0.1	-3	0.6	15	3.5	88
US 30	West	0-445	2	La. 2	03	34.32	871.6	4.5	115	0.0	0	2.0	52	0.8	20	-0.1	-4	0.8	19	3.4	86
US 30	West	0-445	2	La. 2	04	46.31	1176.3	4.6	117	0.1	2	1.8	46	0.6	16	-0.2	-5	0.6	15	3.5	90
US 30	West	0-445	2	La. 2	05	58.32	1481.4	4.6	118	0.1	3	1.9	48	0.7	19	-0.3	-7	0.7	17	3.5	90
US 30	West	0-445	2	La. 2	06	70.35	1786.8	4.7	118	0.1	4	1.7	43	0.6	15	-0.3	-7	0.5	13	3.6	93
US 30	West	0-445	2	La. 2	07	82.33	2091.1	4.7	119	0.2	5	1.7	43	0.7	18	-0.3	-7	0.6	16	3.6	92
US 30	West	0-445	2	La. 2	08	94.45	2399.1	4.7	120	0.2	5	1.5	37	0.6	15	-0.4	-10	0.5	12	3.7	95
US 30	West	0-445	2	La. 2	09	106.39	2702.4	4.7	119	0.2	5	1.4	36	0.6	16	-0.3	-8	0.5	14	3.7	93
US 30	West	0-445	2	La. 2	10	118.85	3018.8	4.7	120	0.2	5	1.1	27	0.3	8	-0.1	-2	0.3	8	3.8	97
US 30	West	0-440	3	La. 2	01	5.08	129.0	4.0	101	-0.6	-14	3.3	84	2.7	68	-2.1	-54	1.6	41	2.4	61
US 30	West	0-440	3	La. 2	02	16.68	423.8	4.1	103	-0.4	-11	1.4	36	0.5	12	0.5	12	0.0	-1	3.3	84
US 30	West	0-440	3	La. 2	03	28.94	735.0	4.1	104	-0.4	-11	2.0	51	0.5	12	0.0	1	0.5	12	3.1	79
US 30	West	0-440	3	La. 2	04	40.92	1039.4	4.2	105	-0.4	-9	2.2	55	0.7	19	0.1	1	0.7	19	3.0	77
US 30	West	0-440	3	La. 2	05	52.96	1345.1	4.2	108	-0.3	-7	2.2	55	0.6	16	0.0	0	0.6	16	3.2	81
US 30	West	0-440	3	La. 2	06	64.93	1649.2	4.3	109	-0.2	-6	2.3	58	0.7	18	0.0	0	0.7	18	3.2	81
US 30	West	0-440	3	La. 2	07	76.96	1954.9	4.3	109	-0.2	-5	2.2	56	0.6	16	0.1	2	0.6	16	3.2	82
US 30	West	0-440	3	La. 2	08	88.97	2259.9	4.4	111	-0.2	-4	2.2	56	0.8	19	0.0	-1	0.8	19	3.2	82
US 30	West	0-440	3	La. 2	09	101.04	2566.5	4.3	109	-0.2	-5	2.1	53	0.7	17	0.0	0	0.7	17	3.2	82
US 30	West	0-440	3	La. 2	10	113.07	2871.9	4.3	110	-0.2	-5	2.1	52	0.7	19	-0.1	-2	0.7	19	3.2	81
US 30	West	0-440	3	La. 2	11	125.19	3179.8	4.3	110	-0.2	-5	1.9	47	0.6	15	-0.2	-5	0.6	14	3.3	84
US 30	West	0-435	4	La. 2	01	8.38	212.8	3.9	98	-0.6	-16	1.7	42	0.7	19	0.6	16	0.4	11	2.9	74
US 30	West	0-435	4	La. 2	02	20.77	527.6	4.0	100	-0.6	-14	1.6	40	0.4	11	0.0	-1	0.4	11	3.0	76
US 30	West	0-435	4	La. 2	03	32.71	831.0	4.0	102	-0.5	-12	1.7	43	0.6	15	-0.1	-2	0.6	15	3.0	76
US 30	West	0-435	4	La. 2	04	44.81	1138.3	4.0	102	-0.5	-12	1.6	41	0.5	13	0.0	-1	0.5	13	3.0	77
US 30	West	0-435	4	La. 2	05	56.77	1441.9	4.1	104	-0.4	-11	1.6	42	0.6	16	-0.1	-3	0.6	16	3.0	77
US 30	West	0-435	4	La. 2	06	68.81	1747.8	4.1	104	-0.4	-10	1.6	40	0.6	15	-0.1	-2	0.6	14	3.1	78
US 30	West	0-435	4	La. 2	07	80.85	2053.5	4.1	104	-0.4	-10	1.7	43	0.6	16	-0.1	-2	0.6	16	3.0	77
US 30	West	0-435	4	La. 2	08	92.84	2358.0	4.1	104	-0.4	-10	1.6	41	0.5	14	-0.1	-2	0.5	14	3.1	78
US 30	West	0-435	4	La. 2	09	104.86	2663.4	4.1	104	-0.4	-11	1.7	43	0.6	15	-0.1	-2	0.6	15	3.0	77
US 30	West	0-435	4	La. 2	10	117.05	2973.1	4.1	103	-0.4	-11	1.6	41	0.6	15	-0.1	-2	0.6	15	3.0	77
US 30	West	1-430	5	La. 2	01	0.06	1.4	3.6	91	-0.9	-23	3.0	76	1.2	29	0.3	8	1.1	28	2.3	58
US 30	West	1-430	5	La. 2	02	11.53	292.9	3.9	98	-0.6	-16	2.4	61	1.1	28	-0.6	-14	1.0	24	2.6	67
US 30	West	1-430	5	La. 2	03	23.92	607.6	3.9	99	-0.6	-15	2.0	50	0.6	16	-0.3	-7	0.6	15	2.9	73
US 30	West	1-430	5	La. 2	04	35.96	913.5	4.0	101	-0.5	-13	2.0	50	0.8	20	-0.3	-9	0.7	19	2.9	73

US 30	West	1-430	5	La. 2	06	48.03	1219.9	3.9	100	-0.6	-15	1.6	42	0.5	12	-0.3	-9	0.3	8	3.0	77
US 30	West	1-430	5	La. 2	07	60.00	1524.1	4.0	101	-0.6	-14	1.6	42	0.5	13	-0.3	-8	0.4	10	3.0	76
US 30	West	1-430	5	La. 2	08	71.97	1828.1	3.9	99	-0.6	-16	1.4	36	0.5	13	-0.3	-9	0.4	9	3.0	75
US 30	West	1-430	5	La. 2	09	83.90	2131.1	4.1	104	-0.4	-10	1.7	43	0.7	17	-0.4	-9	0.6	15	3.1	78
US 30	West	1-430	5	La. 2	10	95.96	2437.3	4.0	102	-0.5	-13	1.5	39	0.6	14	-0.2	-5	0.5	13	3.0	76
US 30	West	1-430	5	La. 2	11	107.93	2741.3	4.4	112	-0.1	-2	-0.3	-7	0.2	6	-0.2	-6	-0.1	-2	3.6	92
US 30	West	1-430	5	La. 2	13	120.03	3048.9	3.9	98	-0.7	-17	1.3	33	0.6	16	-0.2	-5	0.6	16	2.8	71
US 30	West	1-425	6	La. 2	01	6.85	174.0	4.0	101	-0.5	-13	-1.7	-44	1.0	25	0.7	17	-0.7	-18	2.9	73
US 30	West	1-425	6	La. 2	02	19.95	506.7	4.0	102	-0.5	-12	-1.4	-36	0.7	17	0.0	0	-0.7	-17	2.9	75
US 30	West	1-425	6	La. 2	03	31.94	811.2	4.0	102	-0.5	-12	-1.0	-24	0.4	11	0.0	0	-0.4	-11	3.1	78
US 30	West	1-425	6	La. 2	04	43.95	1116.3	4.0	103	-0.5	-12	-1.1	-27	0.5	13	0.1	3	-0.5	-13	3.0	77
US 30	West	1-425	6	La. 2	05	55.93	1420.6	4.1	104	-0.4	-10	-0.2	-4	0.1	4	0.1	3	-0.1	-2	3.3	84
US 30	West	1-425	6	La. 2	06	67.97	1726.3	4.1	104	-0.4	-10	-0.7	-18	0.3	8	0.1	2	-0.3	-7	3.2	82
US 30	West	1-425	6	La. 2	07	79.92	2029.9	4.1	105	-0.4	-9	0.7	17	0.4	10	0.0	0	0.4	10	3.2	81
US 30	West	1-425	6	La. 2	08	92.05	2338.1	4.1	105	-0.4	-9	0.5	14	0.3	8	0.0	0	0.3	8	3.2	82
US 30	West	1-425	6	La. 2	09	103.99	2641.4	4.0	102	-0.5	-13	0.8	21	0.5	13	0.0	1	0.5	13	3.0	76
US 30	West	1-425	6	La. 2	10	115.80	2941.3	4.0	102	-0.5	-12	0.2	4	0.2	5	0.1	1	0.2	5	3.2	81
US 30	West	1-425	6	La. 2	11	128.23	3257.1	4.3	108	-0.2	-6	-0.9	-24	0.0	1	0.0	-1	0.0	1	3.5	89
US 30	West	1-420	7	La. 2	01	10.20	259.0	3.7	95	-0.8	-20	0.4	10	2.9	74	2.9	74	-0.2	-4	2.9	73
US 30	West	1-420	7	La. 2	02	23.22	589.8	3.7	94	-0.8	-21	1.0	26	0.2	6	0.0	1	0.2	6	2.8	72
US 30	West	1-420	7	La. 2	03	35.19	893.9	3.7	94	-0.8	-20	1.2	32	0.4	10	0.1	3	0.4	10	2.8	70
US 30	West	1-420	7	La. 2	04	47.26	1200.3	3.9	98	-0.6	-16	1.3	33	0.3	8	0.1	3	0.3	7	3.0	76
US 30	West	1-420	7	La. 2	05	59.28	1505.7	3.9	98	-0.7	-17	1.5	37	0.4	9	0.0	1	0.4	9	2.9	74
US 30	West	1-420	7	La. 2	06	71.30	1811.1	3.9	98	-0.6	-16	1.5	37	0.3	8	0.2	5	0.2	6	3.0	76
US 30	West	1-420	7	La. 2	07	83.26	2114.7	3.9	98	-0.6	-16	1.6	40	0.4	10	0.1	2	0.4	9	2.9	75
US 30	West	1-420	7	La. 2	08	95.36	2422.1	3.9	99	-0.6	-16	1.5	38	0.4	10	-0.1	-1	0.4	9	3.0	75
US 30	West	1-420	7	La. 2	09	107.33	2726.1	3.9	98	-0.6	-16	1.5	39	0.5	13	0.0	0	0.5	13	2.9	73
US 30	West	1-420	7	La. 2	10	119.53	3036.0	3.9	99	-0.6	-15	1.4	35	0.3	8	-0.1	-2	0.3	8	3.0	76
US 30	West	1-415	8	La. 2	01	4.17	106.0	4.3	109	-0.2	-5	0.4	11	0.3	7	-0.3	-7	-0.1	-3	3.5	89
US 30	West	1-415	8	La. 2	02	16.23	412.3	4.0	102	-0.5	-13	0.7	17	0.3	7	-0.1	-4	0.2	6	3.1	80
US 30	West	1-415	8	La. 2	03	28.03	711.9	3.9	99	-0.6	-15	0.6	16	0.3	7	-0.2	-6	0.1	3	3.1	78
US 30	West	1-415	8	La. 2	04	39.95	1014.8	4.0	101	-0.5	-13	1.0	25	0.4	9	-0.1	-3	0.3	9	3.1	78
US 30	West	1-415	8	La. 2	05	52.05	1322.1	4.0	102	-0.5	-12	0.9	23	0.2	6	-0.1	-2	0.2	5	3.2	80
US 30	West	1-415	8	La. 2	06	64.05	1626.9	4.0	102	-0.5	-12	1.1	28	0.5	11	-0.1	-3	0.4	11	3.1	78
US 30	West	1-415	8	La. 2	07	76.10	1933.0	4.0	103	-0.5	-12	0.9	23	0.3	7	-0.1	-3	0.3	6	3.2	80
US 30	West	1-415	8	La. 2	08	88.07	2237.1	4.0	103	-0.5	-12	1.0	26	0.4	11	-0.1	-3	0.4	11	3.1	78
US 30	West	1-415	8	La. 2	09	100.08	2542.1	4.0	101	-0.5	-13	0.7	19	0.2	6	-0.1	-2	0.2	6	3.1	79
US 30	West	1-415	8	La. 2	10	112.09	2847.0	4.0	101	-0.5	-13	0.9	23	0.4	11	-0.1	-2	0.4	11	3.0	77

US 30	West	1-415	8	La. 2	11	124.21	3155.0	4.0	101	-0.5	-13	0.4	10	0.2	5	-0.1	-3	0.1	4	3.2	80
US 30	West	1-410	9	La. 2	01	2.21	56.3	4.2	108	-0.3	-7	0.2	6	1.7	42	-1.4	-35	0.9	23	3.0	77
US 30	West	1-410	9	La. 2	03	14.65	372.1	4.1	105	-0.4	-9	1.0	26	0.5	12	-0.3	-7	0.4	9	3.2	81
US 30	West	1-410	9	La. 2	04	26.69	677.9	4.1	103	-0.4	-11	1.1	28	0.3	8	0.1	2	0.3	7	3.2	81
US 30	West	1-410	9	La. 2	05	38.61	980.7	4.0	103	-0.5	-12	1.4	36	0.5	13	0.2	4	0.5	13	3.0	77
US 30	West	1-410	9	La. 2	06	50.63	1286.0	4.1	105	-0.4	-10	1.4	35	0.4	9	0.2	4	0.3	8	3.2	81
US 30	West	1-410	9	La. 2	07	62.64	1591.0	4.1	104	-0.4	-10	1.6	40	0.5	12	0.2	5	0.4	11	3.1	80
US 30	West	1-410	9	La. 2	08	74.64	1895.9	4.1	104	-0.4	-10	1.6	40	0.4	10	0.2	4	0.4	9	3.2	80
US 30	West	1-410	9	La. 2	09	86.63	2200.5	4.1	103	-0.5	-11	1.7	44	0.5	13	0.1	1	0.5	13	3.0	77
US 30	West	1-410	9	La. 2	10	98.74	2508.0	4.0	103	-0.5	-12	1.6	40	0.5	14	0.1	3	0.5	13	3.0	77
US 30	West	1-410	9	La. 2	11	110.65	2810.6	3.9	99	-0.6	-15	1.7	43	0.7	17	-0.2	-4	0.6	16	2.8	72
US 30	West	1-410	9	La. 2	12	122.77	3118.4	3.9	98	-0.6	-16	1.4	36	0.4	11	0.2	4	0.4	10	2.9	74
US 30	West	1-405	10	La. 2	01	9.52	241.8	4.0	102	-0.5	-12	2.5	62	0.7	19	-0.3	-9	0.7	17	2.9	75
US 30	West	1-405	10	La. 2	02	21.85	554.9	4.0	102	-0.5	-13	2.4	60	0.6	16	-0.3	-8	0.6	14	3.0	76
US 30	West	1-405	10	La. 2	03	33.77	857.8	4.0	103	-0.5	-12	2.4	61	0.8	21	-0.3	-8	0.8	20	2.9	74
US 30	West	1-405	10	La. 2	04	45.83	1164.2	4.0	101	-0.5	-13	2.3	58	0.6	15	-0.4	-9	0.5	12	3.0	76
US 30	West	1-405	10	La. 2	05	57.86	1469.7	4.0	102	-0.5	-13	2.3	58	0.6	16	-0.2	-6	0.6	15	3.0	75
US 30	West	1-405	10	La. 2	06	69.92	1776.0	4.0	102	-0.5	-13	2.1	52	0.6	15	-0.3	-8	0.5	13	3.0	76
US 30	West	1-405	10	La. 2	07	81.86	2079.2	4.0	102	-0.5	-13	2.0	50	0.7	18	-0.4	-9	0.6	15	2.9	75
US 30	West	1-405	10	La. 2	08	93.95	2386.3	4.1	105	-0.4	-10	1.7	43	0.8	21	-0.5	-13	0.6	16	3.1	78
US 30	West	1-405	10	La. 2	09	105.82	2687.9	4.0	102	-0.5	-13	1.5	39	0.7	17	-0.4	-10	0.5	14	3.0	76
US 30	West	1-405	10	La. 2	10	118.00	2997.3	4.0	101	-0.5	-14	1.3	32	0.4	10	-0.3	-7	0.3	6	3.1	79
US 30	West	2-400	11	La. 2	03	32.53	826.2	5.5	140	1.0	25	-3.2	-81	1.1	29	0.8	21	-0.8	-20	4.4	111
US 30	West	2-400	11	La. 2	04	43.30	1099.9	3.7	95	-0.8	-19	-4.6	-116	2.3	59	2.3	58	-0.5	-12	2.7	70
US 30	West	2-400	11	La. 2	05	55.07	1398.7	3.9	99	-0.6	-15	-2.9	-74	3.0	76	2.6	66	1.4	36	2.4	62
US 30	West	2-400	11	La. 2	06	66.82	1697.3	3.9	98	-0.6	-16	-3.4	-86	3.2	81	3.0	76	-1.0	-26	2.6	66
US 30	West	2-400	11	La. 2	07	78.74	2000.0	4.0	103	-0.5	-12	-1.6	-41	3.8	96	3.7	95	-0.5	-12	3.1	78
US 30	West	2-400	11	La. 2	08	90.79	2306.2	4.0	101	-0.5	-14	*	*	*	*	*	*	*	*	*	*
US 30	West	2-400	11	La. 2	09	102.81	2611.4	3.9	100	-0.6	-15	*	*	*	*	*	*	*	*	*	*
US 30	West	2-400	11	La. 2	10	114.68	2912.9	3.9	99	-0.6	-16	*	*	*	*	*	*	*	*	*	*
US 30	West	2-400	11	La. 2	11	125.68	3192.4	5.2	132	0.7	18	-3.7	-94	3.7	95	2.1	53	-3.1	-79	2.9	74

Appendix C: PCC laboratory test data
C1: Compressive strength test data

Compressive strength test data (English units)

Route	Core	Length (in)	D1 (in)	D2 (in)	D (in)	P (lb)	A (in^2)	f'c (psi)	Direction average (psi)	Coefficient of Variation (%)
I-70	E7	8.0	4.007	3.997	4.000	109500	12.5664	8710	8340	10.28%
I-70	E8	8.0	4.006	4.002	4.000	112520	12.5664	8950		
I-70	E12	8.0	4.004	4.003	4.000	92500	12.5664	7360		
I-70	W1	8.0	4.004	4.005	4.000	137160	12.5664	10920	10310	7.46%
I-70	W2	8.0	4.002	4.003	4.000	132960	12.5664	10580		
I-70	W14	8.0	4.001	4.003	4.000	118700	12.5664	9450		
I-77	N2	7.9	3.971	3.975	3.970	108380	12.3786	8760	8920	1.57%
I-77	N4	7.8	3.958	3.982	3.970	111800	12.3786	9030		
I-77	N15	7.4	3.711	3.707	3.710	96900	10.8103	8960		
I-77	S2	7.4	3.704	3.710	3.710	103440	10.8103	9570	8720	8.49%
I-77	S4	7.4	3.700	3.704	3.700	89500	10.7521	8320		
I-77	S7	7.5	3.705	3.702	3.700	88780	10.7521	8260		
I-90	L2 (EB)	8.0	3.951	3.962	3.957	83000	12.295	6750	7180	7.74%
I-90	L6 (EB)	8.0	3.958	3.956	3.957	85940	12.298	6990		
I-90	L17 (WB)	8.0	3.959	3.960	3.960	96200	12.313	7810		
US-30	A3 (EB)	7.8	3.938	4.000	3.969	112920	12.371	9130	8710	5.97%
US-30	A4 (EB)	8.1	4.063	4.031	4.047	114160	12.863	8880		
US-30	A6 (EB)	8.0	4.031	4.000	4.016	102900	12.665	8130		

Compressive strength test data (metric units)

Route	Core	Length (mm)	D1 (mm)	D2 (mm)	D (mm)	P (kN)	A (mm^2)	f'c (MPa)	Direction average (MPa)	Coefficient of Variation (%)
I-70	E7	203	101.78	101.52	101.60	487.08	8107.3	60.05	57.50	10.28%
I-70	E8	203	101.75	101.65	101.60	500.51	8107.3	61.71		
I-70	E12	203	101.70	101.68	101.60	411.46	8107.3	50.75		
I-70	W1	203	101.70	101.73	101.60	610.12	8107.3	75.29	71.13	7.46%
I-70	W2	203	101.65	101.68	101.60	591.44	8107.3	72.95		
I-70	W14	203	101.63	101.68	101.60	528.00	8107.3	65.16		
I-77	N2	201	100.86	100.97	100.84	482.10	7986.2	60.40	61.48	1.57%
I-77	N4	198	100.53	101.14	100.84	497.31	7986.2	62.26		
I-77	N15	188	94.26	94.16	94.23	431.03	6974.4	61.78		
I-77	S2	188	9.408	9.423	9.423	460.12	69.744	65.98	60.10	8.49%
I-77	S4	188	9.398	9.408	9.398	398.12	69.368	57.36		
I-77	S7	191	9.411	9.403	9.398	394.91	69.368	56.95		
I-90	L2 (EB)	20.3	10.036	10.063	10.051	369.20	79.322	46.54	49.53	7.74%
I-90	L6 (EB)	20.3	10.053	10.048	10.051	382.28	79.342	48.19		
I-90	L17 (WB)	20.3	10.056	10.058	10.058	427.92	79.439	53.85		
US-30	A3 (EB)	19.8	10.003	10.160	10.081	502.29	79.813	62.95	60.08	5.97%
US-30	A4 (EB)	20.6	10.320	10.239	10.279	507.81	82.987	61.23		
US-30	A6 (EB)	20.3	10.239	10.160	10.201	457.72	81.710	56.05		

C2: Splitting tensile strength test data

Splitting tensile strength test data (English units)

Route	Core	Length (in)	D1 (in)	D2 (in)	D (in)	P (lb)	Tensile strength (psi)	Direction average (psi)	Coefficient of Variation (%)
I-70	E10	8.0	4.003	4.012	4.010	35320	700	655	6.23%
I-70	E13	8.0	3.995	3.999	4.000	32000	635		
I-70	E14	8.0	4.002	4.010	4.010	31600	625		
I-70	W5	8.0	4.010	4.005	4.010	28480	565	720	19.75%
I-70	W9	8.0	4.012	4.009	4.010	37460	745		
I-70	W13	8.0	4.015	4.010	4.010	42660	845		
I-77	N5	8.0	3.975	3.972	3.970	43440	870	880	3.79%
I-77	N9	7.8	3.979	3.971	3.980	44540	915		
I-77	N16	7.4	3.705	3.702	3.700	36520	850		
I-77	S5	7.4	3.700	3.699	3.700	41660	970	875	12.16%
I-77	S6	7.4	3.704	3.712	3.710	38560	895		
I-77	S18	7.5	3.704	3.706	3.710	33260	760		
I-90	L7 (EB)	8.1	3.953	3.959	3.960	30060	595	635	5.37%
I-90	L8 (WB)	8.1	3.962	3.960	3.960	32440	645		
I-90	L12 (WB)	8.1	3.960	3.961	3.960	33300	660		
US-30	A8 (EB)	8.0	4.021	4.008	4.01	29380	580	630	16.47%
US-30	A11 (WB)	7.8	4.031	4.018	4.02	27200	555		
US-30	A12 (WB)	8.0	4.015	4.003	4.01	37700	745		

Splitting tensile strength test data (metric units)

Route	Core	Length (mm)	D1 (mm)	D2 (mm)	D (mm)	P (kN)	Tensile strength (MPa)	Direction average (MPa)	Coefficient of Variation (%)
I-70	E10	203	101.68	101.90	101.85	157.11	4.83	4.50	6.23%
I-70	E13	203	101.47	101.57	101.60	142.34	4.38		
I-70	E14	203	101.65	101.85	101.85	140.56	4.31		
I-70	W5	203	101.85	101.73	101.85	126.69	3.90	4.95	19.75%
I-70	W9	203	101.90	101.83	101.85	166.63	5.14		
I-70	W13	203	101.98	101.85	101.85	189.76	5.83		
I-77	N5	203	100.97	100.89	100.84	193.23	6.00	6.06	3.79%
I-77	N9	198	101.07	100.86	101.09	198.12	6.31		
I-77	N16	188	94.11	94.03	93.98	162.45	5.86		
I-77	S5	188	93.98	93.95	93.98	185.31	6.69	6.03	12.16%
I-77	S6	188	94.08	94.28	94.23	171.52	6.17		
I-77	S18	191	94.08	94.13	94.23	147.95	5.24		
I-90	L7 (EB)	206	100.41	100.56	100.58	133.71	4.10	4.37	5.37%
I-90	L8 (WB)	206	100.63	100.58	100.58	144.30	4.45		
I-90	L12 (WB)	206	100.58	100.61	100.58	148.13	4.55		
US-30	A8 (EB)	203	102.13	101.80	101.85	130.69	4.00	4.32	16.47%
US-30	A11 (WB)	198	102.39	102.06	102.11	120.99	3.83		
US-30	A12 (WB)	203	101.98	101.68	101.85	167.70	5.14		

C3: Elastic Modulus and Poisson's Ratio test data

Elastic modulus test data (English units at top, metric units at bottom)

Route	Core	L (in)	D (in)	A (in^2)	P1 (lb)	P2 (lb)	S1 (psi)	S2 (psi)	ε2	E (psi)
I-70	E12	8	4	12.59	4020	39700	319.34	3153.7	1.07E-03	2.80E+06
I-70	W14	8	4	12.58	2630	39200	209.08	3116.32	7.09E-04	4.41E+06
I-77	N15	7.4	3.71	10.80	18300	40000	1693.74	3702.17	5.50E-04	4.02E+06
I-77	S7	7.5	3.7	10.77	12200	39200	1132.52	3638.91	5.50E-04	5.01E+06
I-90	L2 (EB)	8	4	12.29	6172	35004	502.01	2847.12	6.45E-04	3.94E+06
US-30	A15 (WB)	7.9	3.94	12.18	2570	40000	211.06	3284.95	7.44E-04	4.45E+06

Route	Core	L (mm)	D (mm)	A (mm^2)	P1 (kN)	P2 (kN)	S1 (MPa)	S2 (MPa)	ε2	E (MPa)
I-70	E12	203.2	101.6	8122.56	17.88	176.59	2.202	21.744	1.07E-03	19305
I-70	W14	203.2	101.6	8116.11	11.70	174.37	1.442	21.486	7.09E-04	30406
I-77	N15	188.0	94.2	6967.73	81.40	177.93	11.678	25.526	5.50E-04	27717
I-77	S7	190.5	94.0	6948.37	54.27	174.37	7.808	25.089	5.50E-04	34543
I-90	L2 (EB)	203.2	101.6	7929.02	27.45	155.71	3.461	19.630	6.45E-04	27165
I-90	L2 (EB)	200.7	100.1	7858.05	11.43	177.93	1.455	22.649	7.44E-04	30682

Poisson's Ratio test data

Route	Core	εt1	εt2	υ
I-70	E12	4.98E-05	2.71E-04	0.22
I-70	W14	2.37E-06	9.54E-05	0.15
I-77	N15	4.48E-06	8.87E-05	0.17
I-77	S7	8.89E-06	9.00E-05	0.16
I-90	L2	1.09E-05	1.23E-04	0.19
US-30	A15	9.39E-06	1.61E-04	0.22

C4: CTE test data

Coefficient of Thermal Expansion (CTE) test data (Metric units at top. English units at bottom)

Route	Core	V1	T1 (°C)	V2	T2 (°C)	V3	T3 (°C)	L (mm)	CTE1 (1/°C)	CTE2 (1/°C)	CTE (1/°C)
I-70	E16	1.137	11.4	1.221	50.1	1.151	12.9	182.9	7.91E-06	6.91E-06	7.41E-06
I-70	W15	0.57	12.7	0.65	50.1	0.577	13.6	177.7	8.01E-06	7.51E-06	7.76E-06
I-77	N17	3.133	12.3	3.228	50.1	3.136	12.7	179.5	9.26E-06	9.07E-06	9.17E-06
I-77	S16	1.499	12.2	1.59	49.9	1.509	14.2	177.0	9.03E-06	8.51E-06	8.77E-06
I-90	L17 (WB)	1.544	11.7	1.66	50.3	1.544	12.3	191.9	1.05E-05	1.06E-05	1.05E-05
US-30	A13 (WB)	0.891	13.9	0.995	50	0.902	12.6	178.0	1.08E-05	9.38E-06	1.01E-05

Route	Core	V1	T1 (°F)	V2	T2 (°F)	V3	T3 (°F)	L (in)	CTE1 (1/°F)	CTE2 (1/°F)	CTE (1/°F)
I-70	E16	1.137	52.5	1.221	122.2	1.151	55.2	7.199	4.39E-06	3.84E-06	4.12E-06
I-70	W15	0.57	54.9	0.65	122.2	0.577	56.5	6.998	4.45E-06	4.17E-06	4.31E-06
I-77	N17	3.133	54.1	3.228	122.2	3.136	54.9	7.066	5.14E-06	5.04E-06	5.09E-06
I-77	S16	1.499	54.0	1.59	121.8	1.509	57.6	6.97	5.02E-06	4.73E-06	4.87E-06
I-90	L17 (WB)	1.544	53.1	1.66	122.5	1.544	54.1	7.554	5.83E-06	5.89E-06	5.81E-06
US-30	A13 (WB)	1.544	57.0	1.66	122.0	1.544	54.7	7.006	6.00E-06	5.21E-06	5.61E-06

C5: Core Logs (NCHRP forms)

I-70 Madison County Eastbound

PAVEMENT FORENSIC INVESTIGATION	CORE LOG (Multi Core)	Form #17b
Investigation Name	Forensic Study of Early Failures with UBCOs	Investigation #
Plan Reference		Date Sampled 8/19/2015
Drill Notes		Core Size D: 100mm
		Coolant A ☐ W ☒

Core#	Location	Layer Thickness			Observations and Distress Description	Photo
1	EB 766+17	N/A	N/A		wheelpath, spalled joint; shattered	E1
2	EB 766+17	220.4	N/A		center of lane, spalled joint; horizontally cracked	E2
3	EB 766+24	223.1	27.1		center of slab, core for additional testing	E3
4	EB 766+20	223.3	24.0		center of lane, 3' from joint, control for E1&E2	E4
5	EB 768+35	256.4	35.2		center of slba, control for E15	E5
6	EB 769+12	221.2	26.3		midslab crack; vertically cracked	E6
7	EB 769+19	222.8	N/A			E7
8	EB 769+48	221.0	N/A		overlay core	E8
9	EB 769+48	228.4	N/A		old concrete core	E9
10	EB 769+48	222.8	20.1			E10
11	EB 769+11	220.0	26.5		control for E6	E11
12	EB 768+72	236.1	39.0			E12
13	EB 768+64	234.0	50.0			E13
14	EB 768+49	247.5	34.1			E14
15	EB 768+42	245.6	N/A		center of lane, joint of no surface distress;	E15
16	EB 768+20	246.1	28.0			E16
17						
18						
19						
20						
21						
22						
23						
24						
25						

	Notes

Evaluator		Date	

I-70 Madison County Westbound

PAVEMENT FORENSIC INVESTIGATION		CORE LOG (Multi Core)				Form #17b
Investigation Name	Forensic Study of Early Failures with UBCOs			Investigation #		
Plan Reference				Date Sampled	8/19/2015	
Drill Notes				Core Size	D: 100 mm	
				Coolant	A ☐	W ☒

Core#	Location	Layer Thickness			Observations and Distress Description	Photo
1	WB 610+27	230.6	45.5			W1
2	WB 609+99	230.0	52.5		next to a crack	W2
3	WB 609+69	231.5	50.0		center of slab, control for W4, W6&W7	W3
4	WB 609+69	229.9	52.2		wheelpaht, hairline crack	W4
5	WB 609+68	231.5	52.4		center of lane, joint of no surface distress	W5
6	WB 609+61	234.0	47.7			W6
7	WB 609+54	230.6	50.9		center of lane, midslab crack; vertically cracked	W7
8	WB 609+52	230.0	49.0		center of lane, control for W7 or additional test	W8
9	WB 609+40	226.5	50.4			W9
10	WB 609+25	225.0	49.0		center of lane, control for W11&W12	W10
11	WB 609+15	N/A	N/A		wheelpath, spalled joint; shattered	W11
12	WB 609+15	N/A	44.0		center of lane, spalled joint; broken	W12
13	WB 609+07	226.0	44.5			W13
14	WB 608+75	232.2	38.6		next to a core taken at conctruction	W14
15	WB 608+48	232.5	37.4			W15
16						
17						
18						
19						
20						
21						
22						
23						
24						
25						

	Notes

Evaluator		Date	

I-77 Washington/Noble County Northbound

PAVEMENT FORENSIC INVESTIGATION		CORE LOG (Multi Core)				Form #17b
Investigation Name	Forensic Study of Early Failures with UBCOs			Investigation #		
Plan Reference				Date Sampled	10/8/2015	
Drill Notes				Core Size	D: 100 mm	
				Coolant	A ☐	W ☒

Core#	Location	Layer Thickness			Observations and Distress Description	Photo
1	NB 824+9	206.7	69.3			N1
2	NB 824+39	206.5	72.0			N2
3	NB 824+69	207.5	74.7			N3
4	NB 824+99	210.5	74.5			N4
5	NB 825+29	213.4	70.5			N5
6	NB 825+59	210.0	74.1			N6
7	NB 825+67	208.8	82.1		horizontal crack	N7
8	NB 825+67	205.0	77.1			N8
9	NB 825+65	209.5	81.0			N9
10	NB 824+69	207.5	76.0			N10
11	NB 824+69	209.5	73.0			N11
12	NB 824+69	216.2	57.5			N12
13	NB 824+69	213.1	71.5			N13
14	NB 824+61	198.0	75.2			N14
15	NB 825+14	211.2	73.7			N15
16	NB 825+34	210.9	77.0			N16
17	NB 825+64	206.5	78.0			N17
18						
19						
20						
21						
22						
23						
24						
25						

	Notes

Evaluator		Date	

I-77 Washington/Noble County Southbound

PAVEMENT FORENSIC INVESTIGATION		CORE LOG (Multi Core)				Form #17b
Investigation Name	Forensic Study of Early Failures with UBCOs			Investigation #		
Plan Reference				Date Sampled	10/8/2015	
Drill Notes				Core Size	D: 100mm	
				Coolant	A ☐	W ☒

Core#	Location	Layer Thickness			Observations and Distress Description	Photo
1	SB 25+30	214.0	70.0			S1
2	SB 25+15	214.0	64.7			S2
3	SB 25+19	209.8	N/A			S3
4	SB 24+85	220.0	N/A			S4
5	SB 25+00	221.0	59.9			S5
6	SB 25+00	225.0	65.1			S6
7	SB 24+70	213.1	N/A			S7
8	SB 24+25	210.0	28.5			S8
9	SB 24+25	210.1	68.4			S9
10	SB 24+26	210.0	40.0			S10
11	SB 24+25	218.0	66.1			S11
12	SB 24+25	220.0	52.5			S12
13	SB 24+25	217.2	63.7			S13
14	SB 24+17	205.0	35.5		horizontal crack in approach slab	S14
15	SB 23+94	215.0	65.0			S15
16	SB 23+79	214.1	63.1			S16
17	SB 23+64	209.5	65.5			S17
18	SB 23+49	208.8	33.1			S18
19						
20						
21						
22						
23						
24						
25						

	Notes

Evaluator		Date	

I-90 Lake County Eastbound

PAVEMENT FORENSIC INVESTIGATION	CORE LOG (Multi Core)	Form #17b

Investigation Name	Forensic Study of Early Failures with UBCOs	Investigation #	
Plan Reference		Date Sampled	8/30/2016
Drill Notes		Core Size	D: 100mm
		Coolant	A ☐ W ☒

Core#	Location	Layer Thickness			Observations and Distress Description	Photo
1	EB 1561+14	252.5	27.5			L1
2	EB 1561+21	247.6	22.5			L2
3	EB 1561+44	248.0	34.3			L3
4	EB 1561+51	246.5	24.6			L4
5	EB 1561+64	245.5	28.0			L5
6	EB 1562+26	226.9	27.5			L6
7	EB 1562+40	237.5	31.3			L7
8						
9						
10						
11						
12						
13						
14						
15						
16						
17						
18						
19						
20						
21						
22						
23						
24						
25						

	Notes

Evaluator		Date	

I-90 Lake County Westbound

PAVEMENT FORENSIC INVESTIGATION		CORE LOG (Multi Core)				Form #17b
Investigation Name		Forensic Study of Early Failures with UBCOs			Investigation #	
Plan Reference					Date Sampled	8/30/2016
Drill Notes					Core Size	D: 100 mm
					Coolant	A ☐ W ☒

Core#	Location	Layer Thickness			Observations and Distress Description	Photo
1	WB 517+43	246.0	26.6			L8
2	WB 516+85	246.0	24.5			L9
3	WB 516+85	242.0	31.5			L10
4	WB 516+7	245.2	30.3			L11
5	WB 516+7	246.8	41.0			L12
6	WB 516+7	244.0	35.5			L13
7	WB 518+86	247.3	31.5			L14
8	WB 518+86	241.0	33.0			L15
9	WB 518+86	238.0	34.0			L16
10	WB 518+62	233.7	34.8			L17
11	WB 518+10	239.0	32.0			L18
12						
13						
14						
15						
16						
17						
18						
19						
20						
21						
22						
23						
24						
25						

	Notes

Evaluator		Date	

US-30 Ashland County Eastbound

PAVEMENT FORENSIC INVESTIGATION		CORE LOG (Multi Core)				Form #17b
Investigation Name		Forensic Study of Early Failures with UBCOs			Investigation #	
Plan Reference					Date Sampled	9/20/2016
Drill Notes					Core Size	D: 100 mm
					Coolant	A ☐ W ☒

Core#	Location	Layer Thickness			Observations and Distress Description	Photo
1	EB 0+272	231.8	25.4			A1
2	EB 0+272	233.4	25.4			A2
3	EB 0+272	231.8	34.9			A3
4	EB 0+289	233.4	25.4			A4
5	EB 0+293	235.0	27.0			A5
6	EB 0+292	233.4	25.4			A6
7	EB 0+255	N/A	N/A			A7
8	EB 0+266	228.6	30.2			A8
9	EB 0+268	N/A	N/A			A9
10	EB 0+250	N/A	N/A			A10
11						
12						
13						
14						
15						
16						
17						
18						
19						
20						
21						
22						
23						
24						
25						

	Notes

Evaluator		Date	

US-30 Ashland County Westbound

PAVEMENT FORENSIC INVESTIGATION		CORE LOG (Multi Core)				Form #17b
Investigation Name	Forensic Study of Early Failures with UBCOs			Investigation #		
Plan Reference				Date Sampled	8/30/2016	
Drill Notes				Core Size	D: 100 mm	
				Coolant	A ☐	W ☒

Core#	Location	Layer Thickness			Observations and Distress Description	Photo
1	WB 0+294	246.1	20.6			A11
2	WB 0+285	236.5	19.1			A12
3	WB 0+275	225.4	22.2			A13
4	WB 0+278	225.4	20.6			A14
5	WB 0+266	228.6	20.6			A15
6						
7						
8						
9						
10						
11						
12						
13						
14						
15						
16						
17						
18						
19						
20						
21						
22						
23						
24						
25						

	Notes

Evaluator		Date	

Appendix D: Supplemental HIPERPAV data

D1: MAD-70, August 17-September 2, 1999 and May 12-June 1, 2000

Aug. 17, 1999 Moist base

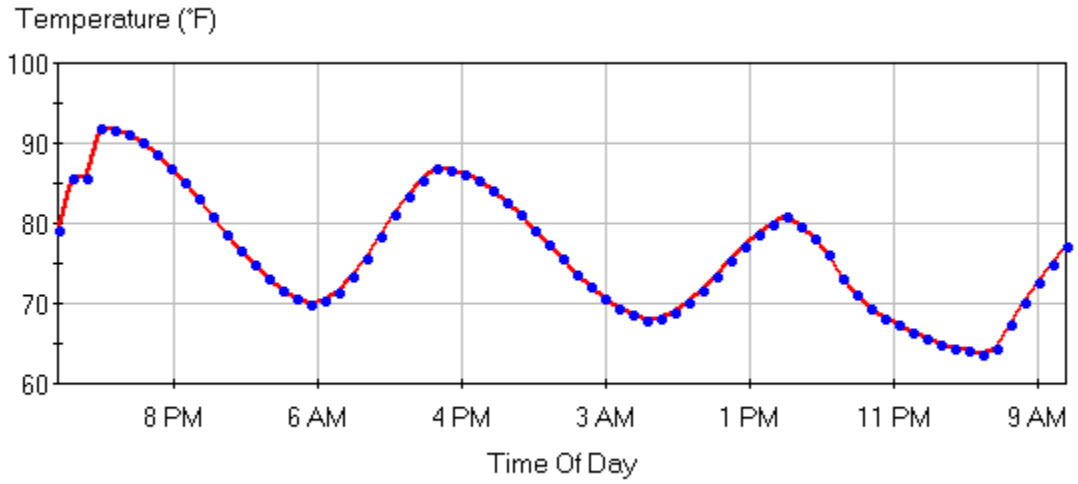

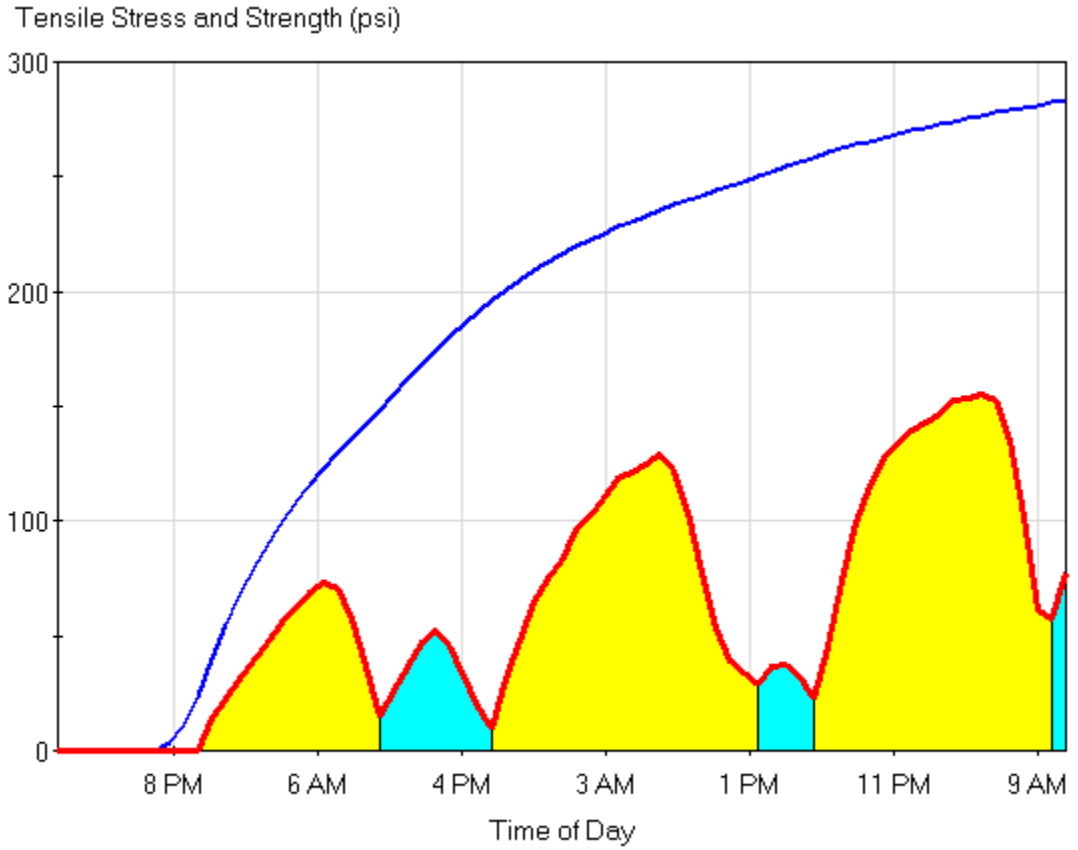

Aug. 17, 1999 Dry Base

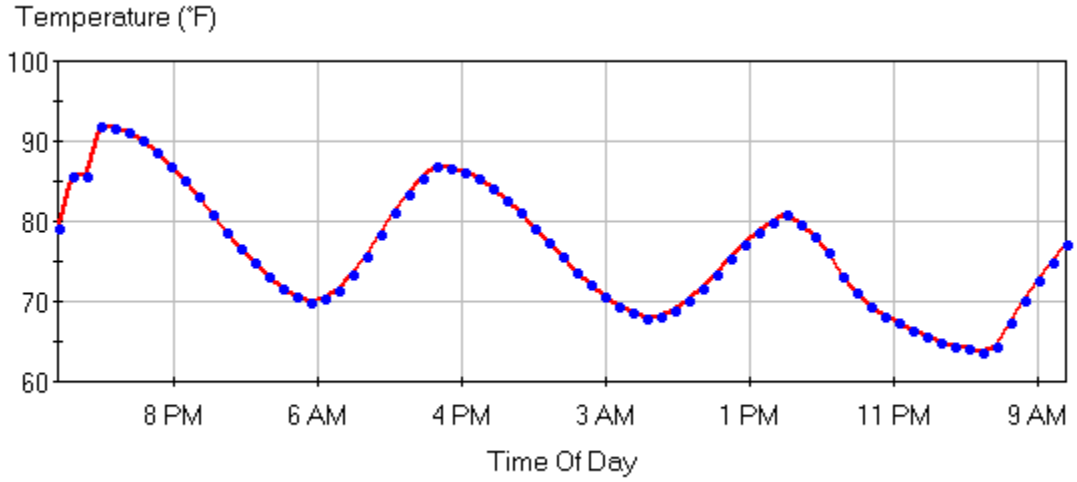

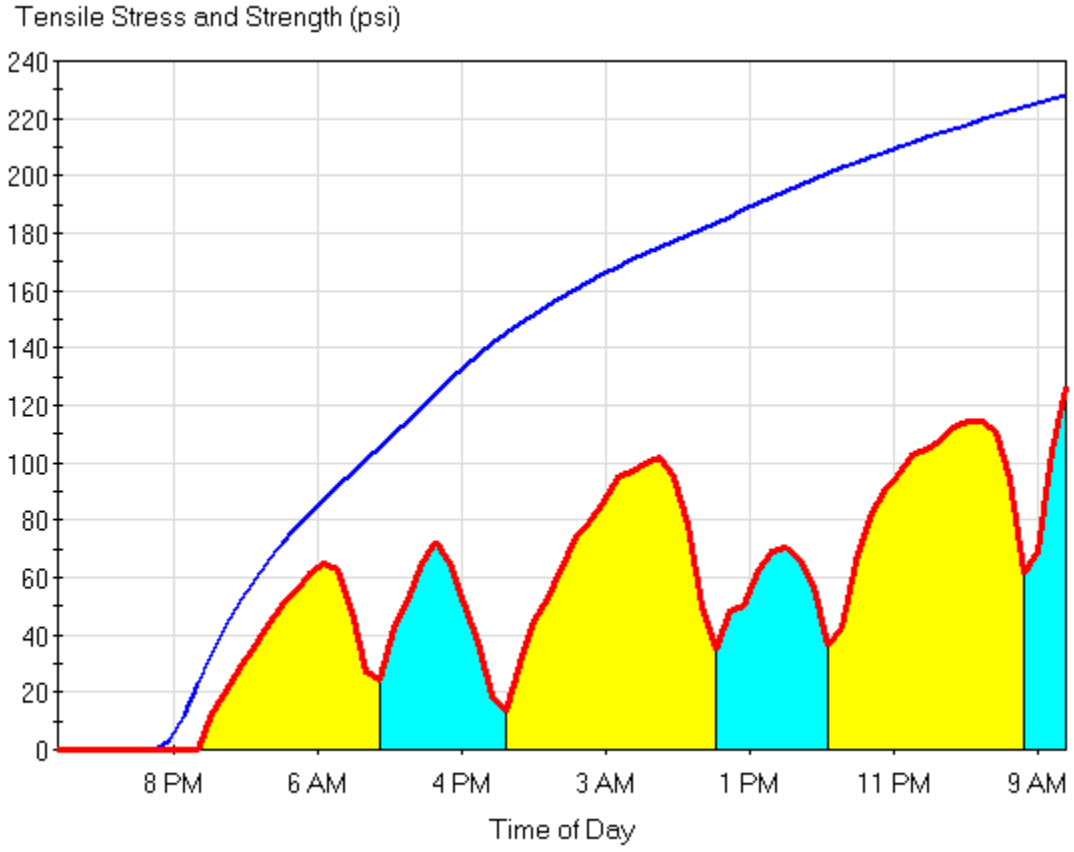

Aug. 18, 1999 Moist base

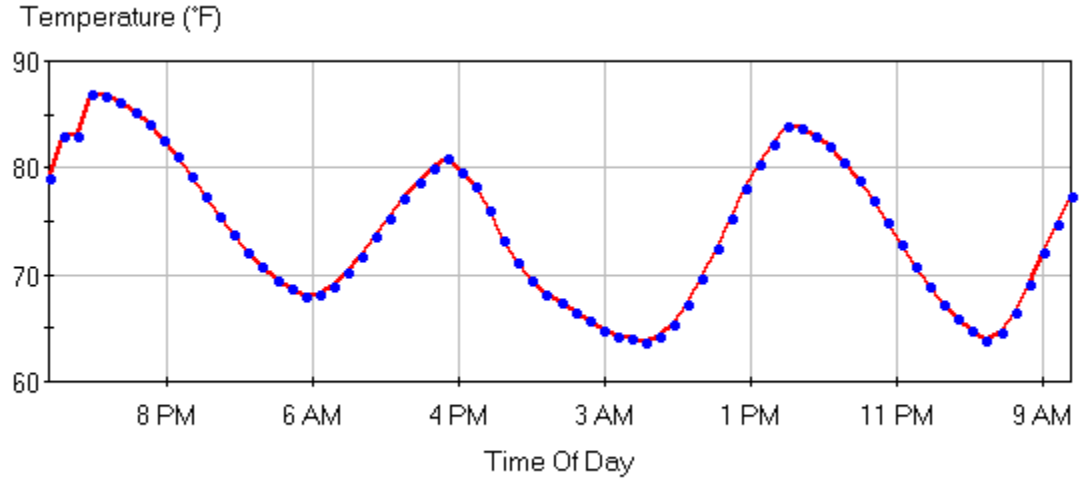

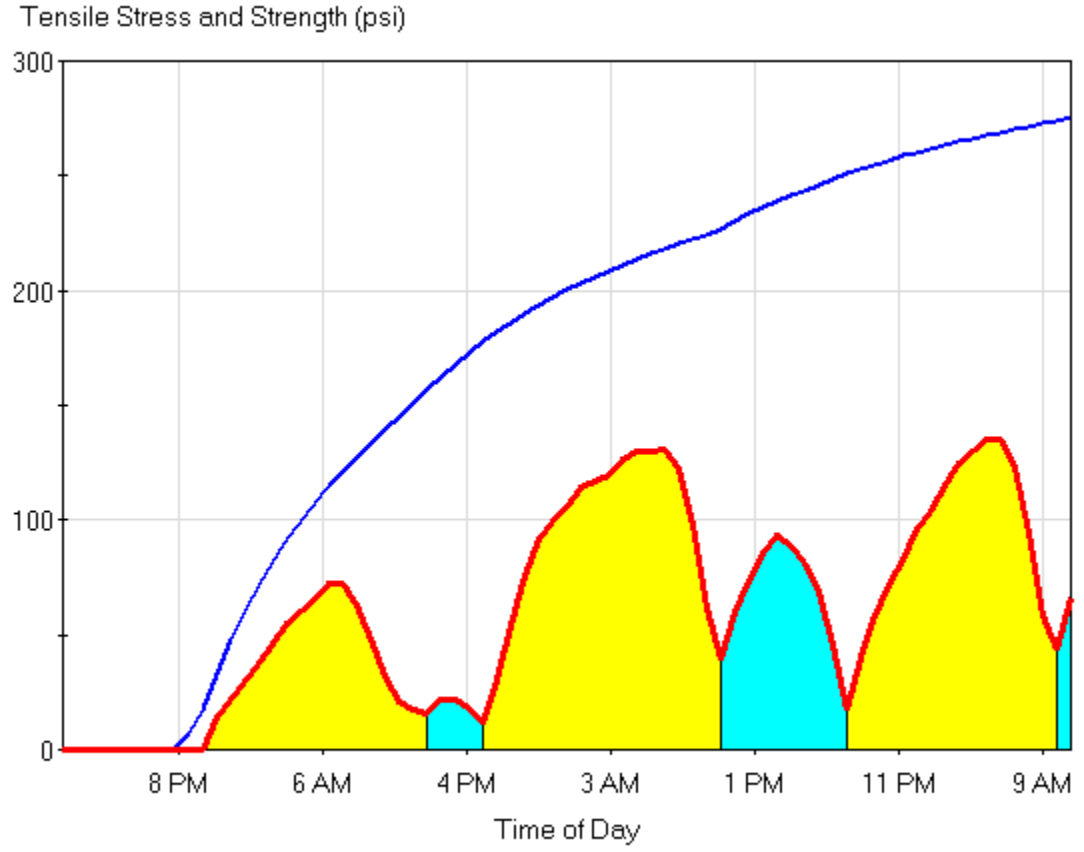

Aug. 18, 1999 Dry base

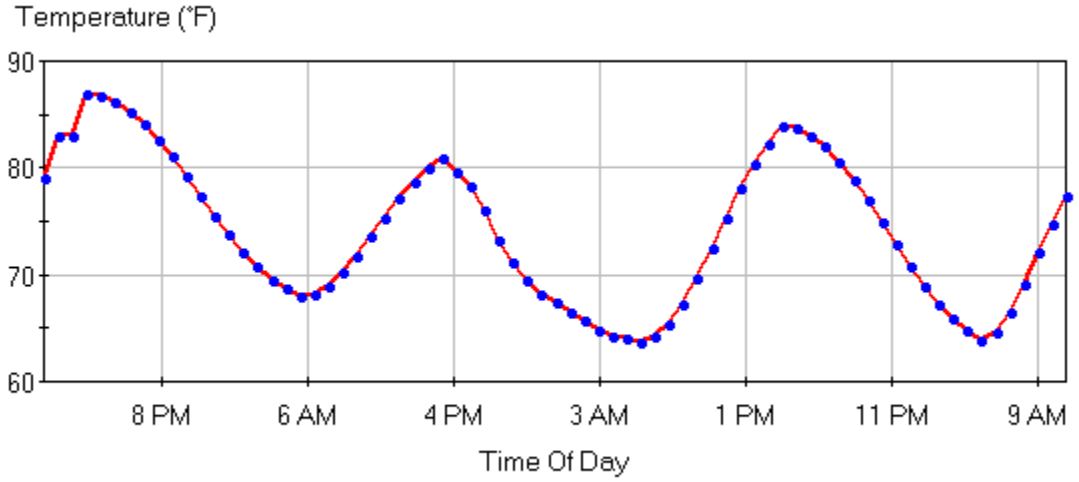

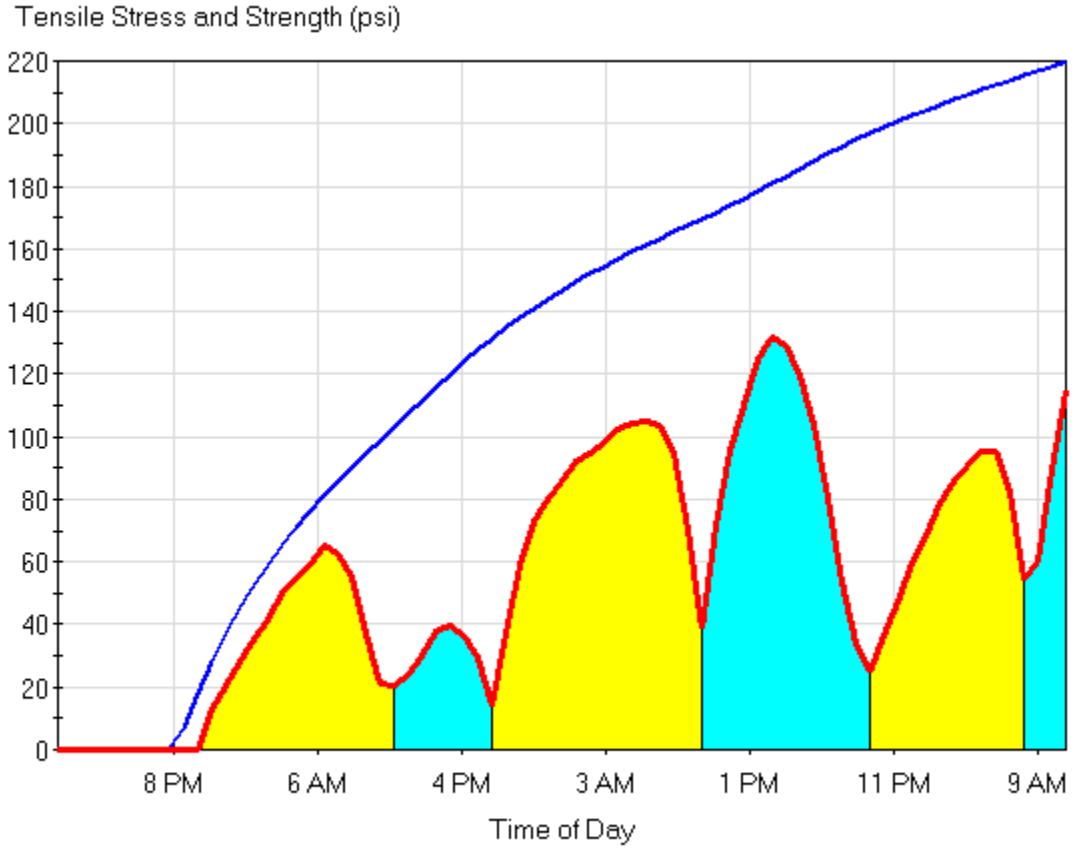

Aug. 20, 1999 Moist base

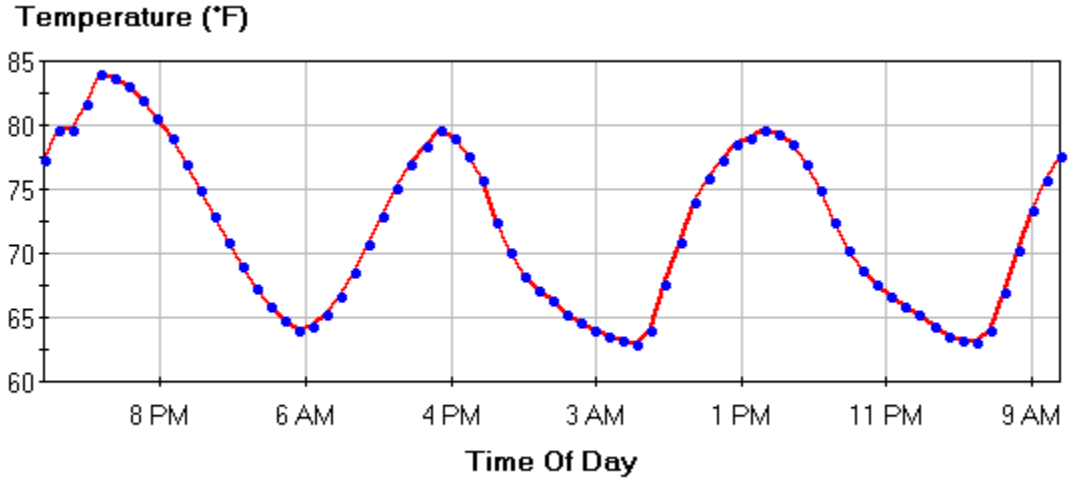

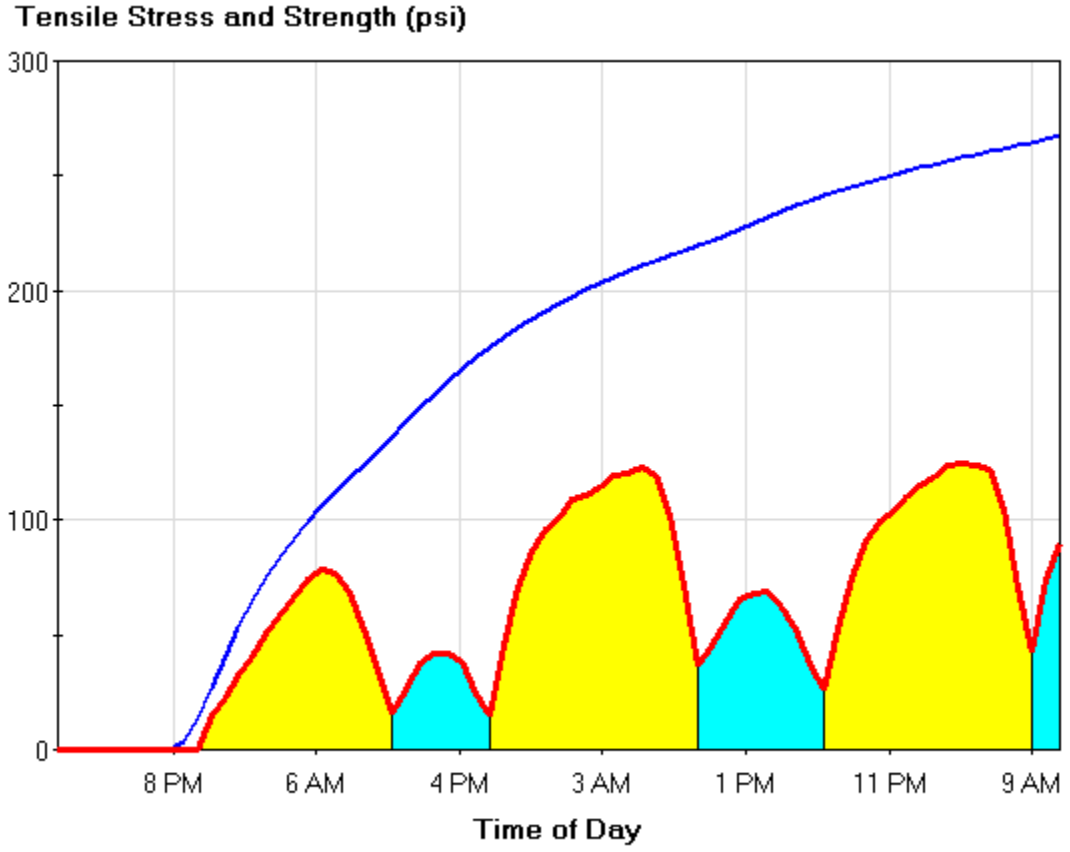

Aug. 20, 1999 Dry base

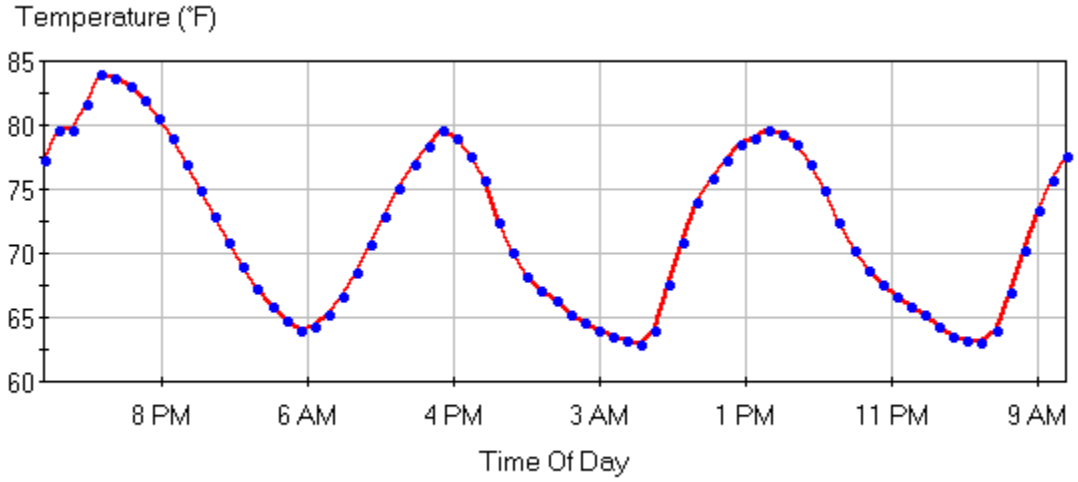

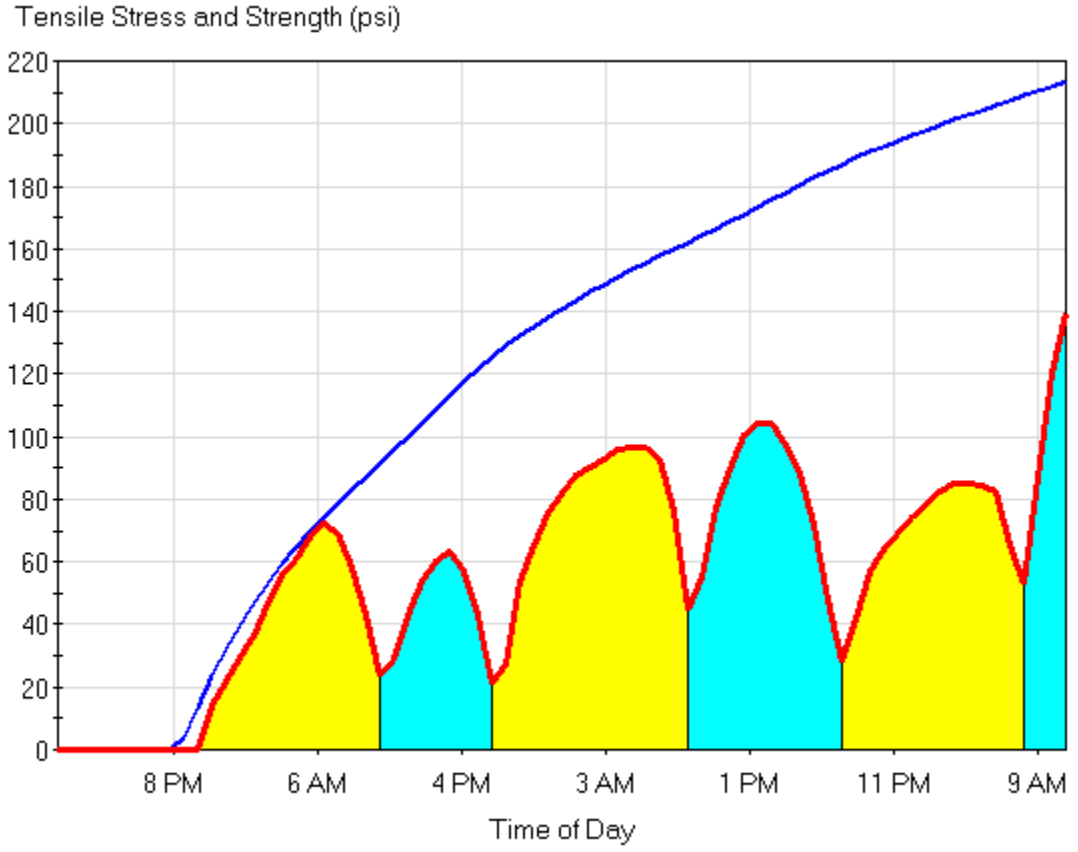

Aug. 23, 1999 Moist base

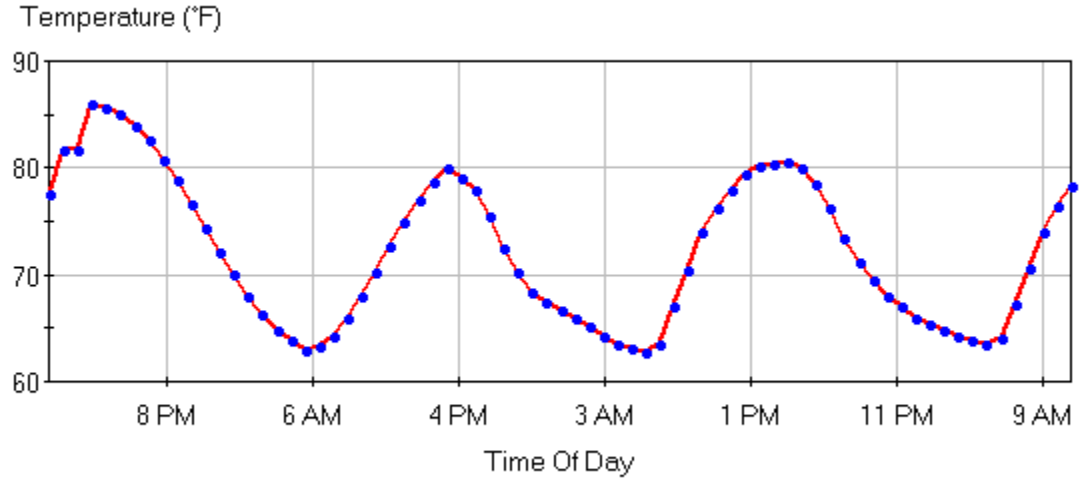

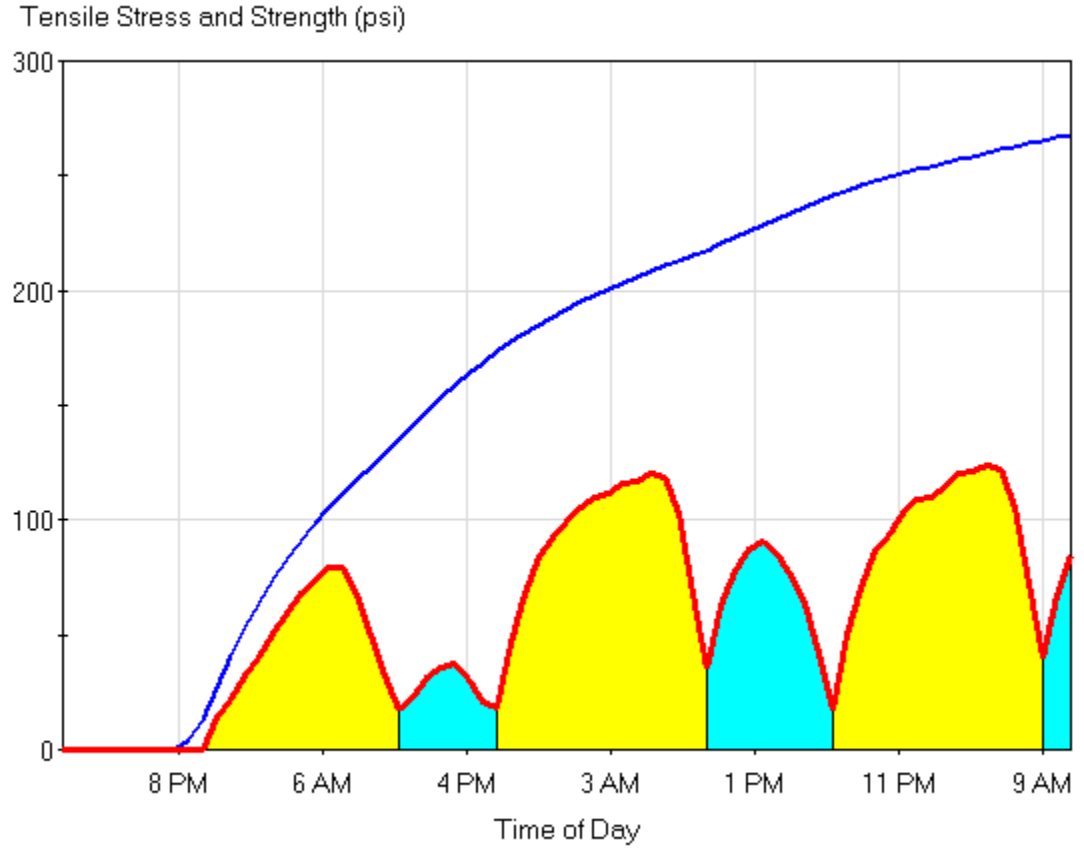

Aug. 23, 1999 Dry base

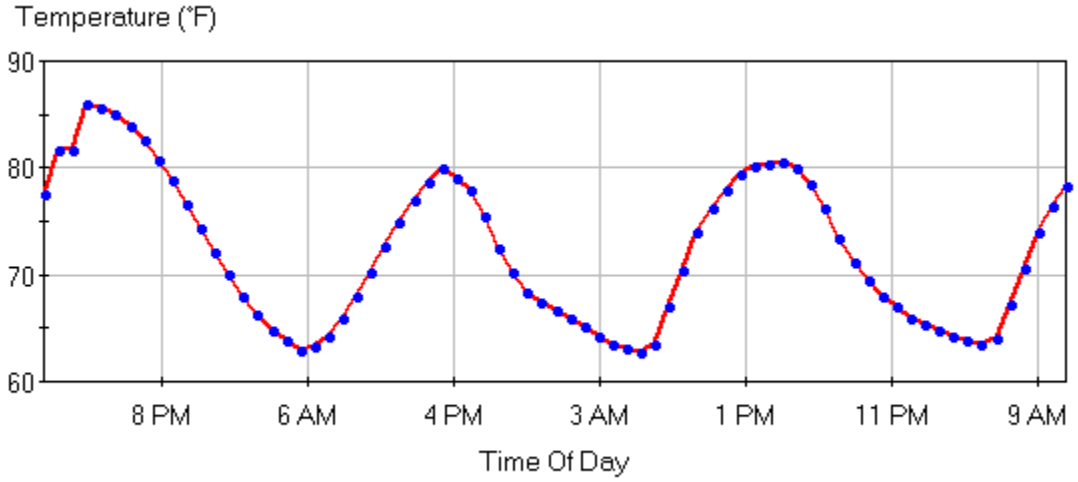

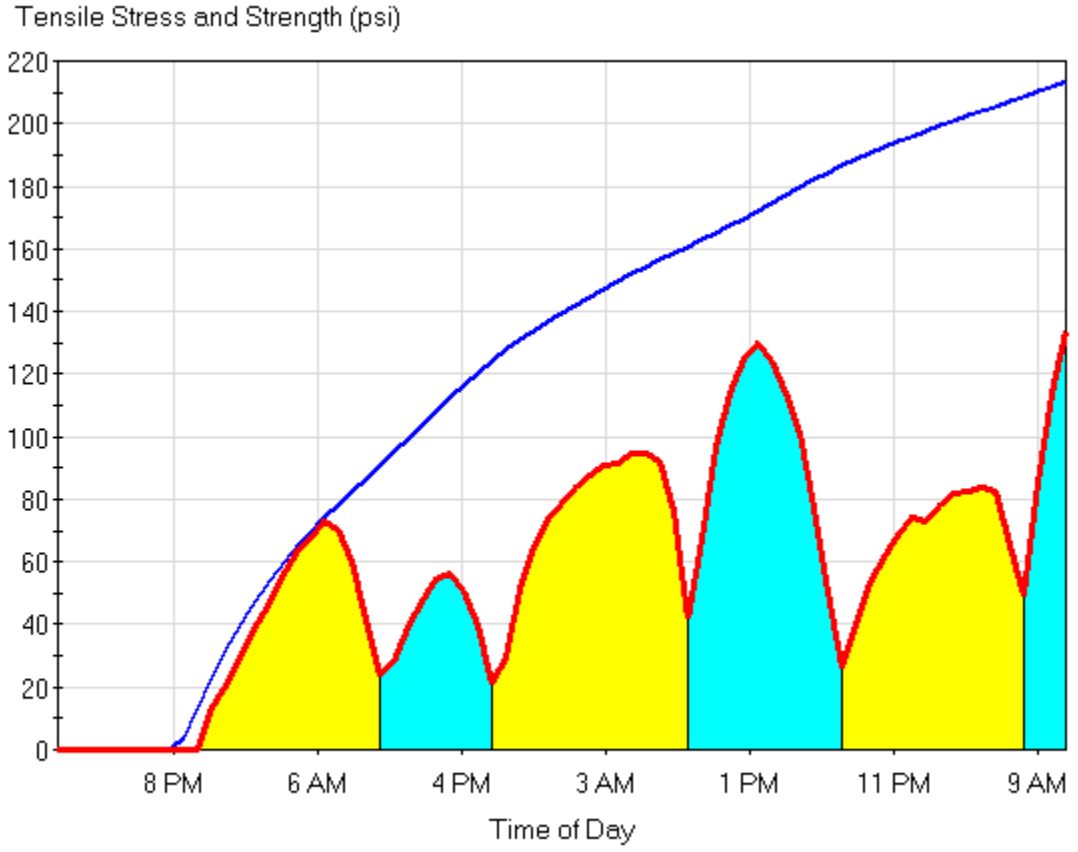

Aug. 27, 1999 Moist base

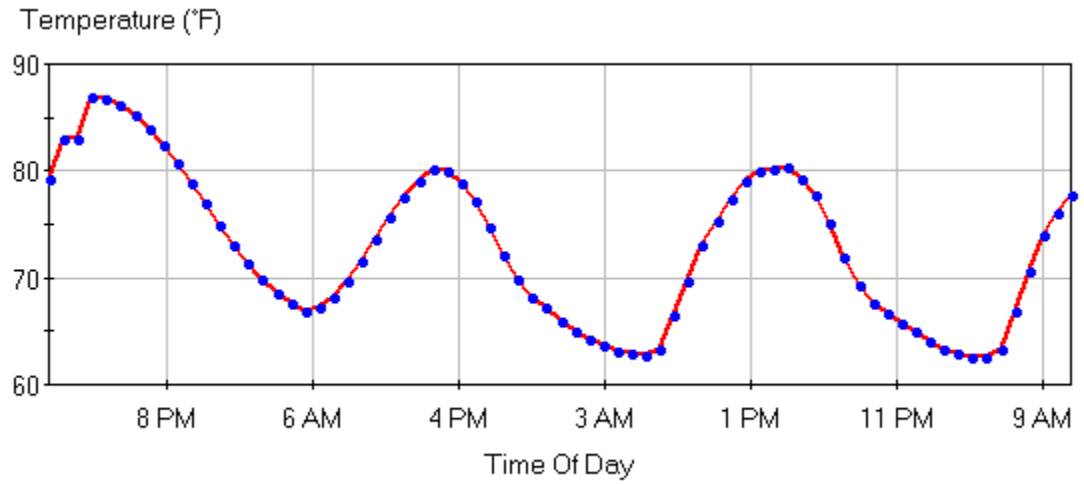

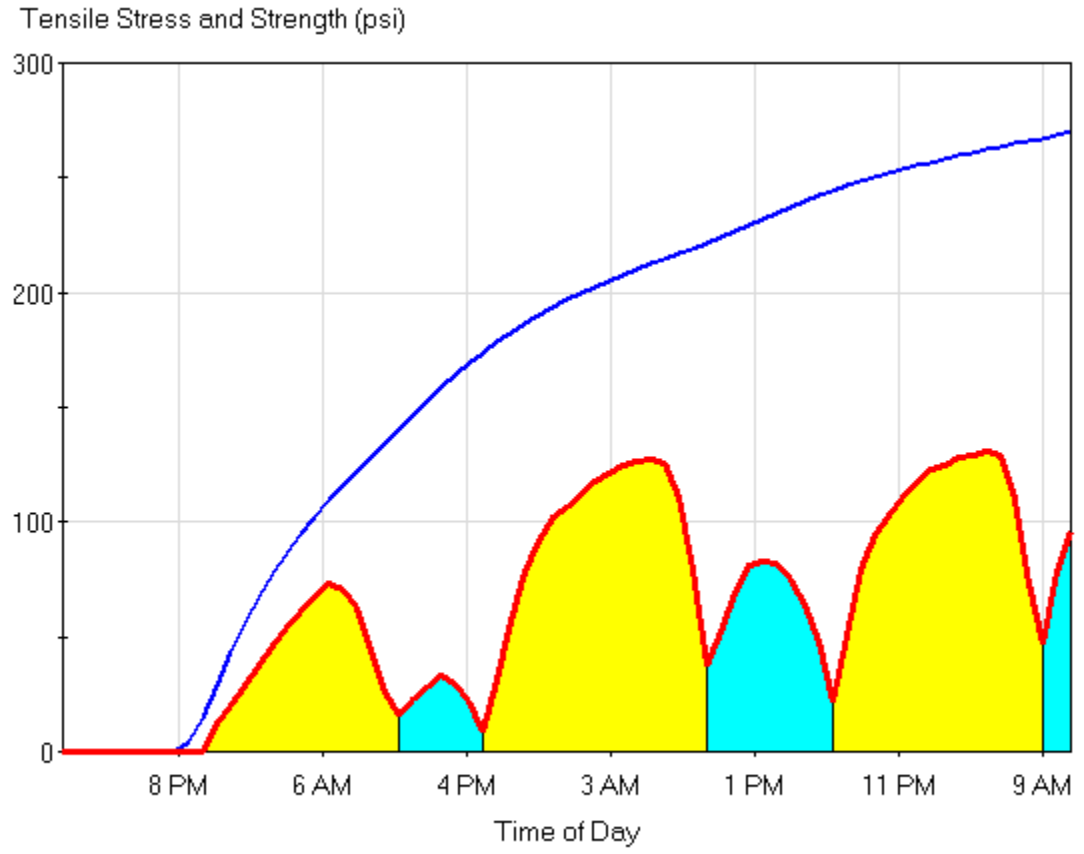

Aug. 27, 1999 Dry base

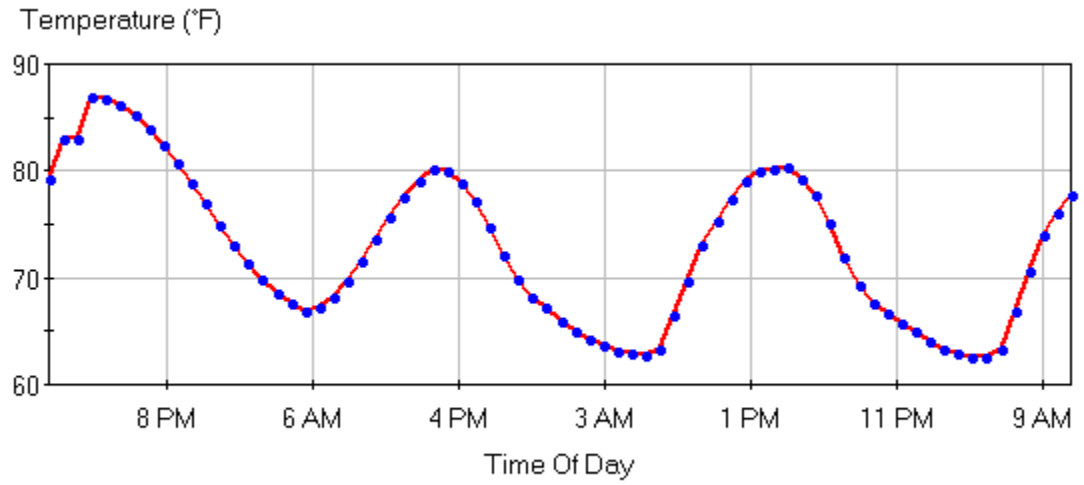

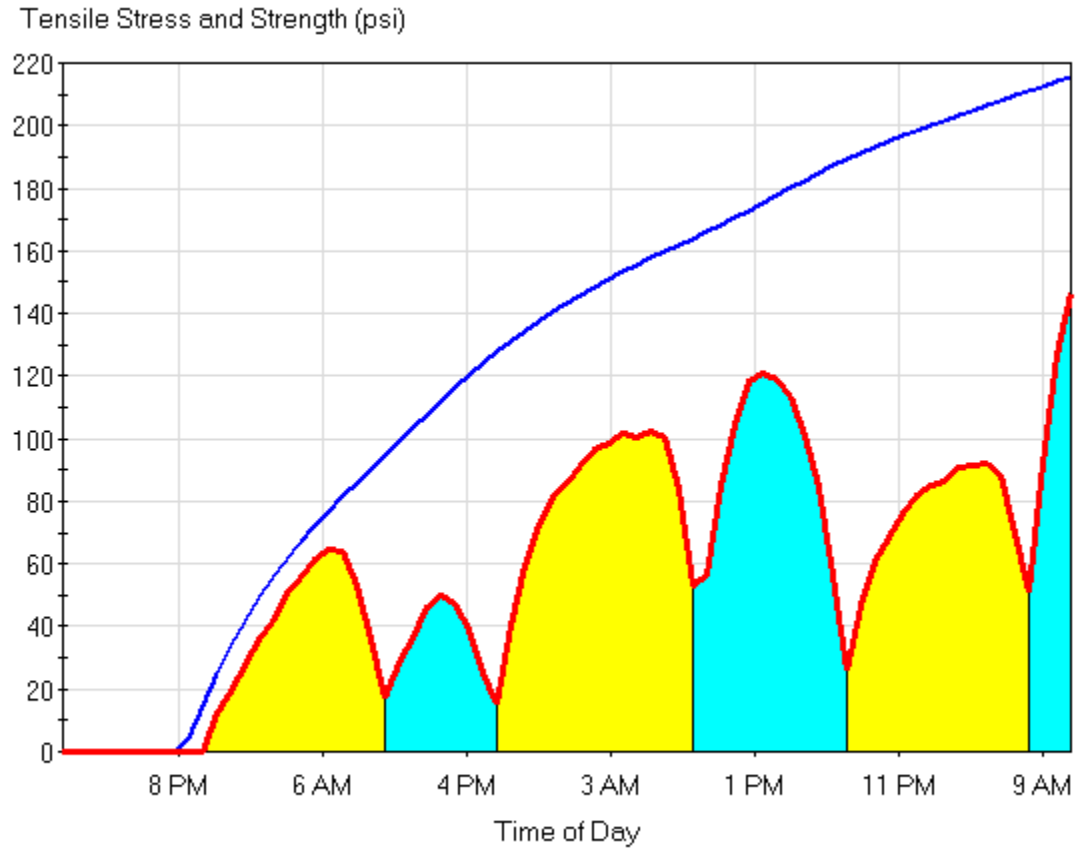

Aug. 30, 1999 Moist base

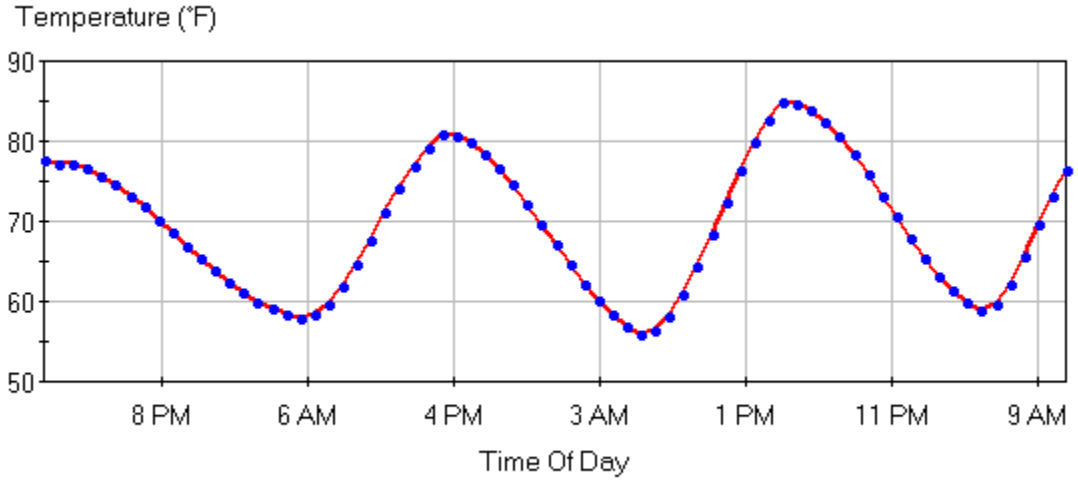

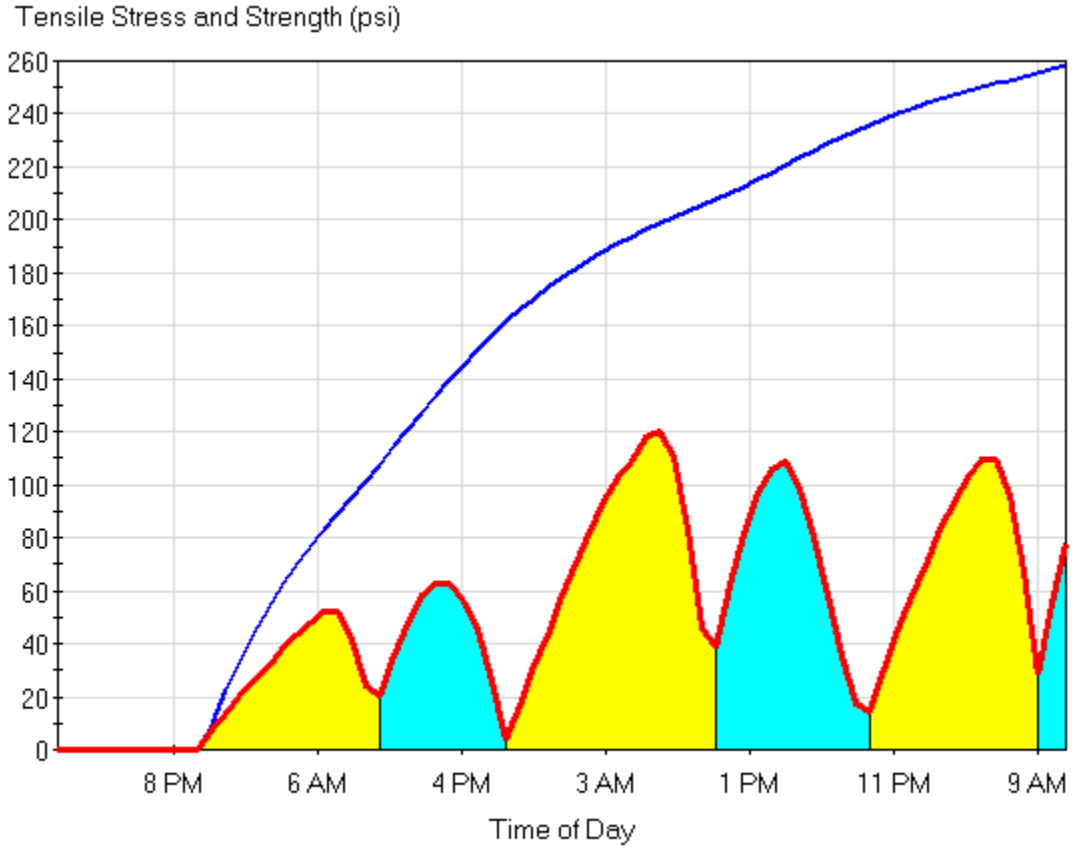

Aug. 30, 1999 Dry base

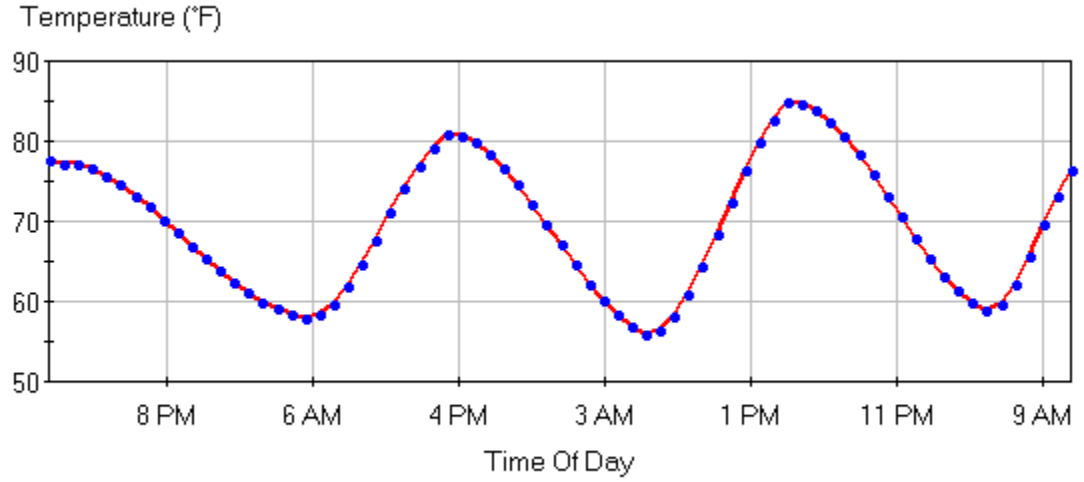

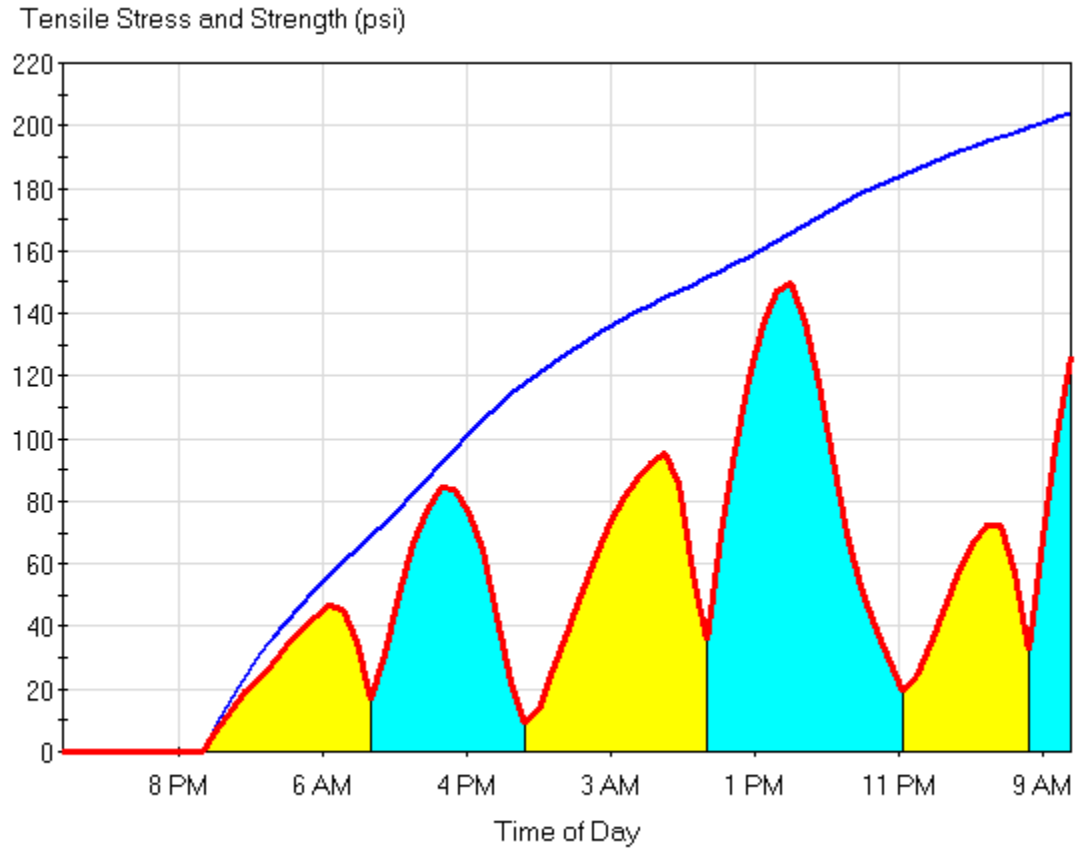

Aug. 31, 1999 Moist base

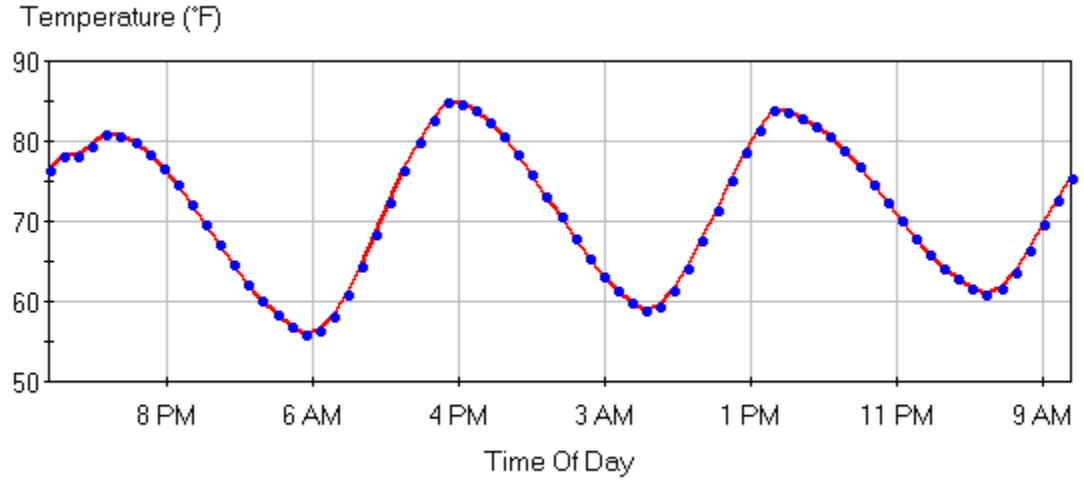

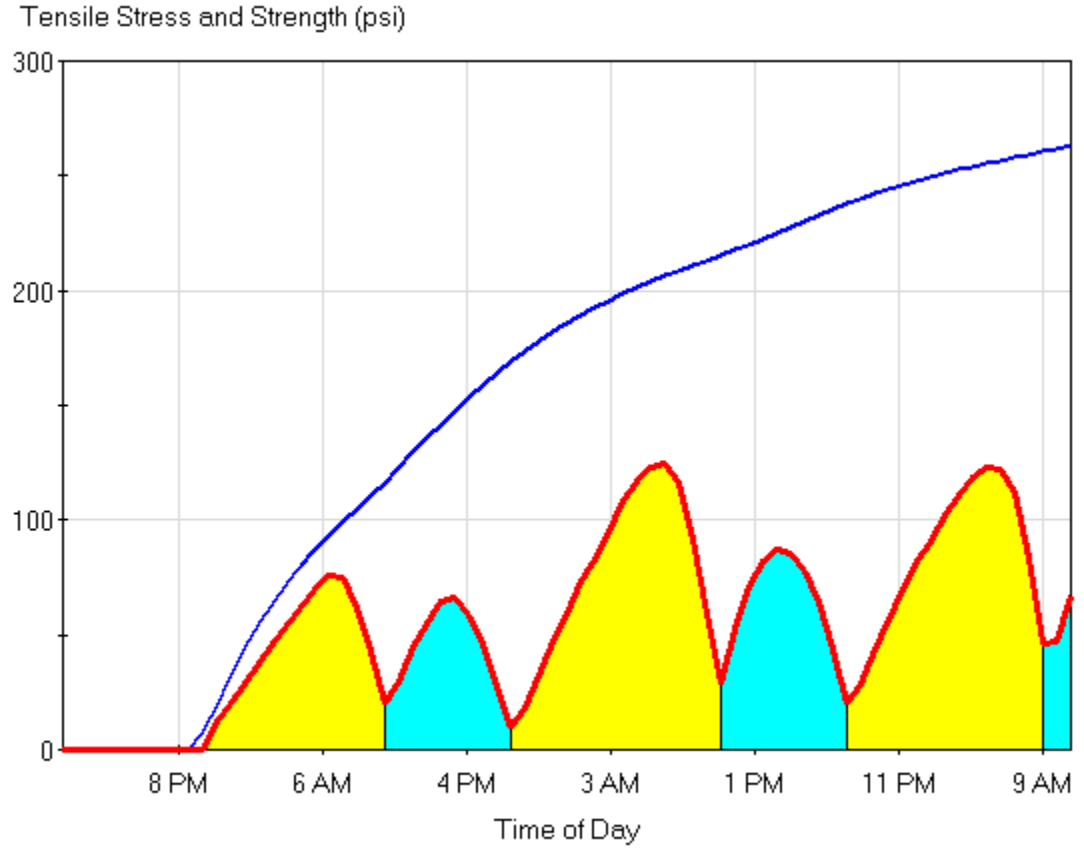

Aug. 31, 1999 Dry base

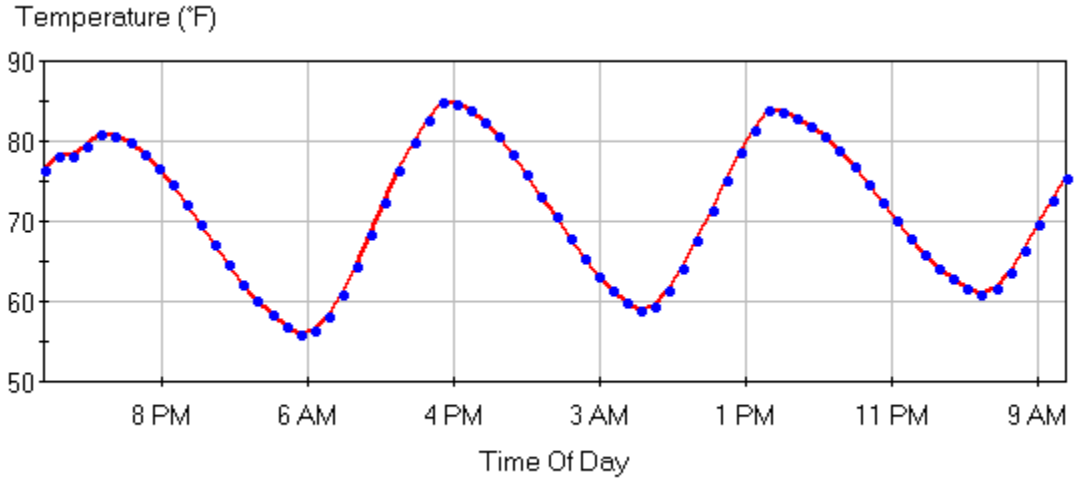

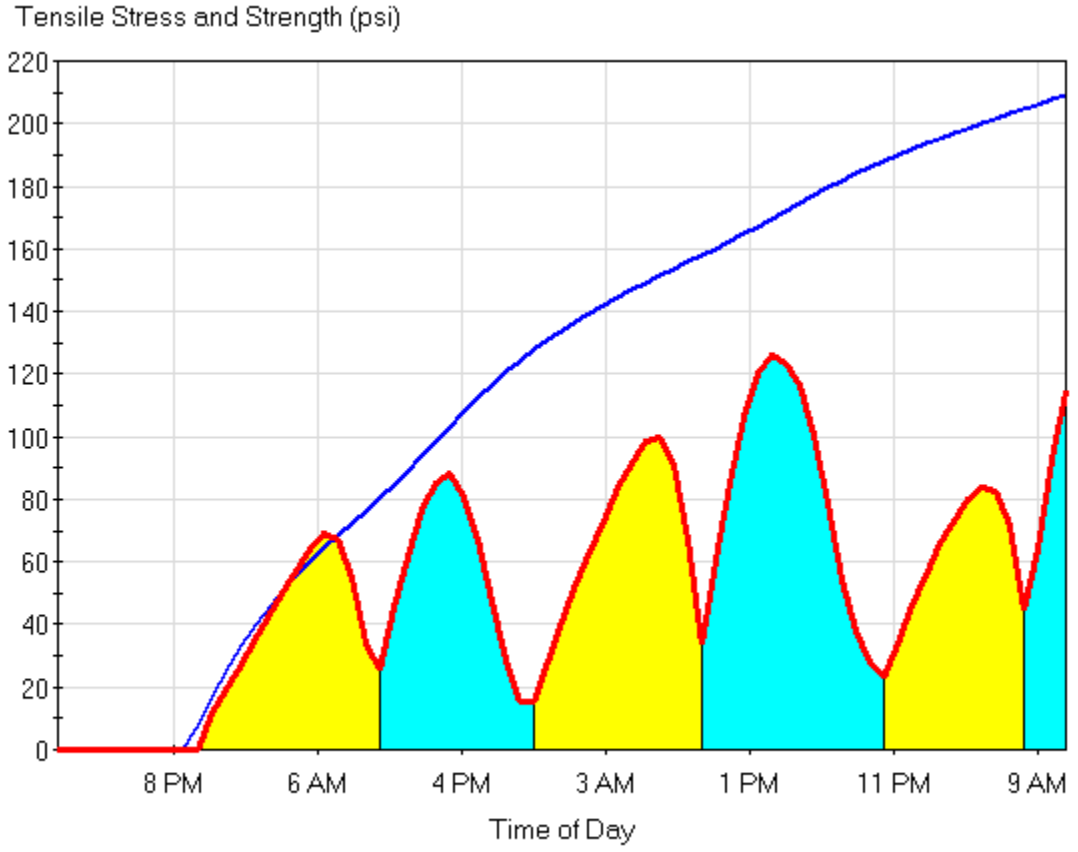

Sept. 2, 1999 Moist base

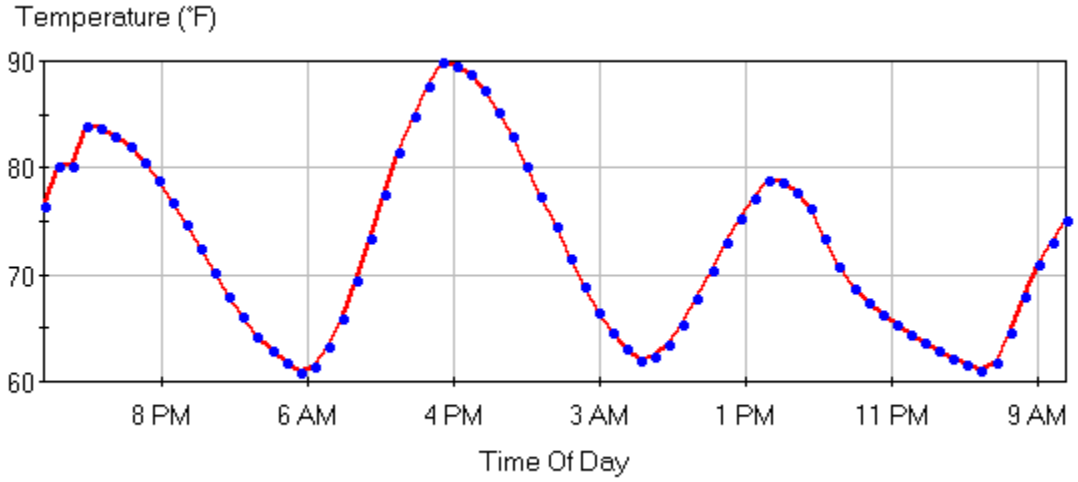

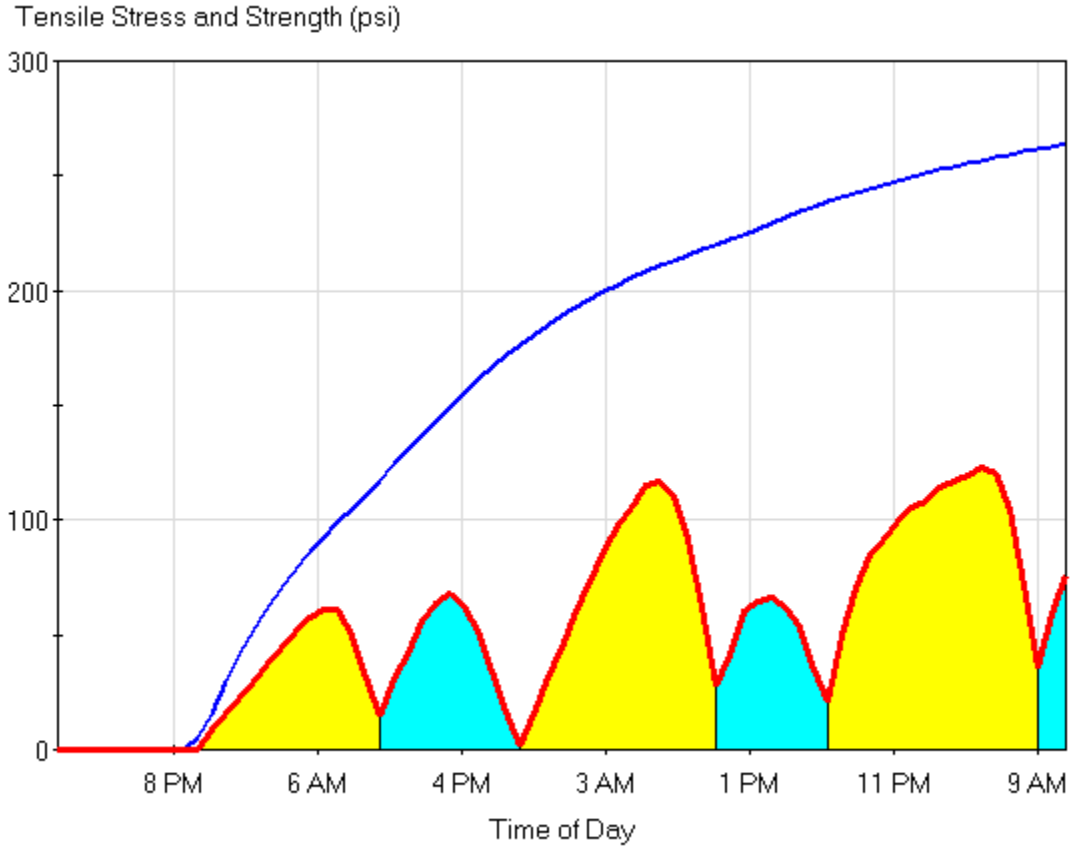

Sept. 2, 1999 Dry base

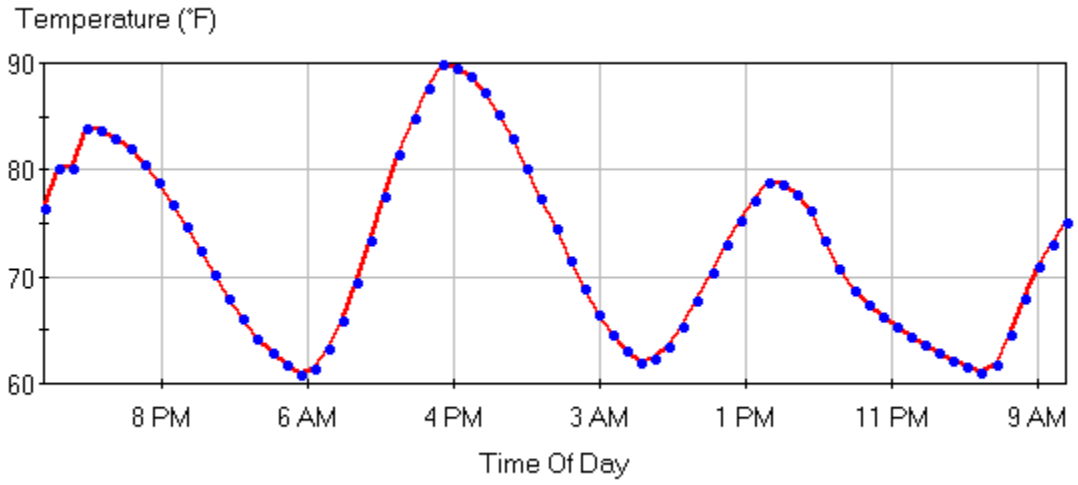

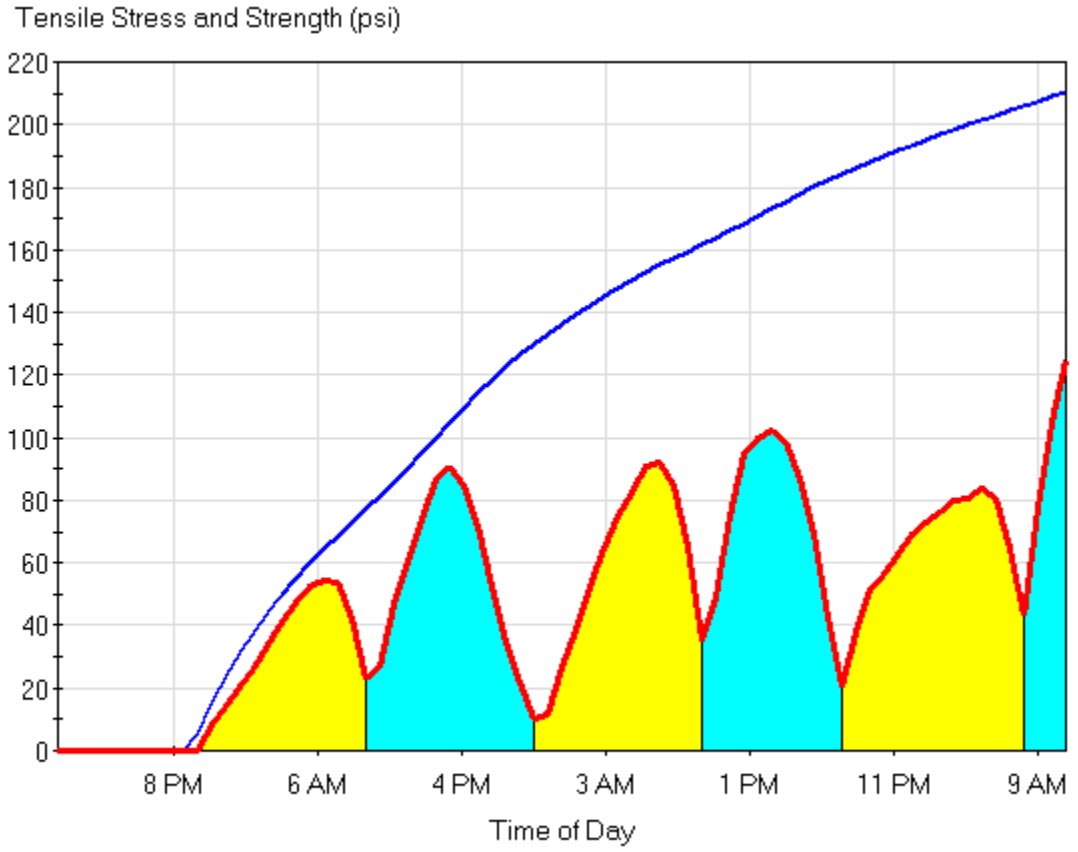

May 12, 2000 Moist base

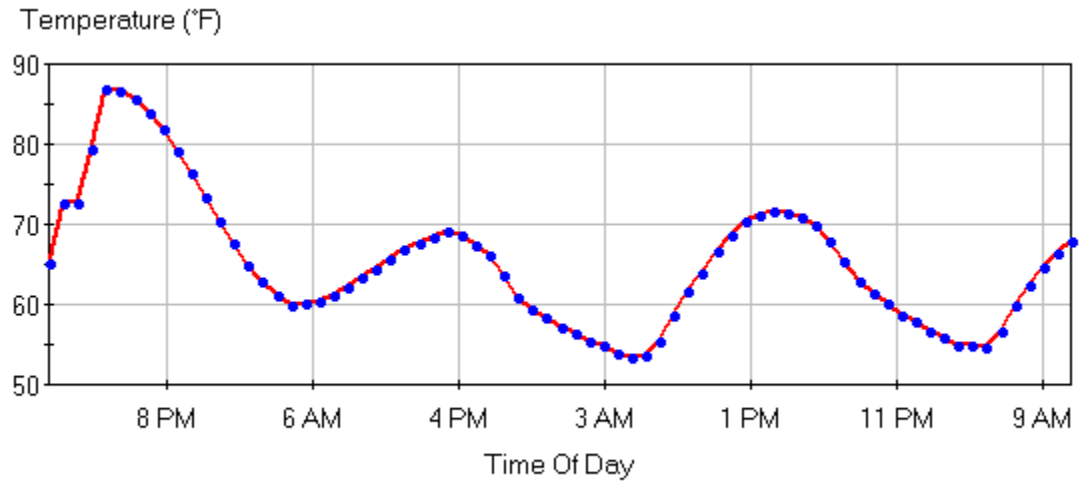

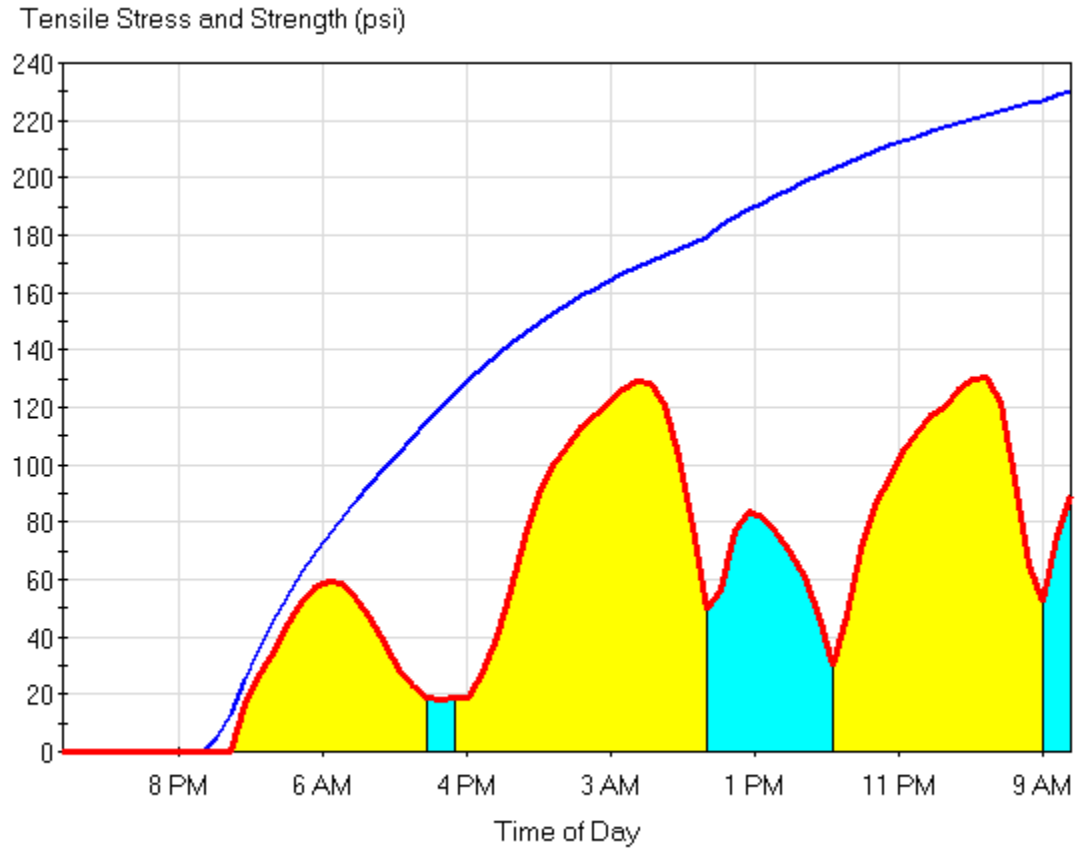

May 12, 2000 Dry base

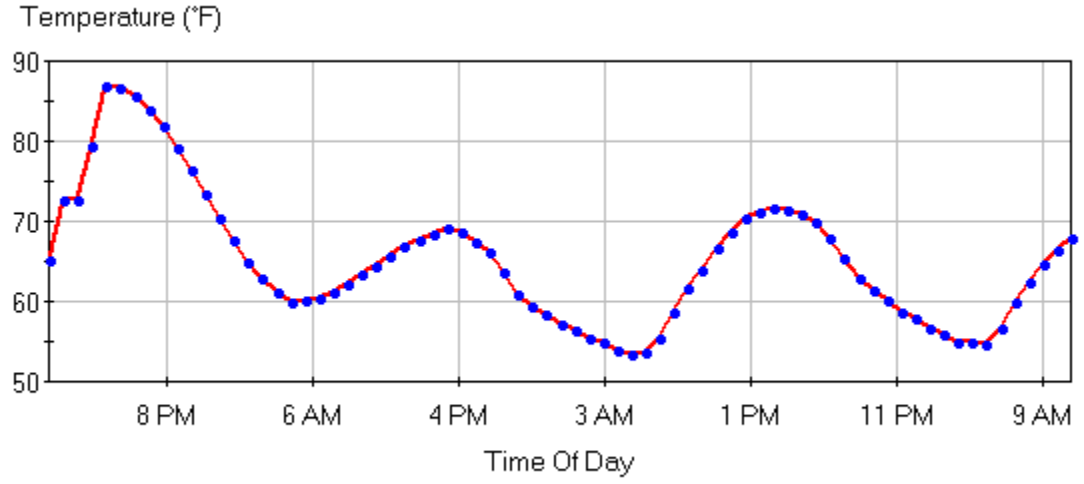

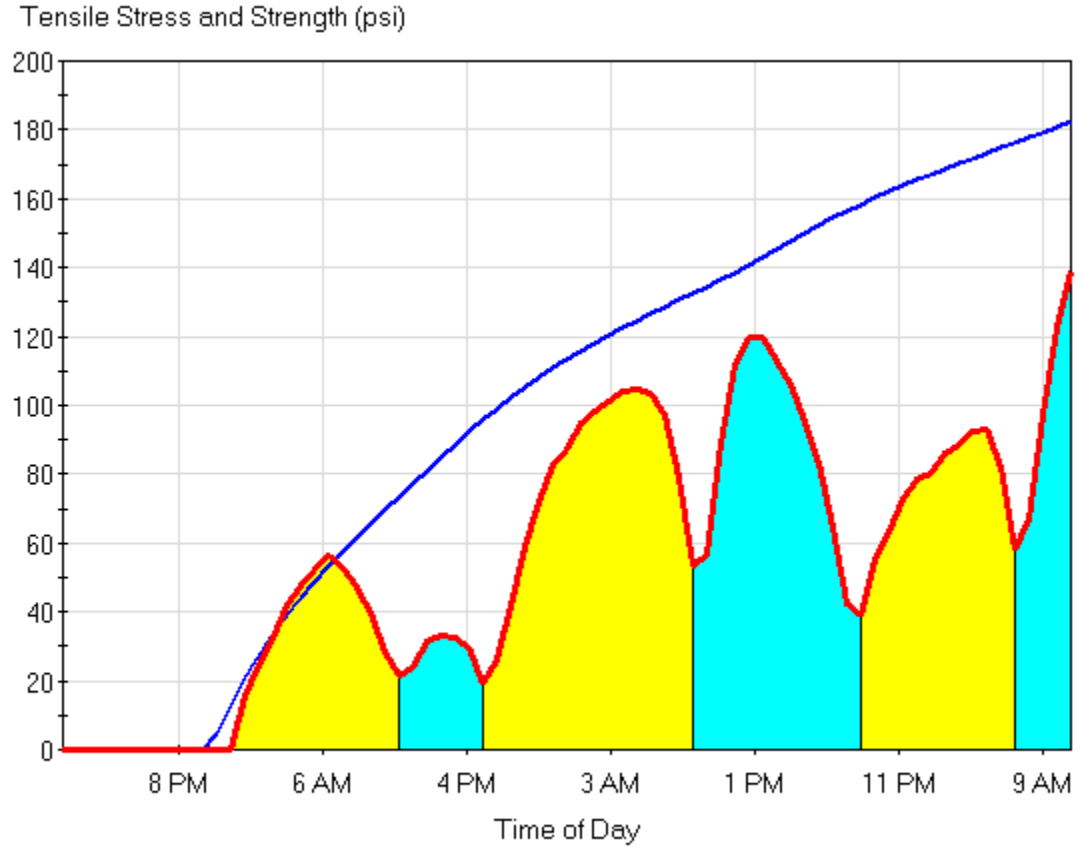

May 15, 2000 Moist base

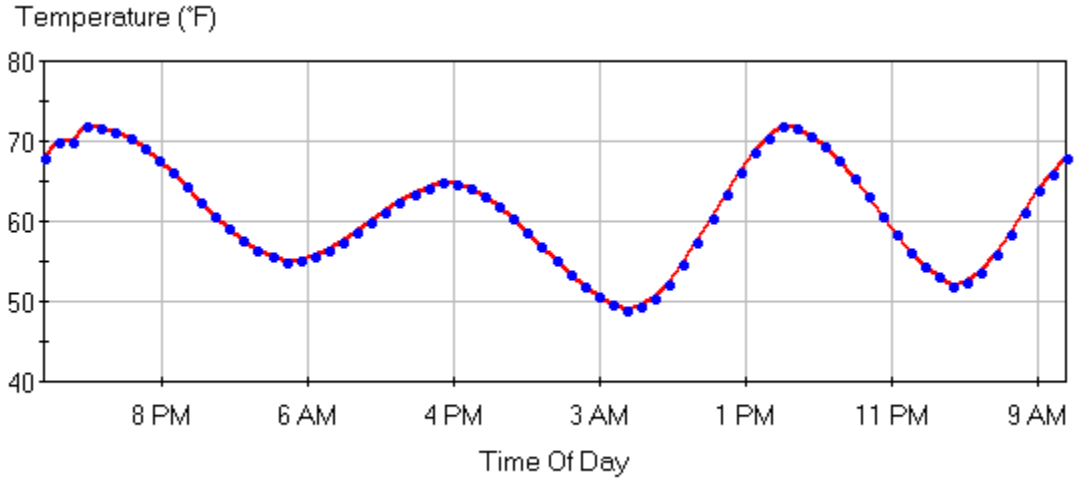

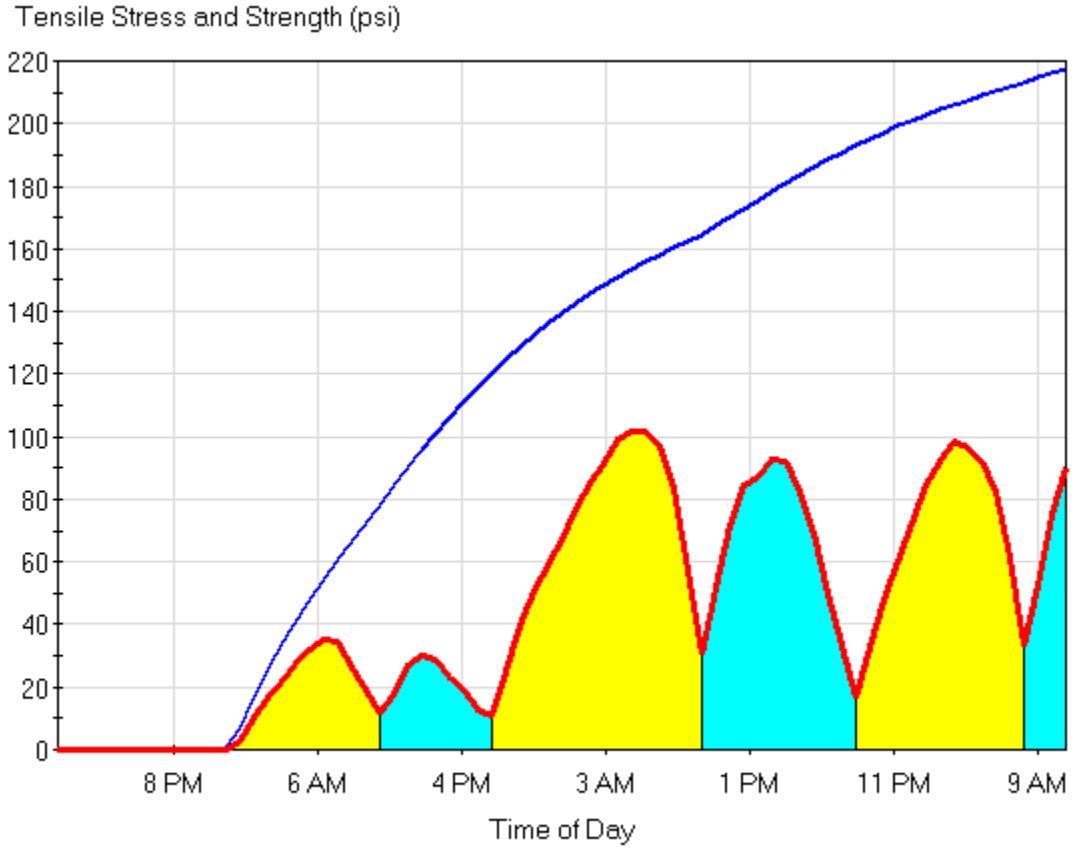

May 15, 2000 Dry base

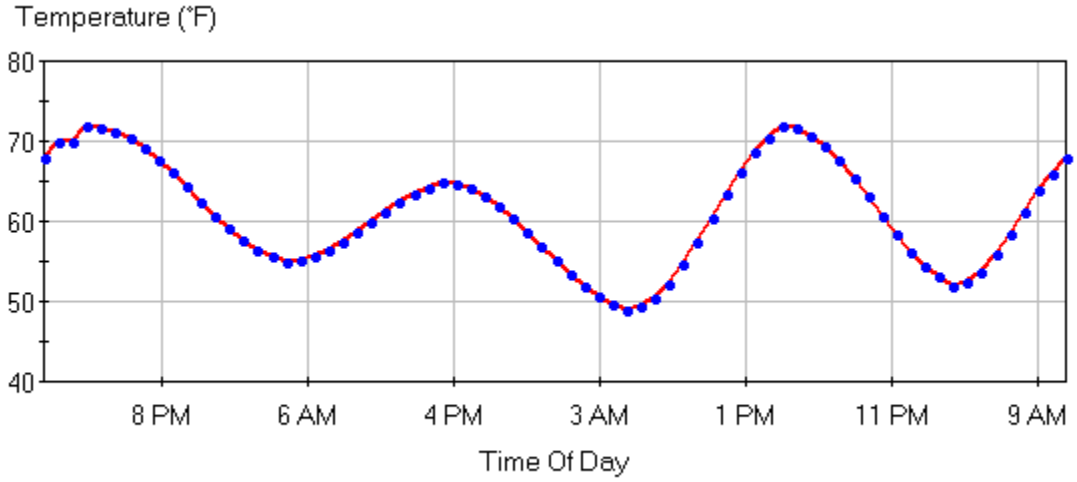

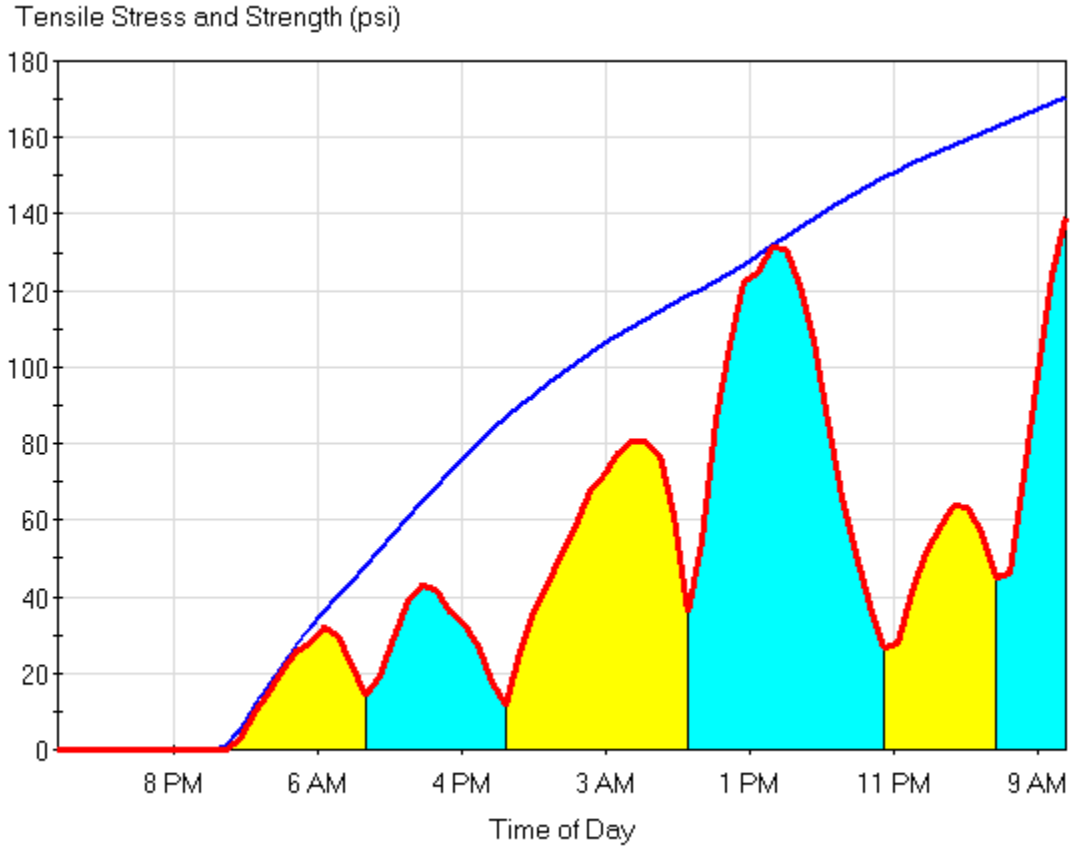

May 16, 2000 Moist base

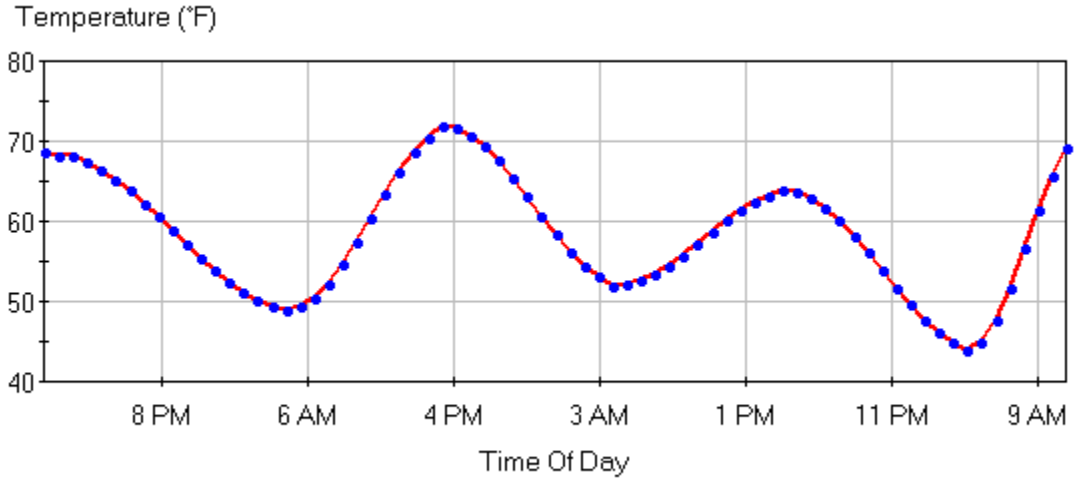

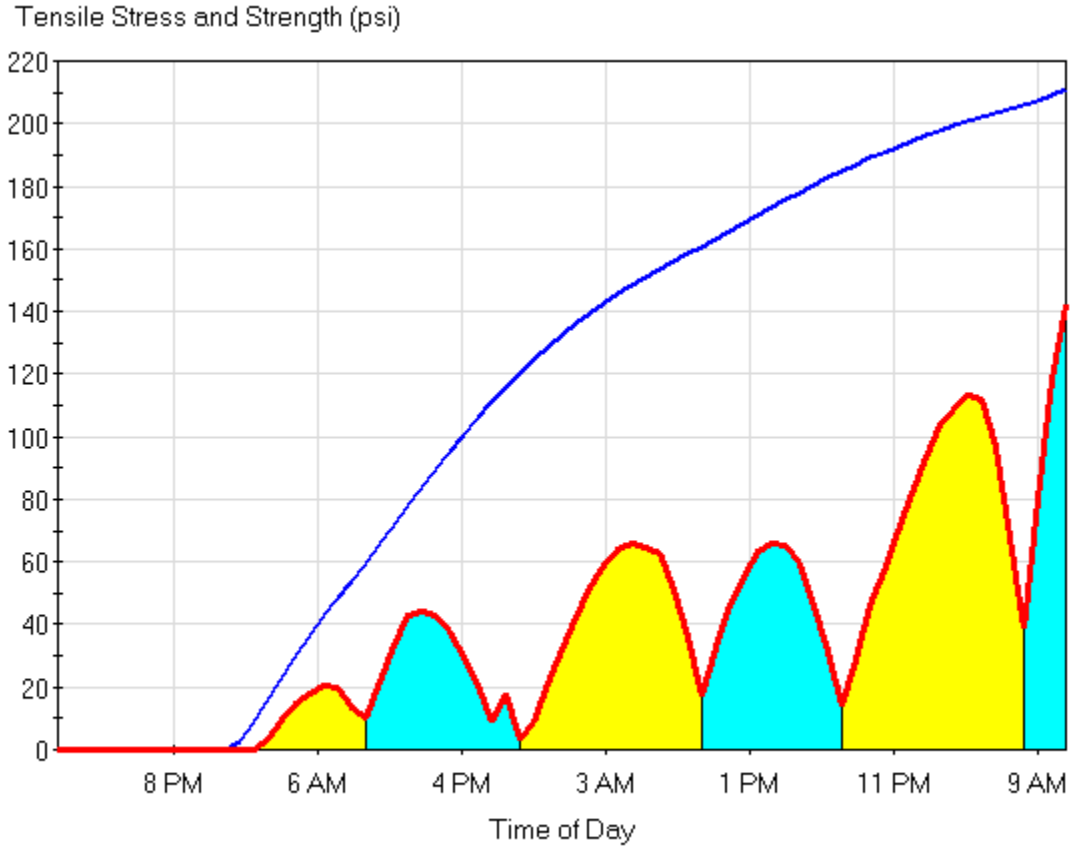

May 16, 2000 Dry base

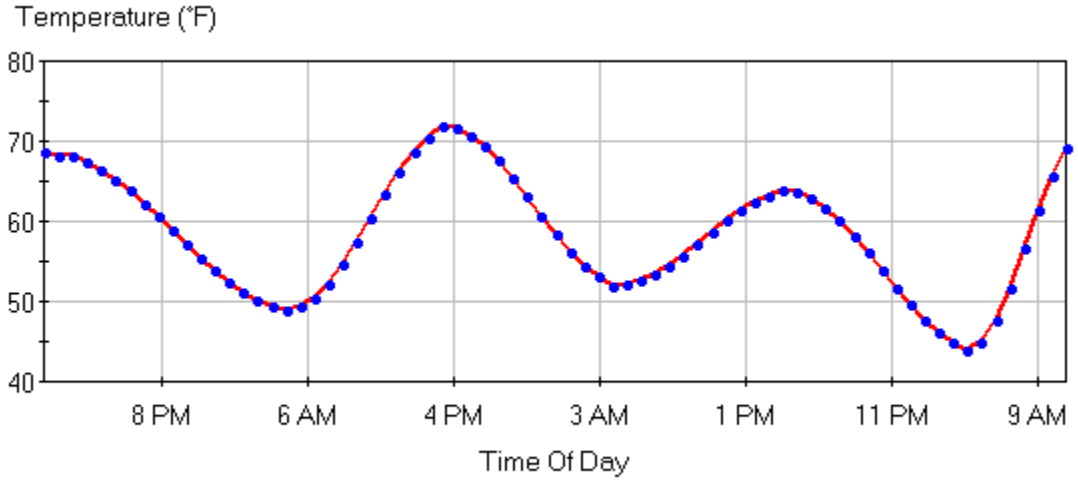

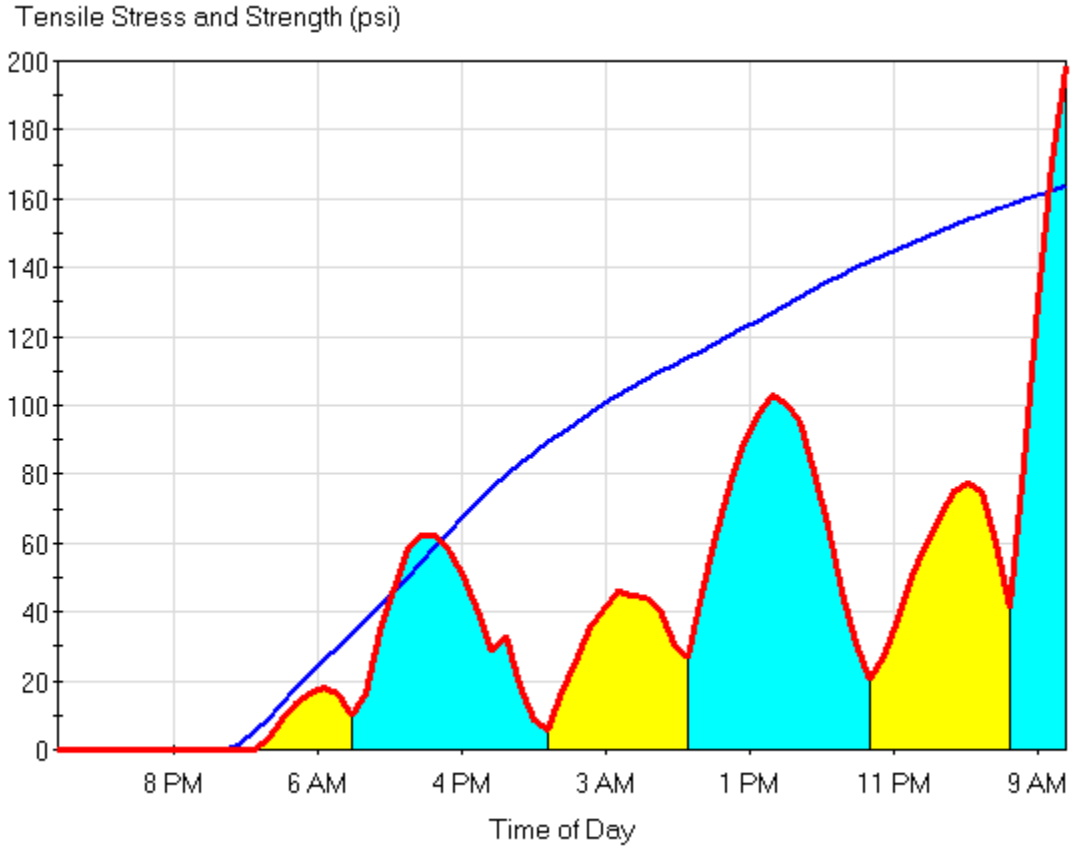

May 17, 2000 Moist base

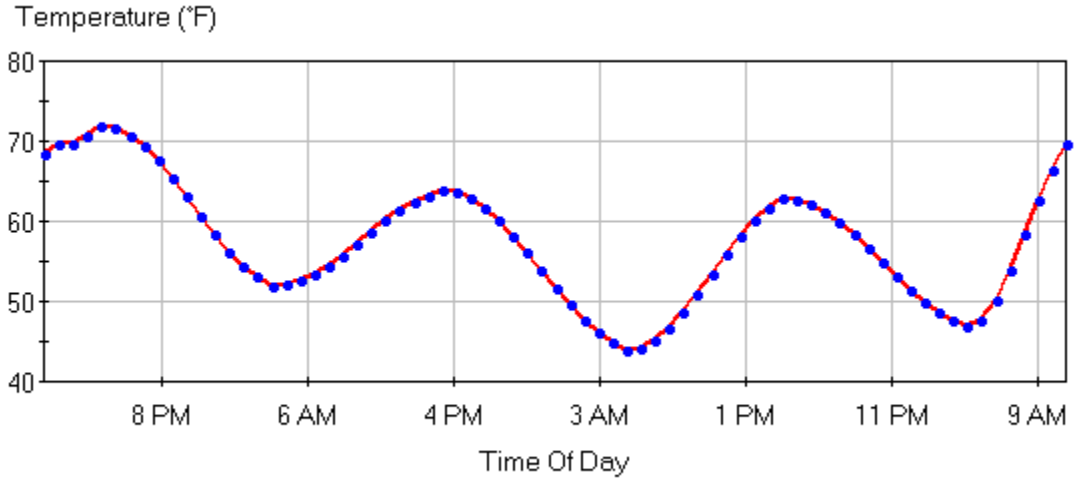

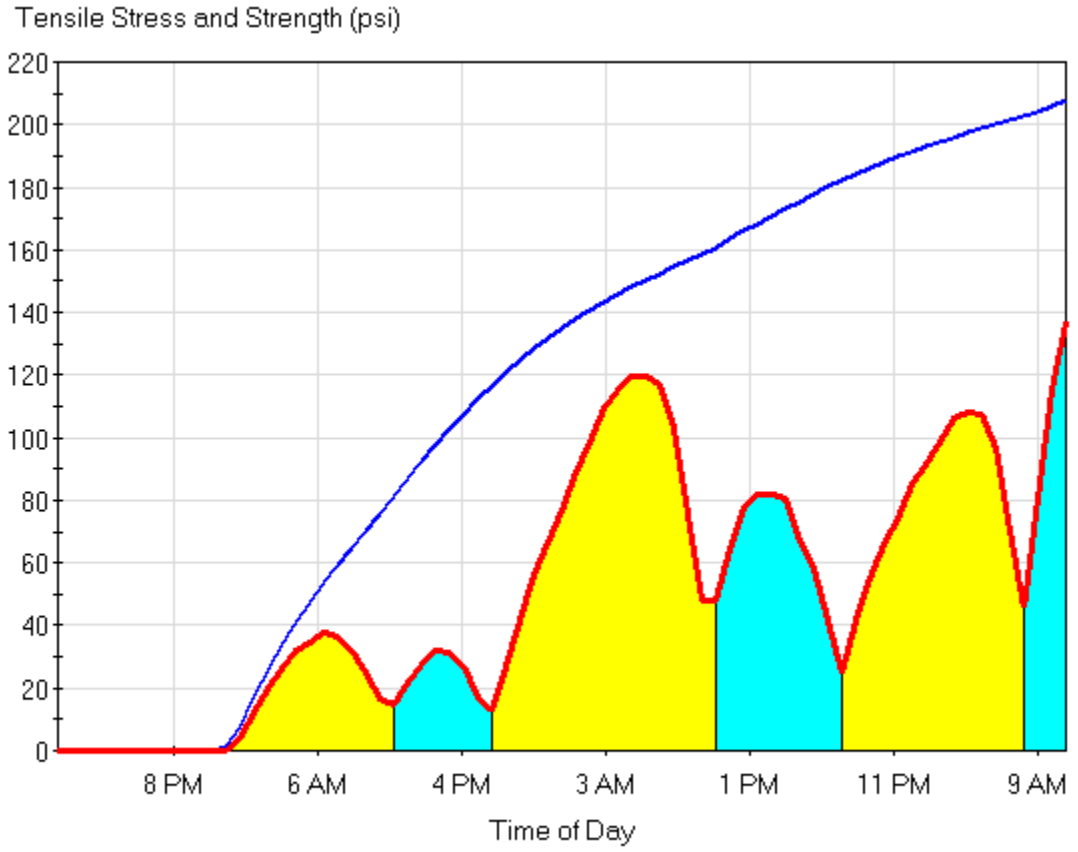

May 17, 2000 Dry base

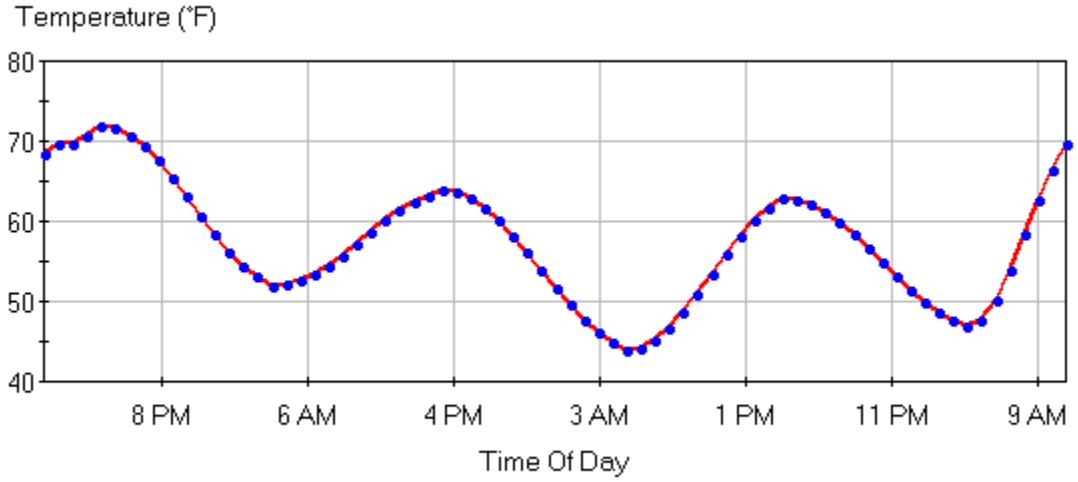

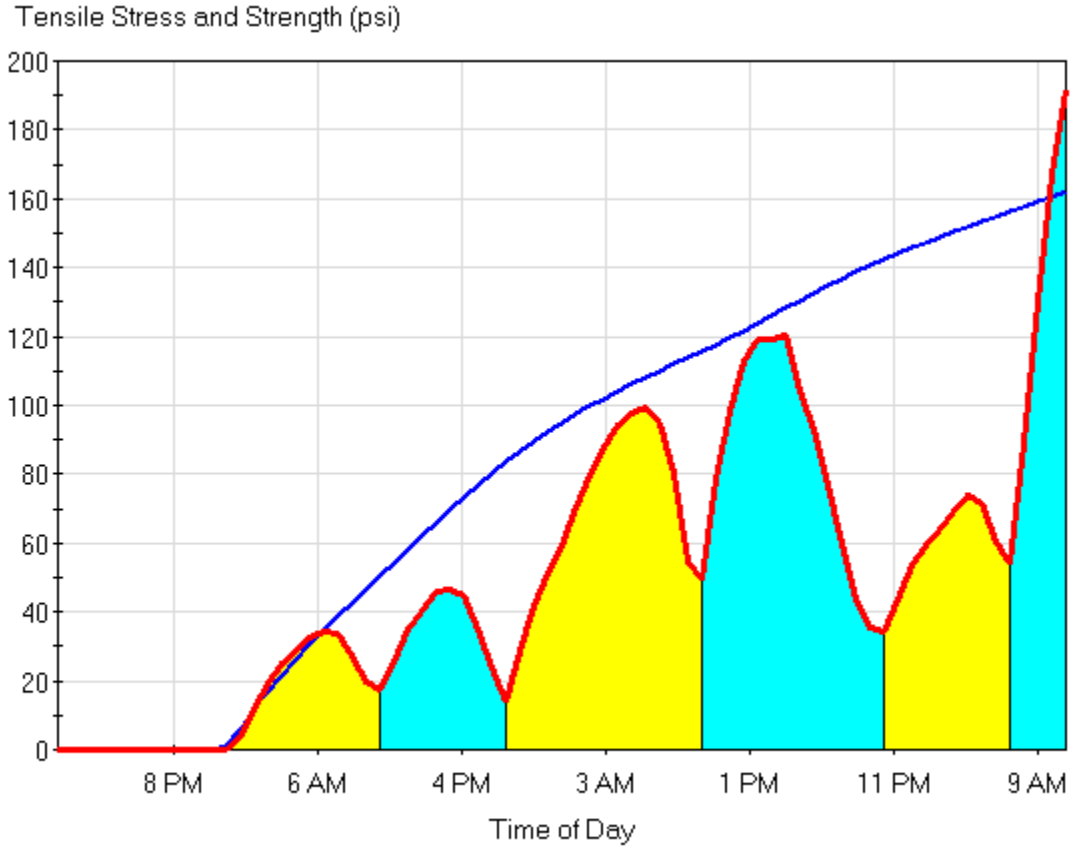

May 18, 2000 Moist base

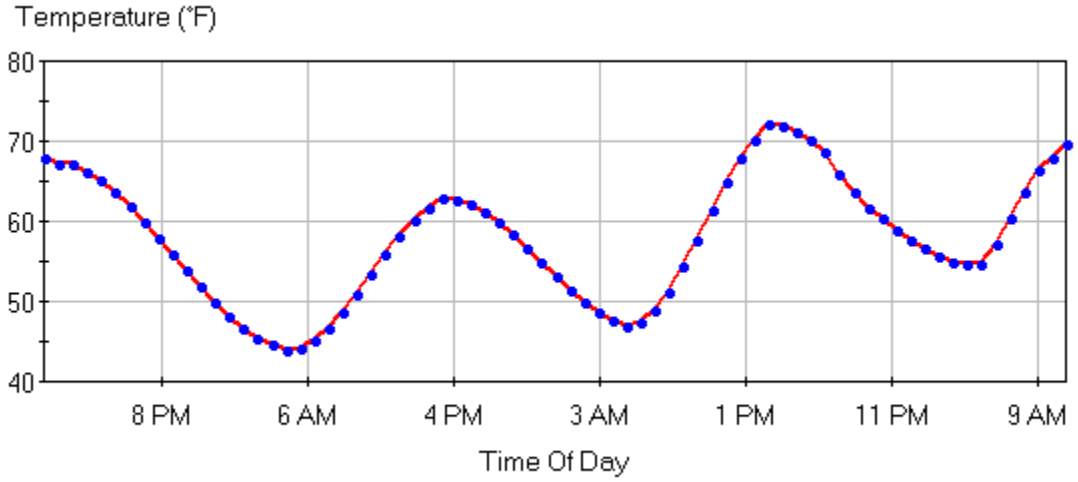

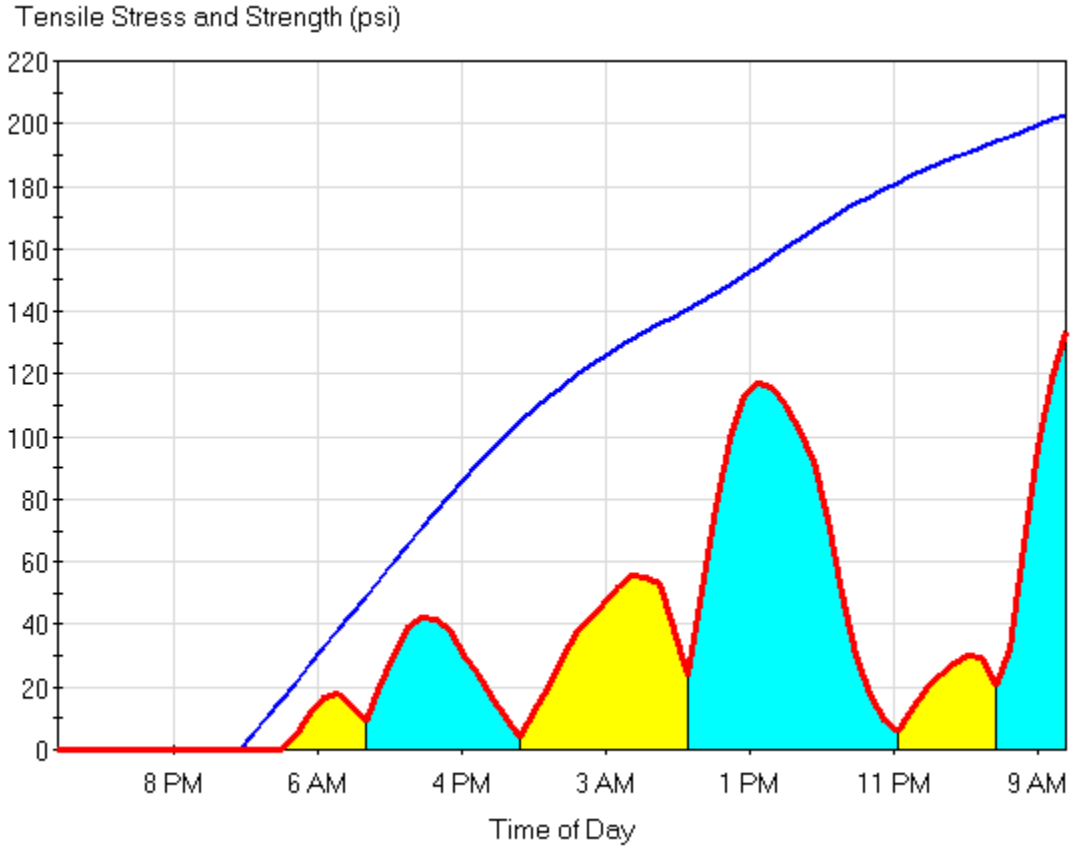

May 18, 2000 Dry base

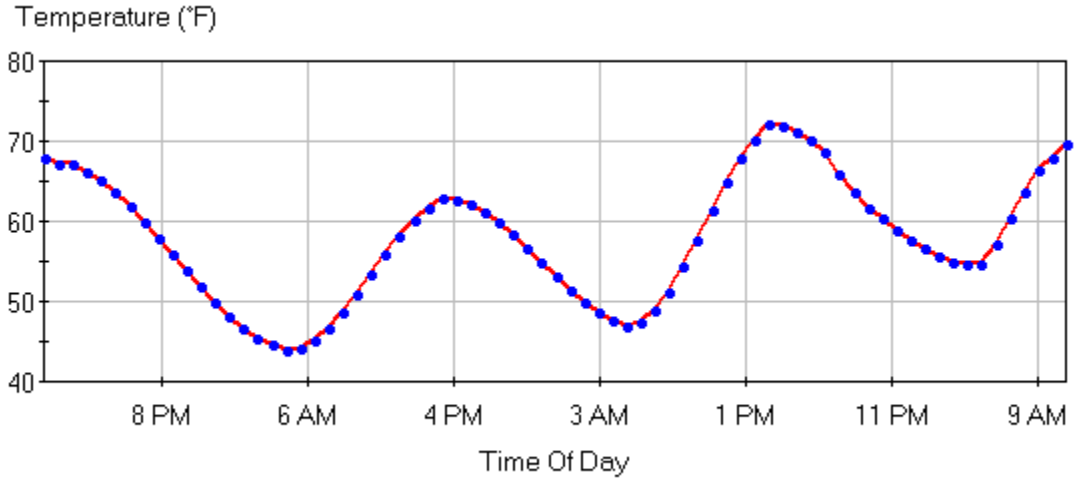

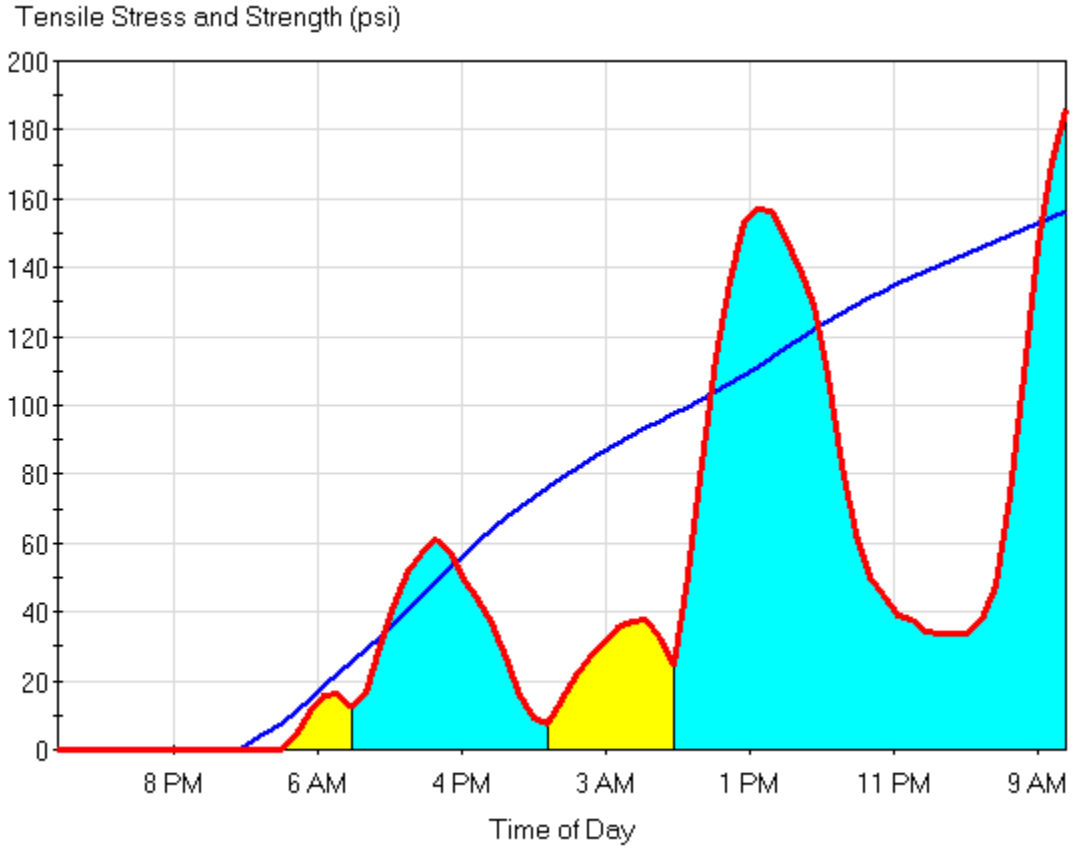

May 19, 2000 Moist base

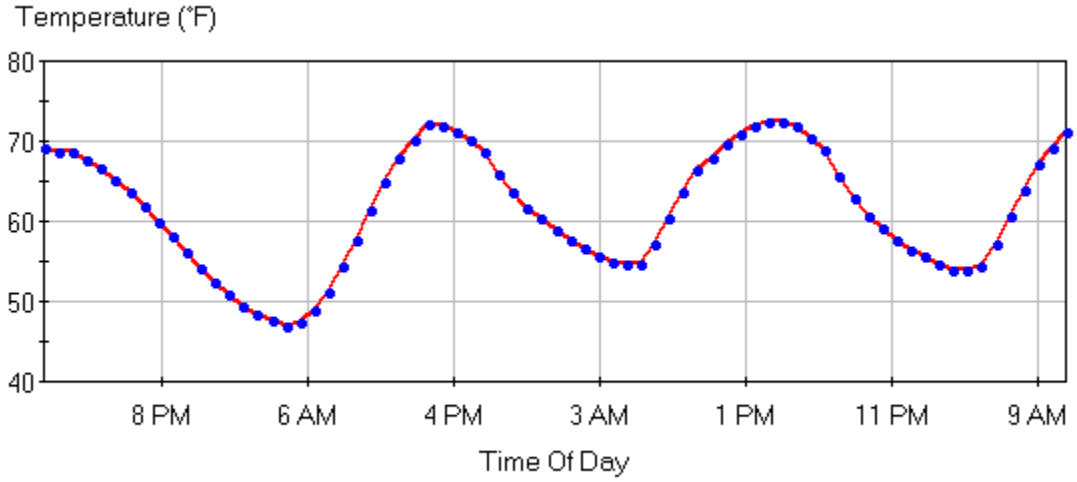

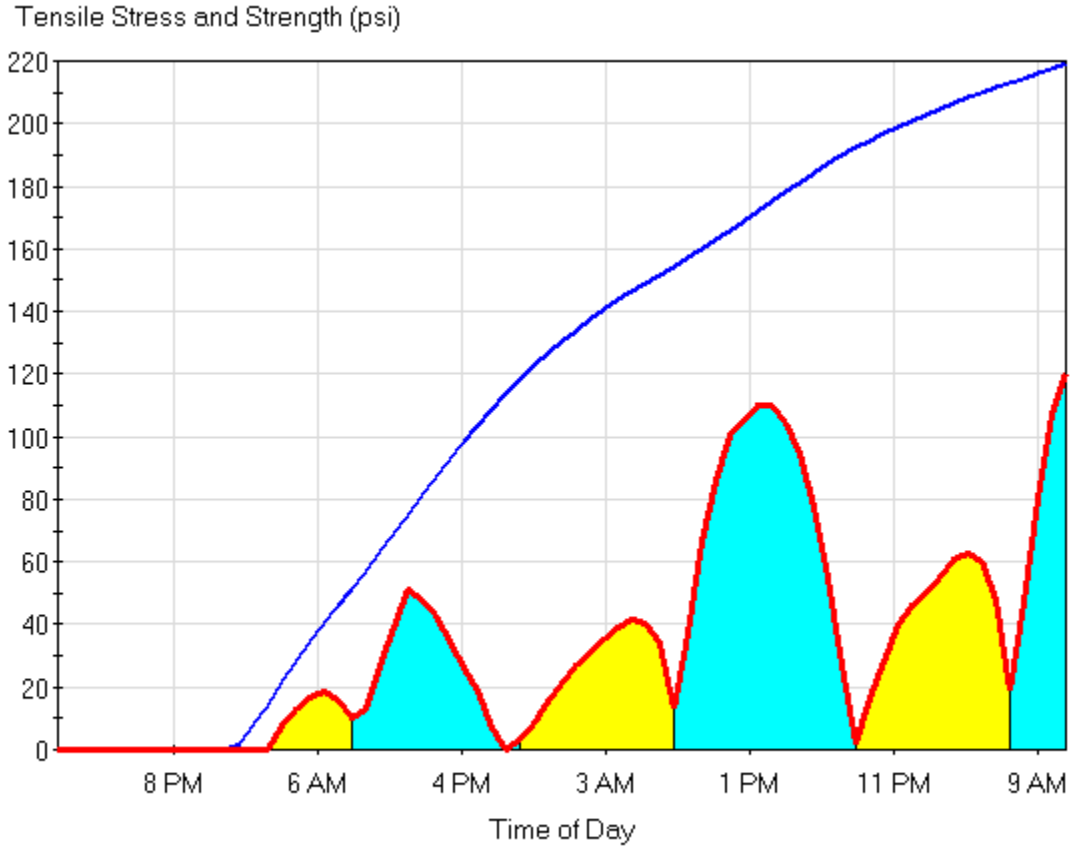

May 19, 2000 Dry base

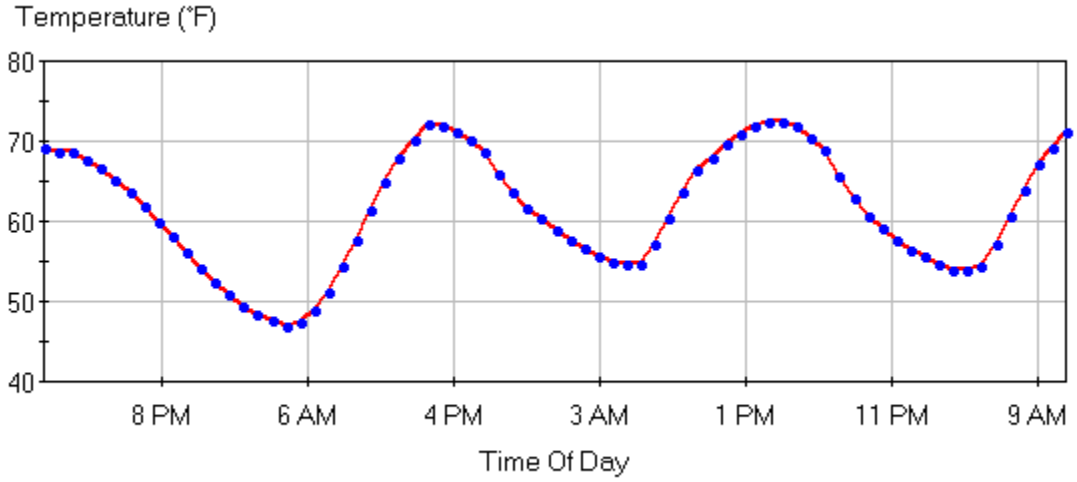

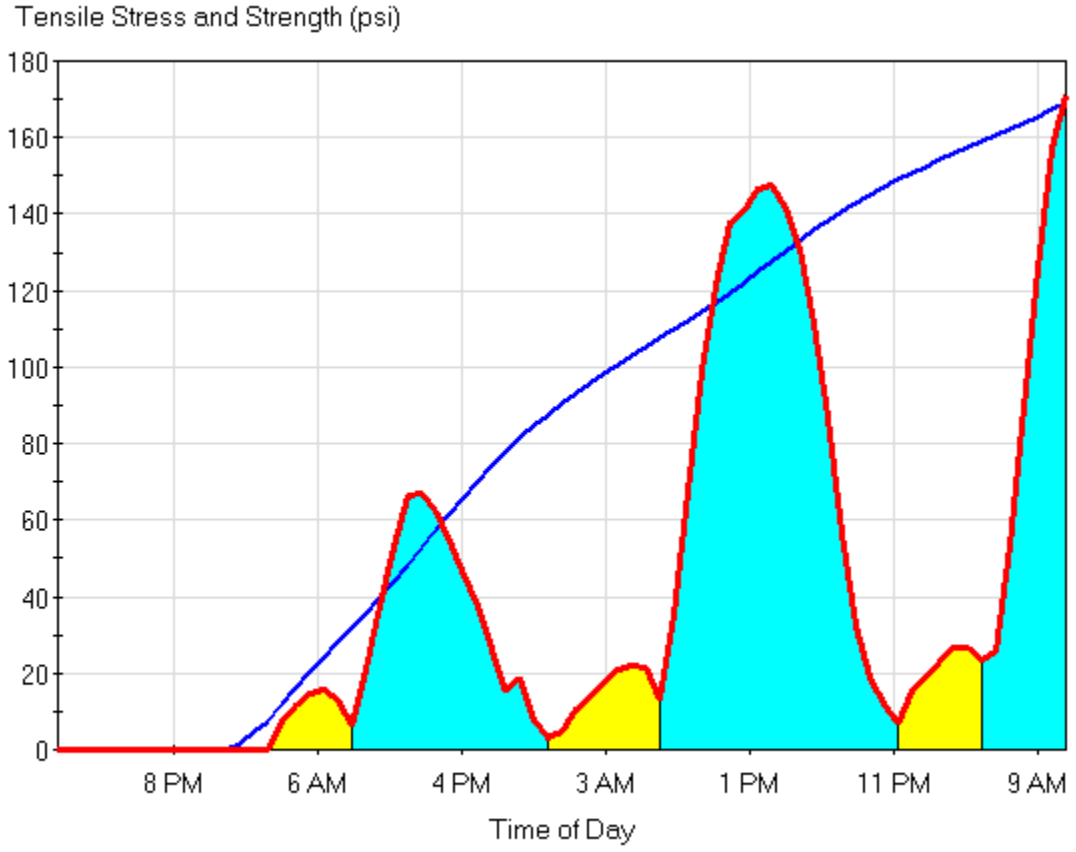

May 24, 2000 Moist base

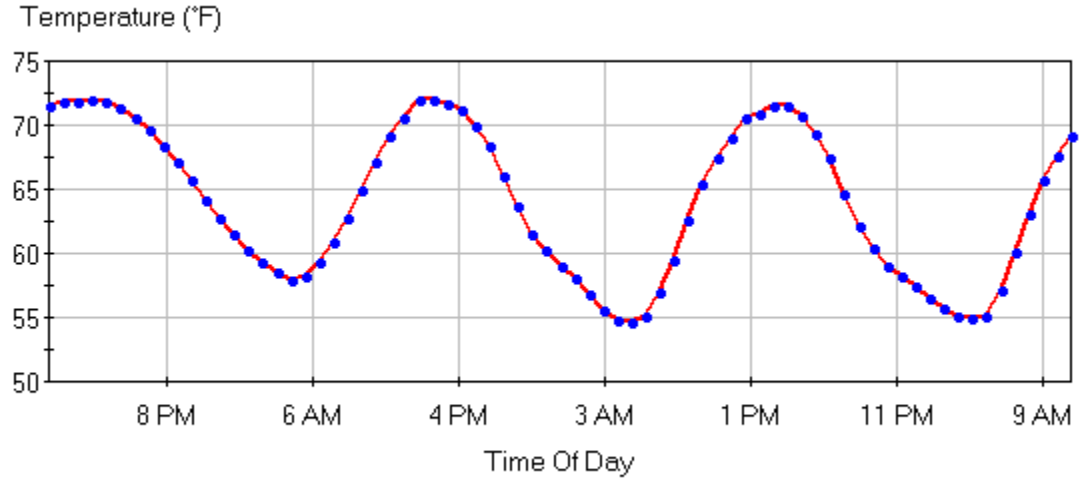

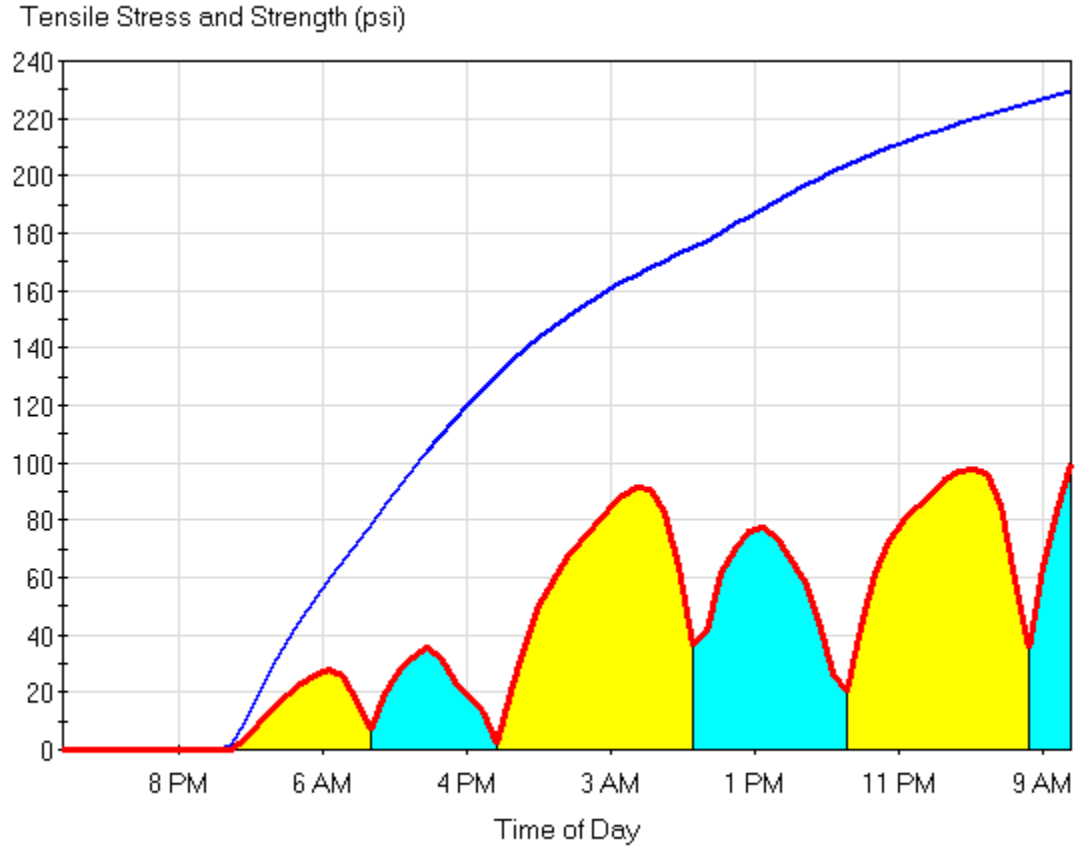

May 24, 2000 Dry base

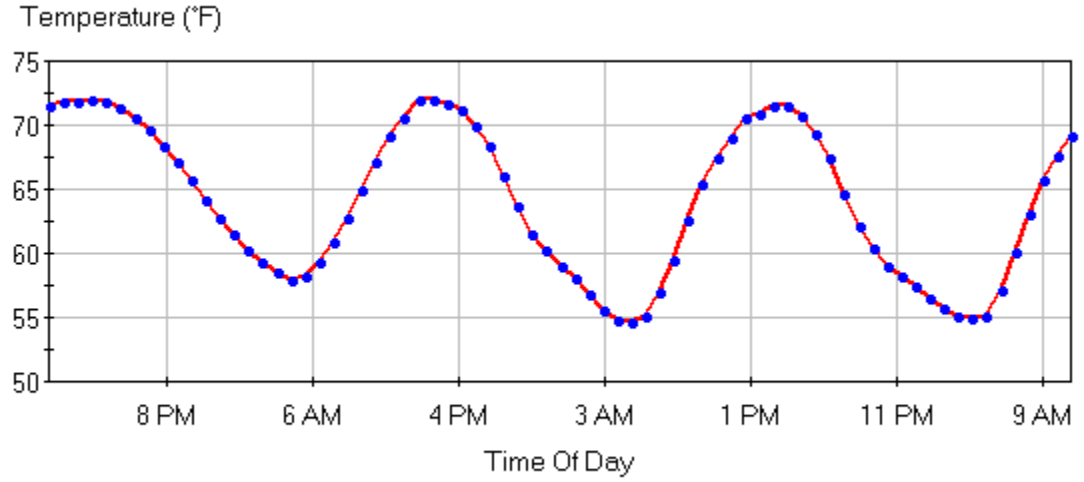

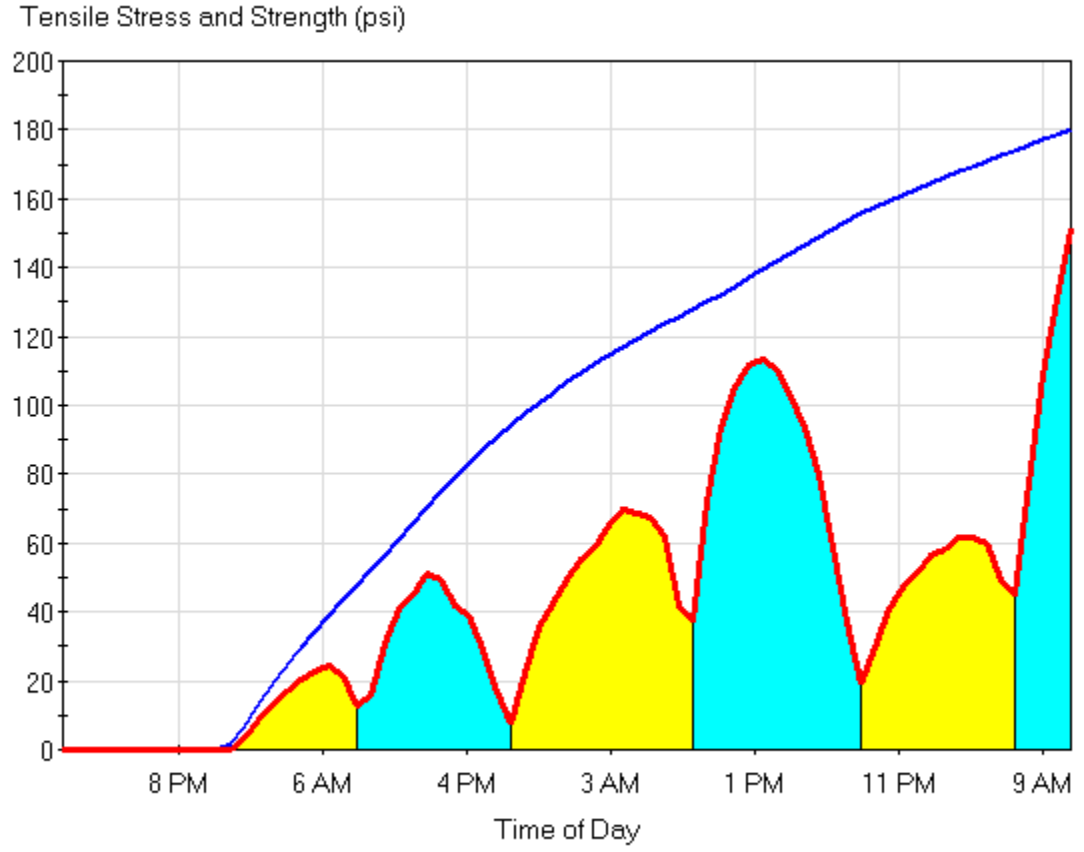

May 30, 2000 Moist base

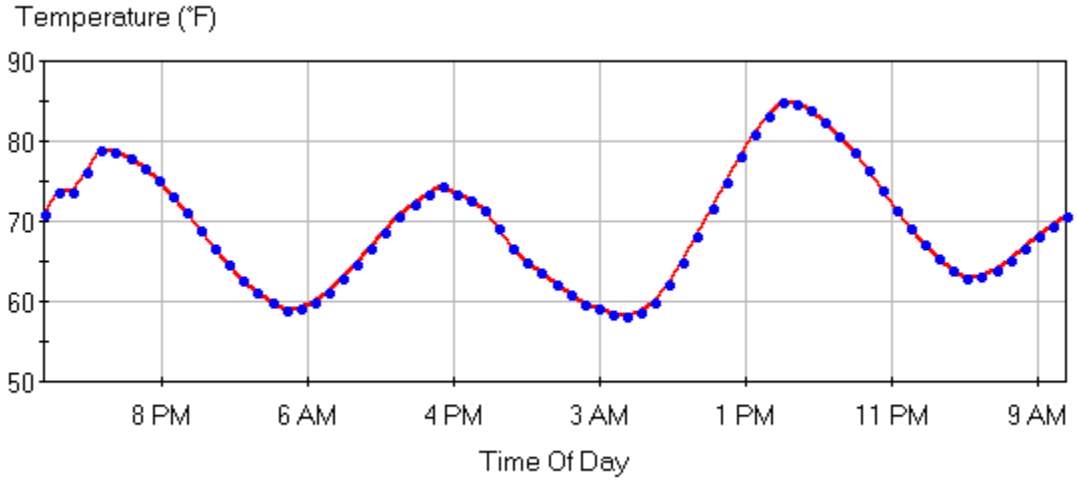

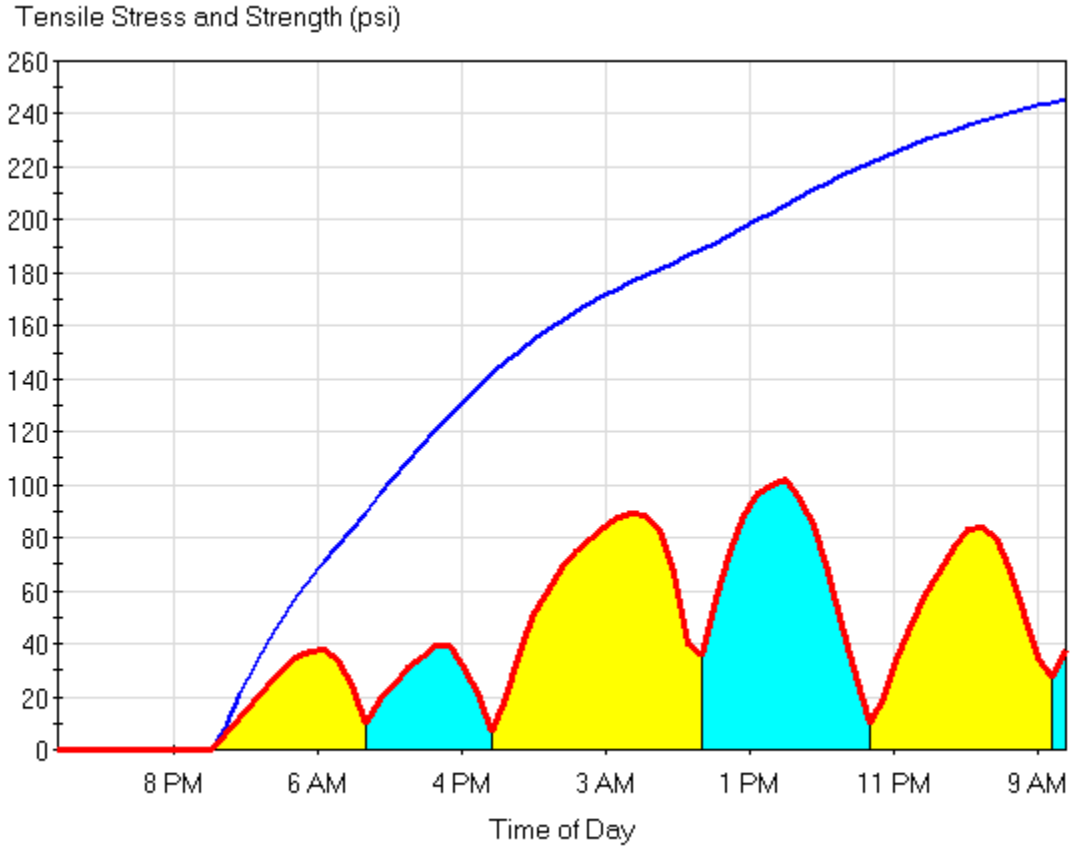

May 30, 2000 Dry base

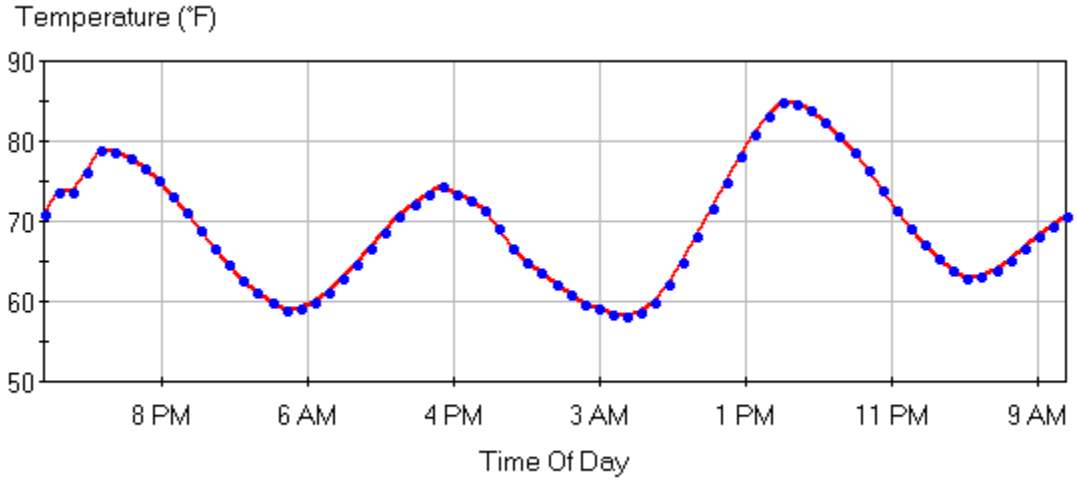

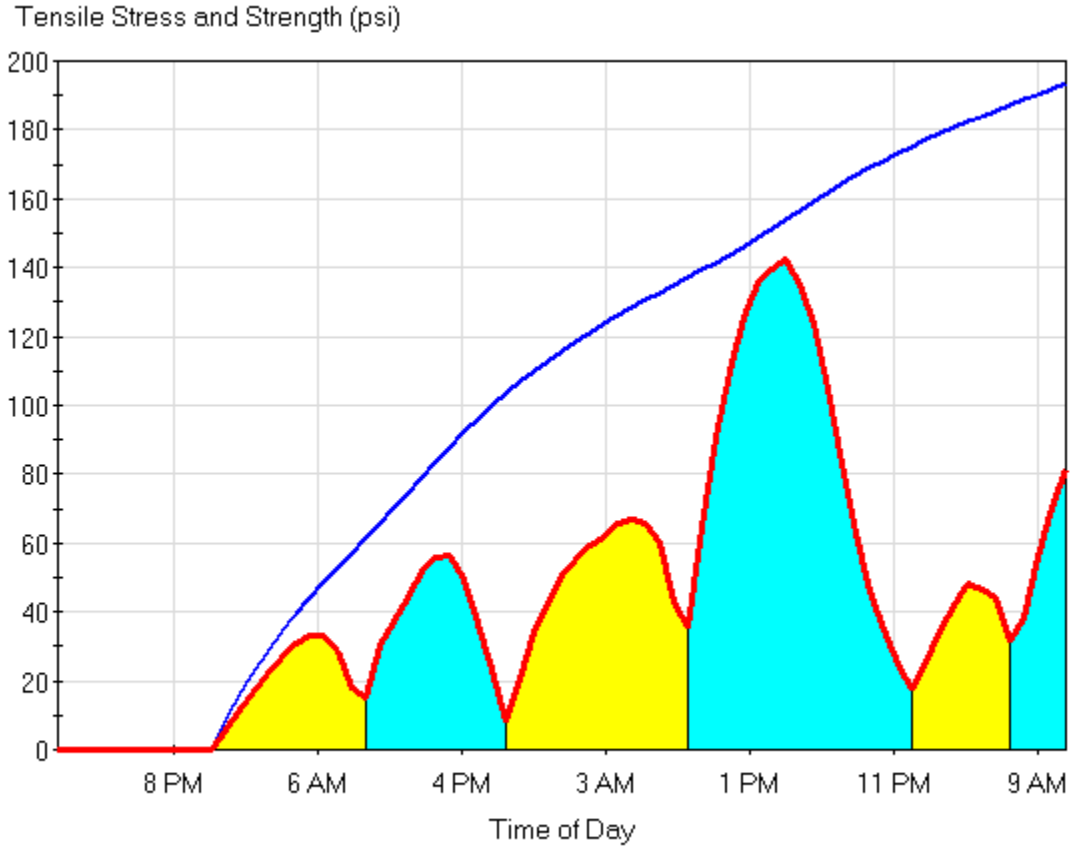

June 1, 2000 Moist base

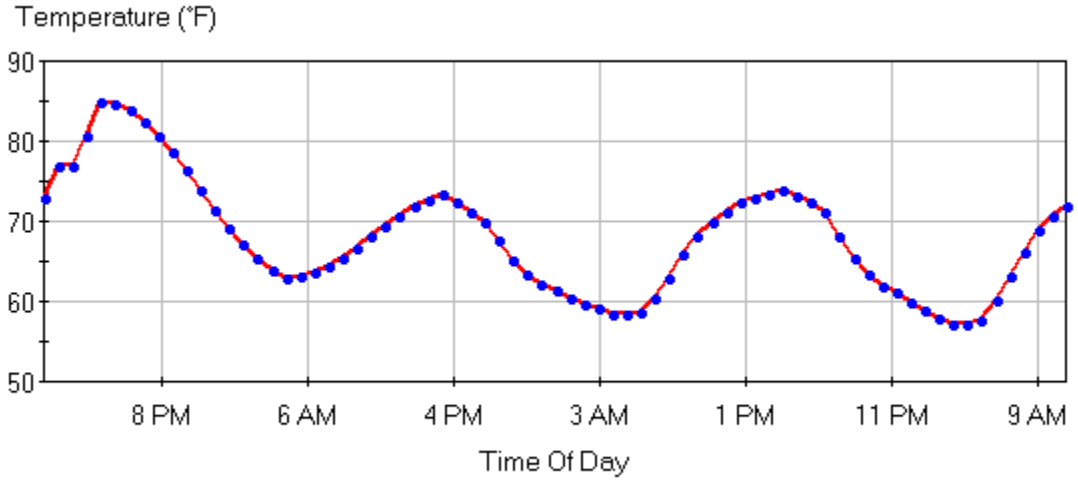

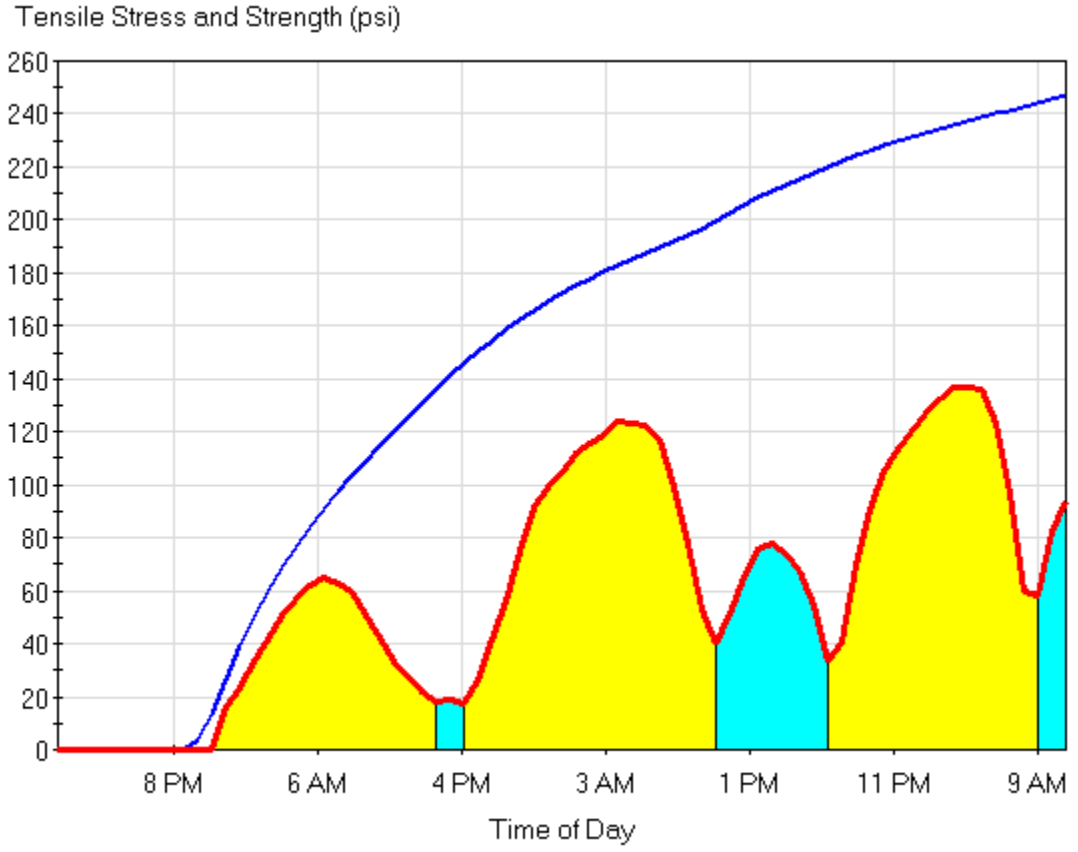

June 1, 2000 Dry base

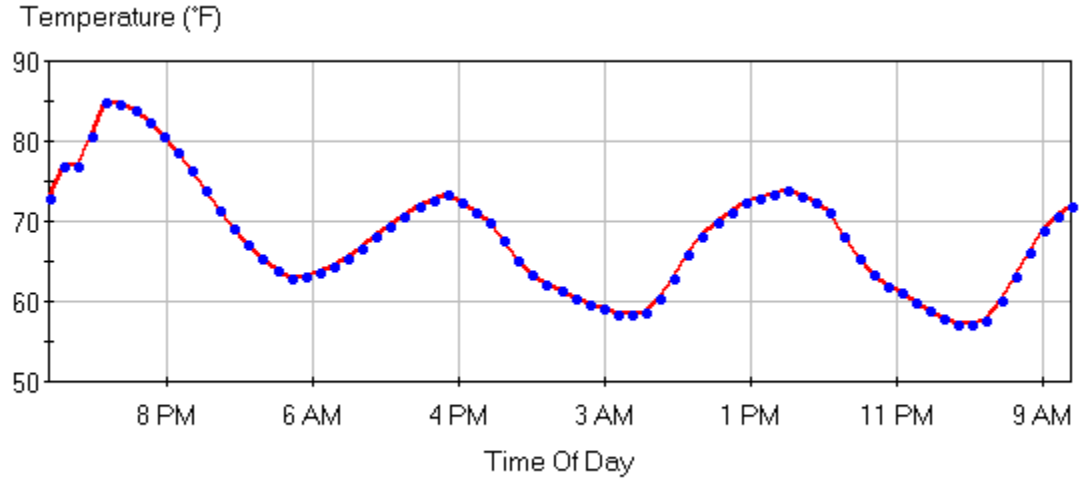

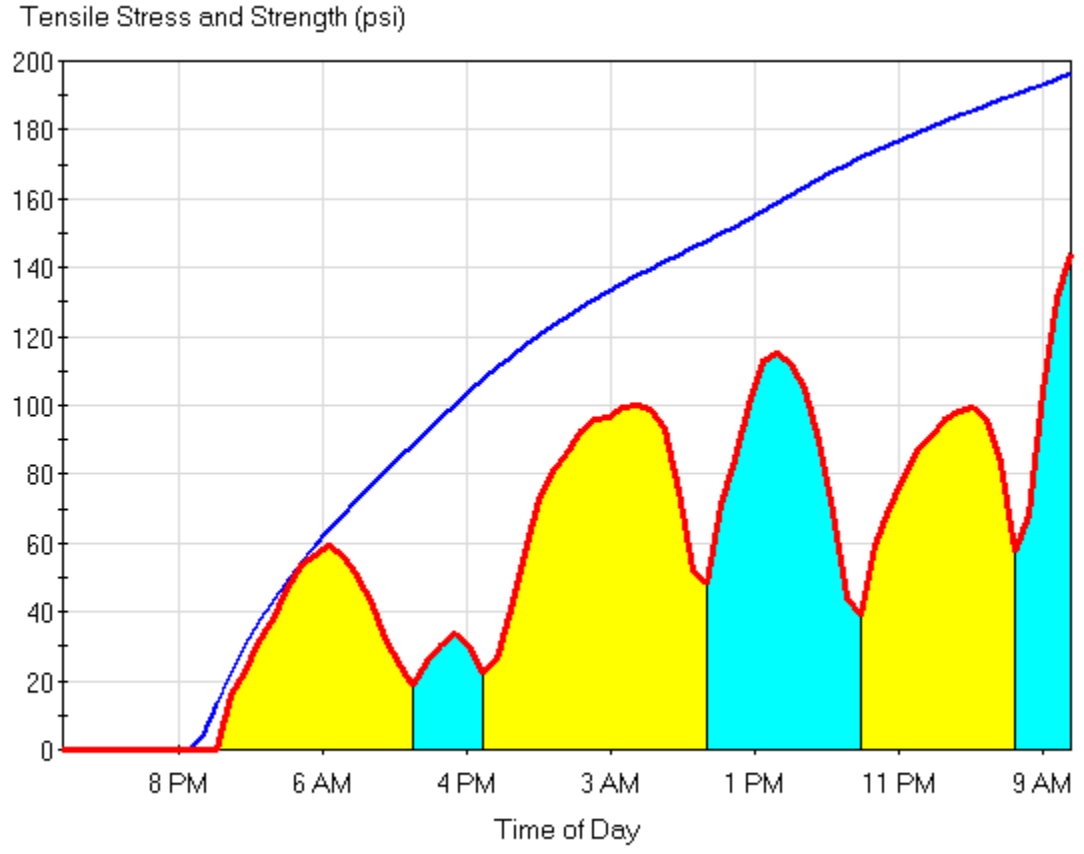

D2: WAS/NOB-77, May 24 – September 15, 2006
Note: All runs assume moist base.

May 24, 2006

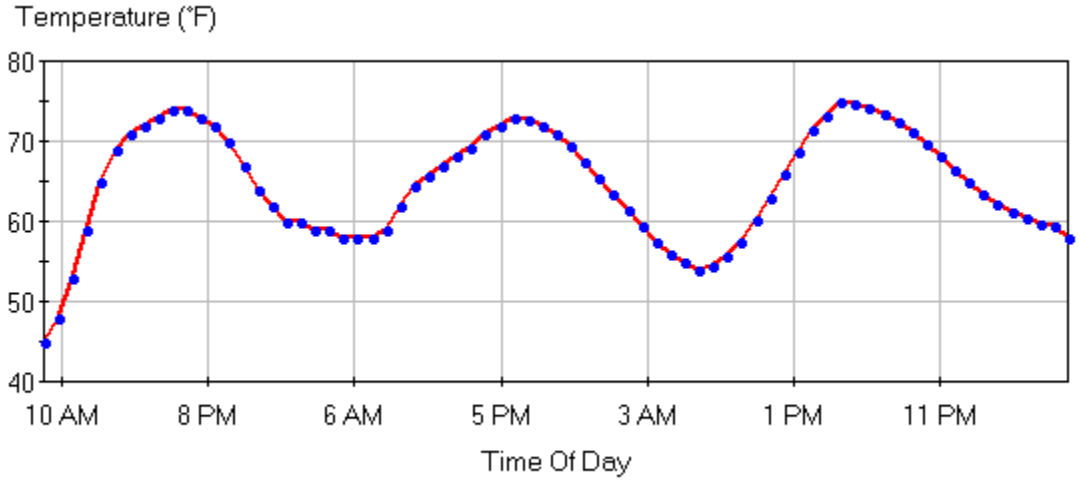

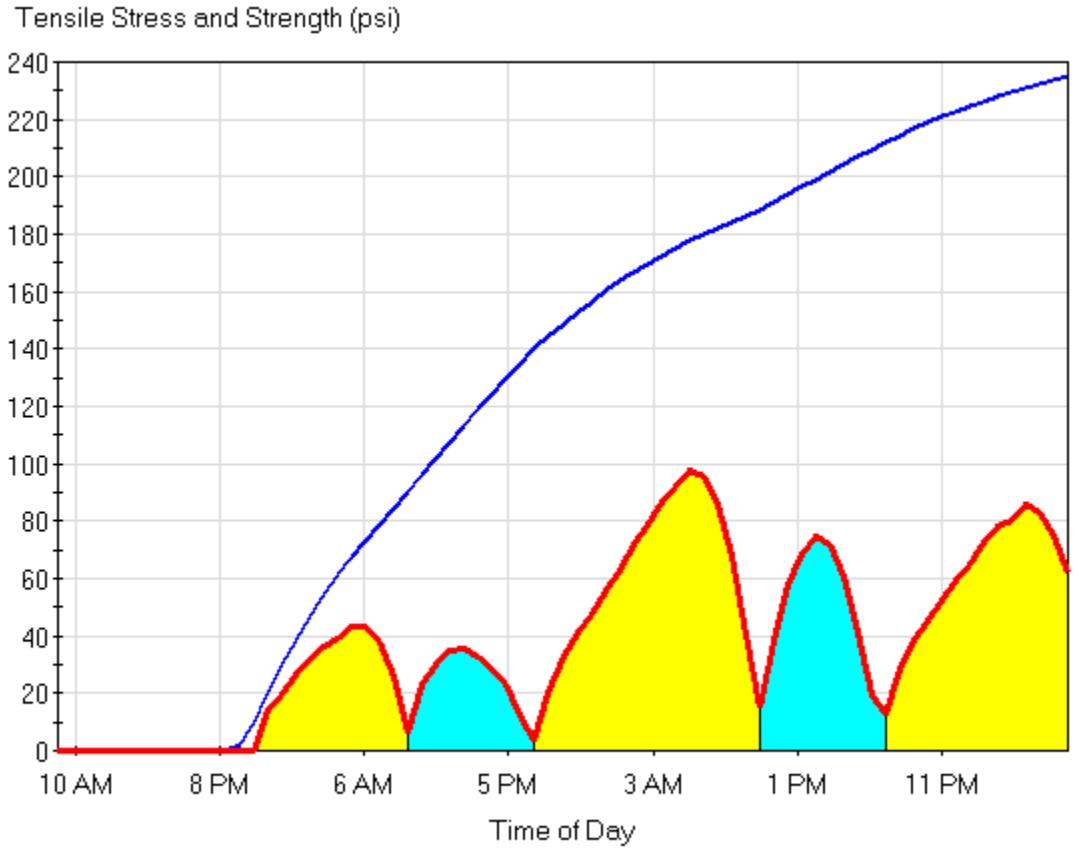

May 30, 2016

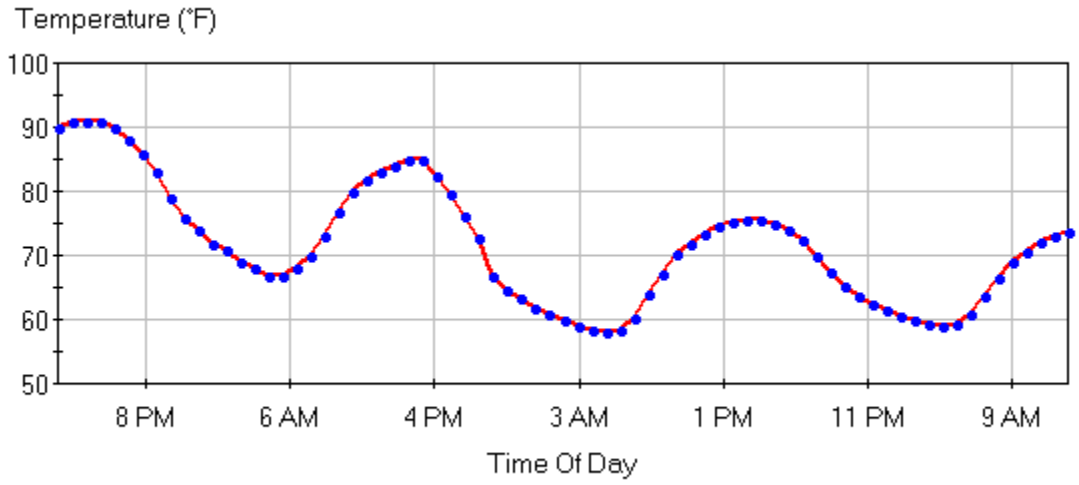
Temperature (°F)
100
90
80
70
60
50
8 PM
6 AM
4 PM
3 AM
1 PM
11 PM
9 AM
Time Of Day

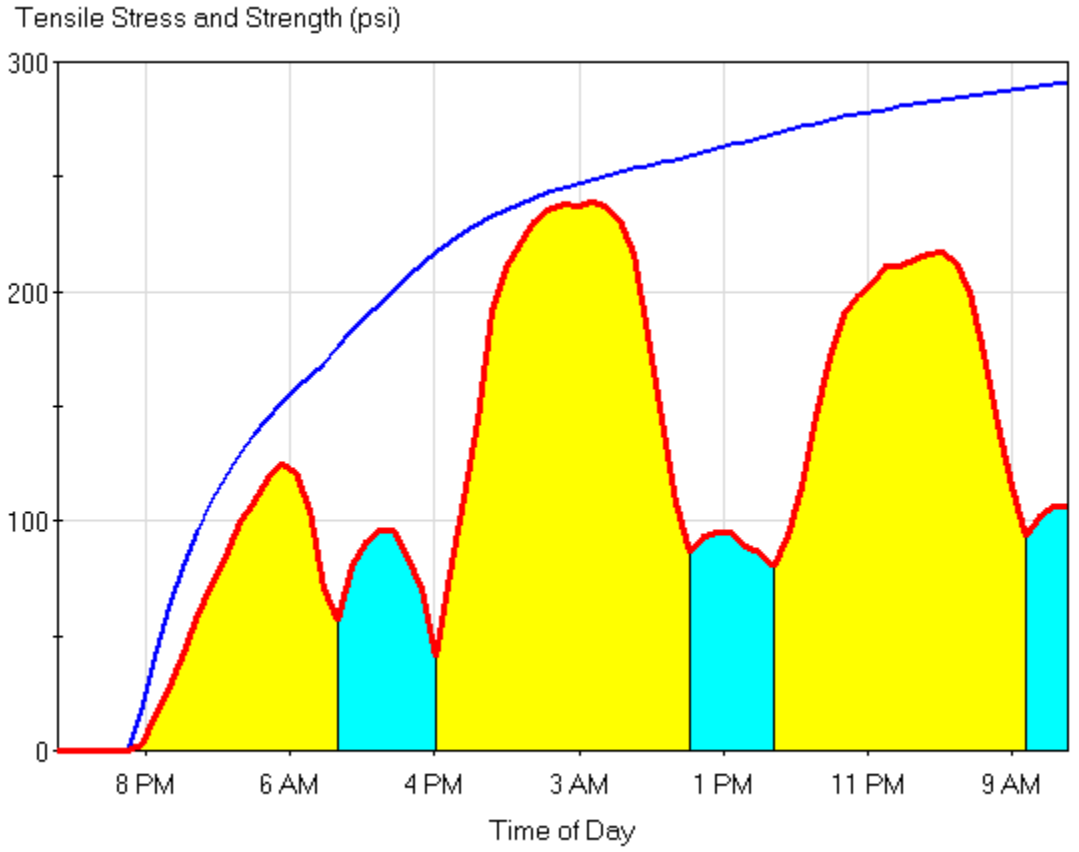
Tensile Stress and Strength (psi)
300
200
100
0
8 PM
6 AM
4 PM
3 AM
1 PM
11 PM
9 AM
Time of Day

June 7, 2016

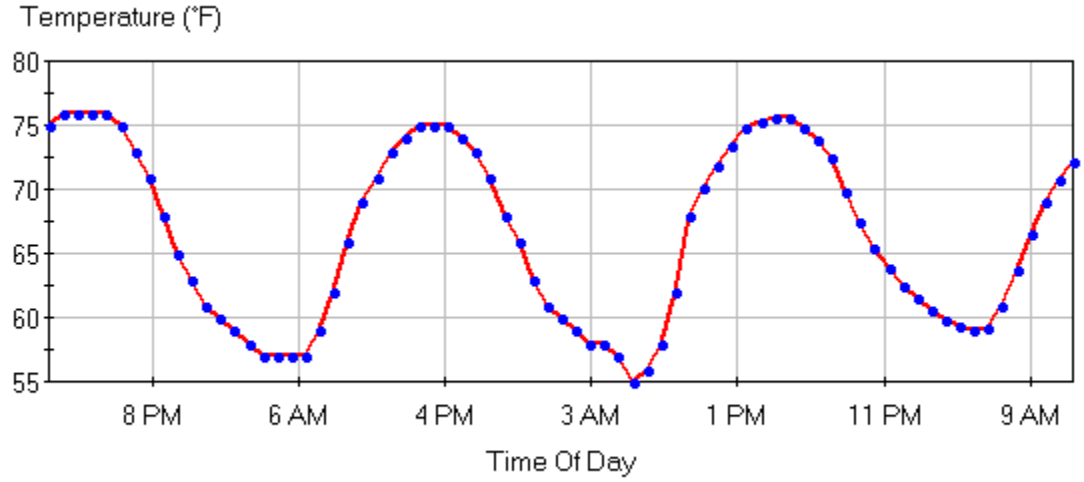
Temperature (°F)
80
75
70
65
60
55
8 PM
6 AM
4 PM
3 AM
1 PM
11 PM
9 AM
Time Of Day

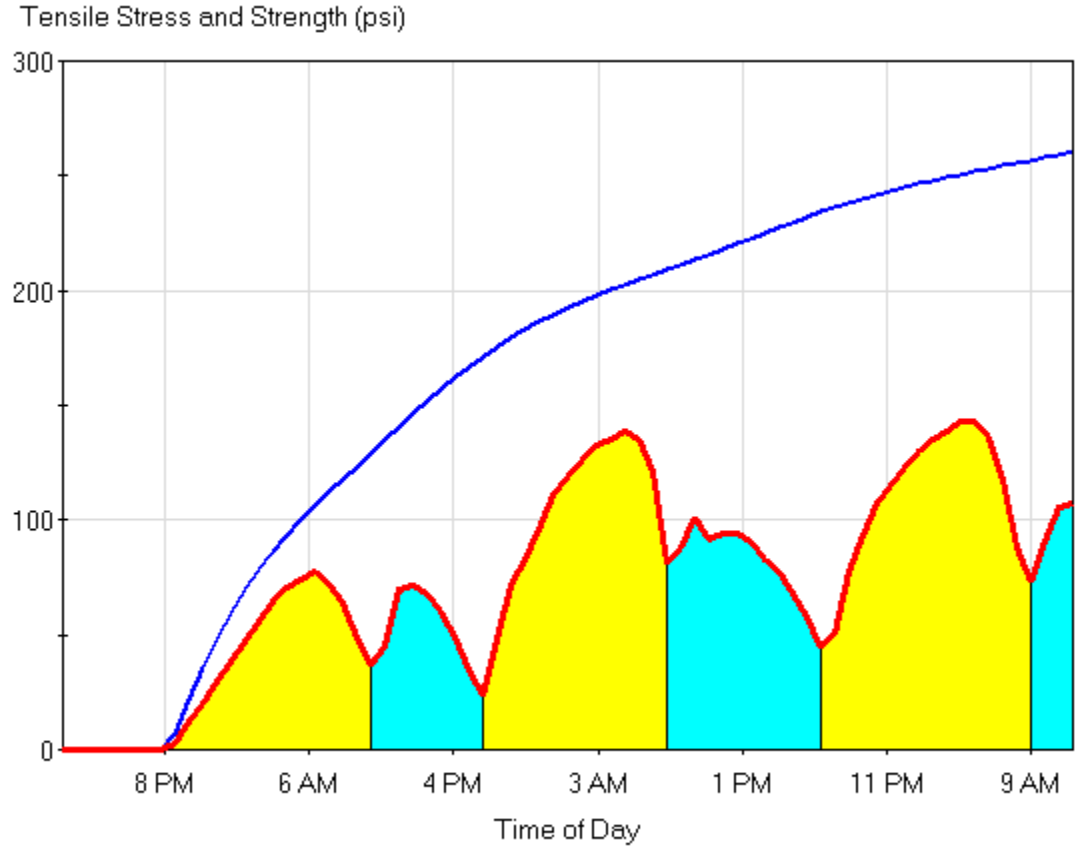
Tensile Stress and Strength (psi)
300
200
100
0
8 PM
6 AM
4 PM
3 AM
1 PM
11 PM
9 AM
Time of Day

June 8, 2006

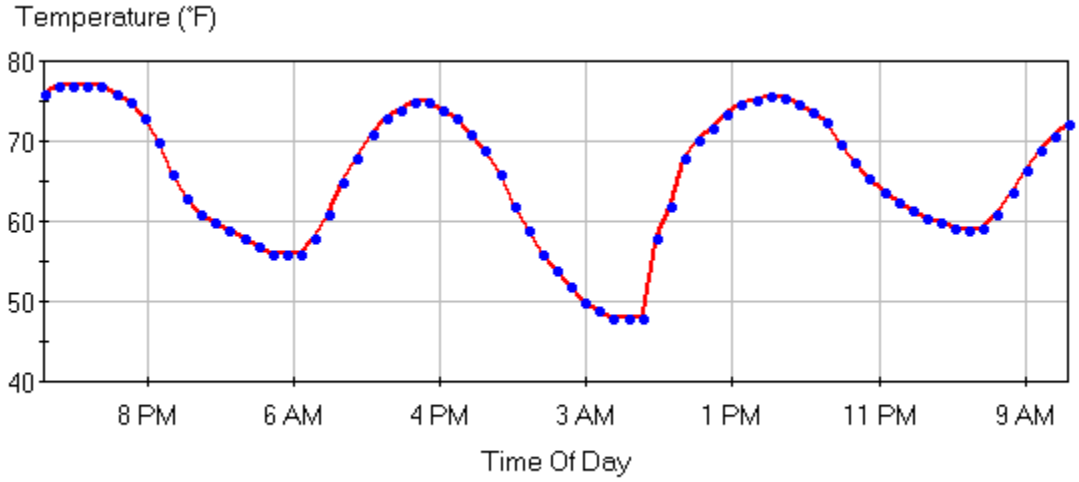
Temperature (°F)
80
70
60
50
40
8 PM
6 AM
4 PM
3 AM
1 PM
11 PM
9 AM
Time Of Day

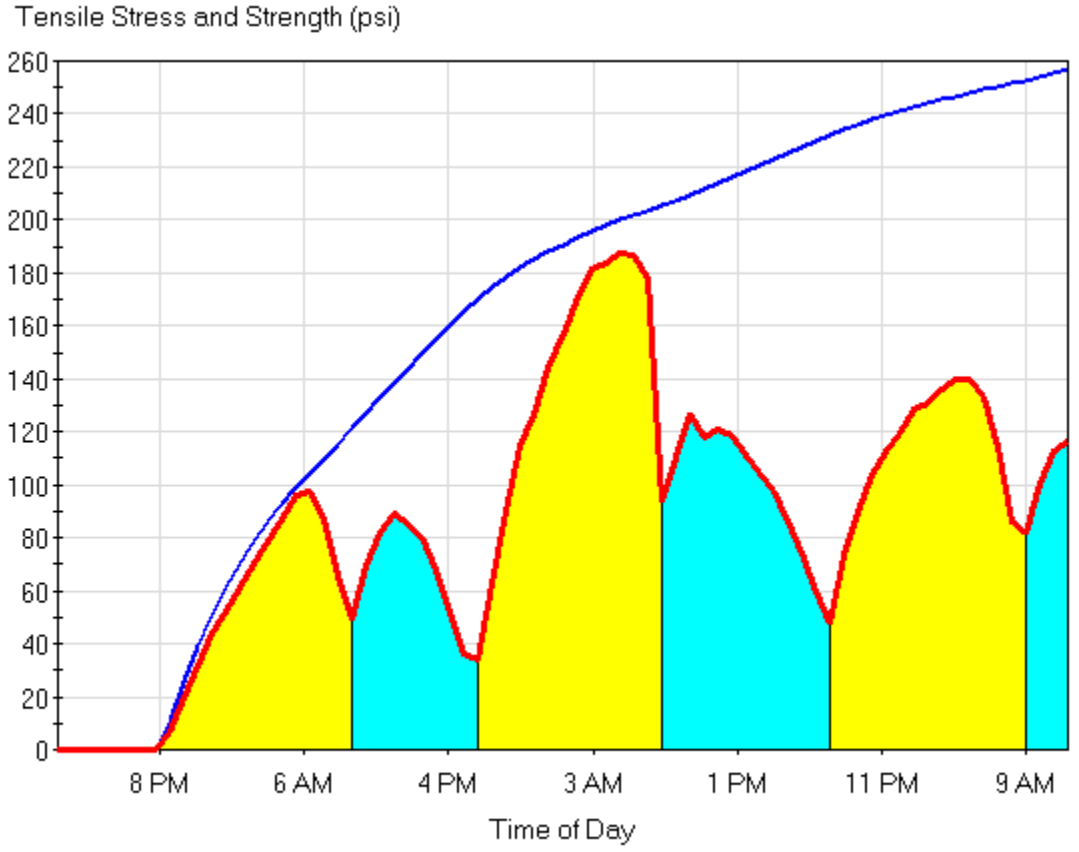
Tensile Stress and Strength (psi)
260
240
220
200
180
160
140
120
100
80
60
40
20
0
8 PM
6 AM
4 PM
3 AM
1 PM
11 PM
9 AM
Time of Day

June 9, 2006

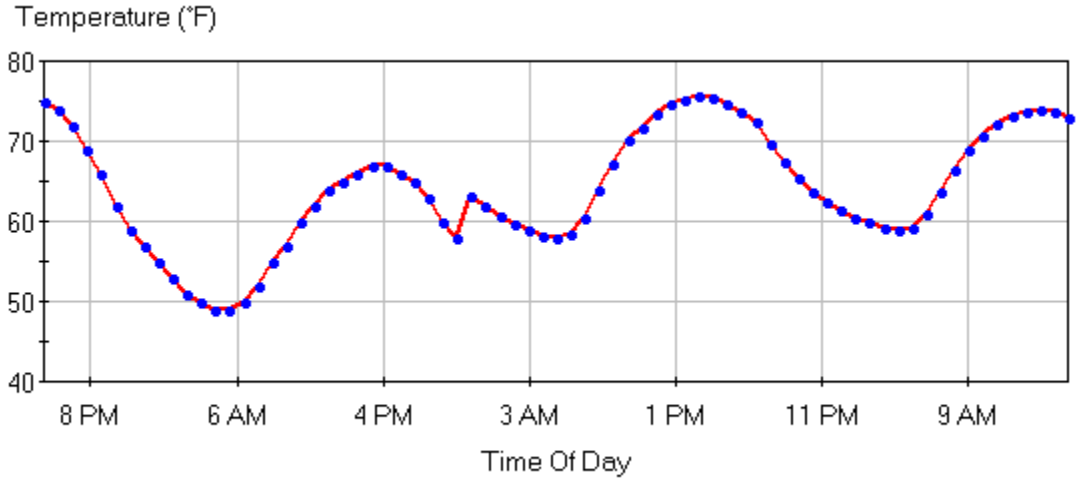
Temperature (°F)
80
70
60
50
40
8 PM
6 AM
4 PM
3 AM
1 PM
11 PM
9 AM
Time Of Day

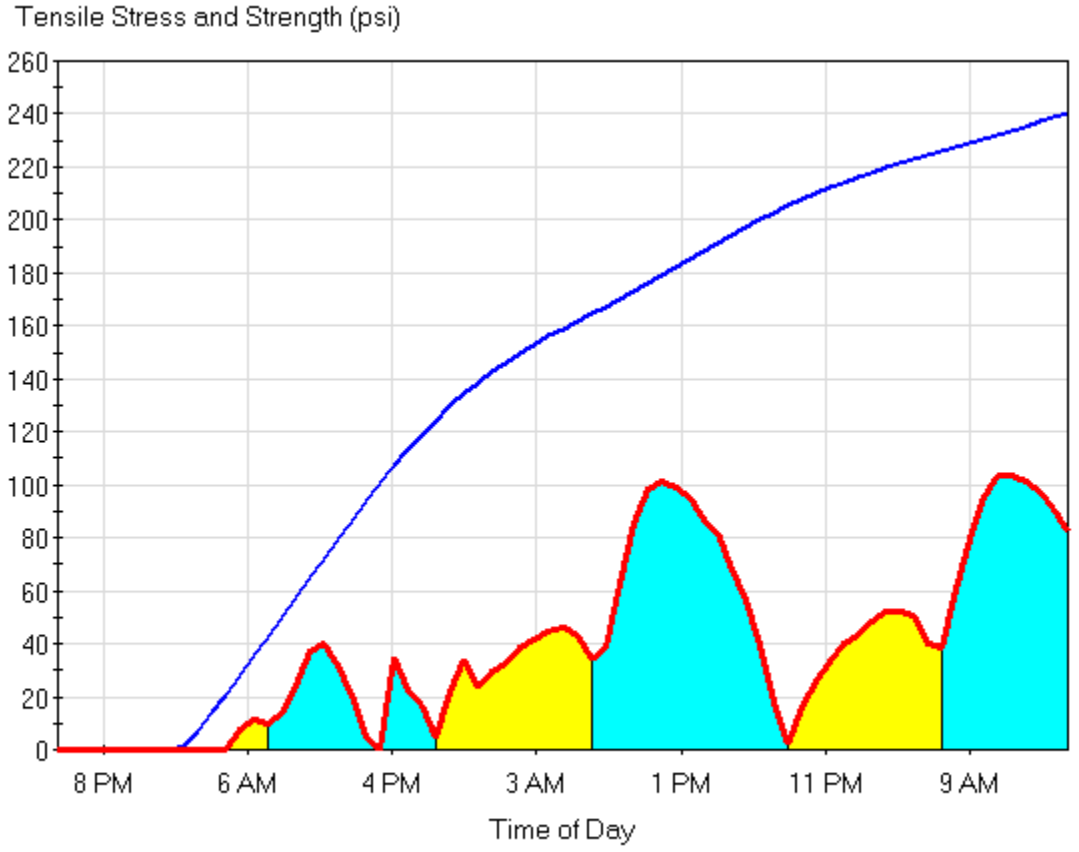
Tensile Stress and Strength (psi)
260
240
220
200
180
160
140
120
100
80
60
40
20
0
8 PM
6 AM
4 PM
3 AM
1 PM
11 PM
9 AM
Time of Day

July 6, 2006

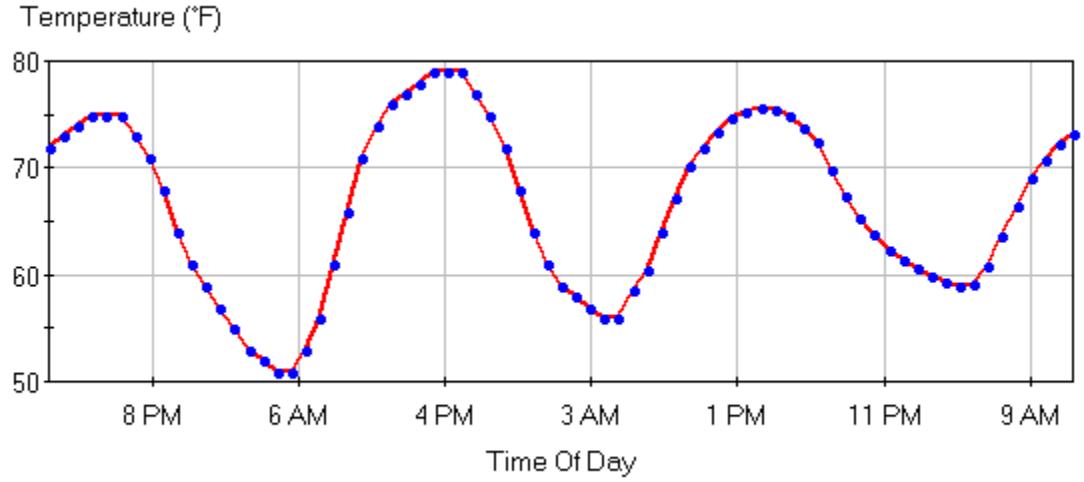
Temperature (°F)
80
70
60
50
8 PM
6 AM
4 PM
3 AM
1 PM
11 PM
9 AM
Time Of Day

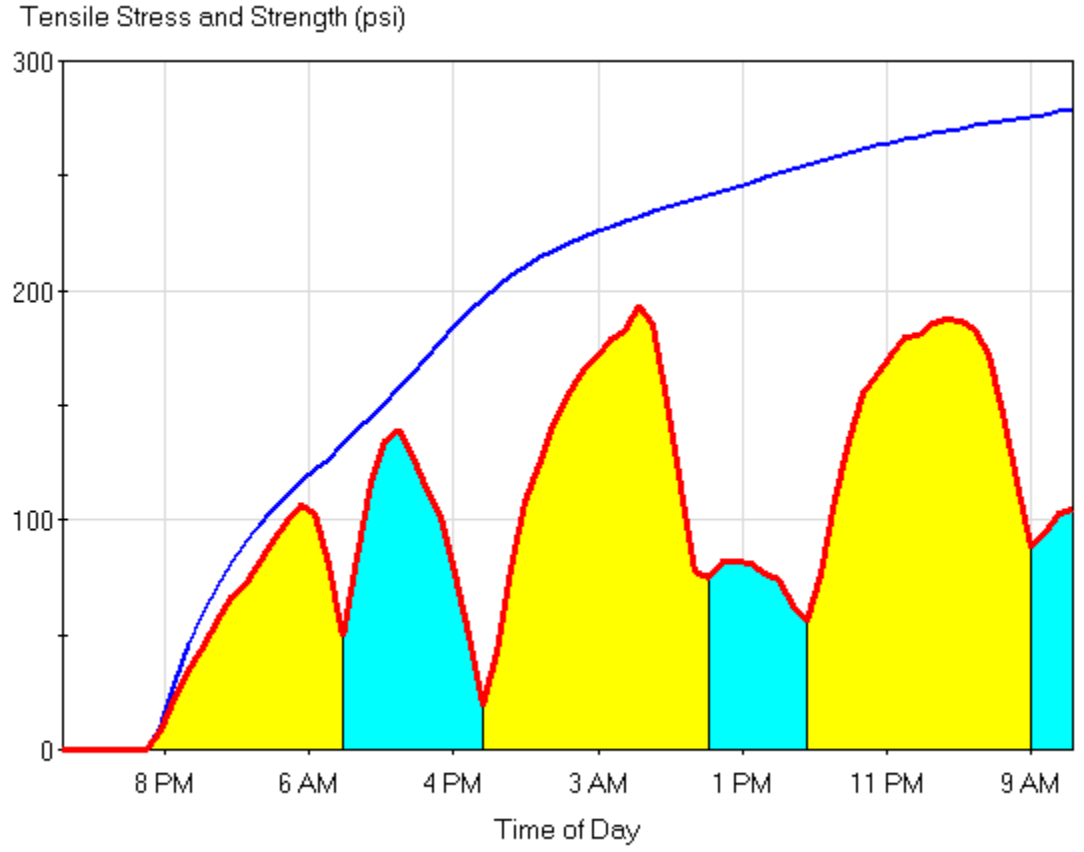
Tensile Stress and Strength (psi)
300
200
100
0
8 PM
6 AM
4 PM
3 AM
1 PM
11 PM
9 AM
Time of Day

July 7, 2006

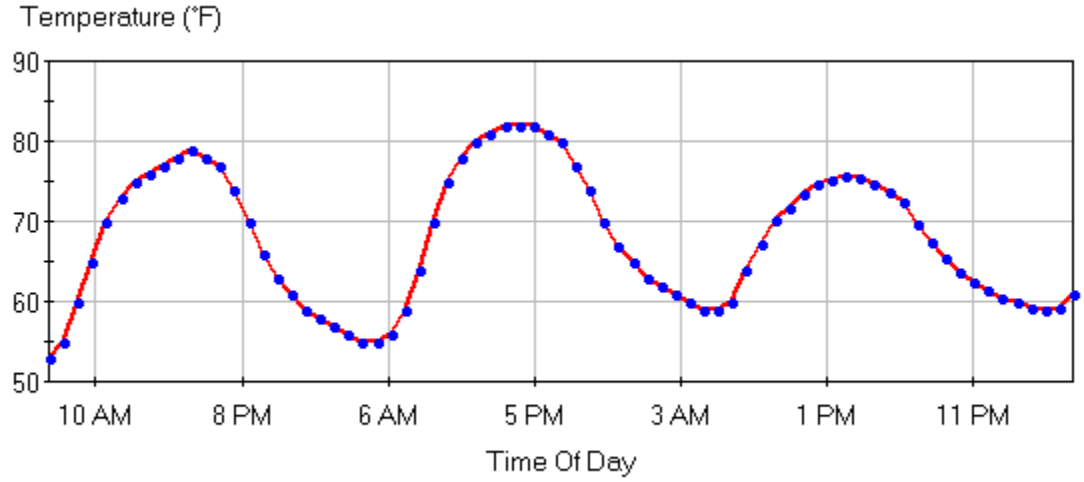
Temperature (°F)
90
80
70
60
50
10 AM
8 PM
6 AM
5 PM
3 AM
1 PM
11 PM
Time Of Day

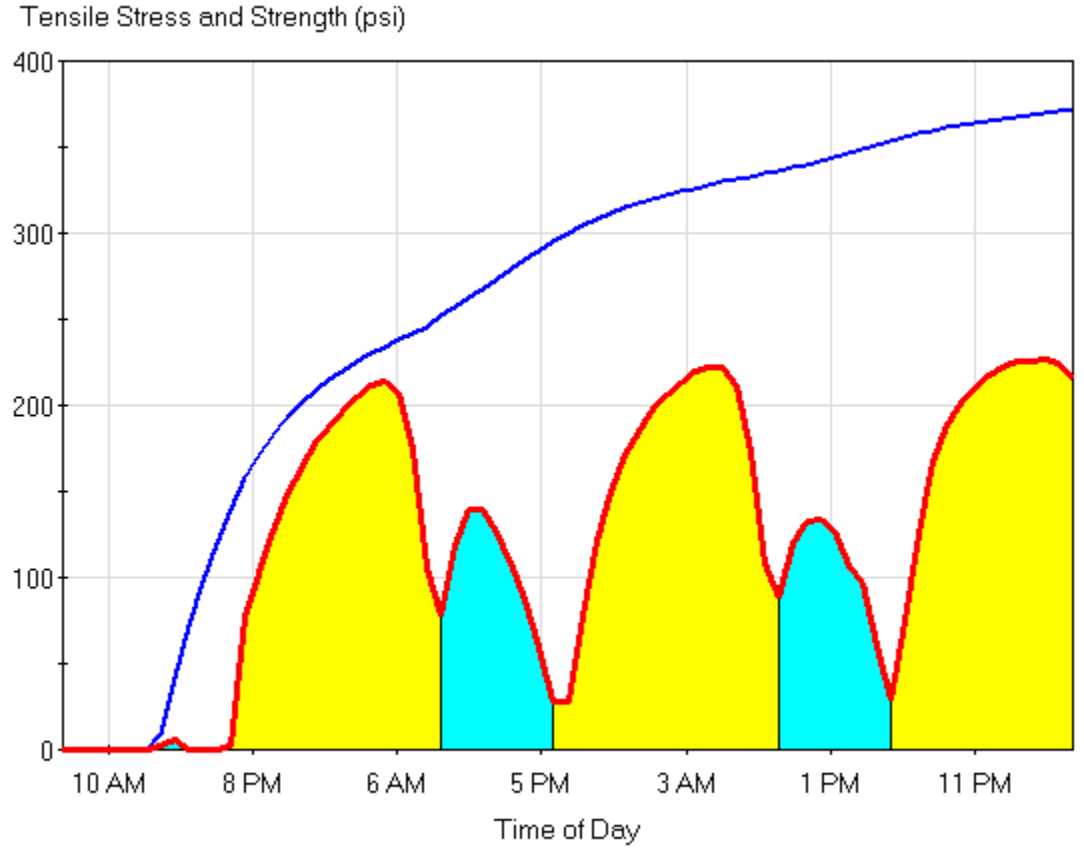
Tensile Stress and Strength (psi)
400
300
200
100
0
10 AM
8 PM
6 AM
5 PM
3 AM
1 PM
11 PM
Time of Day

July 14, 2006

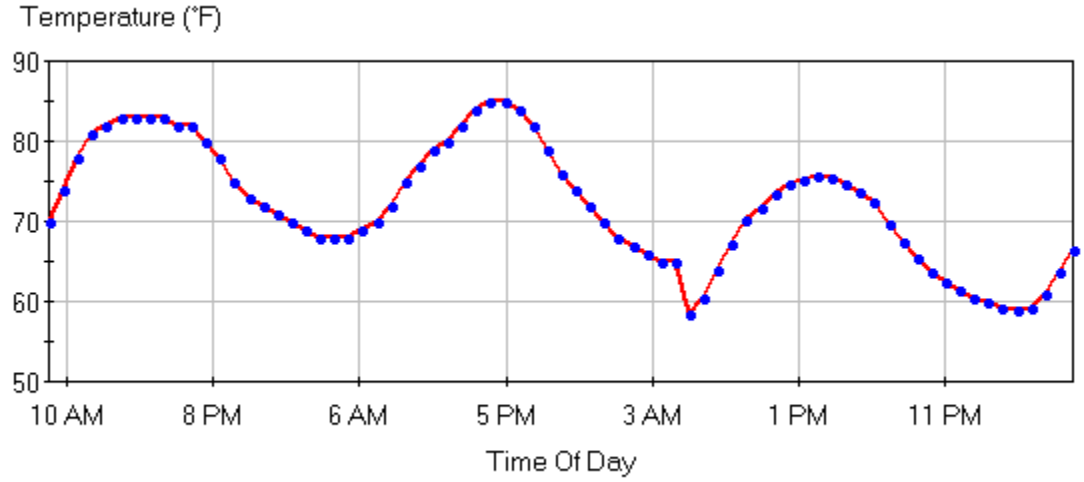
Temperature (°F)
90
80
70
60
50
10 AM
8 PM
6 AM
5 PM
3 AM
1 PM
11 PM
Time Of Day

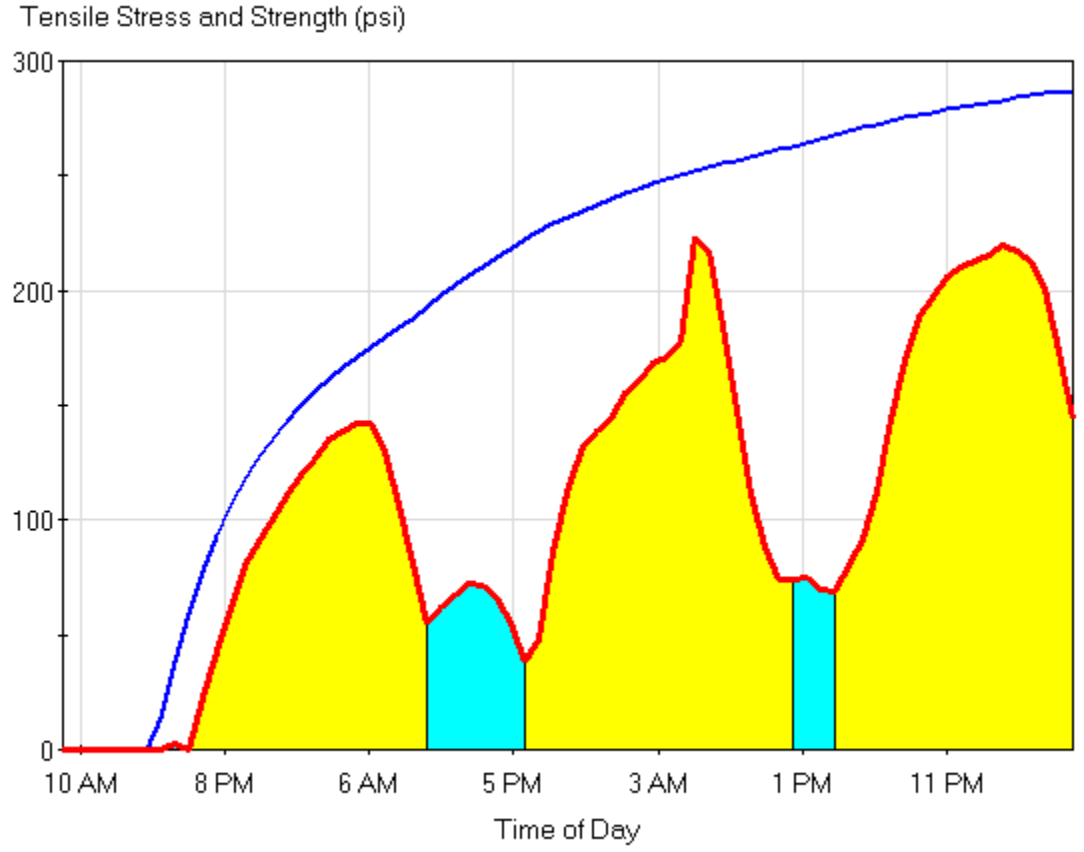
Tensile Stress and Strength (psi)
300
200
100
0
10 AM
8 PM
6 AM
5 PM
3 AM
1 PM
11 PM
Time of Day

September 7, 2006

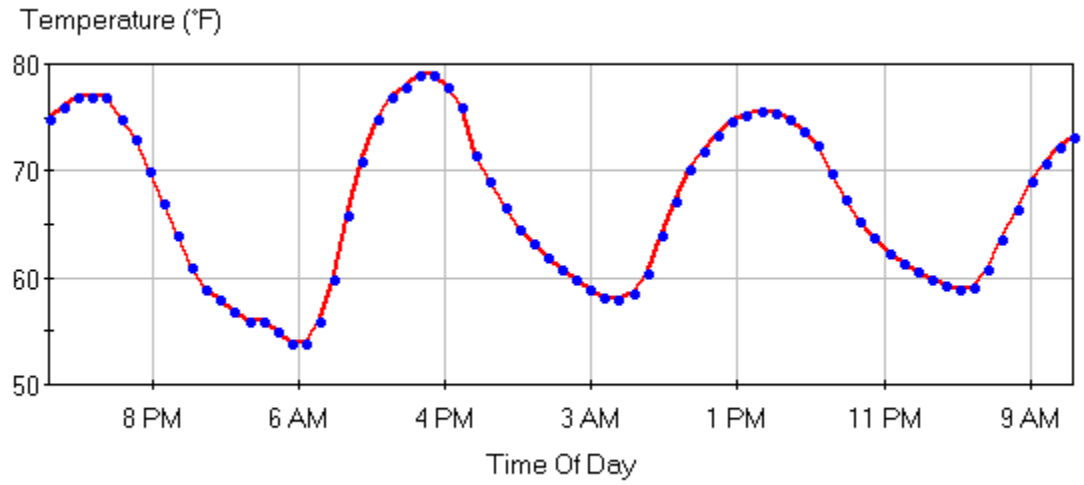

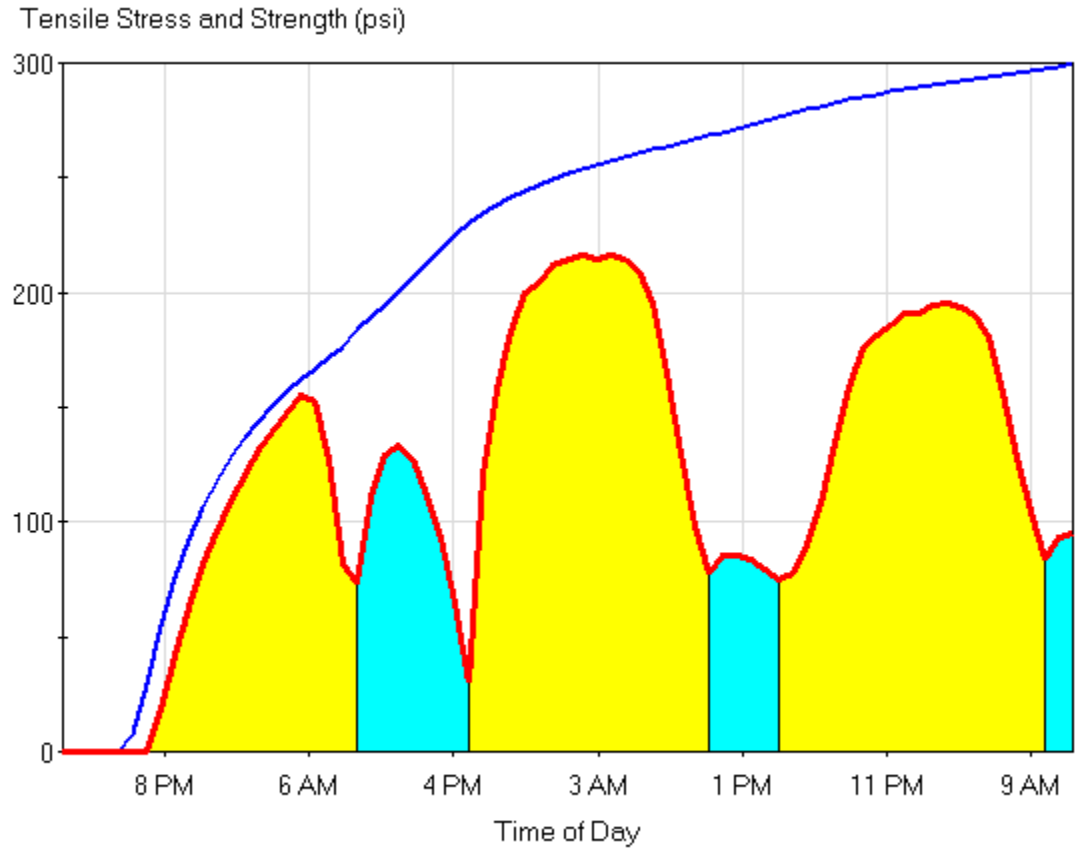

September 8, 2006

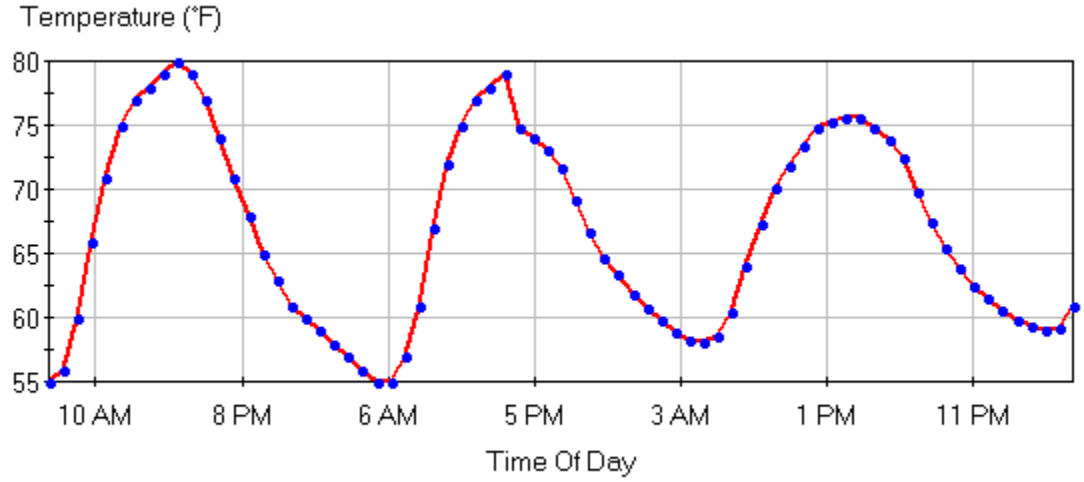

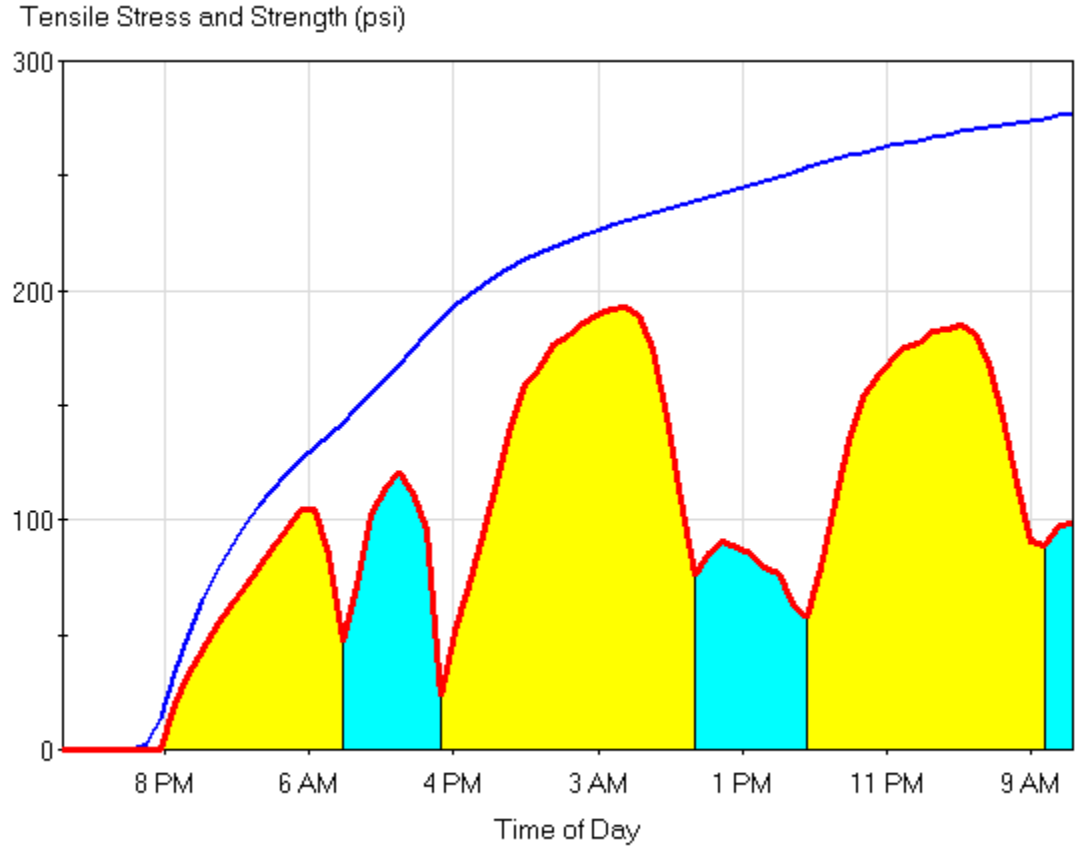

September 11, 2006 saw cutting

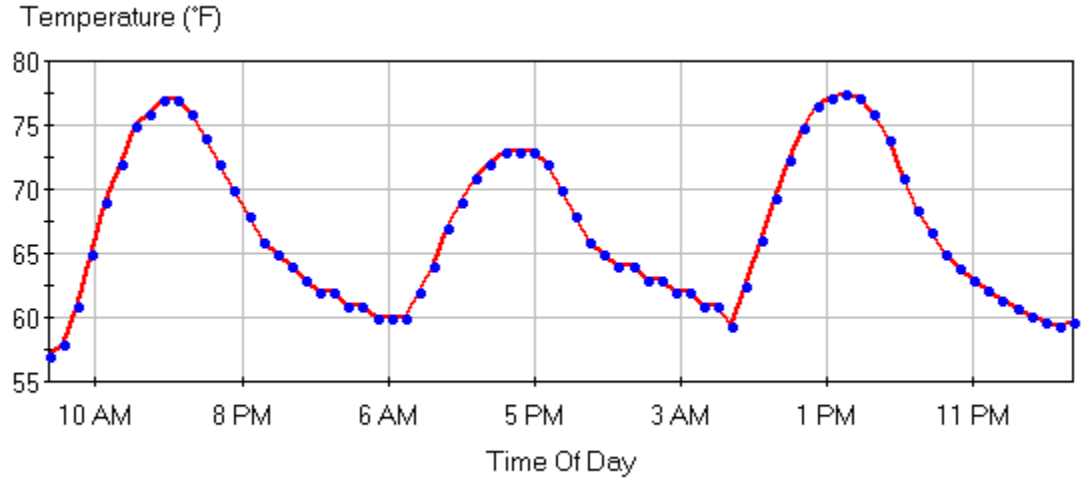

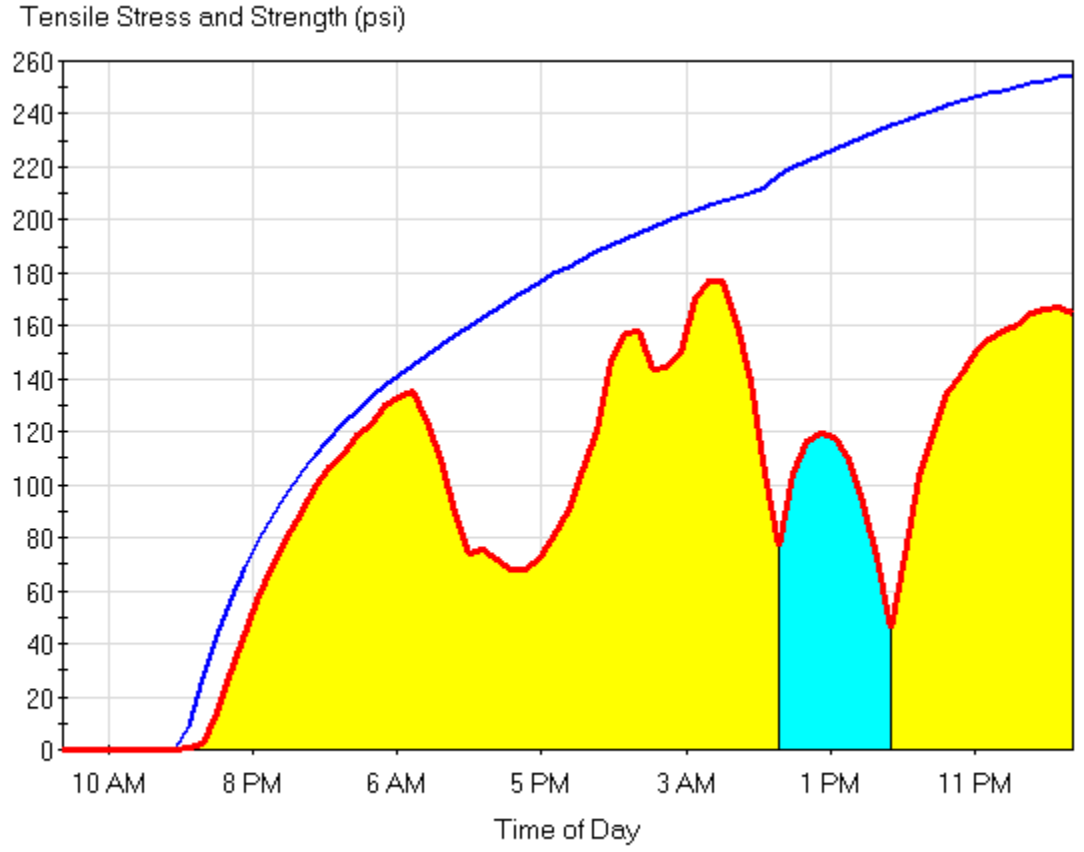

September 14, 2006

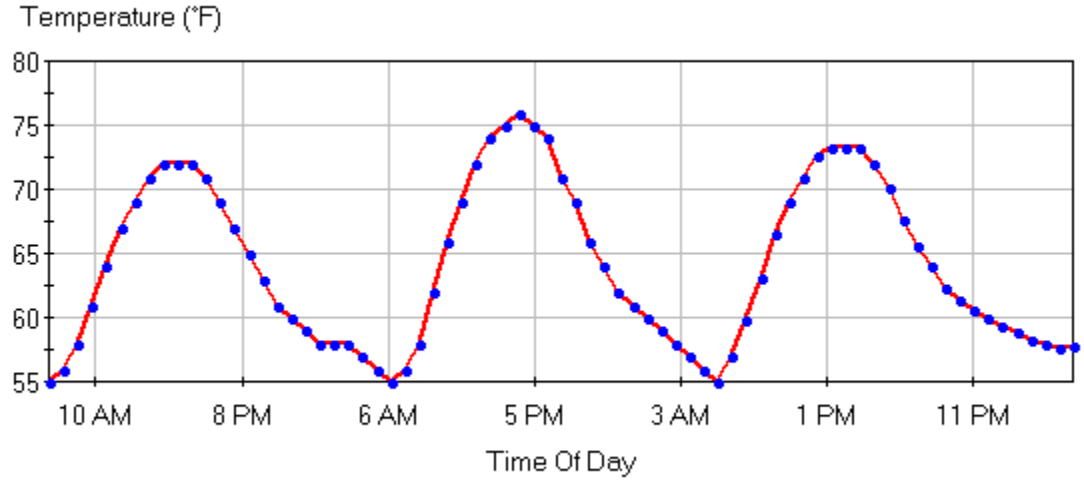

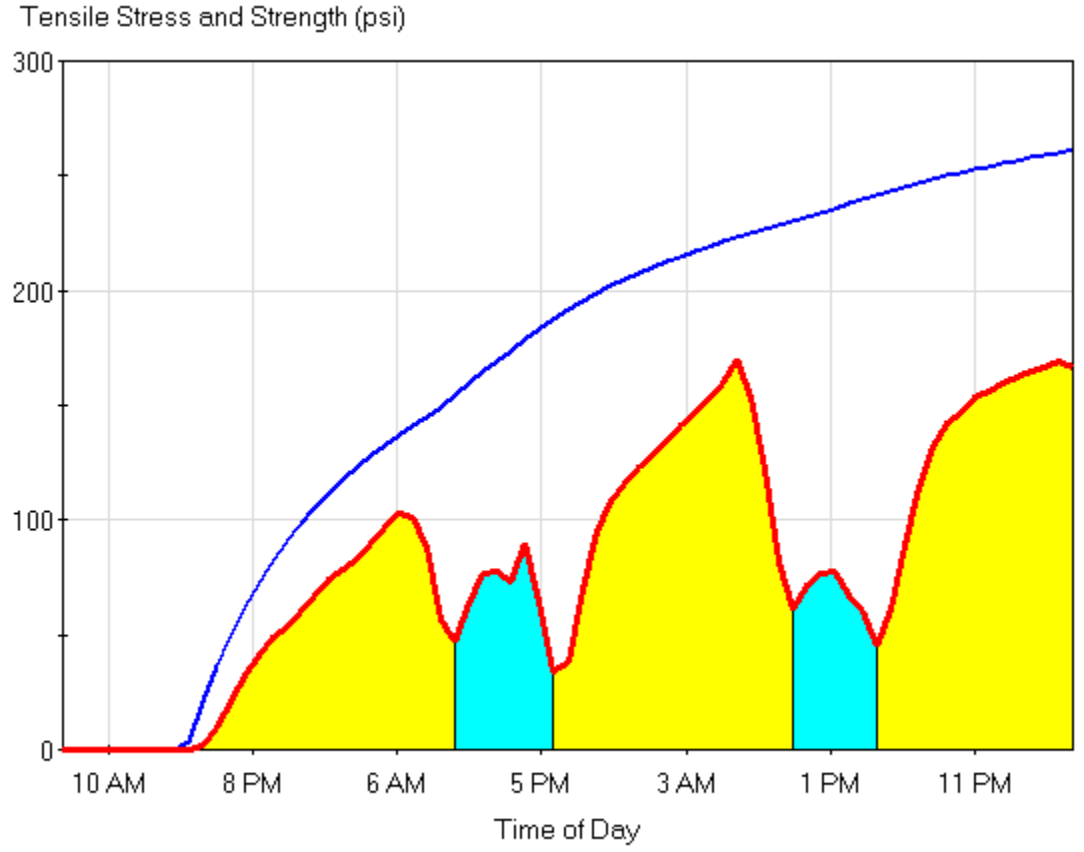

September 15, 2006

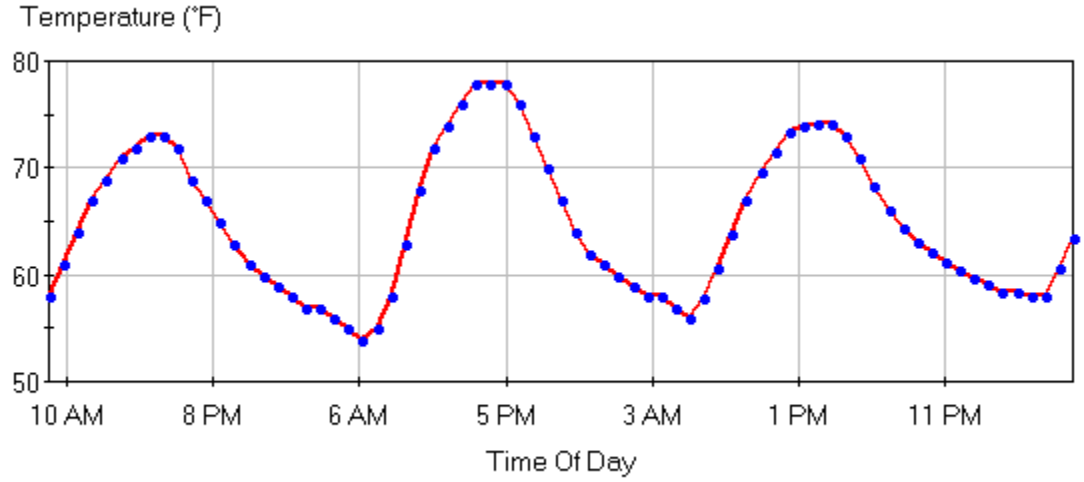

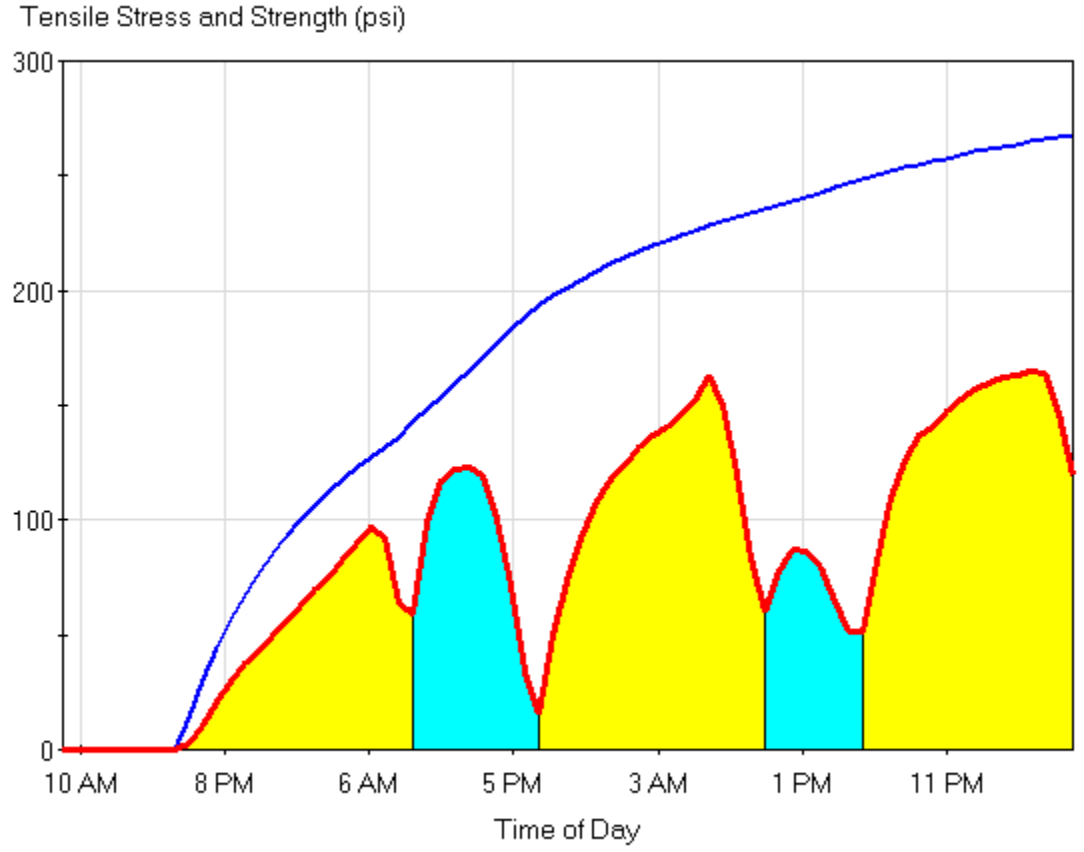

D3: LAK-90, Oct. 10-25, 2006

Oct. 10, 2006

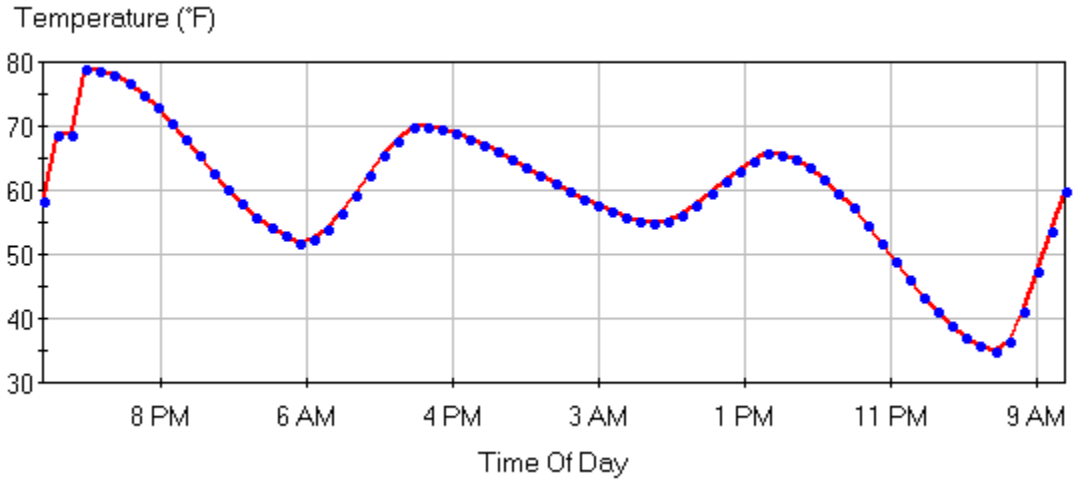

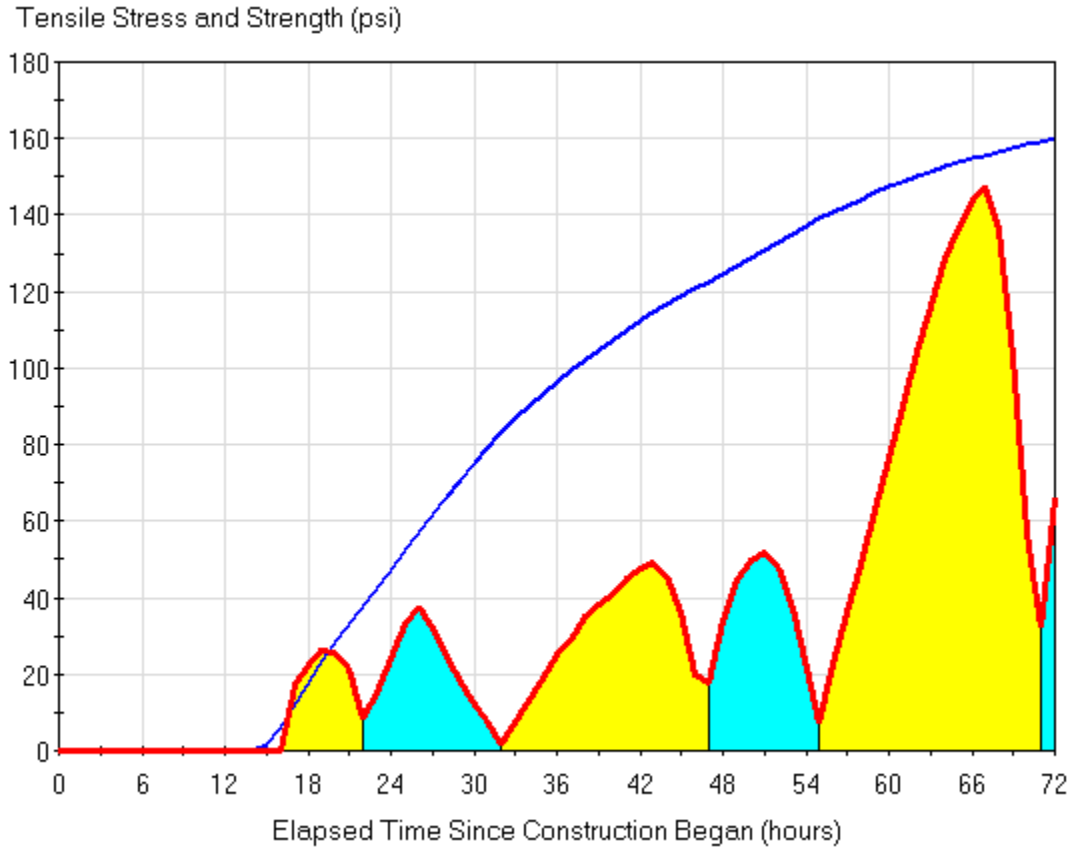

Oct. 11, 2006

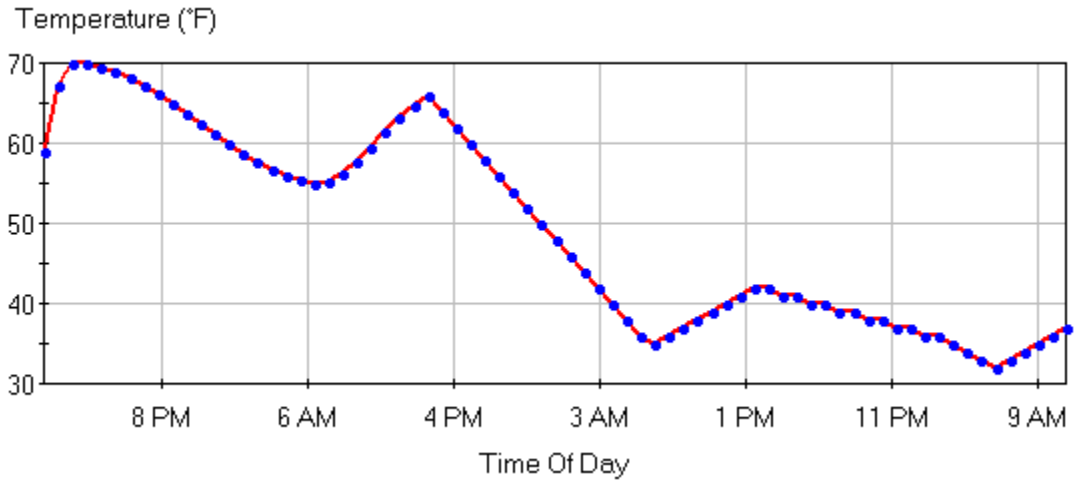
Temperature (°F)
70
60
50
40
30
8 PM
6 AM
4 PM
3 AM
1 PM
11 PM
9 AM
Time Of Day

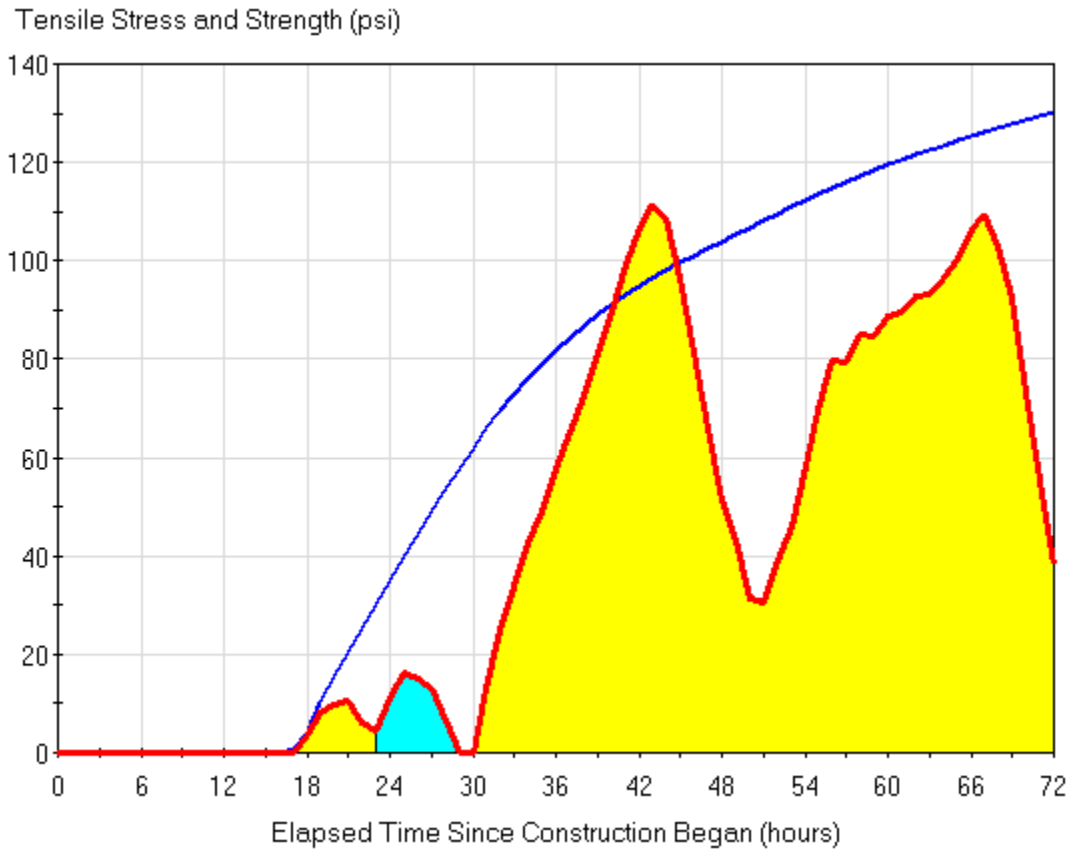
Tensile Stress and Strength (psi)
140
120
100
80
60
40
20
0
0
6
12
18
24
30
36
42
48
54
60
66
72
Elapsed Time Since Construction Began (hours)

Oct. 12, 2006

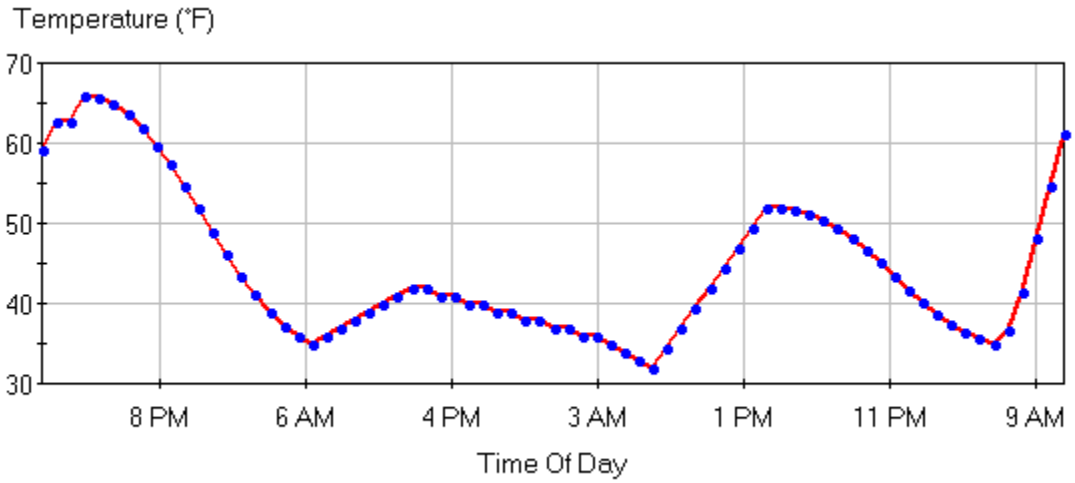
Temperature (°F)
70
60
50
40
30
8 PM
6 AM
4 PM
3 AM
1 PM
11 PM
9 AM
Time Of Day

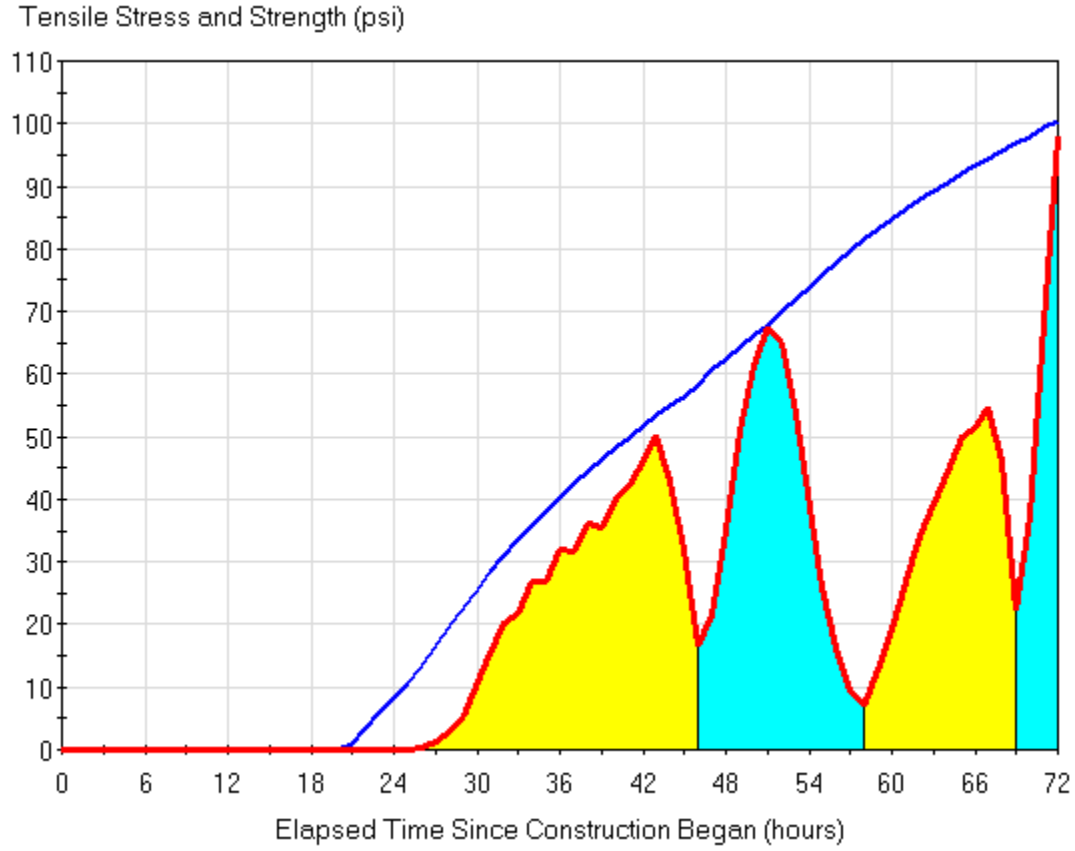
Tensile Stress and Strength (psi)
110
100
90
80
70
60
50
40
30
20
10
0
0
6
12
18
24
30
36
42
48
54
60
66
72
Elapsed Time Since Construction Began (hours)

Oct. 13, 2006

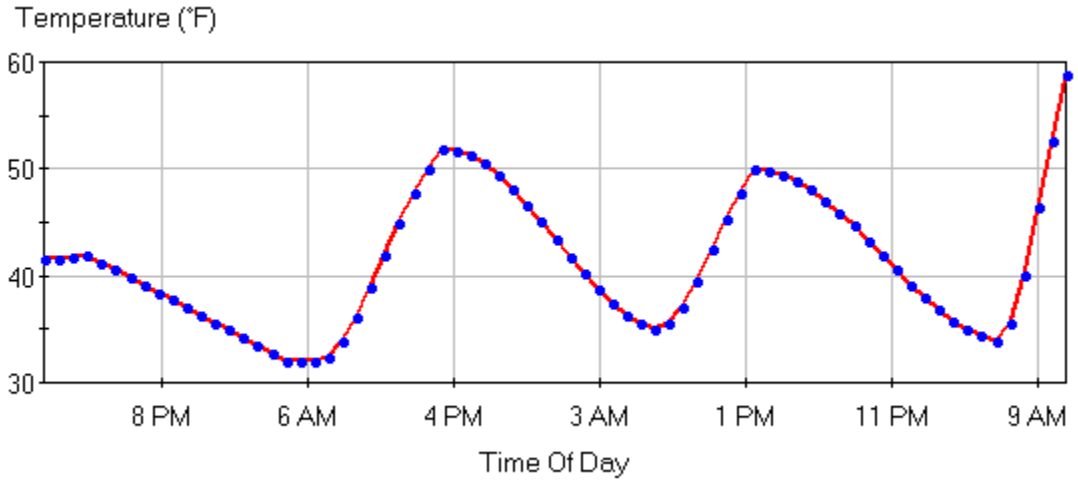
Temperature (°F)
60
50
40
30
8 PM
6 AM
4 PM
3 AM
1 PM
11 PM
9 AM
Time Of Day

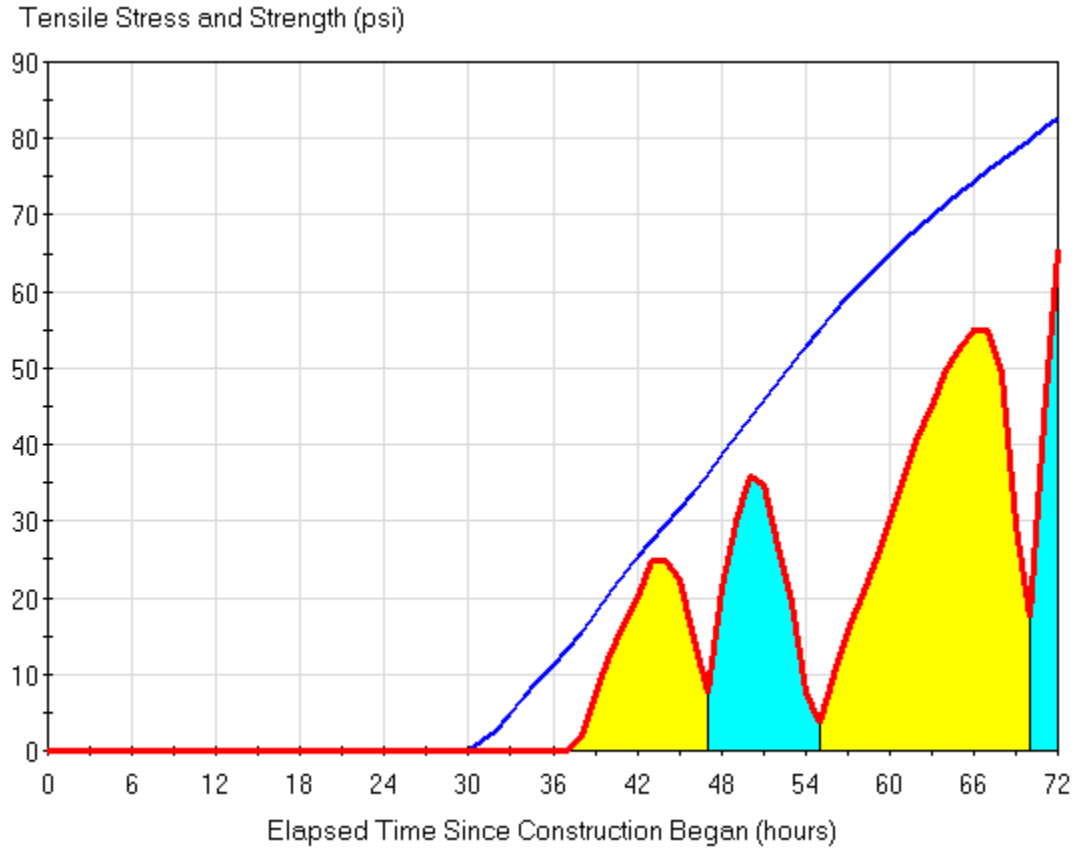
Tensile Stress and Strength (psi)
90
80
70
60
50
40
30
20
10
0
0
6
12
18
24
30
36
42
48
54
60
66
72
Elapsed Time Since Construction Began (hours)

Oct. 14, 2006

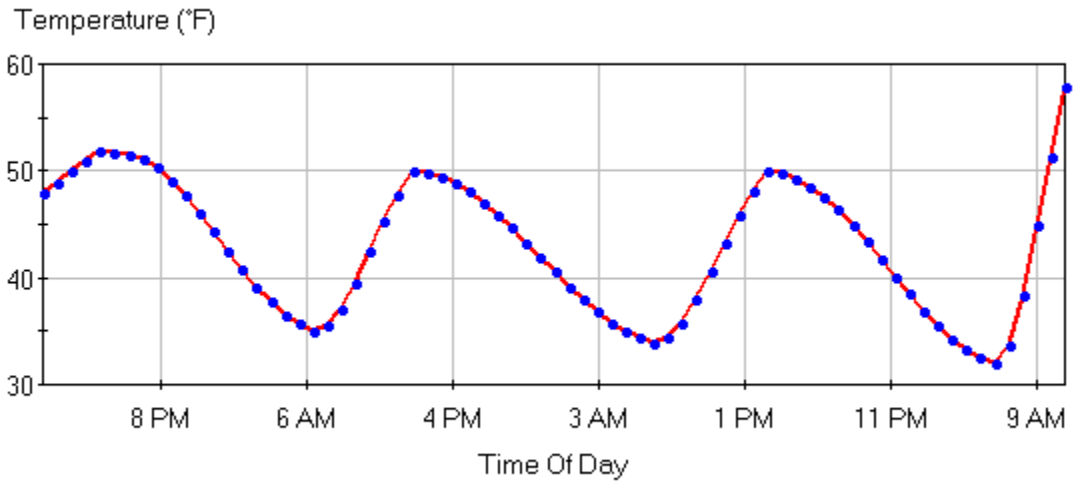
Temperature (°F)
60
50
40
30
8 PM
6 AM
4 PM
3 AM
1 PM
11 PM
9 AM
Time Of Day

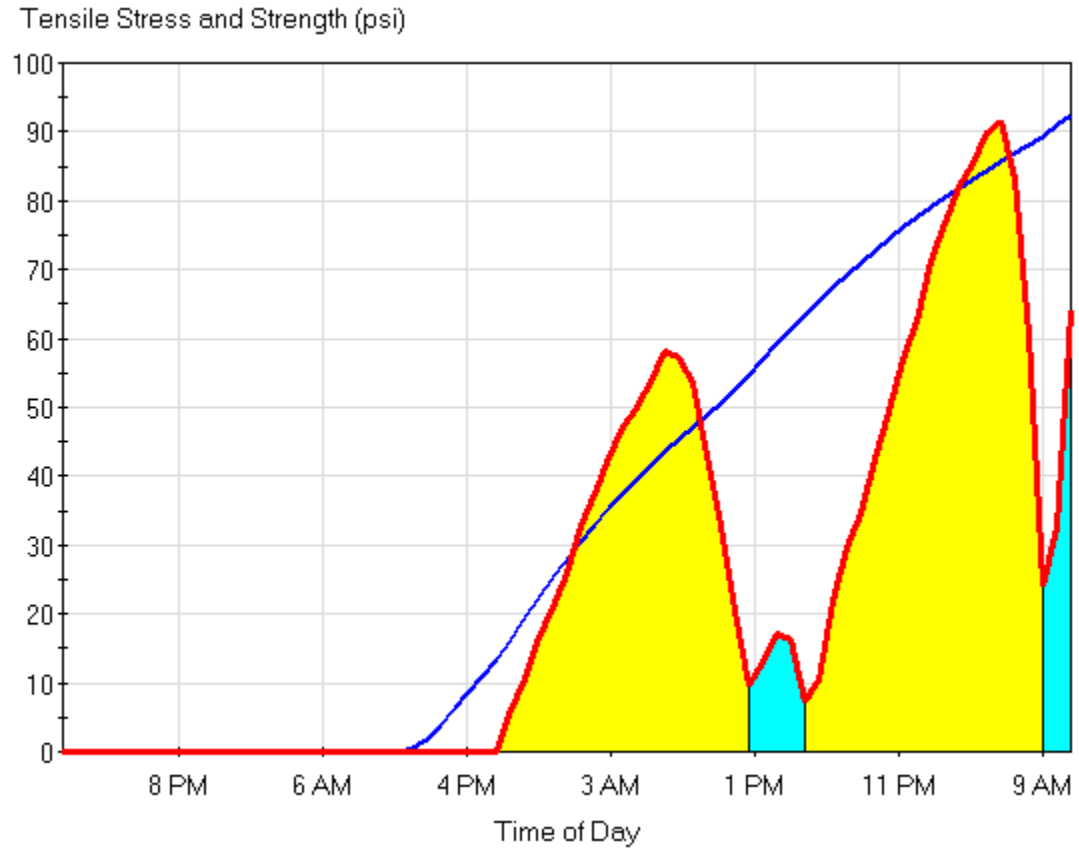
Tensile Stress and Strength (psi)
100
90
80
70
60
50
40
30
20
10
0
8 PM
6 AM
4 PM
3 AM
1 PM
11 PM
9 AM
Time of Day

Oct. 15, 2006

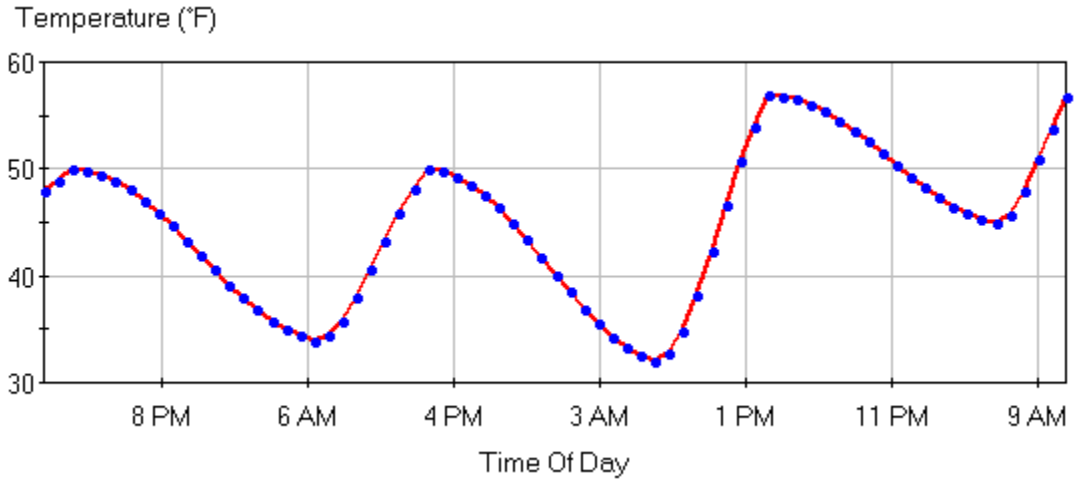
Temperature (°F)
60
50
40
30
8 PM
6 AM
4 PM
3 AM
1 PM
11 PM
9 AM
Time Of Day

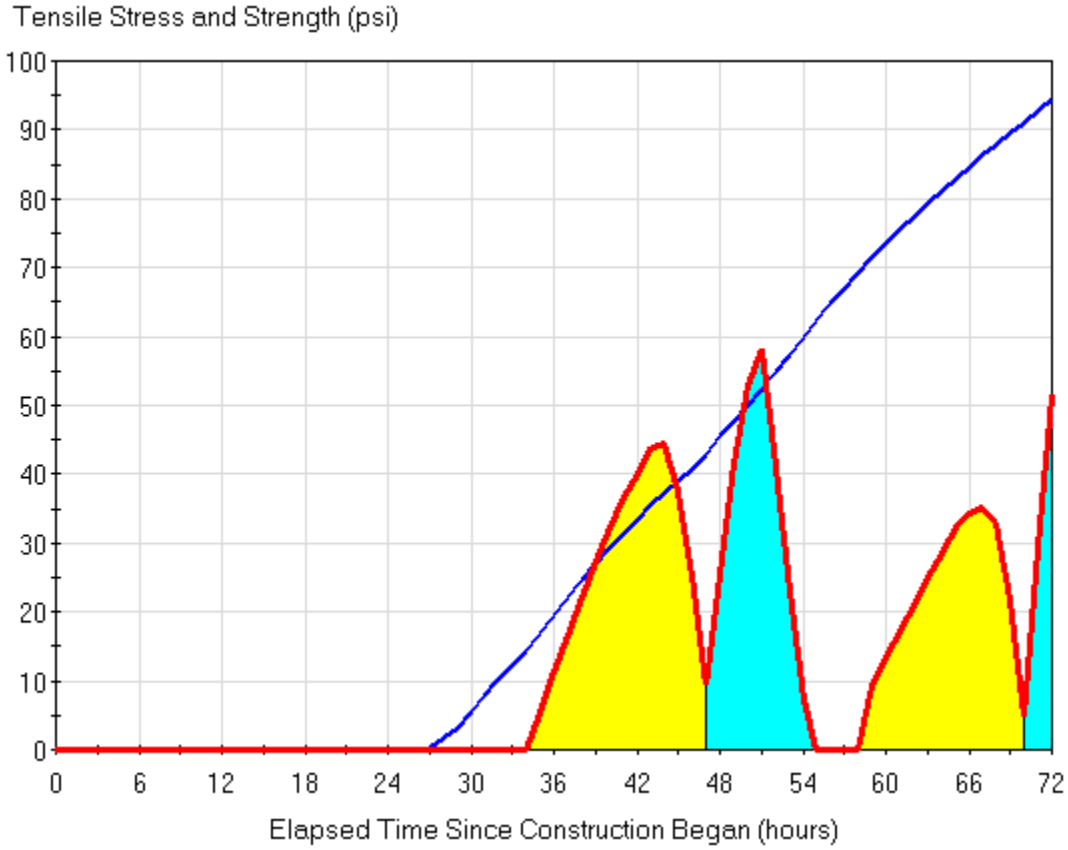
Tensile Stress and Strength (psi)
100
90
80
70
60
50
40
30
20
10
0
0
6
12
18
24
30
36
42
48
54
60
66
72
Elapsed Time Since Construction Began (hours)

Oct. 16, 2006

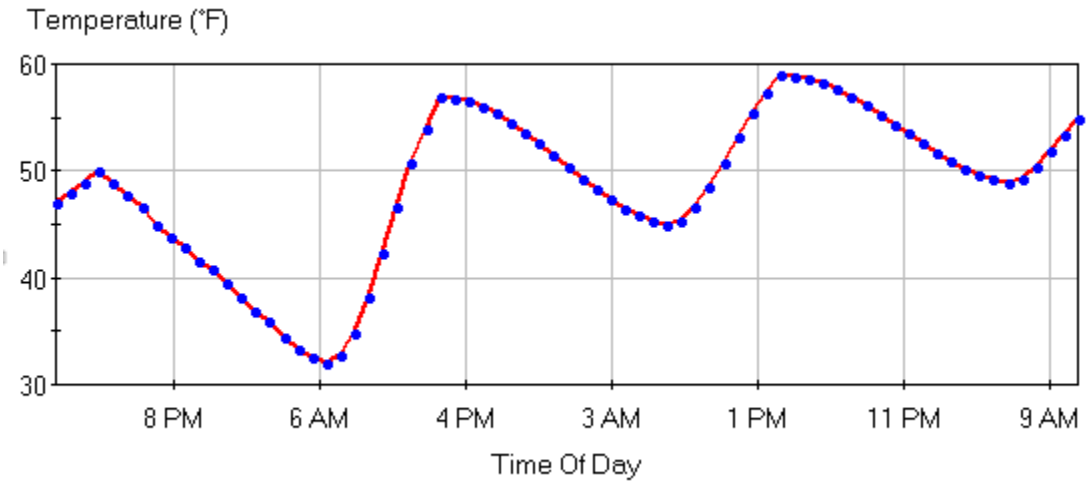
Temperature (°F)
60
50
40
30
8 PM
6 AM
4 PM
3 AM
1 PM
11 PM
9 AM
Time Of Day

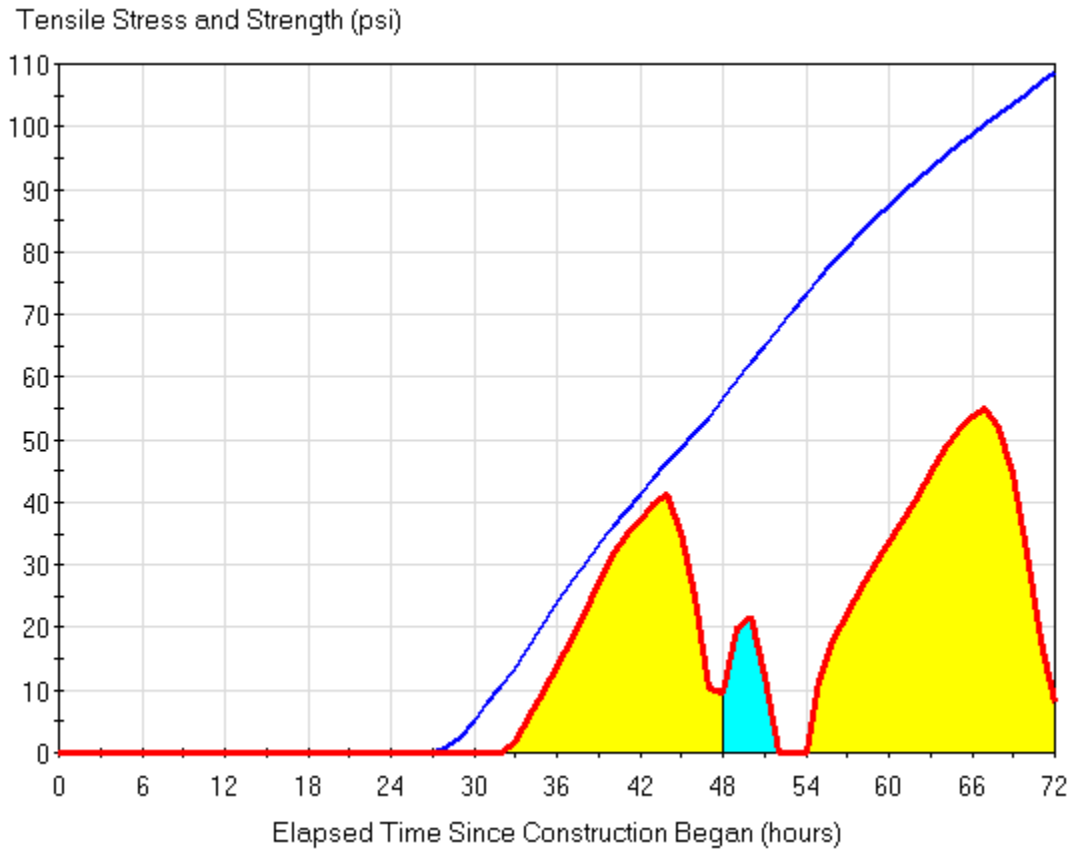
Tensile Stress and Strength (psi)
110
100
90
80
70
60
50
40
30
20
10
0
0
6
12
18
24
30
36
42
48
54
60
66
72
Elapsed Time Since Construction Began (hours)

Oct. 17, 2006

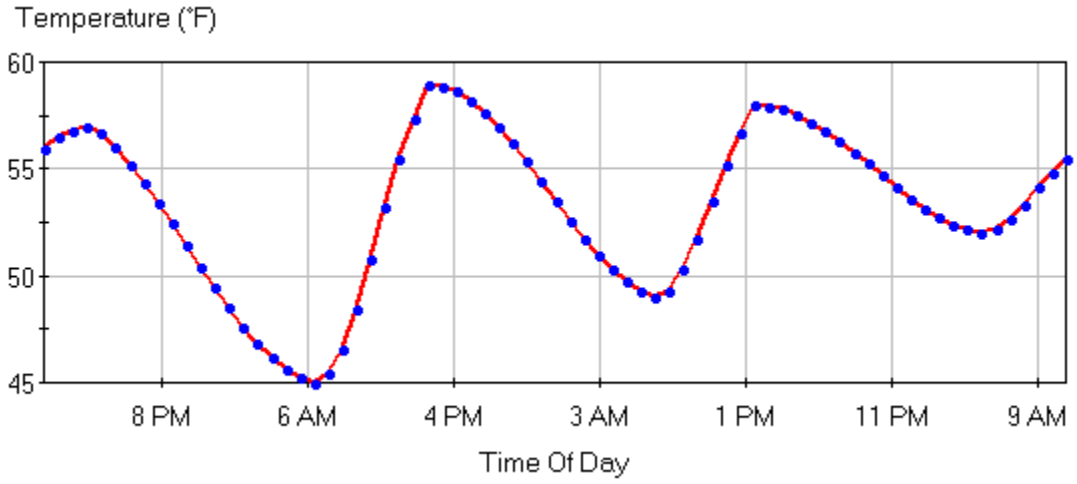
Temperature (°F)
60
55
50
45
8 PM
6 AM
4 PM
3 AM
1 PM
11 PM
9 AM
Time Of Day

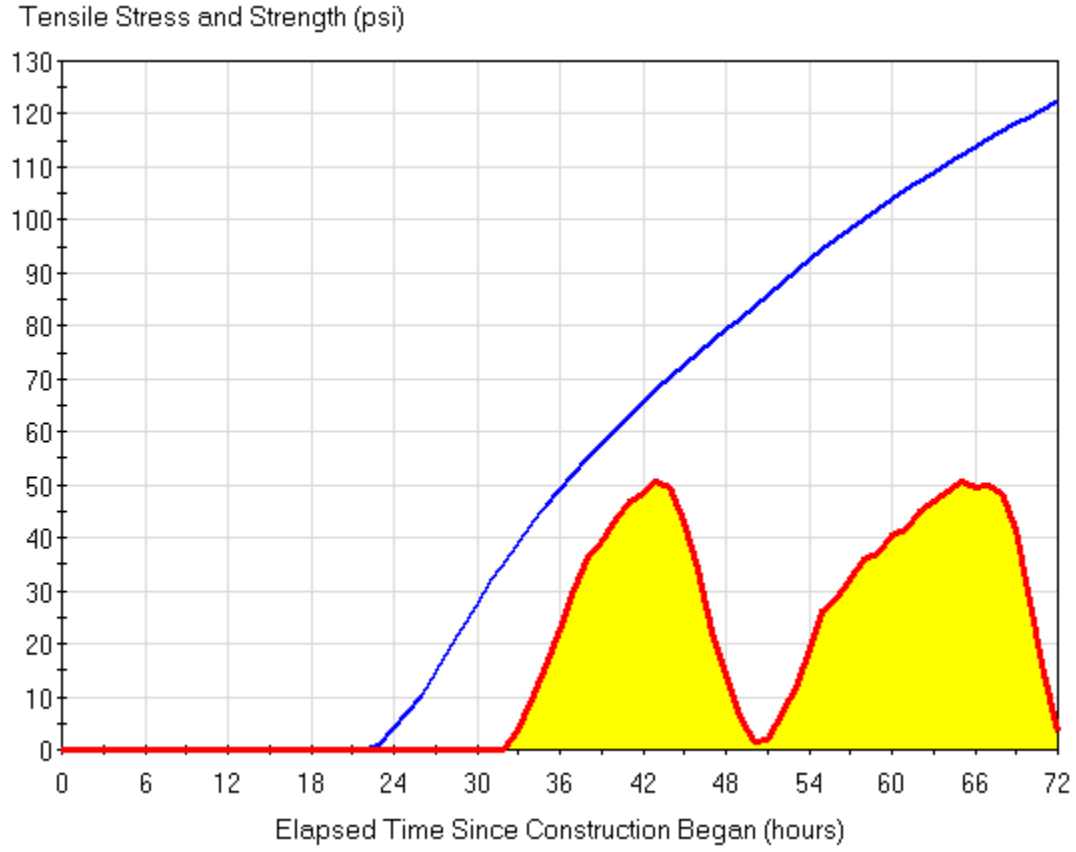
Tensile Stress and Strength (psi)
130
120
110
100
90
80
70
60
50
40
30
20
10
0
0
6
12
18
24
30
36
42
48
54
60
66
72
Elapsed Time Since Construction Began (hours)

Oct. 18, 2006

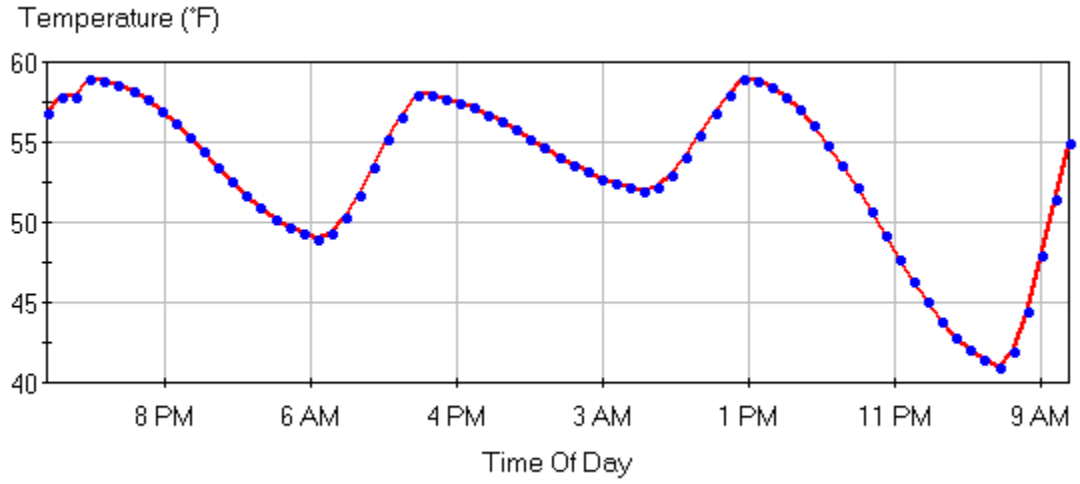
Temperature (°F)
60
55
50
45
40
8 PM
6 AM
4 PM
3 AM
1 PM
11 PM
9 AM
Time Of Day

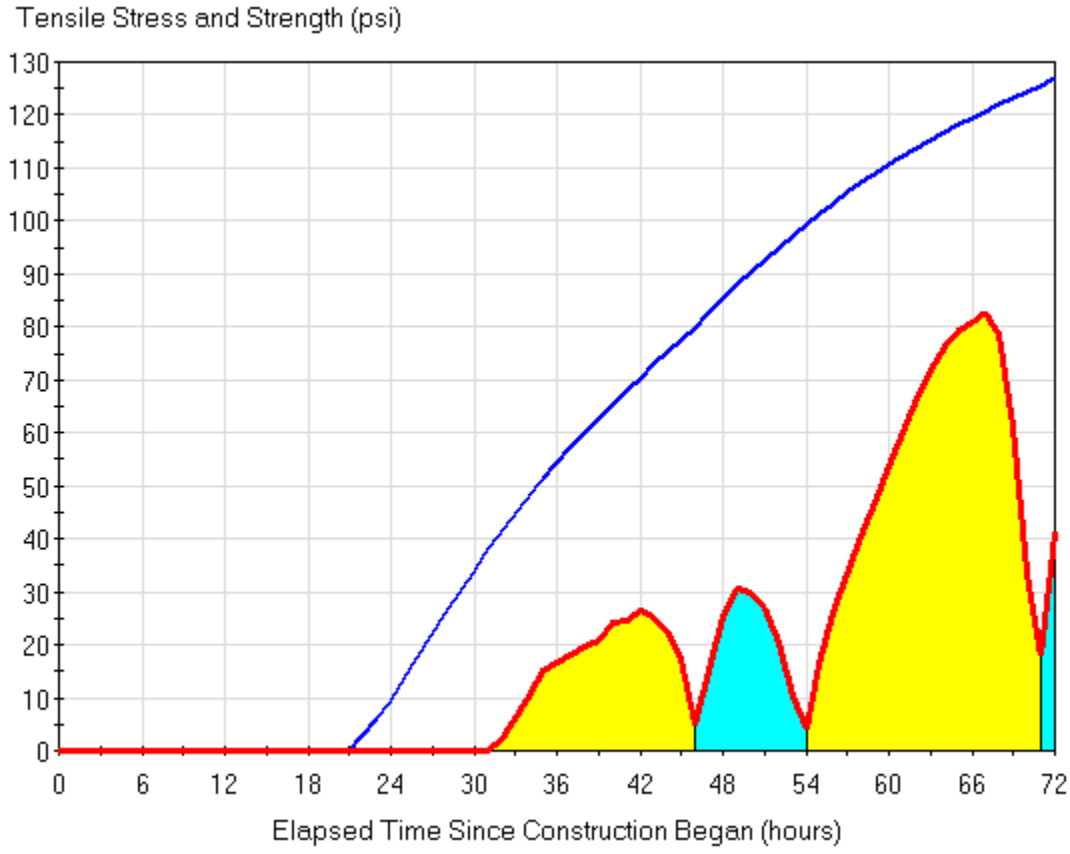
Tensile Stress and Strength (psi)
130
120
110
100
90
80
70
60
50
40
30
20
10
0
0
6
12
18
24
30
36
42
48
54
60
66
72
Elapsed Time Since Construction Began (hours)

Oct. 19, 2006

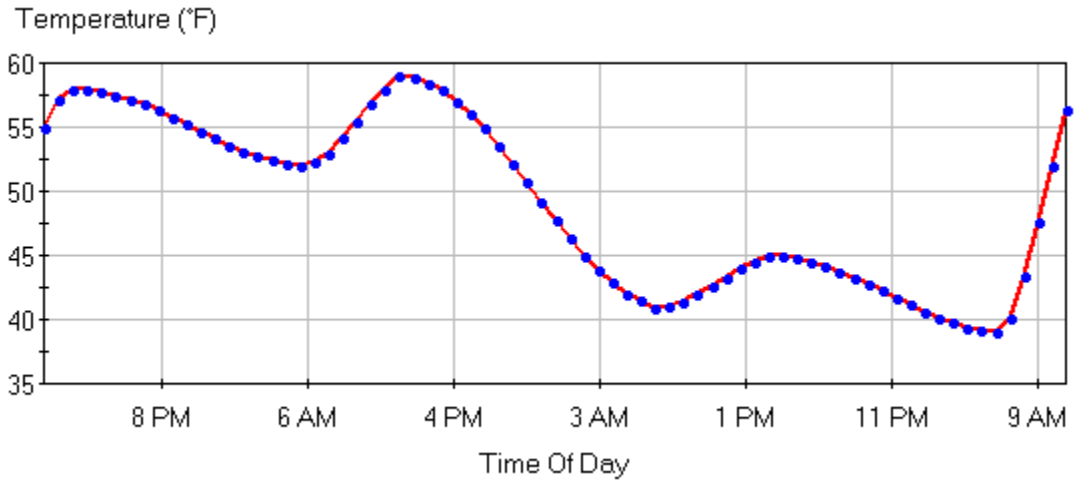
Temperature (°F)
60
55
50
45
40
35
8 PM
6 AM
4 PM
3 AM
1 PM
11 PM
9 AM
Time Of Day

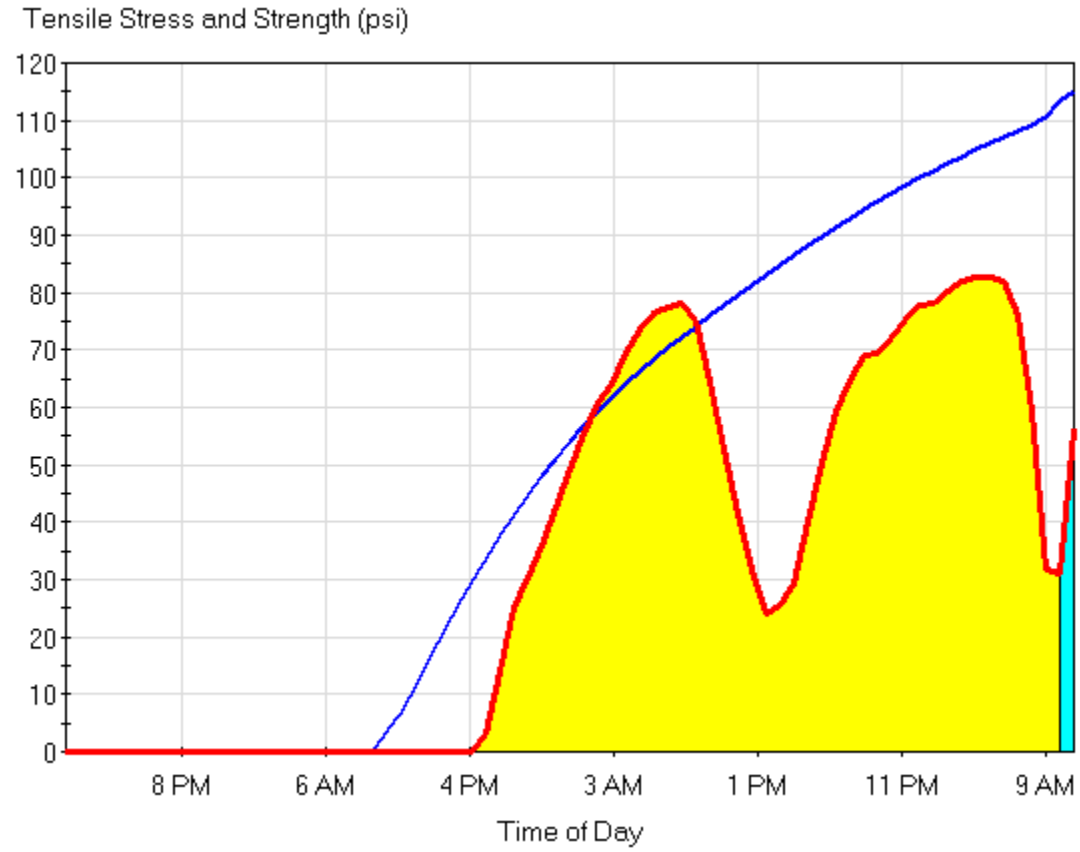
Tensile Stress and Strength (psi)
120
110
100
90
80
70
60
50
40
30
20
10
0
8 PM
6 AM
4 PM
3 AM
1 PM
11 PM
9 AM
Time of Day

Oct. 20, 2006

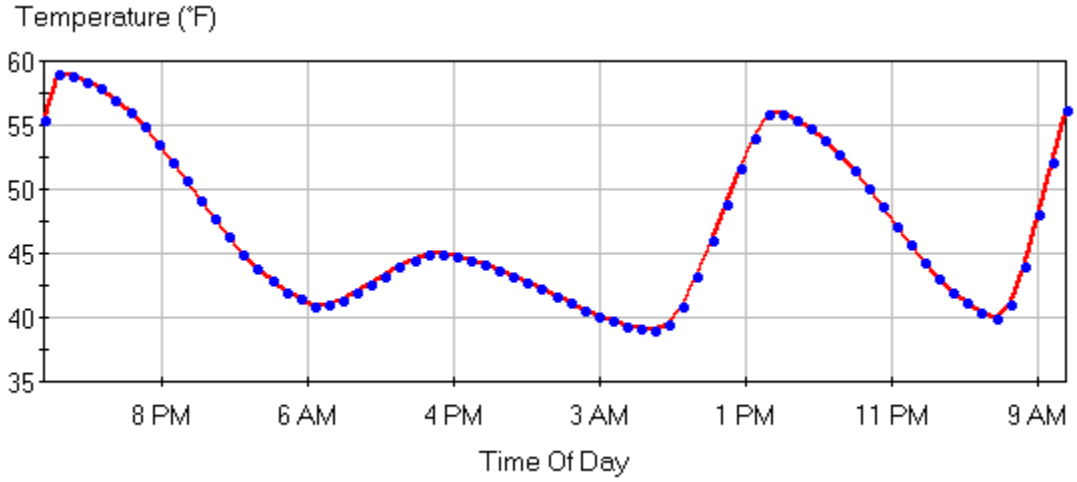
Temperature (°F)
60
55
50
45
40
35
8 PM
6 AM
4 PM
3 AM
1 PM
11 PM
9 AM
Time Of Day

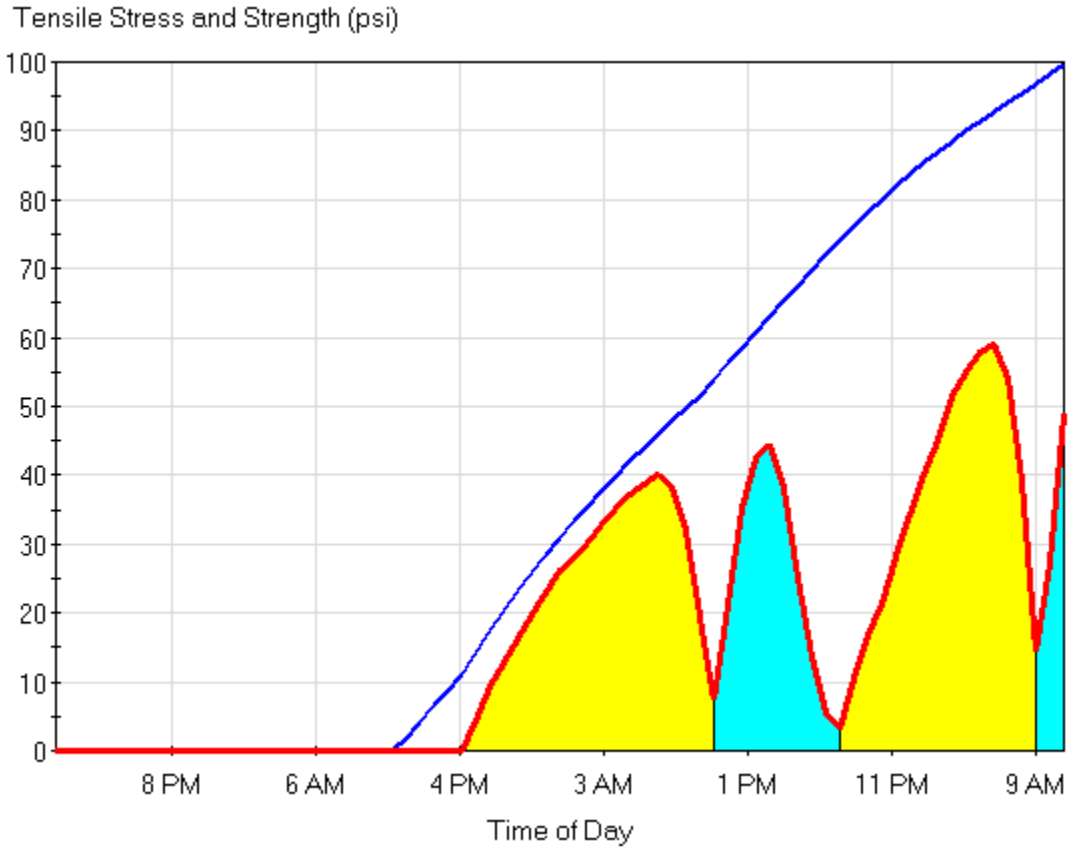
Tensile Stress and Strength (psi)
100
90
80
70
60
50
40
30
20
10
0
8 PM
6 AM
4 PM
3 AM
1 PM
11 PM
9 AM
Time of Day

Oct. 21, 2006

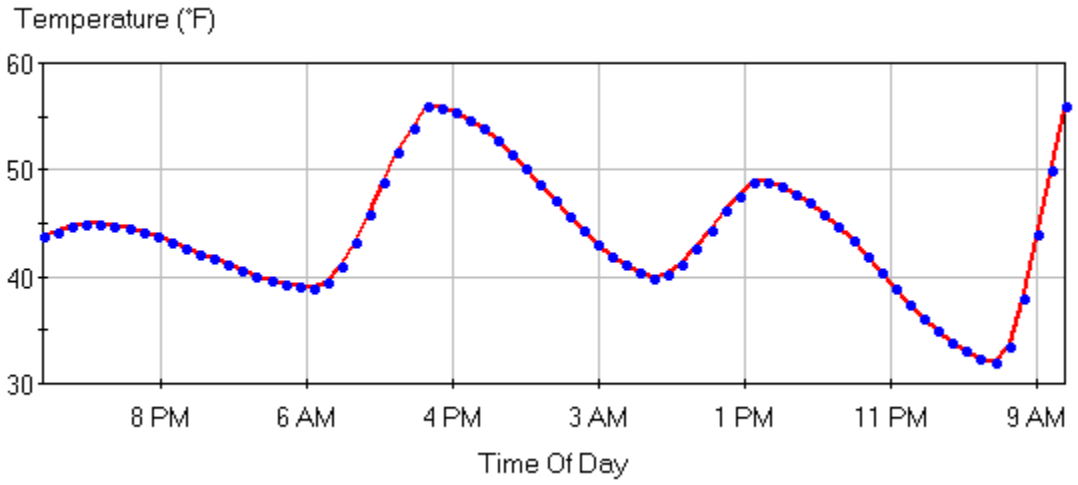
Temperature (°F)
60
50
40
30
8 PM
6 AM
4 PM
3 AM
1 PM
11 PM
9 AM
Time Of Day

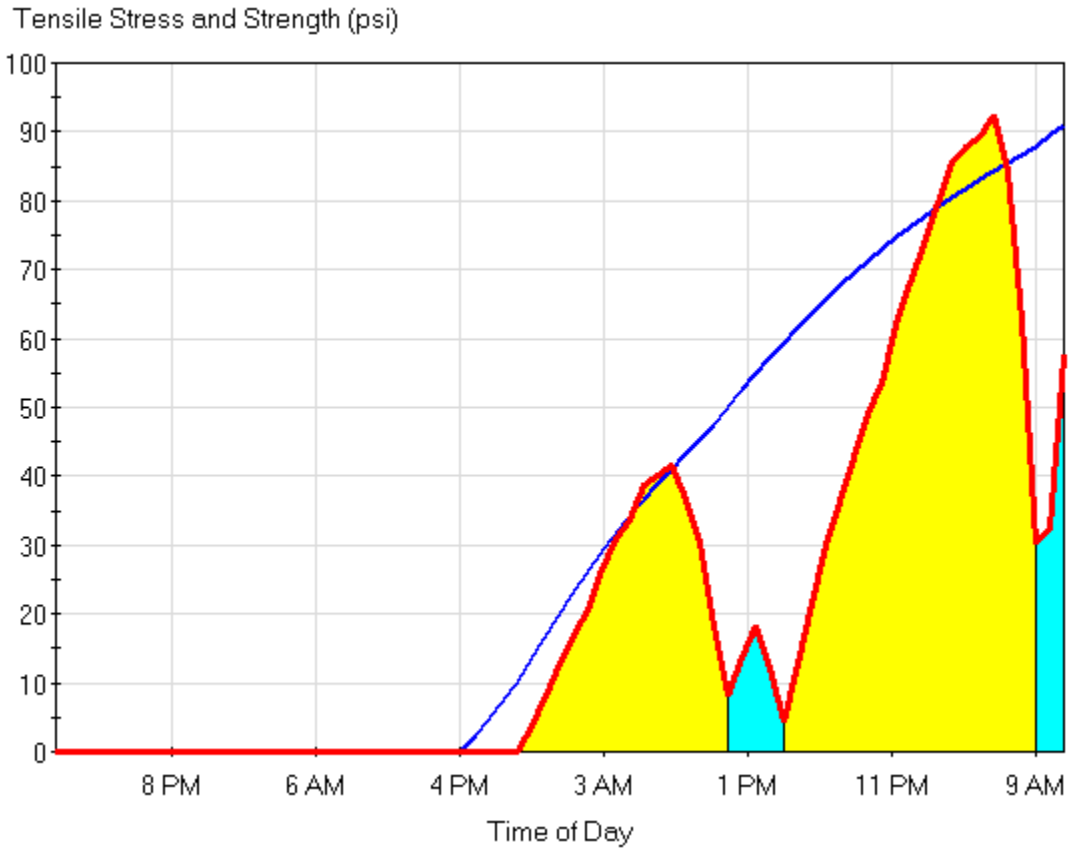
Tensile Stress and Strength (psi)
100
90
80
70
60
50
40
30
20
10
0
8 PM
6 AM
4 PM
3 AM
1 PM
11 PM
9 AM
Time of Day

Oct. 22, 2006

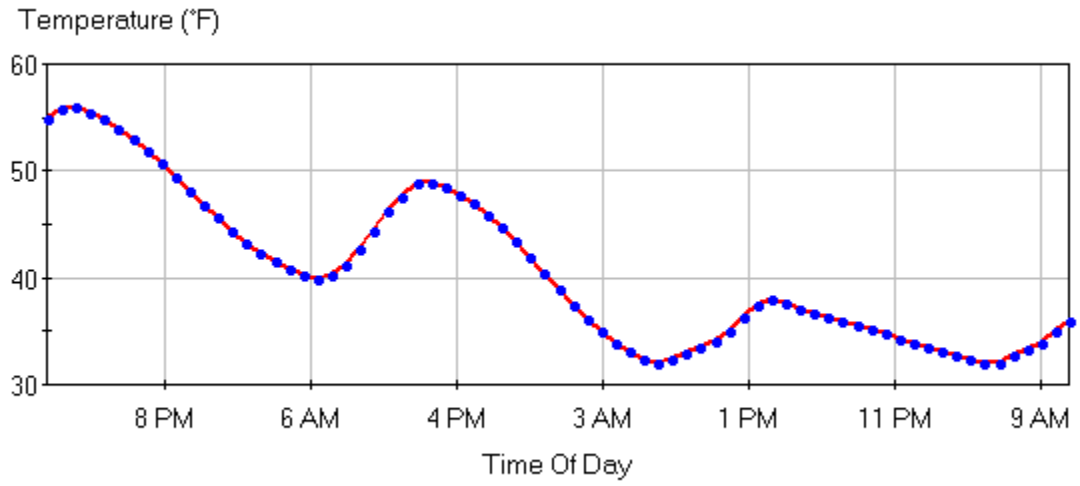
Temperature (°F)
60
50
40
30
8 PM
6 AM
4 PM
3 AM
1 PM
11 PM
9 AM
Time Of Day

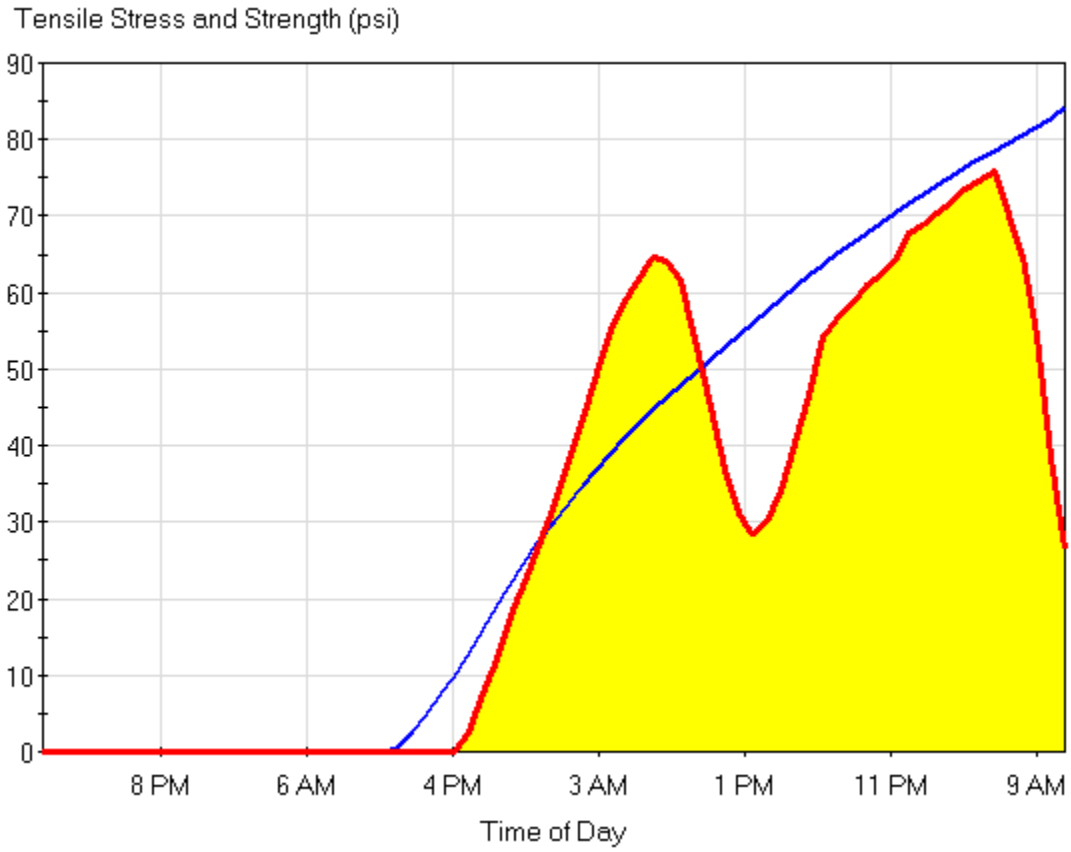
Tensile Stress and Strength (psi)
90
80
70
60
50
40
30
20
10
0
8 PM
6 AM
4 PM
3 AM
1 PM
11 PM
9 AM
Time of Day

Oct. 23, 2006

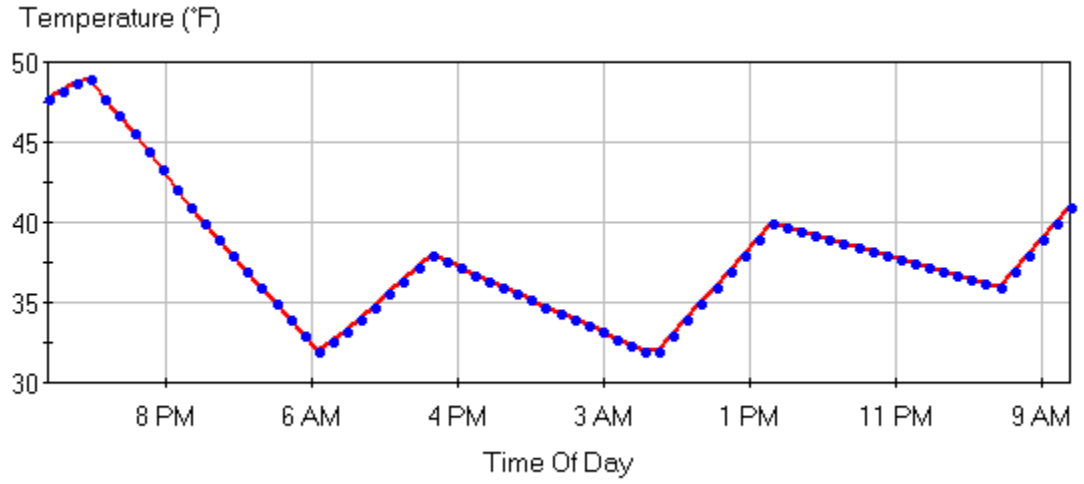
Temperature (°F)
50
45
40
35
30
8 PM
6 AM
4 PM
3 AM
1 PM
11 PM
9 AM
Time Of Day

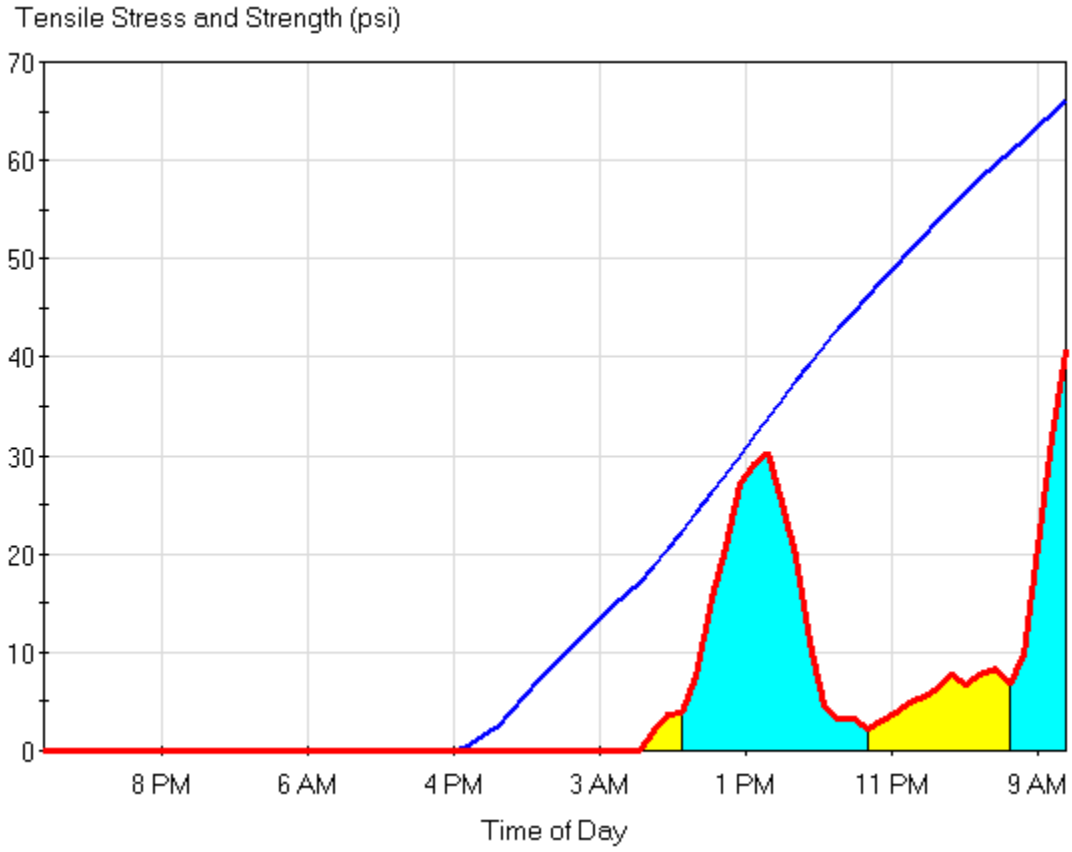
Tensile Stress and Strength (psi)
70
60
50
40
30
20
10
0
8 PM
6 AM
4 PM
3 AM
1 PM
11 PM
9 AM
Time of Day

Oct. 24, 2006

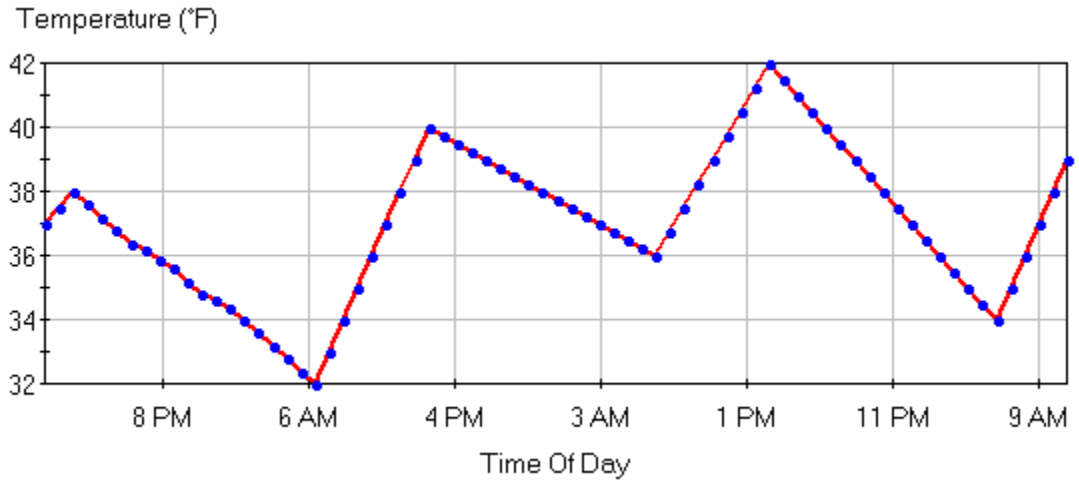
Temperature (°F)
42
40
38
36
34
32
8 PM
6 AM
4 PM
3 AM
1 PM
11 PM
9 AM
Time Of Day

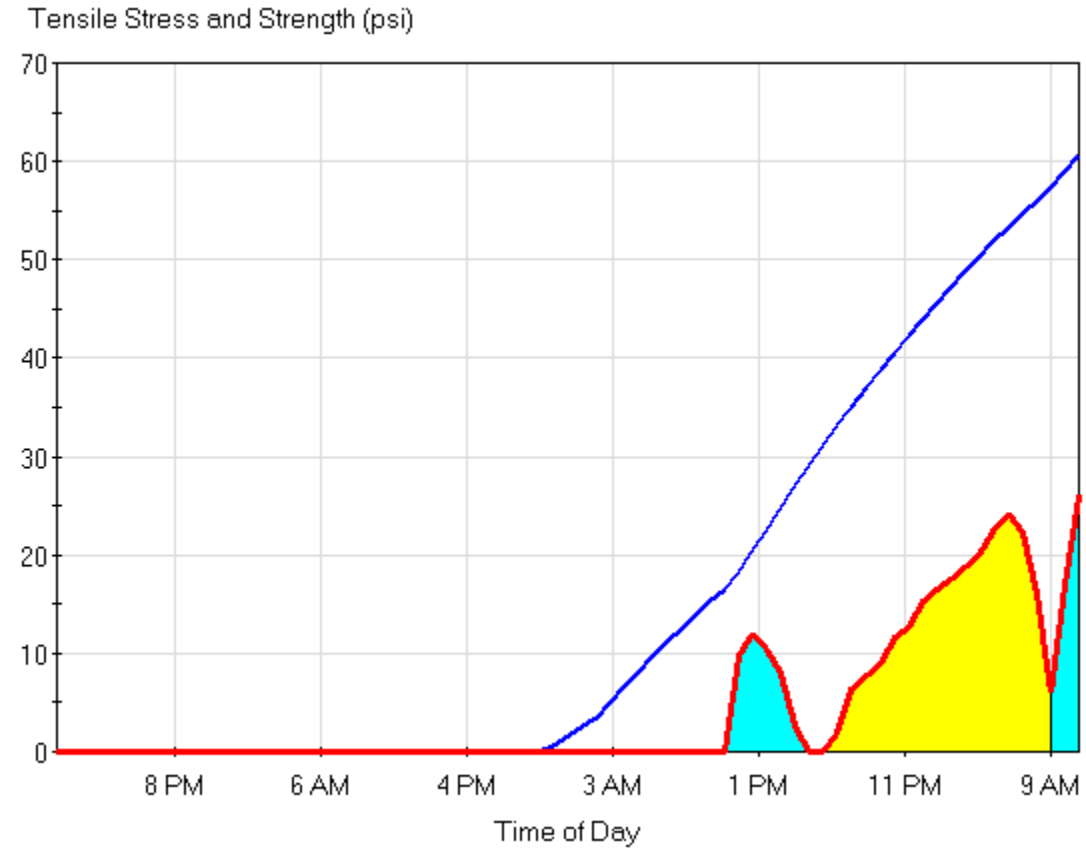
Tensile Stress and Strength (psi)
70
60
50
40
30
20
10
0
8 PM
6 AM
4 PM
3 AM
1 PM
11 PM
9 AM
Time of Day

Oct. 25, 2006

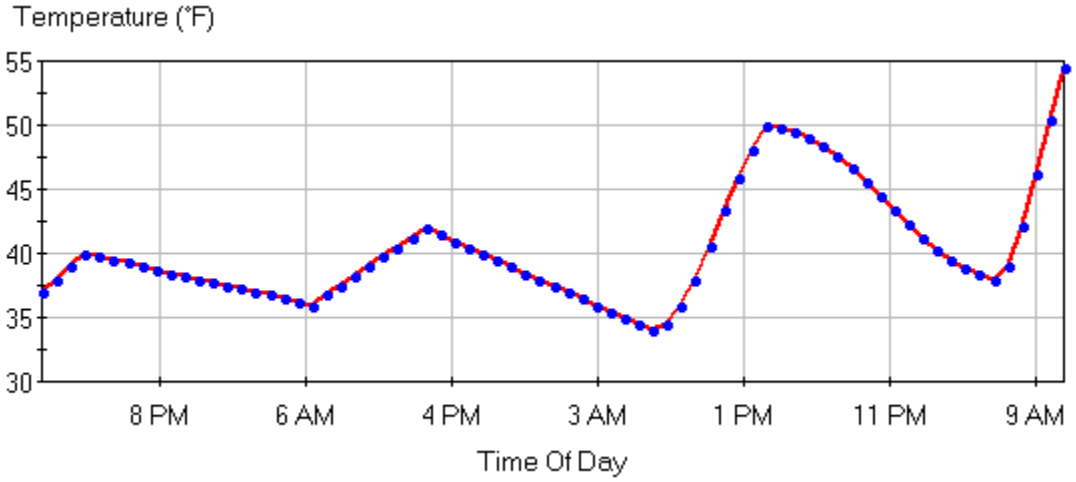
Temperature (°F)
55
50
45
40
35
30
8 PM
6 AM
4 PM
3 AM
1 PM
11 PM
9 AM
Time Of Day

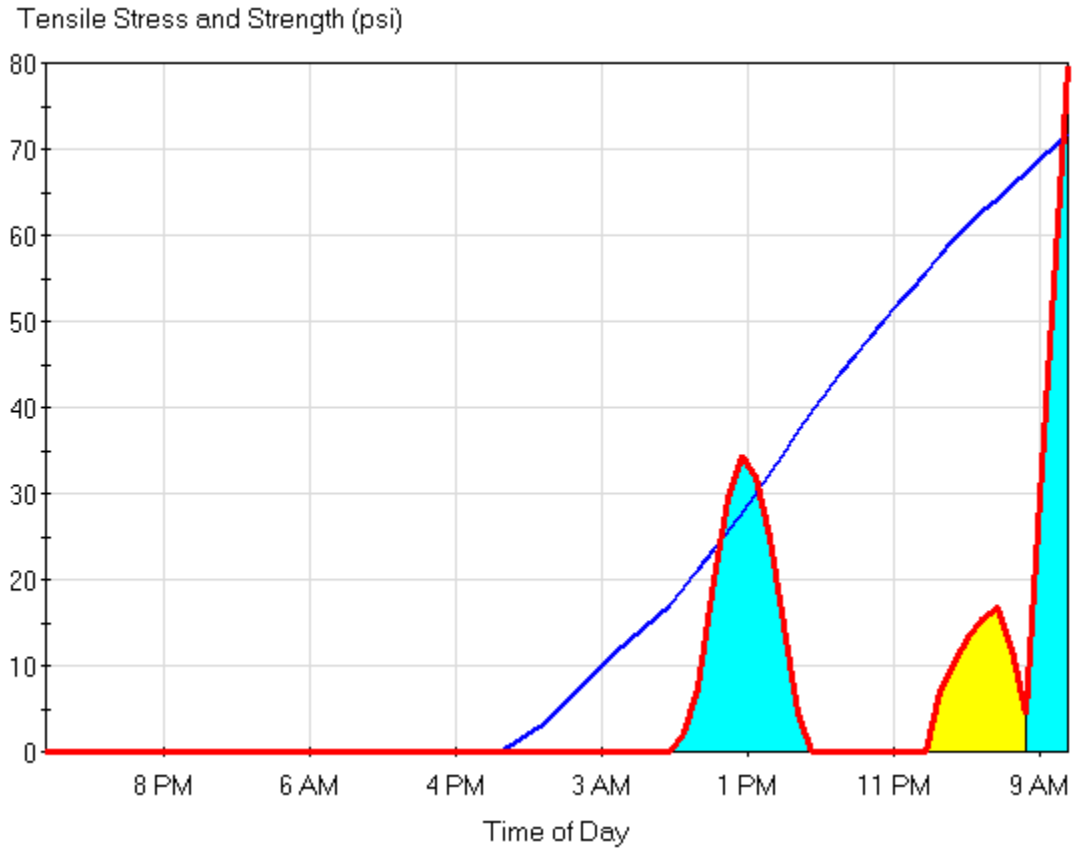
Tensile Stress and Strength (psi)
80
70
60
50
40
30
20
10
0
8 PM
6 AM
4 PM
3 AM
1 PM
11 PM
9 AM
Time of Day

ORITE • 233 Stocker Center • Athens, Ohio 45701-2979 • 740-593-0430
Fax: 740-593-0625 • orite@ohio.edu • http://www.ohio.edu/orite/